UNIVERSITY OF SOUTHAMPTON

FACULTY OF ENGINEERING AND PHYSICAL SCIENCES

School of Chemistry

Active template synthesis of chiral interlocked molecules

by

Florian Modicom

Thesis for the degree of Doctor of Philosophy

December 2018

UNIVERSITY OF SOUTHAMPTON

ABSTRACT

Faculty of engineering and physical sciences

School of Chemistry

Thesis for the degree of Doctor of Philosophy

Active template synthesis of chiral interlocked molecules

by

Florian Modicom

Mechanically interlocked molecules are very interesting compounds for their architecture. The core of these molecules is readily accessible using a large range of synthetic approaches that give access to a wide range of functional group for applications such as sensors, molecular machines or catalyst. This last field attracts attention with the recent emergence of enantioselective catalytic platform and tuneable catalysts, such as on and off switchable or stimuli response catalysts.

In this thesis, the starting chapter highlights the evolution of the synthesis of mechanically interlocked molecules and a selection of chiral systems with recent applications in enantioselective transformations. The following chapter illustrates the influence of the mechanical bond in copper-catalysed transformations. This involved the synthesis of a model rotaxane and the application of rotaxane-based ligand in various copper-catalysed transformations with improvement in terms of diastereoselectivity and conversion. The third chapter is an illustration of a modification of reactivity related to the mechanical bond. The unprecedented tandem reaction, of an otherwise stable moiety, for the synthesis of rotaxanes highlighted in this chapter was a feature of the mechanical bond. The fourth chapter is dedicated to the improvement of an existing approach for the production of simple catenanes in excellent yield. The approach developed in this chapter was extended to multicomponent systems with unprecedented success. The last chapter in an extension of the fourth chapter to access chiral catenanes. The development of a new approach for the accessible synthesis of topologically chiral catenanes enabled the access of usually very complicated molecules.

Table of Contents

Table of Contents ..... *iii*

DECLARATION OF AUTHORSHIP ..... *vi*

Acknowledgements ..... *vii*

Definitions and Abbreviations ..... *viii*

Chapter 1: Introduction 11

1.1. Introduction *12*

1.1.1. Mechanically Interlocked Molecules (MIMs) 12

1.1.2. Synthesis of [2]catenanes and [2]rotaxanes 13

1.1.2.1. Early synthesis 13

1.1.2.2. Passive template synthesis 14

1.1.2.3. Active template metal based synthesis 19

1.1.3. Chirality in rotaxanes and catenanes 25

1.1.3.1. Chiral covalent stereogenic units 26

1.1.3.2. Mechanically planar chiral rotaxane 33

1.1.3.3. Topologically chiral catenane 36

1.2. Conclusions *38*

1.3. Aims of this project *38*

1.4. Bibliography *39*

Chapter 2: The effect of the mechanical bond in copper-catalysed transformations 45

2.1. Introduction *46*

2.1.1. Bipyridine function in macrocycles and AT-CuAAC 46

2.1.2. Introduction to carbene chemistry 49

2.1.2.1. Free carbene 49

2.1.2.2. Fischer-type metal carbene 49

2.1.2.3. Schrock-type metal carbene 50

2.1.2.4. Copper carbene complex reactivity 51

2.1.2.5. Bipyridine ligands in copper catalysis 54

2.1.3. Aims of the project 56

2.2. Results and Discussion *57*

2.2.1. Synthesis of the rotaxane model 57

2.2.1.1. Synthesis of macrocycle **78** 57

2.2.1.2. Synthesis of the two stoppers **30** and **32** 59

2.2.1.3. Synthesis of the rotaxane model **104** 59

2.2.1.4. Complexation of rotaxane **104** with Cu^{I} 61

2.2.2. Evaluation of the behaviour in copper catalysed reactions using an achiral ligand .. 62

2.2.2.1. Henry reaction....63
2.2.2.2. Cyclopropanation reaction....64
2.2.2.3. Insertion of carbenoid in NH bond....68
2.3. Conclusions and Future Work....70
2.4. Experimental....71
2.5. Bibliography....92
Chapter 3: Chemical consequences of the mechanical bond: a tandem active template-rearrangement reaction....95
3.1. Introduction....96
3.1.1. Synthesis of the 1,2,3-triazole motif....96
3.1.2. Transformations of 1,2,3-triazoles....96
3.1.2.1. Dimroth rearrangement....96
3.1.2.2. Thermal induced transformation....97
3.1.2.3. 1-Sulfonyl-1,2,3-triazole....98
3.1.3. Aims and objectives....102
3.2. Results and Discussion....103
3.2.1. Starting material syntheses....103
3.2.2. Isolation and characterisation of the novel interlocked structure....105
3.2.3. Optimisation of the reaction....109
3.2.4. Scope of the reaction....112
3.2.5. Mechanistic investigations....117
3.3. Conclusions and Future Work....122
3.4. Experimental....123
3.5. Bibliography....197
Chapter 4: Efficient multicomponent active template synthesis of catenanes....199
4.1. Introduction....200
4.2. Results and Discussion....201
4.2.1. Synthesis of azide-alkyne functionalised precursor....201
4.2.2. Optimisation of the [2]catenane synthesis using **236**....202
4.2.3. Variation of the bipyridine functionalised macrocycle....204
4.2.4. Multicomponent AT-CuAAC approach for the synthesis of [2]catenane....208
4.3. Conclusions and Future Work....218
4.4. Experimental....219
4.5. Bibliography....291
Chapter 5: Stereoselective synthesis of a topologically chiral [2]catenane....293
5.1. Introduction....294
5.2. Results and Discussion....295
5.2.1. Synthesis of a precursor bearing a chiral centre....295
5.2.2. Synthesis of triazole-containing macrocycles **272** and **274**....296

5.2.3. Attempts to synthesise and separate diastereoisomeric mixture of catenanes..... 296
5.2.4. Synthesis of macrocycle **274** 297
5.2.5. Separation of a diastereoisomeric mixture of catenanes. 298
5.2.6. Attempts to remove the stereogenic centre 301
5.3. Conclusions and Future Work *306*
Experimental *307*
5.4. Bibliography *349*

DECLARATION OF AUTHORSHIP

I, Florian Modicom, declare that this thesis and the work presented in it are my own and has been generated by me as the result of my own original research.

Active template synthesis of chiral interlocked molecules

I confirm that:

1. This work was done wholly or mainly while in candidature for a research degree at this University;

2. Where any part of this thesis has previously been submitted for a degree or any other qualification at this University or any other institution, this has been clearly stated;

3. Where I have consulted the published work of others, this is always clearly attributed;

4. Where I have quoted from the work of others, the source is always given. With the exception of such quotations, this thesis is entirely my own work;

5. I have acknowledged all main sources of help;

6. Where the thesis is based on work done by myself jointly with others, I have made clear exactly what was done by others and what I have contributed myself;

7. Parts of this work have been published as:

E. M. G. Jamieson, F. Modicom and S. M. Goldup, "*Chirality in rotaxanes and catenanes*", *Chem*. *Soc*. *Rev*. 2018, **47**, 5266-5311.
J. E. M. Lewis, F. Modicom, S. M. Goldup, "*Efficient multicomponent active template synthesis of catenanes*" *J*. *Am*. *Chem*. *Soc*., **2018**, 140, 4787-4791.

M. A. Jinks, A. de Juan, M. Denis, C. J. Fletcher, M. Galli, E. M. G. Jamieson, F. Modicom, Z. Zhang, S. M. Goldup, "*Stereoselective synthesis of mechanically planar chiral rotaxanes*" *Angew*. *Chem*. *Int*. *Ed*. Accepted (DOI 10.1002/anie.201808990)

Signed:.....

Date:.....

Acknowledgements

I would like to thank the most important person in the Goldup lab, Steve for being a source of motivation and guidance over the past three years. I would like to thank Steve and Mike for proof reading my thesis and helping me to improve my annoying writing style. A big thank would go to the Goldup group and all the members I had the opportunity to work with over my thesis.

I would like to thank Jamie for his human and scientific lessons as well as his help when times were darker in my research. He was a fantastic “lab manager” and example for the lab.

I would like to thank Ellen for her energy and constant motivation when the project was not the best.

I would like to thank Mathieu for his happiness and helping me to be more organised and by making my writing easier. I would like to thank Jack for being so happy and playing his old music every morning. I would like to thank Peggy, she is an amazing cook outside the lab. I would like to thank Mike for being a “papa” in the lab and being also keen for a beer.

I would like to thank Marzia and Elise for forcing me to go to Circuits twice a week. I would like to thank Andrew and Alberto for their excellent scientific discussions. I would like to thank the rest of the lab, Poom, Aman, Amanda, Shu, for being good co-workers.

I would like to thank Neil and Julie for their assistance with NMR and mass spectrometry

I would like to thank my family, especially Mom, for always being here to listen to me during those long years studying chemistry at university.

Finally, I would like to thank the most fabulous person I met in my life, Cyrielle. You are more than my life partner, you also are my example for life.

Definitions and Abbreviations

δ ..... Chemical shift

Ac ..... Acetyl

AIBN ..... Azobisisobutyronitrile

Aq. ..... Aqueous

Ar ..... Aromatic

AT-CuAAC ..... Active-template Cu-catalysed azide-alkyne cycloaddition

Boc ..... *t*-Butyloxycarbonyl

Bz ..... Benzoyl

CAN ..... Cerium Ammonium Nitrate

CD ..... Circular dichroism

COSY ..... Correlation spectroscopy

CSP-HPLC ..... Chiral stationary phase high-performance liquid chromatography

Cy ..... Cyclohexyl

DDQ 2,3-Dichloro-5,6-dicyano-1,4-benzoquinone

de ..... diastereoisomeric excess

DMF ..... *N,N*-Dimethylformamide

DMSO ..... Dimethylsulfoxide

EDTA ..... *N,N,N',N'*-ethylenediamine tetraacetate

ee ..... Enantiomeric excess

EI ..... Electron Ionisation

Equiv. ..... Equivalent

ESI ..... Electrospray ionisation

EtOAc ..... Ethyl acetate

EtOH ..... Ethanol

h ..... Hours

HMBC ..... Heteronuclear multiple-bond correlation

HPLC ..... High performance liquid chromatography

HRMS ..... High resolution mass spectrometry

HSQC ..... Heteronuclear single quantum correlation

J ..... Coupling constant

JMOD ..... J-modulation spin-echo

LRMS ..... Low resolution mass spectrometry

M ..... Molar

Me ..... Methyl

min ..... Minute

m.p. ..... Melting point

Ms ..... Methanesulfonyl

MS ..... Mass spectrometry

NBS ..... N-Bromosuccinimide

NMR ..... Nuclear magnetic resonance

Ppm ..... Parts per million

quant. ..... Quantitative

R_{mp} ..... *R* isomer (mechanically planar chiral)

R_{mt} ..... *R* isomer (topological chiral)

rt ..... Room temperature

S_{mp} ..... *S* isomer (mechanically planar chiral)

S_{mt} ..... *R* isomer (topological chiral)

TBAF ..... Tetrabutyl Ammonium Fluoride

TFA ..... Trifluoroacetic acid

TfO ..... Trifluoromethanesulfonate

THF ..... Tetrahydrofuran

TLC ..... Thin layer chromatography

Ts 4-Toluenesulfonyl

Chapter 1: Introduction

Abstract: Among Mechanically Interlocked Molecules (MIMs), catenanes are molecules containing two or more interlocked macrocycles, and they are the main subject of this chapter. The evolution of the synthesis of catenanes scaffold is reported. The second part of this chapter is focused on chirality in mechanically interlocked molecules and their applications in assymetric catalysis. Chirality arising from the mechanical bond is also discussed.

Figures 1.21-1.36 appeared in part in our recently published review prepared in collaboration with Ellen Jamieson.

Prior publication: E. M. G. Jamieson, F. Modicom and S. M. Goldup, "Chirality in rotaxanes and catenanes", *Chem*. *Soc*. *Rev*. 2018, **47**, 5266-5311.

1.1. Introduction

1.1.1. Mechanically Interlocked Molecules (MIMs)

Mechanically Interlocked Molecules (MIMs),[1] such as rotaxanes and catenanes (Figure 1.1), have attracted attention not only for their interesting structures, but also for their potential applications in nanotechnology, e.g. molecular machines, switches, wires and motors.[2] In 2016, the Nobel Prize in Chemistry was awarded to Ben Feringa, Jean-Pierre Sauvage and Sir Fraser Stoddart for "*the design and synthesis of molecular machines*".[3]

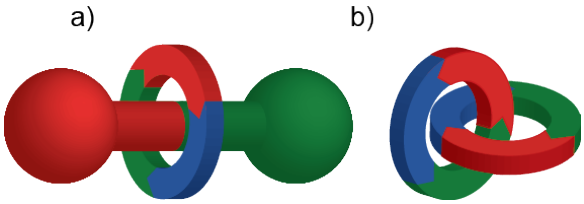

Figure 1.1 Schematic representation of a) [2]rotaxane b) [2]catenane.

A rotaxane is a mechanically interlocked molecule composed of one or more macrocycles threaded on one or more dumbbell shaped molecules (axles). The terminal part of the axle is named a stopper; this group has to be bulky in order to prevent the macrocycle from escaping the architecture ("dethreading"). A catenane is composed of two or more interlocked macrocycles.[4] Rotaxanes and catenanes are considered as single molecules; the separation of each sub-unit requires the breaking of at least one covalent bond. The combination of two separated units into a single molecule is named "mechanical bond". One of the main difference between these two interlocked structures is that the structure of a catenane cannot be altered except by breaking a covalent bond. However, in rotaxane structures, the stretching of the macrocycle may allow the macrocycle to escape over one stopper, resulting in the separation of both sub-units. Mechanically interlocked molecules are generally defined as a kinetically stable multicomponent structure without covalent bond between components. This stability is the direct consequence of the mechanical bond. The nomenclature of mechanically interlocked molecules is determined by the topology of the structure and the number of interlocked components. A number in square bracket is included as a prefix indicating the number of interlocked components, e.g. a catenane containing two macrocycles is written "[2]catenane".

1.1.2. Synthesis of [2]catenanes and [2]rotaxanes

1.1.2.1. Early synthesis

In the early stages, efforts focused on the synthesis of [2]catenanes. The initial attempt by Cramer and co-workers on the synthesis of [2]catenane **3** was unsuccessful using pre-assembly followed by macrocyclisation (Figure 1.2).[5]

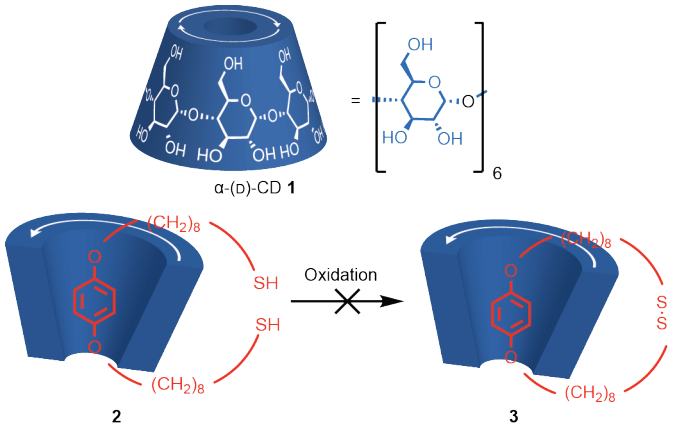

Figure 1.2 Cramer's first attempt to synthesise catenane **3**.

The first synthetic [2]catenane was reported by Wasserman using a statistical approach. However, the yield of the reaction was very low (0.0001%).[6,7] In order to overcome the synthetic challenge for the synthesis of [2]catenane, a new "directed synthesis" to access interlocked molecules was imagined. In the stepwise synthesis reported by Schill and co-workers,[8] the key intramolecular macrocyclisation gave pre-catenane **5** in 30% yield (Figure 1.3). The aniline inside the cavity of **4** and the quaternary carbon centre orientating each electrophile in both side of the plane of the macrocycle were the key factors for this step. [2]Catenane **6** was obtained from **5** in near quantitative yield. The same approach was used for the synthesis of the first [3]catenane by Schill and co-workers.[9,10]

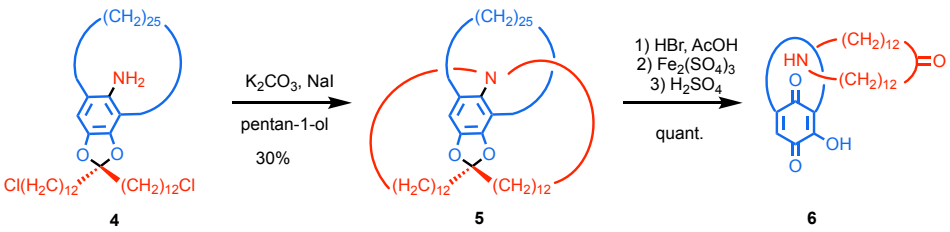

Figure 1.3 Schill's directed synthesis of [2]catenane **6**.

The directed synthesis was the best approach for the synthesis of a [2]catenane for almost twenty years until the approach developed by Sauvage in the early 1980's which was based on a passive template synthesis. However, the directed synthesis was a long and difficult route to obtain an interlocked molecule.

1.1.2.2. Passive template synthesis

In order to overcome the poor yield of the statistical and directed synthesis approaches, passive template synthesis was developed. This approach relies upon the use of non-covalent chemical interactions to hold together the interlocked structure precursors. The supramolecular assembly can be used as reactive structure and undergoes chemical reactions to produce the desired mechanically interlocked structure. The capacity for molecules to interact with one another has been previously studied.[13,14] The crown ether synthesis by Pederson and the studies of cryptands by Lehn and Cram were awarded the 1987 Nobel Prize in Chemistry for "*development and use of molecules with structure-specific interactions of high selectivity*".

Two main strategies were identified to synthesise [2]rotaxanes, as displayed in Figure 1.4 a. The first one involved a pseudo-rotaxane complex in which non-covalent interactions between the pre-axle and the macrocycle were responsible for the stable architecture. The capping of the axle with bulky stoppers generated a rotaxane, in which the macrocycle was not able to slip off the axle. This approach was named stoppering or capping.[15] Catenanes can be produce from the same pseudo-rotaxane by cyclisation of the axle (Figure 1.4 b).[16] On the other hand, the clipping strategy was developed. In this approach, an axle interacts with a pre-macrocycle unit. Then this pre-macrocycle unit is involved in a ring closing reaction in order to form a new covalent bond. This reaction leads to the trapping of the macrocycle around the axle and the generation of the new mechanically interlocked rotaxane.[17] Construction of the mechanical bond in catenane can happen using the same clipping approach by association of two linear units prior to a double cyclisation.[18]

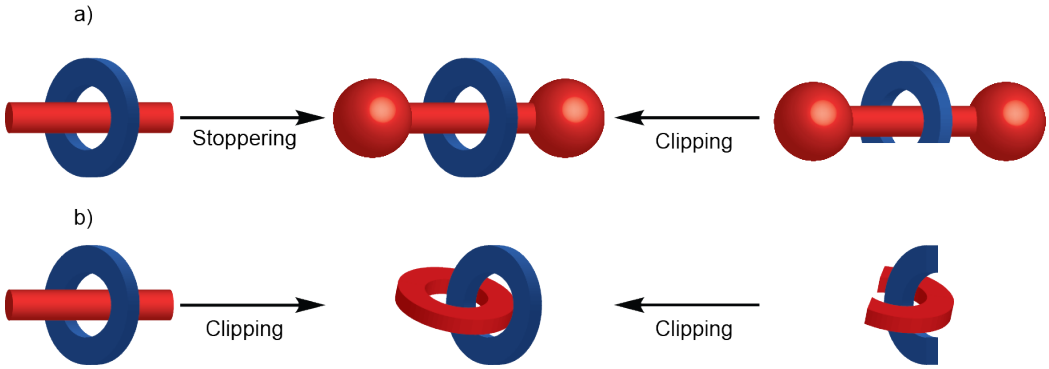

Figure 1.4 Stoppering and clipping approaches in the synthesis of a) [2]rotaxanes and b) [2]catenanes.

The full potential of the passive template for the synthesis of mechanically interlocked molecules was identified by Sauvage. The revolution for the synthesis of mechanically interlocked molecules started with the formation of the [2]catenane using a tetrahedral Cu^{I} template.

The tetrahedral coordination geometry of a Cu^{I} cation allowed the complexation of two phenanthroline-containing ligands orthogonally, responsible for the creation of the crossing point in catenanes. The first passive template synthesis of a [2]catenane using this approach was performed by Sauvage and co-workers in 1983, using Cu^{I} to prepare the catenane precursor **9** followed by macrocyclisation. This yielded Cu^{I} [2]catenane **10** complex in 42% yield (Figure 1.5).[16] The following year, the double clipping approach was employed to form **10** from two equivalents of **8** and a double Williamson macrocyclisation in 27% yield.[18] Tetrahedral Cu^{I} has proven to be an excellent template to access very complex interlocked structures from simple building blocks.[19] In addition, a large range of metals with different coordination spheres were exploited to hold building block and create crossing point in final products.

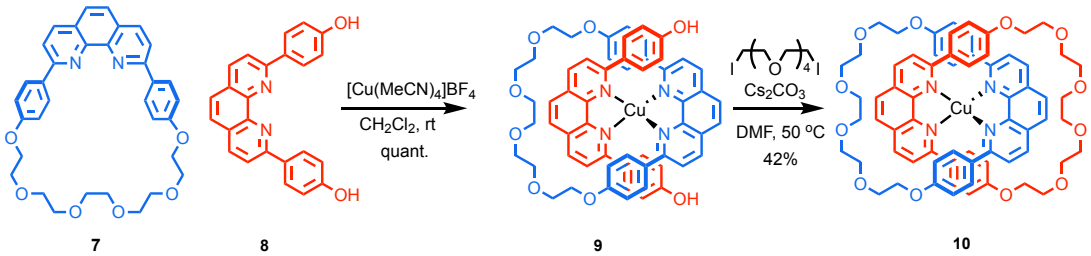

Figure 1.5 Sauvage's passive template approach for the synthesis of [2]catenane **10**. Counter ions omitted for clarity.

The capacity of Zn^{II} to adopt four, five and six ligands was exploited by Sauvage and co-workers in the formation of catenane **13** (Figure 1.6).[20] The complexation of Zn^{II} with tridentate macrocycle **11** and bidentate phenanthroline precursor **12** resulted in the *in-situ* formation of a trigonal bipyramidal arrangement. Pre-organised architecture underwent ring closure metathesis followed by hydrogenation of the internal olefin. The metal free [2]catenane **13** was obtained after demetalation in 40% yield.

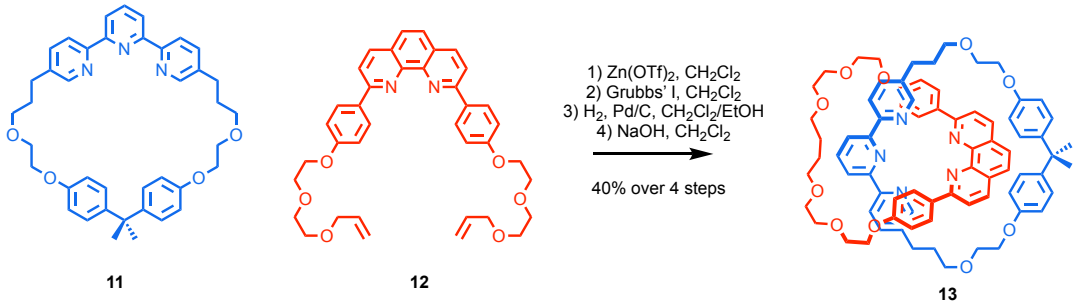

Figure 1.6 Sauvage's passive template synthesis of **13**.

Octahedral metal templates were well exploited for the synthesis of catenanes, rotaxanes and knots.[21] The possibility of having six ligands around a metal centre allowed different combinations of ligands. Sauvage and co-workers were the first to report the use of an octahedral metal template. The combination of two equivalents of a terpyridine-containing ligand with Ru^{II} resulted, after double Williamson cyclisation, in the formation of a [2]catenane in a low 11% yield.[22] This kind of geometry was used by Leigh and co-workers for the synthesis of [2]catenane in higher yield (Figure 1.7).[23] The potential for a 2,6-diiminopyridine-containing ligand **14** to coordinate Zn^{II} resulted after ring closure metathesis in the formation of the interlocked product **15** in 81% yield. Leigh and co-workers also reported the synthesis of rotaxane with octahedral metal under thermodynamic control of the reversible imine-containing axle in near quantitative yield.[24] Following the successful synthesis of interlocked structures using two terpyridine-containing ligands, Sauvage and co-workers focused their attention on the use of three bidentate ligands, resulting in the formation of various rotaxanes[25–28] and catenanes.[29,30]

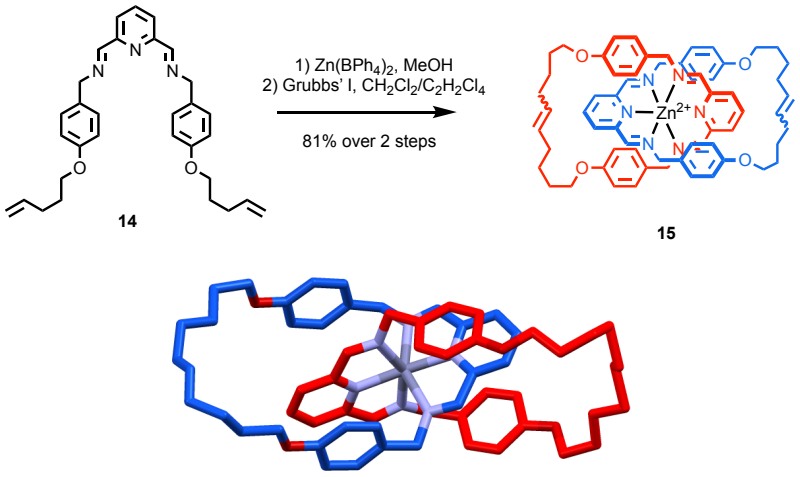

Figure 1.7 Leigh's passive template synthesis of catenane **15**. Counter ions omitted for clarity.

Leigh and co-workers used the linear coordination geometry of Au^{I} for the synthesis of [2]catenane **17** (Figure 1.8).[31] Au^{I} was coordinated by two pyridine ligands **16** followed by ring closing metathesis to obtain **17** in 41% yield. Leigh and co-workers also reported the possibility to use square planar Pd^{II} for the synthesis of rotaxanes and catenanes.[32]

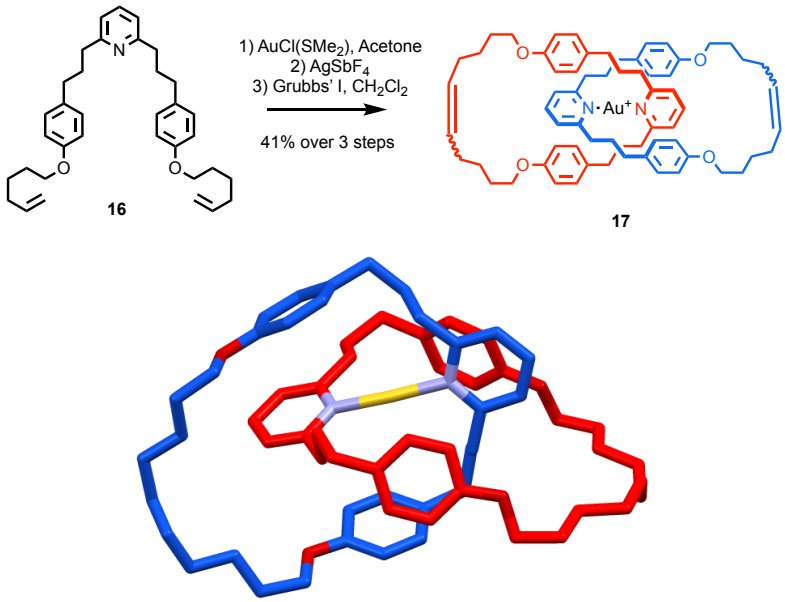

Figure 1.8 Leigh's gold passive template synthesis of catenane **17**. Counter ions omitted for clarity

The passive template is not limited to coordination of metal ions.[21,33,34] Stoddart and co-workers developed the synthesis of [2]catenane using electron donor-acceptor interactions (Figure 1.9).[35] The addition of **18** to electron donor macrocycle **20** in presence of the 1,4-

bis(bromomethyl)benzene **20** resulted in 70% yield of **22**. The electron-deficient bipyridinium intermediate **21** resulting from alkylation of the pyridine with **20** formed a 1:1 inclusion complex in solution, which allowed the organisation of the structure. This electron donor-acceptor interaction was extensively used in the synthesis of [2]catenanes as well as [2]rotaxanes.[36–38] Stoddart and co-workers recently developed a passive template based on radical-paring interactions enabling the access to rotaxanes, catenanes, or molecular pumps.[39]

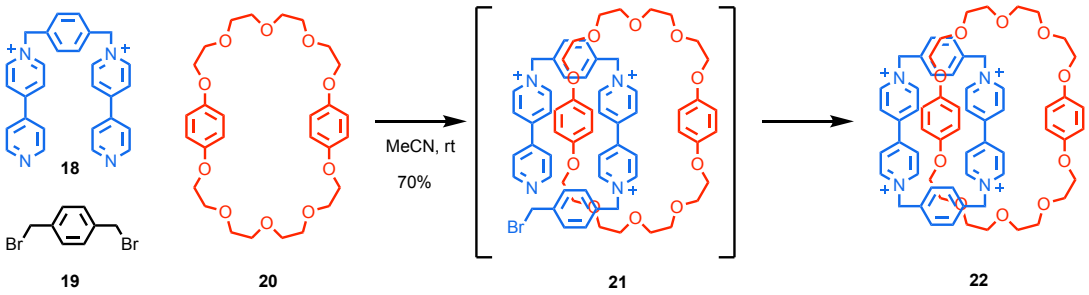

Figure 1.9 Stoddart and co-workers synthesis of [2]catenane **22** *via* electron donor-acceptor interaction.

In a different study, Hunter reported the synthesis of a [2]catenane based on hydrogen-bond interactions. The one-pot synthesis of **25** involved two macrocyclisations (Figure 1.10).[40,41] The initial cyclisation of **24** with isophthaloyl dichloride **23** generated the first macrocycle. The second macrocyclisation occurred through the cavity of the macrocycle in a good 36% yield overall.

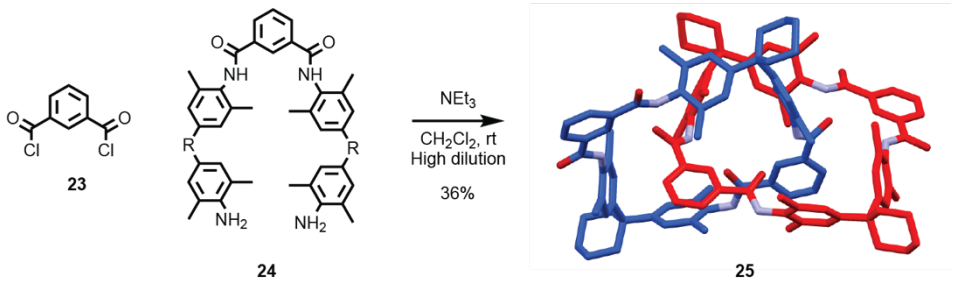

Figure 1.10 Hunter's synthesis of an amide-functionalised [2]catenane. R = 1,1-cyclohexyl.

Many other passive template examples exist for the synthesis of [2]catenanes which involve interactions such as hydrogen bonding, halogen bonding, metal complexation, hydrophobic or electronic and electrostatic interactions.[21,33,42]

The passive template is well exploited in the synthesis of interlocked structure due to the large range of possible interactions.[43–47] However, the passive template is not the only approach available for the synthesis of mechanically interlocked molecules.

1.1.2.3. Active template metal based synthesis

The passive template, presented in the previous section, highlighted the importance of the geometry of the metal for the pre-organisation of the architecture. The possibility to incorporate metals such as Cu^{I}, Zn^{II} or Pd^{II} illustrated the large range of possible combinations. The presence of a metal centre in the cavity of a macrocycle can also play a crucial role for the synthesis of interlocked structures. Leigh and co-workers introduced a new concept for the synthesis of interlocked structures based on an active template (AT), which constituted the evolution of the passive metal template approach used by Sauvage (Figure 1.11).[48,49] As in the passive template, the metal centre played a key role for the spatial organisation of each half-axle component on either side of the macrocycle. In addition to the spatial pre-organisation, the metal centre was also mediating the formation of the new covalent bond through the macrocycle, thus leading to the interlocked structure.

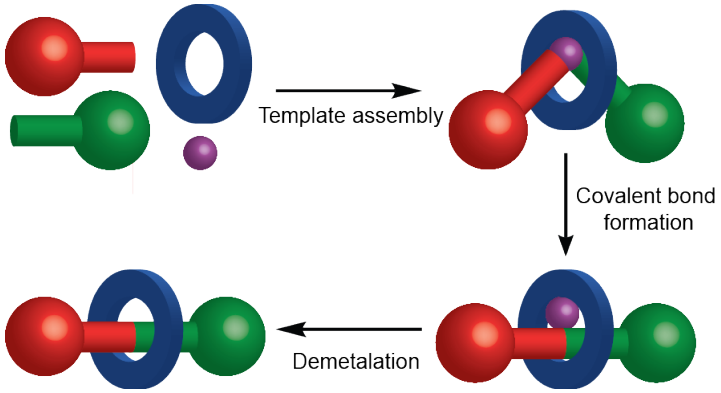

Figure 1.11 Active template metal-based synthesis involving the pre-organisation and the formation of the new covalent bond.

Although very similar, the difference between the passive template and the active template relies on the driving force of the mechanical bond formation. The passive template, as described previously, is based on a thermodynamically stable pre-organisation. However, in the case of the active template, the formation of the mechanical bond is directly linked to the ability of the metal in the cavity of the macrocycle to catalyse the bond forming reaction.

The covalent bond formation happens faster through the macrocycle than in solution, thus resulting in kinetic control. The difference between the passive and active template is significant during the optimisation of a reaction. In the case of the active template, addition of an excess of half-axles can significantly improve the production of the interlocked structure.

The tetrahedral Cu^{I} approach used by Sauvage for the synthesis of interlocked molecules suggested the possibility to orientate two half-axle components in opposite faces of the macrocycle. The Cu^{I}-catalysed azide alkyne cycloaddition (CuAAC) appeared to be an excellent candidate for the synthesis of interlocked molecules using the active template approach. The reaction rate for the copper catalysed reaction was found to be seven to eight orders of magnitude higher than the uncatalysed reaction.[50]

Leigh and co-workers were the first to report the use of the AT-CuAAC for the synthesis of interlocked molecules (Figure 1.12).[51] When the reaction was performed using equimolar mixture of pyridine-containing macrocycle **28**, half-axles **26** and **27** and $[Cu(MeCN)_4]PF_6$, rotaxane **29** was isolated in good yield, after demetalation using KCN (57% yield). The yield was significantly increased to 94% by addition of 5 equivalents of each half-axle components. The authors also highlighted the possibilty to use sub-stoichiometric amount of Cu^{I}, resulting in excellent outcome with an excess of half-axles (82% yield using 5 equivalents of half-axle **26** and **27**). The ability to obtain turn-over for the active template approach showed that the active template did not require the formation of a kinetically stable complex.

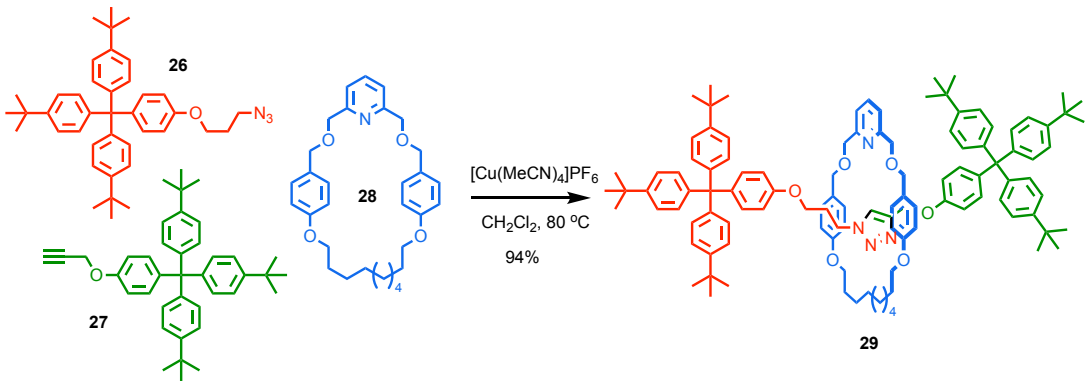

Figure 1.12 Leigh's active template approach in the synthesis of rotaxanes using CuAAC.

As well as the AT-CuAAC, use of a metal promoted covalent bond formation enabled successful syntheses of interlocked structures using different reactions such as a Cadiot-Chodkiewicz reaction,[52] the Glaser alkyne homocoupling,[53–55] Pd catalysed oxidative Heck coupling,[56] the Ni-mediated alkyne homocoupling,[57] and a Diels-Alder cycloaddition.[58]

These examples illustrate the broad range of bond forming reactions for the active template synthesis of rotaxanes.[59]

Goldup and co-workers developed a methodology for the synthesis of small crowded rotaxanes using a bipyridine macrocycle and the AT-CuAAC methodology to prepare different rotaxanes in excellent yield.[60] This methodology was optimised a few years later by the addition of a hindered base. When the base was added to the reaction mixture, the concentration of the Cu-acetylide **31** increased, which accelerated the reaction at room temperature. Goldup and co-workers explored the possibility to form oligomeric [n]rotaxanes using an iterative synthesis based on the AT-CuAAC and were able to obtain approximately 90% yield for each mechanical bond forming step.[61,62]

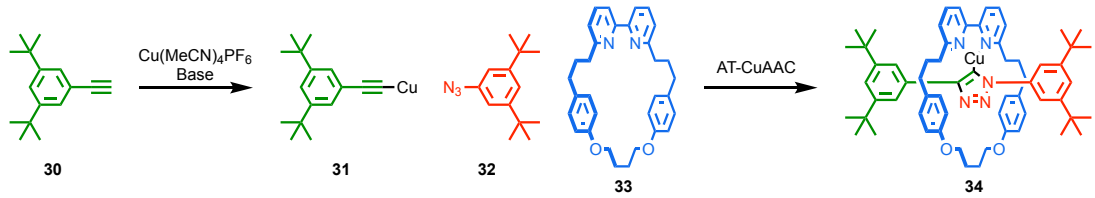

Figure 1.13 Goldup's optimised conditions for the synthesis of copper-triazolide **34**.

The addition of a base enabled the isolation of copper-triazolide complex **34**, which was proposed as an intermediate of the CuAAC before demetalation. The steric hindrance around the metal centre was a key factor for the stability of the organometallic species and prevented the proto-demetalation (Figure 1.14).[63]

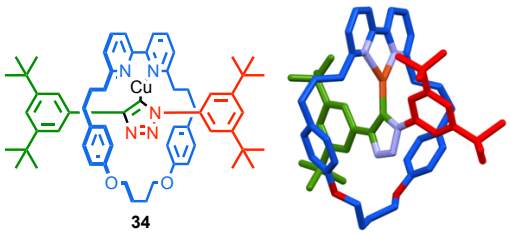

Figure 1.14 Structure of copper-triazolide complex **34** isolated by Goldup and co-workers.

In a different study, Goldup and co-workers focused their attention on the possibility to form a [3]rotaxane in a single event.[64,65] [3]Rotaxane **35** was obtained in 50% yield when the reaction was performed in CH_2Cl_2 at elevated temperature (100 °C) while [2]rotaxane **36** was obtained in quantitative yield in THF at room temperature.

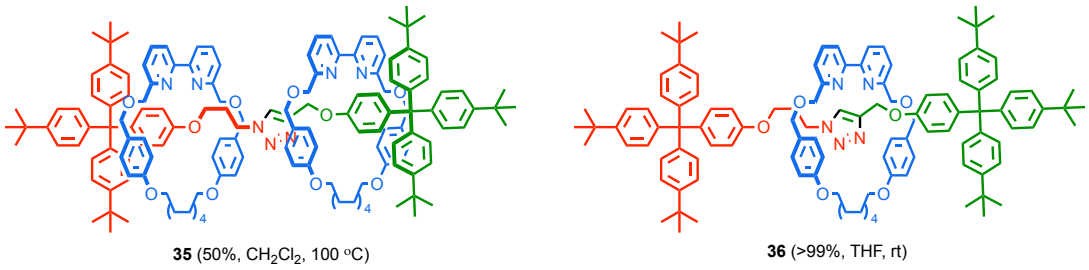

Figure 1.15 Goldup's synthesis of homo [3]rotaxane **35** and [2]rotaxane **36**.

The possibility of obtaining two different products from the same starting material suggested the competition between two different pathways for the AT-CuAAC. Both pathways were in accordance with the mono-nuclear mechanism and the binuclear pathways for the CuAAC proposed by Fokin and co-workers.[50,66] When the reaction was performed at low temperature in coordinating solvent, the formation of [2]rotaxanes suggested a mononuclear pathways. This can be explained by the steric hindrance of the architecture around the copper centre limiting the possibility to have two macrocycles next to each other, thus [2]rotaxanes appeared as the kinetic product of the reaction. However, the introduction of energy via thermal heating increased the possibility to have two macrocycle-copper complexes next to each other, when the reaction was performed at elevated temperature in non-coordinating solvent, the dinuclear pathway was more important resulting in an increase in the formation of [3]rotaxanes. The [3]rotaxanes can be defined as the thermodynamic product of the reaction (Figure 1.16). During this study, the authors highlighted that the repartition of products was very sensitive to the temperature which confirmed that in the case of the AT-CuAAC both pathways are possible but in competition.

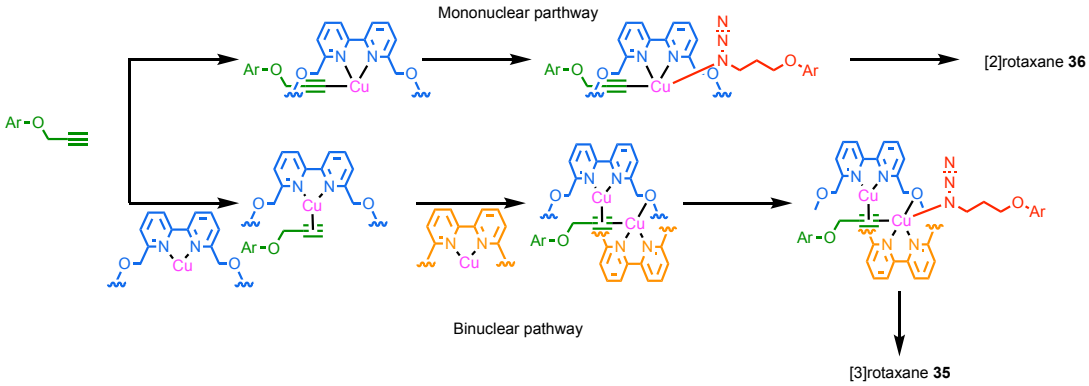

Figure 1.16 Mononuclear pathway and binuclear pathway for the AT-CuAAC. Counter ions omitted for clarity.

More recently, Goldup and co-workers reported the synthesis of a rotaxane **37** capable of exohedral coordination to Au^{I}.[67] This ligand was able to induce an excellent activity and diastereoselectivity in the Ohe-Uemura cyclopropanation reaction (Figure 1.17). The cationic gold complex **38** generated by abstraction of the chloride with the silver salt was a latent catalyst with activation achieved by addition of a second metal centre (additive) leading to the structure **39**. The gold centre coordinated initially inside the rotaxane **38** cavity was displaced by a second cation in order to afford a highly active catalyst **39** (>90% diastereoselectivity).

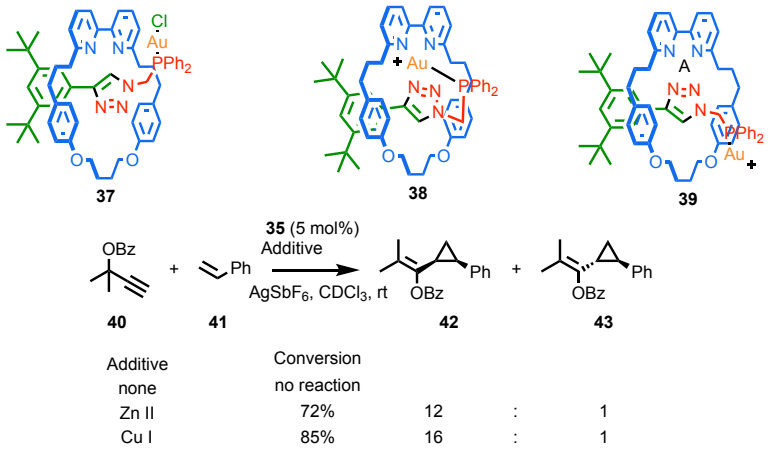

Figure 1.17 Goldup's diastereoselective gold catalyst rotaxane **37**.

In contrast, examples of synthesis of [2]catenanes using the active template approach are more limited with only three reports prior to our contribution. One explanation for the difficult development of active template for the synthesis of [2]catenanes is directly related to the pre-assembly of the macrocycle precursor. The necessity of having the reactive unit in opposite faces of the macrocycle required long and flexible precursor. These precursors, due to the flexibility, can be involved in oligomerisation and non-productive macrocyclisation, thus resulting in non-interlocked macrocycles.

The first active template approach to synthesise catenanes was reported by Saito and co-workers (Figure 1.18).[68] The Cu^{I}-mediated oxidative intramolecular diyne coupling was used for the catenane forming step. The treatment of copper-macrocycle complex **45** with a large excess of diyne **44** (5 equivalents) in presence of K_2CO_3 and I_2, followed by removal of the metal afforded the corresponding [2]catenane **46** in 64% yield after 6 days. They were also able to obtain 27% yield when the reaction was performed using only one equivalent of **44** after 48 hours of reaction.

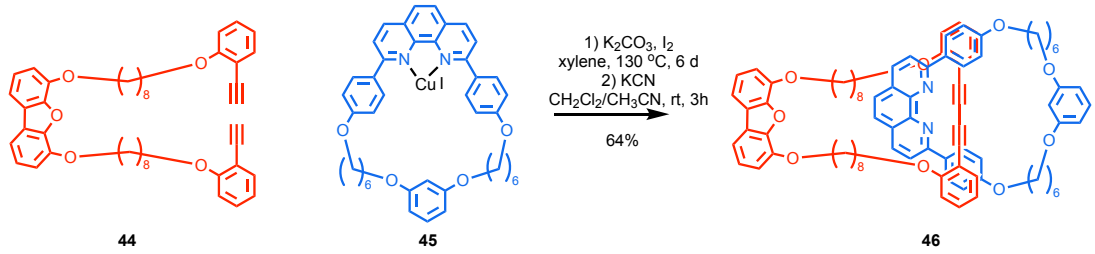

44 45 46

Figure 1.18 Saito's active template synthesis of [2]catenane **46**.

Leigh and co-workers reported an AT-CuAAC approach to generate [2]catenanes (Figure 1.19). The reaction was first performed using one equivalent of **47** at room temperature and after 24 hours, only traces of hetero [2]catenane **49** were observed. After optimisation, the hetero [2]catenane **49** was isolated in a reasonable yield (50%) using five equivalents of **47** at 80 °C for three weeks (500 h) (Figure 1.19).[69] The same approach was used for the homo [2]catenane **51** synthesis which resulted in a good 46% yield *via* a double macrocyclisation. The first macrocycle was formed by macrocyclisation of **50**. The macrocyclisation of the second equivalent of **50** occurred through the cavity of the newly formed macrocycle leading to the formation of the homo [2]catenane **51**. Leigh and co-workers also reported the possibility of using Cadiot-Chodkiewicz coupling between a terminal alkyne and a bromoalkyne to generate [2]catenanes. However, the isolated yield of the product was low (21% yield) using a large excess of macrocycle precursor.[69]

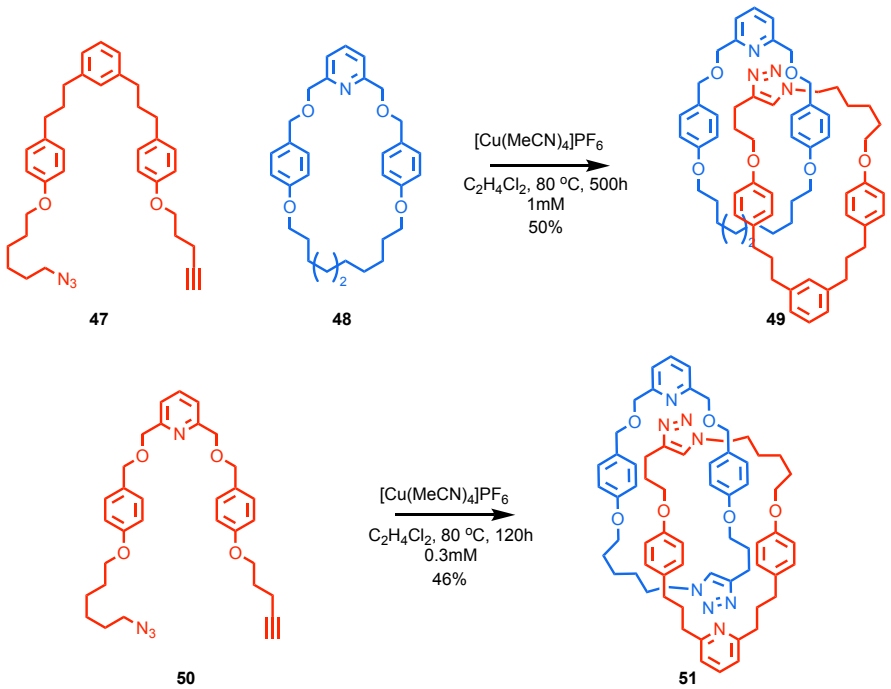

47 48 49 50 51

Figure 1.19 Leigh's AT-CuAAC synthesis of [2]catenanes.

More recently, Saito reported the synthesis of a [2]catenane using copper mediated intramolecular Castro Stevens reaction (Figure 1.20).[70] When five equivalents of **53** were added to **52** in xylene in presence of K_2CO_3 at high temperature, [2]catenane **54** was isolated in 64% yield after 48 hours. The size of the macrocycle **42** was crucial for the efficiency of the catenane formation; when the macrocycle was four methylene groups larger, the isolated yield dropped to 24%.

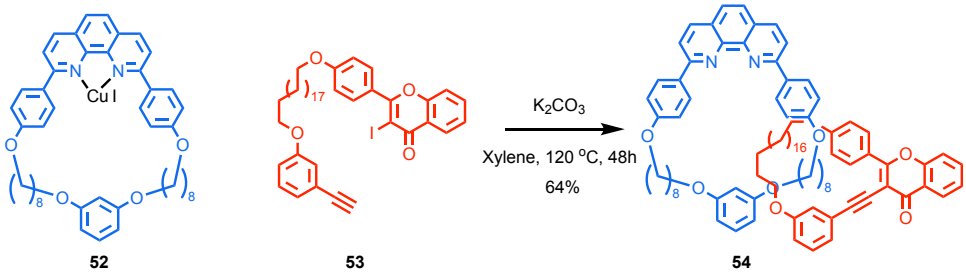

Figure 1.20 Saito's active template synthesis of [2]catenane **54**.

Active template approaches for the synthesis of [2]catenanes have proven to be successful. However, none of them are practical as they require a large excess of precursors to produce [2]catenanes and involve long reaction times.

Development of practical methodologies for the synthesis of catenanes and rotaxanes may allow for the unique properties of interlocked molecules to be widely explored.

1.1.3. Chirality in rotaxanes and catenanes

This section focuses on the chirality present in rotaxanes and catenanes. Chiral interlocked molecules have received a considerable interest for the past 30 years.[71,72] Chiral interlocked structures encountered promising results in enantioselective catalysis or as enantioselective hosts for chiral small molecules. The chirality from covalent stereogenic unit will be first discussed followed by the chirality arising from the mechanical bond, that cannot be found in non-interlocked molecules.

1.1.3.1. Chiral covalent stereogenic units

The generation of chiral interlocked structures can come from the connection of an interlocked molecule and a group bearing a chiral stereogenic unit or by directly integrating a chiral stereogenic unit in the core of the interlocked structure.

Leigh and co-workers reported the effect of the crowded environment of the mechanical bond in the enhancement of the selectivity in catalysis (Figure 1.21).[73] The chirality in rotaxane (*R*,*R*)-**55** came from the macrocycle bearing two chiral centres. When the Ni^{II}-mediated Michael addition reaction used (*R*,*R*)-**55** as ligand, the product was obtained in higher enantioselectivity than the acyclic ligand (*R*,*R*)-**56**. The enhancement of the enantioselectivity was attributed to the steric hindrance of the rotaxane. The steric hindrance also was drastically slowing down the catalytic process.

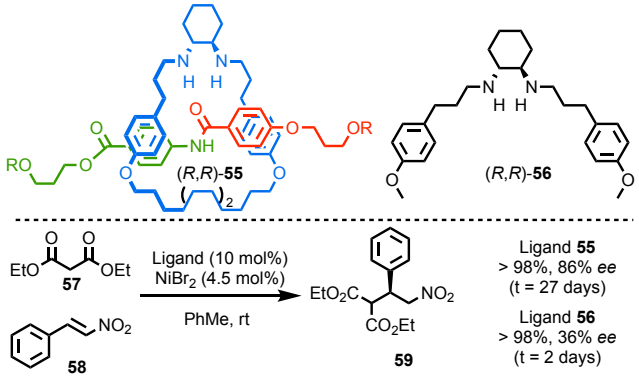

Figure 1.21 Leigh's chiral rotaxane ligand (*R*,*R*)-**55** in the Ni(II)-catalysed Michael addition. R= 4-(C_6H_4)-C(4-(C_6H_4)-*t*Bu)$_3$.

Takata and co-workers demonstrated the faculty to create a chiral environment on an achiral catalytic moiety using the mechanical bond (Figure 1.22).[74] Rotaxane (*R*)-**60** is composed of a binaphthyl-functionalised macrocycle and an achiral thread bearing a thiazolium unit. The non-interlocked axle of (*R*)-**60** catalysed the formation of a racemic benzoin product. However, when the rotaxane (*R*)-**60** was used, the same reaction afforded an enantioselectivity of 23% *ee*. The improvement of the enantioselectivity illustrated the ability to transfer stereochemical information from each sub-unit of the rotaxane. Decreasing the steric congestion in rotaxane (*R*)-**61** resulted in diminished enantioselectivity of the reaction. The mechanical bond in rotaxane (*R*)-**62** allowed the enhancement of the enantioselectivity;

the axle from (*R*)-**62** only gave 3% *ee* while the rotaxane (*R*)-**62** afforded the product in 24% *ee*.

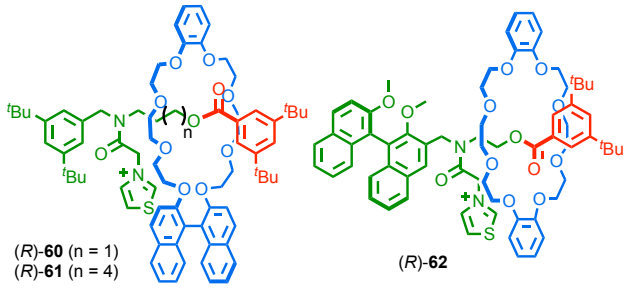

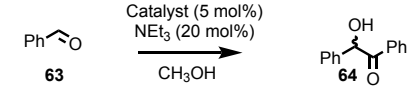

Catalyst	Temperature (°C)	Yield (%)	*ee* (%)
(*R*)-**60**	0	34	23 (*R*)
(*R*)-**61**	0	34	16 (*R*)
(*R*)-**60**	-20	17	27 (*R*)
(*R*)-**62**	-20	7	24 (*S*)
axle of (*R*)-**62**	-20	56	3 (*S*)

Figure 1.22 Takata's thiazolium rotaxane catalysts. Counter ions omitted for clarity.

Takata and co-workers recently reported enantioselective acyl transfer catalysis using rotaxane (*R*)-**65** for the desymmetrisation of *meso* diol **66** (Figure 1.23).[75] (1*R*,2*S*)-**67** was produced in 78% *ee* with quantitative yield of the diol when the reaction was performed with (*R*)-**65**. When the reaction was performed using the axle only, the racemic product was obtained in 47% yield. When the macrocycle was combined to the axle, moderate yield was observed (46%) with low enantioselectivity (3%). When the reaction was performed at lower temperature, the enantioselectivity induced by the rotaxane (*R*)-**65** was increased to 98% *ee* with quantitative yield.

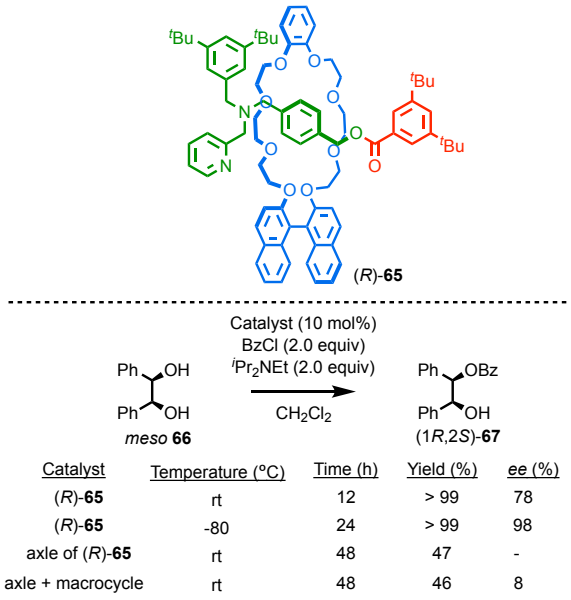

Catalyst	Temperature (°C)	Time (h)	Yield (%)	*ee* (%)
(*R*)-**65**	rt	12	> 99	78
(*R*)-**65**	-80	24	> 99	98
axle of (*R*)-**65**	rt	48	47	-
axle + macrocycle	rt	48	46	8

Figure 1.23 Takata's pyrdine-rotaxane (*R*)-**65** for enantioselective acyl transfer catalysis.

Another example of the effect of the mechanical bond was reported by Niemeyer and co-workers in the hydrogenation of quinoline **70** catalysed by a Bronsted acid (Figure 1.24).[76] Bis-phosphoric acid-functionalised chiral catenane (*S*,*S*)-**68** gave a high yield (90%) with an impressive enantioselectivity of 84% *ee*. When the reaction was carried out using the non-interlocked macrocycle or the acyclic phosphoric acid (*S*)-**69**, the enantioselectivity obtained was considerably lower than the one observed with the interlocked catalyst (12% *ee* and 9% *ee*, respectively). The acyclic phosphoric acid (*S*)-**69** displayed a concentration dependent enantioselectivity with greater selectivity at higher concentration. The enhancement of the enantioselectivity at higher concentration was attributed to the formation of a dimeric phosphoric acid active catalyst as evidenced by molecular modelling. In the case of the catenane, the dimeric pathway was ensured due to the proximity of both phosphoric acids, resulting in high enantioselectivity of the catalytic process.

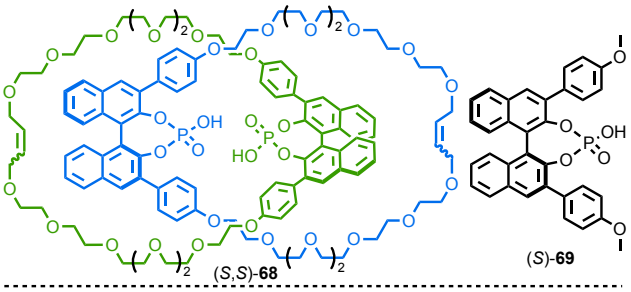

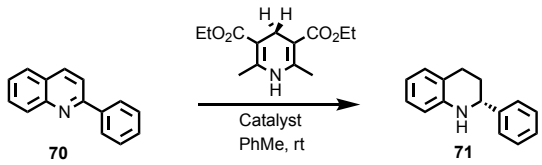

70 71

Catalyst	Loading (mol%)	Yield (%)	*ee* (%)
68	2.5	90	84 (R)
macrocycle	2.5	82	12 (S)
macrocycle	10	82	10 (R)
69	2.5	94	9 (R)
69	10	80	58 (R)

Figure 1.24 Niemeyer's chiral phosphoric acid catenane (*S*,*S*)-**68** in the transfer hydrogenation of quinoline **70**.

Leigh and co-workers were able to combine catalytic activity and molecular shuttling, generating switchable catalysts (Figure 1.25).[77–80] Chiral stereogenic secondary amine in rotaxane (*S*)-**72** proved to be active in a large range of organocatalytic transformations.[81] Protonated rotaxane (*S*)-**72** was catalytically inactive as the macrocycle was located around the ammonium which inhibited the catalytic activity. However, deprotonation of the ammonium shuttled the macrocycle to the triazolium station, thus allowing the catalytic activity of the amine to be restored. (*S*)-**73** catalysed the Michael addition of diketone **75** to crotonaldehyde **74** to produce **76** in high enantioselectivity (80% *ee*), which was found to be similar to the non-interlocked axle (84% *ee*).

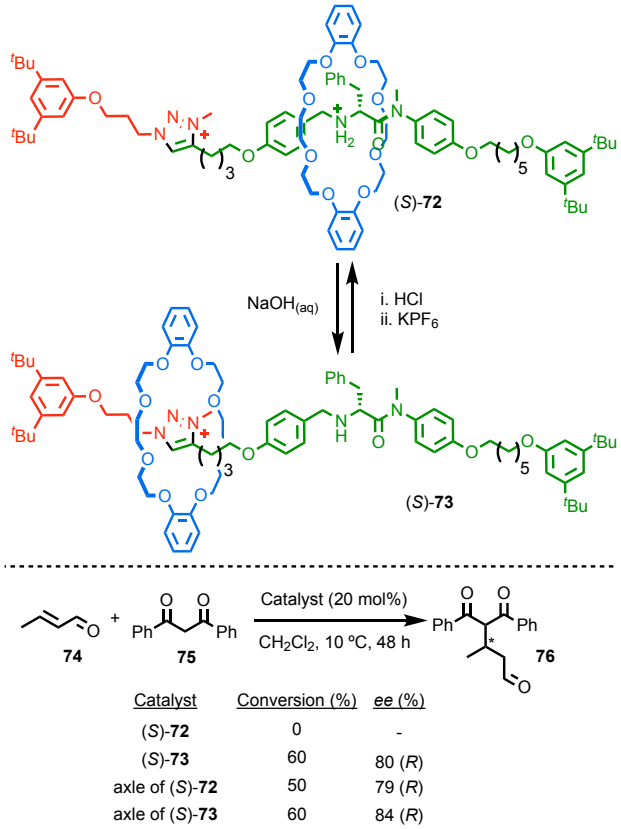

Figure 1.25 Leigh's switchable chiral rotaxane catalyst (*S*)-**73**. Counter ions omitted for clarity.

The expression of chirality in interlocked molecules is not limited to the enantioselectivity of catalytic processes, it can also directly affect the synthesis of these interlocked structures. One of the common manifestation of the chirality in interlocked molecules is the complexity of the NMR spectra.

Goldup and co-workers reported the synthesis of a D-glucose-derived rotaxane (D)-**77** using the AT-CuAAC (Figure 1.26).[60] The macrocycle component of (D)-**77** was desymmetrised by the presence of the glucose-derivate in the small, crowded environment.

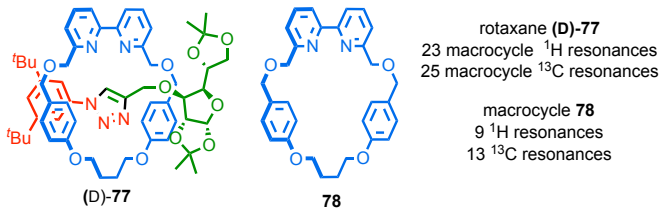

Figure 1.26 Goldup's chiral, crowded D-glucose-based rotaxane (D)-**77**.

The introduction of covalent stereogenic elements in both components of the interlocked molecules increased the molecular complexity as the formation of a mixture of diastereoisomers became possible. Stoddart and co-workers reported the diastereoselective formation of (*R*,*R*)-**81** when enantiopure macrocycle precursor (*R*)-**80** was combined with racemic macrocycle **79** (Figure 1.27).[82] The selectivity came from different rates for the ring closure of each diastereoisomeric intermediates, resulting in a kinetic control of the diastereoselectivity.[47]

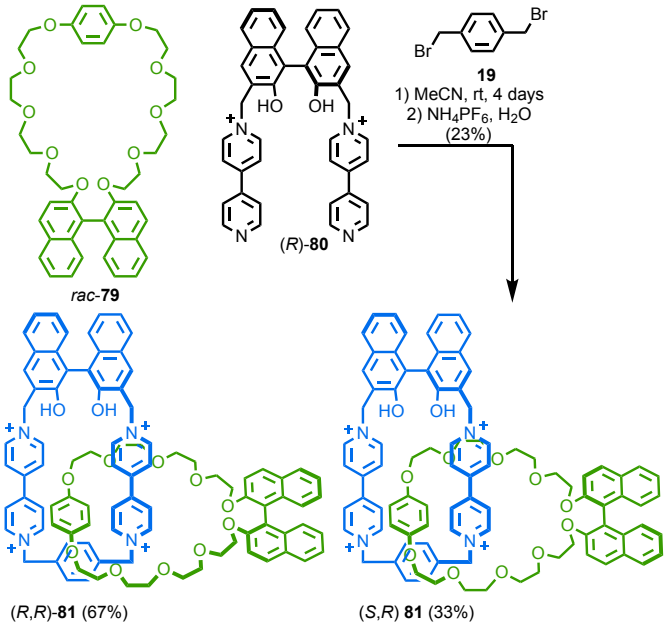

Figure 1.27 Stoddart's diastereoselective synthesis of catenane **81** under kinetic control. Counter ions omitted for clarity.

Takata and co-workers reported diastereoselective post-synthetic transformation of rotaxanes highlighting the influence of the stereogenic element of one component on the other one (Figure 1.28).[83] Diastereoselective Michael addition was used in the stoppering reaction of the pseudo-rotaxane (*R*,*R*)-**82** affording rotaxane (*R*/*S*,*R*,*R*)-**83** in low yield with diastereoselectivity (6% *de*). Takata and co-workers reported the diastereoselective *N*-oxidation of rotaxane (*R*)-**84** when treated with dimethyldioxirane.[84] The excellent diastereoselectivity observed for the most crowded rotaxane (*R*)-**84** decreased considerably with the increase of the length of the axle.

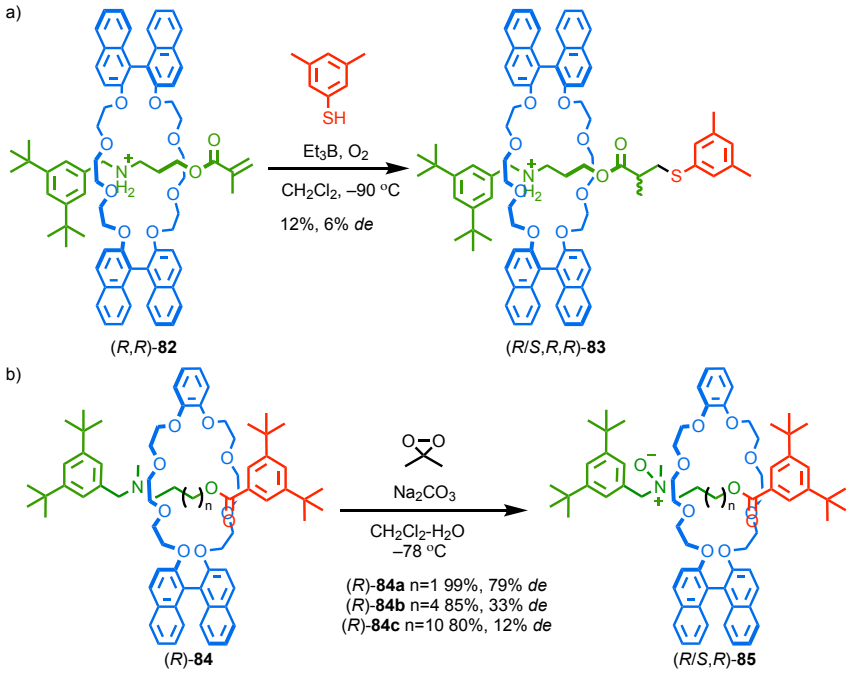

Figure 1.28 Takata's post-synthetic diastereoselective modification.

Hirose and co-workers reported the effect of chirality in the dethreading of meta-stable pseudo rotaxane (*R*/*S*,*S*,*S*)-**86** (Figure 1.29).[85] Nearly one fold difference was observed for the dethreading rates of each diastereoisomers. The proposed mechanism of dethreading suggested a pre-equilibium *via* an activated complex (*R*/*S*,*S*,*S*)-**87**. The pre-equilibrium appeared to be different for each diastereoisomer which led to different rates of dethreading.

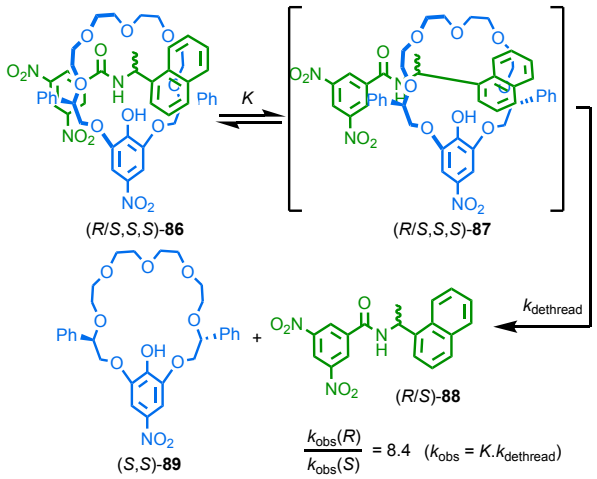

Figure 1.29 Hirose's observation of the kinetic effect of diastereoisomerism of dethreading rates of pseudorotaxane (*R*/*S*,*S*,*S*)-**86**.

All the examples presented above involve chiral covalent stereogenic units. However, one of the feature of interlocked molecules is the possibility to have a chiral molecule arising from the mechanical bond only.

1.1.3.2. Mechanically planar chiral rotaxane

Schill identified, in 1970, that the combination of a C_{nh} symmetric macrocycle and a C_{nv} axle would result in a chiral rotaxane (Figure 1.30 b). The skeleton of a macrocycle showing C_{nh} symmetry is considered as orientated. Although, the possibility of having a C_{nh} symmetric macrocycle is theoretically real, the majority of mechanically planar chiral rotaxanes possesses a C_{1h} symmetric macrocycle. Goldup and co-workers named this type of chirality "mechanical planar chirality" in order to highlight the importance of the mechanical bond. The suffix "*mp*" is added to the stereodescriptor so as to distinguish the mechanical planar chirality from the absolute configuration of other stereogenic units.[86] As shown in Figure 1.30 c, it is possible to extend the concept of the mechanical planar chirality to rotaxanes containing more than one ring.

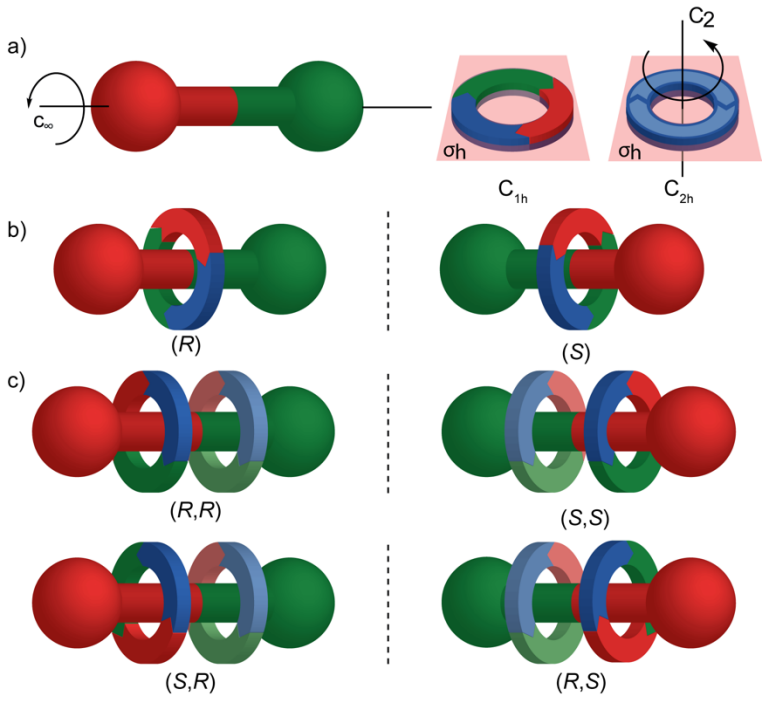

Figure 1.30 Cartoon representation of mechanically planar chiral rotaxanes and their components. a) Axle and macrocycle (C_{1h}, C_{2h}). b) two enantiomers of a mechanically planar chiral [2]rotaxane. c) Four stereoisomers possible for a mechanically planar chiral [3]rotaxanes.

In order to assign the stereochemistry of the mechanical bond, rules were proposed by Vögtle.[87] The highest priority atom of the axle is assigned using the Cahn, Ingold and Prelog rules and labelled as A. Once A is defined, the highest priority atom substituting A is determined and labelled B, which enables the determination of the orientation of the axle. The same approach is used to determine the direction of the macrocycle. Observation of the macrocycle from A to B allows the determination of the orientation of the macrocycle, clockwise direction is defined as (R_{mp}) and anticlockwise as (S_{mp}).

Vögtle and co-workers were the first to illustrate mechanical planar chirality when they managed to separate a racemic mixture of **90** using chiral stationary phase HPLC (CSP-HPLC) (Figure 1.31).[88] They did not manage to obtain single crystal for X-ray diffraction, and thus labelled the enantiomers by their optical rotation. Vögtle and co-workers studied mechanically planar chiral rotaxanes over a number of years, but the limitation of the studies was related to the necessity to use CSP-HPLC which is not scalable.[87,89]

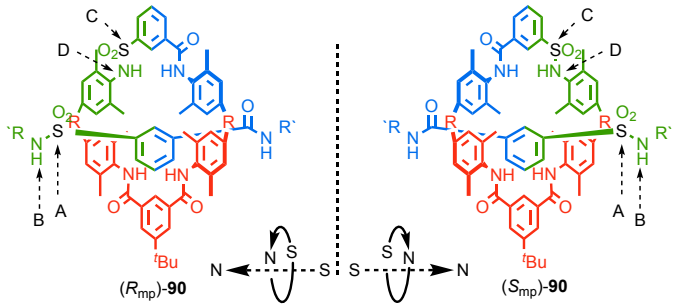

Figure 1.31 Vögtle's mechanically planar chiral rotaxane **86**. R = 1,1-cyclohexyl, R' = C_6H_4-Tr

Takata and co-workers were interested in the synthesis of enantiopure mechanically planar chiral rotaxanes using a dynamic kinetic resolution of pseudorotaxanes **91** (Figure 1.32).[90] The application of enantiopure phosphine catalyst **92** for the acylation of pseudorotaxanes **91** in equilibrium in solution resulted in the formation of rotaxane **93** with 4% *ee*. Once again, the separation of each enantiomers had to be performed using CSP-HPLC. Takata and co-workers reported different examples of mechanically planar chiral rotaxanes, all of which containing separations performed by CSP-HPLC.[91]

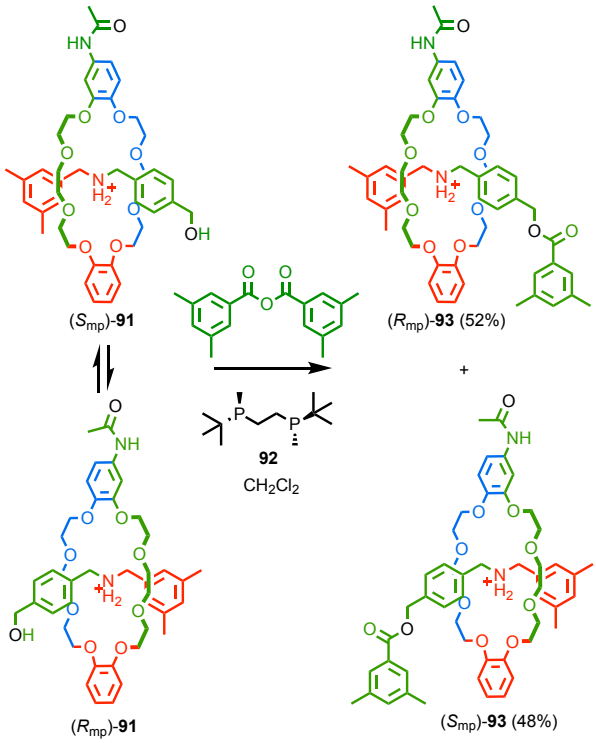

Figure 1.32 Takata's enantioselective dynamic kinetic resolution of pseudorotaxanes **91**. Counter ions omitted for clarity.

Goldup and co-workers developed a new approach for the synthesis of mechanically planar chiral rotaxanes without the need to CSP-HPLC purification (Figure 1.33).[86] The principle of the approach relied on combining mechanically planar chirality with a covalent stereogenic unit, resulting in the formation of diastereoisomers. The use of protected (D)-glucose derived azide **94** led to separable mechanically epimeric chiral rotaxanes **95** using the AT-CuAAC reaction. Once the individual diastereoisomers were in hand, the replacement of the sugar-based stopper by an achiral group was performed by aminolysis. The production of enantiopure (*S*)-**97** and (*R*)-**97** was successfully achieved without the need of CSP-HPLC.

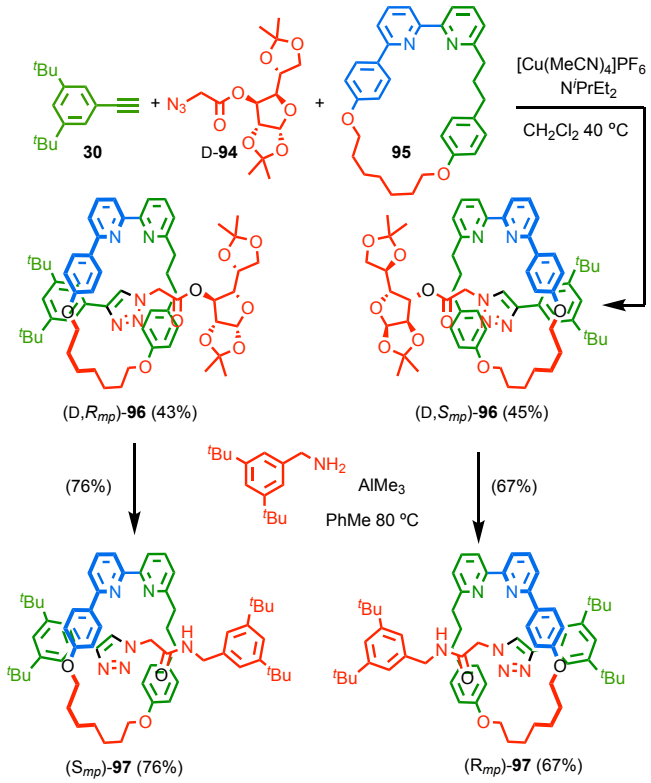

Figure 1.33 Goldup's chiral derivatisation approach to mechanically planar chiral rotaxanes **97**.

Further studies of mechanically planar chiral rotaxanes were really slow due to the difficulty to access enantiopure materials. Goldup and co-workers developed an efficient and scalable approach to generate enantiopure rotaxanes which is expected to allow the application of this kind of chirality to other fields.

1.1.3.3. Topologically chiral catenane

Similarly to the mechanical planar chirality, when two C_{nh}-symmetric orientated macrocycles are combined in a [2]catenane, the resulting structure is chiral. These types of structures were named "topologically chiral catenanes". This kind of chirality was poorly studied due to the complexity to access the material. Nevertheless, most examples about topologically chiral involve the combination of two C_{1h}-symmetric macrocycles (Figure 1.34 a). The topological chirality can be extended to linear [3]catenanes (Figure 1.34 b).

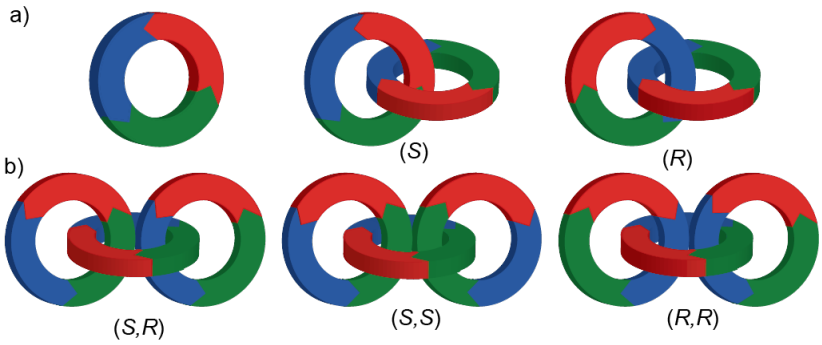

Figure 1.34 Schematic representation of a) topologically chiral homo [2]catenane, b) three strereoisomers of a topologically chiral homo [3]catenane.

The first example of a topologically chiral [2]catenane was reported by Sauvage and co-workers in 1988. However, the interlocked structure was isolated as a racemic mixture (Figure 1.35).[92] They were able to illustrate the chirality of **98** by addition of a chiral alcohol (Pirkle's reagent). [93] In presence of a chiral environment, they were able to observe diastereomeric signals by ^{1}H NMR analysis. A few years later, they were able to isolate enantiopure samples of **98** using CSP-HPLC. The absolute stereochemistry of the **98** was not determined.[94]

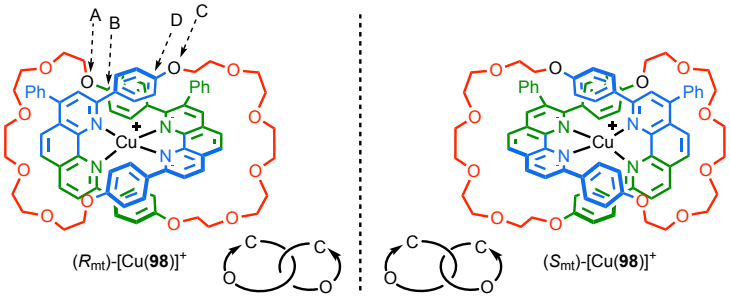

Figure 1.35 Sauvage's topologically chiral catenane **98**.

Vögtle and co-workers reported the synthesis and separation of a topologically chiral [2]catenane using CSP-HPLC (Figure 1.36).[95] The comparison between Sauvage's catenane **98** and Vögtle's catenane **99** highlighted the possibility of having more flexible structures in the case of Vögtle's system. They were able to evaluate the optical property of the enantiopure structure, showing a perfect mirror image by circular dichroism.

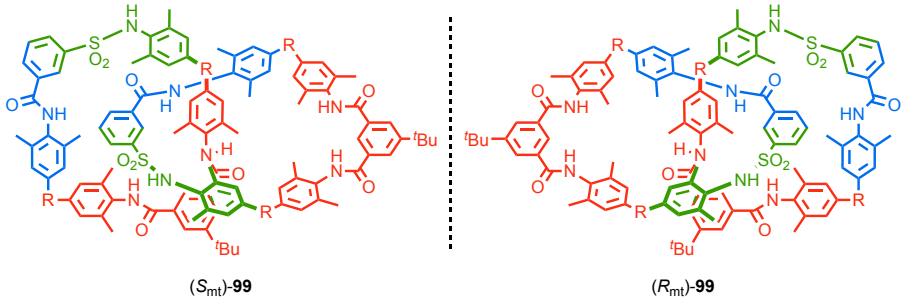

Figure 1.36 Vögtle's topologically chiral catenane **96**. R = 1,1-cyclohexyl.

Both aforementioned examples showed the possibility to prepare enantiopure topological chiral catenanes. However, the need to use CSP-HPLC limits the scale of the reaction.

1.2. Conclusions

The synthesis of interlocked structures evolved from a scientific curiosity to accessible structures thanks to the development of passive and active template for their synthesis. Interlocked molecules displace properties that non-interlocked molecules do not have such as novel reactivity and catalysis. The chirality in interlocked structures can come from covalent stereogenic units or arise from the feature of the mechanical bond, thus the generation of a new type of chirality which remains unavailable in non-interlocked molecules.

1.3. Aims of this project

Mechanical planar chiral rotaxanes are a relatively unexplored class of chiral molecules. The improved synthesis of mechanically chiral rotaxane by Goldup and co-workers using a chiral auxiliary opened a new direction in the development of chiral rotaxanes.[67] Mechanical chirality has yet to be explored in asymmetric catalysis and will be discussed in Chapter 2. The potential to have a reactive species in a confined space allows the discovery of novel reactivities which are inaccessible in non-interlocked molecules and will be discussed in Chapter 3. The active template approach for the synthesis of [2]catenanes suffers from under-development. Recent improvements in the AT-CuAAC reaction for the synthesis of [2]catenanes are discussed in Chapter 4 allowed the subsequent development of an efficient approach for the high yielding synthesis of enantiopure topologically chiral [2]catenanes as presented in Chapter 5.

1.4. Bibliography

[1] J. F. Stoddart, *Chem. Soc. Rev.* **2009**, *38*, 1802–1820.

[2] E. R. Kay, D. A. Leigh, F. Zerbetto, *Angew. Chem. Int. Ed.* **2007**, *46*, 72–191.

[3] D. A. Leigh, *Angew. Chem. Int. Ed.* **2016**, *55*, 14506–14508.

[4] C. J. Bruns and J. F. Stoddart, The Nature of the Mechanical Bond: From Molecules to Machines, Wiley, 2016

[5] A. Lüttringhaus, F. Cramer, H. Prinzbach, F. M. Henglein, *Justus Liebigs Ann. Chem.* **1958**, *613*, 185–198.

[6] E. Wasserman, *J. Am. Chem. Soc.* **1960**, *82*, 4433–4434.

[7] H. L. Frisch, E. Wasserman, *J. Am. Chem. Soc.* **1961**, *83*, 3789–3795.

[8] G. Schill, A. Lüttringhaus, *Angew. Chem. Int. Ed. Engl.* **1964**, *3*, 546–547.

[9] G. Schill, C. Zürcher, *Angew. Chem. Int. Ed. Engl.* **1969**, *8*, 988–988.

[10] G. Schill, C. Zürcher, *Chem. Ber.* **1977**, *110*, 2046–2066.

[11] I. T. Harrison, S. Harrison, *J. Am. Chem. Soc.* **1967**, *89*, 5723–5724.

[12] G. Schill, H. Zollenkopf, *Justus Liebigs Ann. Chem.* **1969**, *721*, 53–74.

[13] D. J. Cram, J. M. Cram, *Science* **1974**, *183*, 803–809.

[14] B. Dietrich, J. M. Lehn, J. P. Sauvage, *Tetrahedron Lett.* **1969**, *10*, 2889–2892.

[15] A.-M. Fuller, D. A. Leigh, P. J. Lusby, I. D. H. Oswald, S. Parsons, D. B. Walker, *Angew. Chem. Int. Ed.* **2004**, *43*, 3914–3918.

[16] C. O. Dietrich-Buchecker, J. P. Sauvage, J. P. Kintzinger, *Tetrahedron Lett.* **1983**, *24*, 5095–5098.

[17] J. Yin, S. Dasgupta, J. Wu, *Org. Lett.* **2010**, *12*, 1712–1715.

[18] C. O. Dietrich-Buchecker, J. P. Sauvage, J. M. Kern, *J. Am. Chem. Soc.* **1984**, *106*, 3043–3045.

[19] J.-P. Sauvage, *Angew. Chem. Int. Ed.* **2017**, *56*, 11080–11093.

[20] C. Hamann, J.-M. Kern, J.-P. Sauvage, *Inorg. Chem.* **2003**, *42*, 1877–1883.

[21] G. Gil-Ramírez, D. A. Leigh, A. J. Stephens, *Angew. Chem. Int. Ed.* **2015**, *54*, 6110–6150.

[22] J. P. Sauvage, M. Ward, *Inorg. Chem.* **1991**, *30*, 3869–3874.

[23] D. A. Leigh, P. J. Lusby, S. J. Teat, A. J. Wilson, J. K. Y. Wong, *Angew. Chem. Int. Ed.* **2001**, *40*, 1538–1543.

[24] L. Hogg, D. A. Leigh, P. J. Lusby, A. Morelli, S. Parsons, J. K. Y. Wong, *Angew. Chem. Int. Ed.* **2004**, *43*, 1218–1221.

[25] D. Pomeranc, D. Jouvenot, J.-C. Chambron, J.-P. Collin, V. Heitz, J.-P. Sauvage, *Chem. – Eur. J.* **2003**, *9*, 4247–4254.

[26] J.-P. Collin, D. Jouvenot, M. Koizumi, J.-P. Sauvage, *Eur. J. Inorg. Chem.* **2005**, *2005*, 1850–1855.

[27] A. I. Prikhod'ko, F. Durola, J.-P. Sauvage, *J. Am. Chem. Soc.* **2008**, *130*, 448–449.

[28] A. I. Prikhod′ko, J.-P. Sauvage, *J. Am. Chem. Soc.* **2009**, *131*, 6794–6807.

[29] P. Mobian, J.-M. Kern, J.-P. Sauvage, *J. Am. Chem. Soc.* **2003**, *125*, 2016–2017.

[30] J.-C. Chambron, J.-P. Collin, V. Heitz, D. Jouvenot, J.-M. Kern, P. Mobian, D. Pomeranc, J.-P. Sauvage, *Eur. J. Org. Chem.* **2004**, *2004*, 1627–1638.

[31] S. M. Goldup, D. A. Leigh, P. J. Lusby, R. T. McBurney, A. M. Z. Slawin, *Angew. Chem. Int. Ed.* **2008**, *47*, 6999–7003.

[32] A.-M. L. Fuller, D. A. Leigh, P. J. Lusby, A. M. Z. Slawin, D. B. Walker, *J. Am. Chem. Soc.* **2005**, *127*, 12612–12619.

[33] N. H. Evans, P. D. Beer, *Chem. Soc. Rev.* **2014**, *43*, 4658–4683.

[34] M. Xue, Y. Yang, X. Chi, X. Yan, F. Huang, *Chem. Rev.* **2015**, *115*, 7398–7501.

[35] P. R. Ashton, T. T. Goodnow, A. E. Kaifer, M. V. Reddington, A. M. Z. Slawin, N. Spencer, J. F. Stoddart, C. Vicent, D. J. Williams, *Angew. Chem. Int. Ed. Engl.* **1989**, *28*, 1396–1399.

[36] D. B. Amabilino, P. R. Ashton, A. S. Reder, N. Spencer, J. F. Stoddart, *Angew. Chem. Int. Ed. Engl.* **1994**, *33*, 433–437.

[37] D. B. Amabilino, P. R. Ashton, S. E. Boyd, J. Y. Lee, S. Menzer, J. F. Stoddart, D. J. Williams, *Angew. Chem. Int. Ed. Engl.* **1997**, *36*, 2070–2072.

[38] R. A. Bissell, E. Córdova, A. E. Kaifer, J. F. Stoddart, *Nature* **1994**, *369*, 133–137.

[39] Y. Wang, M. Frasconi, J. F. Stoddart, *ACS Cent. Sci.* **2017**, *3*, 927–935.

[40] C. A. Hunter, *J. Am. Chem. Soc.* **1992**, *114*, 5303–5311.

[41] H. Adams, F. J. Carver, C. A. Hunter, *J. Chem. Soc. Chem. Commun.* **1995**, *0*, 809–810.

[42] N. H. Evans, P. D. Beer, *Angew. Chem. Int. Ed.* **2014**, *53*, 11716–11754.

[43] P. R. Aston, P. T. Glink, J. F. Stoddart, P. A. Tasker, A. J. P. White, D. J. Williams, *Chem. – Eur. J.* **1996**, *2*, 729–736.

[44] P. D. Beer, M. R. Sambrook, D. Curiel, *Chem. Commun.* **2006**, 2105–2117.

[45] A. Harada, Y. Takashima, H. Yamaguchi, *Chem. Soc. Rev.* **2009**, *38*, 875–882.

[46] J. A. Faiz, V. Heitz, J.-P. Sauvage, *Chem. Soc. Rev.* **2009**, *38*, 422–442.

[47] W. R. Dichtel, O. Š. Miljanić, W. Zhang, J. M. Spruell, K. Patel, I. Aprahamian, J. R. Heath, J. F. Stoddart, *Acc. Chem. Res.* **2008**, *41*, 1750–1761.

[48] J. D. Crowley, S. M. Goldup, A.-L. Lee, D. A. Leigh, R. T. McBurney, *Chem. Soc. Rev.* **2009**, *38*, 1530–1541.

[49] M. Denis, S. M. Goldup, *Nat. Rev. Chem.* **2017**, *1*, 0061.

[50] F. Himo, T. Lovell, R. Hilgraf, V. V. Rostovtsev, L. Noodleman, K. B. Sharpless, V. V. Fokin, *J. Am. Chem. Soc.* **2005**, *127*, 210–216.

[51] V. Aucagne, K. D. Hänni, D. A. Leigh, P. J. Lusby, D. B. Walker, *J. Am. Chem. Soc.* **2006**, *128*, 2186–2187.

[52] J. Berná, S. M. Goldup, A.-L. Lee, D. A. Leigh, M. D. Symes, G. Teobaldi, F. Zerbetto, *Angew. Chem. Int. Ed.* **2008**, *47*, 4392–4396.

[53] S. Saito, E. Takahashi, K. Nakazono, *Org. Lett.* **2006**, *8*, 5133–5136.

[54] M. J. Langton, J. D. Matichak, A. L. Thompson, H. L. Anderson, *Chem. Sci.* **2011**, *2*, 1897–1901.

[55] L. D. Movsisyan, D. V. Kondratuk, M. Franz, A. L. Thompson, R. R. Tykwinski, H. L. Anderson, *Org. Lett.* **2012**, *14*, 3424–3426.

[56] J. D. Crowley, K. D. Hänni, A.-L. Lee, D. A. Leigh, *J. Am. Chem. Soc.* **2007**, *129*, 12092–12093.

[57] J. D. Crowley, S. M. Goldup, N. D. Gowans, D. A. Leigh, V. E. Ronaldson, A. M. Z. Slawin, *J. Am. Chem. Soc.* **2010**, *132*, 6243–6248.

[58] J. D. Crowley, K. D. Hänni, D. A. Leigh, A. M. Z. Slawin, *J. Am. Chem. Soc.* **2010**, *132*, 5309–5314.

[59] J. E. M. Lewis, M. Galli, S. M. Goldup, *Chem. Commun.* **2016**, *53*, 298–312.

[60] H. Lahlali, K. Jobe, M. Watkinson, S. M. Goldup, *Angew. Chem. Int. Ed.* **2011**, *50*, 4151–4155.

[61] J. E. M. Lewis, J. Winn, L. Cera, S. M. Goldup, *J. Am. Chem. Soc.* **2016**, *138*, 16329–16336.

[62] J. Lewis, J. Winn, S. Goldup, J. E. M. Lewis, J. Winn, S. M. Goldup, *Molecules* **2017**, *22*, 89.

[63] J. Winn, A. Pinczewska, S. M. Goldup, *J. Am. Chem. Soc.* **2013**, *135*, 13318–13321.

[64] E. A. Neal, S. M. Goldup, *Chem. Sci.* **2015**, *6*, 2398–2404.

[65] E. A. Neal, S. M. Goldup, *Angew. Chem. Int. Ed.* **2016**, *55*, 12488–12493.

[66] B. T. Worrell, J. A. Malik, V. V. Fokin, *Science* **2013**, *340*, 457–460.

[67] M. Galli, J. E. M. Lewis, S. M. Goldup, *Angew. Chem. Int. Ed.* **2015**, *54*, 13545–13549.

[68] Y. Sato, R. Yamasaki, S. Saito, *Angew. Chem. Int. Ed.* **2009**, *48*, 504–507.

[69] S. M. Goldup, D. A. Leigh, T. Long, P. R. McGonigal, M. D. Symes, J. Wu, *J. Am. Chem. Soc.* **2009**, *131*, 15924–15929.

[70] K. Ito, Y. Mutoh, S. Saito, *J. Org. Chem.* **2017**, *82*, 6118–6124.

[71] N. H. Evans, *Chem. – Eur. J.* **2018**, *24*, 3101–3112.

[72] N. Pairault, J. Niemeyer, *Synlett* **2018**, *29*, 689–698.

[73] S. Hoekman, M. O. Kitching, D. A. Leigh, M. Papmeyer, D. Roke, *J. Am. Chem. Soc.* **2015**, *137*, 7656–7659.

[74] Y. Tachibana, N. Kihara, T. Takata, *J. Am. Chem. Soc.* **2004**, *126*, 3438–3439.

[75] K. Xu, K. Nakazono, T. Takata, *Chem. Lett.* **2016**, *45*, 1274–1276.

[76] R. Mitra, H. Zhu, S. Grimme, J. Niemeyer, *Angew. Chem. Int. Ed.* **2017**, *56*, 11456–11459.

[77] V. Blanco, A. Carlone, K. D. Hänni, D. A. Leigh, B. Lewandowski, *Angew. Chem. Int. Ed.* **2012**, *51*, 5166–5169.

[78] V. Blanco, D. A. Leigh, U. Lewandowska, B. Lewandowski, V. Marcos, *J. Am. Chem. Soc.* **2014**, *136*, 15775–15780.

[79] J. Beswick, V. Blanco, G. D. Bo, D. A. Leigh, U. Lewandowska, B. Lewandowski, K. Mishiro, *Chem. Sci.* **2014**, *6*, 140–143.

[80] V. Blanco, D. A. Leigh, V. Marcos, *Chem. Soc. Rev.* **2015**, *44*, 5341–5370.

[81] V. Blanco, D. A. Leigh, V. Marcos, J. A. Morales-Serna, A. L. Nussbaumer, *J. Am. Chem. Soc.* **2014**, *136*, 4905–4908.

[82] P. R. Ashton, A. M. Heiss, D. Pasini, F. M. Raymo, A. N. Shipway, J. F. Stoddart, N. Spencer, *Eur. J. Org. Chem.* **1999**, *1999*, 995–1004.

[83] Y. Tachibana, N. Kihara, Y. Ohga, T. Takata, *Chem. Lett.* **2000**, *29*, 806–807.

[84] K. Xu, K. Nakazono, T. Takata, *Tetrahedron Lett.* **2016**, *57*, 4356–4359.

[85] K. Hirose, Y. Nakamura, Y. Tobe, *Org. Lett.* **2009**, *11*, 145–147.

[86] R. J. Bordoli, S. M. Goldup, *J. Am. Chem. Soc.* **2014**, *136*, 4817–4820.

[87] C. Reuter, A. Mohry, A. Sobanski, F. Vogtle, *Chem. Weinh. Bergstr. Ger.* **2000**, *6*, 1674–1682.

[88] C. Yamamoto, Y. Okamoto, T. Schmidt, R. Jäger, F. Vögtle, *J. Am. Chem. Soc.* **1997**, *119*, 10547–10548.

[89] C. A. Schalley, K. Beizai, F. Vögtle, *Acc. Chem. Res.* **2001**, *34*, 465–476.

[90] Y. Makita, N. Kihara, N. Nakakoji, T. Takata, S. Inagaki, C. Yamamoto, Y. Okamoto, *Chem. Lett.* **2006**, *36*, 162–163.

[91] F. Ishiwari, K. Nakazono, Y. Koyama, T. Takata, *Angew. Chem. Int. Ed.* **2017**, *56*, 14858–14862.

[92] D. K. Mitchell, J.-P. Sauvage, *Angew. Chem. Int. Ed. Engl.* **1988**, *27*, 930–931.

[93] J. C. Chambron, D. K. Mitchell, J. P. Sauvage, *J. Am. Chem. Soc.* **1992**, *114*, 4625–4631.

[94] J.-C. Chambron, C. Dietrich-Buchecker, G. Rapenne, J.-P. Sauvage, *Chirality* **1998**, *10*, 125–133.

[95] A. Mohry, F. Vögtle, M. Nieger, H. Hupfer, *Chirality* **2000**, *12*, 76–83.

Chapter 2: The effect of the mechanical bond in copper-catalysed transformations

Abstract: This chapter reports the initial investigation on the use of a model rotaxane as a ligand for copper-catalysed transformations such as cyclopropanation of carbenoids, insertion of carbenoid in NH bond. During this study, it was found that the bipyridine-containing rotaxane can be used as ligand for a range of transformations. The mechanical bond was found to have an improvement in the diastereoselectivity of simple reactions.

Prior publication: None of this work has been previously published.

2.1. Introduction

2.1.1. Bipyridine function in macrocycles and AT-CuAAC

The first examples of macrocycles bearing a bipyridine functional group able to form a 1:1 inclusion complex were reported by Sauvage and co-workers in 1986.[1,2] These macrocycles **100** and **101** (Figure 2.1) were composed of two coordination sites, a bipyridine and a phenanthroline. In presence of $[Cu(MeCN)_4]BF_4$, the copper complex **102** was obtained in a folded conformation in a 1:1 mixture of MeCN-CH_2Cl_2. When a second phenanthroline-functionalised molecule was added to **102**, the unfolding of the structure was not observed. Ultimately, the addition of Ru^{II} resulted in selective complexation with the bipyridine functional group. The addition of one equivalent of $[Cu(MeCN)_4]BF_4$ and a second phenanthroline-functionalised molecule resulted in the formation of the hetero-bimetallic complex **103**.

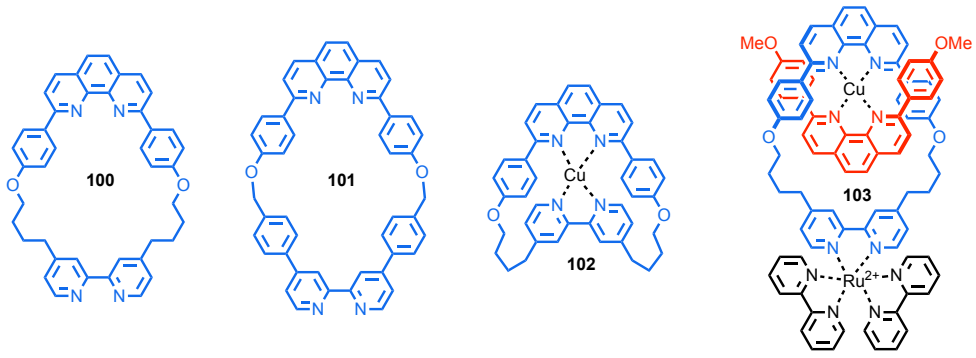

Figure 2.1 Macrocycles bearing a bipyridine unit.

The bipyridine functional group demonstrated to be an efficient coordination site for Cu^{I} in the synthesis of rotaxanes, using the AT-CuAAC approach. Goldup and co-workers reported the high yielding synthesis of [2]rotaxane **104**, from azide **32** and alkyne **30** as the half-axle.[3] A bipyridine based macrocycle **78** was used to promote the cycloaddition product inside the macrocycle cavity (Figure 2.2).

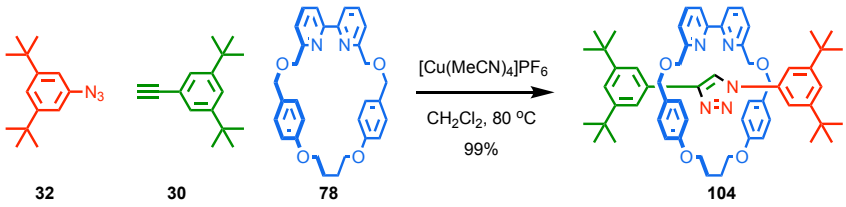

Figure 2.2 Synthesis of rotaxane **104** with a bipyridine based macrocycle **78**.

When the reaction was performed using the bipyridine-functionalised macrocycle **33** in presence of a hindered base, *N*,*N*-diisopropylethylamine, the concentration of the copper-acetylide species increased in the media which speed up the reaction.[4] The presence of the tertiary amine enabled the isolation of the copper-triazolide complex **34** by trapping the proton released during the AT-CuAAC (Figure 2.3).

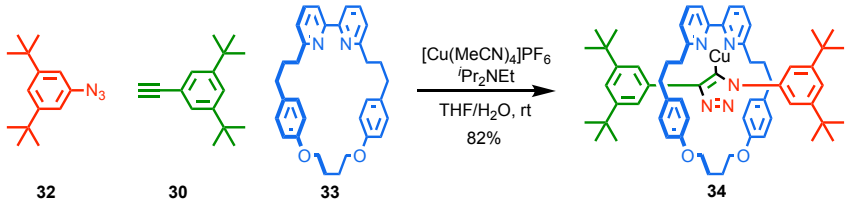

Figure 2.3 Synthesis of complex **34**.

In order to access the bipyridine functionalised macrocycle, two approaches were developed. The first one was reported by Leigh and co-workers in which the closure of the macrocycle was done by a double Williamson etherification reaction (Figure 2.4).[5] This synthesis involved a nickel catalysed homo-coupling reaction of bromopyridine **105** leading to bipyridine **106**. The alcohol function was then alkylated to give **107** and the allyl protecting group was removed using Pd^0, thus leading to **108**. Cyclisation, under high dilution conditions, yielded macrocycle **109** in 19% yield over 4 steps.

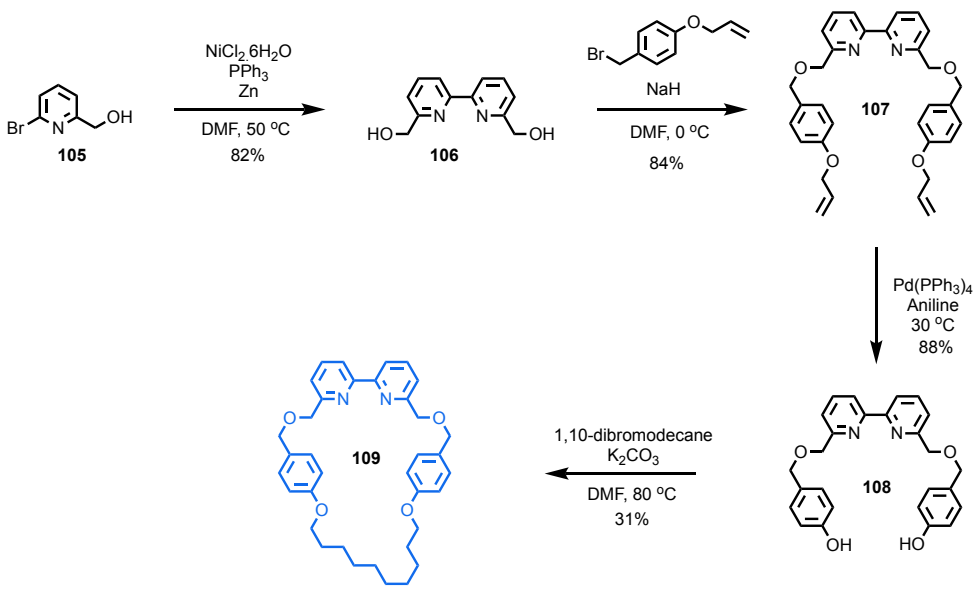

Figure 2.4 Synthesis of macrocycle **109**.

Following this, Goldup and co-workers developed a new methodology for the synthesis of bipyridine macrocyclic compounds.[6] In this new method, the closure of the macrocycle occurred *via* an intramolecular nickel catalysed coupling reaction of two bromopyridines, thus resulting in the formation of a new carbon-carbon bond (highlighted in red in Figure 2.5). Macrocycle **109** was also synthesised in a high yield using this approach (67% yield).

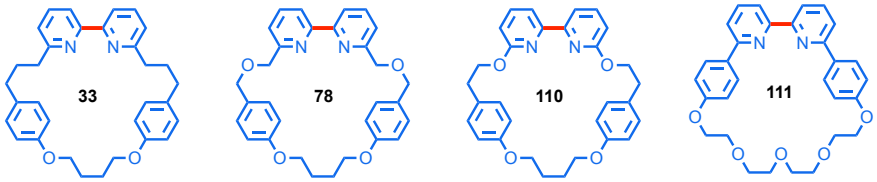

Figure 2.5 Nickel mediated ring closure affording a large range of bipyridine macrocycles.

2.1.2. Introduction to carbene chemistry

2.1.2.1. Free carbene

In 1988, Bertrand and co-workers reported the first synthesis of a free carbene.[7] Flash thermolysis of the diazo compound **112** at 250 °C under vacuum generated the free carbene **113**, in which the carbene is stabilised by the presence of adjacent phosphorus and silicon substituents. In 1991, Arduengo and co-workers reported the first example of a stable N-heterocyclic carbene (NHC) **115** by deprotonation of the imidazolium salt **114** using potassium *tert*-butoxide.[8]

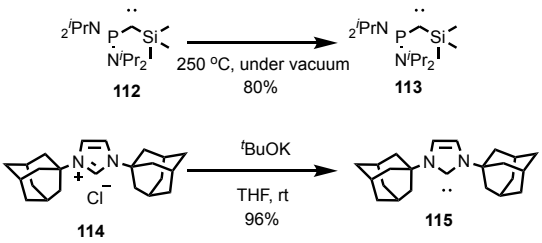

Figure 2.6 Synthesis of stable free carbenes **113** and **115**.

Metal carbene complexes are a type of organometallic compounds in which the metal is bond to a neutral divalent carbon ligand. Over the past 50 years, people have studied this type of organometallic compound. All of this research resulted in the discovery of two type of metal carbenoids.

2.1.2.2. Fischer-type metal carbene

In 1964, Fischer and Maasböl reported the first example of a Fischer-type carbene complex.[9],[10] The treatment of tungsten (0) hexacarbonyl **116** with phenyl lithium followed by methylation using diazomethane resulted in the formation of a new organometallic complex **116** (Figure 2.7). The characterisation of this species revealed for the first time the metal carbene bond. In this complex, the carbene is in the singlet state, due to the presence of two electrons in the same orbital, in which the carbenic carbon has a sp^2-hybridised lone pair (σ electron) and an unoccupied *p*-orbital. The singlet state corresponds to the spin-paired state with both spin in the same orbital resulting in only one combination. The lone

pair donated to the vacant *d*-orbital of the metal and π–back-donation occurred from a second metal *d*-orbital to the unoccupied *p*-orbital of the carbene. This constitutes the metal-carbene bond in the Fischer-type carbene complexes. Fischer-type carbenes are generally found for middle to late transition metals with a low oxidation state with a π-donating substituent, such as alkoxy or amino group, on the carbene centre. These complexes are electrophilic on the carbenic carbon and tend to undergo nucleophilic attack.

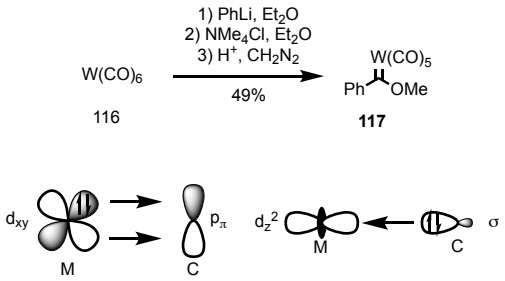

Figure 2.7 Synthesis of Fischer-type metal carbene complex.

2.1.2.3. Schrock-type metal carbene

In 1974, Schrock reported the synthesis of a second type of metal-carbene complex (Figure 2.8).[11] The reaction of tantalum complex **118** with two equivalents of neopentyl lithium followed by α–hydrogen abstraction afforded the tantalum complex **119** in quantitative yield. This type of alkylcarbene complex was defined as the Schrock-type carbene complex. The carbenic carbon is in a triplet state in which the two unpaired electrons of the carbenic carbon interacted with the metal d-orbital forming a covalent double bond between the carbon and the metal. Schrock-type carbene are generally found for early transition metal with high oxidation states with no π-donating substituents on the carbene centre. The carbenic carbon is nucleophilic and can react with electrophiles.

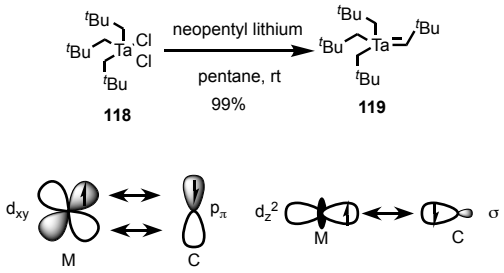

Figure 2.8 Synthesis of Schrock-type metal carbene complex.

Metal carbene complexes have been used in modern organic reactions. Olefin metathesis reaction is one of the most famous applications reported with the use of ruthenium based catalysts bearing carbene ligand such as Grubbs' first and second-generation catalyst **120** and **121** or Hoveyda-Grubbs II catalyst **122** (Figure 2.9).[12–14] The metal carbene bond in the ruthenium based metathesis catalyst is similar to those of the Schrock-type carbenes. However, the carbenic carbon in Schrock-type carbene is nucleophilic, the same carbon is electrophilic in Grubbs' type catalysts.[15]

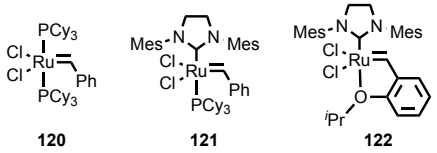

Figure 2.9 Ruthenium-based catalyst for the olefin metathesis reaction.

2.1.2.4. Copper carbene complex reactivity

Controlling the selectivity of reactive intermediates is one of the major objectives in the development of organic reactions. The thermal or photochemical generation of carbenes from a diazo compound by extrusion of nitrogen tends to give a complex mixture of products.[16] However, the controlled decomposition of a diazo compound in presence of a metal leading to a carbenoid intermediate is a useful tool towards the formation of new bonds (Figure 2.10). Carbene transfer from the carbenoid to π–systems such as alkene, alkyne or arene leads to the formation of three-membered rings (Figure 2.10, pathway 1). X-H bonds such as C-H, O-H, N-H reacts with formal insertion of the carbenoid to afford a tertiary carbon while nucleophiles lead to ylides (Figure 2.10, pathway 2 and 3, respectively).

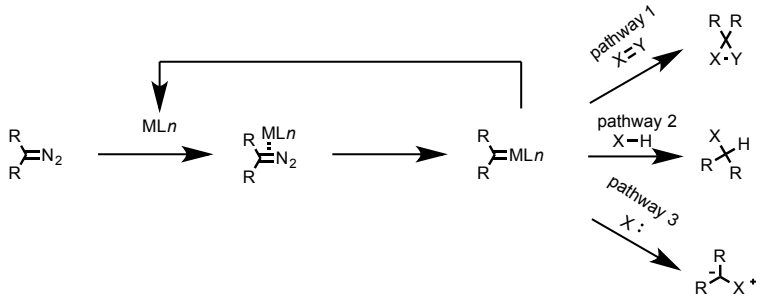

Figure 2.10 Catalysed decomposition of diazo compound and reactivity.

Yates was the first to observe the copper-catalysed decomposition of a diazoketone in 1952.[17] During this study, α-diazoacetophenone (**123**) was dissolved in methanol in presence of copper and the formation of N_2 gas was observed. The only product isolated during this reaction was the methoxyacetophenone **124** (Figure 2.11). Yates proposed in this report that a carbenic entity could be bound to the copper surface with the valence electrons of the copper completing the octet of the carbenic carbon. The second step of the reaction would be the attack of the electron-deficient carbenic carbon by the lone pair of the methanol. In this publication, the author is also reported the possibility to use thiols and amines instead of alcohols.

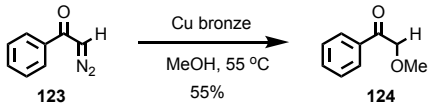

Figure 2.11 Yates' first observation of the copper-catalysed decomposition of **123** in presence of copper.

In 2001, Straub and Hoffman were able to observe for the first time a persistent copper carbene complex in solution.[18] This observation confirmed the hypothesis made by Yates 50 years earlier in which a carbenic complex was generated in presence of copper. The design of a highly basic, sterically hindered iminophosphanamide ligand allowed the formation of a stable Cu^{I} carbenoid. A few years following this, the same group isolated a new copper α-carbonyl carbene **125**, which was characterised using single crystal x-ray crystallography (Figure 2.12).[19] This copper-carbene species is a new example of Fischer-type carbene complex.

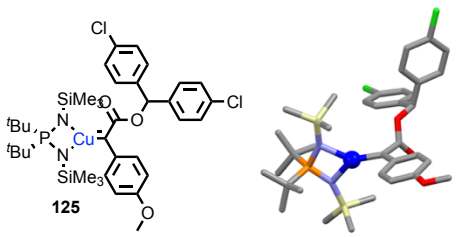

Figure 2.12 Single crystal X-ray structure of copper α-carbonyl carbene **125**. Deep blue ball represents the copper centre.

In 1972, Salomon and Kochi studied the Cu^{I} catalysed cyclopropanation with diazocompounds in presence of olefins.[20] The $CuOTf(C_6H_6)_{0.5}$ was used as organic soluble copper catalyst. In presence of ethyl diazoacetate **127**, *cis* and *trans*-but-2-ene **126** were converted to ethyl 2,3-dimethylcyclopropanecarboxylates **128** in 50% yield after distillation (Figure 2.13 a). The mechanism of the cyclopropanation reaction has extensively studied. In 2002, Norrby and co-workers proposed a concerted mechanism with an asynchronous transition state. In this mechanism, the authors proposed that the bond between the carbenic carbon and the β–carbon of the olefin is formed before the bond to the α–carbon as presented in Figure 2.13 b.[21]

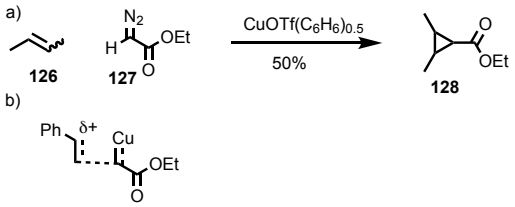

Figure 2.13 a) Cyclopropanation reaction; b) Transition state proposed by Norrby and co-workers.

In the absence of carbene acceptors, such as olefin or X-H bond or nucleophile, the carbenoid complex decomposed slowly, thus leading to the carbene dimer. The homo-coupled product is considered as a side product of many copper catalysed reactions. This dimerization was observed by Noyori and co-workers in 1966 when diphenyldiazomethane **129** afforded tetraphnylethylene **131** in excellent yield in presence of bis(acetylacetonato)copper (II) **130** (Figure 2.14).[22]

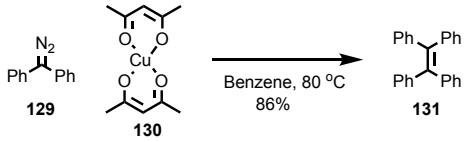

Figure 2.14 Dimerisation of diphenyldiazomethane in presence of copper (II).

Sun and co-workers proposed a mechanism for the homo-coupling reaction of aryldiazoacetate (Figure 2.15).[23] The nucleophilic attack of the diazo carbon on the copper followed by extrusion of N_2 gas leads to the copper carbene species. The presence of a second metal activating the carbenoid species enables the nucleophilic attack of a second diazocompound leading to the formation of the new double bond after extrusion of N_2 molecule.

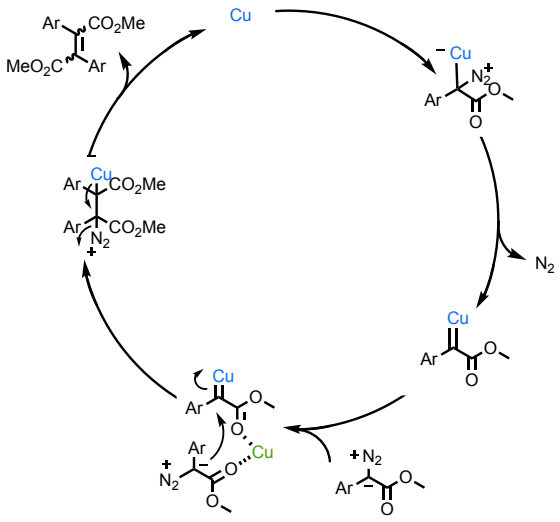

Figure 2.15 Proposed mechanism for homo-coupling reaction of a carbenoid.

2.1.2.5. Bipyridine ligands in copper catalysis

The initial reports on copper carbene complexes involved inorganic copper. In order to have a better control of the outcome of the reaction, the development of a large range of catalysts have been investigated. The inorganic copper bronze source used by Yates in 1951 was replaced by well-defined organic copper source such as bis(acetylacetonato)copper (II) by Noyori in 1966. The development of enantioselective reaction to generate chiral molecules

has been a real challenge. Enantioselective catalysis requires the use of a chiral coordination complex typically by the coordination of enantiopure ligands to the metal.[24] It is worth noting that examples of catalysts displaying chirality-at-metal have been used for enantioselective transformations.[25,26] Many different families of ligands are commonly used in copper catalysed transformations but bipyridine ligands have encountered a great success. This can be explained by their extreme stability in aqueous solution and to atmospheric oxygen simplifying their preparation and long-term storage.

The reaction of styrene with diazoacetate in presence of copper catalyst is well established model to evaluate the efficiency of a ligand in asymmetric cyclopropanation. A selection of chiral bipyridine ligand presenting C_1 or C_2 symmetry is presented in Figure 2.16.

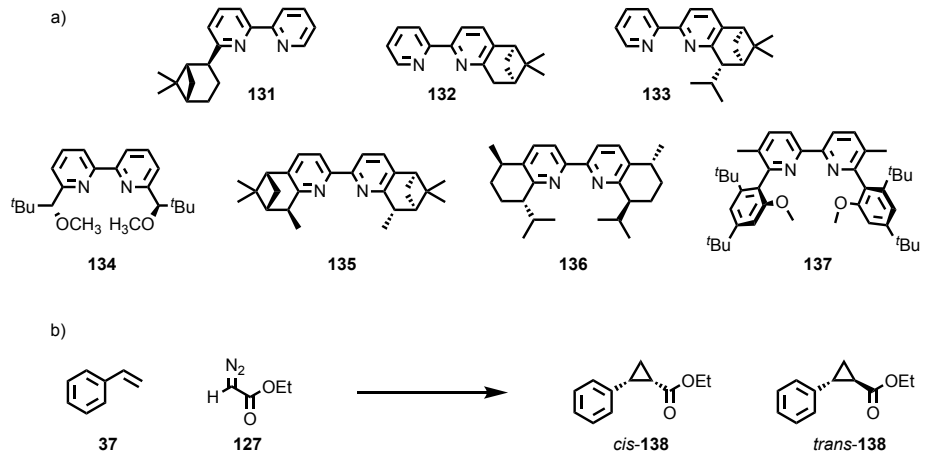

Figure 2.16 a) Selection of chiral bipyridine ligands used in copper catalysis. b) Cyclopropanation of styrene with diazoacetate.

In 1986, Botteghi and co-workers focused their attention in the synthesis of C_1-symmetric enantiopure bipyridine.[27] The application of **131** into the cyclopropanation reaction revealed a poor selectivity for the *cis*/*trans* ratio of the product, however, 20% enantiomeric excess was obtained for the *trans*-cyclopropane. Following the idea of having a C_1-symmetric bipyridine, von Zelewsky and Hayoz prepared **132** from α-pinene and eight years later Chelucci and co-workers evaluated the potential as ligand for cyclopropanation.[28,29] This ligand showed an improvement of the selectivity to the *trans*-isomers but only negligible enantiomeric excess was obtained (10% for the *cis*-isomer). Good enantiomeric excess for the *cis* and *trans*-isomers, respectively 51 and 58%, were obtained when ligand **133** was

used.[30] C_2-symmetric ligand **134** displayed incredible enantioselectivity for the *trans*-isomer as well as for the *cis*-isomer (89% and 74% respectively).[31] Ligands **135** and **136** gave similar selectivity for the cyclopropanation with enantioselectivity higher than 70% for both isomers.[30] Ultimately, ligand **137** with atropisomeric stereochemistry was efficient in driving the reaction towards the *trans*-isomer with an excellent 80% enantiomeric excess.[32]

2.1.3. Aims of the project

Based on the group expertise in the synthesis of "small" rotaxanes as well as the first example of a gold rotaxane as switchable and diastereoselective catalyst,[33] the aim of this project is to develop new rotaxane-based enantioselective and/or diastereoselective catalysts. These new ligands are aimed to be involved in copper catalysed processes. A selected example of rotaxane will be used as a model to explore its potential to act as a ligand for copper and will then be screened in a series of copper catalysed reactions that would create at least one chiral centre. The evaluation of the effect of the mechanical bond on diastereoselectivity, regioselectivity or chemoselectivity will be investigated.

2.2. Results and Discussion

The first part of this section consists in the synthesis of a model rotaxane for the evaluation of the potential of bipyridine-functionalised rotaxane as ligands for copper catalysed reactions. With the potential ligands in hand, different copper-catalysed reactions will be carried out to evaluate the effect of the mechanical bond.

2.2.1. Synthesis of the rotaxane model

*2.2.1.1. Synthesis of macrocycle **78***

The synthesis of macrocycle precursor **142** was performed using optimised conditions reported by Goldup and co-workers (Figure 2.14).[34] This synthesis started with a double Williamson etherification reaction of **139** and 1,4-dibromobutane leading to **140**. The conversion of the hydroxyl group of **140** to bromide was performed using HBr in CH_2Cl_2. The bromide intermediate **141** reacted with 2-bromo-6-hydroxymethylpyridine in presence of sodium hydride, resulting in macrocycle precursor **142**. The overall reported yield for the synthesis of the precursor was 70% and can be performed on a large scale with purification after the final step.

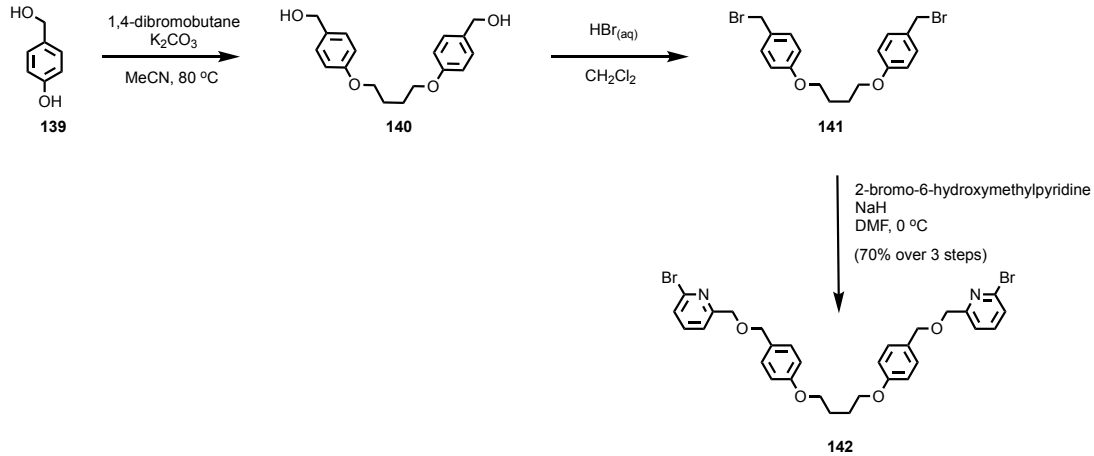

Figure 2.17 Synthesis of macrocycle precursor **142**.

The macrocyclisation of **142** generating **78** was performed on a 2 mmol scale following the reported procedure (Figure 2.18). The *pseudo* high dilution conditions were obtained by slow addition over four hours of precursor **142** into a suspension containing the nickel catalyst mixture, resulting in macrocycle **78** in a 52% yield, slightly lower than the 70% reported yield due to co-elution of the oligomers during the column chromatography.

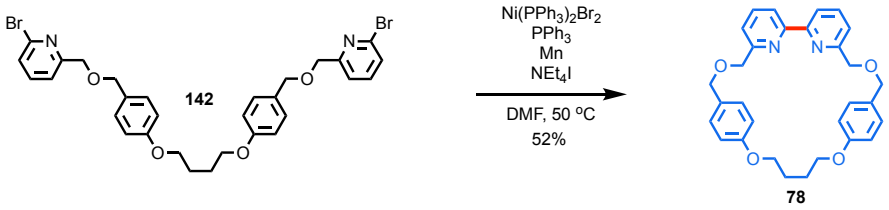

Figure 2.18 Macrocyclisation reaction of **142** into **78**.

Kelsey and Jutand proposed a mechanism for the nickel catalysed homo-coupling reaction involving a Ni^{I}/Ni^{III} active catalyst as reported in Figure 2.19.[35,36] The first step of this mechanism involved a classic oxidative addition of the Ni^{0} into the aryl bromide bond. The Ni^{II} was then reduced to Ni^{I} by single electron transfer for a zinc metallic, or manganese metallic in our procedure. The Ni^{I} intermediate was then involved in a second oxidative addition resulting in the formation of a Ni^{III} intermediate. Reductive elimination generated the homo-coupled product as well as a new Ni^{I} intermediate which can be reduced to Ni^{0} by a second single electron transfer.

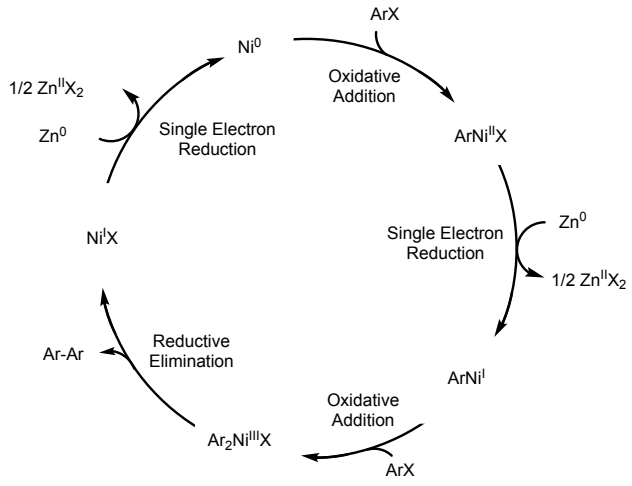

Figure 2.19 Proposed mechanism for the nickel mediated homo-coupling reaction.

*2.2.1.2. Synthesis of the two stoppers **30** and **32***

1-Bromo-3,5-di-*tert*-butylbenzene **143** was the starting material for the synthesis of both stoppers (Figure 2.20). Azide stopper **30** was prepared in 76% yield by a bromide/lithium exchange followed by a nucleophilic attack on the organic tosyl azide. Alkyne **32** was prepared in a two steps procedure involving a Sonogashira reaction with trimethylsilylacetylene followed by the desilylation using K_2CO_3 in a 1:1 mixture of CH_2Cl_2 and MeOH mixture, resulting in a 90% yield over two steps.

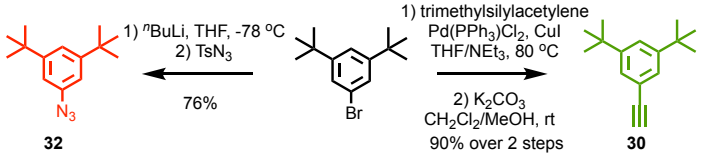

Figure 2.20 Synthesis of stoppers **30** and **32**.

*2.2.1.3. Synthesis of the rotaxane model **104***

The rotaxane model was prepared using the AT-CuAAC approach, resulting in the formation of a 1,4-disubstituted 1,2,3-triazole moiety (Figure 2.21). The more favourable formation of the rotaxane compared to the axle is explained by the fast complexation of the copper by the bipyridine macrocycle. This adduct can catalyse the [2+3] cycloaddition through the cavity of the macrocycle.

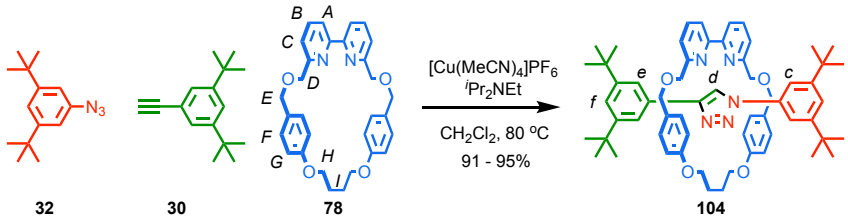

Figure 2.21 Rotaxane synthesis under thermal conditions

The use of 0.96 equivalents of copper is key in this procedure. The stacked ^{1}H NMR plot in Figure 2.22 compares the ^{1}H NMR spectra of macrocycle **78**, rotaxane **104** and axle **145** (Figure 2.22). The distinctive signal of the triazole proton H_d shifted from 8.10 ppm for the axle to 10.50 ppm for the rotaxane, as a result of the hydrogen bonding interaction between

the bipyridine moiety and the triazole proton. In addition, the aromatic protons of the phenyl rings H_F and H_G in the macrocycle are shielded due to the anisotropic effect of the triazole moiety present in the cavity of the rotaxane. Finally, the benzylic proton H_E was observed as a singlet in the macrocycle due to the C_2-symmetry macrocycle. H_E appeared as two doublets in the ^{1}H NMR of rotaxane **104**, this is due to the loss of one plane of symmetry by the presence of the non-symmetrical axle which make H_E diastereotopic.

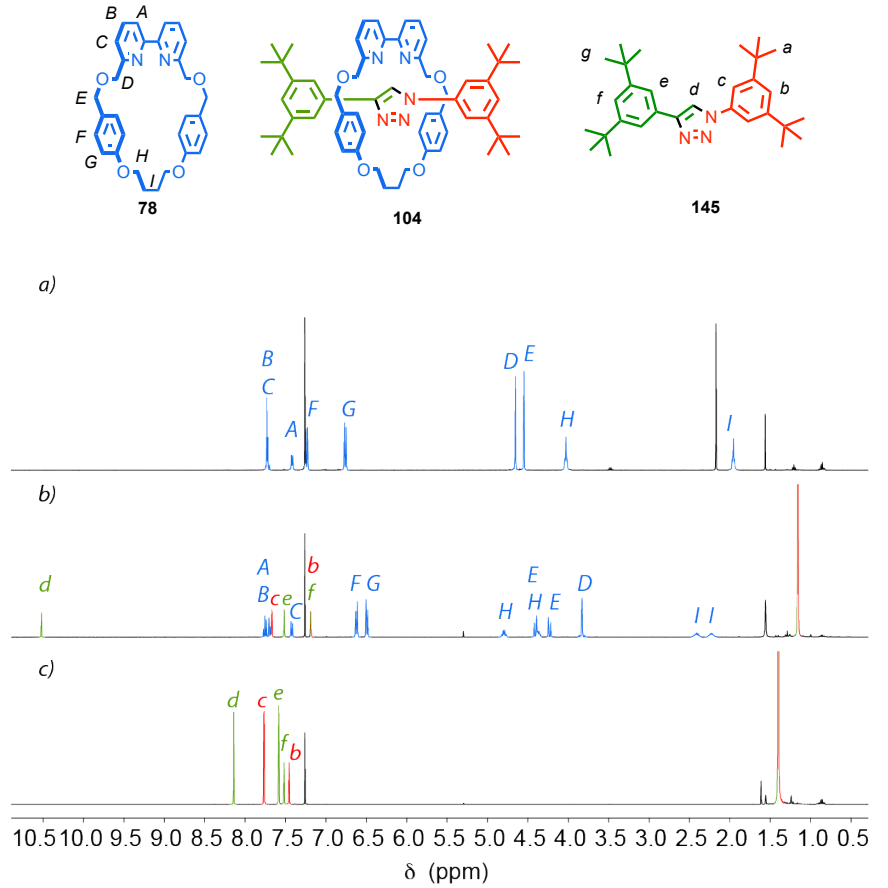

Figure 2.22 Stack ^{1}H NMR (400 MHz, $CDCl_3$, 298K) of a) macrocycle **78**, b) rotaxane **104** and c) axle **145**.

Subsequently, the reaction was scaled up to produce enough material for the catalyst screening. The rotaxane synthesis was initially performed on 0.025 or 0.05 mmol scale that results in ~ 40 mg of product. The scale of the reaction was increased from 0.05 mmol to 0.2 mmol with no loss in yield. The limitation of the vessel size used to perform the reaction forced us to increase the concentration of the reaction from 10 mM to 40 mM, enabling the increase of the scale up to 0.8 mmol without drop of the yield (Table 2.1) affording ~ 650 mg of rotaxane **104** after purification.

Table 2.1 Scaling up of the rotaxane synthesis

Scale	Concentration	Isolated yield[a]
0.05 mmol	0.01 mmol/mL	93%
0.2 mmol	0.01 mmol/mL	94%
0.2 mmol	0.04 mmol/mL	95%
0.8 mmol	0.04 mmol/mL	91%

Conditions: Stoppers (1.5 equiv.), Macrocycle (1 equiv.), $[Cu(MeCN)_4PF_6]$ (0.96 equiv.), $^{i}Pr_2NEt$ (10 equiv.), CH_2Cl_2, 80 °C, 16h. [a] Isolation by column chromatography on silica.

*2.2.1.4. Complexation of rotaxane **104** with Cu^{I}*

In the perspective of applying the model rotaxane in catalysis, it was crucial to verify the ability of **104** to bind Cu^{I} or Cu^{II}. Cu^{I} was chosen for the complexation using rotaxane model **104** resulting in the complex **104-Cu**. Indeed, Cu^{I} is a diamagnetic species, which allowed the ^{1}H NMR study of the complexation. The copper source used in this study was $[Cu(MeCN)_4PF_6]$. The addition of one equivalent of copper to the rotaxane solution resulted in a single well-defined species, which was characterised by its ^{1}H NMR spectrum (Figure 2.23).

The chemical shift of H_d appeared at 6.85 ppm in the complex **104-Cu** while H_d is at 10.50 ppm in the ligand. The explanation of this chemical shift difference is explained by a flipping of the triazole moiety in the axle. The copper centre is now coordinated by two nitrogen atoms from the bipyridine moiety and one nitrogen atom from the triazole ring. The hydrogen bonding interaction between the bipyridine moiety and the triazole proton is not possible, which explain the difference of chemical shifts for H_d.

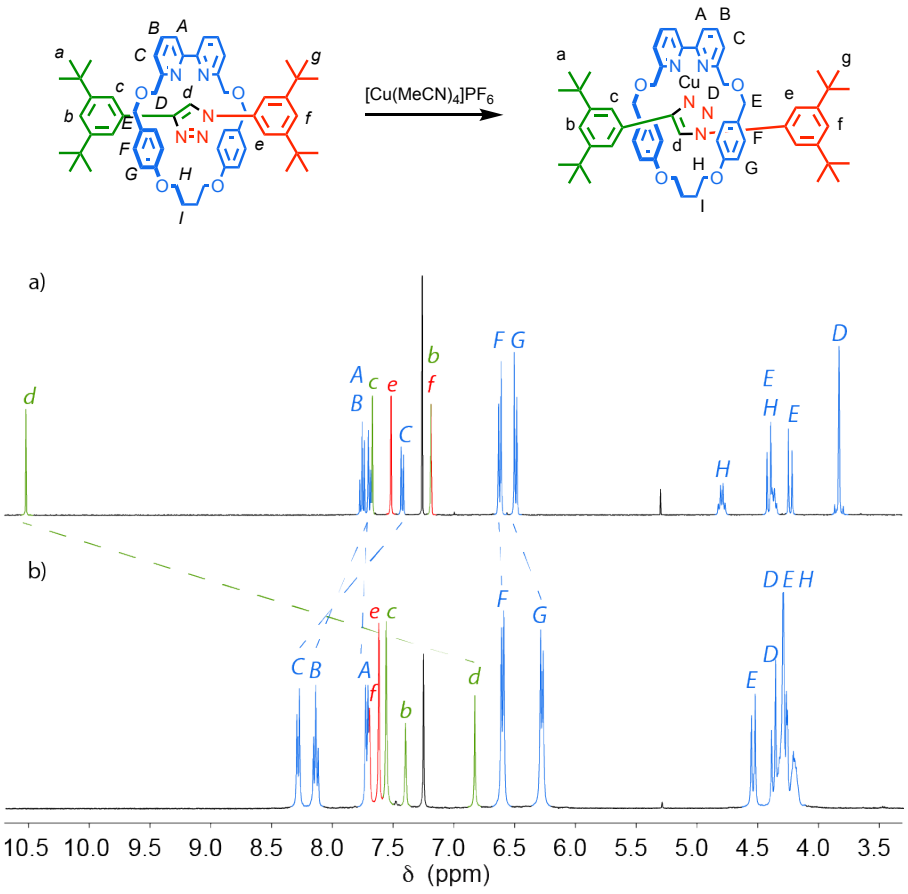

Figure 2.23 Partial Stack ^{1}H NMR (400 MHz, $CDCl_3$, 298K) of a) Rotaxane **104**, b) Rotaxane **104** + 1 equiv. of $[Cu(MeCN)_4]PF_6$.

2.2.2. Evaluation of the behaviour in copper catalysed reactions using an achiral ligand

With the evidence of being able to chelate a cationic copper with the rotaxane 9, the catalysis using copper can be envisaged. In order to do so, the ligands used in this section are presented in Figure 2.24. The effect of the mechanical bond can be evaluated by comparison of the results obtained using **144** and those obtained using an equimolar mixture of **74** and **145**. As our long-term aim was to investigate chiral ligands, only reactions forming one or more chiral centres were investigated.

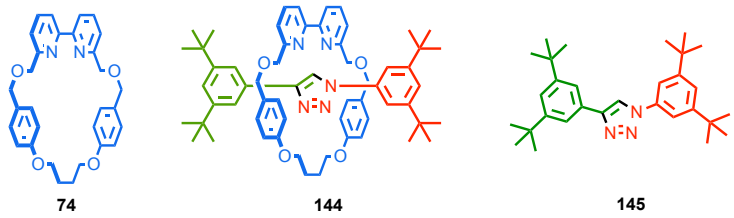

Figure 2.24 Ligands used in the catalysis experiments

2.2.2.1. Henry reaction

The first attempted catalytic process was the Henry reaction of aldehyde with nitromethane resulting in the formation of nitroaldol. This reaction is known to be catalysed by a combination of Brønsted base and Lewis acid activations. Deprotonation of nitromethane by the base generates the activated nitronate. The nitronate can undergo a nucleophilic attack on the aldehyde activated by the Lewis acid resulting in formation of the nitroalcohol product after protonation (Figure 2.25).

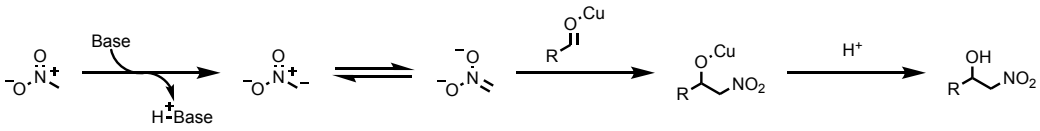

Figure 2.25 Henry reaction mechanism.

The system used in this study was the reaction between nitromethane and *p*-nitrobenzaldehyde **146** in dry methanol leading to nitroalcohol **147**. When the reaction was performed in absence of Lewis acid and base, no reaction was observed (Table 2.2, Entry 1). Addition of macrocycle **78** or rotaxane **104** in absence of metal did not provide any reaction (Table 2.2, Entries 2 and 4). When the macrocycle was combined with axle **145**, conversion was still not observed (Table 2.2, Entry 3). Addition of CuBr alone as Lewis acid, resulted in marginal conversion with 4% of nitroalcohol **147** formed potentially due to the heterogeneity of the reaction mixture (Table 2.2, Entry 5). Addition of a slight excess of macrocycle compared to the copper, resulted in a significant increase of the conversion (50%) (Table 2.2, Entry 6). When the macrocycle was combined with axle **145**, the conversion was slightly lower with 44% (Table 2.2, Entry 7). Finally, when a slight excess of rotaxane **104** was used in presence of CuBr, the obtained conversion was 41% (Table 2.2, Entry 8). The reaction mixture was homogeneous in presence of ligands and metal. The presence of the slight

excess of bipyridine-functionalised ligand can play the role of the base to deprotonate the nitromethane as proposed in the mechanism (Figure 2.25).

Table 2.2 Henry reaction of p-nitrobenzaldehyde with nitromethane

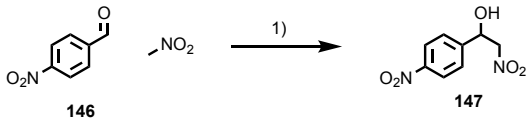

146 **147**

Entry	Copper source	Ligand	Conversion[a]
1	none	none	0%
2	none	**78**	0%
3	none	**78** + **145**	0%
4	none	**104**	0%
5	CuBr	none	4%
6	CuBr	**78**	50%
7	CuBr	**78** + **145**	44%
8	CuBr	**104**	41%

Conditions: 1) Copper source (5% mol), Ligand (6% mol), MeOH, rt, 16h, [a] Determined by ^{1}H NMR

The results did not show significant effects of the mechanical bond. In order to evaluate the effect of the mechanical bond, other systems involving the copper as reaction intermediate were investigated.

2.2.2.2. Cyclopropanation reaction

The controlled decomposition of a diazocompound in presence of a copper source is known to generate a highly reactive copper carbene intermediate. This intermediate can be trapped using different reagents. The reaction of this carbenoid with a reagent bearing unsaturation led to the formation of three-membered ring. The use of olefin-functionalised molecule generates a cyclopropane, whereas triple bond generates a cyclopropene.

When evaluating the diastereoselective and/or enantioselective efficiency of ligand, the reaction between styrene (**41**) and ethyl diazoacetate (**127**) is often used as model reaction. This reaction generates two diasteoreoisomers (*cis* and *trans*-isomers) both existing as mixture of two enantiomers. In addition, two degradation products can also be formed, diethyl maleate **146** and diethyl fumarate **147** (Figure 2.26).

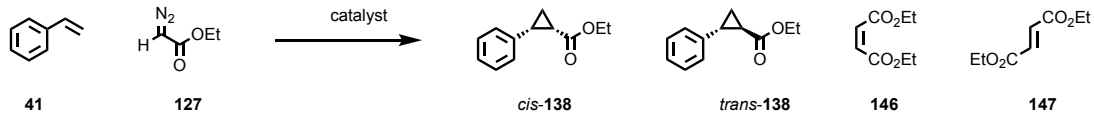

Figure 2.26 Cyclopropanation reaction of styrene with ethyl diazoacetate in presence of copper.

The reaction was achieved by addition of the ethyl diazoacetate into a mixture containing $[Cu(MeCN)_4]PF_6$, ligand and styrene in $CDCl_3$ at room temperature. The mixture was analysed by ^1H NMR spectroscopy after 16 hours. The characteristic peaks used for the analysis were 6.84 ppm for the fumarate (integrating for 2H), 6.24 ppm for the maleate (integrating for 2H), 1.90 ppm for the *trans*-cyclopropane (integrating for 1H) and 2.09 ppm for the *cis*-cyclopropane (integrating for 1H).[20] Control reactions were carried out. Macrocycle **78**, combination of macrocycle **78** and axle **145** or rotaxane **104**, without metal produced no reaction (Table 2.3, Entries 1-4). When copper was included in the reaction mixture, after 16 hours, the ethyl diazoacetate was completely consumed forming each of four products in different ratios. When the copper was used without an added ligand, the major compound formed in 91% was the mixture of *trans*/*cis* cyclopropane **138** obtained, respectively in a ratio of 52% and 39% (Table 2.3, Entry 5). Addition of macrocycle **78** reduced the selectivity slightly towards the cyclopropanes to 81% (Table 2.3, Entry 6). The major cyclopropane formed under those conditions was the *cis*-isomer with 44% whereas the *trans*-isomer was represented 37% of the products formed. The non-interlocked combination of macrocycle **78** and axle **145** led to nearly equivalent ratio of cyclopropanes formed, 40% and 38% respectively for the *trans* and *cis*-isomers (Table 2.3, Entry 7). The addition of rotaxane **104** as ligand significantly favoured the formation of the *trans*-isomer compare to the *cis* with 42% and 16% respectively but decreased the ratio of cyclopropanes in the crude mixture (58% of cyclopropanes formed) (Table 2.3, Entry 8). The selectivity towards the formation of the cyclopropanes appeared to be reduced by increasing the steric hindrance around the copper centre. The steric hindrance around the carbene bond can make the approach of the olefin more difficult to form the cyclopropane. The selectivity for the *trans*-isomer seemed to be improved by increasing the bulkiness of the ligand. The significant difference in term

of *trans*-selectivity between the entries 7 and 8 was the first evidence of an effect of the mechanical bond. The marginal difference between entries 6 and 7 suggested that the combination of the axle and the macrocycle behaved similarly to the macrocycle. This suggested that the triazole was not involved in the coordination of the copper in the non-interlocked combination.

Table 2.3 Cyclopropanation reaction of styrene and ethyl diazoacetate catalysed by a Cu^{I} complex

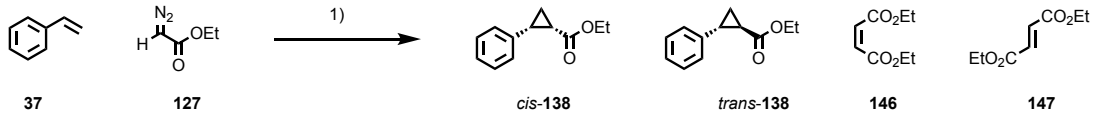

37 **127** *cis*-**138** *trans*-**138** **146** **147**

				Ratio [a]			
Entry	Ligand	[Cu]	Conv. diazo [a]	*cis*-138	*trans*-138	146	147
1	None	None	0%	-	-	-	-
2	**78**	None	0%	-	-	-	-
3	**78** + **145**	None	0%	-	-	-	-
4	**104**	None	0%	-	-	-	-
5	None	$[Cu(MeCN)_4PF_6]$	100%	52%	39%	3%	6%
6	**78**	$[Cu(MeCN)_4PF_6]$	100%	37%	44%	13%	6%
7	**78** + **145**	$[Cu(MeCN)_4PF_6]$	100%	40%	38%	9%	13%
8	**104**	$[Cu(MeCN)_4PF_6]$	100%	16%	42%	17%	24%

Conditions: 1) Styrene (5 equiv.), diazo compound (1 equiv.), $Cu(MeCN)_4PF_6$ (5% mol), ligand (6% mol), CH_2Cl_2, rt, 16h. [a] Determined by ^1H NMR.

The cyclopropanation reaction was extended to 2-aryl-2-diazoacetates leading to a tri-substituted cyclopropane. The diazo compound used in this series of reaction was **148**, which allowed the complete analysis by ^1H NMR. Both homo-coupled olefins were distinct by ^1H NMR. In this case, the only isomer of **149** formed during the reaction was the *trans*. Once again, the control experiments in absence of copper did not show any decomposition of the diazo compound **148** leading to cyclopropane or homo-coupled products (Table 2.4, Entries 1-4). The use of copper without ligand led to exceptional conversion towards the *trans*-cyclcopropane **149** (Table 2.4, Entry 5). However, when the macrocycle **78** or rotaxane **104** were used as ligands, the conversion dropped significantly to 30% and 27% respectively

(Table 2.4, Entries 6 and 8). The combination of non-interlocked macrocycle **78** and axle **145** in the presence of copper was surprisingly inactive (Table 2.4, Entry 7). Other unidentified products were formed during the reaction when macrocycle **78** and rotaxane **104** were used. The presence of water in the $CDCl_3$ used could lead to the insertion of the carbenoid in the OH bond.

Table 2.4 Reaction between styrene and ethyl 2-diazo-2-phenylacetate catalysed by copper

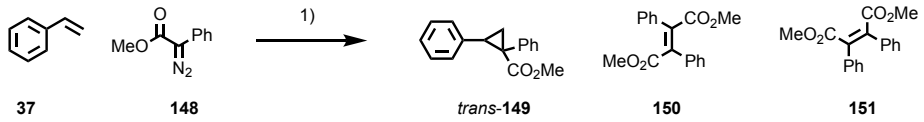

37 **148** *trans*-**149** **150** **151**

Entry	Ligand	[Cu]	Conversion	*trans*-149[a]	150[a]	151[a]
1	None	None	0%	-	-	-
2	**78**	None	0%	-	-	-
3	**78** + **145**	None	0%	-	-	-
4	**104**	None	0%	-	-	-
5	None	$[Cu(MeCN)_4PF_6]$	100%	80%	7%	ND
6	**78**	$[Cu(MeCN)_4PF_6]$	80%	30%	20%	ND
7	**78** + **145**	$[Cu(MeCN)_4PF_6]$	<5%	2%	<5%	ND
8	**104**	$[Cu(MeCN)_4PF_6]$	54%	27%	10%	ND

Conditions: 1) Styrene (5 equiv.), diazo compound (1 equiv.), $[Cu(MeCN)_4PF_6]$ (5% mol), ligand (6% mol), CH_2Cl_2, rt, 16h. [a] Determined by ^1H using 1,1,2,2-tetrachloroethane as internal standard. ND not detected.

The use of an electron-donating group (OMe) on the diazo compound increased the formation of cyclopropane **152** to 61% when rotaxane **104** was used as ligand. This can be explained by a faster reaction of the carbenoid with the styrene due to a more reactive carbenoid. In contrast, the presence of an electron withdrawing group (NO_2) did not give the formation of cyclopropane **153**, where only starting materials were recovered. In this case the diazo compound is less reactive than **148** and did not allow the formation of the

carbenoid intermediate. Variation of the methyl ester of **148** to ethyl ester did not increase the conversion to **154** (25% NMR yield) (Figure 2.27).

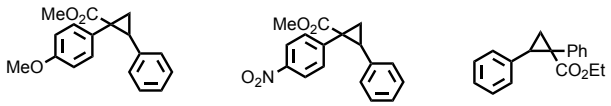

152 (61%) **153** (0%) **154** (25%)

Figure 2.27 Extension of the reaction to different diazocompounds.

The results did show some effect of the mechanical bond with an increase of the diastereoselectivity in the case of ethyl diazoacetate **127**. However, when bulkier diazo compounds were used, the conversion of the diazocompound was lower which suggested that the steric hindrance of the rotaxane as ligand was slowing down the reaction or preventing the reaction of the carbenoid and the styrene.

2.2.2.3. Insertion of carbenoid in NH bond

Copper carbenoid species can react with double bonds, triple bonds but also with an X-H bond where X can be O, N, Si, S or C.[38] The reaction of chiral amine and the copper carbene intermediate from the decomposition of methyl 2-diazo-2-phenylacetate **148** in presence of copper led to the formation of a second chiral centre. The presence of two stereogenic centres in the molecule led to the formation of a mixture of two diastereoisomers. [39]

The first test reaction was performed using (*R*)-1-phenylethan-1-amine **155** and methyl 2-diazo-2-phenylacetate **148** in presence of 5% mol of $[Cu(MeCN)_4]PF_6$ and 6% mol of rotaxane ligand in $CDCl_3$. No reaction was observed in the crude reaction mixture by ^1H NMR. Switching to CH_2Cl_2 solved the reactivity issue observed in the case of $CDCl_3$. The presence of traces of HCl in the $CDCl_3$ was identify as issue due to the possible the protonation of the amine used for the reaction. Addition of diazo compound **148** to a mixture of amine **155** and $[Cu(MeCN)_4]PF_6$ followed by 16 hours of stirring at room temperature led to low conversion to the product of insertion **156** (25%) with only 4% diastereomeric excess (*de*) (Table 2.5, Entry 5). The addition of the macrocycle as ligand increased the conversion to **148** to 34%

and the *de* to 10% (Table 2.5, Entry 6). Surprising result was obtained in Table 2.5, Entry 7, when a combination of the non-interlocked ligand converted the diazo compound **148** into **156** in a really low yield (9%). The best result was obtained when the rotaxane was added as ligand to the copper, which led to 87% conversion to **156** after 16 hours and 23% *de* (Table 2.5, Entry 8). Pleasingly, this study showed that the mechanical bond could influence the diastereoselectivity of a catalytic reaction as well as the reaction yield.

Table 2.5 Insertion of a carbenoid in NH bond

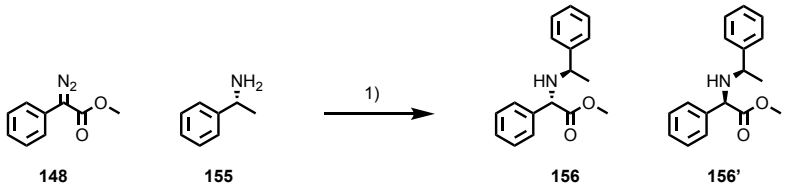

148 **155** **156** **156'**

Entry	Ligand	[Cu]	NMR Yield[a]	Diastereomeric ratio[a]
1	None	None	0%	
2	**78**	None	0%	
3	**78** + **145**	None	0%	
4	**104**	None	0%	
5	None	$[Cu(MeCN)_4PF_6]$	23%	52:48
6	**78**	$[Cu(MeCN)_4PF_6]$	34%	45:55
7	**78** + **145**	$[Cu(MeCN)_4PF_6]$	9%	45:55
8	**104**	$[Cu(MeCN)_4PF_6]$	87%	61:39

Conditions: 1) **155** (1 equiv.), **148** (1 equiv.), $[Cu(MeCN)_4]PF_6$ (5% mol), ligand (6% mol), CH_2Cl_2, rt, 16h.
[a] Determined by ^1H NMR using 1,1,2,2-tetrachloroethane as internal standard.

We tried to widen the scope of the reaction using different chiral amines. Rotaxane **104** was used as ligand in each trial and we observed *de* ranging from 23% to 36%. Furthermore, the conversion was found to be relatively good from 52% to 87% (Figure 2.28). The use of bulkier

amine in the case of the formation of **158** increased the *de* of the reaction. This is can be explained by the steric hindrance around the metal induced by the ligand.

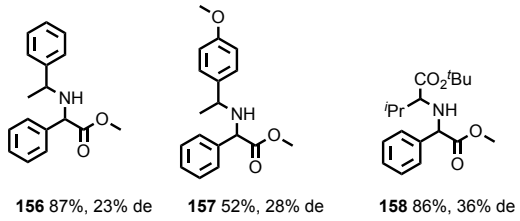

156 87%, 23% de **157** 52%, 28% de **158** 86%, 36% de

Figure 2.28 Scope of the insertion of the carbenoid in the NH bond with conversion and *de*.

2.3. Conclusions and Future Work

We found that the structure of the rotaxane model used in this investigation was suitable for catalysis. The use of a sterically hindered ligand in copper catalysed reactions showed some preliminary positive results. The use of rotaxane as ligand generated a homogeneous catalyst, which presented higher activity than the heterogeneous system used in the Henry reaction. The controlled decomposition of diazocompound was successfully performed using rotaxane **104** as ligand. In the cyclopropanation reaction of ethyldiazoacetate with styrene in presence of copper catalyst, higher diastereoselectivity was observed for the cyclopropanation (14% *de* with no ligand and 44% *de* with rotaxane **104** as ligand). The insertion of carbenoid in a NH bond showed real effects from the mechanical bond on conversion as well as diastereoselectivity (4% *de* with no ligand and 23% *de* with rotaxane **104** as ligand).

The preliminary results obtained during this investigation suggested the possibility to design ligands based on rotaxane for copper-catalysed reactions. The possibility to modify the steric hindrance around the copper could improve the diastereoselectivity of catalytic reactions.

The influence of stereogenic centres in metal catalysed reaction has been recently reported.[40] However, reports on the application of chirality resulting from the mechanical bond (such as mechanically planar chiral rotaxanes or topologically chiral catenanes) have yet to be published. The use of mechanically planar chiral rotaxanes or topologically chiral catenanes constitutes the logic evolution of this project.

2.4. Experimental

General Experimental

Synthesis: Unless otherwise stated, all reagents, including anhydrous solvents, were purchased from commercial sources and used without further purification. All reactions were carried out under an atmosphere of N_2 using anhydrous solvents unless otherwise stated. Petrol refers to the fraction of petroleum ether boiling in the range 40-60 °C. Flash column chromatography was performed using Biotage Isolera-4 automated chromatography system, employing Biotage SNAP or ZIP cartridges. Analytical TLC was performed on precoated silica gel plates (0.25 mm thick, 60F254, Merck, Germany) and observed under UV light.

Analysis: NMR spectra were recorded on Bruker AV400, AV3-400 or AV500 instrument, at a constant temperature of 300 K. Chemical shifts are reported in parts per million from low to high field and referenced to residual solvent. ^{13}C data were typically recorded as phased JMOD experiments. Coupling constants (*J*) are reported in Hertz (Hz). Standard abbreviations indicating multiplicity were used as follows: m = multiplet, quint = quintet, q = quartet, t = triplet, d = doublet, s = singlet, app. = apparent, br = broad. Signal assignment was carried out using 2D NMR methods (HSQC, HMBC, COSY, NOESY) where necessary. In the case of some complex multiplets with contributions from more than one signal absolute assignment was not possible. Here indicative either/or assignments (e.g. $H_{A/B}$ for H_A or H_B) are provided. All melting points were determined using a Griffin apparatus. Low resolution mass spectrometry was carried out by the mass spectrometry services at the University of Southampton (Waters TQD mass spectrometer equipped with a triple quadrupole analyser with UHPLC injection [BEH C18 column; MeCN-hexane gradient {0.2% formic acid}]). High resolution mass spectrometry was carried out by the mass spectrometry services at the University of Southampton (MaXis, Bruker Daltonics, with a Time of Flight (TOF) analyser; samples were introduced to the mass spectrometer via a Dionex Ultimate 3000 autosampler and uHPLC pump in a gradient of 20% acetonitrile in hexane to 100% acetonitrile (0.2% formic acid) over 5 min at 0.6 mL min; column: Acquity UPLC BEH C18 (Waters) 1.7 micron 50 × 2.1mm). As accurate mass measurements are of limited value for compounds with Mw >1000 Da, in these cases a graphical comparison of the observed isotope pattern and the predicted isotopic distribution is provided.

*Synthesis of the rotaxane model **104***

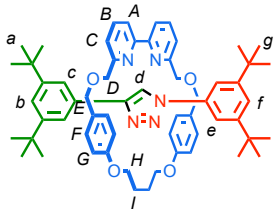

Azide **32** (278 mg, 1.20 mmol, 1.5 eq.), alkyne **30** (257 mg, 1.20 mmol, 1.5 eq), macrocycle **78** (386mg, 0.80 mmol, 1eq.) and $[Cu(MeCN)_4PF_6]$ (286 mg, 0.77 mmol, 0.96 eq.) were placed in a CEM vial under N_2. Dry CH_2Cl_2 (20 mL) was added. Diisopropylethylamine (1.4 mL, 8.00 mmol, 10 eq.) was added. The reaction mixture was stirred overnight at 80 °C. The mixture was cooled to room temperature and diluted with CH_2Cl_2 (100 mL). Then organic phase was washed with EDTA-NH_3 solution (100 mL). The aqueous phase was extracted with CH_2Cl_2 (2 x 50 mL), the combined organic phases was dried ($MgSO_4$), filtered and the solvent removed in vacuo. Purification by column chromatography (Petrol with a 0 to 20% gradient of Et_2O) afforded the product **104** (651 mg, 91%) as white foam.

^{1}H NMR (400 MHz, $CDCl_3$) δ 10.53 (s, 1H, H_d), 7.76 (t, *J* = 7.7, 2H, H_B), 7.70 (d, *J* = 7.8, 2H, H_A), 7.67 (d, *J* = 1.6, 2H, H_e), 7.51 (d, *J* = 1.3, 2H, H_c), 7.42 (d, *J* = 7.6, 2H, H_C), 7.19 (brs, 2H, H_b, H_f), 6.62 (d, *J* = 8.4, 4H, H_F), 6.49 (d, *J* = 8.4, 4H, H_G), 4.80 (dt, *J* = 8.2, 7.4, 2H, two of H_H), 4.41 (d, *J* = 12.2, 2H, two of H_E), 4.40-4.33 (m, 2H, two of H_H), 4.23 (d, *J* = 12.3, 2H, two of H_E), 3.87-3.78 (m, 4H, H_D), 2.48-2.36 (m, 2H, two of H_I), 2.28-2.16 (m, 2H, two of H_I), 1.16 (s, 36H, H_a, H_g); ^{13}C NMR (100 MHz, $CDCl_3$) δ 159.9, 159.4, 155.3, 151.3, 150.2, 146.6, 137.4 (x2), 131.6, 129.1, 127.6, 121.9, 121.0, 120.5, 120.3 (x2), 119.8, 115.0, 114.4, 73.2, 70.2, 66.5, 34.9 (x2), 31.5, 31.4, 25.0;

All data were in accordance with those reported.[3]

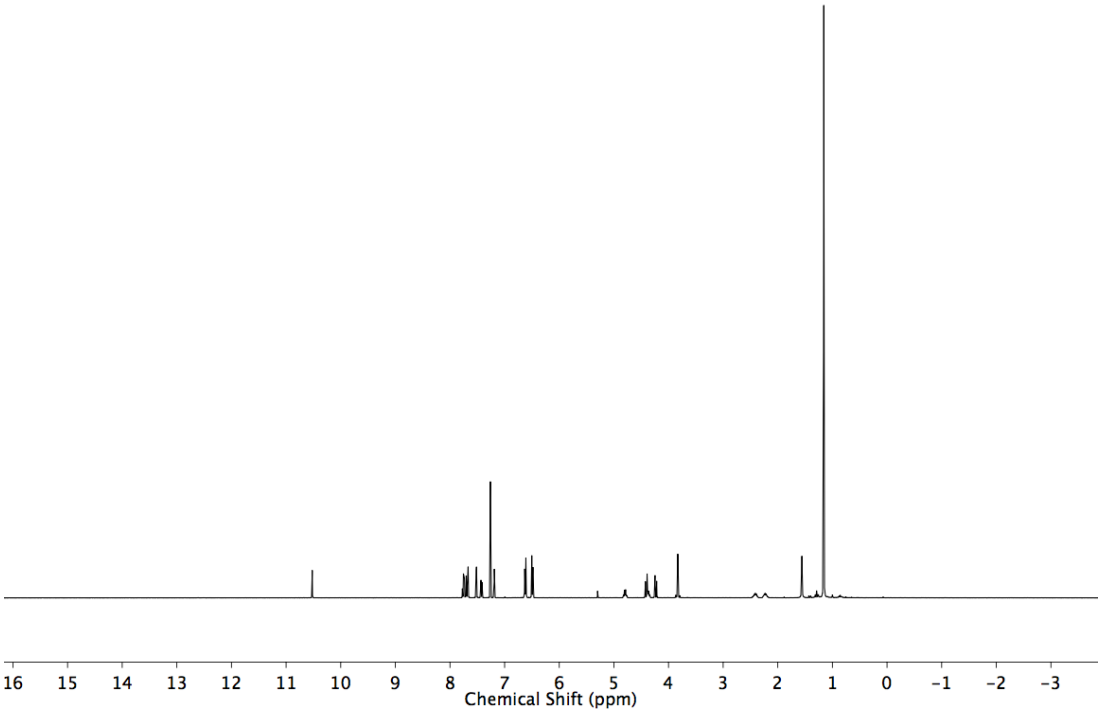

Figure 2.29 ^{1}H NMR ($CDCl_3$, 400 MHz) of **104**

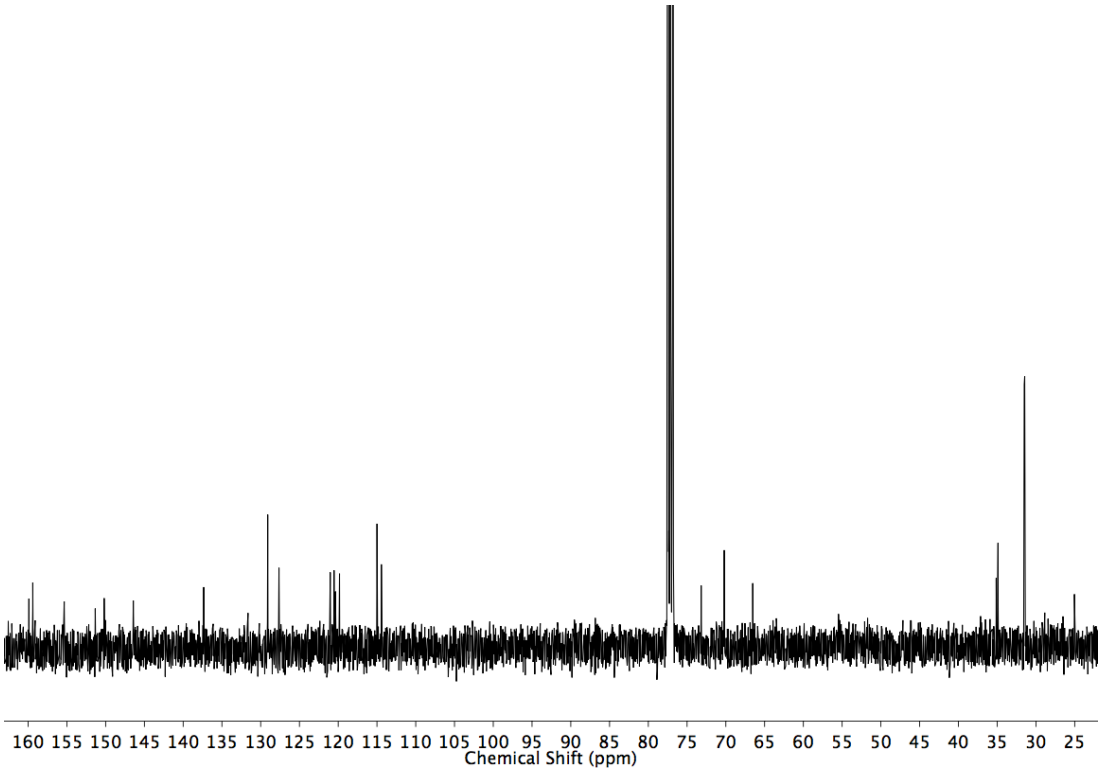

Figure 2.30 ^{13}C NMR ($CDCl_3$, 101 MHz) of **104**

*Complexation of the rotaxane **104** with $[Cu(MeCN)_4]PF_6$*

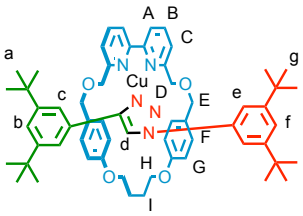

Rotaxane **104** (9.3 mg, 0.01 mmol), $[Cu(MeCN)_4PF_6]$ (3.7 mg, 0.01 mmol) were placed in a NMR tube, then $CDCl_3$ (0.5 mL) was added. The tube was sonicated for 10 minutes to afford an orange solution of **104-Cu**. Then NMR analysis was run without purification.

^{1}H NMR (400 MHz, $CDCl_3$) δ 8.30 (d, *J* = 8.0, 2H, H_C), 8.15 (t, *J* = 8.0, 2H, H_B), 7.73 (d, *J* = 8.0, 2H, H_A), 7.71 (brs, 1H, H_d), 7.63 (brs, 2H, H_e), 7.57 (brs, 2H, H_c), 7.41 (brs, 1H, H_b), 6.84 (s, 1H, H_d), 6.61 (d, *J* = 6.6 Hz, 4H, H_F), 6.29 (d, *J* = 6.6, 4H, H_G), 4.60-4.15 (m, 12H, H_D, H_E, H_H), 2.30 (m, 4H, H_I), 1.51 (s, 18H, H_g), 1.23 (s, 18H, H_a). ^{13}C NMR (101 MHz, $CDCl_3$) δ 158.5, 157.9, 153.5, 152.2, 151.2, 145.6, 140.7, 136.7, 130.1, 129.7, 127.8, 125.2, 124.1, 123.8, 121.8, 121.3, 119.6, 116.7, 114.45, 74.0, 72.1, 67.3, 35.7, 35.3, 31.7, 31.5, 26.0.

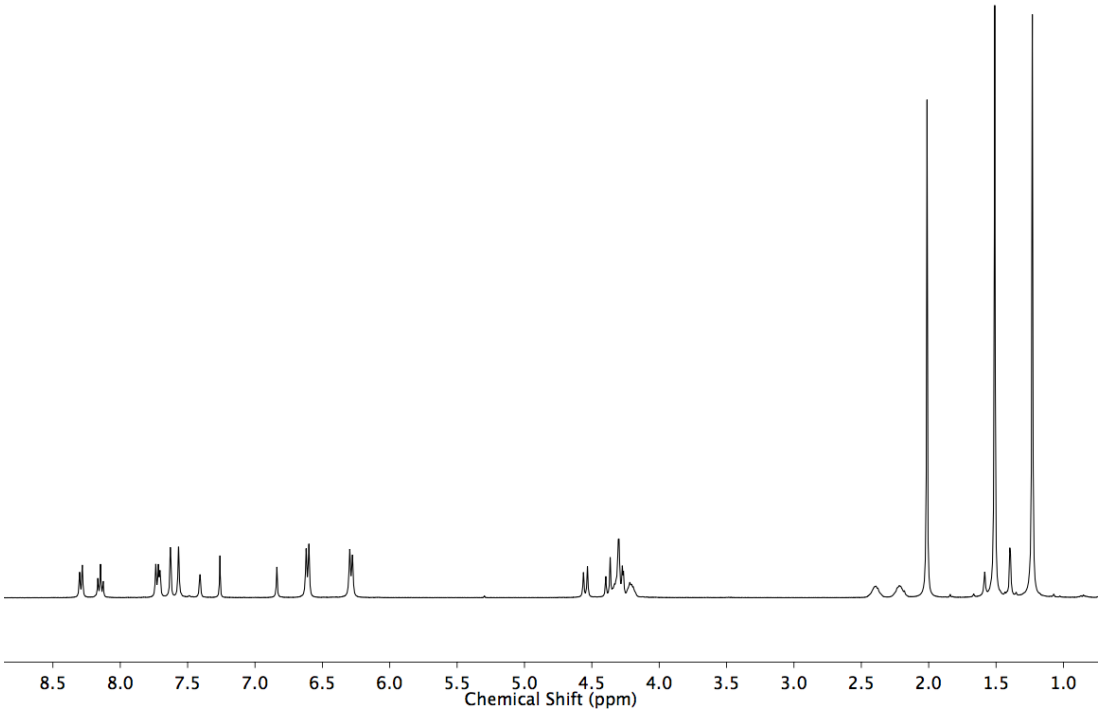

Figure 2.31 ^{1}H NMR ($CDCl_3$, 400 MHz) of **104-Cu**

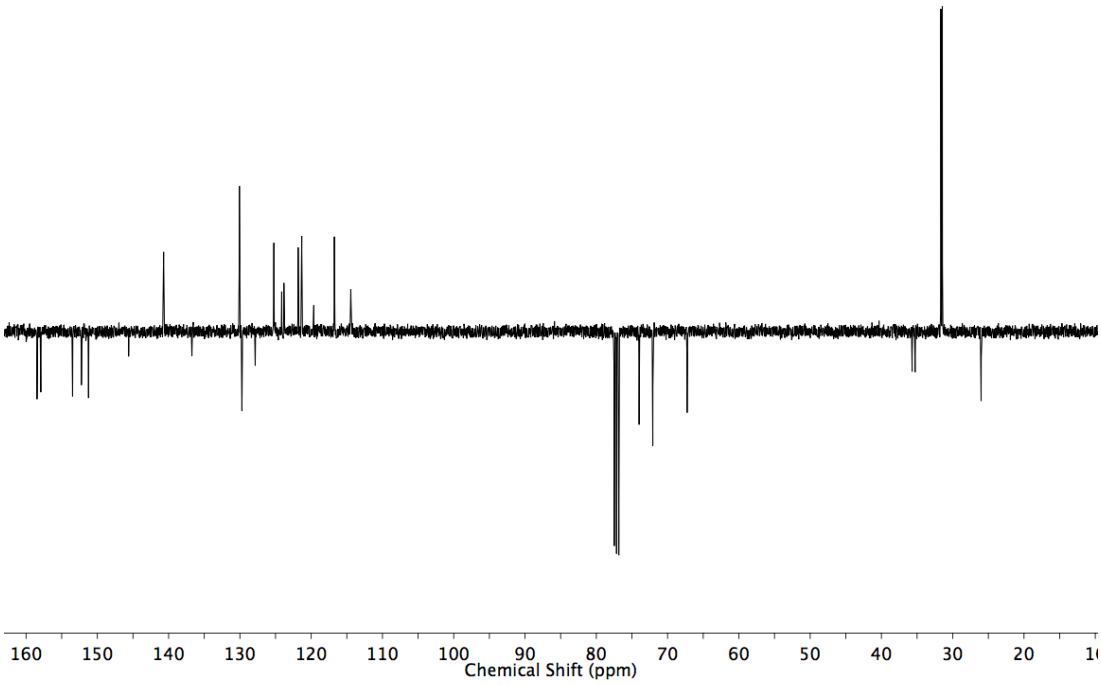

Figure 2.32 JMOD NMR ($CDCl_3$, 101 MHz) of **104-Cu**

General procedure for the Henry reaction.

In a CEM vial under N_2 were placed the ligand (6 mol%), CuBr(5 mol%) in dry MeOH. After 30 minutes, *p*-nitrobenzaldehyde (1 equiv.) was added followed by nitromethane (5 equiv.). The mixture was stirred for 16h at room temperature. The solvent was removed under reduced pressure. The crude reaction mixture was analysed by ^{1}H NMR.

General procedure for the cyclopropanation reaction.

In a CEM vial under N_2 were placed the ligand (6 mol%), $[Cu(MeCN)_4]PF_6$ (5 mol%) in dry CH_2Cl_2. Then a freshly distilled styrene (4 eq) was injected. The mixture was stirred for 10 minutes at room temperature and the diazocompound (1 eq) was injected. Then the mixture was stirred for 16h at room temperature. The solvent was removed under reduced pressure. The crude reaction mixture was analysed by ^{1}H NMR.

General procedure for the insertion of the carbenoid in the NH bond.

In a CEM vial under N_2 were placed the ligand (6 mol%), $[Cu(MeCN)_4]PF_6$ (5 mol%) in dry CH_2Cl_2. The amine (1 eq) was then added to the solution. The mixture was stirred for 10 minutes at room temperature and the diazocompound (1 eq) was injected. Then the mixture was stirred for 16h at room temperature. The solvent was removed *in vacuo* and tetrachloroethane was added as internal standard. The crude reaction mixture was analysed by ^{1}H NMR.

Analytical Data for products of catalysis

*Compound **147***

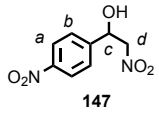

147

^{1}H NMR (400 MHz, $CDCl_3$) δ 8.27 (d, *J* = 8.8, 2H, H_a), 7.63 (d, *J* = 8.8, 2H, H_b), 5.61 (dt, *J* = 8.3, 4.1, 1H, H_c), 4.63-4.56 (m, 2H, H_d), 3.14 (d, *J* = 4.1, 1H, OH). ^{13}C NMR (101 MHz, $CDCl_3$) δ 148.4, 145.2, 127.1, 124.3, 80.8, 70.1. All data were in accordance with those reported.[41]

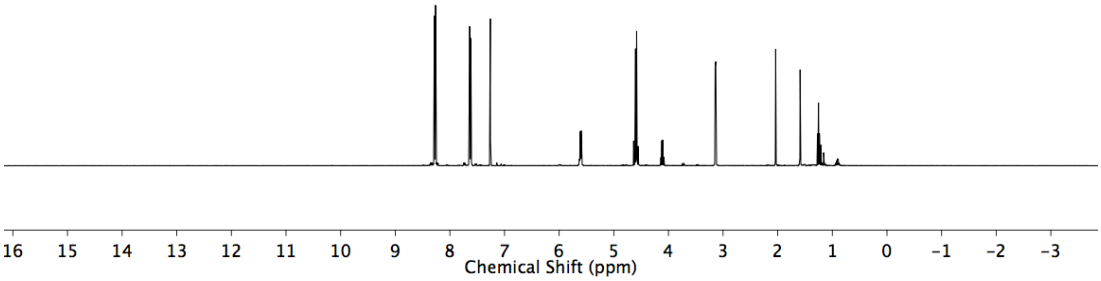

Figure 2.33 ^{1}H NMR ($CDCl_3$, 400 MHz) of **147**

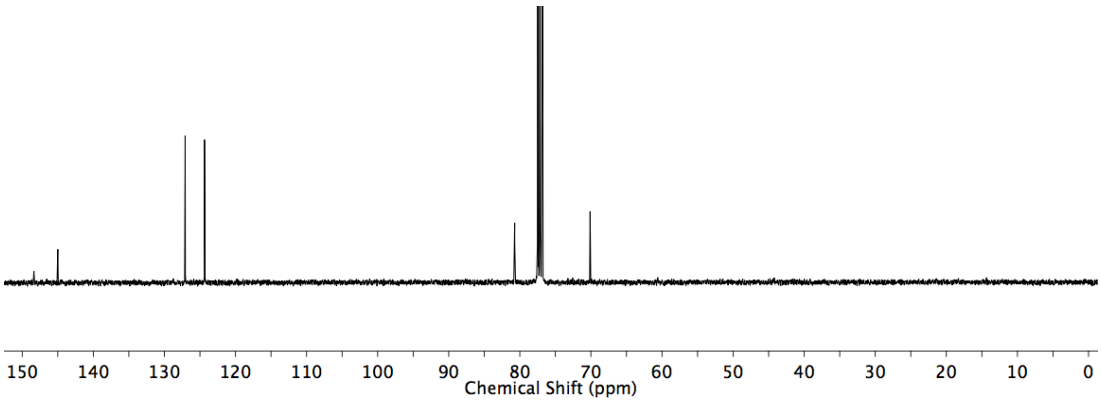

Figure 2.34 ^{13}C NMR ($CDCl_3$, 101 MHz) of **147**

Compound ***138***

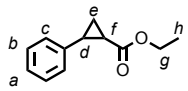

138

trans-isomer: ^{1}H NMR (400 MHz, $CDCl_3$) δ 7.32-7.07 (m, 5H, H_a, H_b, H_c), 4.26 (q, *J* = 7.1, 2H, H_g), 2.54-2.48 (m, 1H, H_d), 1.90 (ddd, *J* = 8.4, 5.3, 4.2, 1H, H_f), 1.63-1.57 (m, 1H, 1 of H_e), 1.37-1.24 (m, 4H, 1 of H_e, H_h). ^{13}C NMR (101 MHz, $CDCl_3$) δ 165.0, 140.1, 128.5, 126.5, 126.2, 61.3, 26.2, 24.2, 17.1, 14.0. All data were in accordance with those reported.[42]

cis-isomer: ^{1}H NMR (400 MHz, $CDCl_3$) δ 7.32-7.07 (m, 5H, H_a, H_b, H_c), 3.87 (q, *J* = 7.1, 2H, H_g), 2.62-2.55 (m, 1H, H_d), 2.08 (ddd, *J* = 9.3, 7.8, 5.6, 1H, H_f), 1.72 (ddd, *J* = 7.5, 5.7, 6.0, 1H, 1 of H_e), 1.37-1.24 (m, 1H, 1 of H_e), 0.97 (t, *J* = 7.2, 3H, H_h). ^{13}C NMR (101 MHz, $CDCl_3$) δ 171.0, 136.4, 129.3, 127.9, 126.6, 60.2, 25.5, 21.8, 14.1, 11.1. All data were in accordance with those reported.[42]

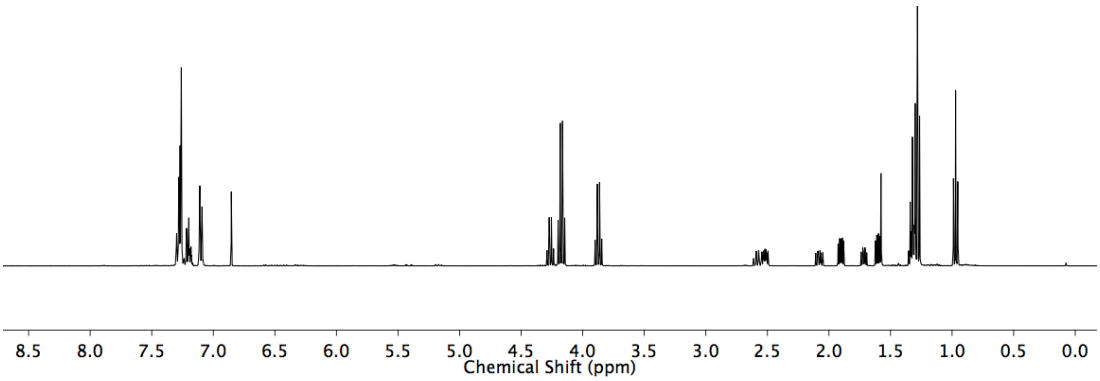

Figure 2.35 ^{1}H NMR ($CDCl_3$, 400 MHz) of a mixture of *cis*-**138** and *trans*-**138**.

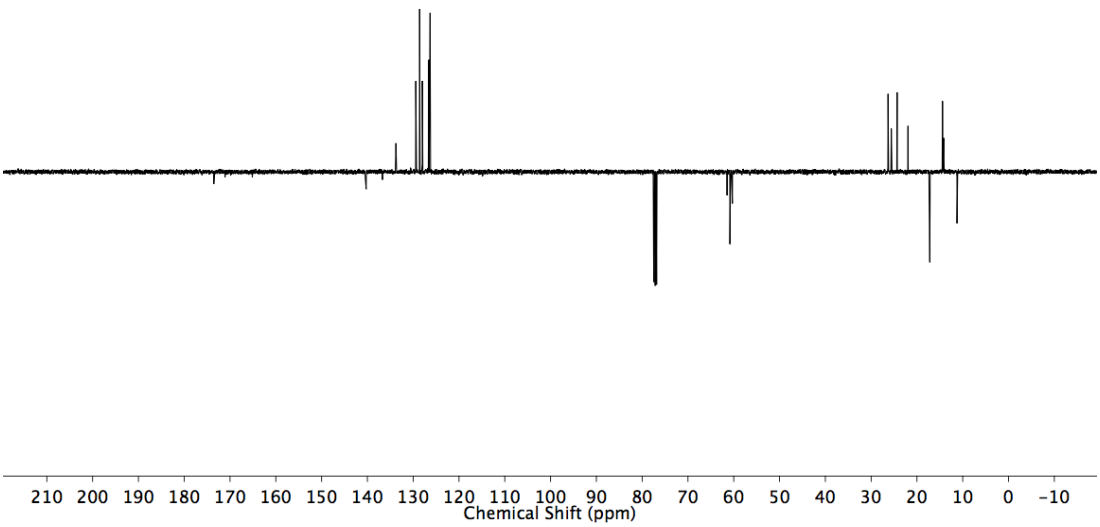

Figure 2.36 JMOD NMR ($CDCl_3$, 101 MHz) of a mixture of *cis*-**138** and *trans*-**138**.

*Compound **149***

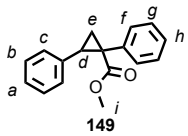

149

trans-isomer: ^{1}H NMR (400 MHz, $CDCl_3$) δ 7.16-7.10 (m, 3H, H_f or H_g, H_h), 7.09-7.00 (m, 5H, H_a, H_b, H_f or H_g), 6.81-6.74 (m, 2H, H_c), 3.67 (s, 3H, H_i), 3.11 (dd, *J* = 9.4, 7.3, 1H, H_d), 2.14 (dd, *J* = 9.4, 4.9, 1H, $H_{e\ trans}$), 1.88 (dd, *J* = 7.3, 4.9, 1H, $H_{e\ cis}$). ^{13}C NMR (101 MHz, $CDCl_3$) 174.5, 136.5, 134.9, 132.1, 128.2, 127.8, 127.8, 127.2, 126.4, 52.8, 37.5, 33.3, 20.6. All data were in accordance with those reported.[43]

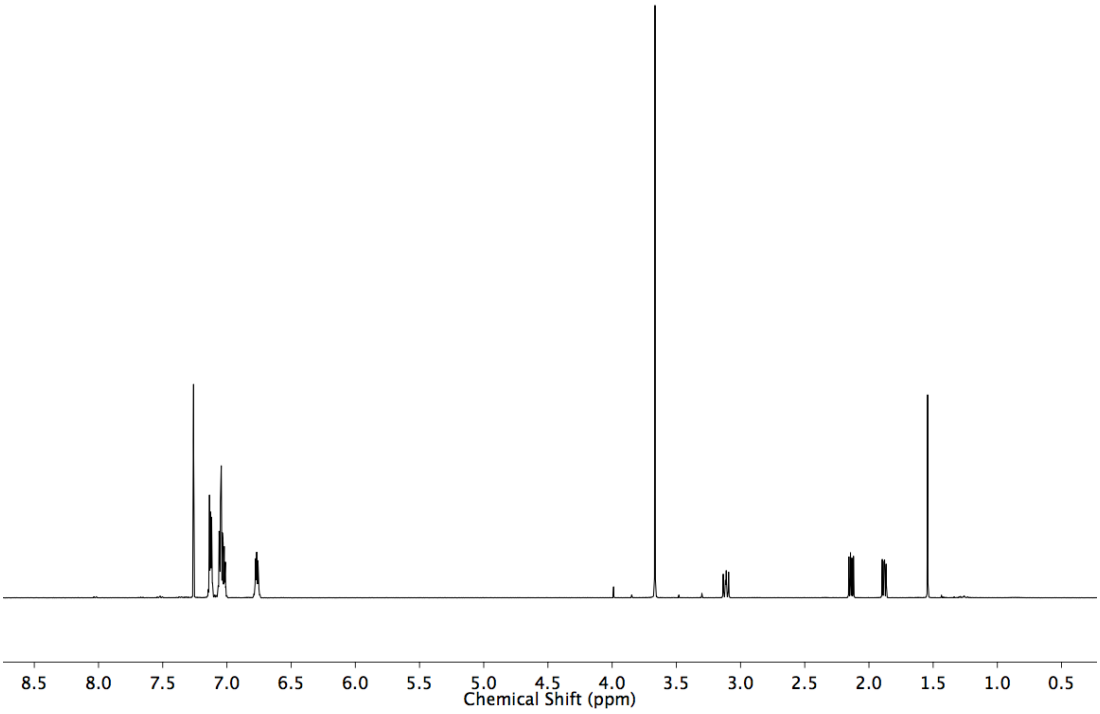

Figure 2.37 ^{1}H NMR ($CDCl_3$, 400 MHz) of *trans*-**149**.

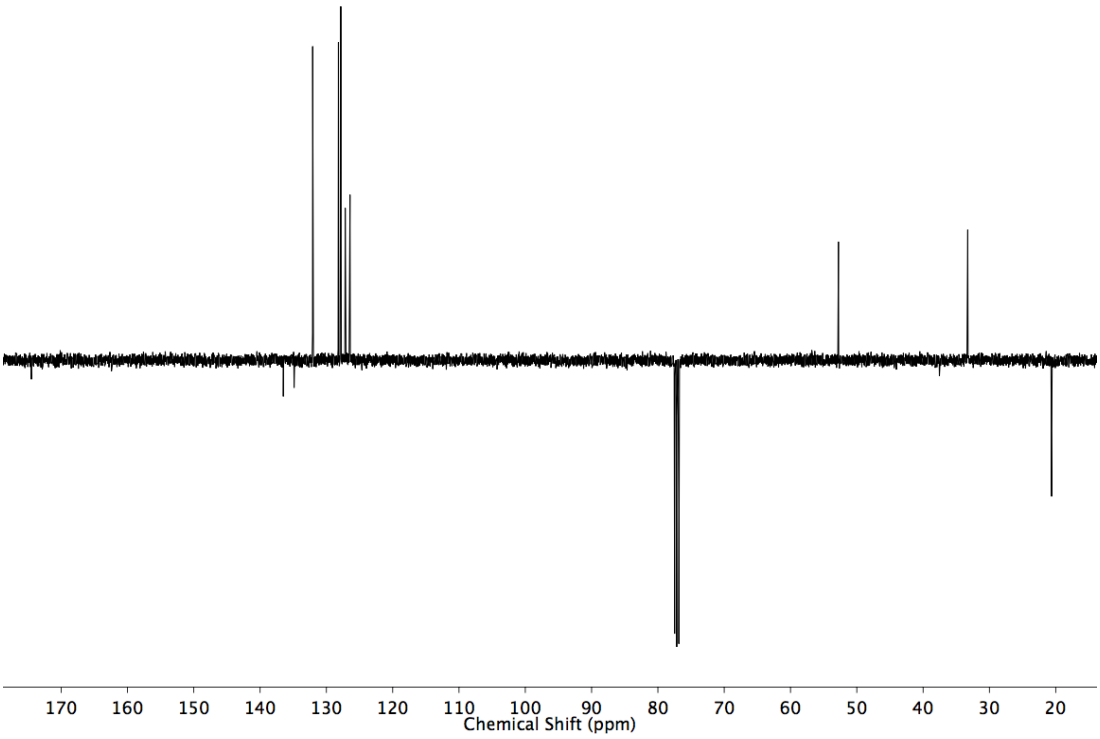

Figure 2.38 JMOD NMR ($CDCl_3$, 101 MHz) of *trans*-**149**.

*Compound **154***

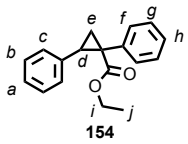

154

trans-isomer: ^{1}H NMR (400 MHz, $CDCl_3$) δ 7.14-7.09 (m, 3H, H_f or H_g, H_h), 7.04-7.00 (m, 5H, H_a, H_b, H_f or H_g), 6.82-6.73 (m, 2H, H_c), 4.25-4.05 (m, 2H, H_i), 3.10 (dd, *J* = 9.4, 7.3, 1H, H_d), 2.13 (dd, *J* = 9.4, 4.8, 1H, $H_{e\ trans}$), 1.88 (dd, *J* = 7.3, 4.8, 1H, $H_{e\ cis}$), 1.18 (t, *J* = 7.1, 3H, H_j). ^{13}C NMR (101 MHz, $CDCl_3$) δ 173.7, 136.5, 134.8, 131.9, 128.0, 127.7, 127.6, 126.9, 126.2, 61.3, 37.6, 32.9, 20.1, 14.2. All data were in accordance with those reported.[44]

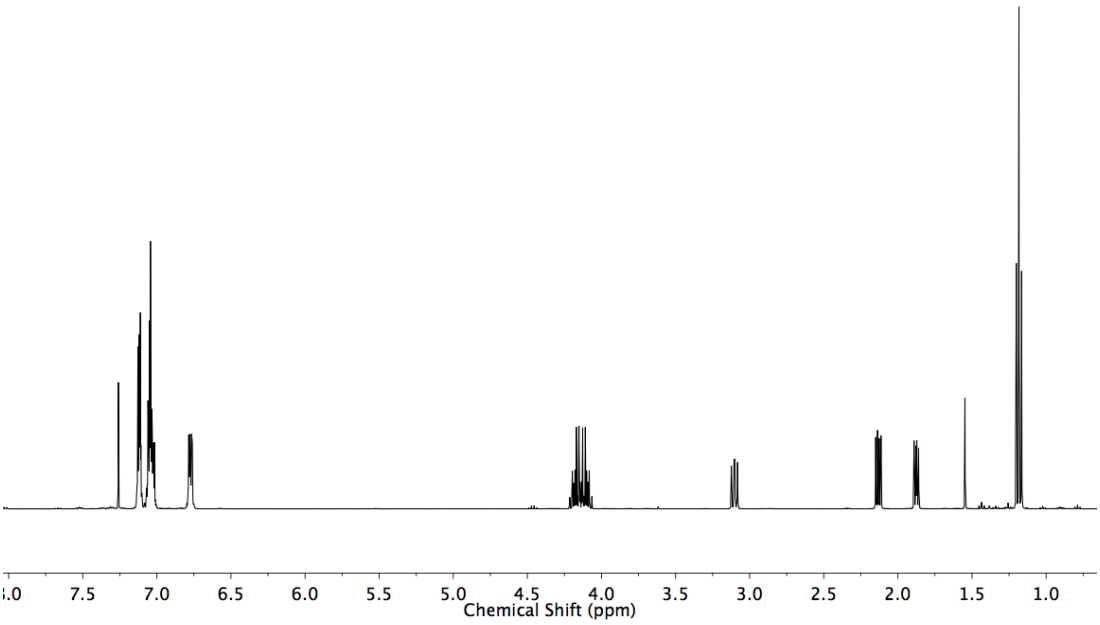

Figure 2.39 ^{1}H NMR ($CDCl_3$, 400 MHz) of *trans*-**154**.

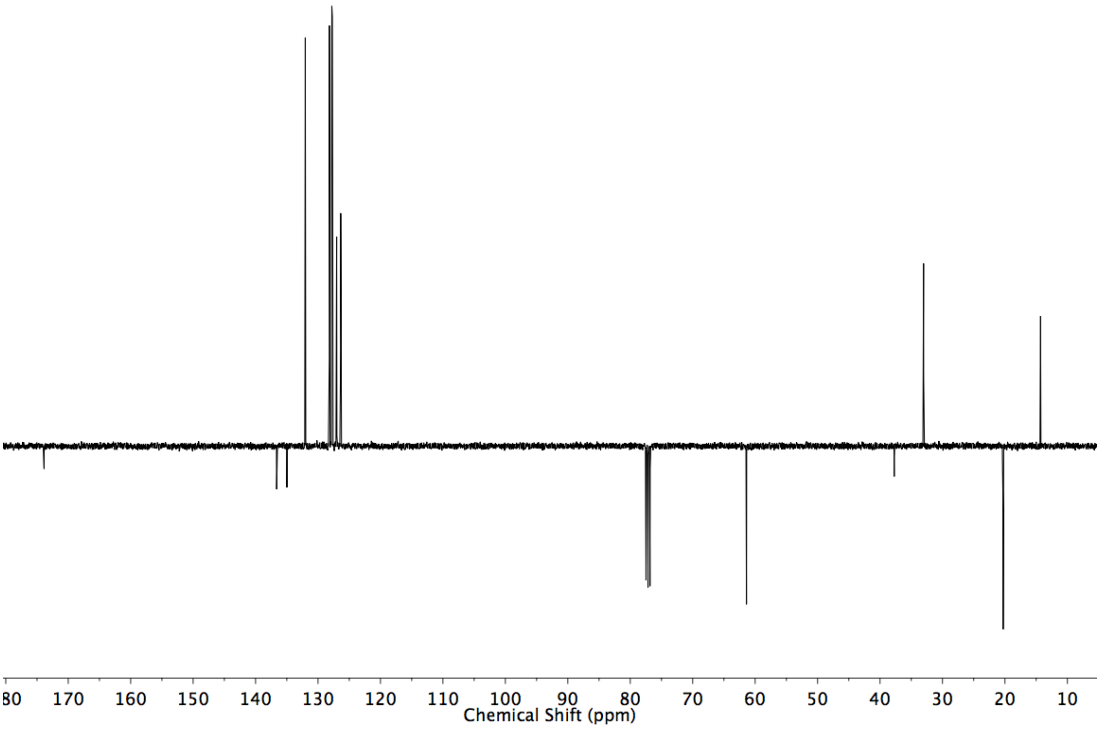

Figure 2.40 JMOD NMR ($CDCl_3$, 101 MHz) of *trans*-**154**.

Compound ***152***

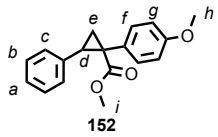

152

trans-isomer: ^{1}H NMR (400 MHz, $CDCl_3$) δ 7.11-7.04 (m, 3H, H_a, H_b,), 6.93 (d, *J* = 8.2, 2H, H_f), 6.80-6.75 (m, 2H, H_c), 6.67 (d, *J* = 8.2, 2H, H_g), 3.72 (s, 3H, H_h), 3.66 (s, 3H, H_i), 3.07 (dd, *J* = 9.4, 7.3, 1H, H_d), 2.12 (dd, *J* = 9.4, 4.8, 1H, $H_{e\ trans}$), 1.82 (dd, *J* = 7.3, 4.8, 1H, $H_{e\ cis}$). ^{13}C NMR (101 MHz, $CDCl_3$) δ 174.8, 158.6, 136.6, 133.0, 128.2, 127.8, 126.9, 126.4, 113.3, 55.2, 52.7, 36.8, 33.3, 20.9. All data were in accordance with those reported.[43]

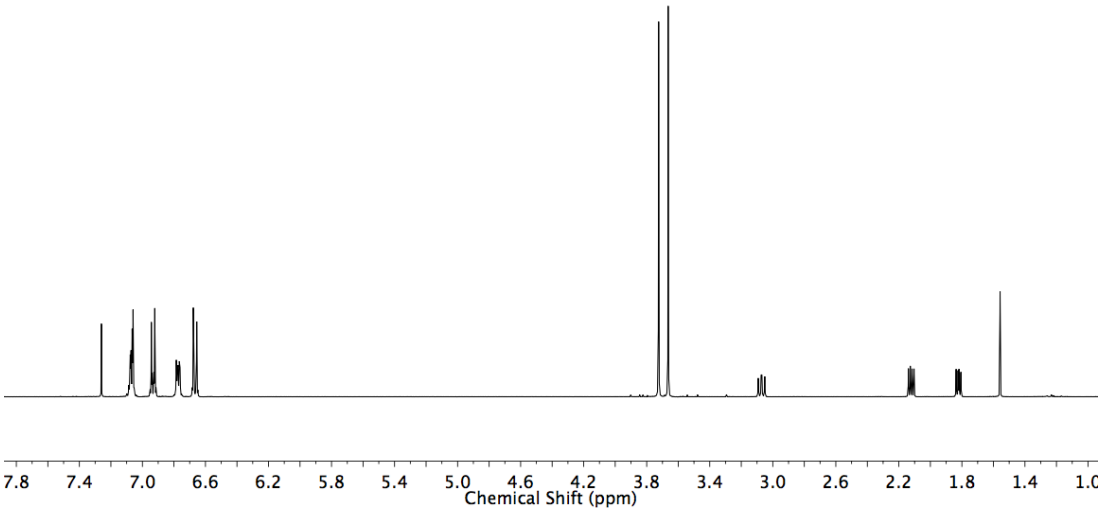

Figure 2.41 ^{1}H NMR ($CDCl_3$, 400 MHz) of *trans*-**152**.

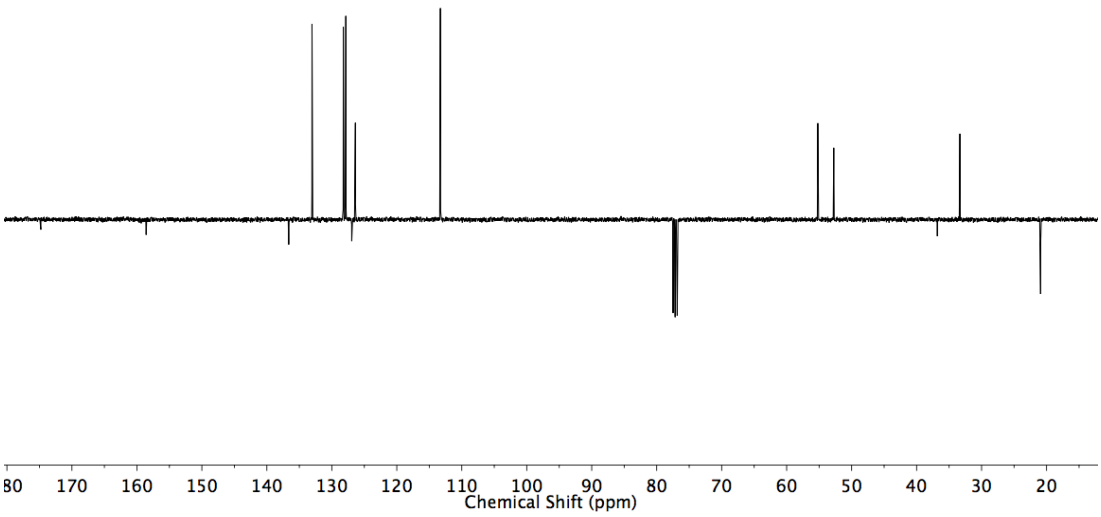

Figure 2.42 JMOD NMR ($CDCl_3$, 101 MHz) of *trans*-**152**.

*Compound **156***

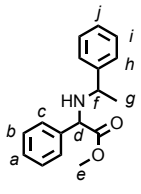

156

Diastereoisomer 1: ^{1}H NMR (400 MHz, $CDCl_3$) δ 7.33-7.15 (m, 10H, H_a, H_b, H_c, H_h, H_i, H_j), 4.17 (s, 1H, H_d), 3.74 (q, *J* = 6.5, 1H, H_f), 3.65 (s, 3H, H_e), 2.25 (s, 1H, NH), 1.33 (d, *J* = 6.5, 3H, H_g). ^{13}C NMR (101 MHz, $CDCl_3$) δ 174.4, 144.9, 138.6, 128.8, 128.7, 128.1, 127.3, 127.3, 127.0, 63.1, 56.7, 52.2, 24.8. All data were in accordance with those reported.[45]

Diastereoisomer 2: ^{1}H NMR (400 MHz, $CDCl_3$) δ 7.30-7.13 (m, 10H, H_a, H_b, H_c, H_h, H_i, H_j), 4.12 (s, 1H, H_d), 3.51 (s, 3H, H_e), 3.48 (q, *J* = 6.5, 1H, H_f), 2.34 (s, 1H, NH), 1.26 (d, *J* = 6.5, 3H, H_g). ^{13}C NMR (101 MHz, $CDCl_3$) δ 173.4, 144.7, 138.4, 128.8, 128.6, 128.1, 127.9, 127.3, 127.0, 62.8, 54.9, 52.3, 24.5. All data were in accordance with those reported.[45]

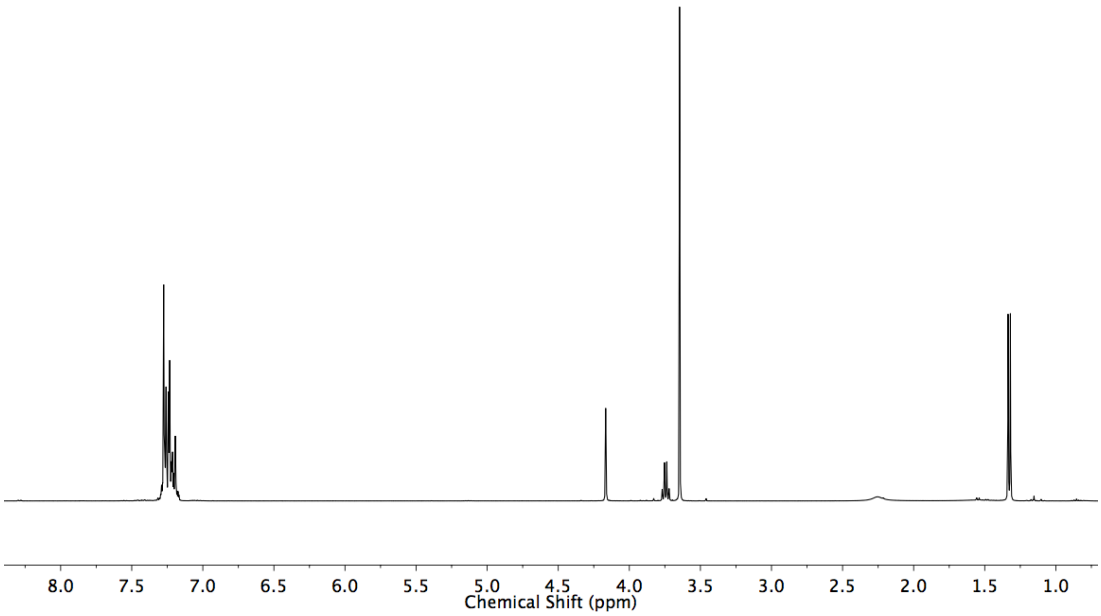

Figure 2.43 ^{1}H NMR ($CDCl_3$, 400 MHz) of first diastereoisomer of **156**.

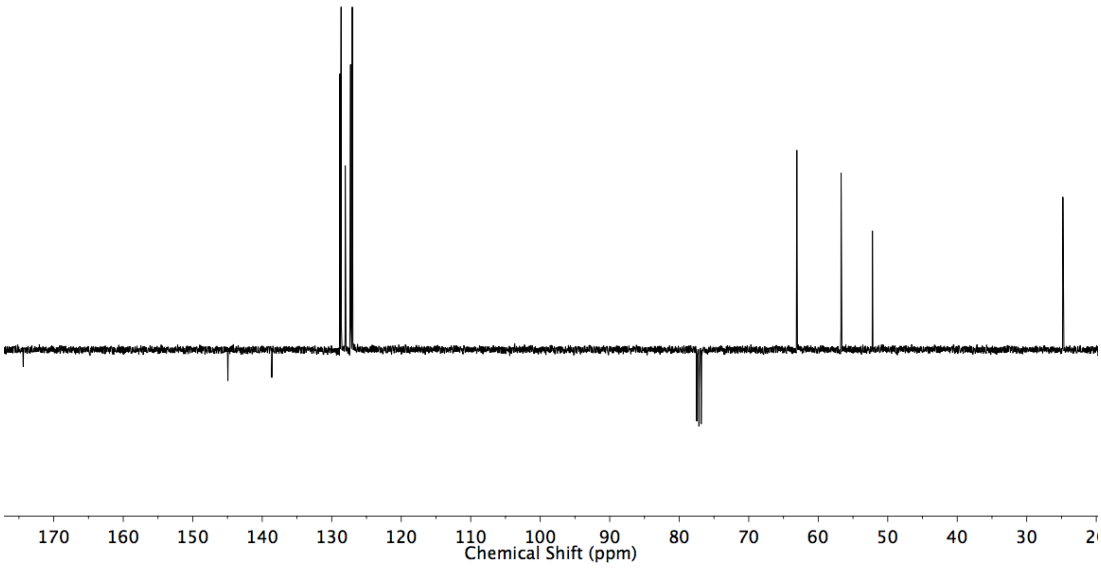

Figure 2.44 JMOD NMR ($CDCl_3$, 400 MHz) of first diastereoisomer of **156**.

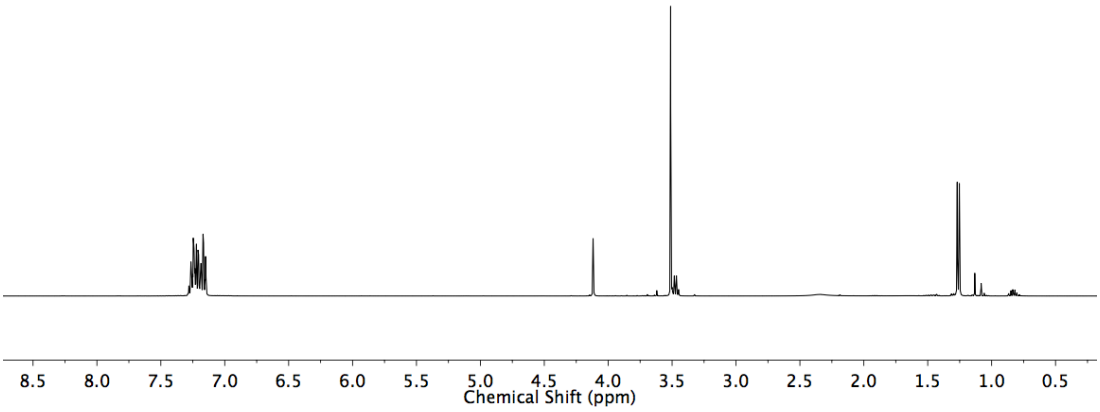

Figure 2.45 ^{1}H NMR ($CDCl_3$, 400 MHz) of second diastereoisomer of **156**.

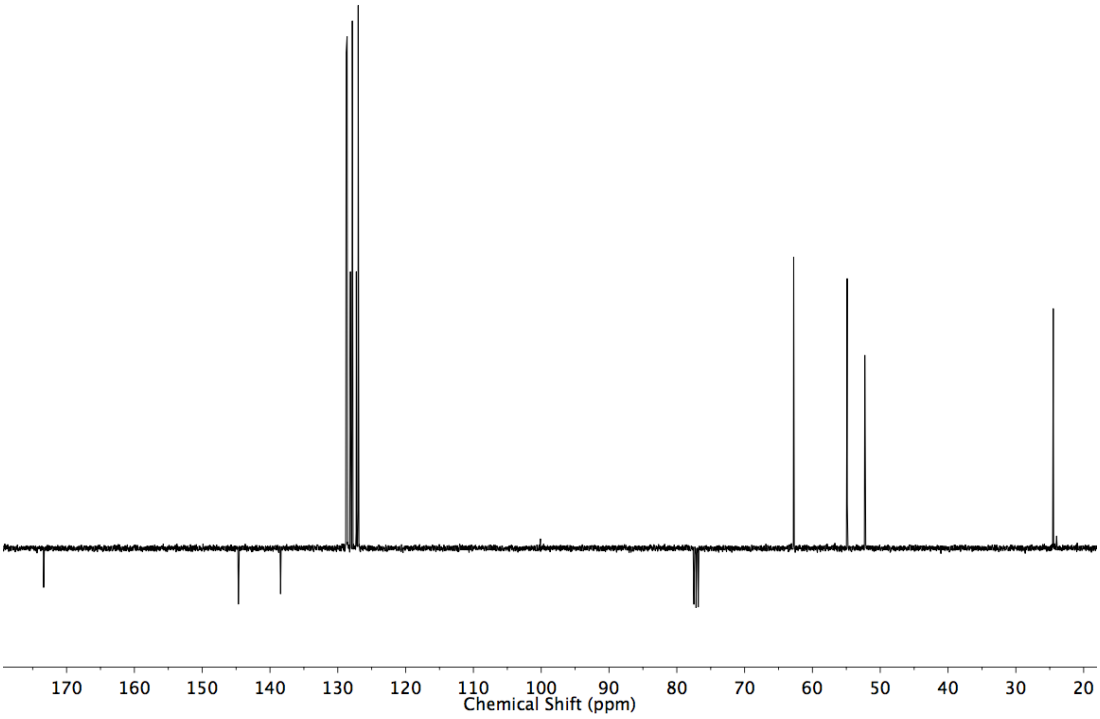

Figure 2.46 JMOD NMR ($CDCl_3$, 400 MHz) of second diastereoisomer of **156**.

*Compound **157***

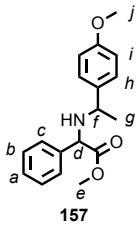

157

Diastereoisomer 1: ^{1}H NMR (400 MHz, $CDCl_3$) δ 7.27-7.12 (m, 7H, H_a, H_b, H_c, H_h,), 6.78 (d, *J* = 8.9, 2H, H_i), 4.13 (s, 1H, H_d), 3.71 (s, 3H, H_j), 3.68 (q, *J* = 6.5, 1H, H_f), 3.61 (s, 3H, H_e), 2.15 (s, 1H, NH), 1.28 (d, *J* = 6.5, 3H, H_g). ^{13}C NMR (101 MHz, $CDCl_3$) δ 174.4, 158.9, 138.7, 136.9, 128.8, 128.1, 128.0, 127.3, 114.0, 63.0, 56.0, 55.4, 52.2, 24.8. HR-ESI-MS *m/z* =322.1409 $[M+Na]^+$ calc. 322.1414.

Diastereoisomer 2: ^{1}H NMR (400 MHz, $CDCl_3$) δ 7.42-7.27 (m, 5H, H_a, H_b, H_c), 7.16 (d, *J* = 8.7, 2H, H_h), 6.88 (d, *J* = 8.7, 2H, H_i), 4.20 (s, 1H, H_d), 3.81 (s, 3H, H_j), 3.61 (s, 3H, H_e), 3.52 (q, *J* = 6.5, 1H, H_f), 2.33 (s, 1H, NH), 1.33 (d, *J* = 6.5, 3H, H_g). ^{13}C NMR (101 MHz, $CDCl_3$) δ 173.4, 158.9, 138.5, 137.7, 128.7, 128.1, 128.0, 127.8, 114.0, 62.7, 55.4, 54.2, 52.2, 24.5. HR-ESI-MS *m/z* =322.1409 $[M+Na]^+$ calc. 322.1414.

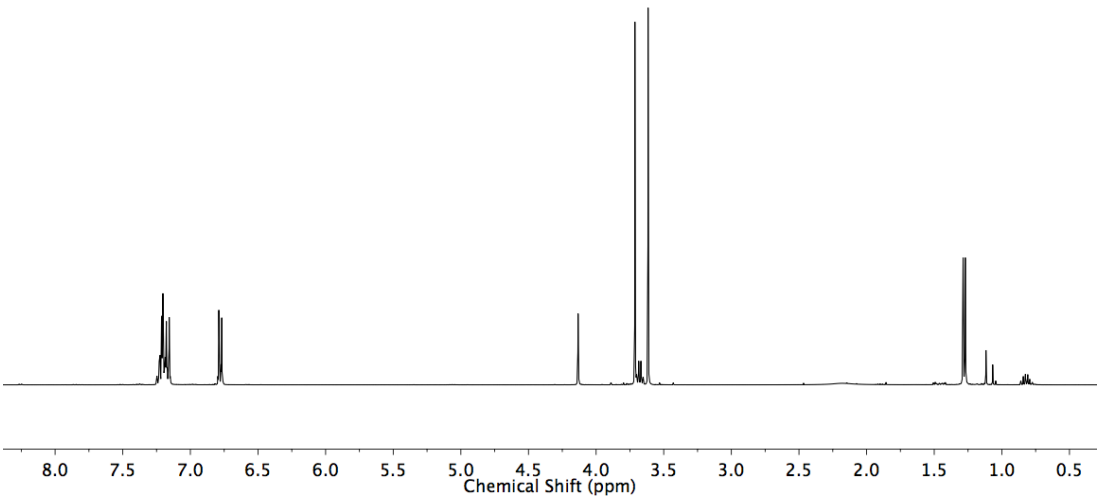

Figure 2.47 ^{1}H NMR ($CDCl_3$, 400 MHz) of first diastereoisomer of **157**.

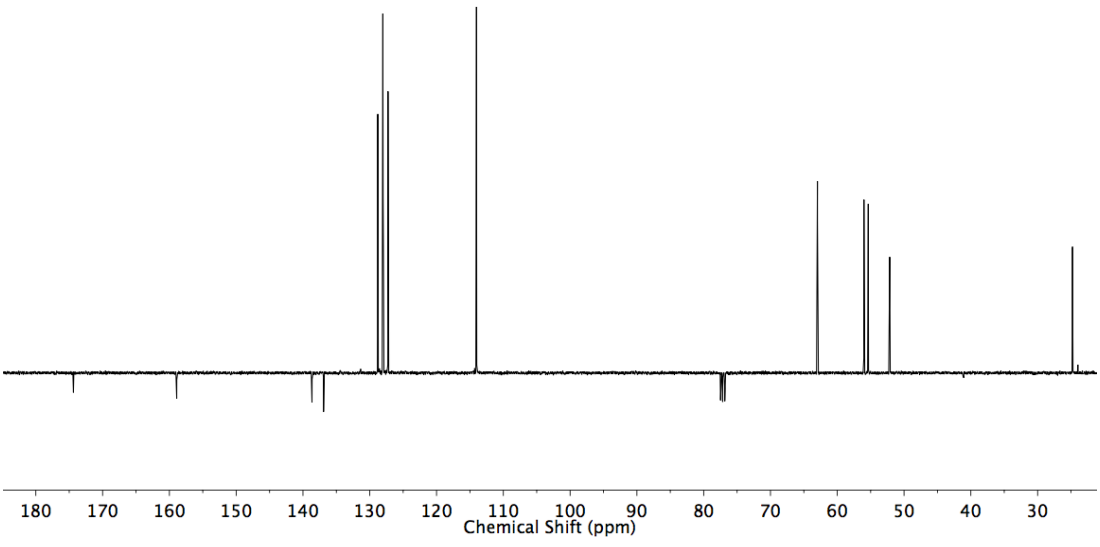

Figure 2.48 JMOD NMR ($CDCl_3$, 400 MHz) of first diastereoisomer of **157**.

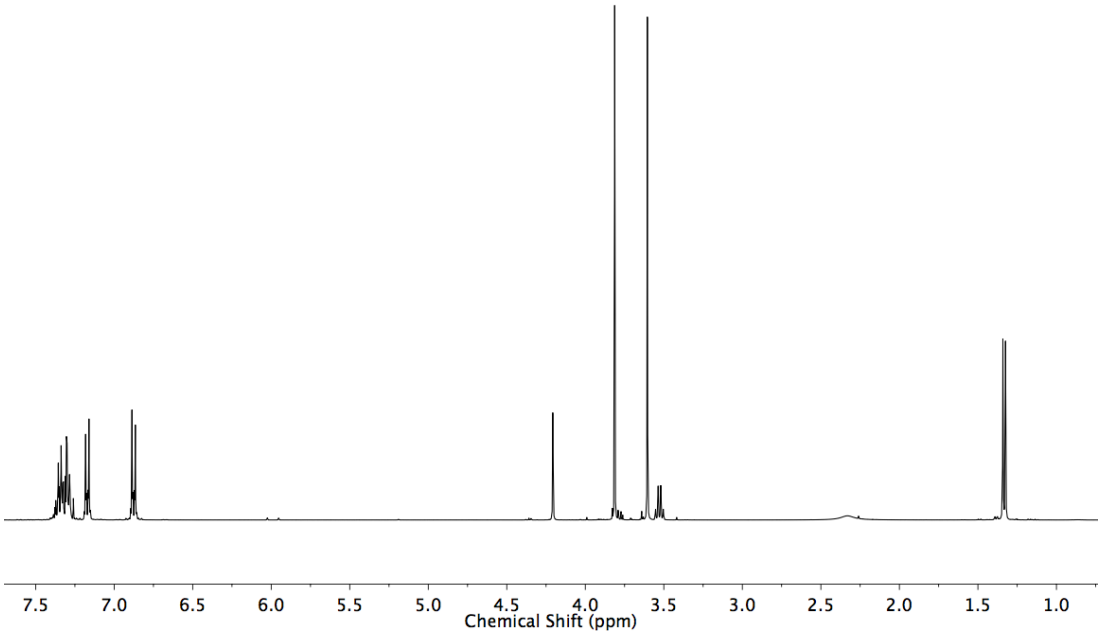

Figure 2.49 ^{1}H NMR ($CDCl_3$, 400 MHz) of second diastereoisomer of **157**.

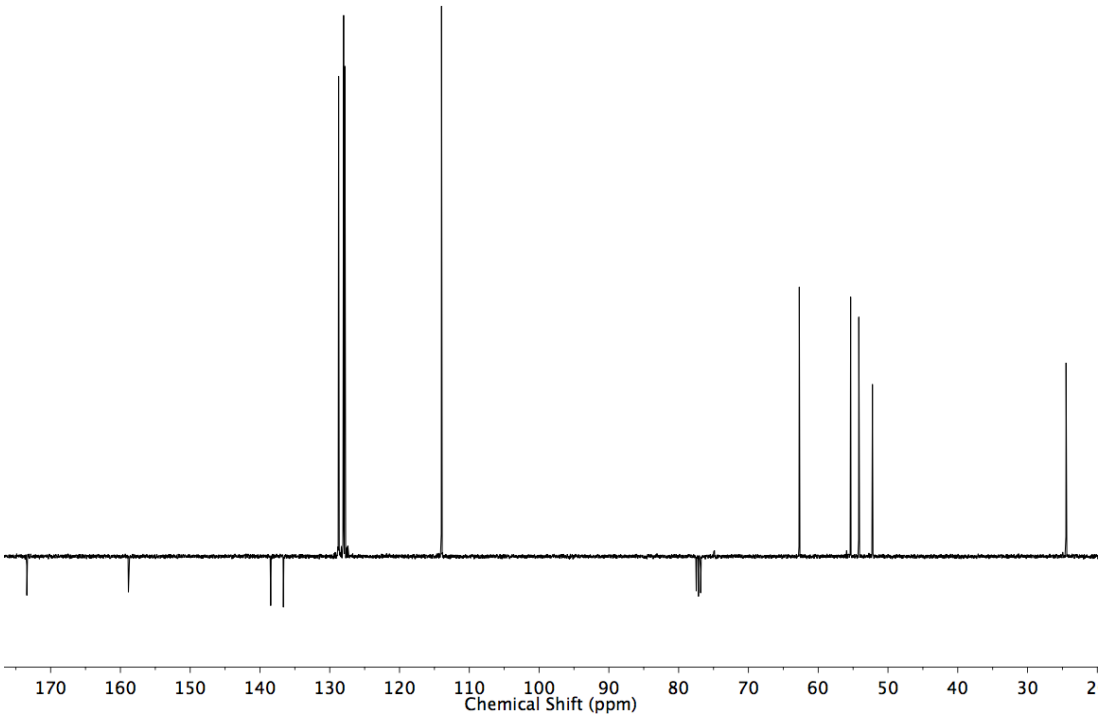

Figure 2.50 JMOD NMR ($CDCl_3$, 400 MHz) of second diastereoisomer of **157**.

*Compound **158***

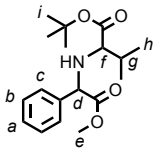

158

Diastereoisomer 1: ^{1}H NMR (400 MHz, $CDCl_3$) δ 7.44-7.27 (m, 5H, H_a, H_b, H_c), 4.38 (s, 1H, H_d), 3.69 (s, 3H, H_e), 2.95 (d, *J* = 5.6, 1H, H_f), 2.04-1.88 (m, 1H, H_g), 1.42 (s, 9H, H_i), 1.00 (d, *J* = 6.7, 3H, 3 of H_h), 0.97 (d, *J* = 6.7, 3H, 3 of H_h). ^{13}C NMR (101 MHz, $CDCl_3$) δ 173.6, 172.9, 138.4, 128.6, 128.2, 127.8, 80.9, 65.6, 65.0, 52.0, 31.8, 28.1, 19.1, 18.3. HR-ESI-MS *m/z* = 344.1839 $[M+Na]^+$ calc. 344.1832.

Diastereoisomer 2: ^{1}H NMR (400 MHz, $CDCl_3$) δ 7.44-7.27 (m, 5H, H_a, H_b, H_c), 4.33 (s, 1H, H_d), 3.67 (s, 3H, H_e), 2.71 (d, *J* = 5.6, 1H, H_f), 2.04-1.88 (m, 1H, H_g), 1.49 (s, 9H, H_i), 0.94 (d, *J* = 6.7, 3H, 3 of H_h), 0.92 (d, *J* = 6.7, 3H, 3 of H_h). ^{13}C NMR (101 MHz, $CDCl_3$) δ 173.6, 172.8, 138.2, 128.4, 128.3, 128.0, 81.0, 64.7, 64.0, 64.0, 52.3, 31.6, 28.2, 19.4, 18.2. HR-ESI-MS *m/z* = 344.1839 $[M+Na]^+$ calc. 344.1832.

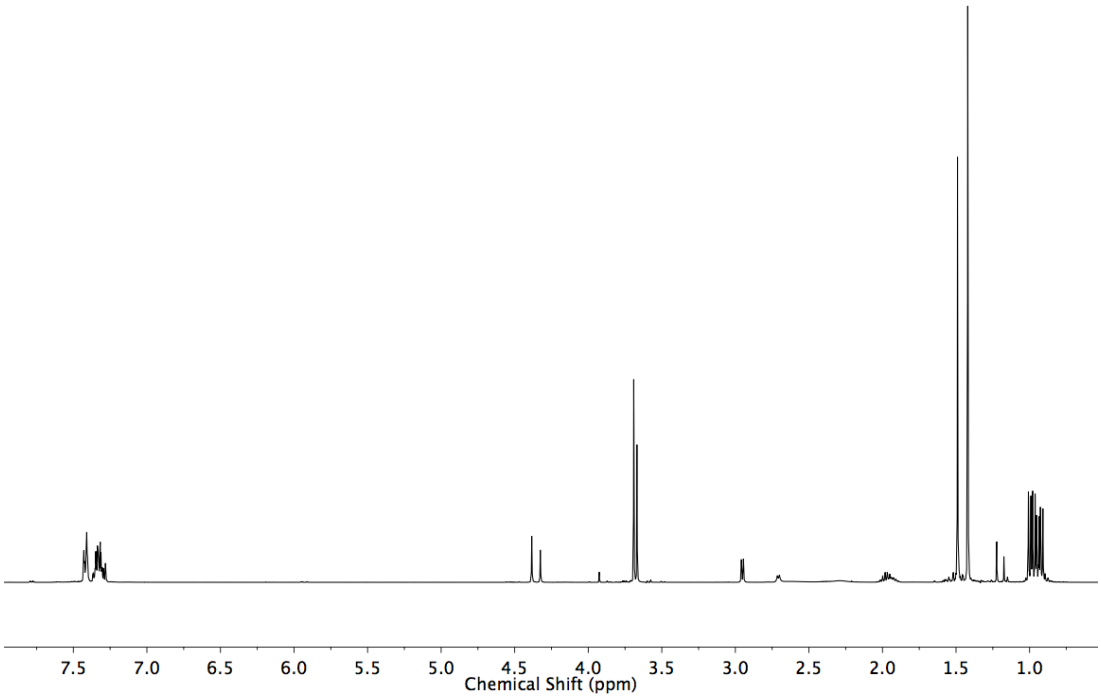

Figure 2.51 ^{1}H NMR ($CDCl_3$, 400 MHz) of a diastereoisomer mixture of **158**.

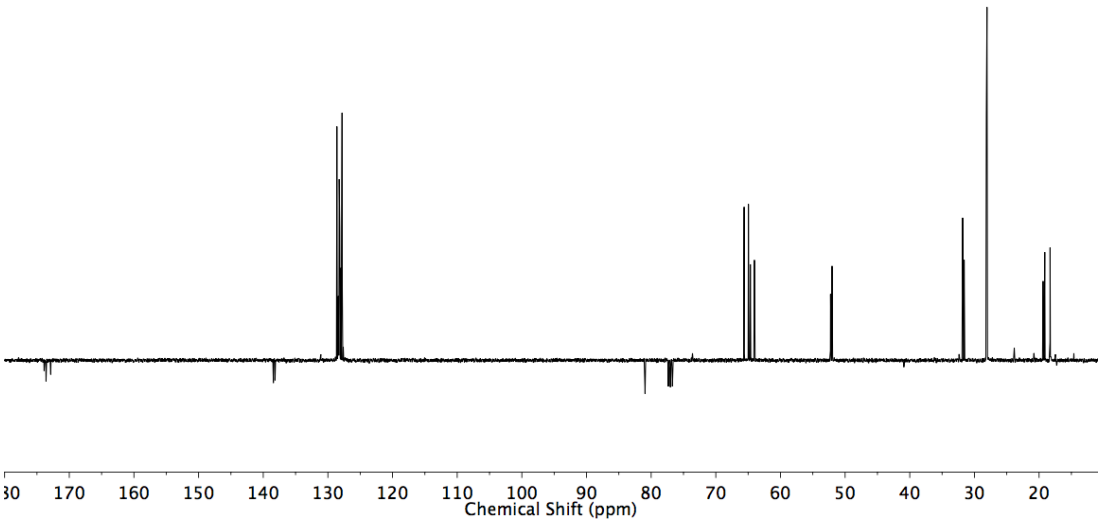

Figure 2.52 JMOD NMR ($CDCl_3$, 400 MHz) of a diastereoisomer mixture of **158**.

2.5. Bibliography

[1] J.-C. Chambron, J.-P. Sauvage, *Tetrahedron Lett.* **1986**, *27*, 865–868.

[2] J.-C. Chambron, J.-P. Sauvage, *Tetrahedron* **1987**, *43*, 895–904.

[3] H. Lahlali, K. Jobe, M. Watkinson, S. M. Goldup, *Angew. Chem. Int. Ed.* **2011**, *50*, 4151–4155.

[4] J. Winn, A. Pinczewska, S. M. Goldup, *J. Am. Chem. Soc.* **2013**, *135*, 13318–13321.

[5] J. Berná, J. D. Crowley, S. M. Goldup, K. D. Hänni, A.-L. Lee, D. A. Leigh, *Angew. Chem. Int. Ed.* **2007**, *46*, 5709–5713.

[6] J. E. M. Lewis, R. J. Bordoli, M. Denis, C. J. Fletcher, M. Galli, E. A. Neal, E. M. Rochette, S. M. Goldup, *Chem. Sci.* **2016**, *7*, 3154–3161.

[7] A. Igau, H. Grutzmacher, A. Baceiredo, G. Bertrand, *J. Am. Chem. Soc.* **1988**, *110*, 6463–6466.

[8] A. J. Arduengo, R. L. Harlow, M. Kline, *J. Am. Chem. Soc.* **1991**, *113*, 361–363.

[9] E. O. Fischer, A. Maasböl, *Angew. Chem. Int. Ed. Engl.* **1964**, *3*, 580–581.

[10] E. O. Fischer, A. Maasböl, *Chem. Ber.* **1967**, *100*, 2445–2456.

[11] R. R. Schrock, *J. Am. Chem. Soc.* **1974**, *96*, 6796–6797.

[12] P. Schwab, M. B. France, J. W. Ziller, R. H. Grubbs, *Angew. Chem. Int. Ed. Engl.* **1995**, *34*, 2039–2041.

[13] M. Scholl, T. M. Trnka, J. P. Morgan, R. H. Grubbs, *Tetrahedron Lett.* **1999**, *40*, 2247–2250.

[14] J. S. Kingsbury, J. P. A. Harrity, P. J. Bonitatebus, A. H. Hoveyda, *J. Am. Chem. Soc.* **1999**, *121*, 791–799.

[15] G. Occhipinti, V. R. Jensen, *Organometallics* **2011**, *30*, 3522–3529.

[16] K. P. Kornecki, J. F. Briones, V. Boyarskikh, F. Fullilove, J. Autschbach, K. E. Schrote, K. M. Lancaster, H. M. L. Davies, J. F. Berry, *Science* **2013**, 1243200.

[17] P. Yates, *J. Am. Chem. Soc.* **1952**, *74*, 5376–5381.

[18] B. F. Straub, P. Hofmann, *Angew. Chem.* **2001**, *113*, 1328–1330.

[19] I. V. Shishkov, F. Rominger, P. Hofmann, *Organometallics* **2009**, *28*, 1049–1059.

[20] R. G. Salomon, J. K. Kochi, *J. Am. Chem. Soc.* **1973**, *95*, 3300–3310.

[21] T. Rasmussen, J. F. Jensen, N. Østergaard, D. Tanner, T. Ziegler, P.-O. Norrby, *Chem. – Eur. J.* **2002**, *8*, 177–184.

[22] H. Nozaki, S. Moriuti, M. Yamabe, R. Noyori, *Tetrahedron Lett.* **1966**, *7*, 59–63.

[23] C. Zhu, G. Xu, D. Ding, L. Qiu, J. Sun, *Org. Lett.* **2015**, *17*, 4244–4247.

[24] X. Zhao, Y. Zhang, J. Wang, *Chem. Commun.* **2012**, *48*, 10162–10173.

[25] J. Ma, X. Zhang, X. Huang, S. Luo, E. Meggers, *Nat. Protoc.* **2018**, *13*, 605–632.

[26] E. B. Bauer, *Chem. Soc. Rev.* **2012**, *41*, 3153–3167.

[27] C. Botteghi, C. Chelucci, G. Chessa, G. Delogu, S. Gladiali, F. Soccolini, *J. Organomet. Chem.* **1986**, *304*, 217–225.

[28] P. Hayoz, A. von Zelewsky, *Tetrahedron Lett.* **1992**, *33*, 5165–5168.

[29] G. Chelucci, S. Gladiali, M. G. Sanna, H. Brunner, *Tetrahedron Asymmetry* **2000**, *11*, 3419–3426.

[30] D. Lötscher, S. Rupprecht, H. Stoeckli-Evans, A. von Zelewsky, *Tetrahedron Asymmetry* **2000**, *11*, 4341–4357.

[31] H.-L. Kwong, W.-S. Lee, H.-F. Ng, W.-H. Chiu, W.-T. Wong, *J. Chem. Soc. Dalton Trans.* **1998**, *0*, 1043–1046.

[32] H. L. Wong, Y. Tian, K. S. Chan, *Tetrahedron Lett.* **2000**, *41*, 7723–7726.

[33] M. Galli, J. E. M. Lewis, S. M. Goldup, *Angew. Chem. Int. Ed.* **2015**, *54*, 13545–13549.

[34] J. E. M. Lewis, R. J. Bordoli, M. Denis, C. J. Fletcher, M. Galli, E. A. Neal, E. M. Rochette, S. M. Goldup, *Chem. Sci.* **2016**, *7*, 3154–3161.

[35] I. Colon, D. R. Kelsey, *J. Org. Chem.* **1986**, *51*, 2627–2637.

[36] C. Amatore, A. Jutand, *Organometallics* **1988**, *7*, 2203–2214.

[37] T. Godau, S. M. Bleifuß, A. L. Müller, T. Roth, S. Hoffmann, F. W. Heinemann, N. Burzlaff, *Dalton Trans.* **2011**, *40*, 6547–6554.

[38] D. Gillingham, N. Fei, *Chem. Soc. Rev.* **2013**, *42*, 4918–4931.

[39] S. Guizzetti, M. Benaglia, S. Rossi, *Org. Lett.* **2009**, *11*, 2928–2931.

[40] S. Hoekman, M. O. Kitching, D. A. Leigh, M. Papmeyer, D. Roke, *J. Am. Chem. Soc.* **2015**, *137*, 7656–7659.

[41] A. Dixit, P. Kumar, G. D. Yadav, S. Singh, *Inorganica Chim. Acta* **2018**, *479*, 240–246.

[42] P. Bajaj, G. Sreenilayam, V. Tyagi, R. Fasan, *Angew. Chem. Int. Ed.* **2016**, *55*, 16110–16114.

[43] F. G. Adly, M. G. Gardiner, A. Ghanem, *Chem. – Eur. J.* **2016**, *22*, 3447–3461.

[44] L. Li, B. Zhou, Y.-H. Wang, C. Shu, Y.-F. Pan, X. Lu, L.-W. Ye, *Angew. Chem. Int. Ed.* **2015**, *54*, 8245–8249.

[45] E. Aller, R. T. Buck, M. J. Drysdale, L. Ferris, D. Haigh, C. J. Moody, N. D. Pearson, J. B. Sanghera, *J. Chem. Soc. Perkin 1* **1996**, *0*, 2879–2884.

Chapter 3: Chemical consequences of the mechanical bond: a tandem active template-rearrangement reaction

Abstract: This chapter reports the unexpected discovery of tandem reaction for the synthesis of rotaxanes. The acrylamide containing rotaxanes were produced *via* tandem active template CuAAC-rearrangement reaction in moderate to excellent yield (16% to 97% yield). Mechanistic investigations indicated that this tandem reaction was directly related to the mechanical bond *via* the stability of Cu^{I}-triazolide intermediate; when the reaction was performed without mechanical bond no traces of acrylamide-containing rotaxanes were observed.

This project was performed, and the results reported herein were obtained in equal collaboration with Ellen Jamieson. Crystallography was performed by Ellen Jamieson.

Prior publication: The majority of this chapter has been submitted as part of:

F. Modicom, E. M. G. Jamieson and S. M. Goldup, "*Chemical Consequences of the Mechanical Bond: A Tandem Active Template-Rearrangement Reaction*", *Angew. Chem. Int. Ed*. Under revision.

3.1. Introduction

3.1.1. Synthesis of the 1,2,3-triazole motif

The 1,2,3-triazole motif became ubiquitous in organic chemistry following the reports on the copper(I) catalysed azide-alkyne cycloaddition (Cu-AAC) by both Sharpless and co-workers and Medal and co-workers in 2002.[1,2] This methodology allowed the selective formation of the 1,4-disubstituted 1,2,3-triazoles under mild conditions, rather than a mixture of 1,4 and 1,5-disubstituted 1,2,3-triazole when the Huisgen's cycloaddition is performed under thermal conditions.

More recently, Folkin and co-workers reported a selective synthesis of 1,5-disubstituted 1,2,3-triazole when the reaction is catalysed by [Cp*Ru(PPh_3)$_2$Cl] (Figure 3.1).[3] The ruthenium azide-alkyne cycloaddition (Ru-AAC) can also be used with internal alkyne providing a 1,4,5-trisubstituted 1,2,3-triazole.

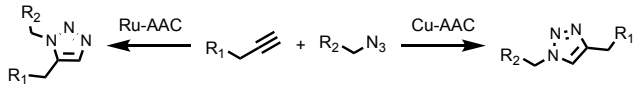

Figure 3.1 Examples of RuAAC and CuAAC reactions.

3.1.2. Transformations of 1,2,3-triazoles

The 1,2,3-triazole motif has been used in synthesis due to the stability of this functional group.[4,5] However, there have been reports on transformations of the 1,2,3-triazole functionality over the years.[6] 1,2,3-Triazoles bearing a strongly electron-withdrawing group at the N^1 position displace the equilibrium towards the ring-opened isomer.[7,8] This property was extensively used in organic synthesis.[9]

3.1.2.1. Dimroth rearrangement

The first example of rearrangement was reported in 1909 by Dimroth in which endocyclic and exocyclic nitrogens switch places (Figure 3.2).[10,11] The reaction mechanism consisted in a ring-opening and ring-closure reaction and is known as Dimroth rearrangement.

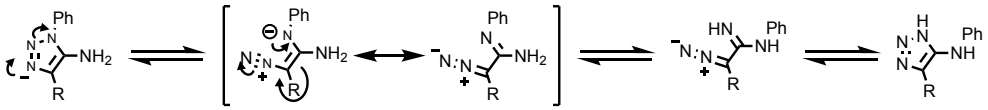

Figure 3.2 Dimroth rearrangement of 1,2,3-triazole.

3.1.2.2. Thermal induced transformation

Rees and co-workers reported a study on the behaviour of the 1,2,3-triazoles under thermal conditions in 1975.[12] The vapour phase pyrolysis of 1,4-diphenyl-1,2,3-triazoles **159** led to the formation of 3-phenylindoles **161**. The formation of the indole motif was explained by the in-situ formation of a carbene intermediate **160** which can react with the phenyl ring to form the 5-membered ring (Figure 3.3).

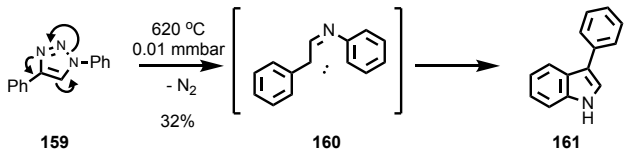

Figure 3.3 Synthesis of indole **161** *via* pyrolysis of 1,4-diphenyl-1,2,3-triazole **159**.

Latyshez and co-workers reported a cascade transformation of 5-iodo-1,2,3-triazole to benzoxazoles.[13] During this process, the first step was an intramolecular nucleophilic displacement of the iodide by the phenolate formed *in-situ*. This resulting triazole-fused heterocyclic intermediate **163** existed in equilibrium with the diazo tautomer **164**. The benzoxazole **165** was then obtained *via* a Bamford-Stevens-type denitrogenation in an excellent yield. The authors were able to isolate and characterise the diazo tautomer **164**, which is a key result. The authors focused on developing a method to trap the diazo tautomer by transition metal such a copper, palladium or rhodium. The metallocabenoid intermediate was then inserted into a range of primary and secondary amines in a good yield.

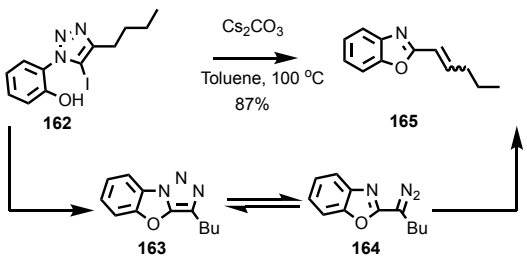

Figure 3.4 Cascade transformation of 5-iodo-1,2,3-triazole to benzoxazoles.

3.1.2.3. 1-Sulfonyl-1,2,3-triazole

Fokin and co-workers investigated the Cu^{I} catalysed reaction of phenyacetylene **167** with *para*-toluenesulphonylazide **166**.[14] The only isolated product after the reaction was a cyclobutene derivative **173** in 31% yield. A proposed mechanism proceeded *via* a similar ring opening presented in the Dimroth rearrangement leading to a toluenesulphonylketenimine intermediate **171** which dimerised and tautomerised to form product **173** (Figure 3.5).

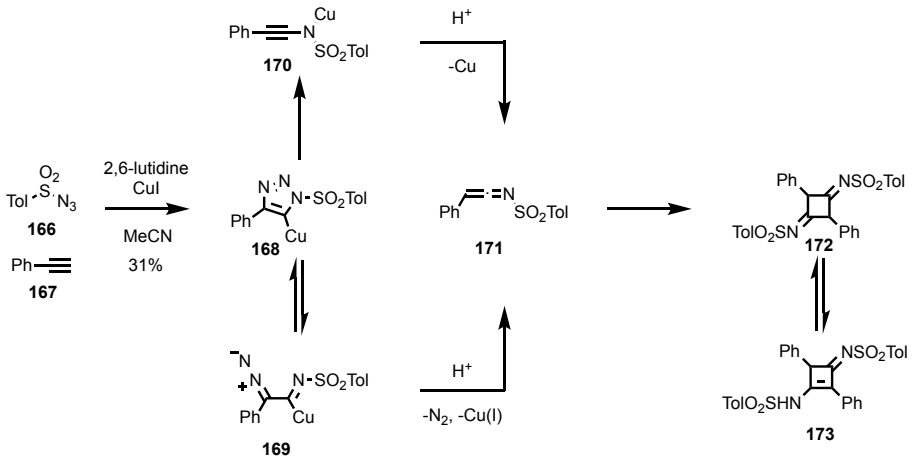

Figure 3.5 Possible mechanistic pathway leading to the cyclobutene **173**.

Following the unexpected reactivity of the *N*-*para*-toluenesulphonyltriazolide copper complex **168**, Fokin and co-workers studied the effect of the substituent on the N^1 of the 1,4-disubstituted 1,2,3-triazoles on the triazole opening process (Figure 3.6).[15] The DFT calculations for the ring opening of the 1,2,3-triazole was performed using *N*-methylsulphonyltriazolide copper complex **177** and the *N*-methyl analogue **174**. In the case of the **174**, the calculated activation barrier was much higher than the calculated one in the

case of the **177**, 148 kJ.mol^{-1} and 64kJ.mol^{-1}, respectively. The ring opening process was more favoured for the sulphonyl complex than the methyl.

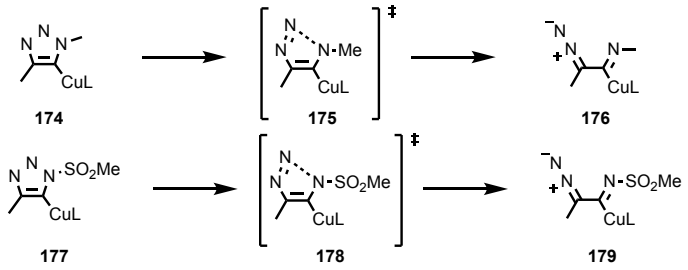

Figure 3.6 Models used for the DFT calculation of the ring opening reaction of 1,2,3-triazoles.

Following these studies, Fokin and co-workers exploited the *in-situ* formation of a reactive ketenimine which reacted with a large number of nucleophiles, such as amines, alcohols and water to form amidines, imidates and amides respectively (Figure 3.7).[16]

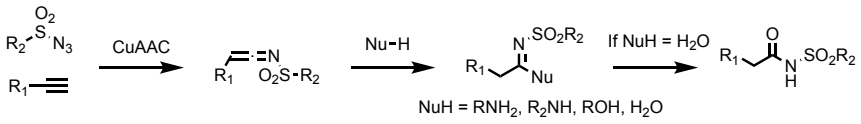

Figure 3.7 Nucleophilic trapping of *N*-sulphonyl ketenimine.

Pitchumani and co-workers developed a one-pot Cu^{I} catalysed azide-alkyne/ ketenimine-nitrone cycloaddition cascades to form imidazolidine-4-ones (Figure 3.8).[17] The first cycloaddition led, after rearrangement, to the formation of the ketenimine **171**, which underwent a second [3+2] cycloaddition with nitrone **180** to form the oxadiazolidine **181** which rearranged to form the imidazolidine-4-one **183**.

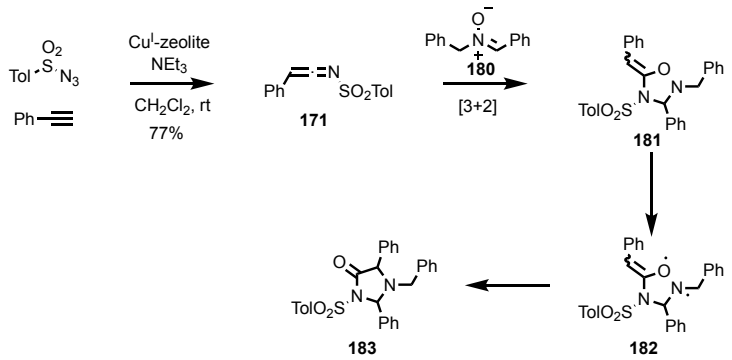

Figure 3.8 Ptichumani's azide-alkyne/ ketenimine-nitrone cycloaddition cascades.

Following this report, Murakami and co-workers reported the synthesis of enaminones by rhodium denitrogenative rearrangement of 1-(*N*-sulfonyl-1,2,3-triazol-4-yl)alkanols.[18] The principle of this approach was to use the equilibrium between the closed and open forms of the triazole. The rhodium reacted with the diazo function to form a rhodium-azavinyl carbene intermediate, which was followed by an alkyl group migration (Figure 3.9). A demetalation led to the expected enaminone. In this report, the authors were able to develop a one-carbon ring expansion strategy using a 1-(*N*-tosyl-1,2,3-triazol-4-yl)cycloalkanols in good yield.

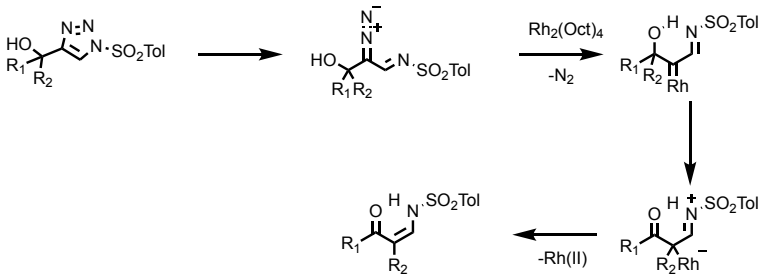

Figure 3.9 Murakami's rhodium denitrogenative rearrangement approach.

Fokin and co-workers reported the exact same study only few months after Murakami's report on the synthesis of enaminone.[19] In addition, they reported an acetate or an amine migration in addition to the alkyl group leading to the formation of an α,β–unsaturated imines (Figure 3.10).

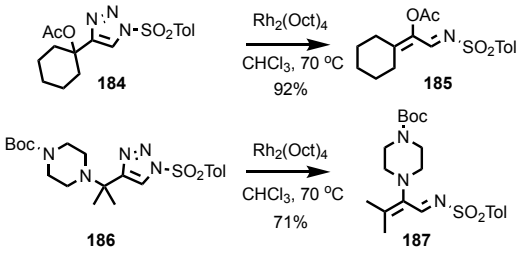

Figure 3.10 Fokin's α,β–unsaturated imine synthesis

In addition to the sulfonyl group, phosphoryl and certain acyl azides can be excellent one-nitrogen sources in the Cu-AAC. As proposed previously for the *N*-sulphonyl derivatives, the use of these two electron-withdrawing groups could generate a reactive ketenimine species, which then could react with nucleophile.

Chang and co-workers were the first to use phosphoryl azides in place of the sulfonyl azide used by Fokin and co-workers (Figure 3.11).[20] When the phosphyl azide **188** was reacted with phenylacetelyne **167** and $HN(^{i}Pr)_2$ in presence of CuI, the corresponding *N*-phosphorylamidine **189** was obtained in excellent yield.

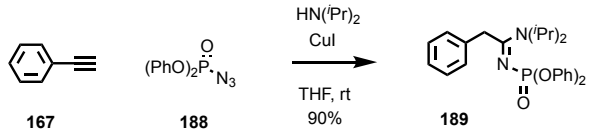

Figure 3.11 Multi-component synthesis of N-phosphorylamidine via Cu-AAC followed by nucleophilic trapping of *N*-phosphoryl ketenimine.

Fokin and co-workers reported the formation of the *N*-acylamidine from the acyl azide **190** in a mediocre yield (Figure 3.12).[16] Once again, the reaction involved the formation of the *N*-acylketenimine.

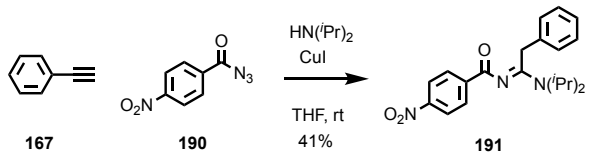

Figure 3.12 Multi-component synthesis of *N*-phosphorylamidine via Cu-AAC followed by nucleophilic trapping of *N*-acyl ketenimine.

Finally, Fokin and co-workers developed an operationally simple and efficient synthesis of 1-sulphonyl-1,2,3-triazoles without observation of side product during the reaction.[21] The terminal alkyne and sulphonylazide were reacted in $CHCl_3$ in presence of CuI and 2,6-lutidine at 0 °C leading to the expected 1-*N*-sulphonyl-1,2,3-triazole. The decrease of the temperature was crucial for this reaction to supress the entropically favoured opening of the triazole ring. Fokin and co-workers reported a second procedure for the exclusive synthesis of triazole using Cu^{I} thiophene-2-carboxylate.[22] During the process, the thiophene ligand was expected to play two rules. The first one was the deprotonation of the terminal alkyne generating the thiophene carboxylic acid. The sulfur present in the thiophene was assuring the coordination of the ligand to the copper centre, in which case the protiolysis step became intramolecular and therefore rapid and facile.

3.1.3. Aims and objectives

The original aim of the project was the development of a methodology to access enantiopure mechanically planar rotaxane which could be tested as ligand for enantioselective catalysis. In order to do so, a group project was started for the stereoselective synthesis of mechanically planar rotaxanes. One of the system used a half-axle bearing a chiral propargylic alcohol in order to generate potentially separable mechanically planar diastereoisomeric rotaxanes which could then be oxidised to the ketone, which would lead to enantiopure ketone-functionalised rotaxane. However, when using the propargylic alcohol **192**, an unexpected, uncharacterised novel interlocked structure was observed by Dr E. Rochette. This product was observed in various percentages; but the structure was not defined at the time.

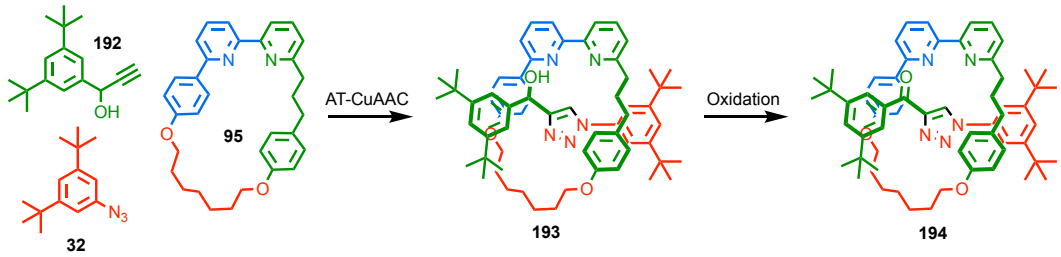

Figure 3.13 Proposed route for the synthesis of enantiopure rotaxane

Because of these preliminary results, we set out to identify and fully characterise this novel interlocked product. The understanding of the factors in favour of the formation of the novel interlocked structure will help in the optimisation of the syntheses of both interlocked structures. During this investigation, we were interested in understanding the importance of the mechanical bond during the process, which would lead to the proposition of a mechanism.

3.2. Results and Discussion

3.2.1. Starting material syntheses

In the case of the chiral rotaxane, the use of enantiopure propargylic alcohol would be required. In the preliminary study, racemic propargylic alcohols were used to avoid the use of expensive and synthetically challenging enantiopure propargylic alcohols. The syntheses of all propargylic alcohols used in this chapter are presented below.

The synthesis of the propargylic alcohol **192** was originally performed in two steps *via* a Bouveault reaction to yield aldehyde **195** followed by a Grignard reaction using ethynyl magnesium chloride.[23] This reaction proceeded well, and was very high yielding (Figure 3.14).

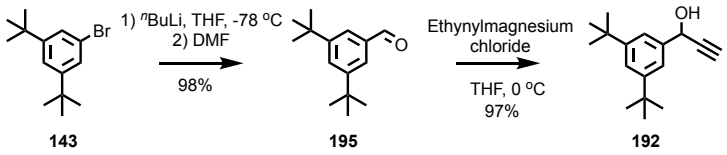

Figure 3.14 Synthesis of propargyl alcohol **192**.

However, an alternative route using Sommelet reaction for the synthesis of aldehyde **195** was used in order to solve the scalability issues involved with butyl lithium reagent, as well as using less expensive starting materials. This synthesis was based on a modified literature procedure, and was very successful with a yield of 77% over two steps on a multi-gram scale (Figure 3.15).[24]

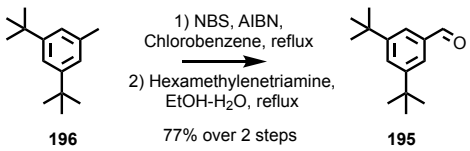

Figure 3.15 Alternative route for the synthesis of **195**.

Alcohol of **192** was alkylated using sodium hydride and iodomethane yielding to **197** in 98% yield.

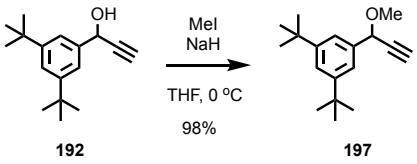

Figure 3.16 Synthesis of **197**.

A quaternary propargylic alcohol **200** was prepared from the carboxylic acid **198** by reaction with methyl lithium to give ketone **199** which was reacted with ethynylmagnesium chloride to afford **200** in 48% yield.[25]

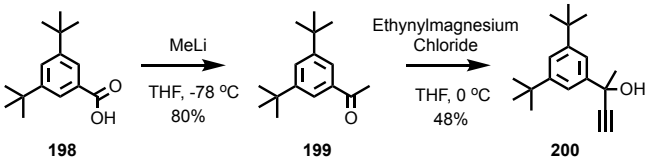

Figure 3.17 Synthesis of quaternary propargylic alcohol **200**.

The synthesis of a propargylic alcohol with an extra carbon between the phenyl ring and the propargylic unit was realised using Diederich's approaches.[26,27] Diederich and co-workers reported two syntheses for the aldehyde **201**, the first one involved the reduction of the nitrile group to an aldehyde whereas the second one involved a Wittig reaction followed by a deprotection.

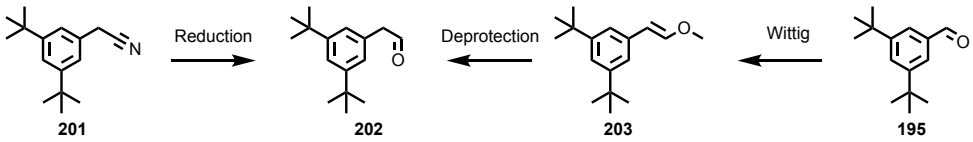

Figure 3.18 Diederich's approaches for the synthesis of **202**.

The first approach appeared to be more straightforward. However, the difficult purification process did not allow the access to the expected aldehyde. The second approach was used in order to prepare the aldehyde **202**.

Once the aldehyde was in hand, the addition of ethynylmagnesium chloride led to the propargylic alcohol **204** in a moderate 36% yield. The treatment of the aldehyde **202** with Bestmann-Ohira reagent led to the formation of the alkyne **205** in 81% yield which is an analogue of **192** lacking the hydroxy group.

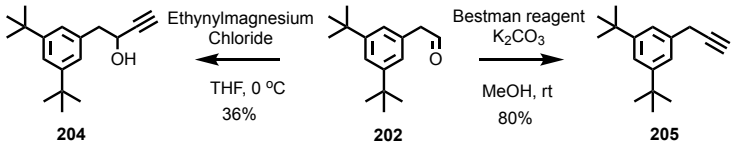

Figure 3.19 Syntheses of **204** and **205**.

3.2.2. Isolation and characterisation of the novel interlocked structure

During the investigation, rotationally symmetrical macrocycle **103** was used instead of the non-symmetrical macrocycle **92** as it makes the analysis of the unexpected structure easier, as well as it being easier to synthesise.

Preliminary results had previously found traces of an unexpected mechanically interlocked molecule for the reaction of **192**, **101** and **103** using our standard rotaxane forming conditions. However, when the reaction was performed with care the product was not detected in the reaction mixture (Table 3.1, Entry 1). Both KCN and EDTA-NH_3 methods were evaluated to remove the copper after the reaction, in both case no traces of side product were observed.

Table 3.6 Attempt of understanding the reason of the formation of the mystery product.

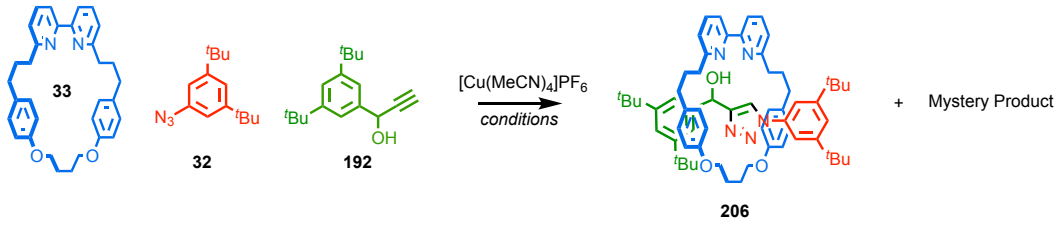

Entry	Conditions	Ratio **206**/mystery product[a]
1	$^{i}Pr_2NEt$, CH_2Cl_2, rt, 48h	> 99:1
2	$^{i}Pr_2NEt$, CH_2Cl_2-H_2O (9:1), rt, 48h	90:10
3	CH_2Cl_2-H_2O (9:1), rt, 48h	40:60

[a] Determined by ^{1}H NMR.

The appearance of the side product could be due to presence of trace of H_2O. When the reaction was performed using a 9:1 mixture of CH_2Cl_2-H_2O, the novel interlocked molecule was formed in higher yield (Table 3.1, Entry 2). Removal of the base from the reaction conditions considerably increased the amount of mystery product (Table 3.1, Entry 3).

The mystery product was purified by column chromatography on silica. The LC-MS analysis revealed a single component displaying a mass peak with *m/z* = 926.6199, corresponding to [**206**+H-N_2]$^+$, suggesting dinitrogen has been extruded.

The ^{1}H NMR of the unknown compound did not display the desymmetrisation of the macrocycle component expected as the result of the presence of a stereogenic centre, whereas the spectrum of **206** displayed two resonances for each proton of the macrocycle component (Figure 3.20). The absence of the desymmetrisation of the macrocycle in the ^{1}H NMR of the mystery product suggested that the stereogenic centre associated with the propargylic alcohol was not present.

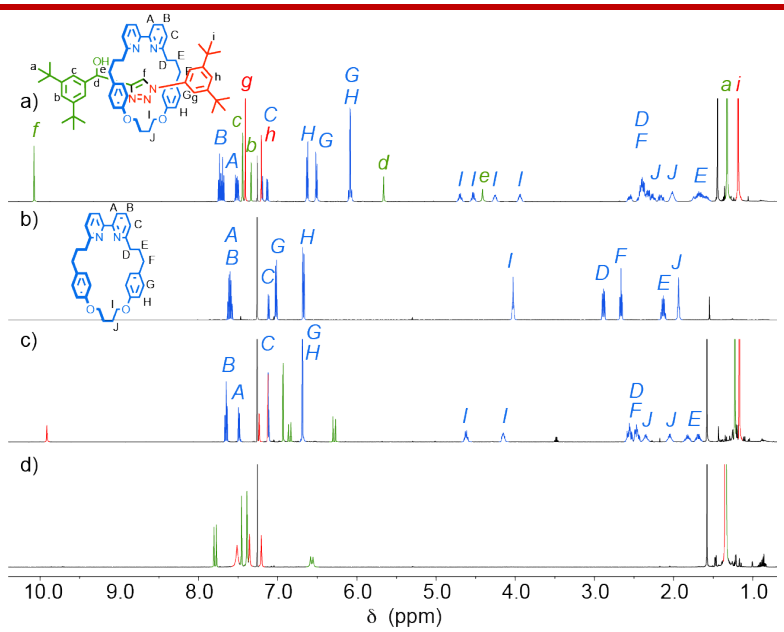

Figure 3.20 Stack ^{1}H NMR (500 MHz, $CDCl_3$, 298K) of a) triazole-functionalised rotaxane **206**, b) macrocycle **33**, c) mystery rotaxane, and d) axle of mystery rotaxane.

The ^{1}H NMR spectrum of the unknown compound contained two doublets at 6.85 and 6.29 ppm with J = 15.5 Hz, consistent with *trans*-related vinyl protons. The presence of a broad singlet at 9.91 ppm was characteristic to hydrogen bond between the proton from the triazole or N-H or O-H and the bipyridine of the macrocycle.

Following the analysis of the NMR spectrum, two structures could be proposed for the unknown interlocked molecule (Figure 3.21).

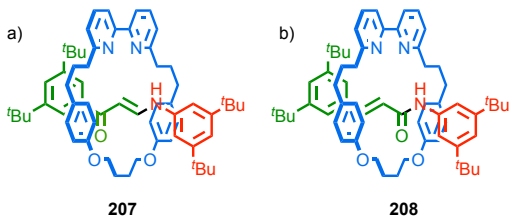

Figure 3.21 Possible structures for the unknown interlocked molecule

The study of the HMBC NMR (Figure 3.22) did not show correlations between the signal at 9.91 ppm and the vinylic carbons at 139.0 and 123.3 ppm which would eliminate the enaminone functionalised structure **207** (Figure 3.21 a). The presence of a correlation with the peak at 163.8 ppm suggested the correlation of a NH with a carbonyl as illustrated in the acrylamide functionalised structure **208** (Figure 3.21 b).

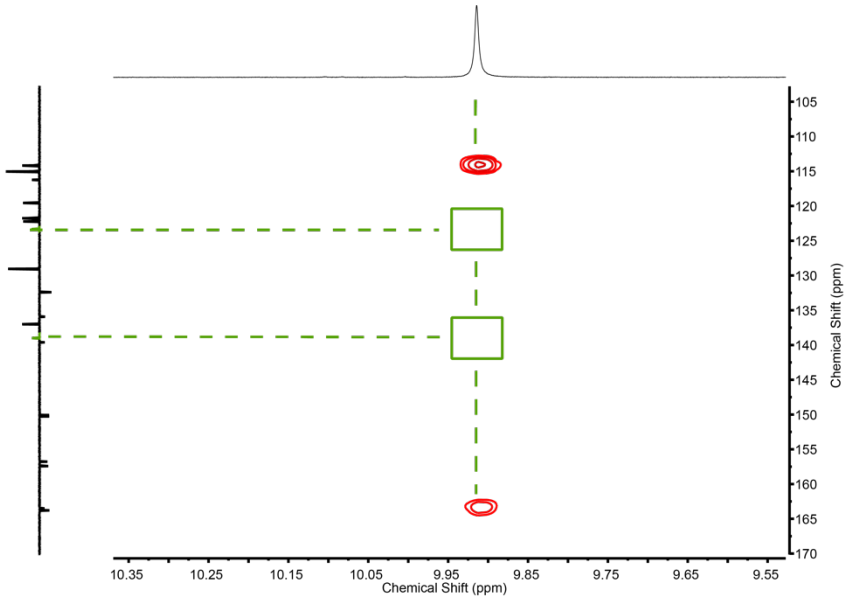

Figure 3.22 Partial HMBC NMR ($CDCl_3$) of the unknown compound revealing the lack of correlation between the NH and the vinylic carbons highlighted in green.

Ultimately, slow diffusion of Et_2O into a CH_2Cl_2 solution of the unknown interlocked structure produced single crystal suitable for x-ray analysis revealing the structure of the unknown product (Figure 3.23). The presence of the *trans*-acrylamide functionality proposed from the NMR analysis was confirmed in the solid state.

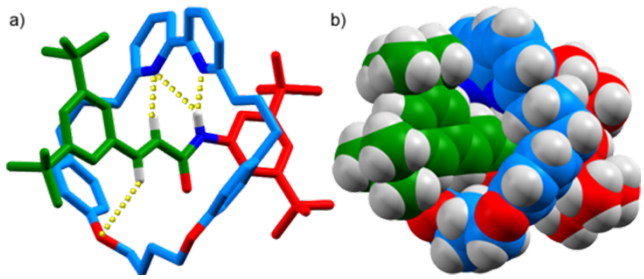

Figure 3.23 Solid-state structures and selected distances and angles of rotaxane **208** in a) sticks representation (selected intercomponent distances in Å: H_d–O = 2.94, H_e–N = 2.79, H_f–N = 2.65, H_f–N = 2.26) and b) spacefilling representations.

3.2.3. Optimisation of the reaction

Although the intentional use of a mixture of CH_2Cl_2 and H_2O as solvent led to the improvement in the formation of the rearranged structure **208**, the structure was still the minor product of the reaction. This could be explained by the immiscibility of the CH_2Cl_2 and H_2O forming a biphasic mixture. In order to have a monophasic mixture, THF was used instead of the CH_2Cl_2 leading to formation of **208** as sole interlocked product after 48 hours of reaction (Table 3.2). However, the reaction was found to be difficult to reproduce, the conversion varied from 24 to 100% to the acrylamide **208**. It is worth noting than the starting material was observed in the crude reaction mixture when the conversion was not complete.

Table 3.2 Effect of the solvent mixture on the conversion.

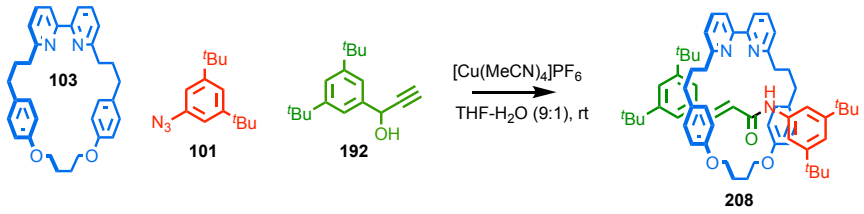

Attempt	Conv.[a]	Ratio **208**/**205**[a]
1	24%	> 99:1
2	30%	> 99:1
3	80%	> 99:1
4	100%	> 99:1

[a] Determined by ^{1}H NMR.

A kinetic study was performed in order to evaluate the kinetic profile of the reaction. Deuterated solvents were used and ^{1}H NMR were recorded every two hours. This study gave us two important pieces of information. During this trial, the product was completely formed after 40 hours and obtained as sole interlocked molecule as expected from the trial with non-deuterated solvent. It was noted that the interlocked structure was not observed during the first three hours of the reaction suggesting an induction period. However, no persistent intermediate species were observed that could give any clues for the mechanistic pathway.

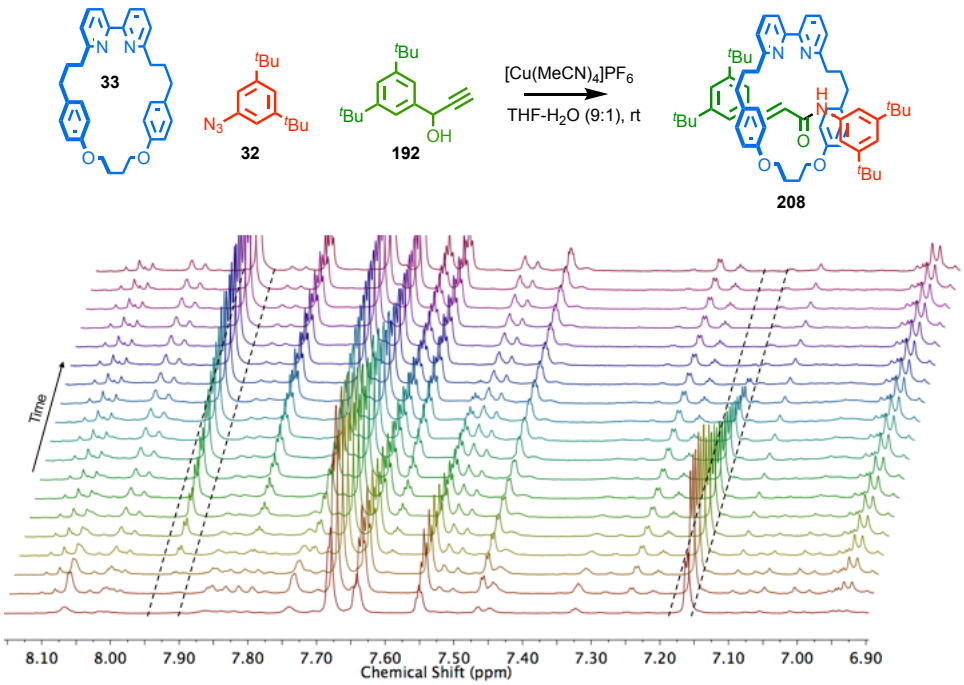

Figure 3.24 Stacked partial ^{1}H NMR (400 MHz, THF-d_8) with formation of **208** and consumption of starting material peaks highlighted.

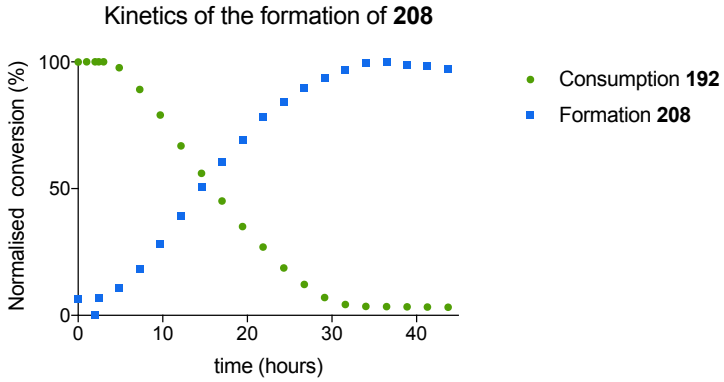

Figure 3.25 Plot of formation of **208** vs consumption of starting material with respect to time with values normalized to the residual solvent peak.

The lag period observed during this study suggested that something was formed during the reaction which was triggering the formation of **208**. From this observation, it was proposed that the PF_6^- ion was decomposing to form F^- ion and PF_5, phenomena that has previously been observed.[28]

When an aqueous solution of KF was used instead of the H_2O, the conversion appeared to be reproducible and near quantitative for each trial (Table 3.3, entries 1-3).

Table 3.3 Effect of addition of KF on the conversion.

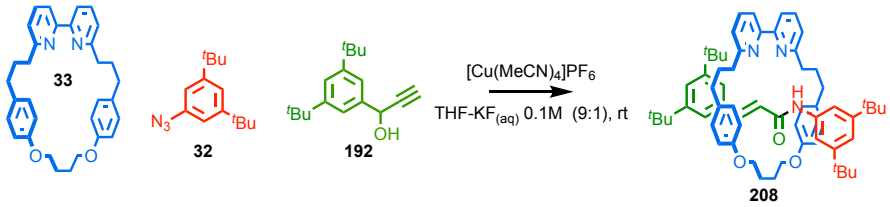

Attempt	Conv.[a]	Ratio **208**/**205**[a]
1	98%	> 99:1
2	98%	> 99:1
3	98%	> 99:1

[a] Determined by ^{1}H NMR.

In order to accelerate the reaction, the procedure was repeated using H_2O in a microwave reactor at 80 °C leading to shorter reaction times. The reaction was stopped after 40 minutes and the conversion varied from 66 to 80% with a complete selectivity (Table 3.4, Entry 1). When the reaction was performed using $KF_{(aq)}$ instead of H_2O, the conversion of macrocycle **103** was every time higher than the reaction with H_2O (Table 3.4, Entry 2). However, the selectivity appeared to decrease slightly. The use of TBAF instead of $KF_{(aq)}$ gave complete consumption of the macrocycle but the ratio **208**/**205** dropped to nearly 1:1 (Table 3.4, Entry 3). The loss of selectivity can be explained by the decomposition of TBAF in presence of water which occurred at 77 °C generating tri-*n*-butylamine;[29] a base which favoured the formation of the triazole-functionalised rotaxane **205**.

In order to increase the selectivity for the acrylamide functional group, a trial using $KF_{(aq)}$ was performed at 70 °C for one hour leading to complete conversion and complete selectivity towards **208** (Table 3.4, Entry 4). The use of TBAF instead of $KF_{(aq)}$ gave complete consumption of the macrocycle with an increase of the amount of the triazole-containing rotaxane **205** (Table 3.4, Entry 5). The conditions presented in Table 3.4, Entry 4 were considered as the optimised conditions for the rest of the investigation.

Finally, in order to discard the effect of the microwave energy on the reaction for the optimised conditions, the reaction was performed under thermal conditions. The excellent

conversion and selectivity (Table 3.4, Entry 6) ruled out the effect of the microwave energy and highlighted that the temperature was important to reduce the reaction time.

Table 3.4 Optimisation of the formation of **208** with respect to solvent, temperature and additive under microwave irradiation.

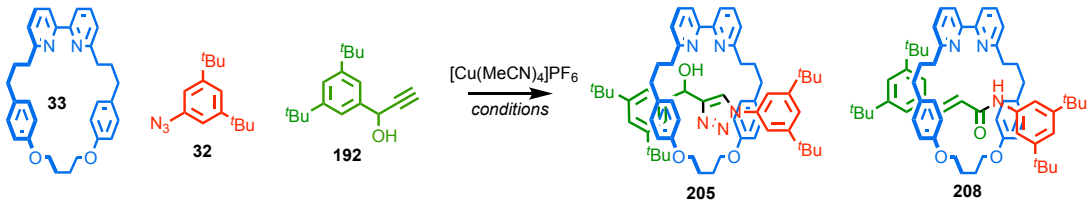

Entry	Time	Solvent	Temperature	Additive	Conv. [a]	Ratio **208**:**205**[a]
1	40 min	THF + 10% H_2O	80 °C	-	66-80%	> 99:1
2	40 min	THF + 10% H_2O	80 °C	KF (0.9 eq)	93-99%	> 99:1 - 96:4
3	40 min	THF + 10% H_2O	80 °C	TBAF (0.9 eq)	100%	57:43
4	**1 h**	**THF + 10% H_2O**	**70 °C**	**KF (0.9 eq)**	**100%**	**> 99/1**
5	1 h	THF + 10% H_2O	70 °C	TBAF (0.9 eq)	100%	92:8
6[b]	1 h	THF + 10% H_2O	70 °C	KF (0.9 eq)	100%	> 99:1

[a] Determined by ^{1}H NMR, [b] Reaction performed under thermal conditions.

3.2.4. Scope of the reaction

In order to evaluate the ratio with the triazole-containing rotaxane, all triazole-containing rotaxanes were prepared with exclusive selectivity using anhydrous solvent in presence of ^{i}Pr$_2$NEt (Figure 3.26). The triazole-functionalised rotaxanes were obtained in good yield except for **210** and **215**. The yield for **210** was lower than expected due to slow reaction. In the case of **215**, the compound was co-eluting with the macrocycle during the purification.

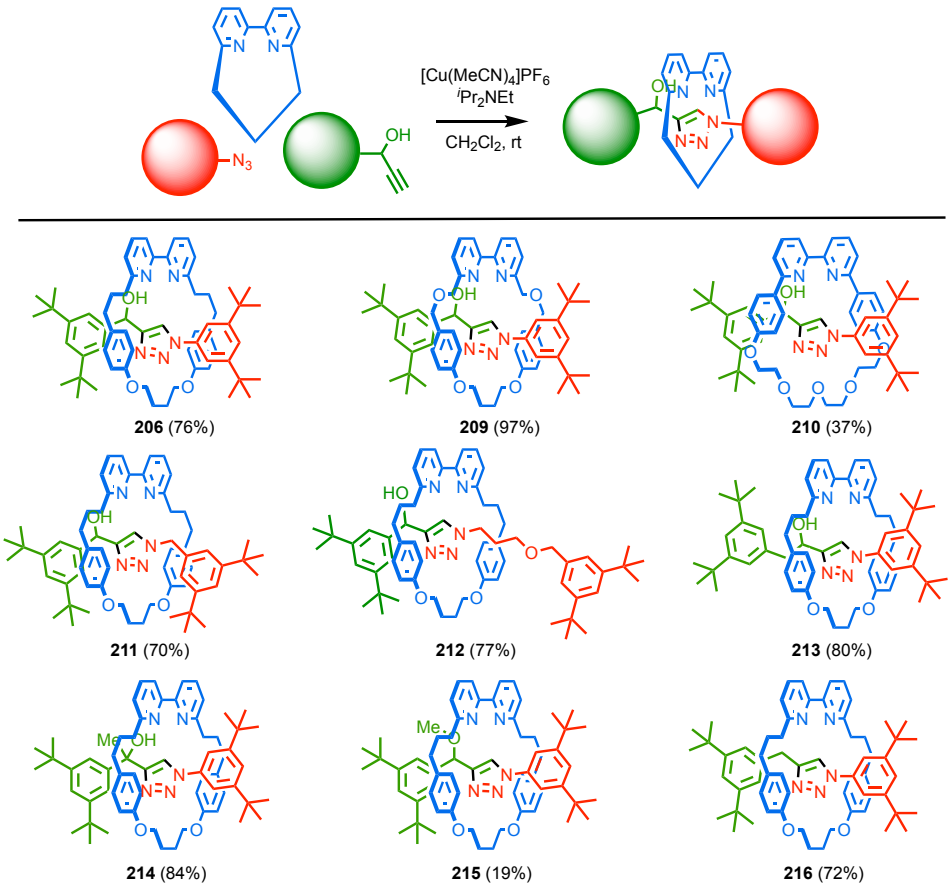

Figure 3.26 Selective triazole-functionalised rotaxane synthesis.

With optimised conditions for the synthesis of acrylamide-functionalised rotaxane in hand, the reaction was performed using different macrocycles to verify that the observed structure was not specific to the macrocycle **110**.

When macrocycle **78** was used, the rearranged structure **217** was formed selectively and isolated in near quantitative yield. However, when macrocycle **110** was used under the optimised conditions, no reaction occurred. In order to combat this lack of reactivity, the temperature was increased to 150 °C and the reaction was run for two hours resulting in 80% conversion of the macrocycle **110** as well as decreasing the selectivity to 70%. The rearranged structure **218** was isolated in 50% yield (Figure 3.27).

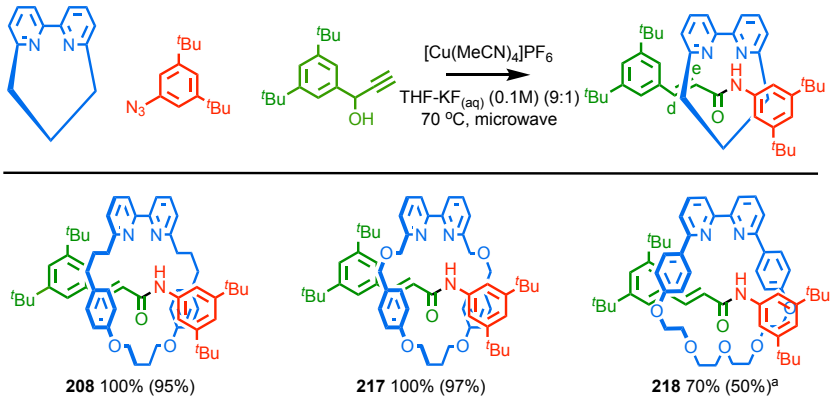

Figure 3.27 Rearranged structure with variation of macrocycle. Percentage shown correspond to the percentage of macrocycle converted into the structure, and figure in brackets is isolated yield. [a] Reaction performed at 150 °C for 2h.

Each rotaxane presented two characteristic doublets with a J = 15.5 Hz, consistent with a *trans*-related vinylic proton (Figure 3.28). In the case of **217**, these two protons H_e and H_d were observed at 5.92 and 6.81 ppm and at 6.46 and 7.27 ppm for **218**. The chemical shift of the NH from the amide functional group was always observed with a high value, 9.94 ppm for **217** and 9.78 ppm for **218**, which was a result of the hydrogen bond between the bipyridine unit of the macrocycle and the NH of the amide.

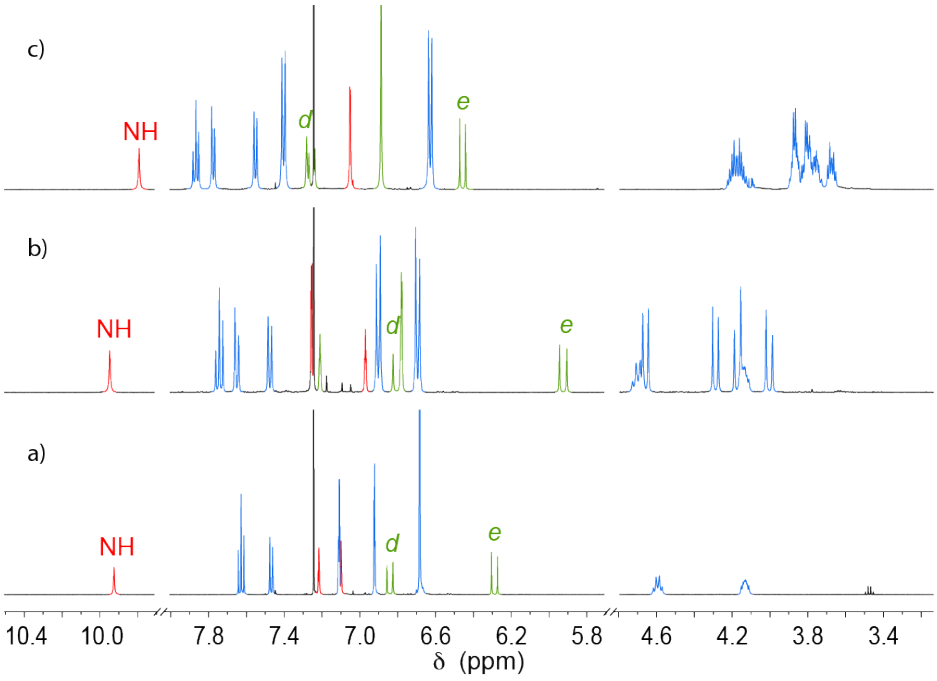

Figure 3.28 Partial Stack ^{1}H NMR (500 MHz, $CDCl_3$, 298K) of a) rotaxane **208**, b) rotaxane **217**, c) rotaxane **218**.

Slow diffusion of Et_2O into a CH_2Cl_2 solution of the **217** produced single crystal suitable for x-ray analysis confirming the structure of the product (Figure 3.29). The presence of the *trans*-acrylamide functionality proposed from the NMR analysis was confirmed in the solid state.

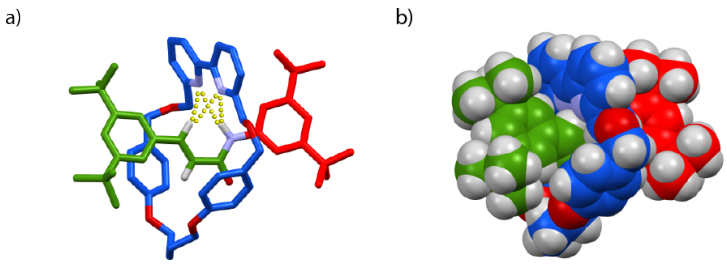

Figure 3.29 Solid-state structures and selected distances and angles of rotaxane **217** in a) sticks representation (selected intercomponent distances in Å: He–N = 2.58, He–N = 2.68, Hf–N = 2.68, Hf–N = 2.54) and b) spacefilling representations.

After the variation of the macrocycle, the next step was the investigation of the effect of the steric hindrance of the stoppers (Figure 3.30). For this investigation, two azide-functionalised stoppers and one alkyne-functionalised stopper were used. The use of benzylic azide **219** stopper reduce the selectivity to 80%, **220** was isolated in 67% yield. Increasing the distance between the aromatic unit and the azide in **221** led to a significant drop of selectivity to 20%, in this case **222** was isolated in 16% yield. The use of **204**, in which one carbon was introduced between the aromatic and the carbon bearing the alcohol, led to a drop of selectivity to **223** to 60% which was isolated in 43% yield.

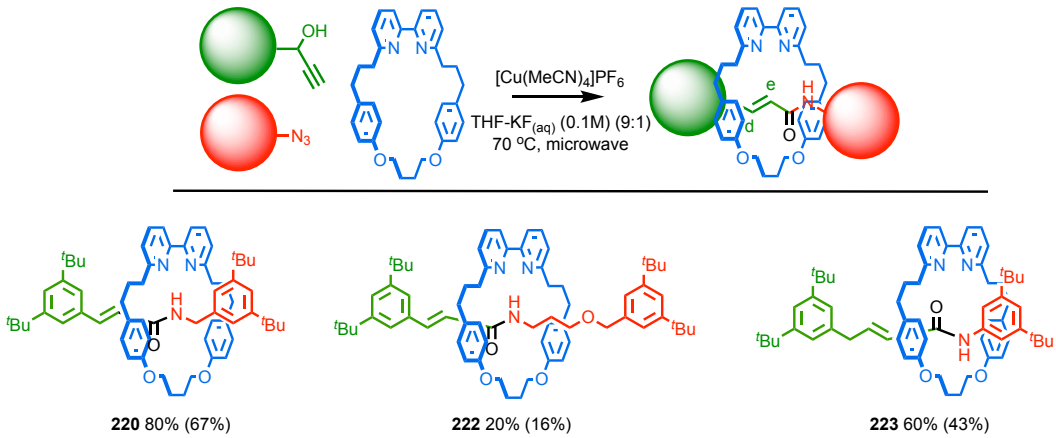

Figure 3.30 Rearranged structure with variation of stoppers. Percentage shown correspond to the percentage of macrocycle converted into the structure, and figure in brackets is isolated yield.

In the case of **220**, the NH from the amide appeared as a triplet with *J* = 4.8 Hz due to the presence of the benzylic CH_2. The vinylic protons appeared at 6.35 and 7.19 ppm with *J* = 16.0 Hz confirming once again the *trans*-related olefin. In the case of **222**, the NH from the amide appeared as a triplet with *J* = 5.4 Hz due to the presence of the CH_2. The *trans*-related vinylic protons appeared at 6.32 and 7.27 ppm with *J* = 16.0 Hz. Finally, in the case of **223**, the trans-related vinylic protons appeared at 5.46 and 6.42 as doublet of triplet with *J* = 15.5, 1.6 Hz and *J* = 15.5, 6.8 Hz respectively. The vinylic proton at 6.42 ppm was assigned as the proton in alpha of the benzylic CH_2 due to the higher value of the coupling constant (6.8 vs 1.6 Hz).

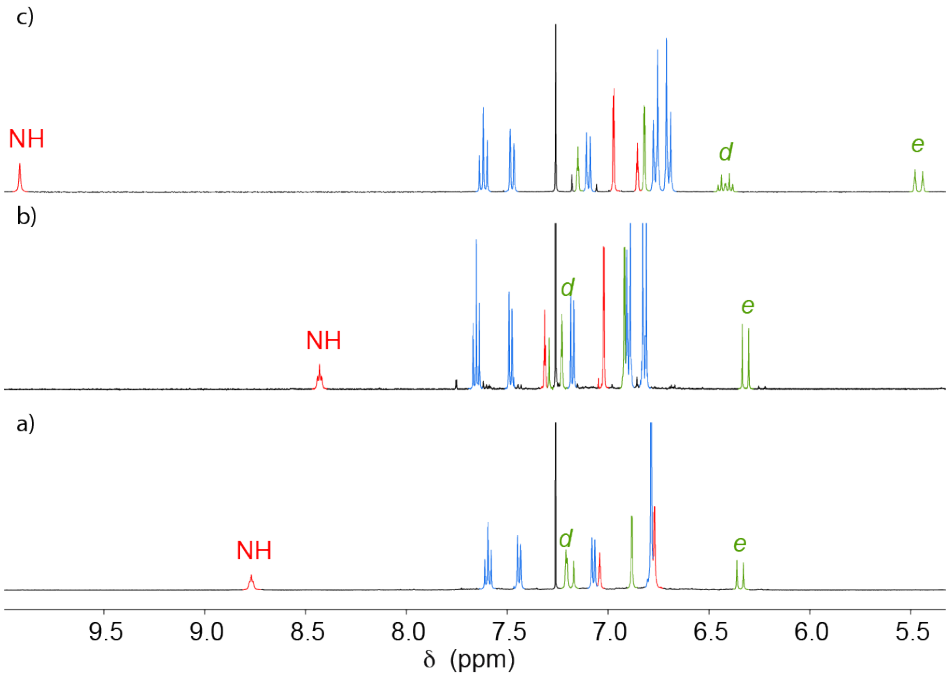

Figure 3.31 Partial Stack ^{1}H NMR (500 MHz, $CDCl_3$, 298K) of a) rotaxane **220**, b) rotaxane **222**, c) rotaxane **223**.

These results suggested a strong influence of the steric hindrance due to the mechanical bond. In order to confirm this hypothesis, two experiments were performed (Figure 3.32). In the first experiment, the reaction was performed using the optimised conditions without macrocycle which only led to the formation of triazole-functionalised axle **224** and no traces of acrylamide-functionalised axle **225** were detected. The second experiment involved the use of a macrocycle which is too large to be retained by the axle and only resulted in the formation of the corresponding triazole-functionalised axle **224**. These two results consolidated the importance of the mechanical bond.

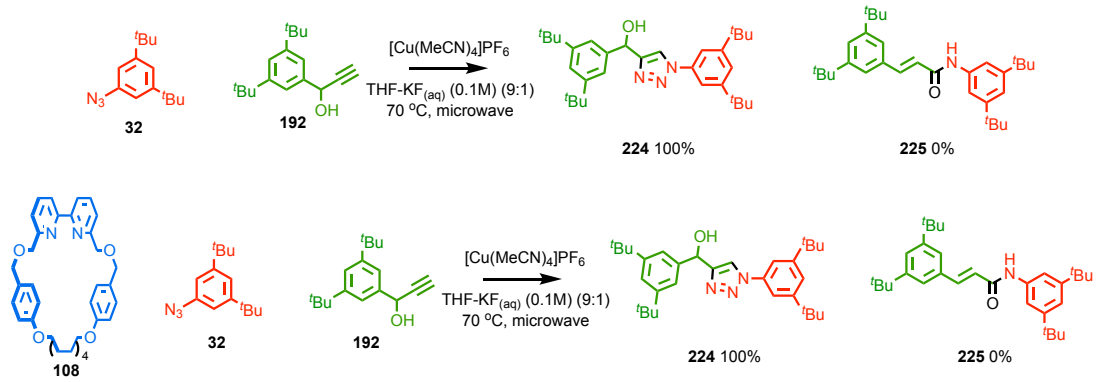

Figure 3.32 Experiments confirming the importance of the mechanical bond. Percentage shown correspond to the ratio of products formed.

3.2.5. Mechanistic investigations

In the context of forming selectively the acrylamide-functionalised rotaxanes, the scope of the reaction appeared to be limited to sterically hindered systems. This observation suggested that one of the key intermediate was stabilised by the mechanical bond.

In order to understand more about the requirement of the reaction, two substrates were tested (Figure 3.33). The use of **205**, in which the hydroxyl group was not present, resulted in complete formation of the triazole-functionalised rotaxane **216** with no traces of acrylamide or other rearrangement products. The use of **197**, where the hydroxyl group is alkylated, surprisingly resulted in complete formation of the acrylamide-functionalised rotaxane **208**.

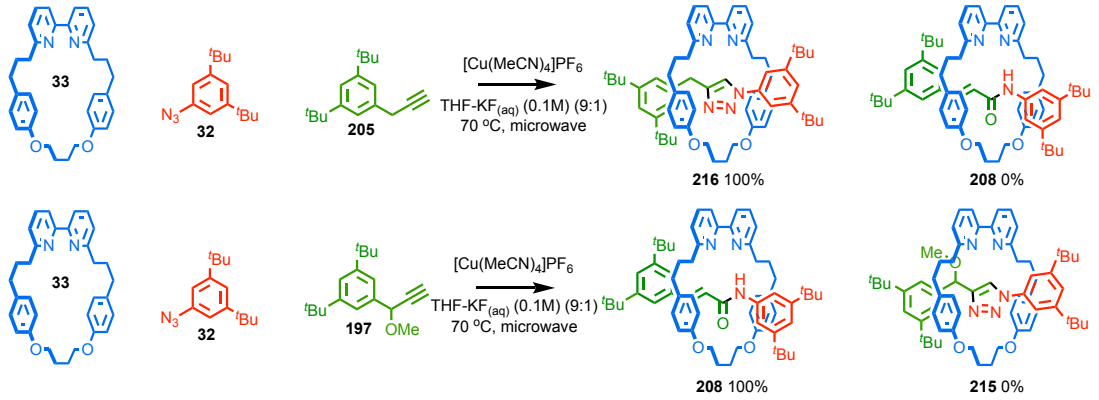

Figure 3.33 Experiments confirming the importance of hydroxyl group. Percentage shown correspond to the ratio of products formed.

The first result confirmed that the hydroxyl group was crucial to the rearrangement process. The importance of the oxygen was confirmed by exclusive formation of **208** in the second experiment, in which a methoxy group was present. A possible explanation for this result could be the in-situ acidic cleavage of the ether resulting in the generation of **192** in the crude reaction mixture. A second possibility would be the elimination of methanol catalysed by acid in the intermediate of the reaction (copper-triazolide intermediate, see proposed mechanism Figure 3.36).

The next substrate **200** was used under the standard conditions and led to the selective formation of one product (Figure 3.34). The product **226** was isolated in 85% yield and characterised as the expected acryclamide-functionalised product. In this case, neither the triazole-functionalised product **214** or other rearrangement products were observed.

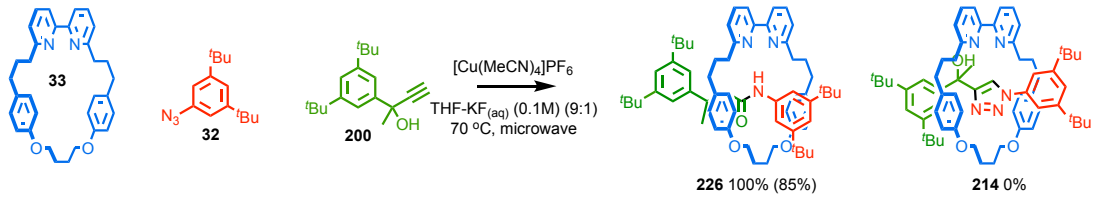

Figure 3.34 Rearranged structure with quaternary stopper **226**. Percentage shown correspond to the percentage of macrocycle converted into the structure, and figure in brackets is isolated yield.

While trying to prepare the triazole-functionalised rotaxane from **214**, we observed the formation of a surprisingly stable intermediate **227**. The LR-MS analysis revealed that the intermediate formed was the copper-triazolide intermediate during the Cu-AAC reaction (Figure 3.35). This compound, however, was decomposed on silica gel to the acrylamide-

containing rotaxane **226** when purification of the compound was attempted. The possibility to generate this copper-triazolide was a key factor for the elucidation of the mechanism.

Instead of isolating the intermediate, the crude reaction mixture containing the copper-triazolide **227** was used, after an aqueous extraction in order to remove traces of base, for the following tests.

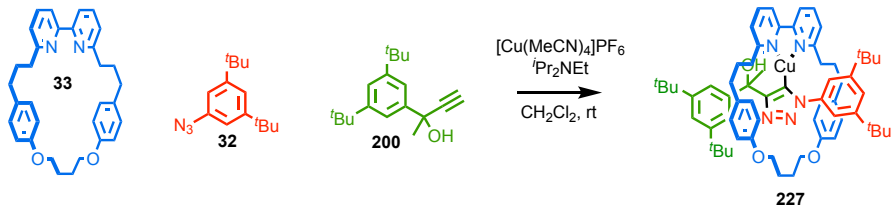

Figure 3.35 In-situ formation of the copper-triazolide intermediate **227**.

By subjecting **227** to the optimised conditions to form the acrylamide-functionalised rotaxane, the corresponding acrylamide-functionalised **226** was observed, however a significant amount of the copper-triazolide was not degraded during the reaction (entry 1). The exact quantification of the conversion was not possible by ^{1}H NMR analysis due to the broadness of the signals corresponding to copper-triazolide **227**. During the AT-CuAAC reaction, the terminal acetylene releases a proton in the reaction media while forming the copper-acetylide complex which would form one equivalent of HPF_6. In order to mimic the AT-CuAAC experimental conditions, the copper-triazolide **227** was subjected to the same conditions with one equivalent of HPF_6 (entry 2). This experiment resulted in near quantitative formation of the acrylamide-functionalised rotaxane. When $KF_{(aq)}$ was omitted, the triazolide **227** was fully converted to **226** (entry 3).

Table 3.5 Rearrangement conditions for the copper triazolide intermediate **227**

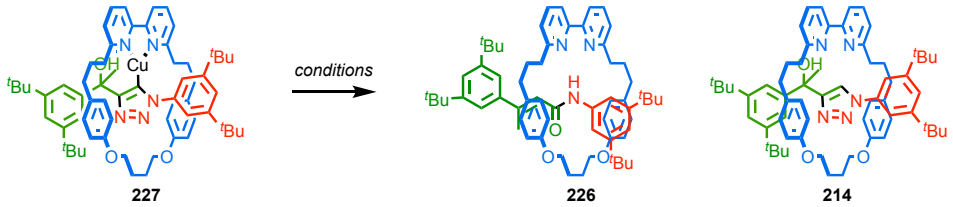

Entry	Conditions	Ratio **226**:**214**[a]
1	THF, 10 % $KF_{(aq)}$ 0.1 M, 70 °C, microwave, 1 h	96:4
2	THF, 10 % $KF_{(aq)}$ 0.1 M, HPF_6 (1 eq.), 70 °C, microwave, 1 h	100:0
3	THF, 10 % H_2O, HPF_6 (1 eq.), 70 °C, microwave, 1 h	100:0

[a] Determined by ^{1}H NMR

In all cases, the only interlocked compound formed was the acrylamide-functionalised rotaxane **226**, and no triazole-functionalised rotaxane **214** were observed during these tests. Those results suggested that the conversion of the copper-triazolide to the corresponding acrylamide-functionalised rotaxane was promoted by acid.

It is worth noting that when the triazole-functionalised rotaxane **214** was subjected to the exact same conditions, in all cases the only product obtained was the triazole starting material. These results confirmed that the acrylamide was not a degradation product of the triazole-functionalised rotaxane.

These results suggested that the acrylamide-functionalised rotaxane was obtained by rearrangement of the copper-triazolide intermediate.

A mechanism was proposed for the formation of the acrylamide-functionalised rotaxane *via* a tandem reaction involving the formation of the copper-triazolide intermediate of the AT-CuAAC followed by the rearrangement of this intermediate (Figure 3.36). As highlighted during the investigation, the presence of the hydroxyl function was crucial to trigger the reaction, as well as the presence of the acid. Finally, these two hypothesises suggested that the alcohol was protonated by the acid in order to increase the leaving group character of the oxonium group. The loss of the water molecule generated a resonance stabilised carbocation. Subsequent loss of N_2 with elimination of the C-Cu bond led to the formation of

a cumulated ketenimine species. The cumulated ketenimine then underwent reaction with a water molecule to generate after tautomerisation the observed acrylamide function. The rule of the KF can be proposed to be a source of F^- which can coordinate to the copper and polarised the C-Cu bond, as well as play the role a weak acid for the protonation of the alcohol function rather than the protodemetalation.

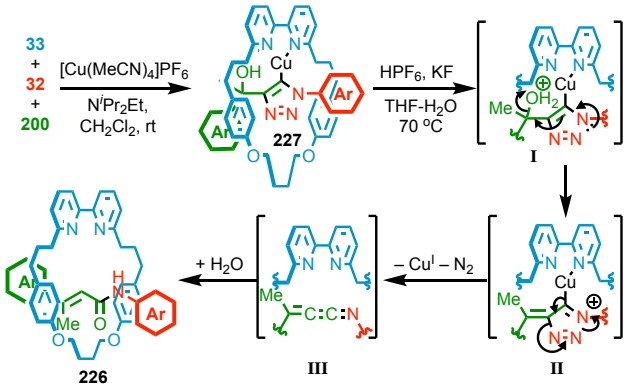

Figure 3.36 Proposed mechanism for the rearrangement process.

Ketenimine species are known to react with water to form an amide (Figure 3.37). Hegarty and co-workers proposed in 1997 that the hydration of the ketenimine in acid condition involved the pre-equilibrium N-protonation followed by the rate determining water attack forming the enol which would tautomerise to the form the amide.[30]

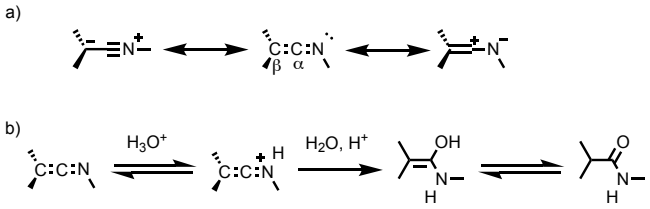

Figure 3.37 a) Resonance forms of ketenimine. b) Hydration of ketenimine under acid condition.

Ren and co-workers reported in 2010 a study for the hydration of ketenimines in non-acidic condition. In these conditions, the oxygen of the water molecule underwent an in-plane attack on the electron-deficient Cα of ketenimine, in addition to having either reversible protonation of the N or the protonation of Cβ.[31] In both conditions, the amide function was generated after tauromerisation. They conducted calculation on the hydration of ketenimine with model involving from one to five water molecules. The result in each case revealed that

the addition was favoured on the C=N bond. However, the calculated energy difference decreased when the number of water molecule increases suggesting that the hydration across the C=C and the C=N was in competition even if the hydration was slightly favoured across the C=N.

3.3. Conclusions and Future Work

We were able to isolate and characterise rotaxane **208**. This rotaxane showed an unexpected acrylamide functional group in the linear unit, which is we believe the first example of the rearrangement of an interlocked structure. High yielding and reproducible conditions were developed to selectively produce either the acrylamide-functionalised rotaxanes or triazole-functionalised rotaxanes.

During the evaluation of the scope of the reaction, the macrocycle variation did not significantly affect the outcome of the reaction. However, the variation of the stoppers influenced the selectivity of the reaction. When the steric hindrance around the copper-triazole unit was reduced by increasing the distance with the stopper unit, the ratio acrylamide:triazole dropped significantly from 100:0 to 25:75. This is directly linked to the stability of the copper-triazolide to the protodemetalation reaction, the more hindered is the system the more stable is the intermediate.

The possibility to observe the rearrangement of a persistent copper-triazolide under the rearrangement conditions suggesting that the organometallic species was the key intermediate to selectively form either the triazole or the acrylamide functionalised rotaxanes.

Although the triazole product of the CuAAC was shown to rearrange when the N^1 was substituted by an electron withdrawing group, the alkynes and azides used during this study do not fit these general substrate classes. We believe that this study is the first example of rearrangement of a triazole moiety not bearing a strongly electron withdrawing group.

The findings presented in this chapter highlights the ability to access products that are not accessible in non-interlocked structures under the same conditions. The possibility to stabilise reactive species with interlocked structure could allow the access to even more complex reaction schemes.

3.4. Experimental

The following compounds were synthesised according to literature procedures:

2-(3,5-di-*tert*-butylphenyl)acetaldehyde **202**,[27] 1-azido-3,5-di-*tert*-butylbenzene **101**,[32] 1-(azidomethyl)-3,5-di-*tert*-butylbenzene **219**,[33] 1-((3-azidopropoxy)methyl)-3,5-di-*tert*-butylbenzene **221**,[34] macrocycles **74**, **103**, **108** and **110**.[35]

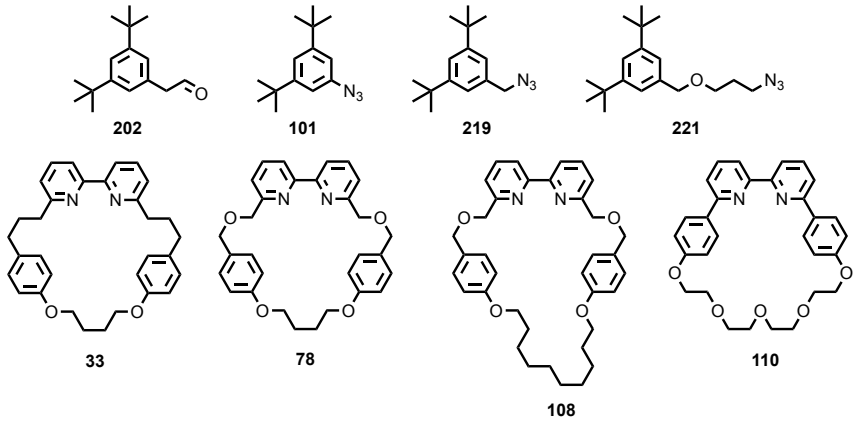

This project was performed, and the results reported herein were obtained in equal collaboration with Ellen Jamieson. Crystals were solved by Ellen Jamieson.

*3,5-Di-tert-butylbenzaldehyde (**195**)*

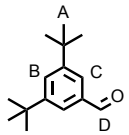

3,5-Di-tert-butyltoluene (6.1 g, 29.9 mmol) was treated with NBS (11.0 g, 62.0 mmol) and AIBN (33.8 mg, 0.2 mmol) in chlorobenzene (150 mL), and stirred for 16 h at 140 °C. The mixture was cooled to room temperature and passed through a Celite plug. The solvent was removed *in vacuo.* The residue was slurried in 20 mL of 1:1 water/ethanol. Hexamethylenetetramine (12.2 g, 86.9 mmol) was added, and the mixture was heated to reflux for 4 h, before being quenched with a toluene/Et_2O mixture (1:1, 130 mL). The organic phase was washed with brine (50 mL), dried ($MgSO_4$), filtered and the solvent removed *in vacuo.* The residue was purified by column chromatography on silica (petrol/Et_2O 95:5) to afford the **195** as white solid (5.0 g, 77%). M.p. 84 - 86 °C. Spectra were consistent with those previously reported.[27] ^{1}H NMR (400 MHz, $CDCl_3$) δ: 10.01 (s, 1H, H_D), 7.75-7.68 (m, 3H, H_B, H_C), 1.37 (s, 18H, H_A). ^{13}C NMR (101 MHz, $CDCl_3$) δ: 193.3, 152.0, 136.3, 129.9, 124.2, 35.2, 31.3.

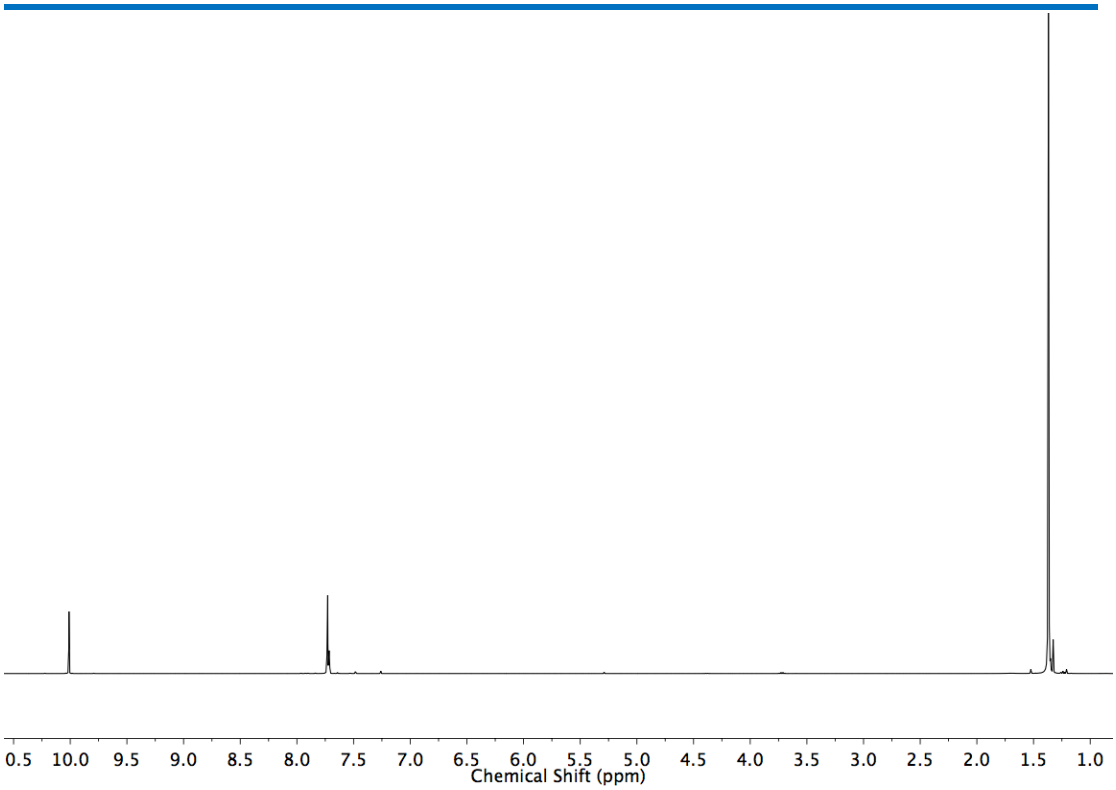

Figure 3.38 ^{1}H NMR ($CDCl_3$, 400 MHz) of **195**.

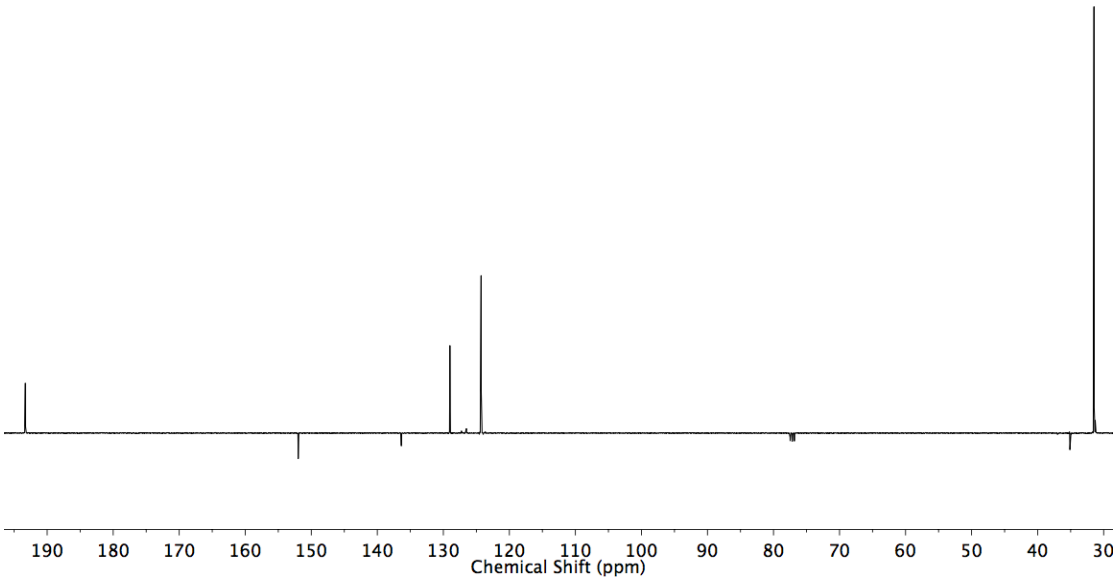

Figure 3.39 JMOD NMR ($CDCl_3$, 101 MHz) of **195**

*1-(3,5-di-tert-butylphenyl)prop-2-yn-1-ol (**192**)*

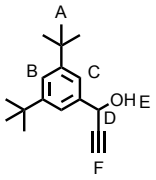

195 (1.4 g, 6.4 mmol) was dissolved in THF (20 mL) at 0 °C under N_2. A solution of ethynylmagnesium chloride (0.6 M, 10 mmol, 16 mL) was added dropwise. The mixture was stirred for 20 h at room temperature. A saturated aqueous NH_4Cl solution (10 mL) was added. The solvent removed *in vacuo*. The residue was extracted with Et_2O (3 x 20 mL). The combined organic layers were washed with brine (10 mL), dried ($MgSO_4$), filtered and the solvent removed *in vacuo.* The residue was purified by column chromatography on silica (petrol/ethyl acetate 9:1) to afford the **192** as light-yellow oil (1.5 g, 97%). ^{1}H NMR (400 MHz, $CDCl_3$) δ: 7.44-7.39 (m, 3H, H_B, H_C), 5.46 (d, *J* =2.2, 1H, H_D), 2.67 (d, *J* =2.2, 1H, H_F), 2.14 (br. s, 1H, H_E), 1.34 (s, 18H, H_A). ^{13}C NMR (101 MHz, $CDCl_3$) δ: 151.2, 139.3, 122.7, 121.0, 84.1, 74.7, 65.1, 35.0, 31.6. HR-EI-MS *m/z* = 244.18118 $M^{+\cdot}$ calc. 244.18217.

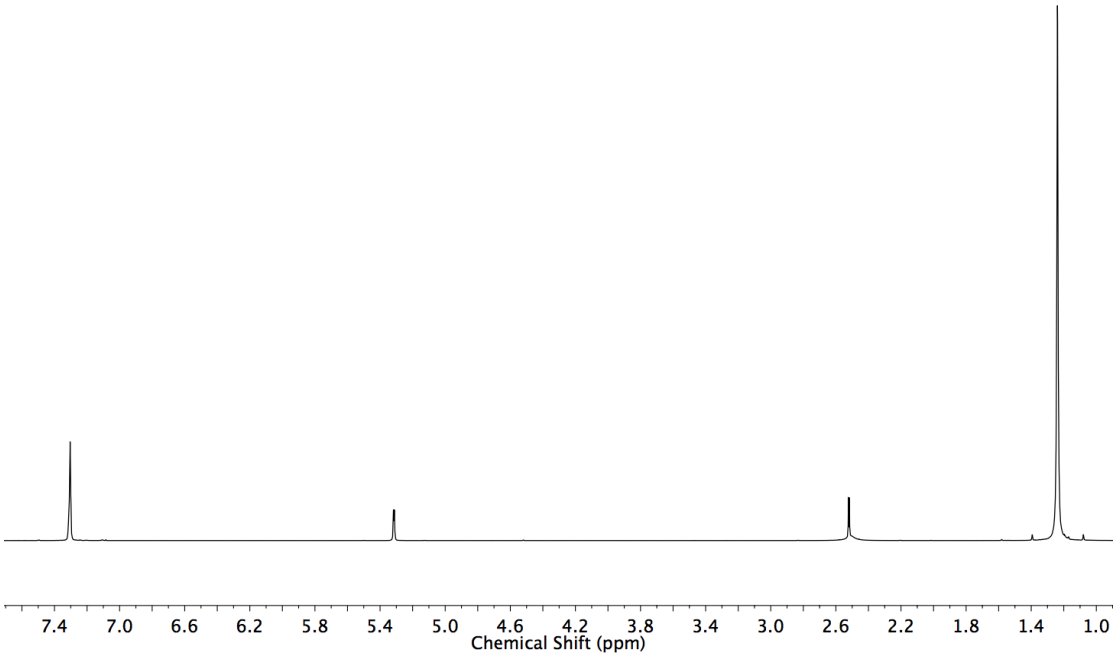

Figure 3.40 ^{1}H NMR ($CDCl_3$, 400 MHz) of **192**.

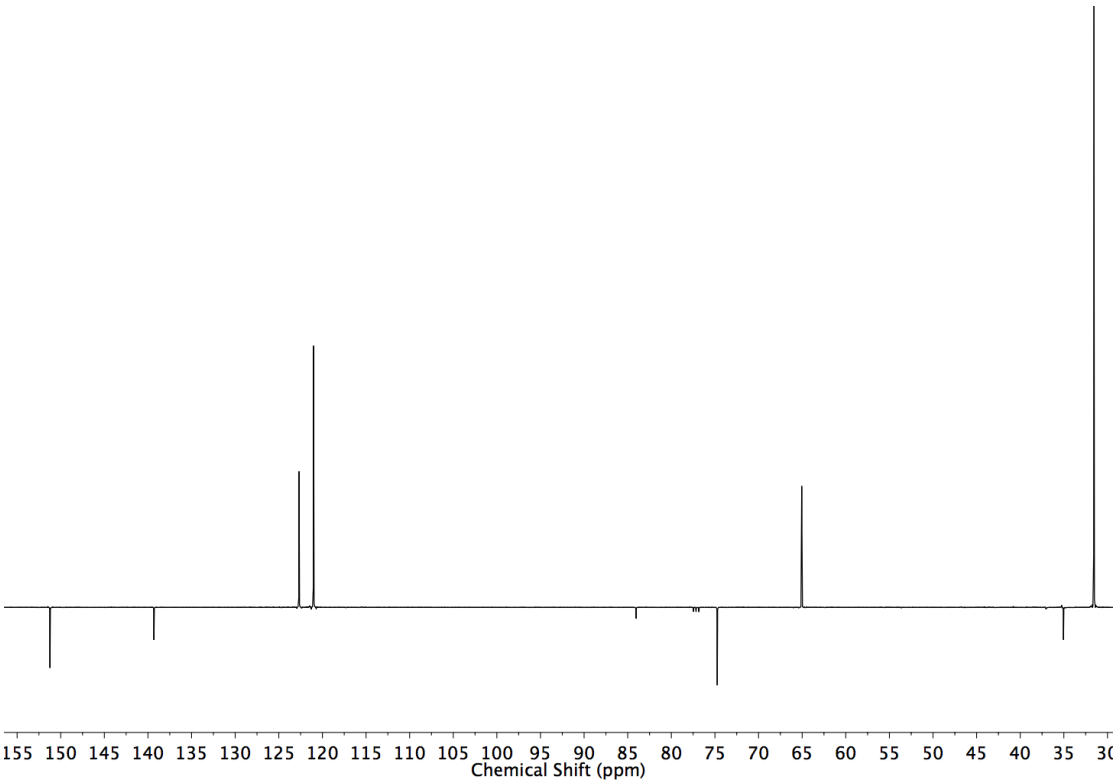

Figure 3.41 JMOD NMR ($CDCl_3$, 101 MHz) of **192**.

*1,3-di-tert-butyl-5-(1-methoxyprop-2-yn-1-yl)benzene (**197**)*

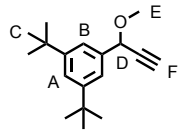

192 (50 mg, 0.2 mmol) was dissolved in THF (1 mL) at 0 °C under N_2. NaH (12 mg, 0.3 mmol) was added in one portion. The mixture was stirred for 10 minutes and iodomethane (26 µL, 0.4 mmol) was added. The mixture was stirred for 3 h at room temperature. A saturated aqueous NH_4Cl solution (5 mL) was added to quench the reaction followed by extraction with Et_2O (3 x 10 mL). The combined organic layers were washed with brine (5 mL), dried ($MgSO_4$), filtered and the solvent removed *in vacuo*. The residue was purified by column chromatography on silica (petrol/Et_2O 95:5) to afford the **197** as yellow oil (52 mg, 98%). ^{1}H NMR (400 MHz, $CDCl_3$) δ: 7.40 (t, *J* =1.8, 1H, H_A), 7.34 (d, *J* =1.8, 2H, H_B), 5.05 (d, *J* =2.2, 1H, H_D), 3.47 (s, 3H, H_E), 2.65 (d, *J* =2.2, 1H, H_F), 1.33 (s, 18H, H_C). ^{13}C NMR (101 MHz, $CDCl_3$) δ: 151.1, 137.1, 122.9, 121.8, 81.9, 75.7, 73.7, 56.3, 35.1, 31.6. HR-EI-MS *m/z* = 258.19835 M^+ calc. 258.19782.

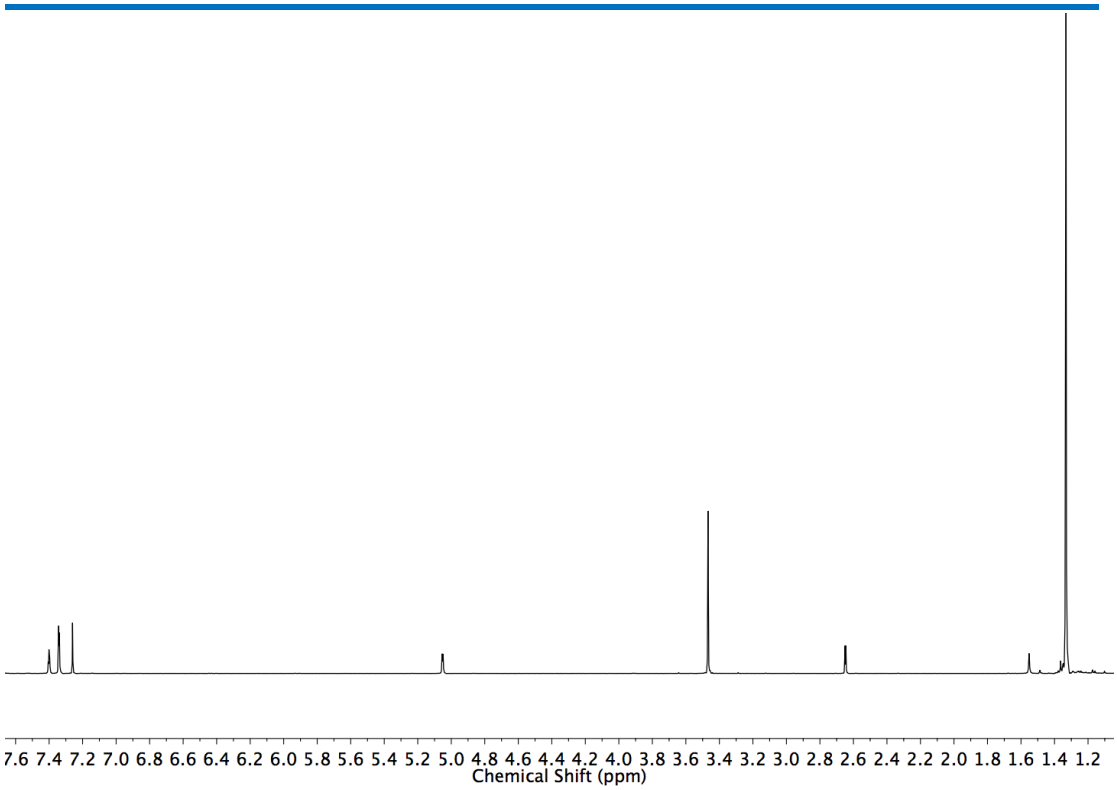

Figure 3.42 ^{1}H NMR ($CDCl_3$, 400 MHz) of **197**.

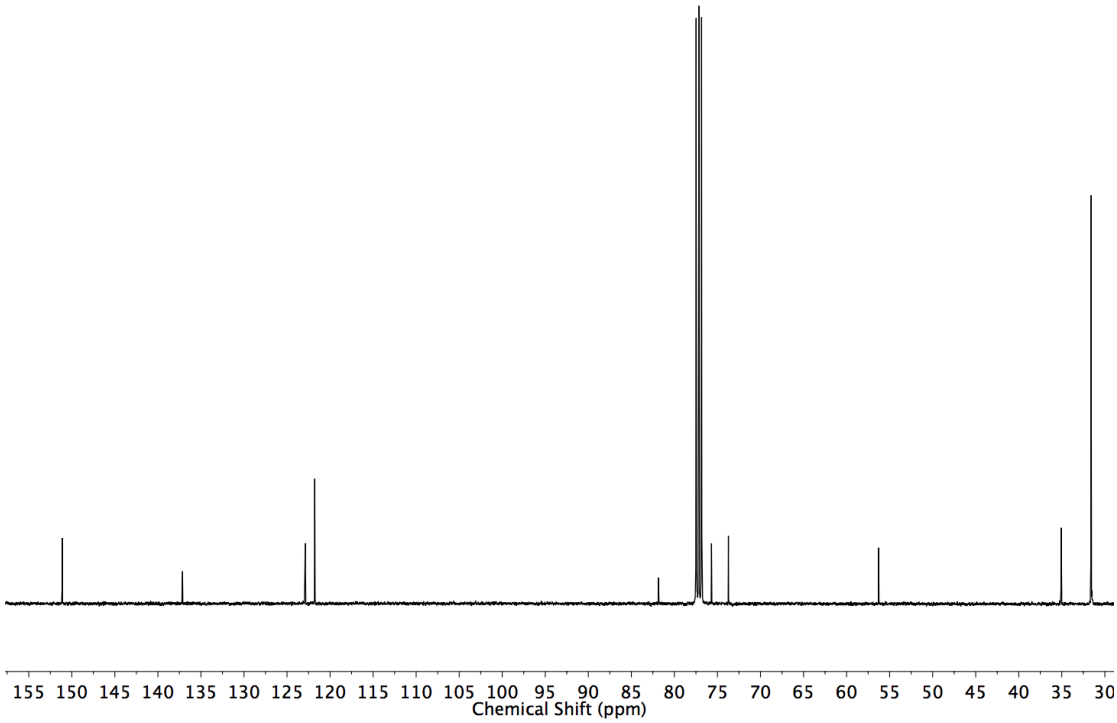

Figure 3.43 ^{13}C NMR ($CDCl_3$, 101 MHz) of **197**.

*1-(3,5-di-tert-butylphenyl)ethan-1-one (**199**)*

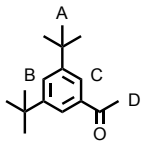

3,5-di-tert-butylbenzoic acid (470 mg, 2 mmol) was dissolved in THF (5 mL) at -78 °C under N_2. A solution of methyl lithium (1.6 M, 2.75 mL, 4.4 mmol) was added dropwise. The mixture was slowly warmed to room temperature and stirred for 30 minutes then a saturated aqueous NH_4Cl solution (10 mL) was added to stop the reaction. The organic product was extracted with petrol (3 x 20 mL), dried ($MgSO_4$), filtered and the solvent removed *in vacuo*. The residue was purified by column chromatography on silica (petrol/ethyl acetate 95:5) to afford **199** as colourless oil (370 mg, 80%). Spectra were consistent with those previously reported.[25] ^{1}H NMR (400 MHz, $CDCl_3$) δ: 7.81 (t, *J* =1.8, 1H, H_B), 7.65 (d, *J* =1.8, 2H, H_C), 2.61 (s, 3H, H_D), 1.36 (s, 18H, H_A). ^{13}C NMR (101 MHz, $CDCl_3$) δ: 199.1, 151.4, 137.0, 127.5, 122.7, 35.1, 31.5, 29.9.

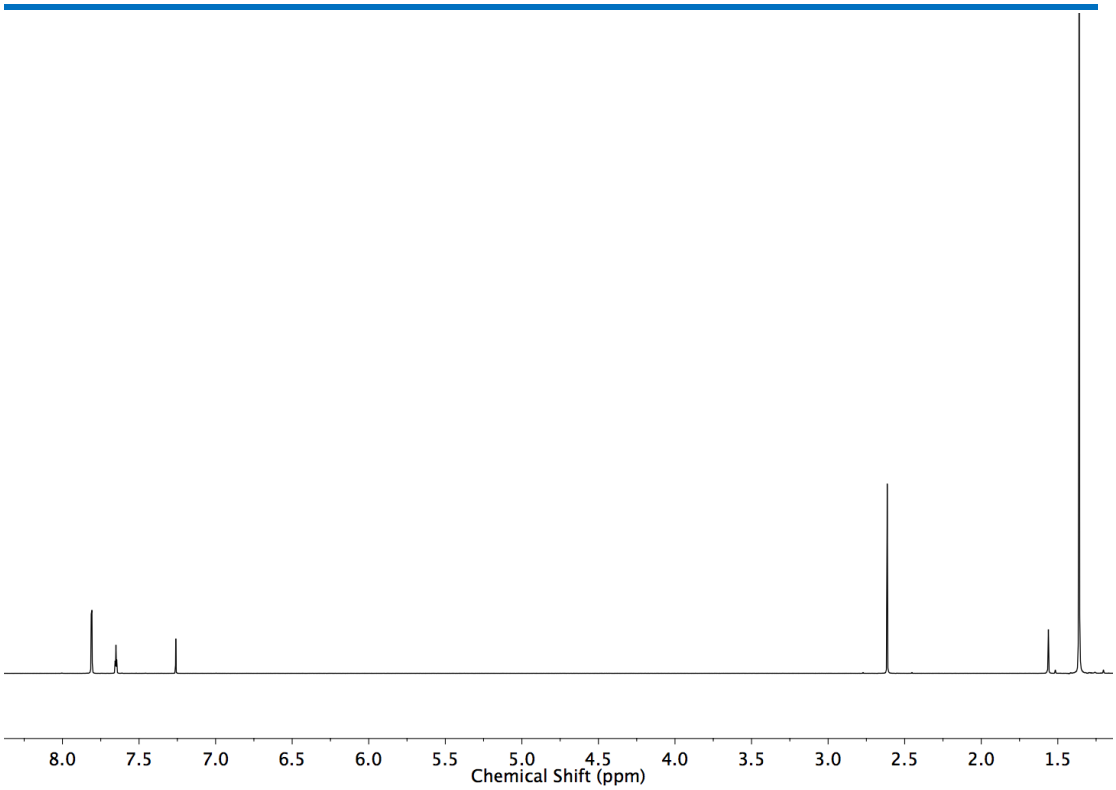

Figure 3.44 ^{1}H NMR ($CDCl_3$, 400 MHz) of **199**.

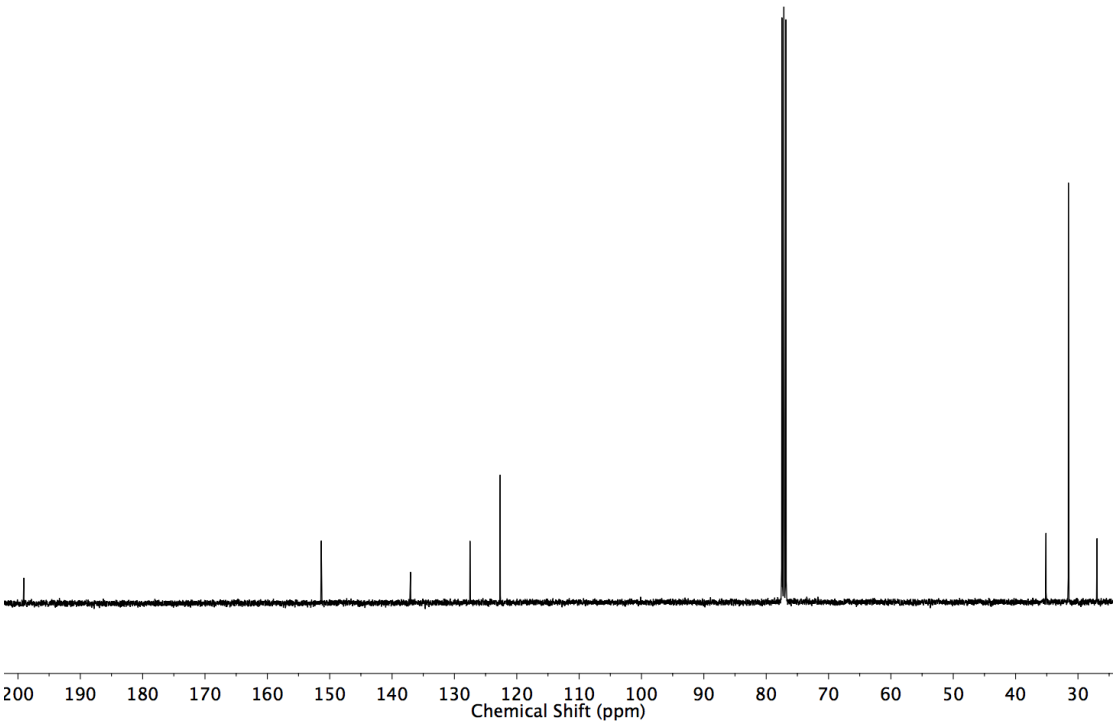

Figure 3.45 ^{13}C NMR ($CDCl_3$, 101 MHz) of **199**.

*2-(3,5-di-tert-butylphenyl)but-3-yn-2-ol (**200**)*

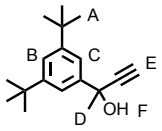

199 (370 mg, 1.6 mmol) was dissolved in THF (3 mL) at 0 °C under N_2. A solution of ethynylmagnesium chloride (0.6 M, 2.4 mmol, 4 mL) was added dropwise. The mixture was stirred for 16 h at room temperature. A saturated aqueous NH_4Cl solution (5 mL) was added. The solvent removed *in vacuo*. The residue was extracted with Et_2O (3 x 20 mL). The combined organic layers were washed with brine (10 mL), dried ($MgSO_4$), filtered and the solvent removed *in vacuo*. The residue was purified by column chromatography on silica (petrol/ethyl acetate 9:1) to afford **200** as colorless oil (200 mg, 48%). ^{1}H NMR (400 MHz, $CDCl_3$) δ: 7.53 (t, *J* =1.8, 1H, H_B), 7.38 (d, *J* =1.8, 2H, H_C), 2.68 (s, 3H, H_D), 2.37 (br. s, 1H, H_F), 1.81 (s, 1H, H_E), 1.35 (s, 18H, H_A). ^{13}C NMR (101 MHz, $CDCl_3$) δ: 150.9, 144.3, 122.1, 119.2, 87.8, 73.0, 70.6, 35.2, 33.3, 31.6. HR-EI-MS *m/z* = 258.19876 M^+ calc. 258.19782.

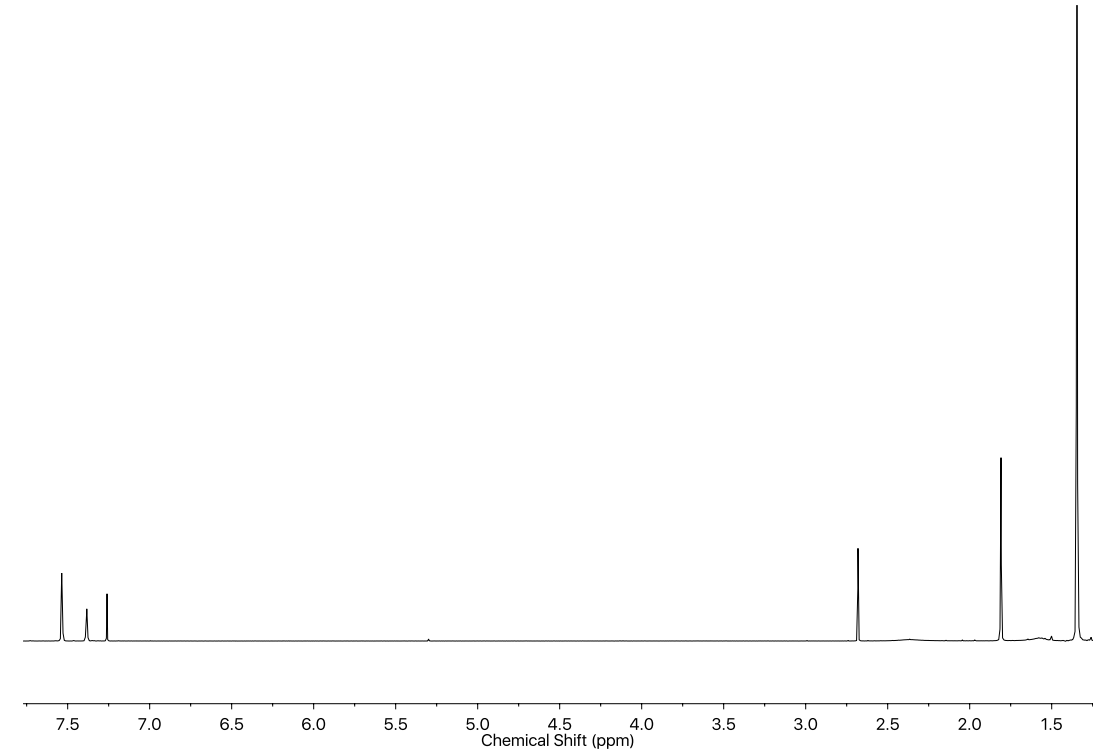

Figure 3.46 ^{1}H NMR ($CDCl_3$, 400 MHz) of **200**.

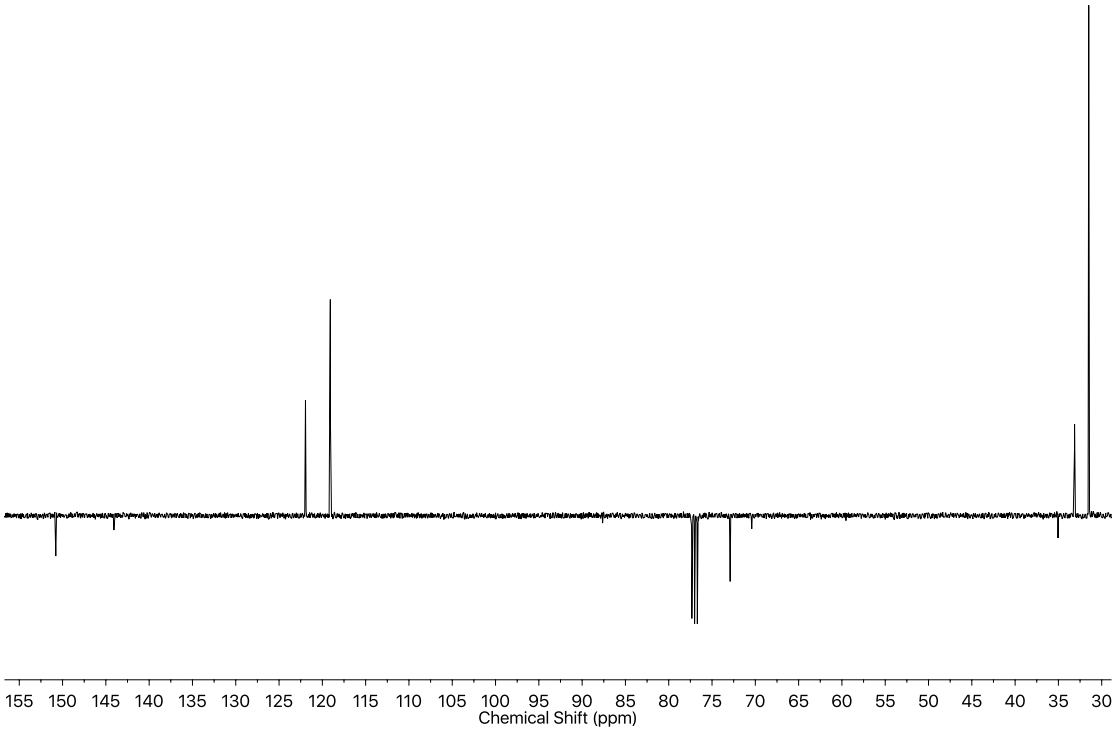

Figure 3.47 JMOD NMR ($CDCl_3$, 101 MHz) of **200**.

*1,3-di-tert-butyl-5-(prop-2-yn-1-yl)benzene (**205**)*

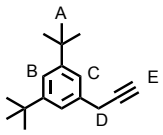

202 (200 mg, 0.86 mmol), dimethyl(1-diazo-2-oxo-propyl)phosphonate (192 mg, 1.00 mmol), and K_2CO_3 (235 mg, 1.7 mmol) were stirred in methanol (2 mL) for 19 h at room temperature. The mixture was diluted with CH_2Cl_2 (10 mL) and filtered. The crude mixture was washed with water (5 mL) and brine (5 mL). The combined aqueous layers were extracted with CH_2Cl_2 (10 mL). The combined organic layers were dried ($MgSO_4$), filtered and the solvent removed *in vacuo.* The residue was purified by column chromatography on silica (petrol) to afford **205** as colorless oil (160 mg, 81%). ^{1}H NMR (400 MHz, $CDCl_3$) δ: 7.31 (t, *J* =1.8, 1H, H_B), 7.20 (d, *J* =1.8, 2H, H_C), 3.60 (d, *J* =2.6, 2H, H_D), 2.18 (t, *J* =2.6, 1H, H_E), 1.33 (s, 18H, H_A). ^{13}C NMR (101 MHz, $CDCl_3$) δ: 151.2, 135.2, 122.3, 120.9, 82.6, 70.4, 35.0, 31.6, 25.3. HR-EI-MS *m/z* = 228.18696 M^+ calc. 228.18725.

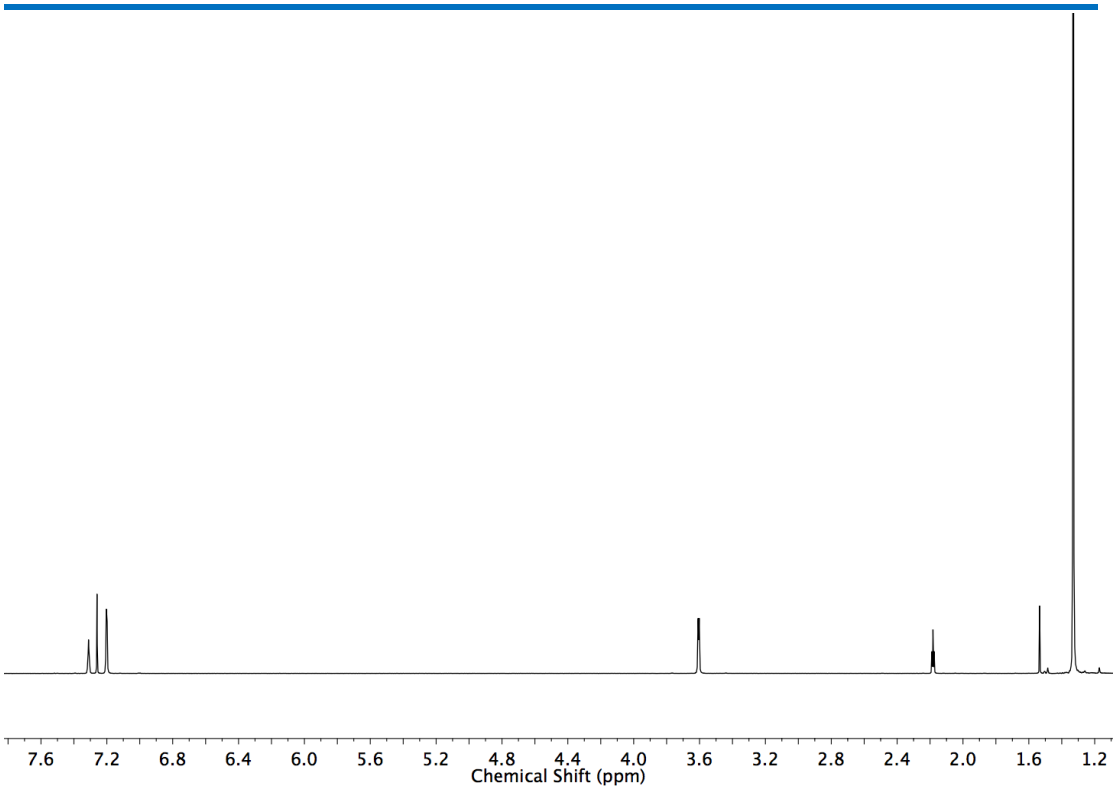

Figure 3.48 ^{1}H NMR ($CDCl_3$, 400 MHz) of **205**.

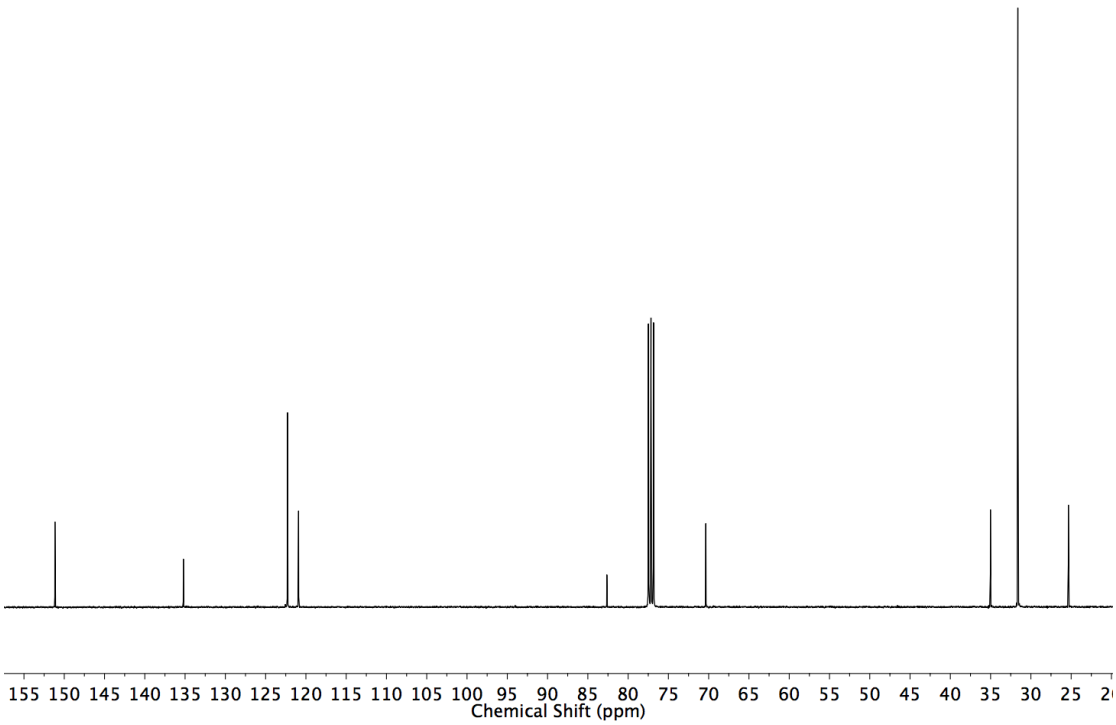

Figure 3.49 ^{13}C NMR ($CDCl_3$, 101 MHz) of **205**.

*1-(3,5-di-tert-butylphenyl)but-3-yn-2-ol (**204**)*

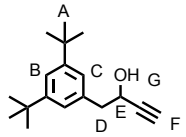

202 (400 mg, 1.7 mmol) was dissolved in THF (3 mL) at 0 °C under N_2. A solution of ethynylmagnesium bromide (0.5 M, 2.0 mmol, 4.0 mL) was added dropwise. The mixture was stirred for 20 h at room temperature. A saturated aqueous NH_4Cl solution (5 mL) was added. The solvent removed *in vacuo*. The residue was extracted with Et_2O (3 x 20 mL). The combined organic layers were washed with brine (10 mL), dried ($MgSO_4$), filtered and the solvent removed *in vacuo.* The residue was purified by column chromatography on silica (petrol/Et_2O 95:5) to afford the **204** as colourless oil (160 mg, 36 %). ^{1}H NMR (400 MHz, $CDCl_3$) δ: 7.33 (t, *J* =1.9, 1H, H_B), 7.13 (d, *J* =1.9, 2H, H_C), 4.58 (app. qd, *J* =6.1, 2.0, 1H, H_E), 3.03 (qd, *J* =16.3, 6.5, 2H, H_D), 2.50 (d, *J* =2.1, 1H, H_F), 1.88 (d, *J* =6.1, 1H, H_G), 1.33 (s, 18H, H_A). ^{13}C NMR (101 MHz, $CDCl_3$) δ: 151.0, 135.1, 124.2, 121.2, 84.6, 73.7, 63.2, 44.6, 34.9, 31.6. HR-EI-MS *m/z* = 258.19765 M^+ calc. 258.19782.

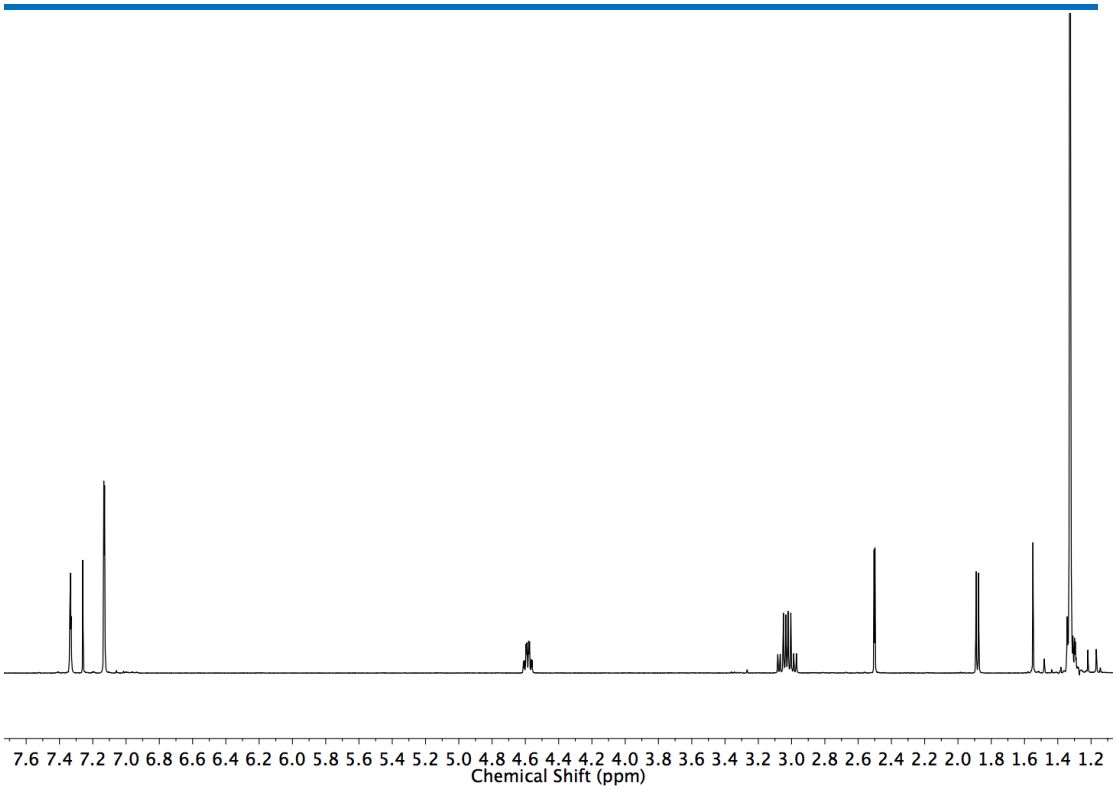

Figure 3.50 ^{1}H NMR ($CDCl_3$, 400 MHz) of **204**.

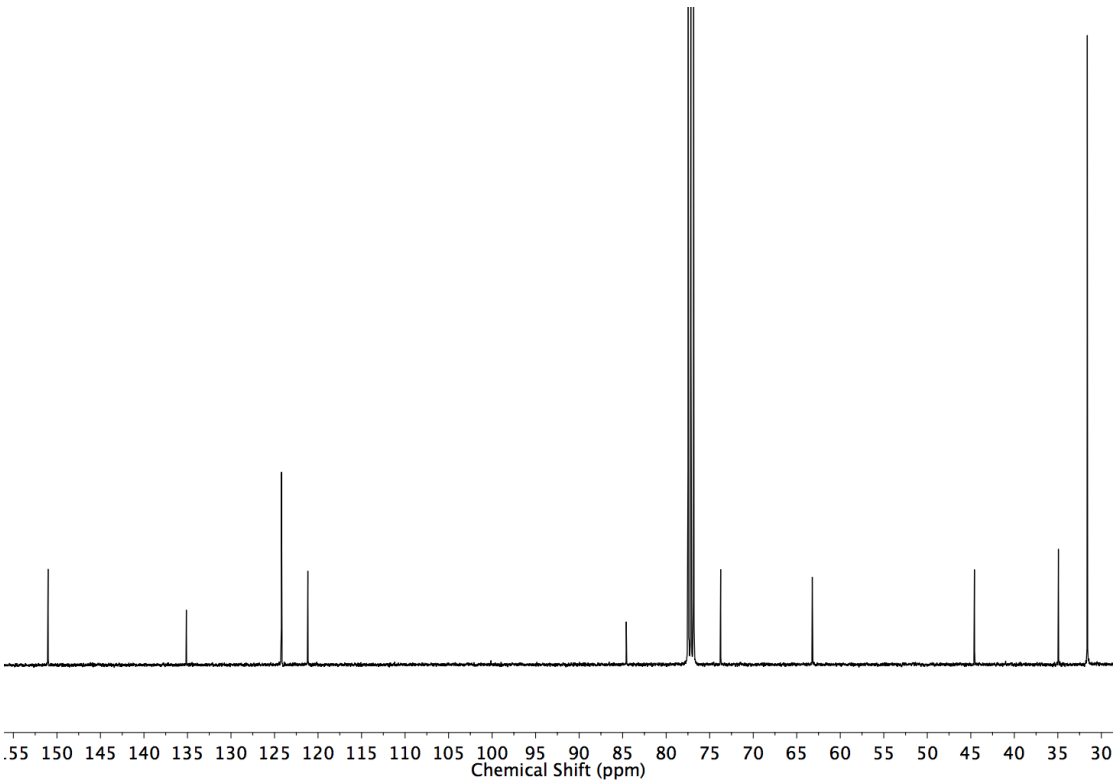

Figure 3.51 ^{13}C NMR ($CDCl_3$, 101 MHz) of **204**.

Synthesis of acrylamide rotaxanes

General Procedure

$KF_{(aq)}$ (0.1M, 0.8 eq.) was added to a solution of **alkyne** (1.2 eq.), **azide** (1.2 eq.), **macrocycle** (1 eq.) and $[Cu(MeCN)_4]PF_6$ (0.96 eq.) in THF (72 mL/mmol) in a microwave vial. The orange mixture was stirred at 70 °C under microwave irradiation for 1 hour. The crude was diluted with CH_2Cl_2 (200 mL/mmol), washed with EDTA-NH_3 solution (100 mL/mmol). The aqueous layer was extracted with CH_2Cl_2 (2 x 100 mL/mmol). Combined organic extracts were washed with brine (100 mL/mmol), dried ($MgSO_4$), filtered and the solvent removed *in vacuo*. Purification by flash column chromatography on silica gel yielded the product.

*Rotaxane **208***

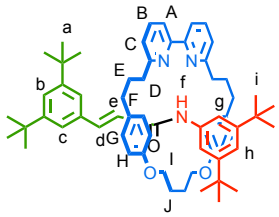

Prepared according to general procedure. **33** (24.0 mg, 0.05 mmol), $[Cu(MeCN)_4]PF_6$ (17.9 mg, 0.048 mmol), **32** (13.8 mg, 0.06 mmol), and **192** (14.6 mg, 0.06 mmol). After purification by column chromatography on silica (petrol with a gradient of 0 to 20% Et_2O) **208** was obtained as a white foam (44.0 mg, 95%). ^{1}H NMR (500 MHz, $CDCl_3$) δ: 9.91 (S, 1H, H_f), 7.65 (t, *J* =7.8, 2H, H_B), 7.49 (dd, *J* =7.8, 1.0, 2H, H_A), 7.23 (t, *J* = 1.8, 1H, H_h), 7.14 – 7.10 (m, 4H, H_g, H_C), 6.94 – 6.92 (m, 3H, H_b, H_c), 6.85 (d, *J* =15.5, 1H, H_d), 6.69 (s, 8H, H_G, H_H), 6.29 (d, *J* =15.5, 1H, H_e), 4.70 - 4.55 (m, 2H, H_I), 4.21 - 4.10 (m, 2H, $H_{I'}$), 2.62 – 2.42 (m, 8H, H_D, H_F), 2.40 – 2.30 (m, 2H, H_J), 2.11 – 2.00 (m, 2H, $H_{J'}$), 1.88 – 1.64 (m, 4H, H_E), 1.23 (s, 18H, H_a), 1.17 (s, 18H, H_i). ^{13}C NMR (126 MHz, $CDCl_3$) δ: 163.8, 163.5, 157.4, 156.8, 150.3, 150.1, 139.6, 139.0, 137.0, 135.9, 132.4, 129.1, 123.3, 122.2, 122.0, 121.8, 119.6, 116.2, 115.0, 114.2, 66.3, 36.6, 35.2, 34.8, 34.8, 31.5, 31.5, 31.3, 25.0. HR-ESI-MS *m/z* = 926.6199 $[M+H]^+$ calc. 926.6194.

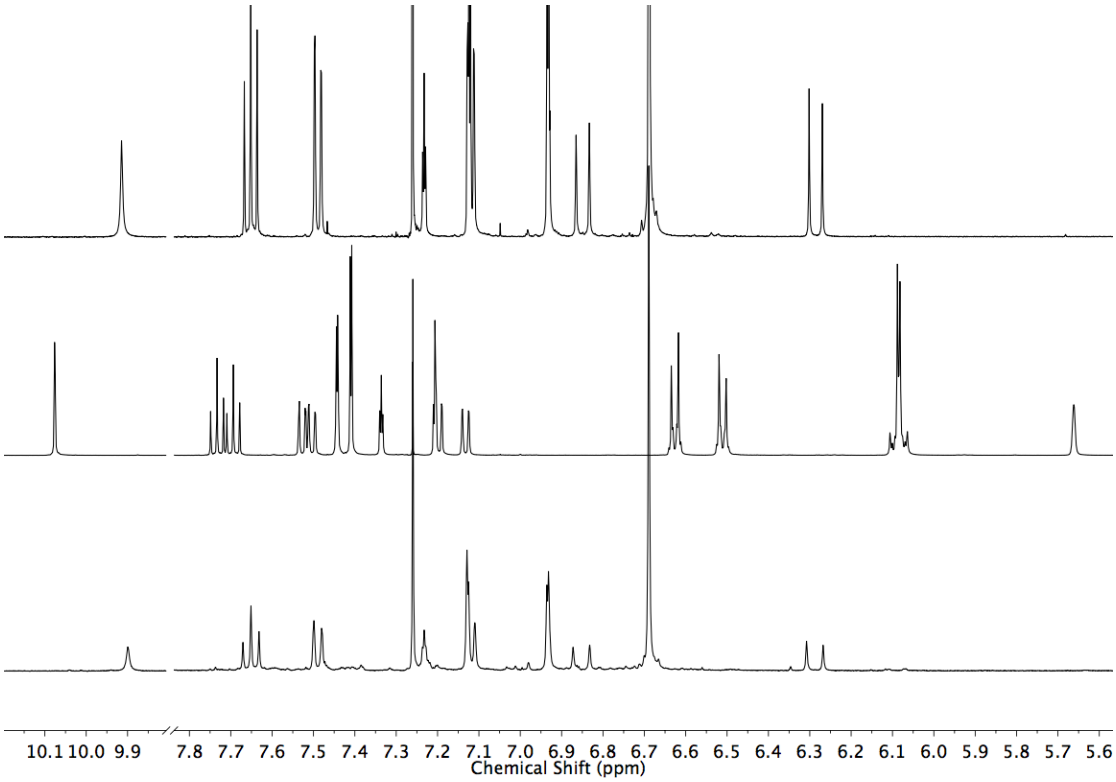

Figure 3.52 Stacked partial ^{1}H NMR (400 MHz, $CDCl_3$) spectra of **208** (top), **206** (middle) and crude reaction mixture (bottom). Ratio of **208**:**206** = 100:0.

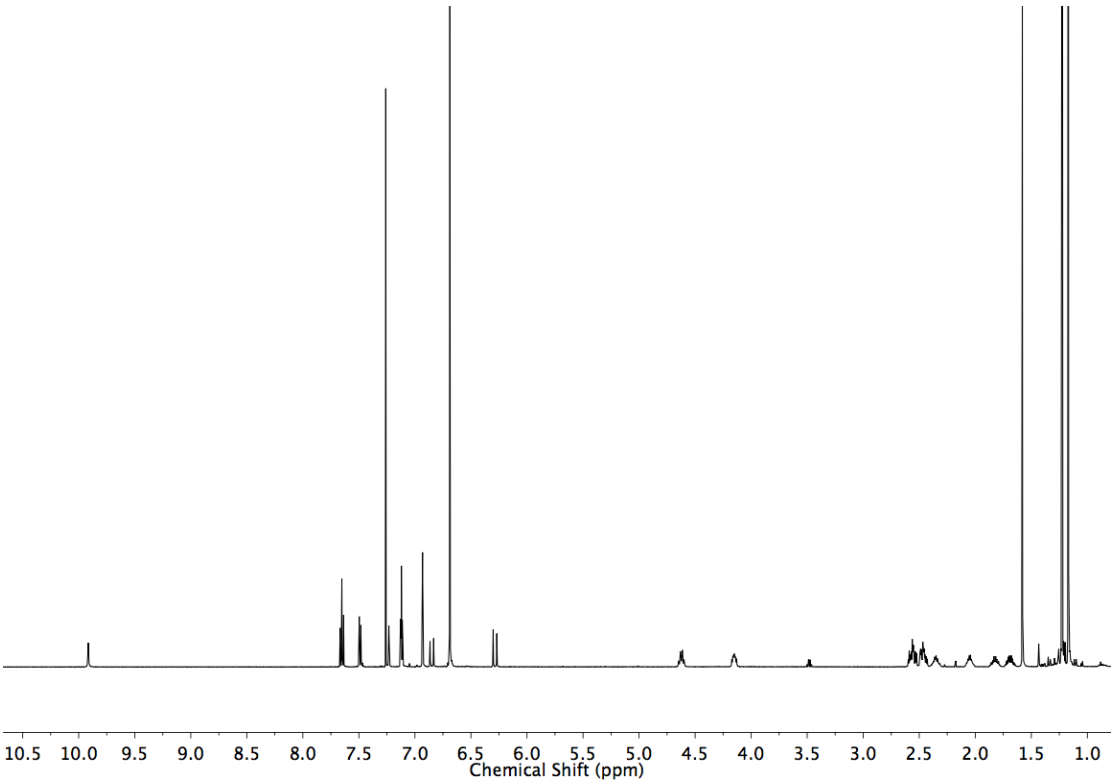

Figure 3.53 ^{1}H NMR ($CDCl_3$, 500 MHz) of **208**

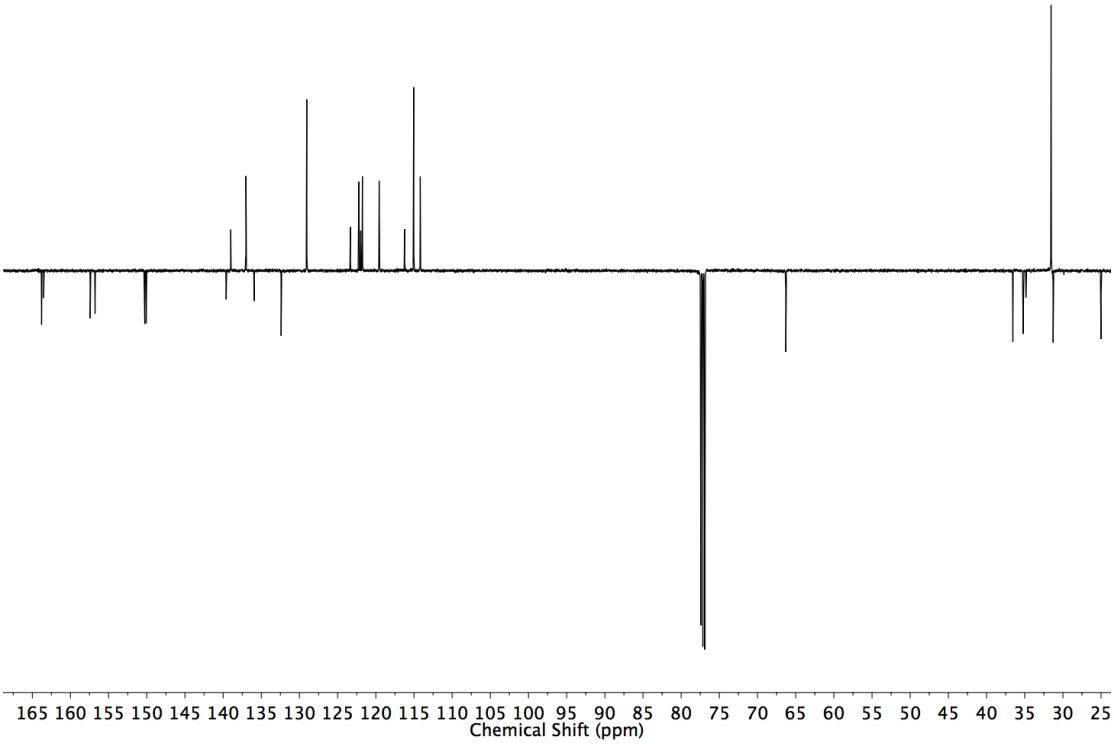

Figure 3.54 JMOD NMR ($CDCl_3$, 126 MHz) of **208**

*Rotaxane **217***

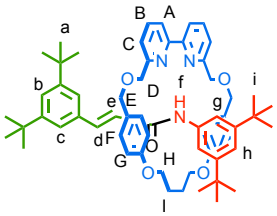

Prepared according to general procedure. **78** (48.3 mg, 0.1 mmol), $[Cu(MeCN)_4]PF_6$ (35.8 mg, 0.096 mmol), **32** (29.3 mg, 0.12 mmol), **192** (27.8 mg, 0.12 mmol). After purification by column chromatography on silica (petrol with a gradient of 0 to 20% Et_2O) **217** was obtained as a white foam (90.0 mg, 97%). ^{1}H NMR (400 MHz, $CDCl_3$) δ: 9.94 (s, 1H, H_f), 7.77 (t, *J* =7.7, 2H, H_B), 7.67 (dd, *J* =7.7, 1.0, 2H, H_A), 7.50 (dd, *J* =7.7, 1.0, 2H, H_C), 7.27 (d, *J* =1.8, 2H, H_g), 7.23 (t, *J* =1.8, 1H, H_b), 6.98 (t, *J* =1.8, 1H, H_h), 6.91 (d, *J* =8.5, 4H, H_F), 6.81 (d, *J* =16.0, 1H, H_d), 6.79 (d, *J* =1.8, 2H, H_c), 6.70 (d, *J* =8.5, 4H, H_G), 5.92 (d, *J* =16.0, 1H, H_e), 4.77 – 4.70 (m, 2H, 2 of H_H), 4.69 (d, *J* =12.0, 2H, 2 of H_D), 4.31 (d, *J* =12.0, 2H, 2 of H_D), 4.19 (d, *J* =13.8, 2H, 2 of H_E), 4.18 – 4.12 (m, 2H, 2 of H_H), 4.02 (d, *J* =13.8, 2H, 2 of H_E), 2.46 – 2.33 (m, 2H, 2 of H_I), 2.11 – 1.99 (m, 2H, 2 of H_I), 1.21 (s, 18H, H_a or H_i), 1.19 (s 18H, H_a or H_i). ^{13}C NMR (101 MHz, $CDCl_3$) δ: 163.3, 160.1, 159.2, 154.9, 150.5, 150.3, 139.6, 139.4, 127.5, 135.6, 129.9, 128.2, 122.9, 122.3, 122.1, 120.8, 119.9, 116.4, 115.1, 114.1, 72.9, 69.5, 66.1, 34.9, 34.8, 31.5, 25.0, 24.8. HR-ESI-MS *m/z* = 930.5763 $[M+H]^+$ calc. 930.5779.

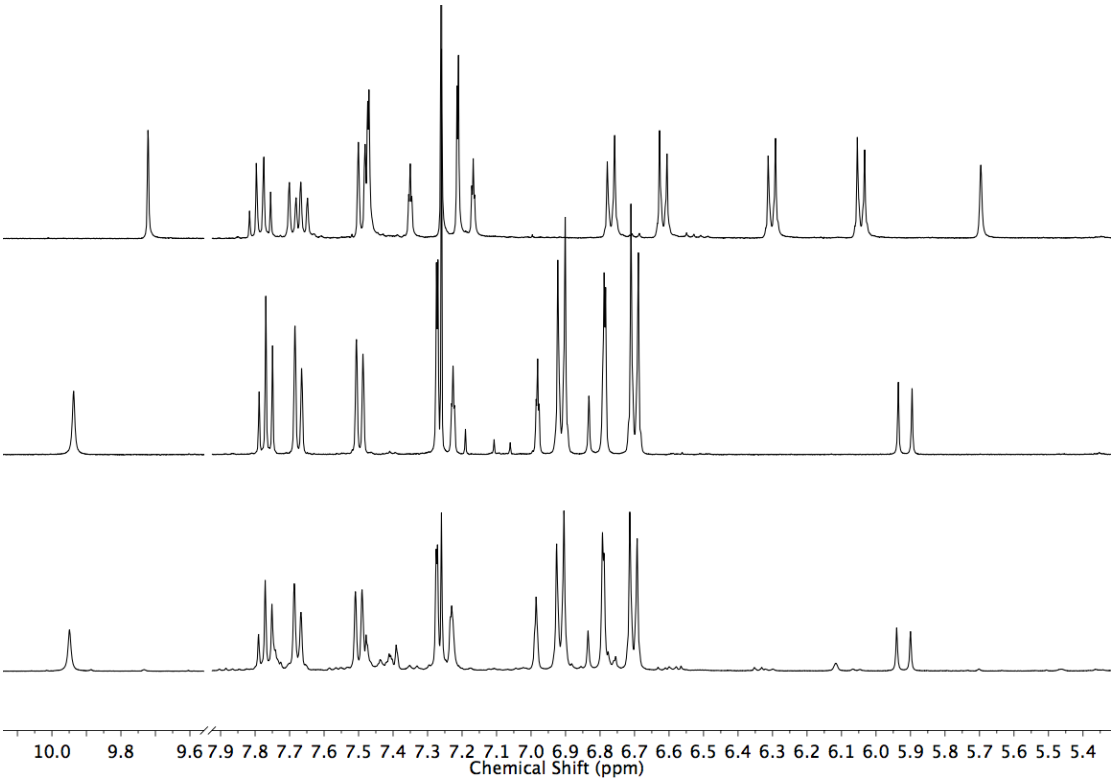

Figure 3.55 Stacked partial ^{1}H NMR (400 MHz, $CDCl_3$) spectra of **209** (top), **217** (middle) and crude reaction mixture (bottom). Ratio of **217**:**209** = 100:0.

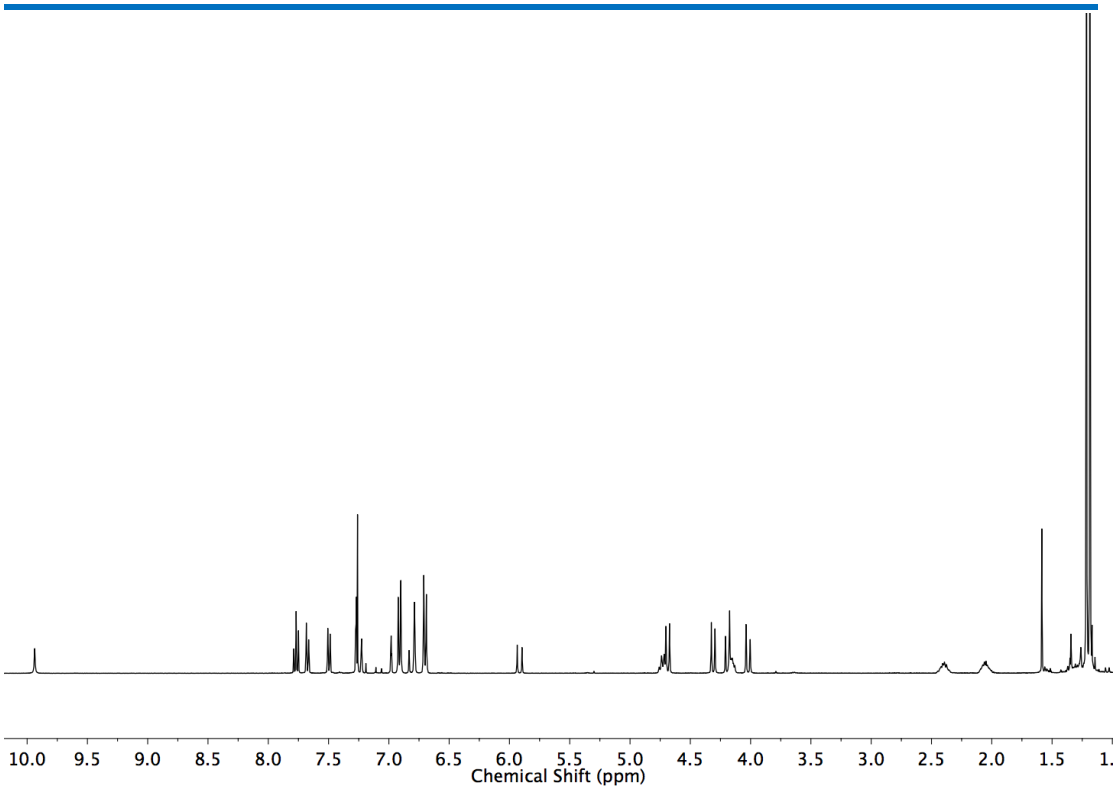

Figure 3.56 ^{1}H NMR ($CDCl_3$, 400 MHz) of **217**

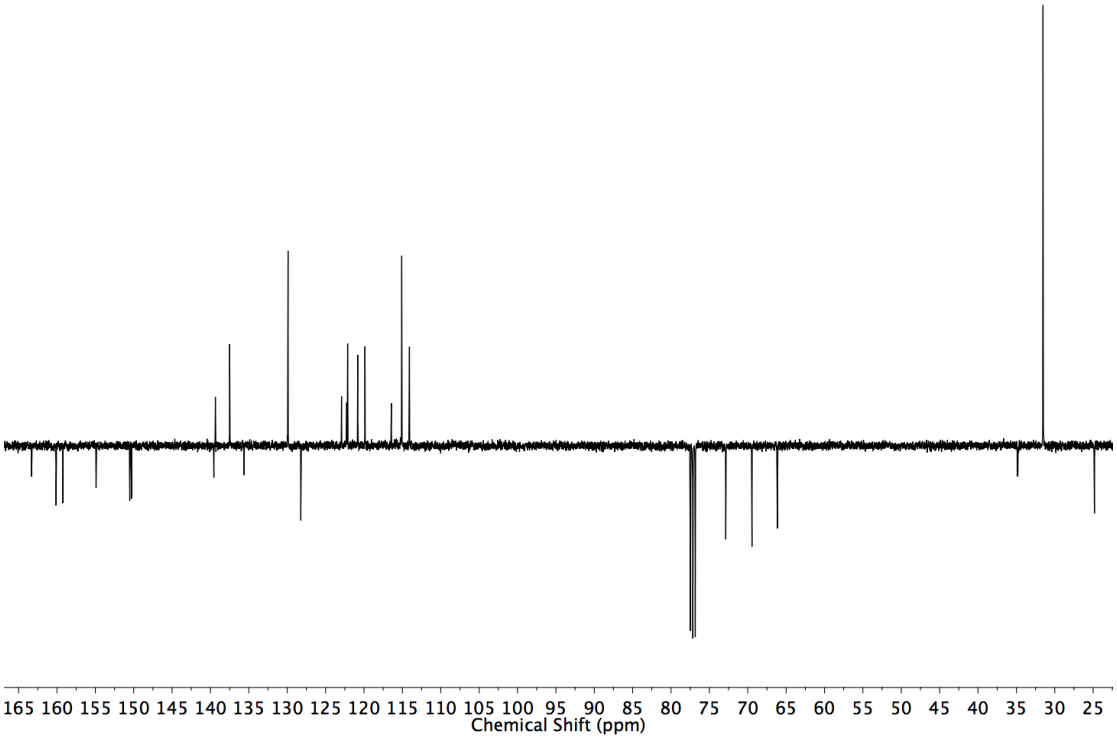

Figure 3.57 JMOD NMR ($CDCl_3$, 101 MHz) of **217**

Rotaxane ***218***

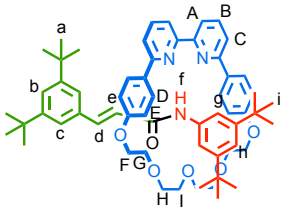

A modification of general procedure was used in which the reaction was stirred at 150 °C for 2 h. **110** (12.5 mg, 0.025 mmol), $[Cu(MeCN)_4]PF_6$ (8.9 mg, 0.024 mmol), **32** (6.9 mg, 0.03 mmol), and **192** (7.3 mg, 0.03 mmol). After purification by column chromatography on silica (petrol with a gradient of 0 to 50% Et_2O) **218** was obtained as a white foam (11.8 mg, 50%). ^{1}H NMR (500 MHz, $CDCl_3$) δ: 9.78 (s, 1H, H_f), 7.90 (t, t, *J* =7.8, 2H, H_B), 7.80 (dd, *J* =7.8, 0.9, 2H, H_A), 7.57 (dd, *J* =7.8, 0.9, 2H, H_C), 7.42 (d, *J* =8.5, 4H, H_D), 7.30 (t, *J* =1.8, 1H, H_b), 7.27 (d, *J* =16.0, H_d), 7.06 (d, *J* =1.8, 2H, Hc), 6.90 (apps, 3H, H_g, H_h), 6.63 (d, *J* =8.5, 4H, H_E), 6.46 (d, *J* =16.0, 1H, H_e), 4.26 – 4.14 (m, 4H, H_F), 3.96 – 3.64 (m, 12H, H_G, H_H, H_I), 1.33 (s, 18H, H_a), 1.12 (s, 18H, H_h). ^{13}C NMR (126 MHz, $CDCl_3$) δ: 163.6, 159.9, 158.9, 157.2, 150.6, 150.2, 138.7, 138.5, 137.7, 135.5, 132.4, 129.4, 124.3, 122.8, 122.1, 120.5, 119.6, 116.7, 115.1, 113.6, 70.3, 70.1, 68.3, 66.9, 34.9, 34.7, 31.5 (×2). HR-ESI-MS *m/z* = 946.5712 $[M+H]^+$ calc. 946.5729.

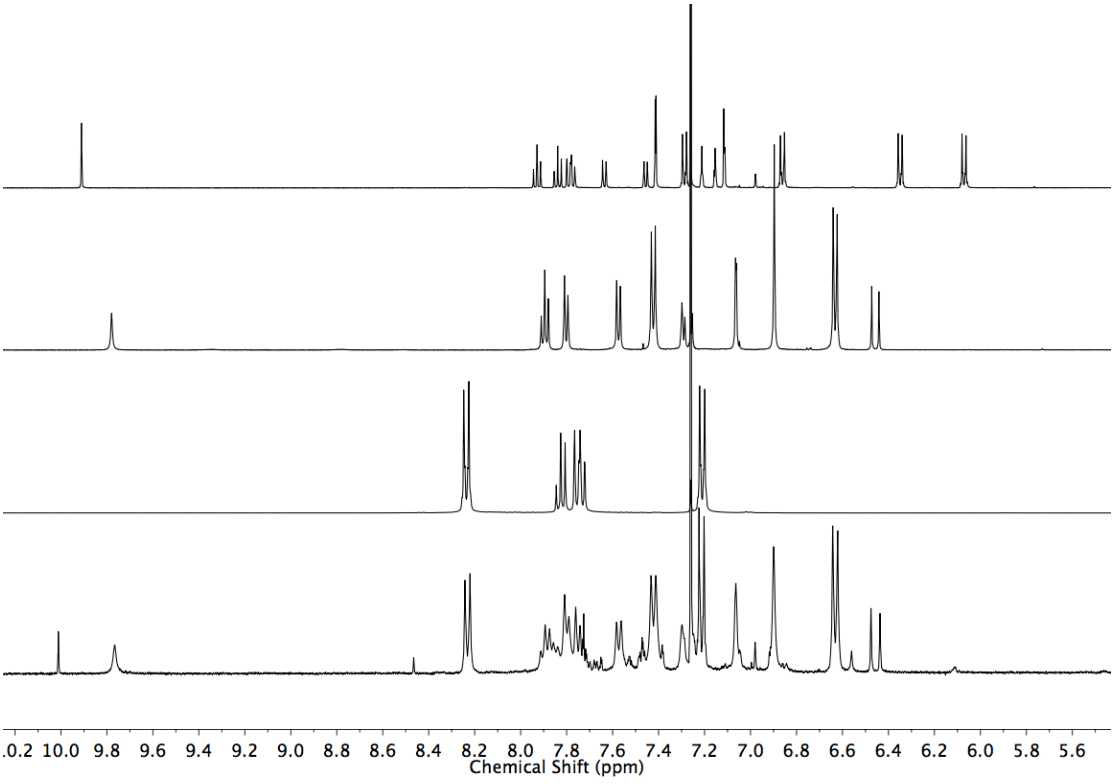

Figure 3.58 Stacked partial ^{1}H NMR (400 MHz, $CDCl_3$) spectra of **210** (top), **218** (upper middle), macrocycle **110** (lower middle) and crude reaction mixture (bottom). Ratio of **218**:oxidised product of **210** = 80:20.

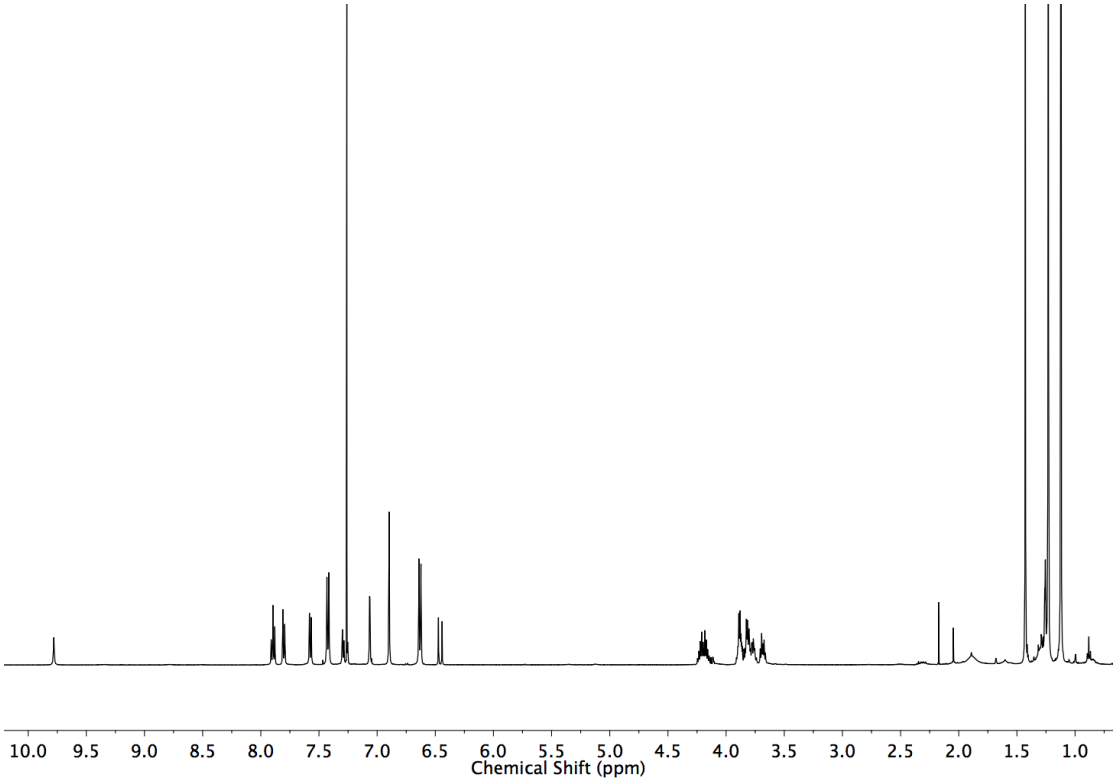

Figure 3.59 ^{1}H NMR ($CDCl_3$, 500 MHz) of **218**

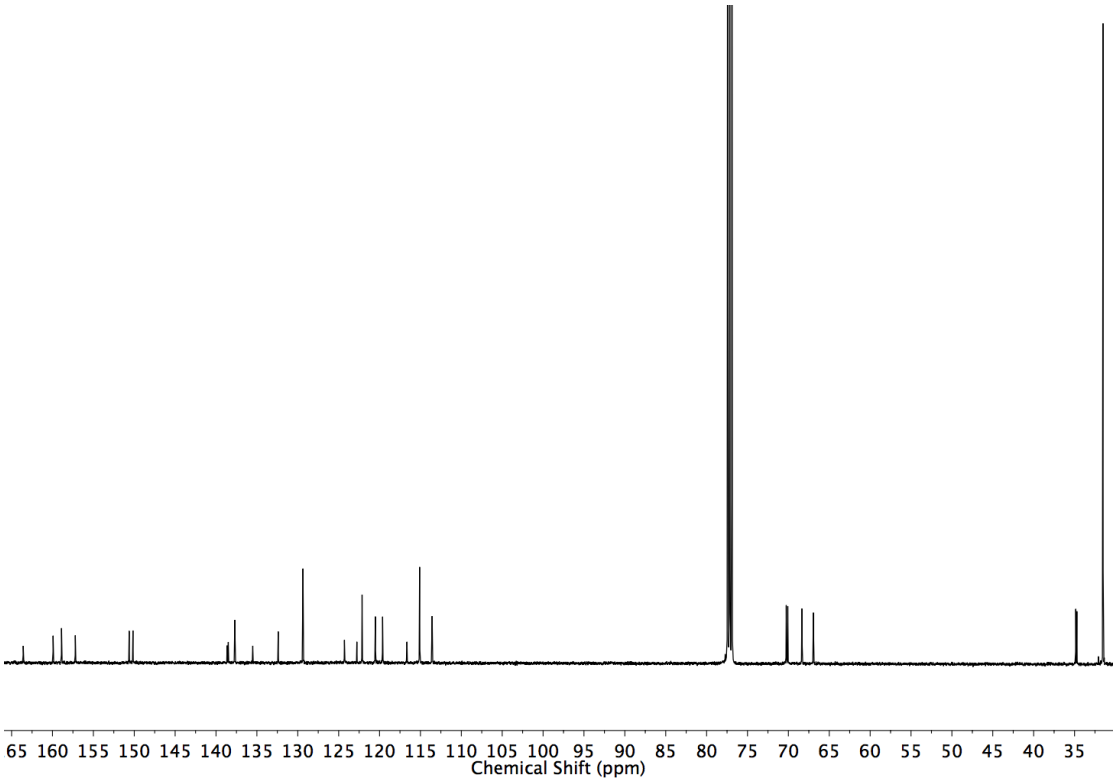

Figure 3.60 ^{13}C NMR ($CDCl_3$, 126 MHz) of **218**

*Rotaxane **220***

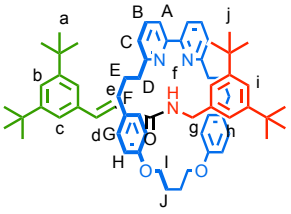

Prepared according to general procedure. **33** (12.0 mg, 0.025 mmol), $[Cu(MeCN)_4]PF_6$ (8.9 mg, 0.024 mmol), **219** (7.3 mg, 0.03 mmol), and **192** (7.3 mg, 0.03 mmol). After purification by column chromatography on silica (petrol with a gradient of 0 to 20% Et_2O) **220** was obtained as a white foam (16.0 mg, 68 %). ^{1}H NMR (500 MHz, $CDCl_3$) δ: 8.77 (t, *J* =4.8, 1H, H_f), 7.60 (t, *J* =7.8, 2H, H_B), 7.44 (dd, *J* =7.8, 1.0, 2H, H_A), 7.21 (t, *J* =1.8, 1H,H_b), 7.19 (d, *J* =16.0, 1H, H_d), 7.07 (dd, *J* =7.8, 1.0, 2H, H_C), 7.04 (j, *J* =1.9, 1H, H_i), 6.88 (d, *J* =1.9, 2H, H_c), 6.79 (s, 8H, H_G, H_H), 6.77 (d, *J* =1.8, 2H, H_h), 6.35 (d, *J* =16.0, 1H, H_e), 4.33 – 4.23 (m, 4H, H_I), 3.41 (d, *J* =4.8, 2H, H_g), 2.61 – 2.47 (m, 4H, H_F), 2.46 – 2.34 (m, 4H, H_D), 2.17 – 2.10 (m, 4H, H_J), 1.83 – 1.70 (m, 4H, H_E), 1.16 (s, 18H, H_a), 1.06 (s, 18H, H_j). ^{13}C NMR (126 MHz, $CDCl_3$) δ: 165.4, 163.6, 157.3, 156.5, 150.4, 149.8, 137.6, 137.2, 136.9, 135.7, 132.6, 129.4, 123.2, 122.9, 122.3, 121.9, 121.9, 120.5, 119.5, 115.2, 66.6, 44.2, 36.5, 35.2, 34.8, 34.7, 31.5, 31.4, 31.4, 25.0; HR-ESI-MS *m/z* = 940.6351 $[M+H]^+$ calc. 940.6351.

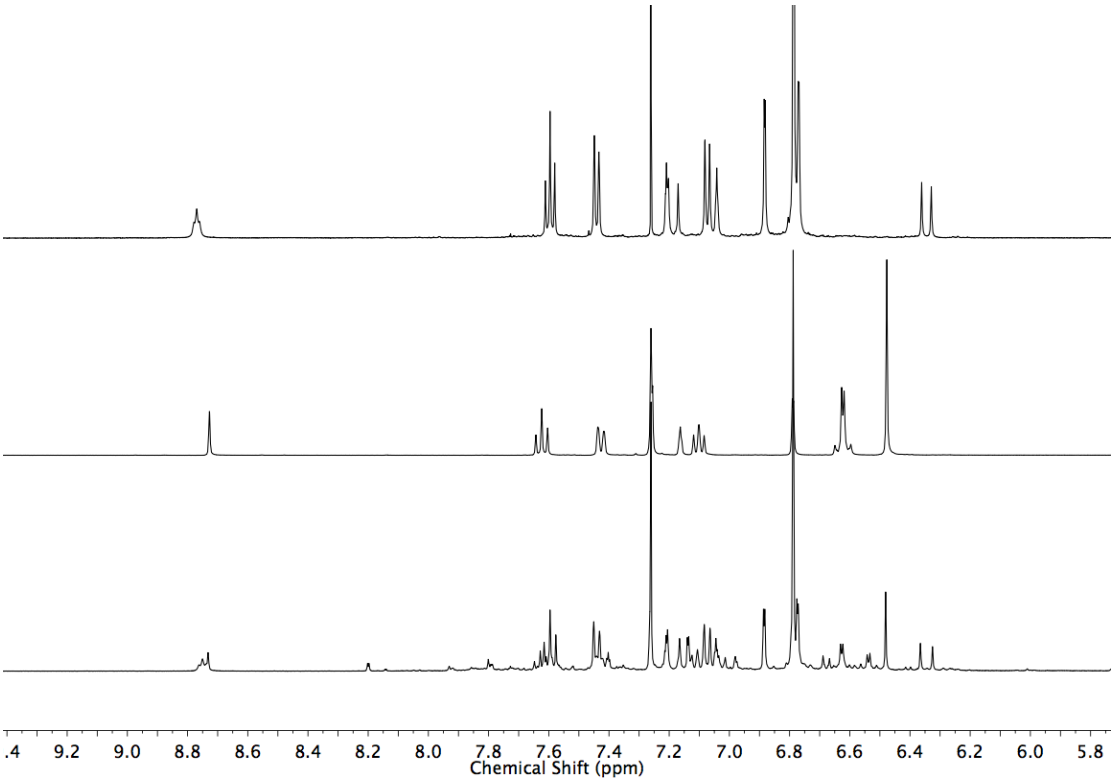

Figure 3.61 Stacked partial ^{1}H NMR (400 MHz, $CDCl_3$) spectra of **220** (top), **211** (middle) and crude reaction mixture (bottom). Ratio of **220**:**211** = 75:25.

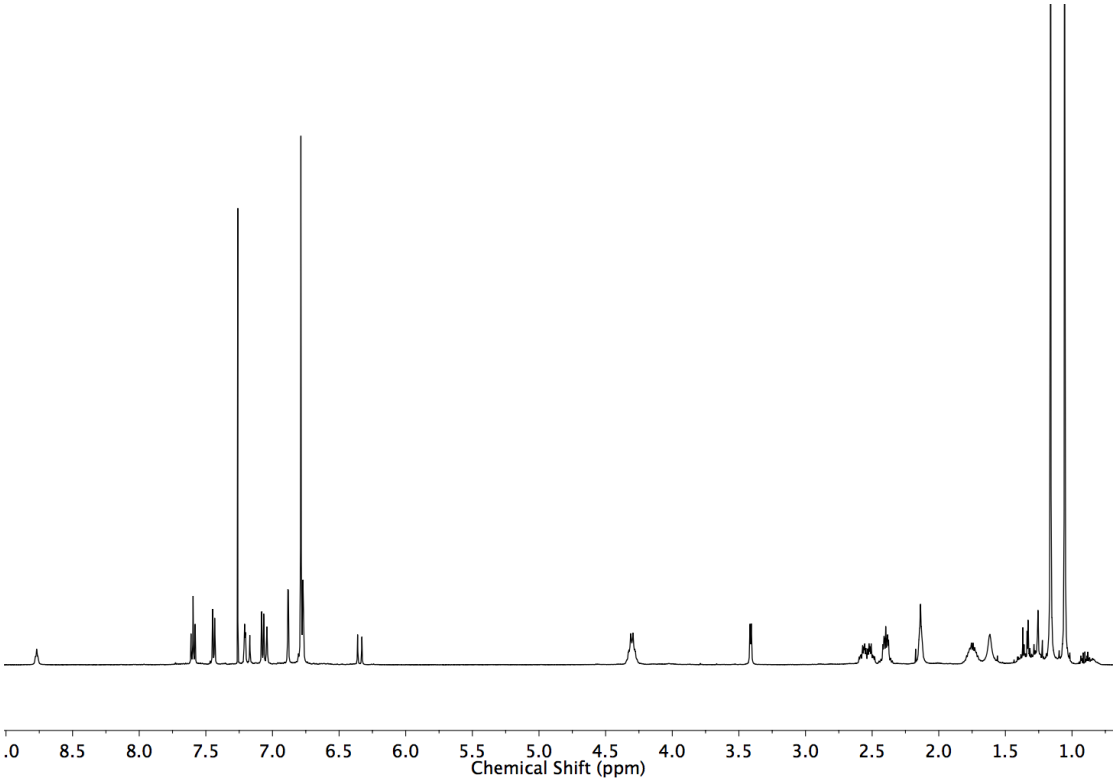

Figure 3.62 ^{1}H NMR ($CDCl_3$, 500 MHz) of **220**

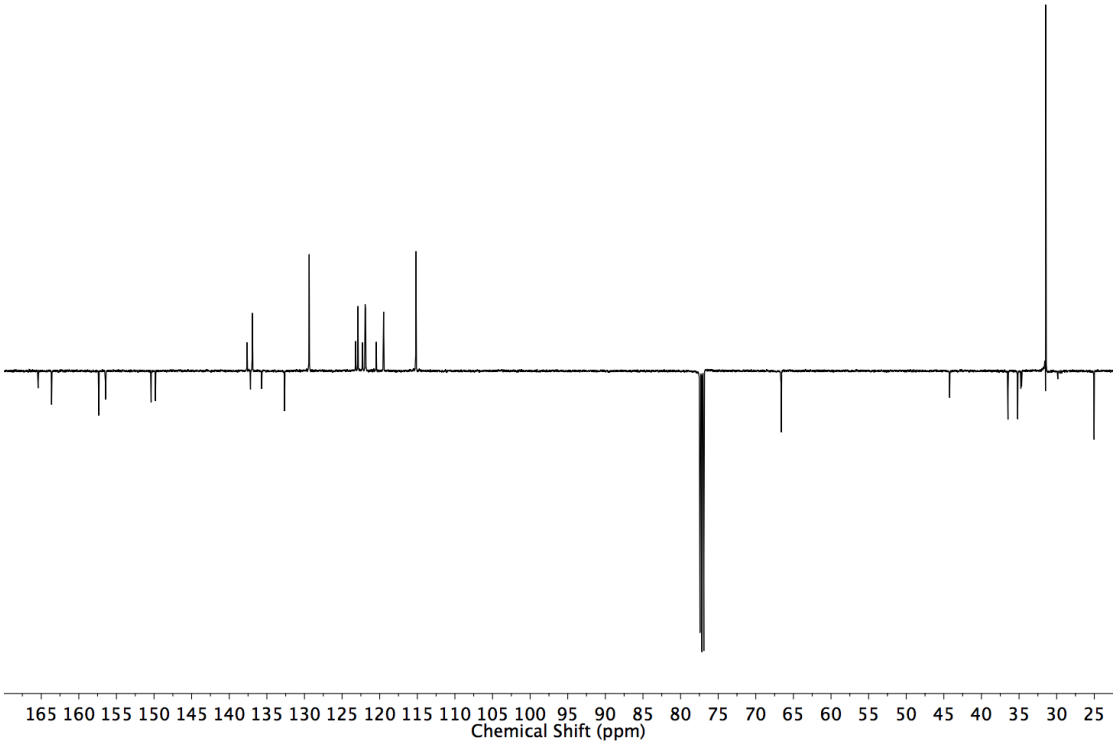

Figure 3.63 JMOD NMR ($CDCl_3$, 126 MHz) of **220**

Rotaxane ***222***

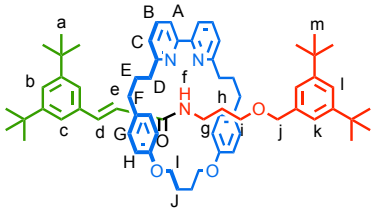

Prepared according to general procedure. **33** (12.0 mg, 0.025 mmol), $[Cu(MeCN)_4]PF_6$ (8.9 mg, 0.024 mmol), **221** (9.1 mg, 0.03 mmol), and **192** (7.3 mg, 0.03 mmol). After purification by column chromatography on silica (petrol with a gradient of 0 to 50% Et_2O) **222** was obtained as a colourless oil (4.0 mg, 16 %). ^{1}H NMR (500 MHz, $CDCl_3$) δ: 8.43 (t, *J* =5.4, 1H, H_f), 7.65 (t, *J* =7.8, 2H, H_B), 7.48 (dd, *J* =7.8, 0.9, 2H, H_A), 7.31 (t, *J* =1.9, 1H, H_l), 7.27 (d, *J* =16.0, 1H, H_d), 7.23 (t, *J* =1.9, 1H, H_b), 7.18 (dd, *J* =7.8, 0.9, 2H, H_C), 7.02 (d, *J* =1.9, 2H, H_k), 6.92 (d, *J* =1.9, 2H, H_c), 6.90 (d, *J* =8.5, 4H, H_G), 6.82 (d, *J* =8.5, 4H, H_F), 6.32 (d, *J* =16.0, 1H, H_e), 4.29 – 4.13 (m, 4H, H_I), 4.08 (s, 2H, H_j), 3.02 (t, *J* =7.2, 2H, H_i), 2.70 – 2.53 (m, 8H, H_D, H_F), 2.29 – 2.23 (m, 2H, H_g), 2.18 – 1.99 (m, 4H, H_J), 1.97 – 1.75 (m, 4H, H_E), 1.30 (s, 18H, H_a), 1.16 (s, 18H, H_m), 0.97 (t, *J* =7.8, 2H, H_h). ^{13}C NMR (126 MHz, $CDCl_3$) δ: 165.4, 163.5, 157.5, 156.6, 150.7, 150.6, 137.9, 137.8, 137.1, 135.5, 132.8, 129.6, 123.2, 122.6, 122.1, 121.9, 121.9, 121.7, 119.8, 115.1, 73.5, 68.8, 66.5, 36.6, 35.5, 35.3, 34.9, 34.8, 31.6, 31.5, 31.4, 28.8, 25.0. HR-ESI-MS *m/z* = 998.6749 $[M+H]^+$ calc. 998.6769.

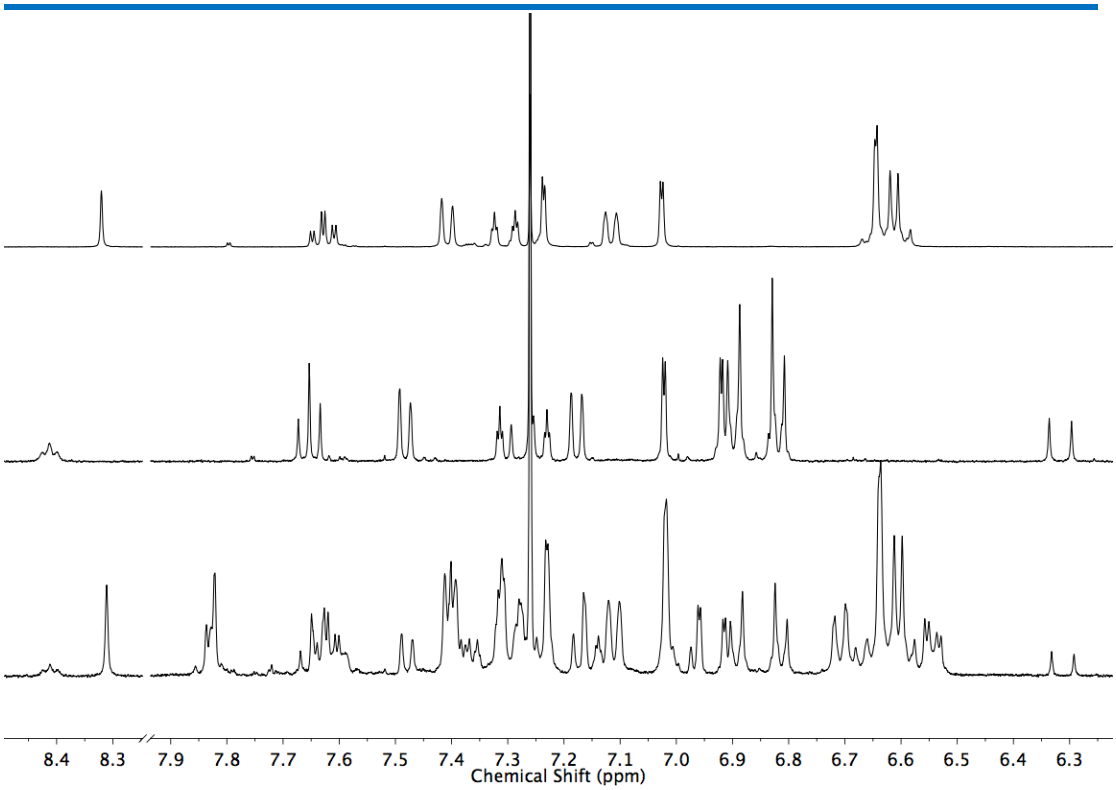

Figure 3.64 Stacked partial ^{1}H NMR (400 MHz, $CDCl_3$) spectra of **212** (top), **222** (middle) and crude reaction mixture (bottom). Ratio of **222**:**212** = 35:65.

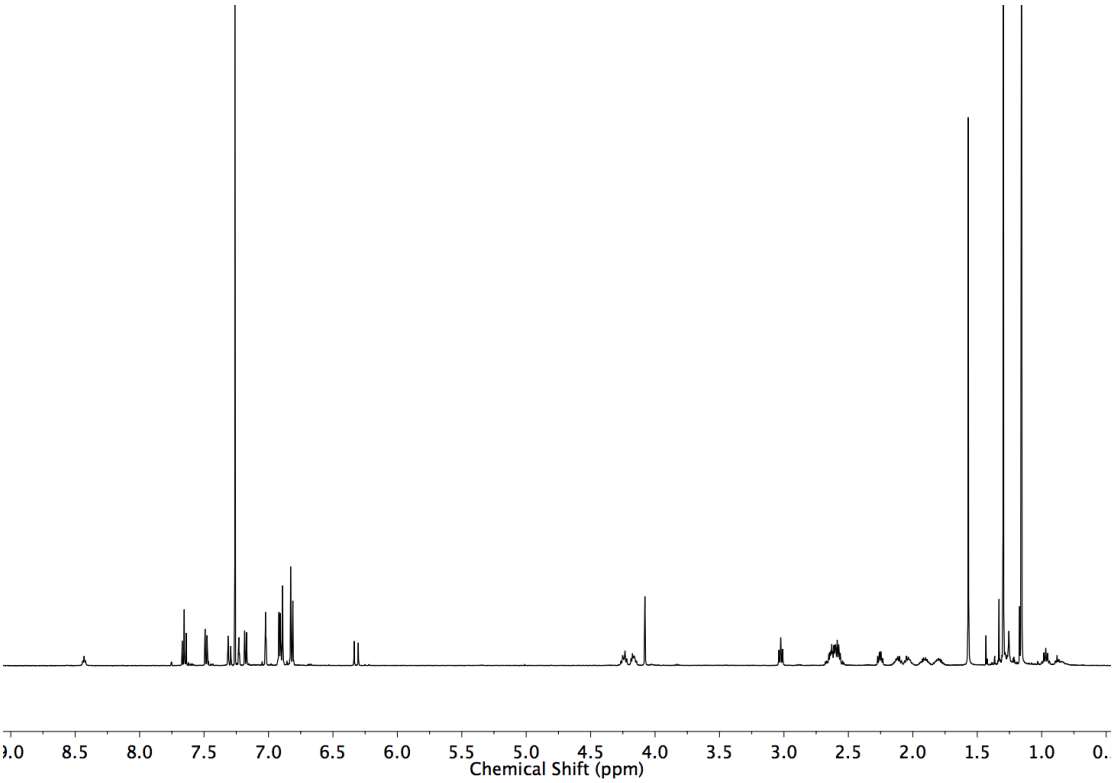

Figure 3.65 ^{1}H NMR ($CDCl_3$, 500 MHz) of **222**

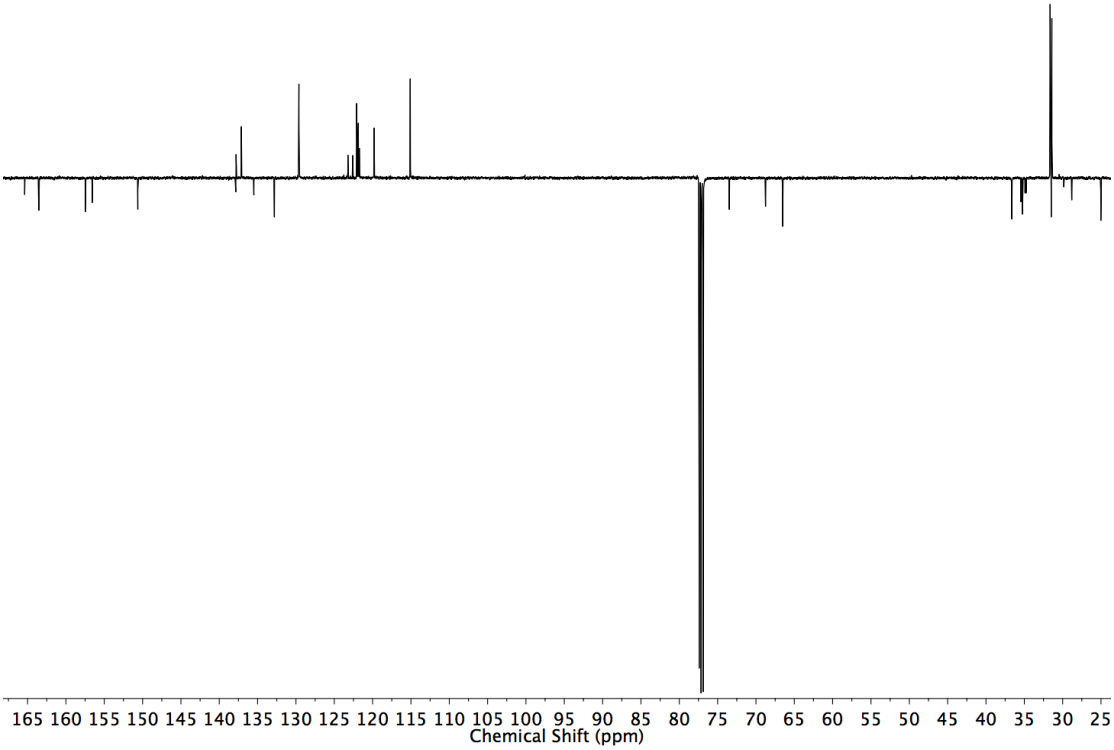

Figure 3.66 JMOD NMR ($CDCl_3$, 126 MHz) of **222**

*Rotaxane **223***

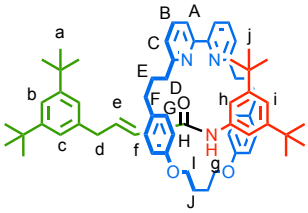

Prepared according to general procedure. **33** (12.0 mg, 0.025 mmol), $[Cu(MeCN)_4]PF_6$ (8.9 mg, 0.024 mmol), **101** (6.9 mg, 0.03 mmol), and **204** (7.8 mg, 0.03 mmol). After purification by column chromatography on silica (petrol with a gradient of 0 to 20% Et_2O) **223** was obtained as a colourless oil (10.0 mg, 43%). ^{1}H NMR (400 MHz, $CDCl_3$) δ: 9.92 (s, 1H, H_g), 7.62 (t, *J* =7.9, 2H, H_B), 7.48 (dd, *J* =7.9, 0.9, 2H, H_A), 7.15 (t, *J* =1.9, 1H, H_b), 7.10 (dd, *J* =7.9, 0.9, 2H, H_C), 6.97 (d, *J* =1.9, 2H, H_h), 6.85 (t, *J* =1.9, 1H, H_i), 6.82 (d, *J* =1.9, 2H, H_c), 6.77 (d, *J* =8.5, 4H, H_G), 6.70 (d, *J* =8.5, 4H, H_H), 6.42 (dt, *J* =15.5, 6.8, 1H, H_e), 5.46 (dt, *J* =15.5, 1.6, 1H, H_f), 4.50 – 4.38 (m, 2H, 2 of H_I), 4.17 – 4.06 (m, 2H, 2 of H_I), 2.93 (d, *J* =6.8, 2H, H_d), 2.63 – 2.41 (m, 8H, H_D, H_F), 2.29 – 2.16 (m, 2H, 2 of H_J), 2.07 – 1.95 (m, 2H, 2 of H_J), 1.90 – 1.67 (m, 4H, H_E), 1.21 (s, 18H, H_a or H_j), 1.10 (s, 18H, H_a or H_j). ^{13}C NMR (101 MHz, $CDCl_3$) δ: 163.6, 163.3, 157.6, 156.3, 150.4, 150.0, 141.3, 139.4, 138.5, 137.0, 132.6, 129.2, 125.6, 122.9, 121.9, 120.2, 119.6, 116.0, 115.1, 114.3, 66.5, 39.4, 36.6, 35.2, 34.8 (×2), 31.6, 31.5, 31.1, 25.2. HR-ESI-MS *m/z* = 940.6367 $[M+H]^+$ calc. 940.6351.

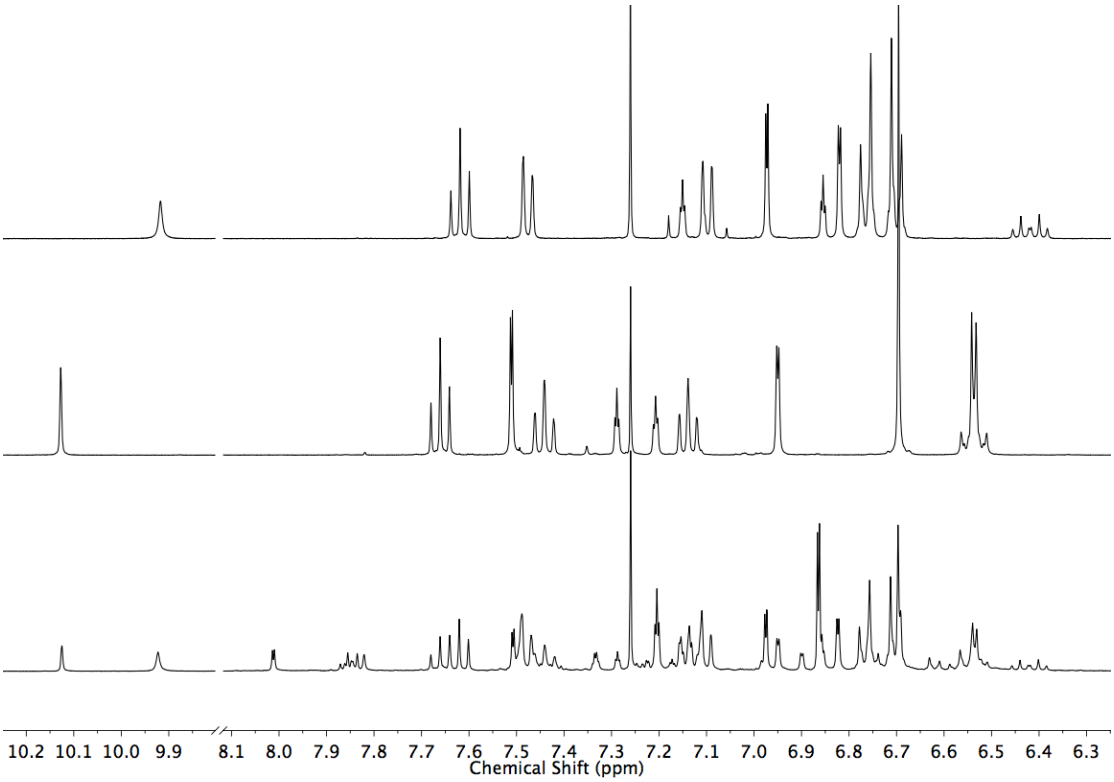

Figure 3.67 Stacked partial ^{1}H NMR (400 MHz, $CDCl_3$) spectra of **223** (top), **213** (middle) and crude reaction mixture (bottom). Ratio of **223**:**213** = 60:40.

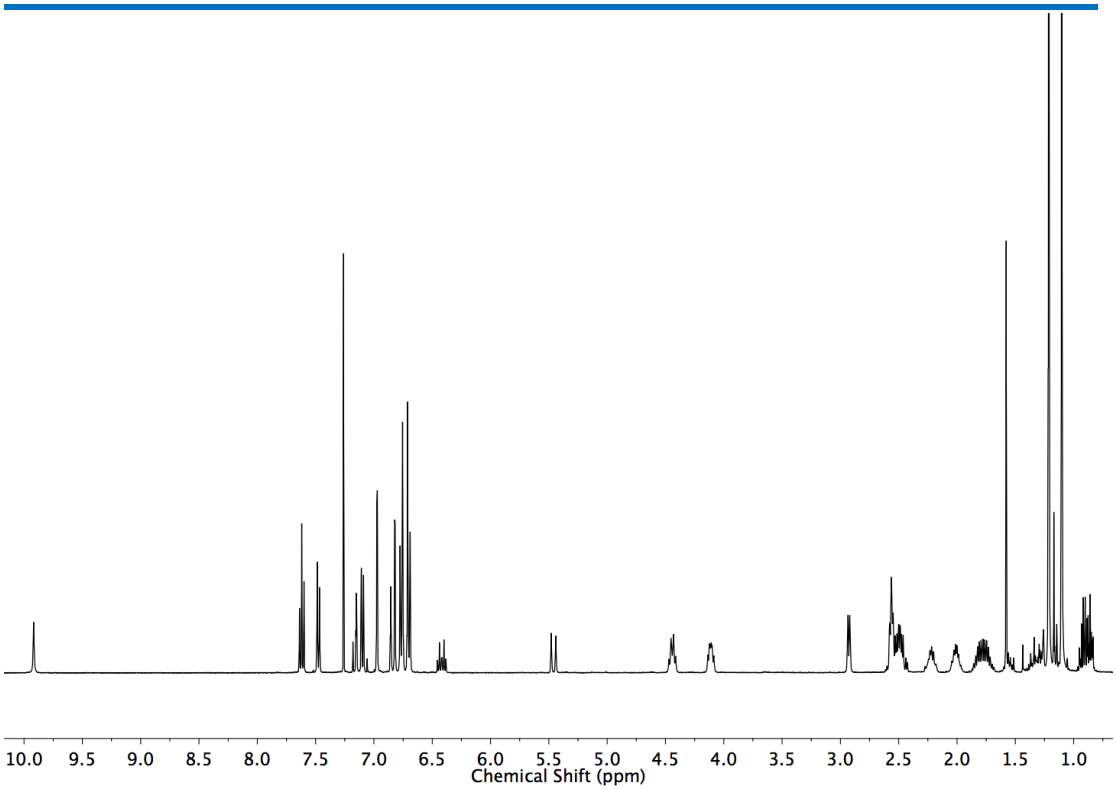

Figure 3.68 ^{1}H NMR ($CDCl_3$, 400 MHz) of **223**

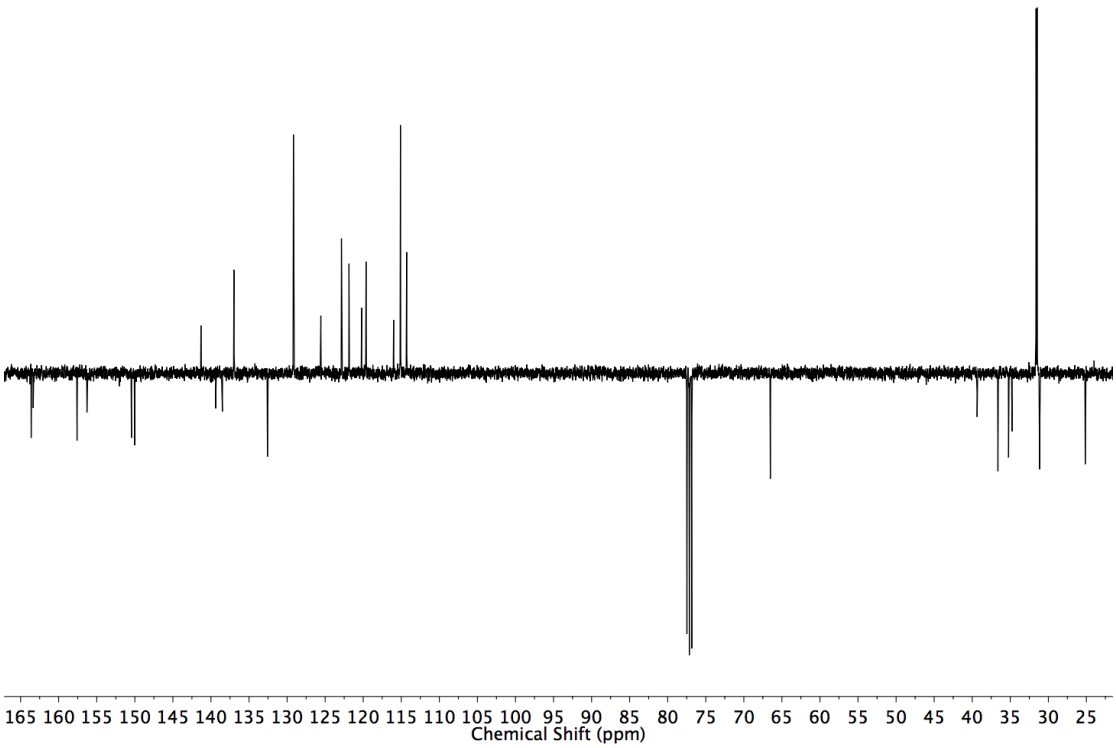

Figure 3.69 JMOD NMR ($CDCl_3$, 101 MHz) of **223**

Rotaxane ***226***

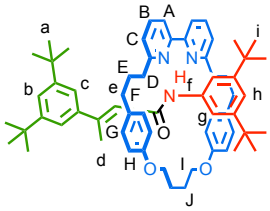

Prepared according to general procedure. **33** (12.0 mg, 0.025 mmol), $[Cu(MeCN)_4]PF_6$ (8.9 mg, 0.024 mmol), **101** (6.9 mg, 0.03 mmol), and **200** (7.7 mg, 0.03 mmol). After purification by column chromatography on silica (petrol with a gradient of 0 to 30% Et_2O) **226** was obtained as a colourless oil (19.9 mg, 85 %). ^{1}H NMR (500 MHz, $CDCl_3$) δ: 10.29 (s, 1H, H_f), 7.66 (t, *J* =7.8, 2H, H_B), 7.55 (dd, *J* =7.8, 0.9, 2H, H_A), 7.24 (d, *J* =1.9, 2H, H_g), 7.17 (t, *J* =1.9, 1H, H_b), 7.13 (dd, *J* =7.8, 0.9, 2H, H_C), 7.05 (d, *J* =1.9, 2H, H_c), 6.93 (t, *J* =1.9, 1H, H_h), 7.74 (d, *J* =8.5, 4H, H_G), 6.61 (d, *J* =8.5, 4H, H_H), 6.54 (q, *J* =1.2, 1H, H_e), 4.72 – 4.64 (m, 2H, 2 of H_I), 4.21 – 4.15 (m, 2H, 2 of H_I), 2.59 – 2.43 (m, 8H, H_D, H_F), 2.35 – 2.25 (m, 2H, 2 of H_J), 2.12 (d, *J* =1.2, 3H, Hd), 2.09 – 1.98 (m, 2H, 2 oh H_J), 1.82 – 1.60 (m, 4H, H_E), 1.19 (s, 18H, H_a), 1.08 (s, 18H, H_i). ^{13}C NMR (126 MHz, $CDCl_3$) δ: 164.0, 163.2, 157.7, 156.5, 150.0, 149.9, 147.5, 142.8, 140.6, 137.0, 132.1, 128.9, 122.2, 122.1, 121.3, 120.5, 119.4, 115.3, 115.2, 113.3, 66.4, 36.8, 35.4, 34.9, 34.8, 31.6, 31.6, 31.4, 25.0, 17.0. HR-ESI-MS *m/z* = 940.6343 $[M+H]^+$ calc. 940.6351.

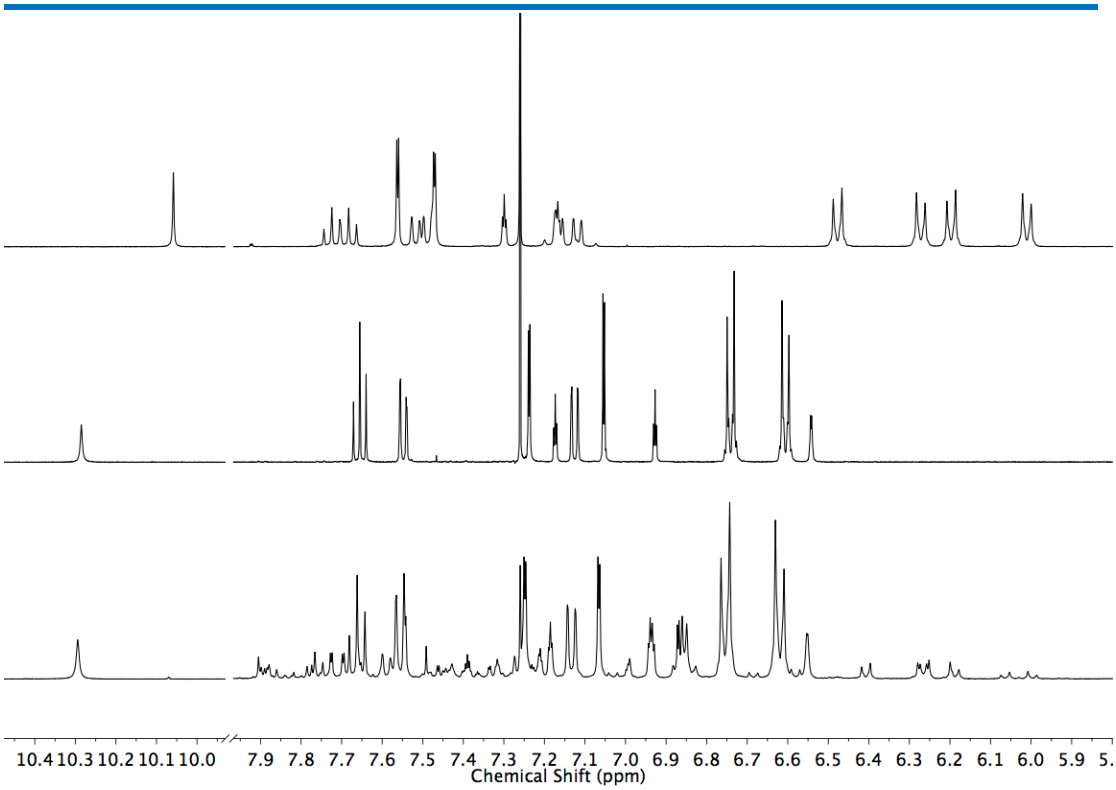

Figure 3.70 Stacked partial ^{1}H NMR (400 MHz, $CDCl_3$) spectra of **214** (top), **226** (middle) and crude reaction mixture (bottom). Ratio of **226**:**214** = 95:5.

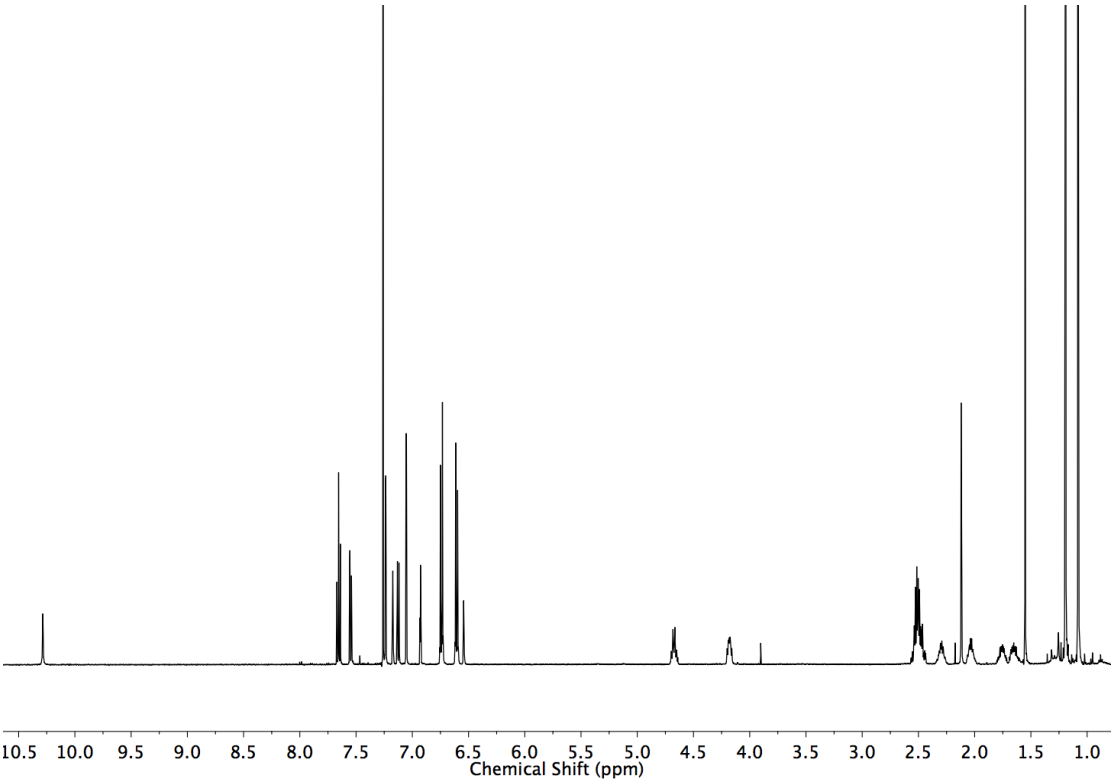

Figure 3.71 ^{1}H NMR ($CDCl_3$, 500 MHz) of **226**

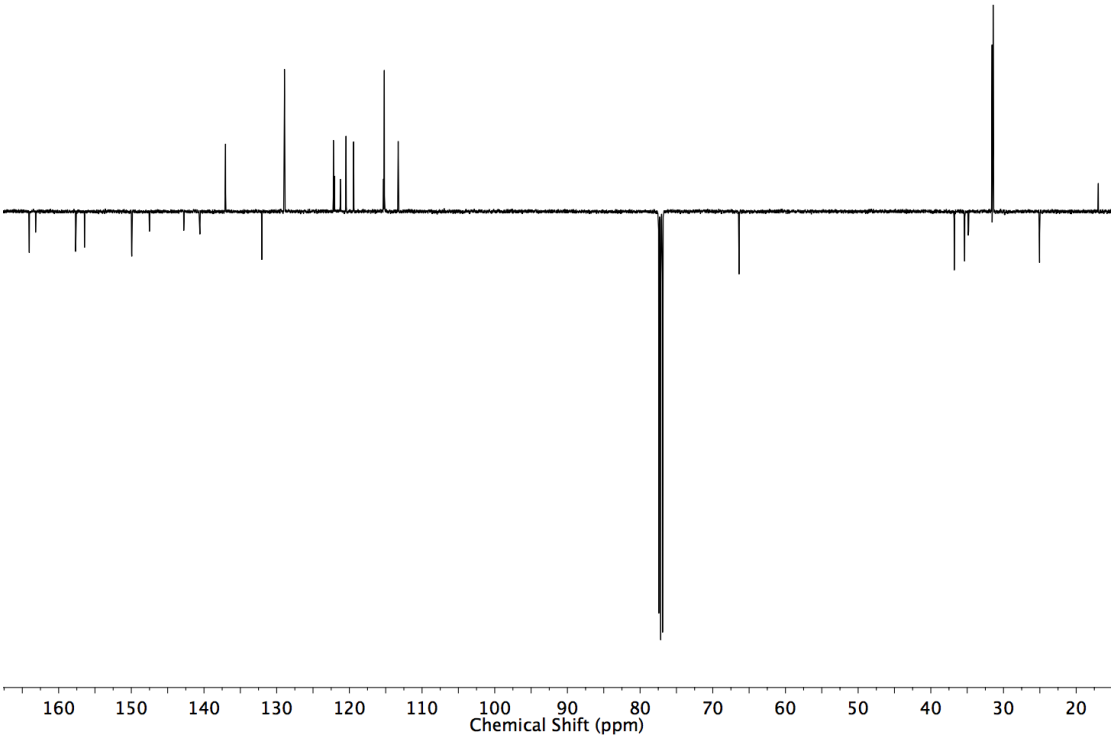

Figure 3.72 JMOD NMR ($CDCl_3$, 126 MHz) of **226**

Synthesis of triazole rotaxanes

General Procedure

N^iPr_2Et (2 eq.) was added to a solution of **alkyne** (1.2 eq.), **azide** (1.2 eq.), **macrocycle** (1 eq.) and $[Cu(MeCN)_4]PF_6$ (0.96 eq.) in CH_2Cl_2 (80 mL/mmol) in a microwave vial. The deep red mixture was stirred at room temperature for 16 hours. The crude was diluted with CH_2Cl_2 (200 mL/mmol), washed with EDTA-NH_3 solution (100 mL/mmol). The aqueous layer was extracted with CH_2Cl_2 (2 x 100 mL/mmol). Combined organic extracts were washed with brine (100 mL/mmol), dried ($MgSO_4$), filtered and the solvent removed *in vacuo*. Purification by flash column chromatography on silica gel yielded the product.

Rotaxane ***206***

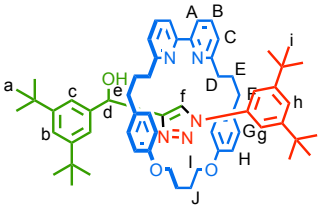

Prepared according to general procedure. **33** (12.0 mg, 0.025 mmol), $[Cu(MeCN)_4]PF_6$ (8.9 mg, 0.024 mmol), **32** (7.0 mg, 0.03 mmol), and **192** (7.3 mg, 0.03 mmol). After purification by column chromatography on silica (petrol with a gradient of 0 to 50% Et_2O) **206** was obtained as a white foam (18.0 mg, 76%). ^{1}H NMR (500 MHz, $CDCl_3$): δ 10.08 (d, *J* =0.8, 1H, H_f), 7.73 (t, *J* =7.8 1H, 1 of H_B), 7.69 (t, *J* =7.8, 1H, 1 of H_B), 7.53 (dd, *J* =7.8, 1.0, 1H, 1 of H_A), 7.50 (dd, *J* =7.8, 1.0, 1H, 1 of H_A), 7.44 (dd, *J* =1.9, 0.6, 2H, H_c), 7.41 (d, *J* =1.8, 2H, H_g), 7.34 (t, *J* =1.9, 1H, H_b), 7.18 – 7.21 (m, 2H, 1 of H_C, H_h), 7.13 (dd, *J* =7.8, 0.8, 1H, 1 of H_C), 6.63 (d, *J* =8.6, 2H, 1 of H_H), 6.51 (d, *J* =8.6, 2H, 1 of H_G), 6.05 – 6.11 (m, 4H, 1 of H_G, 1 of H_H), 5.66 (brds, 1H, H_d), 4.64 – 4.77 (m, 1H, 1 of H_I), 4.49 – 4.60 (m, 1H, 1 of H_I), 4.41 (s, 1H, H_e), 4.21 – 4.30 (m, 1H, 1 of H_I), 3.91 – 4.00 (m, 1H, 1 of H_I), 2.12 – 2.60 (m, 10H, H_D, 2 of H_J, H_F), 1.96 – 2.07 (m, 2H, 2 of H_J), 1.53 – 1.79 (m, 4H, H_E), 1.32 (s, 18H, H_a), 1.19 (s, 18H, H_i). ^{13}C NMR (126 MHz, $CDCl_3$): δ 163.4, 163.1, 157.9, 157.1, 157.1, 156.9, 151.1, 150.0, 149.9, 142.6, 137.3, 137.1, 137.1, 131.7, 151.5, 128.3, 128.2, 122.4, 121.6, 121.5, 121.4, 120.6, 120.2, 120.1, 120.1, 115.4, 114.4, 114.3, 69.9, 66.8, 66.3, 36.9, 36.1, 35.1, 35.1, 35.0, 34.7, 32.3, 31.7, 31.4, 30.0, 25.1, 24.9. HR-ESI-MS *m/z* = 954.6257 $[M+H]^+$ calc. 954.6256.

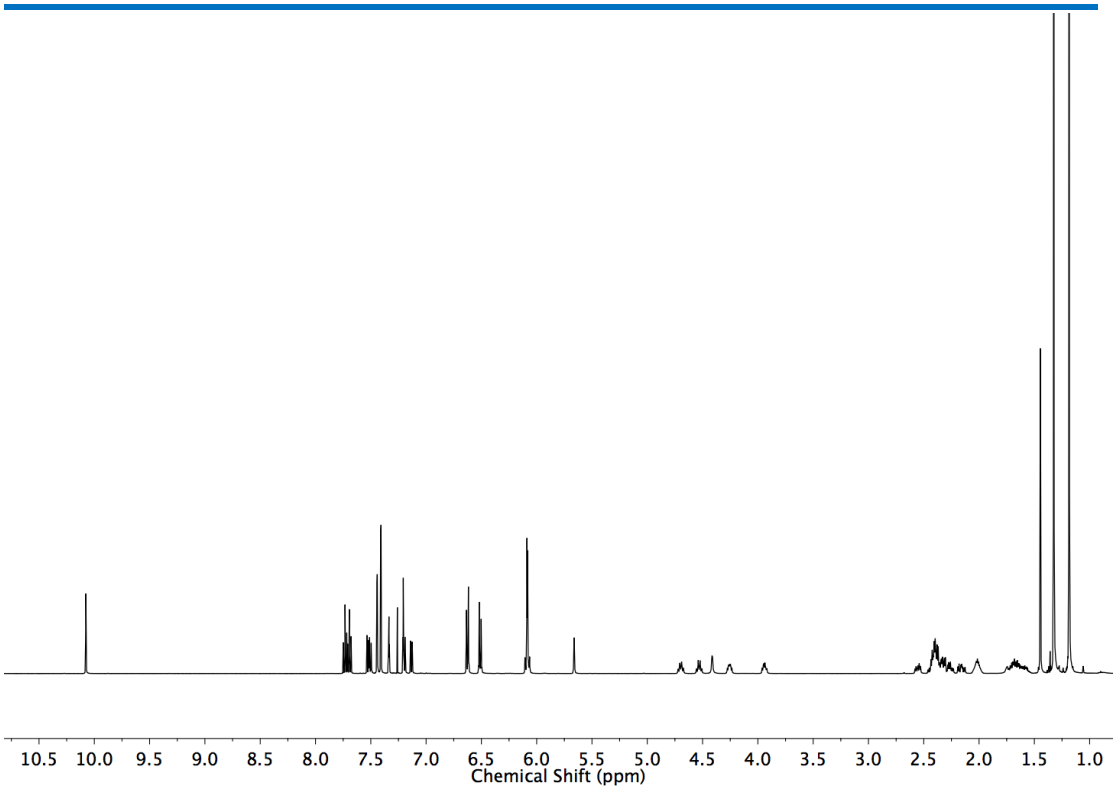

Figure 3.73 ^{1}H NMR ($CDCl_3$, 500 MHz) of **206**

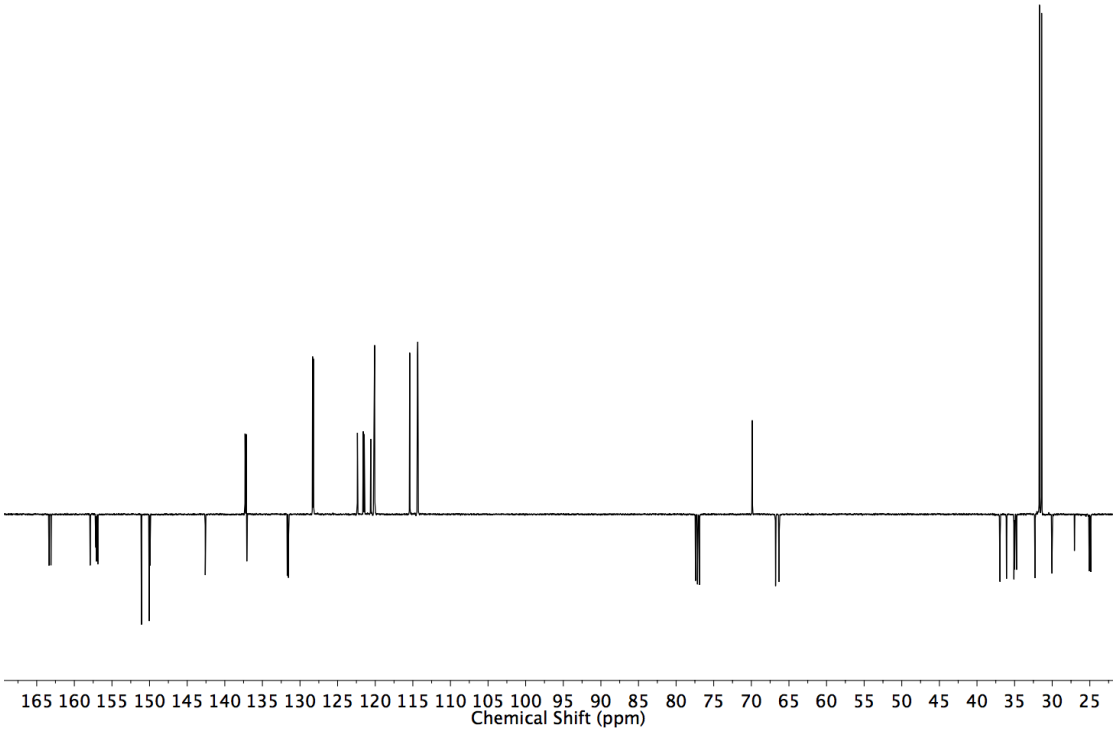

Figure 3.74 JMOD NMR ($CDCl_3$, 126 MHz) of **206**

*Rotaxane **209***

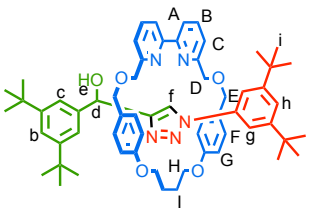

Prepared according to general procedure. **78** (48.3 mg, 0.1 mmol), $[Cu(MeCN)_4]PF_6$ (35.8 mg, 0.096 mmol), **32** (29.3 mg, 0.12 mmol), and **192** (27.8 mg, 0.12 mmol). After purification by column chromatography on silica (petrol with a gradient of 0 to 50% Et_2O) **209** was obtained as a white foam (90.0 mg, 97%). ^{1}H NMR (400 MHz, $CDCl_3$): δ 9.65 (s, 1H, H_f), 7.75 – 7.68 (m, 2H, H_B), 7.62 (dd, *J* =7.8, 1.0, 1H, 1 of H_A), 7.58 (dd, *J* =7.8, 1.0, 1H, 1 of H_A), 7.42 (dd, *J* =7.8, 1.0, 2H, H_C), 7.40 (d, *J* =1.9, 2.H, H_c), 7.28 (t, *J* =1.9, 1H, H_b), 7.14 (d, *J* =1.9, 2H, H_g), 7.10 (t, *J* =1.9, 1H, H_h), 6.70 (d, *J* =8.5, 2H, 2 of H_F), 6.54 (*J* =8.5, 2H, 2 of H_G), 6.23 (d, *J* =8.5, 2H, 2 of H_F), 5.97 (d, *J* =8.5, 2H, 2 of H_G), 5.62 (s, 1H, H_d), 4.68 (q, *J* =7.8, 1H, 1 of H_H), 4.57 (d, *J* =12.2, 1H, 1 of H_E), 4.48 (q, *J* =7.8, 1H, 1 of H_H), 4.36 (d, *J* =12.2, 1H, 1 of H_E), 4.21 (d, *J* =12.2, 1H, 1 of H_E), 4.16 (q, *J* =7.8, 1H, 1 of H_I), 4.02 (t, *J* =12.2, 2H, 1 of H_D, 1 of H_E), 3.95 (q, *J* =12.2, 2H, 2 of H_D), 3.83 (q, *J* =7.8, 1H, 1 of H_I), 3.77 (d, *J* =12.2, 1H, H_D), 2.40 – 2.33 (m, 2H, 2 of H_I), 2.00 – 1.83 (m, 2H, 2 of H_I), 1.27 (s, 18H, H_a or H_h), 1.09 (s, 18H, H_a or H_h). ^{13}C NMR (101 MHz, $CDCl_3$): δ 159.6, 159.6, 159.3, 158.6, 155.2, 155.1, 151.2, 147.9, 149.7, 142.3, 137.6, 137.4, 136.8, 129.4, 128.9, 127.9, 127.2, 121.8, 121.5, 120.9, 120.7, 120.4, 120.2, 120.2, 120.1, 115.3, 114.2, 114.0, 73.0, 72.9, 70.5, 70.0, 69.8, 66.7, 66.0, 34.9, 34.9, 31.6, 31.3, 24.8, 24.7. HR-ESI-MS *m/z* = 958.5843 $[M+H]^+$ calc. 958.5841.

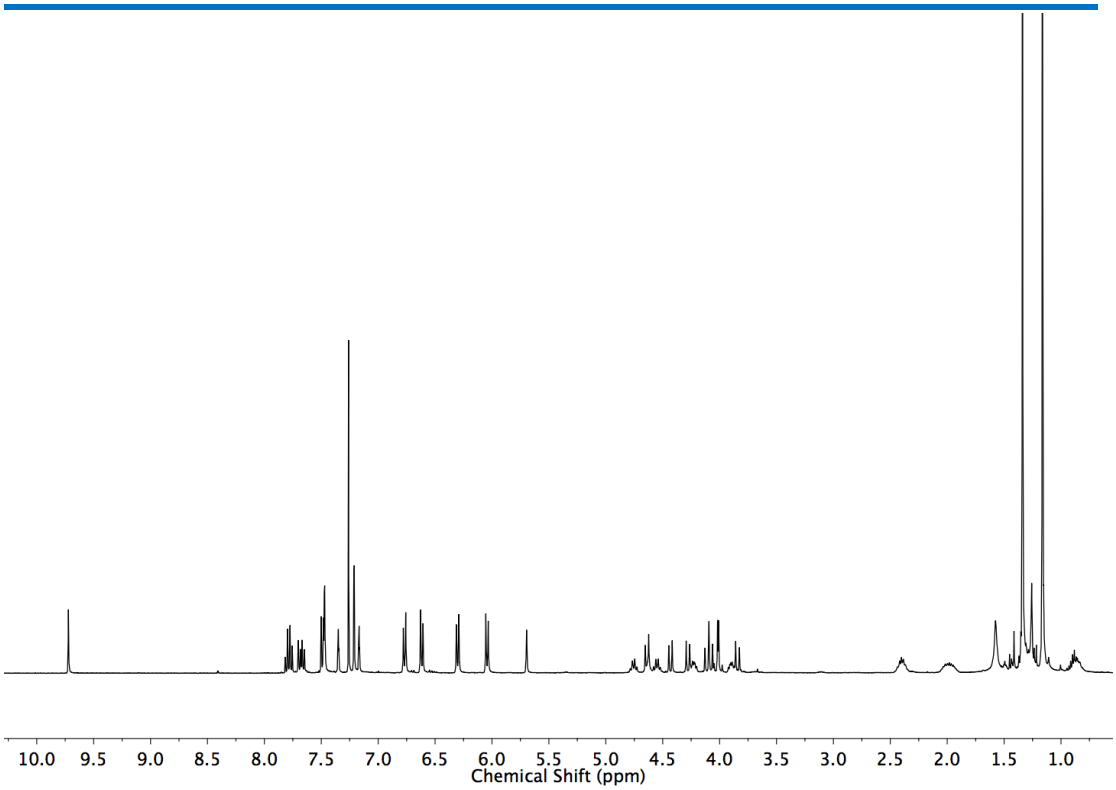

Figure 3.75 ^{1}H NMR ($CDCl_3$, 400 MHz) of **209**

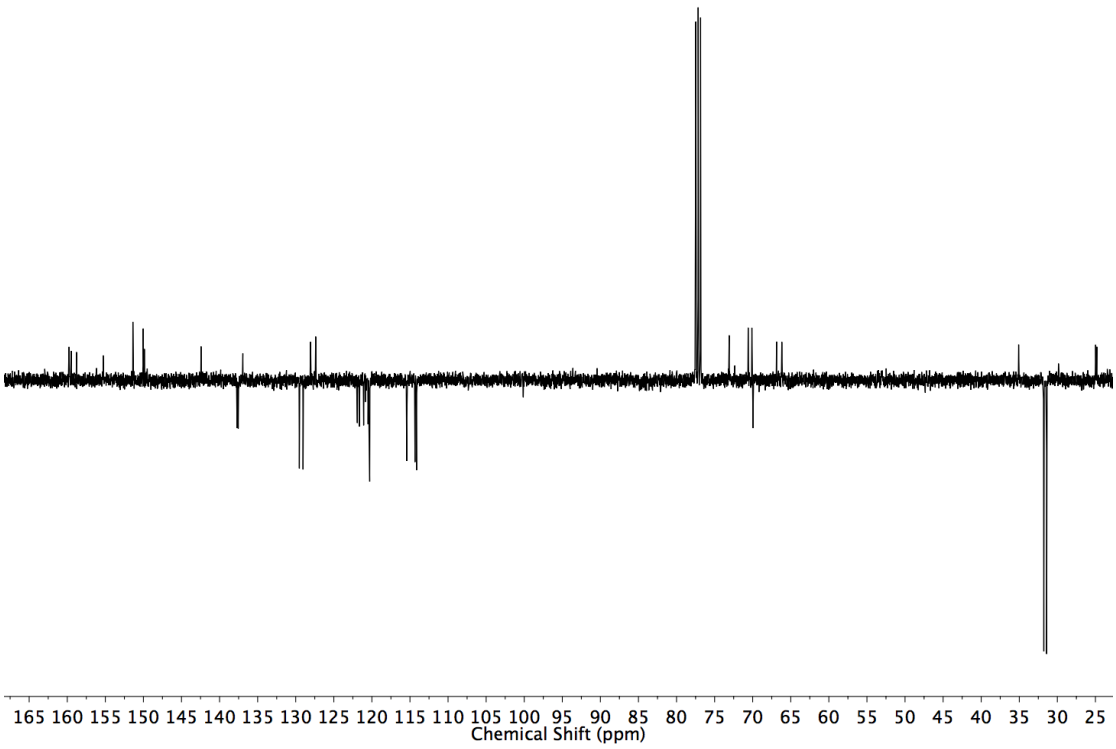

Figure 3.76 JMOD NMR ($CDCl_3$, 101 MHz) of **209**

*Rotaxane **210***

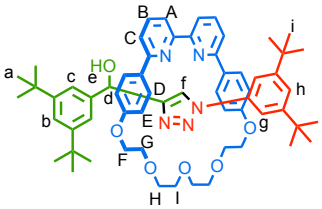

Prepared according to general procedure. **110** (12.0 mg, 0.025 mmol), $[Cu(MeCN)_4]PF_6$ (8.9 mg, 0.024 mmol), **32** (6.9 mg, 0.03 mmol), and **192** (7.3 mg, 0.03 mmol). After purification by column chromatography on silica (petrol with a gradient of 0 to 50% Et_2O) **210** was obtained as a white foam (9.0 mg, 37%). ^{1}H NMR (500 MHz, $CDCl_3$) δ: 9.91 (s, 1H, H_f), 7.93 (t, J = 7.8, 1H, 1 of H_B), 7.84 (t, J = 7.8, 1H, 1 of H_B), 7.79 (dd, J = 7.8, 0.9, 1H, 1 of H_A), 7.77 (dd, J = 7.8, 0.9, 1H, 1 of H_A), 7.64 (dd, J = 7.8, 0.9, 1H 1 of H_C), 7.46 (dd, J = 7.8, 0.9, 1H, 1 of H_C), 7.41 (d, J = 1.8, 2H, H_g), 7.29 (d, J = 8.7, 2H, 2 of H_E), 7.21 (t, J =1.8, 1H, H_h), 7.15 (t, J = 1.8, 1H, H_b), 7.11 (d, J = 1.8, 2H, H_c), 6.86 (d, J = 8.7, 2H, 2 of H_E), 6.35 (d, J = 8.7, 2H, 2 of H_D), 6.07 (d, J = 8.7, 2H, 2 of H_D), 5.00 (d, J = 2.3, 1H, H_d), 4.07 – 3.51 (m, 16H, H_F, H_G, H_H, H_I), 2.99 (d, J = 2.3, 1H, H_e), 1.12 (s, 18H, H_i), 1.09 (s, 18H, H_a). ^{13}C NMR (126 MHz, $CDCl_3$) δ 160.07, 159.47, 159.12, 158.45, 157.67, 157.40, 151.48, 150.44, 149.46, 142.21, 137.60, 137.53, 136.71, 132.80, 132.08, 129.54, 129.13, 125.67, 123.99, 121.90, 121.64, 120.64, 120.35, 120.15, 119.93, 119.62, 114.67, 114.33, 114.15, 70.14, 70.01, 69.91, 69.79, 69.64, 68.85, 68.22, 67.17, 66.09, 34.98, 34.79, 31.47, 31.33. HR-ESI-MS *m/z* = 974.5783 $[M+H]^+$ calc. 974.5790.

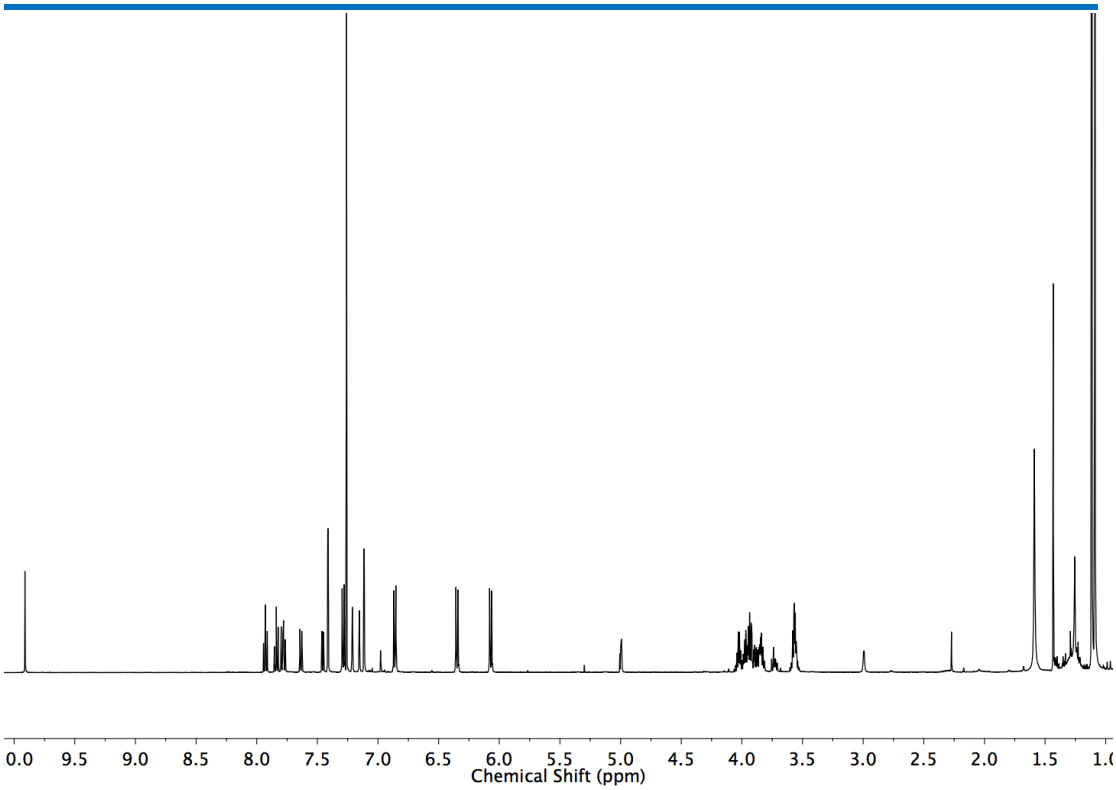

Figure 3.77 ^{1}H NMR ($CDCl_3$, 500 MHz) of **210**

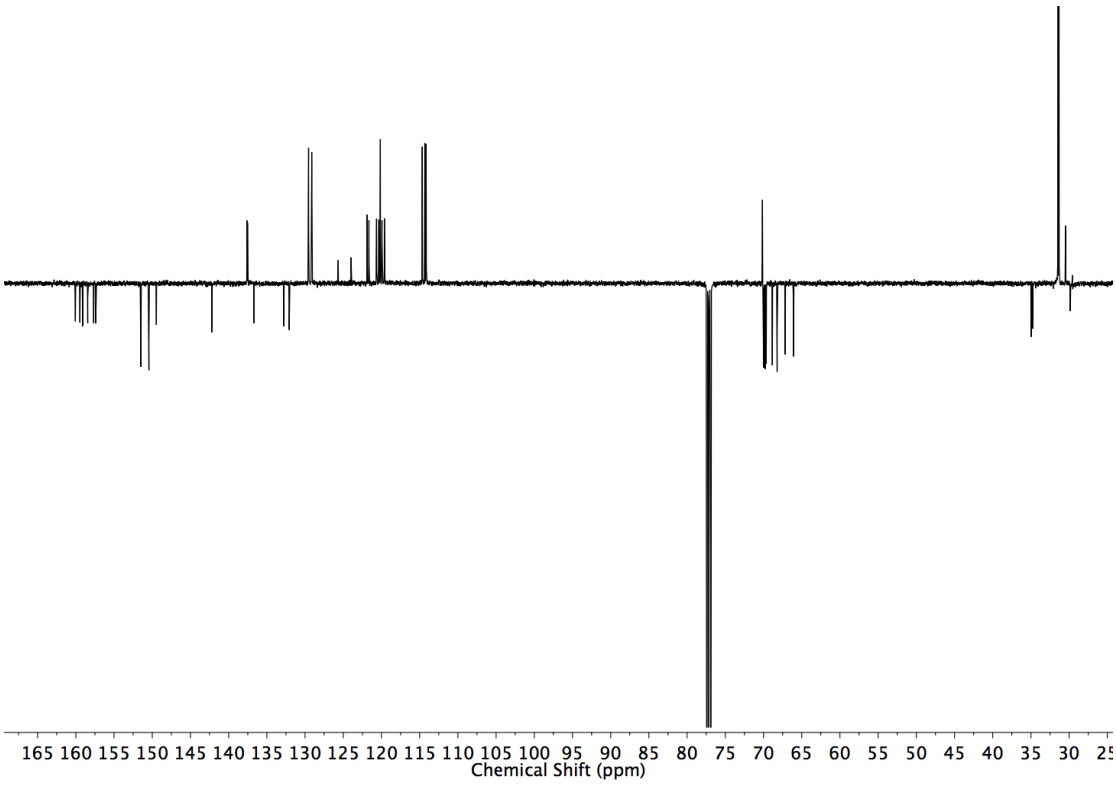

Figure 3.78 JMOD NMR ($CDCl_3$, 126 MHz) of **210**

*Rotaxane **211***

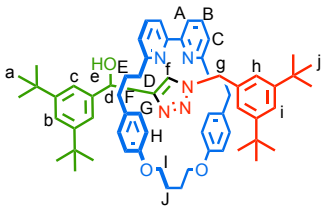

Prepared according to general procedure. **33** (12.0 mg, 0.025 mmol), $[Cu(MeCN)_4]PF_6$ (8.9 mg, 0.024 mmol), **219** (7.3 mg, 0.03 mmol), and **192** (7.3 mg, 0.03 mmol). After purification by column chromatography on silica (petrol with a gradient of 0 to 50% Et_2O) **211** obtained as a white foam (17.0 mg, 70%). ^{1}H NMR (400 MHz, $CDCl_3$): δ 8.73 (s, 1H, H_f), 7.62 (t, *J* =7.8, 2H, H_B), 7.26 (app. s, 3H, H_b, H_c), 7.16 (t, *J* =1.8, 1H, H_i), 7.10 (app. t, *J* =7.7, 2H, H_C) 6.79 (d, *J* =1.8, 2H, H_h), 6.68 – 6.57 (m, 4H, 2 of H_G, 2 of H_H), 6.48 (s, 4H, 2 of H_G, 2 of H_H), 5.38 (br. s, 1H, H_d), 4.67 (d, *J* =3.7, 1H, H_e), 4.65 – 4.52 (m, 2H, 2 of H_I), 4.49 (d, *J* =13.9, 1H, 1 of H_g), 4.25 (d, *J* =13.9, 1H, 1 of H_g), 4.18 – 4.00 (m. 2H, 2 of H_I), 2.68 – 2.15 (m, 10H, H_D, H_F, 2 of H_J), 2.03 – 1.95 (m, 2H, 2 of H_J), 1.85 – 1.49 (m, 4H, H_E), 1.26 (s, 18H, H_a or H_j), 1.11 (s, 18H, H_a or H_j). ^{13}C NMR (101 MHz, $CDCl_3$): δ 162.8, 162.8, 157.6, 157.4, 156.9, 156.7, 150.7, 149.9, 149.2, 142.4, 137.1, 136.9, 133.2, 132.4, 132.3, 128.9, 128.7, 124.2, 123.3, 122.8, 121.7, 121.6, 121.5, 120.7, 120.0, 119.9, 115.2, 114.9, 69.8, 66.7, 66.5, 53.4, 36.6, 36.3, 34.9, 34.9, 34.7, 34.7, 31.7, 31.5, 31.1, 30.5, 25.1, 25.0. HR-ESI-MS *m/z* = 968.6402 $[M+H]^+$ calc. 968.6412.

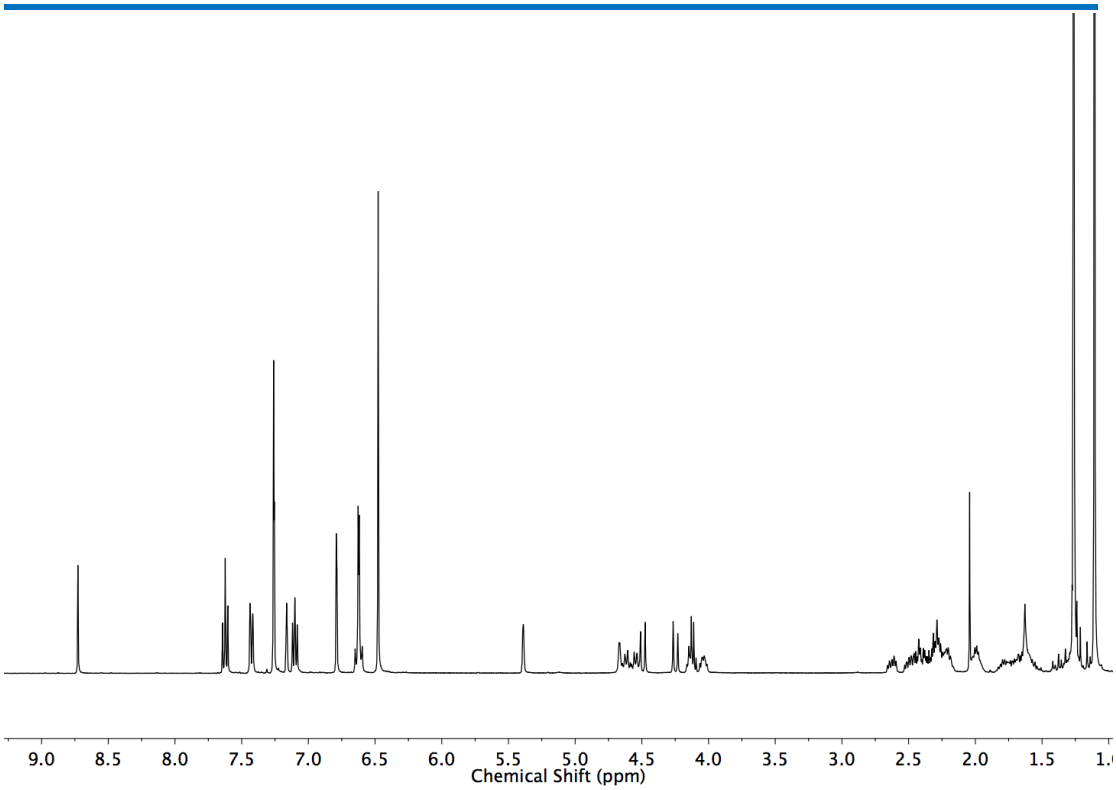

Figure 3.79 ^{1}H NMR ($CDCl_3$, 400 MHz) of **211**

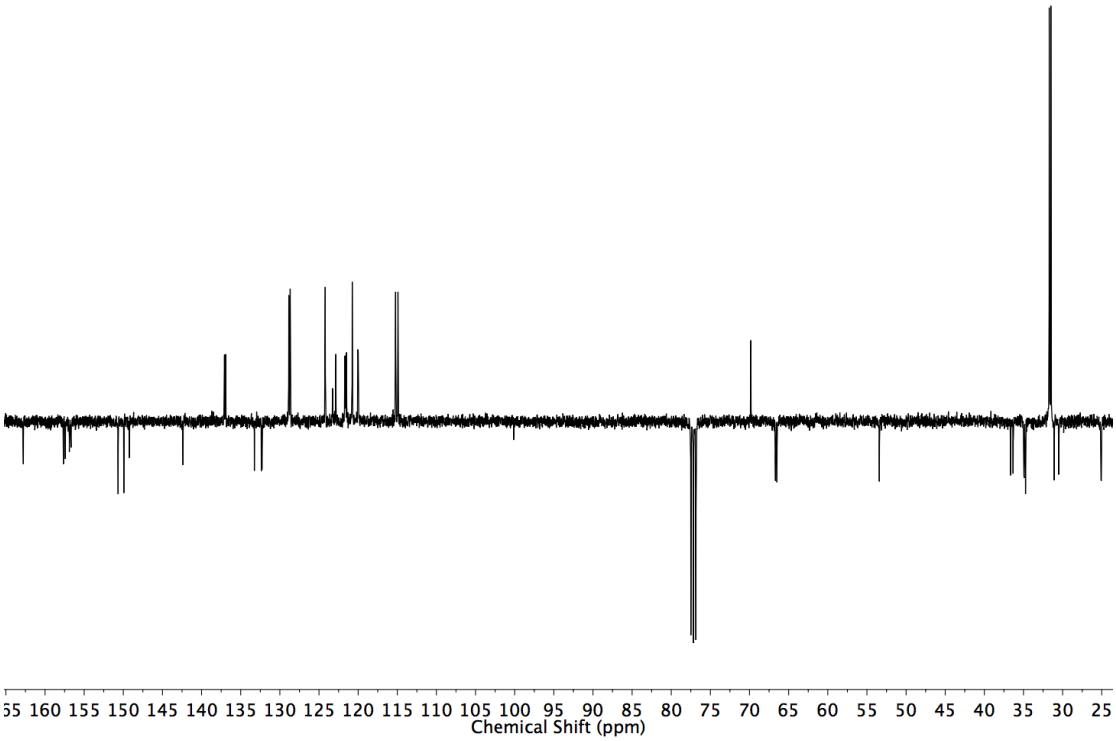

Figure 3.80 JMOD NMR ($CDCl_3$, 101 MHz) of **211**

*Rotaxane **212***

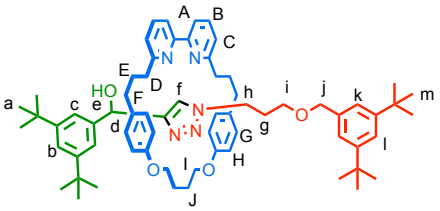

Prepared according to general procedure. **33** (12.0 mg, 0.025 mmol), $[Cu(MeCN)_4]PF_6$ (8.9 mg, 0.024 mmol), **221** (9.1 mg, 0.03 mmol), and **192** (7.3 mg, 0.03 mmol). After purification by column chromatography on silica (petrol with a gradient of 0 to 50% Et_2O) **212** was obtained as a white foam (20.0 mg, 77%). ^{1}H NMR (400 MHz, $CDCl_3$): δ 8.32 (s, 1H, H_f), 7.63 (td, *J* =7.8, 2.6, 2H, H_B), 7.51 (d, *J* =7.7, 2H, H_A), 7.32 (t, *J* =1.9, 1H, H_l), 7.29 (t, *J* =1.9, 1H, H_b), 7.24 (t, *J* =1.9, 2H, H_c), 7.12 (d, *J* =7.7, H_C), 7.03 (d, *J* =1.9, 2H, H_k), 6.68 – 6.57 (m, 8H, H_G, H_H), 5.74 (d, *J* =4.5, 1H, H_d), 4.42 – 4.30 (m, 2H, 2 of H_I), 4.04 (s, 2H, H_j), 4.02 – 3.94 (m, 2H, 2 of H_J), 3.24 (d, *J* =4.7, 1H, H_e), 2.89 (t, *J* =6.7, 2H, H_i), 2.63 – 2.51 (m, 2H, H_g), 2.21 – 2.03 (m, 2H, 2 of H_J), 1.99 – 1.84 (m, 2H, 2 of H_J), 1.77 – 1.64 (m, 4H, H_E), 1.31 (s, 18H, H_a or H_m), 1.23 (s, 18H, H_a or H_m), 1.04 – 0.88 (m, 2H, H_h). ^{13}C NMR (101 MHz, $CDCl_3$) δ 162.8, 162.8, 157.6, 157.6, 157.5 (×2), 150.7, 150.7, 149.8, 142.2, 137.9, 137.0, 136.9, 133.0, 133.0, 129.4 (×2), 123.0, 122.0, 122.0, 121.7, 121.6, 121.6, 120.4, 120.4, 120.4, 115.1, 115.0, 73.0, 70.4, 67.6, 66.5 (×2), 46.7, 37.0 (×2), 36.8 (×2), 34.9, 34.9, 31.8, 31.7, 31.6, 28.8, 24.9, 24.9 (×2). LR-ESI-MS *m/z* = 1026.68 $[M+H]^+$ calc. 1026.68.

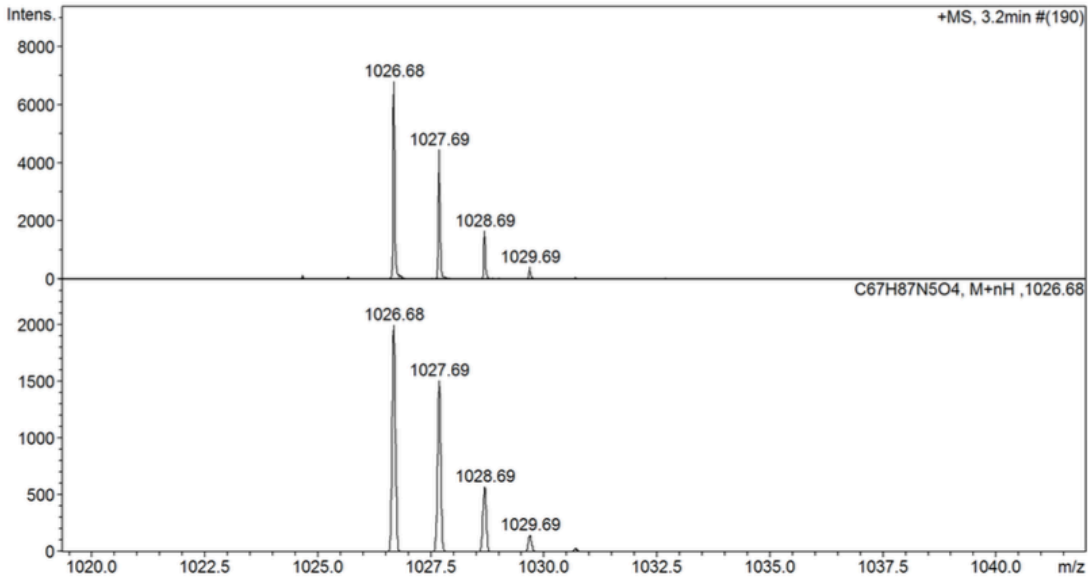

Figure 3.81 Observed (top) and calculated (bottom) isotopic patterns for **212**

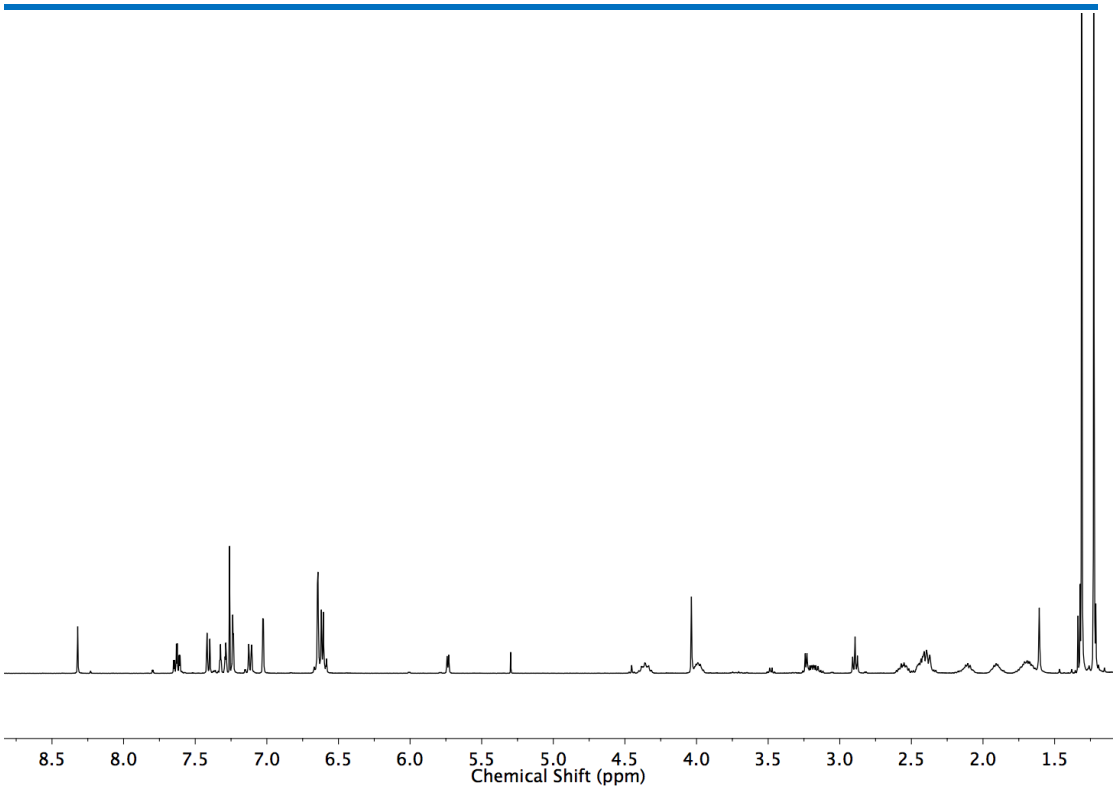

Figure 3.82 ^{1}H NMR ($CDCl_3$, 400 MHz) of **212**

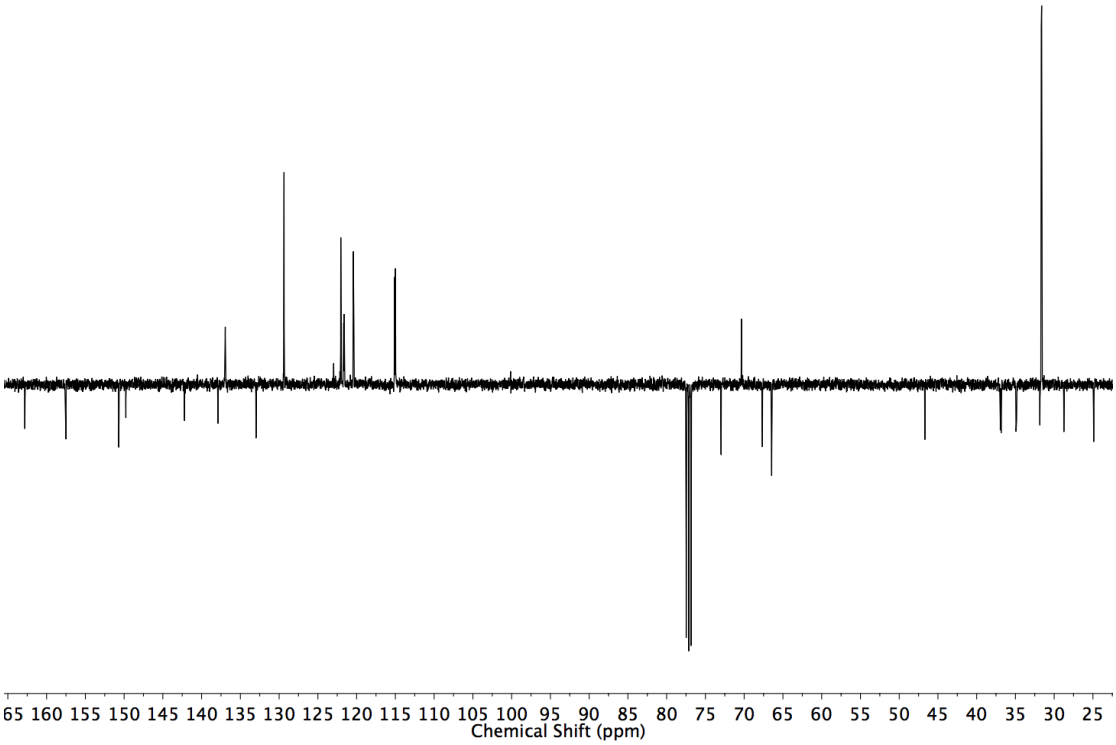

Figure 3.83 JMOD NMR ($CDCl_3$, 101 MHz) of **212**

Rotaxane ***213***

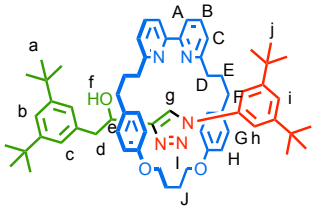

Prepared according to general procedure. **33** (19.1 mg, 0.04 mmol), $[Cu(MeCN)_4]PF_6$ (14.1 mg, 0.038 mmol), **101** (10.4 mg, 0.045 mmol), and **204** (11.6 mg, 0.045 mmol). After purification by column chromatography on silica (petrol with a gradient of 0 to 30% Et_2O) **213** was obtained as a white foam (31.0 mg, 80%). ^{1}H NMR (400 MHz, $CDCl_3$) δ: 10.13 (s, 1H, H_g), 7.66 (t, *J* =7.8, 2H, H_B), 7.51 (d, *J* =1.9, 2H, H_c), 7.44 (td, *J* =8.0, 0.9, 2H, H_A), 7.29 (t, *J* =1.9, 1H, H_i), 7.21 (t, *J* =1.9, 1H, H_b), 7.14 (dt, *J* =8.0, 0.9, 2H, H_C), 6.95 (d, *J* =1.9, 2H, H_c), 6.70 (s, 4H, 2 of H_G, 2 of H_H), 6.58 – 6.48 (m, 4H, 2 of H_G, 2 of H_H), 4.63 – 4.23 (m, 5H, H_I, H_e), 3.78 (s, 1H, H_f), 2.70 – 2.63 (m, 1H, 1 of H_d), 2.63 – 2.26 (m, 8H, H_D, H_F), 2.26 – 2.10 (m, 4H, H_J), 1.98 (dd, *J* =14.6, 11.2, 1H, 1 of H_d), 1.90 – 1.64 (m, 4H, H_E), 1.32 (s,18H, H_a), 1.21 (s, 18H, H_j). ^{13}C NMR (101 MHz, $CDCl_3$) δ 163.4, 163.4, 157.7, 157.7, 157.1, 157.1, 151.9, 149.8 (×2), 138.7 (×2), 137.4, 137.2, 137.1, 132.1, 128.8, 128.7, 123.7, 122.7, 122.0, 122.0, 121.0, 120.1, 120.0, 119.9, 115.4, 114.8, 114.4, 66.6, 66.6, 66.5, 43.6, 36.8 (×2), 35.4, 35.4, 35.2, 34.9, 32.0, 31.8, 31.4, 31.3, 25.1, 24.9. HR-ESI-MS *m/z* = 968.6392 $[M+H]^+$ calc. 968.6412.

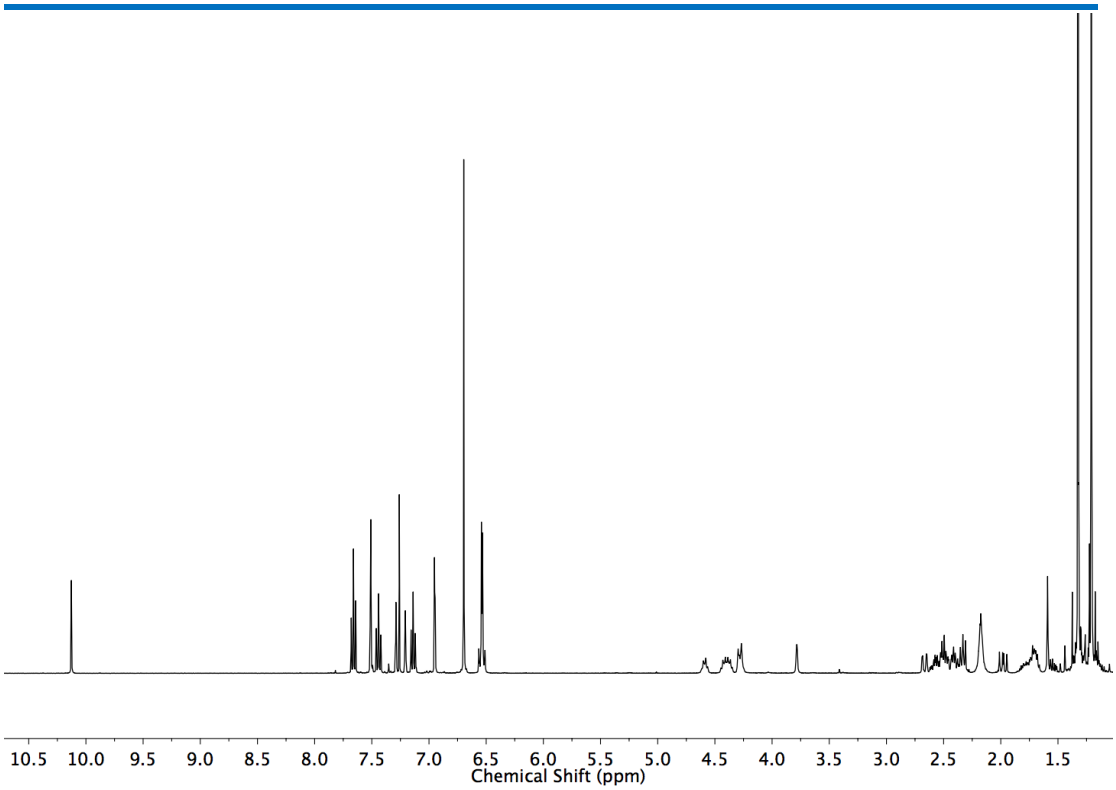

Figure 3.84 ^{1}H NMR ($CDCl_3$, 400 MHz) of **213**

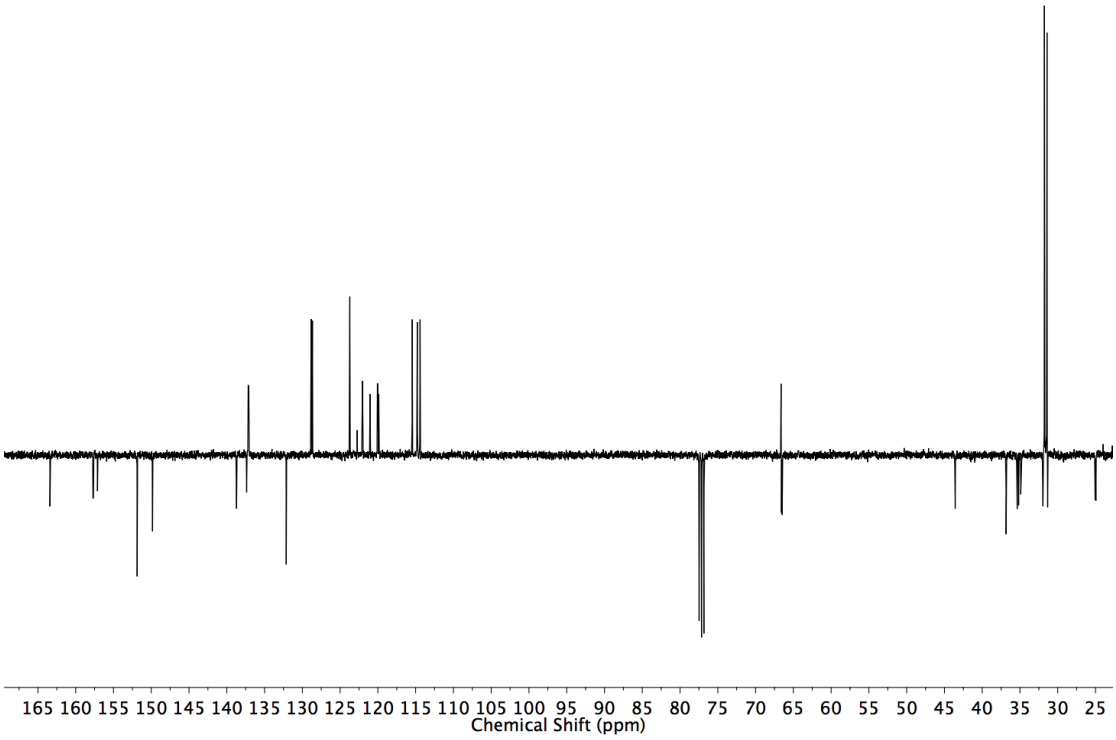

Figure 3.85 JMOD NMR ($CDCl_3$, 101 MHz) of **213**

Rotaxane ***214***

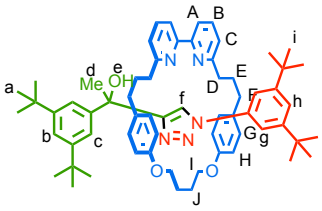

$^{i}Pr_2NEt$ (9.0 µl, 0.05 mmol) was added to a solution of **200** (6.5 mg, 0.025 mmol), **32** (5.8mg, 0.025 mmol), **33** (12.0 mg, 0.025 mmol) and $[Cu(MeCN)_4]PF_6$ (8.9 mg, 0.024 mmol) in CH_2Cl_2 (2.0 mL) in a microwave vial. The deep red mixture was stirred at room temperature for 16 h. TBACN (26.0 mg, 0.097 mmol) in CH_2Cl_2 was added to the mixture and stirred for five days at room temperature until the solution turned black. The solvent was removed via bubbling. The residue was diluted with CH_2Cl_2 (20 mL), washed with water (10 mL). The aqueous layer was extracted with CH_2Cl_2 (2 x 10 mL). Combined organic extracts were washed with brine (10 mL), dried ($MgSO_4$), filtered and the solvent removed *in vacuo*. After purification by column chromatography on silica (petrol:CH_2Cl_2 1:1, with a gradient of 0 to 5% acetonitrile) **214** was obtained as a white foam (20.0 mg, 84%).^{1}H NMR (400 MHz, $CDCl_3$) δ: 10.06 (s, 1H, H_f), 7.72 (app t, *J* = 7.8 1H, 1 of H_B), 7.68 (app t, *J* =7.7, 1H, one of H_B), 7.56 (d, *J* = 1.8, 2H, H_c), 7.52 (dd, *J* = 7.8, 0.9, 1H, one of H_A), 7.50 – 7.46 (m, 3H, H_g, one of H_A,), 7.30 (t, *J* = 1.8, 1H, H_b), 7.18-7.10 (m, 3H, H_h, H_C), 6.48 (d, *J* = 8.6, 2H, 2 of H_G), 6.27 (d, *J* = 8.6, 2H, 2 of H_G) 6.20 (d, *J* = 8.6, 2H, 2 of H_H) 6.01 (d, *J* = 8.6, 2H, 2 of H_H), 4.81 (q, *J* = 7.9, 1H, 1 of H_I), 4.66 (q, *J* = 7.9, 1H, 1 of H_I), 4.19 – 4.10 (m, 1H, 1 of H_I) 4.03 – 3.81 (m, 2H, H_e, 1 of H_I), 2.52 – 1.92 (m, 12H, H_D, H_F, H_J), 1.70-1.50 (m, 7H, H_d, H_E), 1.24 (s, 18H, H_a), 1.09 (s, 18H, H_i). ^{13}C NMR (101 MHz, $CDCl_3$) δ 163.4, 163.4, 157.5, 157.3, 156.9, 153.4, 150.9, 150.9, 149.7, 137.1, 137.1, 137.0, 131.6, 131.5, 128.2, 122.1, 121.8, 121.1, 120.7, 120.4, 120.2,120.0, 129.4, 115.2, 113.6, 114.4, 72.3, 66.3, 66.3, 37.0, 36.8, 35.2, 35.1, 35.1, 31.8, 31.5, 31.4, 31.0, 25.0, 24.3. HR-ESI-MS *m/z* =968.6397 $[M+H]^+$ calc. 968.6412.

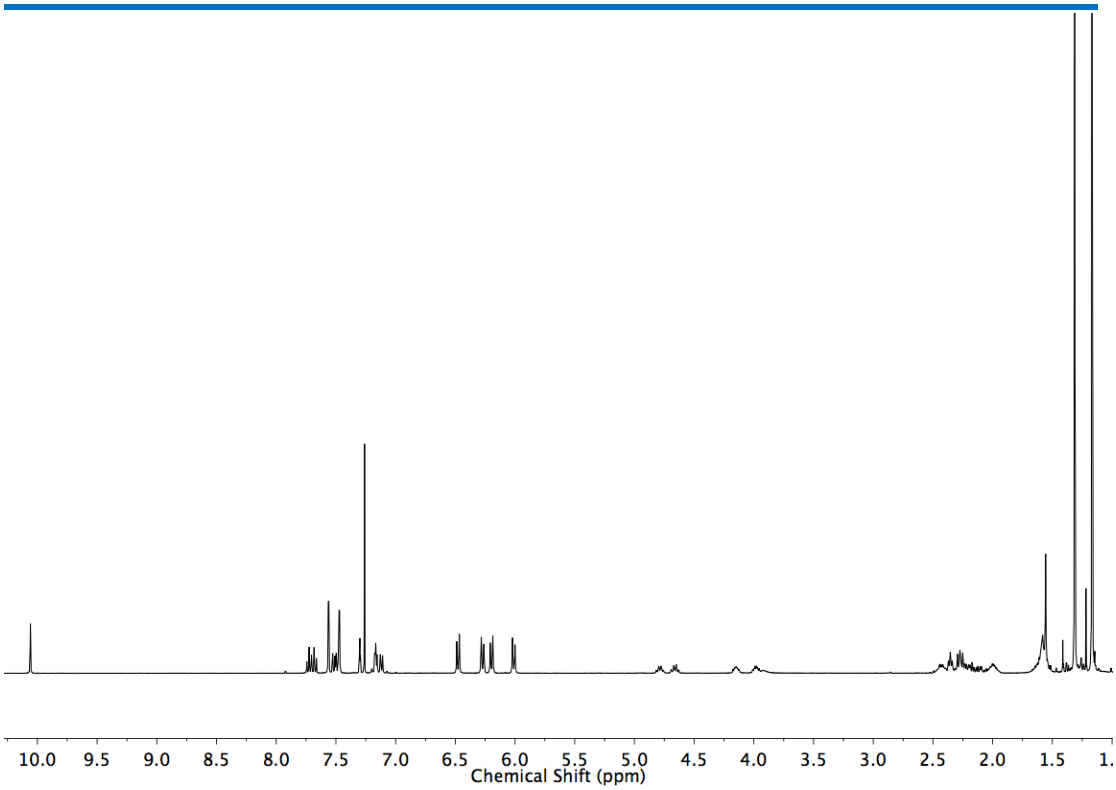

Figure 3.86 ^{1}H NMR ($CDCl_3$, 400 MHz) of **214**

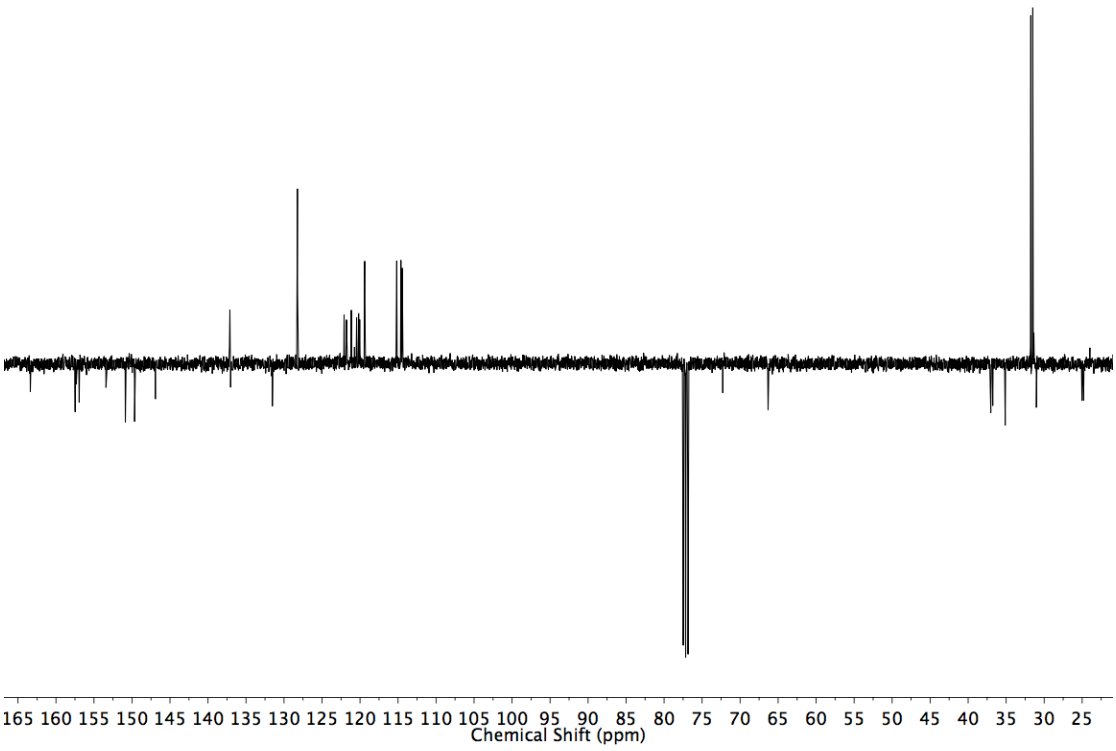

Figure 3.87 ^{13}C NMR ($CDCl_3$, 101 MHz) of **214**

Rotaxane ***215***

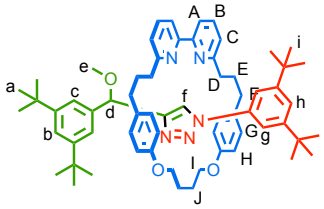

$^{i}Pr_2NEt$ (9.0 µl, 0.05 mmol) was added to a solution of **197** (6.5 mg, 0.025 mmol), **32** (5.8mg, 0.025 mmol), **33** (12.0 mg, 0.025 mmol), and $[Cu(MeCN)_4]PF_6$ (8.9 mg, 0.024 mmol), in CH_2Cl_2 (2.0 mL) in a microwave vial. The deep red mixture was stirred at room temperature for 16 h. KCN (10.0 mg, 0.153 mmol) in CH_2Cl_2 was added to the mixture and stirred for two days at room temperature until the solution turned black. The solvent was removed via bubbling. The residue was diluted with CH_2Cl_2 (20 mL), washed with water (10 mL). The aqueous layer was extracted with CH_2Cl_2 (2 x 10 mL). Combined organic extracts were washed with brine (10 mL), dried ($MgSO_4$), filtered and the solvent removed *in vacuo*. After purification by column chromatography on silica (petrol with a gradient of 0 to 50% ethyl acetate) **215** was obtained as a white foam (4.7 mg, 19%)*.^{1}H NMR (500 MHz, $CDCl_3$) δ: 10.24 (s, 1H, H_f), 7.73 (t, *J* =7.8, 1H, 1 of H_B), 7.69 (t, *J* = 7.8, 1H, 1 of H_B), 7.60 (d, *J* = 1.7, 2H, H_c), 7.54 (ddd, *J* = 7.8, 2.7, 0.9, 2H, H_A), 7.25 (t, *J* = 2.7, 1H, H_h), 7.21 (d, *J* = 2.7, 2H, H_g), 7.18 (t, *J* = 2.7, 1H, H_b), 7.12 (dd, *J* = 7.8, 1.0, 1H, 1 of H_C), 7.07 (dd, *J* = 7.8, 1.0, 1H, 1 of H_C), 6.44 (d, *J* = 8.6, 2H, 2H, 2 of H_H), 6.28 (d, *J* = 8.6, 2H, 2 of H_H), 6.18 (d, *J* = 8.6, 2H, 2 of H_G), 5.97 (d, *J* = 8.6, 2H, H_G), 4.91 (s, 1H, H_d), 4.89 – 4.81 (m, 1H, 1 of H_I), 4.81 – 4.73 (m, 1H, 1 of H_I), 4.19 – 4.11 (m, 1H, 1 of H_I), 4.10 – 4.06 (m, 1H, 1 of H_I), 3.00 (s, 3H , H_e), 2.48 – 1.95 (m, 2H, 2 of H_J), 2.36 – 2.25 (m, 14H, H_D, H_E, H_F, 2 of H_J), 1.17 (s, 36H, H_a, H_i). ^{13}C NMR (126 MHz, $CDCl_3$) δ 163.5, 163.5, 157.6, 157.5, 157.3, 157.1, 150.6, 150.4, 146.3, 141.0, 137.1, 137.0, 136.9, 131.5, 131.5, 128.2, 128.1, 124.2, 122.3, 121.9, 121.8, 121.0, 120.9, 119.9, 119.8, 115.21, 115.1, 114.9, 79.8, 66.7, 66.5, 56.7, 37.2, 37.0, 35.2, 35.2, 35.2, 34.9, 31.9, 31.5, 31.5, 31.4, 24.9, 24.9. HR-ESI-MS *m/z* =968.6402 $[M+H]^+$ calc. 968.6412. *Product decomposed during purification, resulting in the low yield.

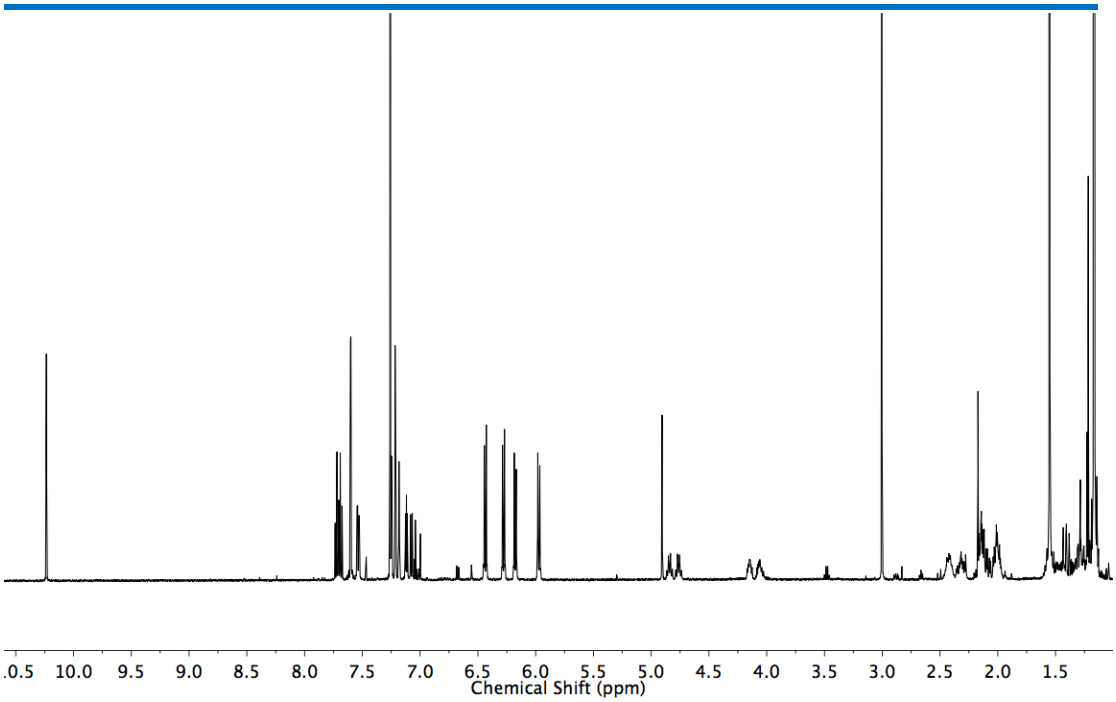

Figure 3.88 ^{1}H NMR ($CDCl_3$, 500 MHz) of **215**

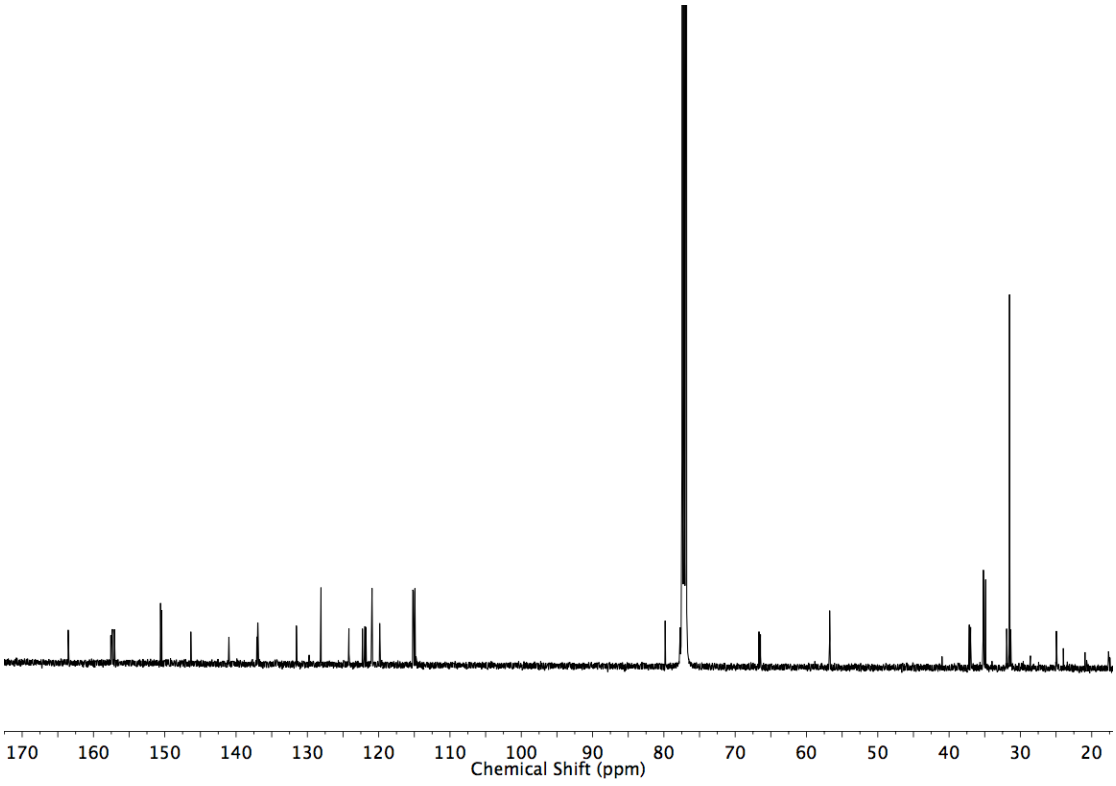

Figure 3.89 ^{13}C NMR ($CDCl_3$, 126 MHz) of **215**

Rotaxane ***216***

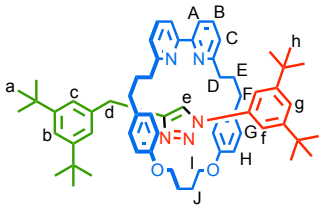

Prepared according to general procedure. **33** (12.0 mg, 0.025 mmol), $[Cu(MeCN)_4]PF_6$ (8.9 mg, 0.024 mmol), **32** (7.0 mg, 0.03 mmol), and **205** (7.0 mg, 0.03 mmol). After purification by column chromatography on silica (petrol with a gradient of 0 to 40% Et_2O) **216** was obtained as a white foam (17.0 mg, 72%). ^{1}H NMR (400 MHz, $CDCl_3$) δ: 10.09 (s, 1H, H_e), 7.69 (t, *J* =7.7, 2H, H_B), 7.51 (dd, *J* =7.8, 0.9, 2H, H_A), 7.45 (d, *J* =1.7, 2H, H_f), 7.18 (t, *J* =1.7, 1H, H_g), 7.16 (t, *J* =1.7, 1H, H_b), 7.09 (dd, *J* =7.8, 0.9, 2H, H_C), 6.95 (d, *J* =1.8, 2H, H_c), 6.40 (d, *J* =8.5, 4H, H_H), 6.16 (d, *J* =8.5, 54H, H_G), 4.72 (q, *J* =7.8, 2H, H_I), 4.26-4.09 (m, 2H, H_I), 3.45 (s, 2H, H_d), 2.45 – 1.98 (m, 12H, H_D, H_F, H_I), 1.57 – 1.29 (m, 4H, H_E), 1.16 (s, 18H, H_h), 1.12 (s, 18H, H_a). ^{13}C NMR (101 MHz, $CDCl_3$) δ: 163.5, 157.6, 157.3, 150.7, 150.5, 145.3, 139.6, 137.3, 136.9, 131.8, 128.2, 123.8, 123.1, 122.0, 120.8, 120.6, 119.7, 115.4, 115.1, 68.8, 37.0, 35.2, 35.1, 34.7, 33.2, 32.2, 31.5, 31.5, 25.0. HR-ESI-MS *m/z* = 938.6307 $[M+H]^+$ calc. 938.6307.

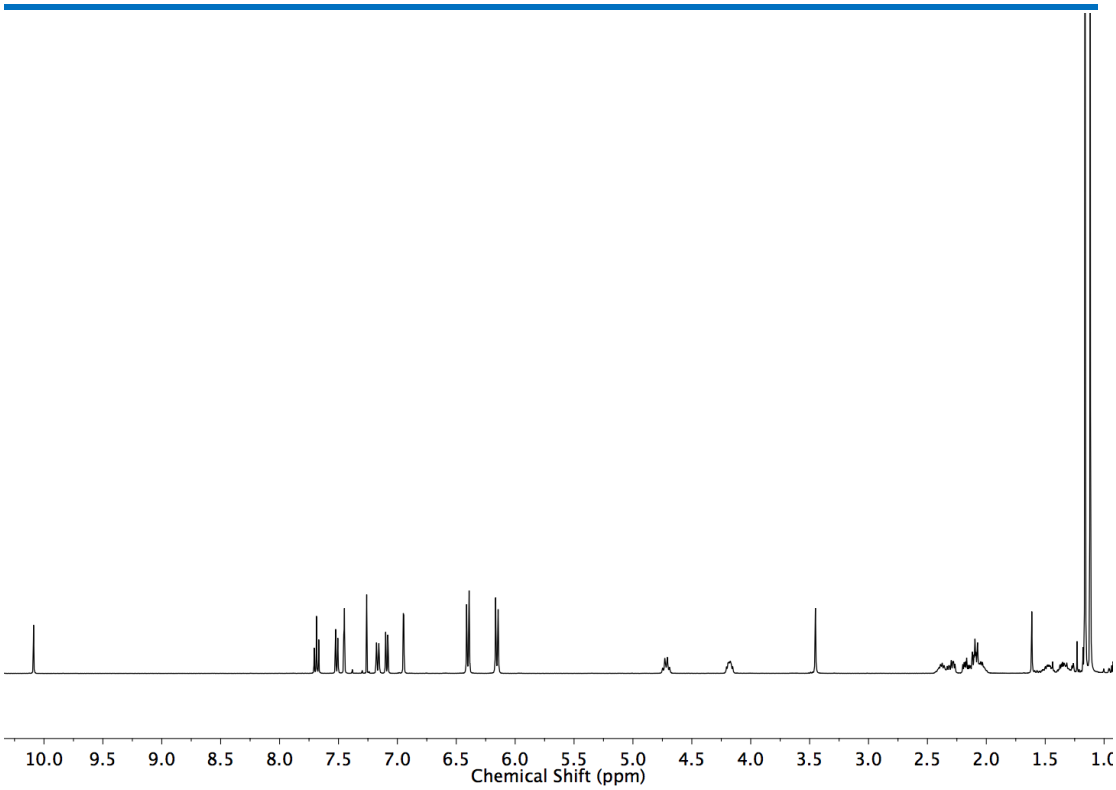

Figure 3.90 ^{1}H NMR ($CDCl_3$, 400 MHz) of **216**

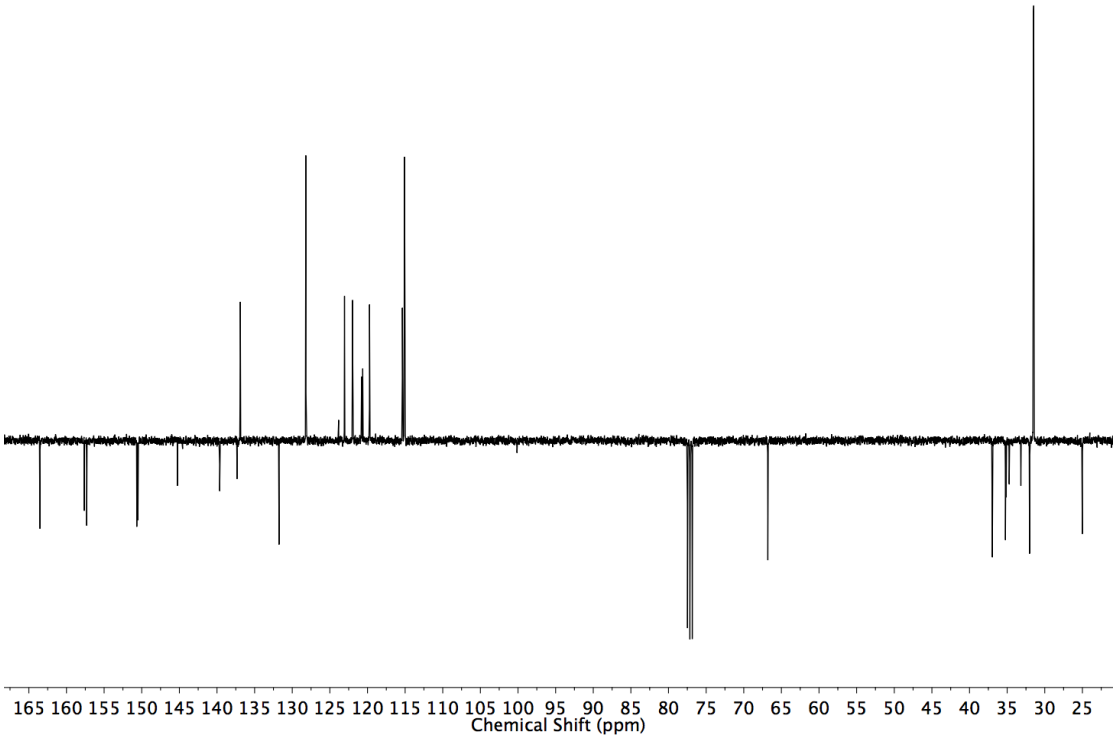

Figure 3.91 JMOD NMR ($CDCl_3$, 101 MHz) of **216**

Axle ***224***

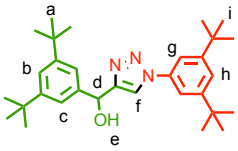

32 (24.4 mg, 0.1 mmol), **192** (23.1 mg, 0.1 mmol), $CuSO_4.5H_2O$ (12.5 mg, 0.05 mmol), and sodium ascorbate (19.8 mg, 0.1 mmol) were placed in a round bottom flask. DMF (2mL) was added and the mixture was stirred for 16 h. The crude mixture was diluted with Et_2O (10 mL), washed with water (2 x 10 mL), brine (5 mL), dried ($MgSO_4$), filtered and the solvent removed *in vacuo*. The residue was purified by column chromatography on silica (petrol with 0 to 50% Et_2O) to afford **224** as white foam (37.0 mg, 78%). ^{1}H NMR (400 MHz, $CDCl_3$): δ 7.74 (s, 1H, H_e), 7.48 (t, *J* =1.7, 1H, H_h), 7.47 (d, *J* =1.7, 2H, H_g) 7.40 (t, *J* =1.7, 1H, H_b), 7.38 (d, *J* =1.7, 2H, H_c), 6.11 (d, *J* =3.7, 1H, H_d), 2.85 (d, *J* =3.7, 1H, H_e), 1.35 (s, 18H, H_i), 1.33 (s, 18H, H_a). ^{13}C NMR (101 MHz, $CDCl_3$): δ 152.9, 151.9, 151.3, 141.2, 136.9, 123.1, 122.4, 121.0, 120.0, 115.7, 70.3, 35.3, 35.1, 31.6, 31.6. HR-ESI-MS *m/z* = 476.3624 $[M+H]^+$ calc. 476.3635.

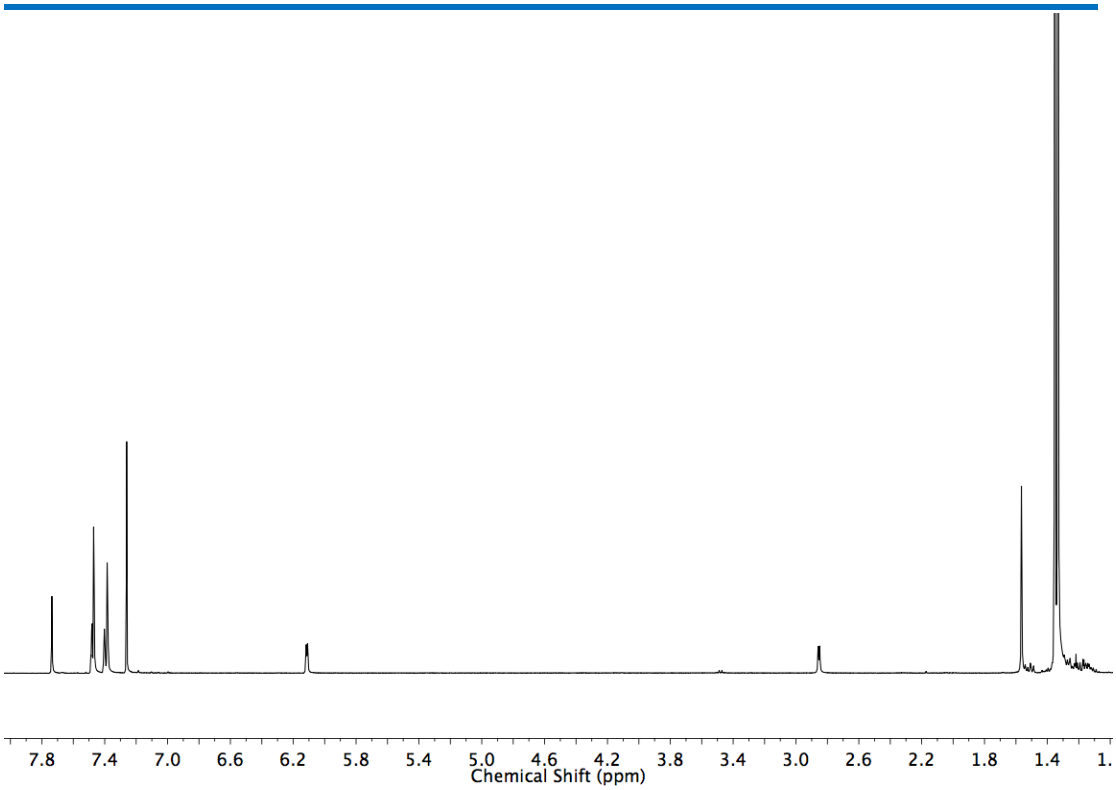

Figure 3.92 ^{1}H NMR ($CDCl_3$, 400 MHz) of **224**

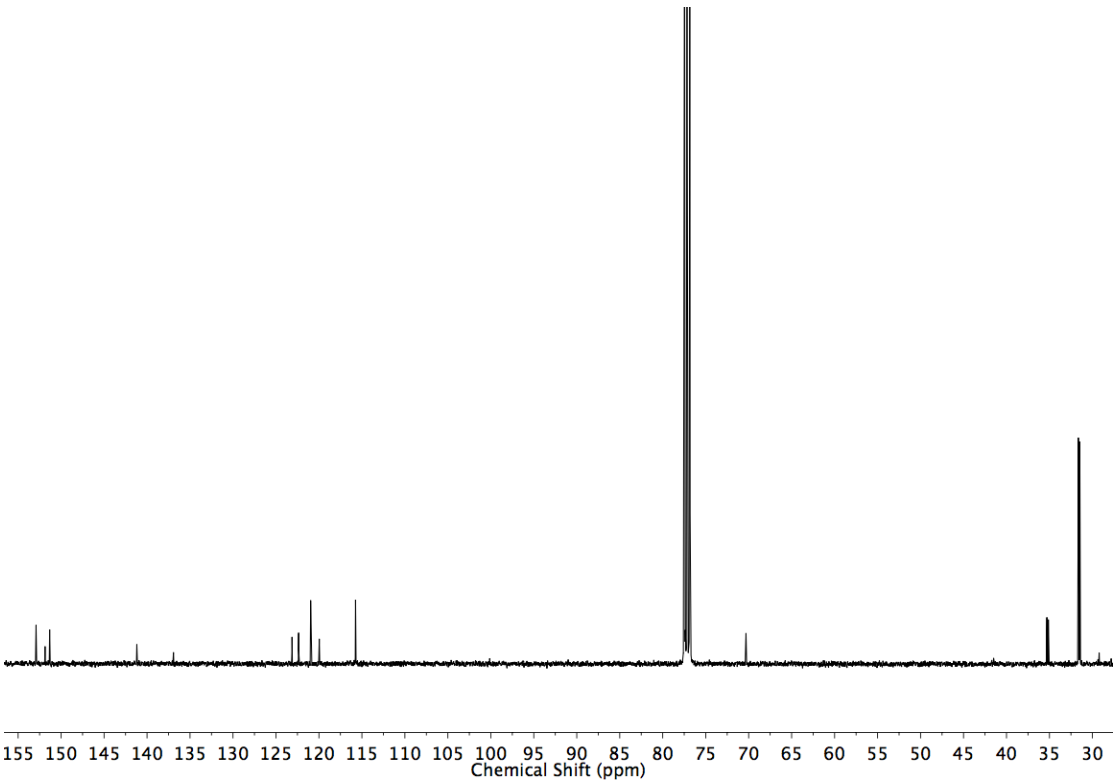

Figure 3.93 ^{13}C NMR ($CDCl_3$, 101 MHz) of **224**

Thread ***225***

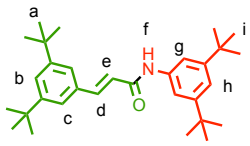

Rotaxane **217** (30.0 mg, 0.03 mmol) was dissolved in CH_2Cl_2 (1.0 mL). Trifluoroacetic acid (0.5 mL) was added and the mixture was stirred for 16 h at room temperature. The mixture was diluted with CH_2Cl_2 (10 mL), washed with $NaHCO_3$(5 mL), brine (5 mL), dried ($MgSO_4$), filtered and the solvent removed *in vacuo*. The residue was purified by column chromatography on silica (petrol and 0 to 10% Et_2O) to afford **225** as white foam (11.0 mg, 82%). ^{1}H NMR (400 MHz, $CDCl_3$): δ 7.79 (d, *J* = 15.5, 1H, H_d), 7.51 (br. s, 2H, H_g), 7.46 (t, *J* =1.7, 1H, H_b) 7.39 (d, *J* =1.7, 2H, H_c), 7.34 (br. s, 1H, H_f), 7.21 (br. s, 1H, H_h), 6.57 (d, *J* = 15.5, 1H, H_e), 1.35 (s, 18H, H_i), 1.34 (s, 18H, H_a). ^{13}C NMR (126 MHz, $CDCl_3$) δ 164.1, 151.7, 151.4, 143.3, 137.5, 134.0, 124.4, 122.3, 120.3, 118.6, 114.5, 35.0, 34.9, 31.4, 31.4. HR-ESI-MS *m/z* = 448.3570 $[M+H]^+$ calc. 448.3574.

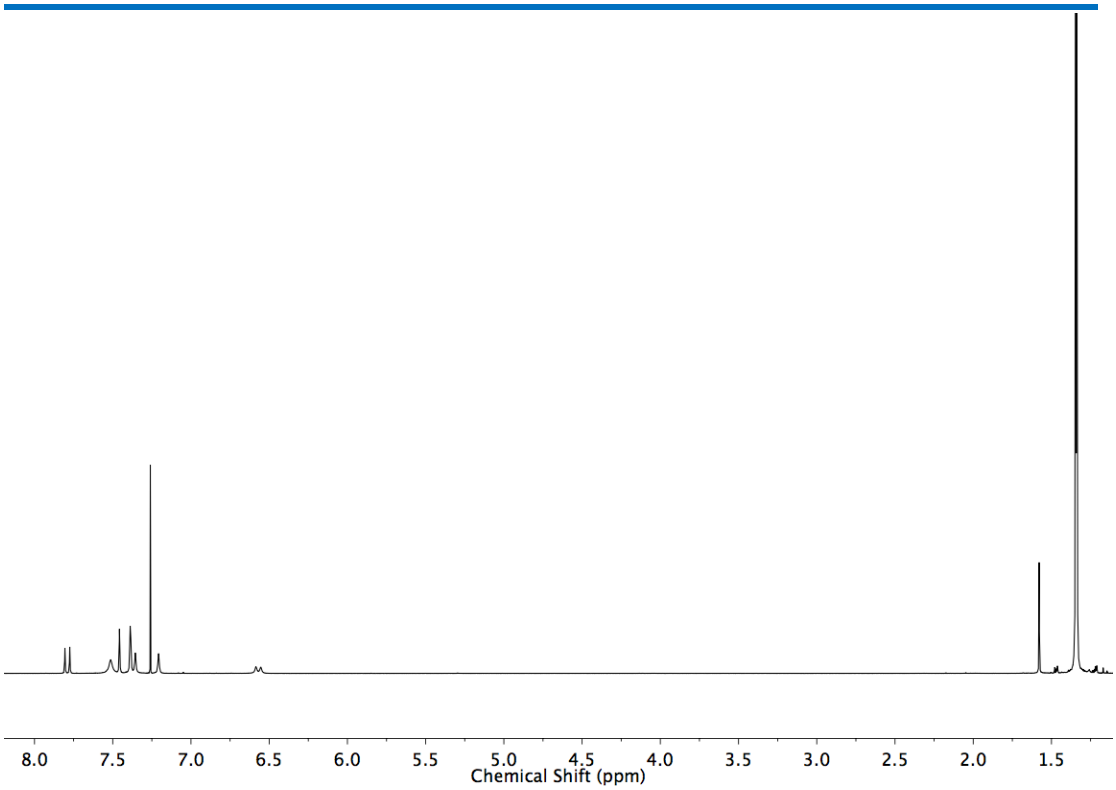

Figure 3.94 ^{1}H NMR ($CDCl_3$, 500 MHz) of **225**

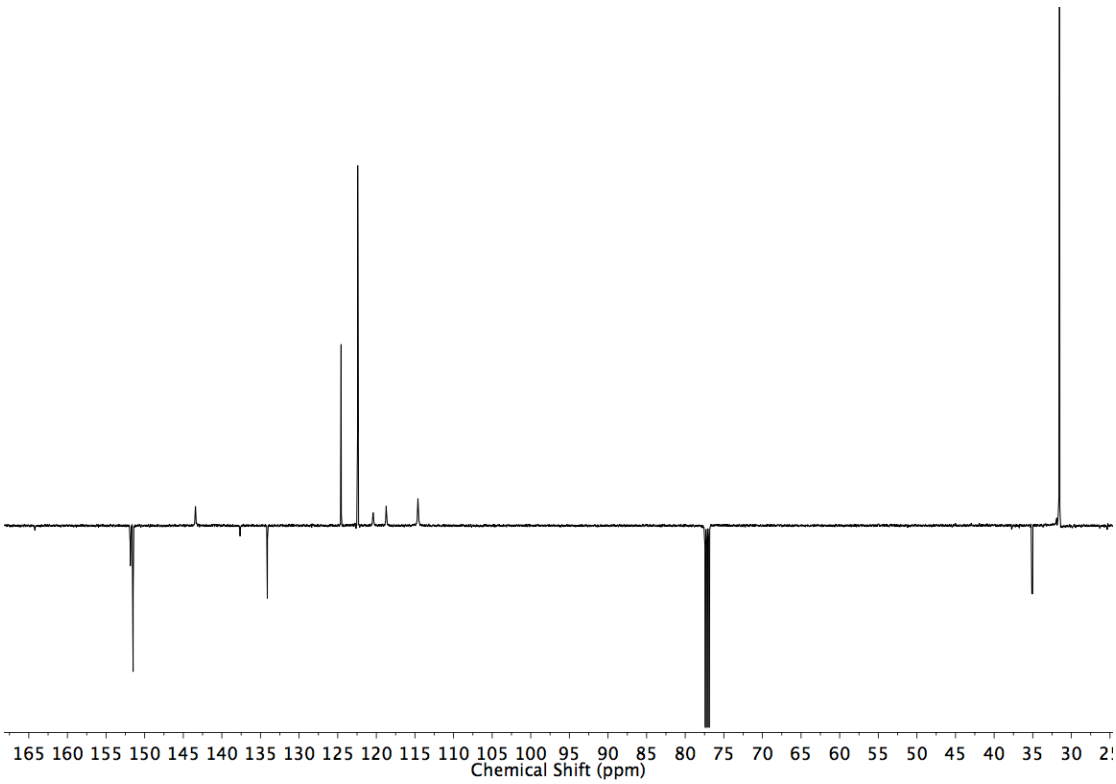

Figure 3.95 JMOD NMR ($CDCl_3$, 126 MHz) of **225**

Table 3.7 Optimisation of the formation of **208** with respect to solvent, temperature and additive.

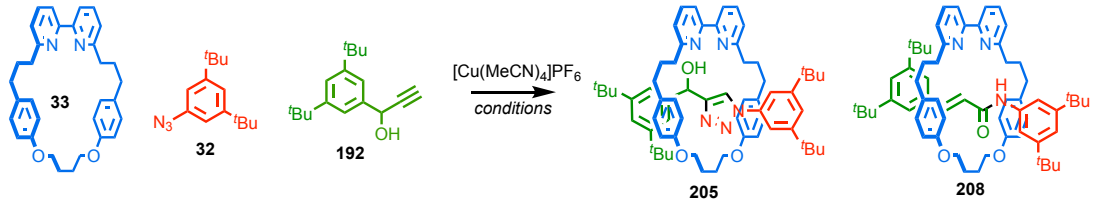

Entry	Time	Solvent	Temp	Additive	Conv.[a]	Ratio 208:205[a]
1	**48 h**	**CH_2Cl_2**	**RT**	**N^{i}Pr$_2$Et (2 eq.)**	**100%**	**>1:99**
2	48 h	CH_2Cl_2 + 10% H_2O	RT	N^{i}Pr$_2$Et (2 eq.)	100%	10:90
3	48 h	CH_2Cl_2 + 10% H_2O	RT	-	100%	60:40
4	48 h	CH_2Cl_2	RT	-	0	-
5	48 h	THF	RT	-	0	-
6	48 h	THF + 10% H_2O	RT	-	24 - 100%*	>99:1
7	48 h	THF + 10% H_2O	RT	KF (0.9 eq.)	97 - 98%	>99:1
8	48 h	THF + 10% H_2O	RT	TBAF (0.9 eq)	29%	92:8
9[b]	40 min	THF + 10% H_2O	80 °C	-	66 - 80%*	>99:1
10[b]	40 min	THF + 10% H_2O	80 °C	KF (0.9 eq)	93 - 99%	>99:1 – 96:4
11[b]	40 min	THF + 10% H_2O	80 °C	TBAF (0.9 eq)	100%	57:43
12[b]	**1 h**	**THF + 10% H_2O**	**70 °C**	**KF (0.9 eq)**	**100%**	**>99:1**
13[b]	1 h	THF + 10% H_2O	70 °C	TBAF (0.9 eq)	100%	92:8
14[c]	**1 h**	**THF + 10% H_2O**	**70 °C**	**KF (0.9 eq)**	**100%**	**>99:1**

[a] Determined by ^{1}H NMR, [b] Reaction performed in a microwave reactor. [c] Reaction performed under thermal conditions. *Reproducibility issues.

Kinetic Study of the reaction

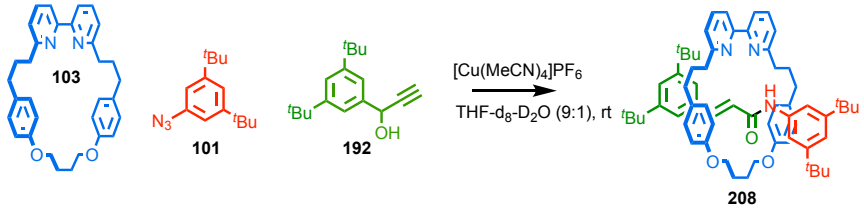

A sample was prepared according to general procedure A. **33** (7.3 mg, 0.0153 mmol), $[Cu(MeCN)_4]PF_6$ (5.5mg, 0.0147 mmol), **32** (4.3mg, 0.0184 mmol), and **192** (4.5 mg, 0.0184 mmol) in the stated deuterated solvents. The crude sample was then passed through a Celite plug and 0.6 ml was transferred into a NMR tube, and a ^{1}H NMR spectrum was recorded on a Bruker Avance 400 in 2 hour intervals. The disappearance of the peak at 7.16 ppm (d, *J* = 1.7, 2H) and the appearance of the peak at 7.91 (d, *J* = 1.7 Hz, 1H) were integrated with respect to the residual THF peak.

*Synthesis of triazolide intermediate **227**.*

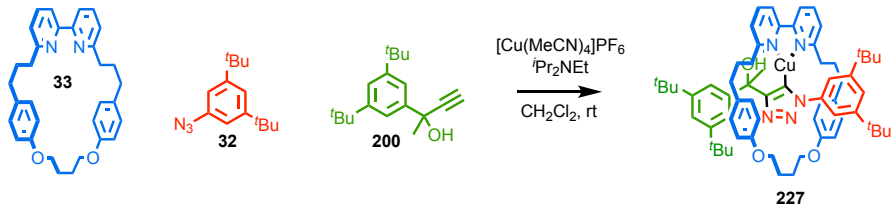

$^{i}Pr_2NEt$ (40.0 µl, 0.23 mmol) was added to a solution of **200** (25.6 mg, 0.10 mmol), **32** (23.1 mg, 0.10 mmol), **33** (48.0 mg, 0.10 mmol) and $[Cu(MeCN)_4]PF_6$ (36.6 mg, 0.098 mmol) in CH_2Cl_2 (8.0 mL) in a microwave vial. The deep red mixture was stirred at room temperature for 16 h. The reaction was diluted in CH_2Cl_2 then washed with water (10 mL), brine (10 mL), dried the solvent removed *in vacuo*. Formation of triazolide **227** was confirmed via LR-ESI-MS *m/z* =1030.9 $[M+H]^+$ calc. 1030.9. The residue was then dissolved in CH_2Cl_2 (8.0 mL), and aliquots (3 x 1.0 mL, hereby referred to as A, B, and C) were transferred into a microwave vial and concentrated *in vacuo*.

*Rearrangement of triazolide intermediate **227** to rotaxane **226**.*

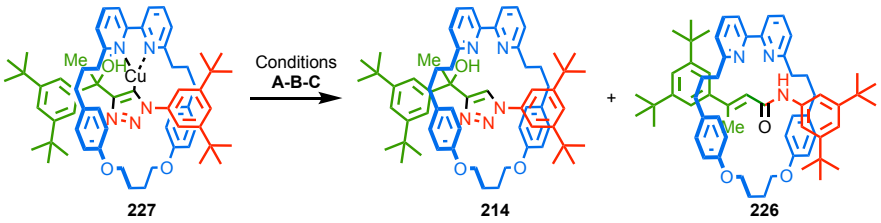

227 **214** **226**

Condition **A**

Crude residue was dissolved in a mixture of $KF_{(aq)}$ (0.1M, 0.1 mL) and THF (0.9 mL). The orange mixture was stirred at 70 °C under microwave irradiation for 1 hour. The reaction mixture was diluted with CH_2Cl_2 (20 mL), washed with EDTA-NH_3 solution (10 mL). The aqueous layer was extracted with CH_2Cl_2 (2 x 10 mL). The combined organic extracts were washed with brine (10 mL), dried ($MgSO_4$) and analysed by ^1H NMR.

Condition **B**

Crude residue was dissolved in a mixture of $KF_{(aq)}$ (0.2 M, 0.05 mL), $HPF_{6(aq)}$ (0.25 M, 0.05 mL) and THF (0.9 mL). The orange mixture was stirred at 70 °C under microwave irradiation for 1 hour. The crude was diluted with CH_2Cl_2 (20 mL), washed with EDTA-NH_3 solution (10 mL). The aqueous layer was extracted with CH_2Cl_2 (2 x 10 mL). Combined organic extracts were washed with brine (10 mL), dried ($MgSO_4$) and analysed by ^1H NMR.

Condition **C**

Crude residue was dissolved in a mixture of $HPF_{6(aq)}$ (0.13 M, 0.1 mL) and THF (0.9 mL). The orange mixture was stirred at 70 °C under microwave irradiation for 1 hour. The crude was diluted with CH_2Cl_2 (20 mL), washed with EDTA-NH_3 solution (10 mL). The aqueous layer was extracted with CH_2Cl_2 (2 x 10 mL). Combined organic extracts were washed with brine (10 mL), dried ($MgSO_4$) and analysed by ^1H NMR.

Production of **226** was confirmed by ^{1}H NMR. For all cases **214** was not observed. Due to broadening of the triazolide intermediate conversion cannot be quantified for the case of **A,** however the presence or absence of the doublet at 6.21 can be used as a qualitative measure.

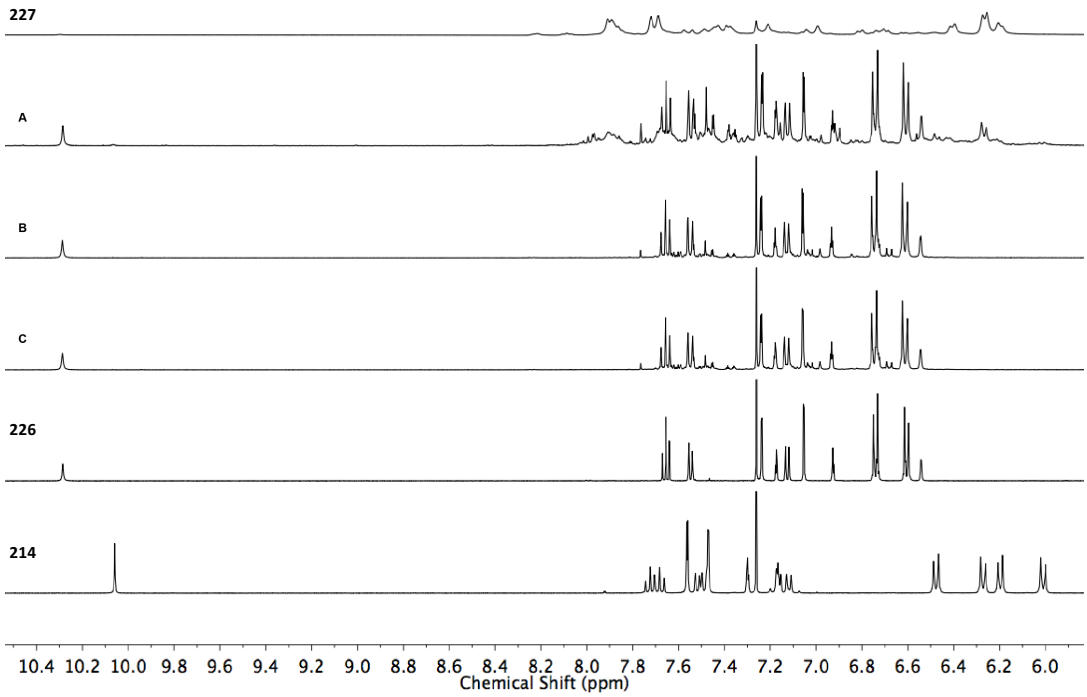

Figure 3.96 Stacked partial ^{1}H NMR (400 MHz, $CDCl_3$) of **227**, conditions A, B, C, **226** and **214** for comparison.

Control experiments

A. A sample of **205** (1.6 mg, 0.0017 mmol) in THF (200 µL) was treated with a solution of $HPF_{6(aq)}$ (20 µL, 0.08 M, 0.0017 mmol), in a sealed microwave vial. The mixture was stirred at 70 °C under microwave irradiation for 1 hour. The crude was diluted with CH_2Cl_2 (10 mL), washed with EDTA-$NH_{3(aq)}$ (5 mL). The aqueous layer was extracted with CH_2Cl_2 (2 x 10 mL). Combined organic extracts were washed with brine (10 mL), dried ($MgSO_4$), filtered and the solvent removed *in vacuo*. Analysis by ^{1}H NMR showed some decomposition but no formation of **11**.

B. A sample of **205** (1.6 mg, 0.0017 mmol) and $[Cu(MeCN)_4]PF_6$ (0.6 mg, 0.0016 mmol) in THF (200 µL) was treated with a solution of $HPF_{6(aq)}$ (20 µL, 0.08 M, 0.0017 mmol), in a sealed microwave vial. The mixture was stirred at 70 °C under microwave irradiation for 1 hour. The crude was diluted with CH_2Cl_2 (10 mL), washed with EDTA-$NH_{3(aq)}$ (5 mL). The aqueous layer was extracted with CH_2Cl_2 (2 x 10 mL). Combined organic extracts were washed with brine (10 mL), dried ($MgSO_4$), filtered and the solvent removed *in vacuo*. Analysis by ^{1}H NMR showed some decomposition but no formation of **11**.

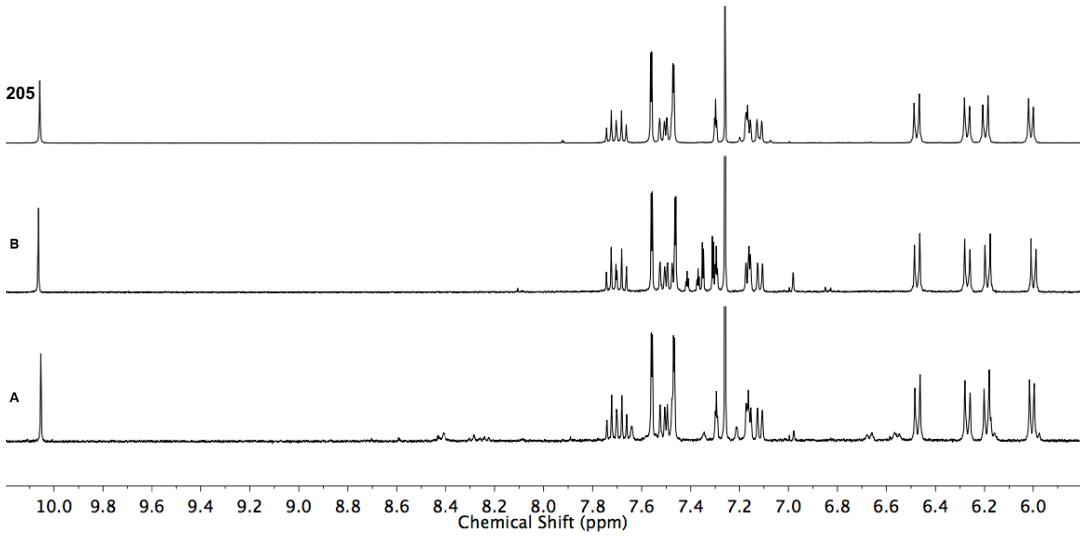

Figure 3.97 Stacked partial ^{1}H NMR (400 MHz, $CDCl_3$) of control experiments, A and B, and **205.**

*Single Crystal X-ray Analysis of rotaxanes **206**, **208**, **217** and **220**.*

Crystals of **206** were grown by vapour diffusion of Et_2O into a CH_2Cl_2 solution. Crystals of **208** and **217** and **220** were grown by vapour diffusion of pentane into a Et_2O solution.

Data were collected at 100 K using a FRE+ HF diffractometer equipped with a Saturn 724+ enhanced sensitivity detector. Cell determination, data collection, data reduction, cell refinement and absorption correction were performed with CrysalisPro. The structures **206** and **217** were solved using SUPERFLIP,[36]-[37] **208** was solved using ShelXT,[38] and **220** was solved using ShelXS.[39] All structures were refined against F_2 using anisotropic thermal displacement parameters for all non-hydrogen atoms using ShelXL[10] and software packages within. Hydrogen atoms were placed in calculated positions, except structure **217** H(1) which was located in the difference map, and all were refined using a riding model.

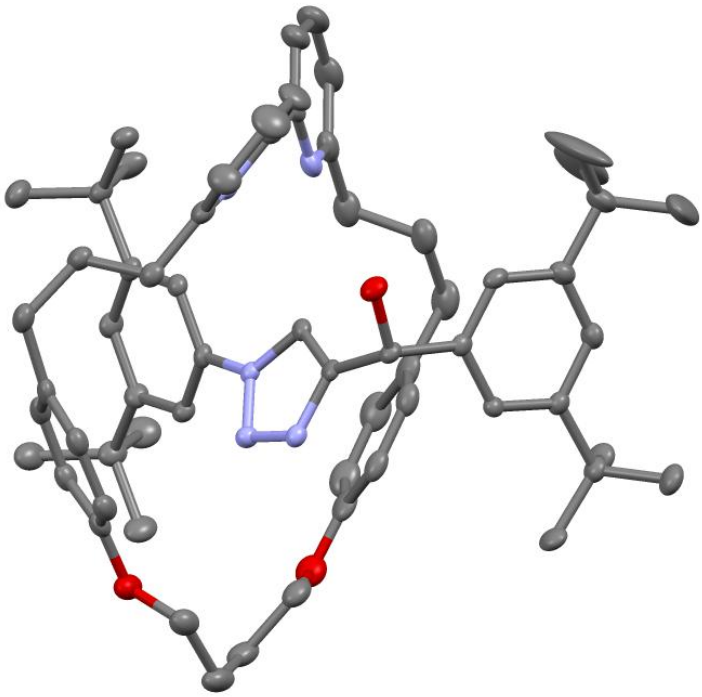

Figure 3.98 Ellipsoid plot of the asymmetric unit of **206** (ellipsoids shown at 50% probability). Hydrogen atoms omitted for clarity

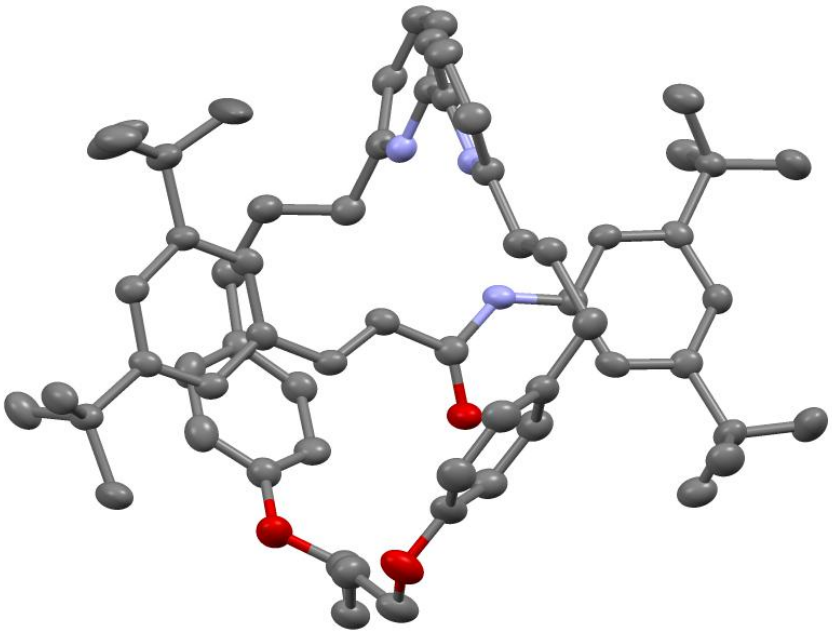

Figure 3.99 Ellipsoid plot of the asymmetric unit of **208** (ellipsoids shown at 50% probability). Hydrogen atoms omitted for clarity

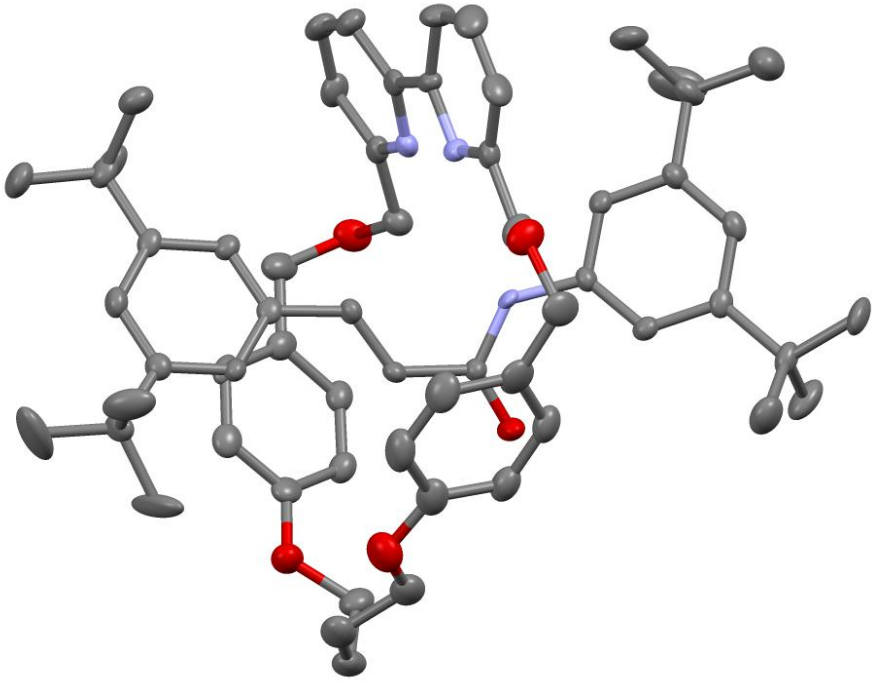

Figure 3.100 Ellipsoid plot of the asymmetric unit of **217** (ellipsoids shown at 50% probability). Hydrogen atoms omitted for clarity

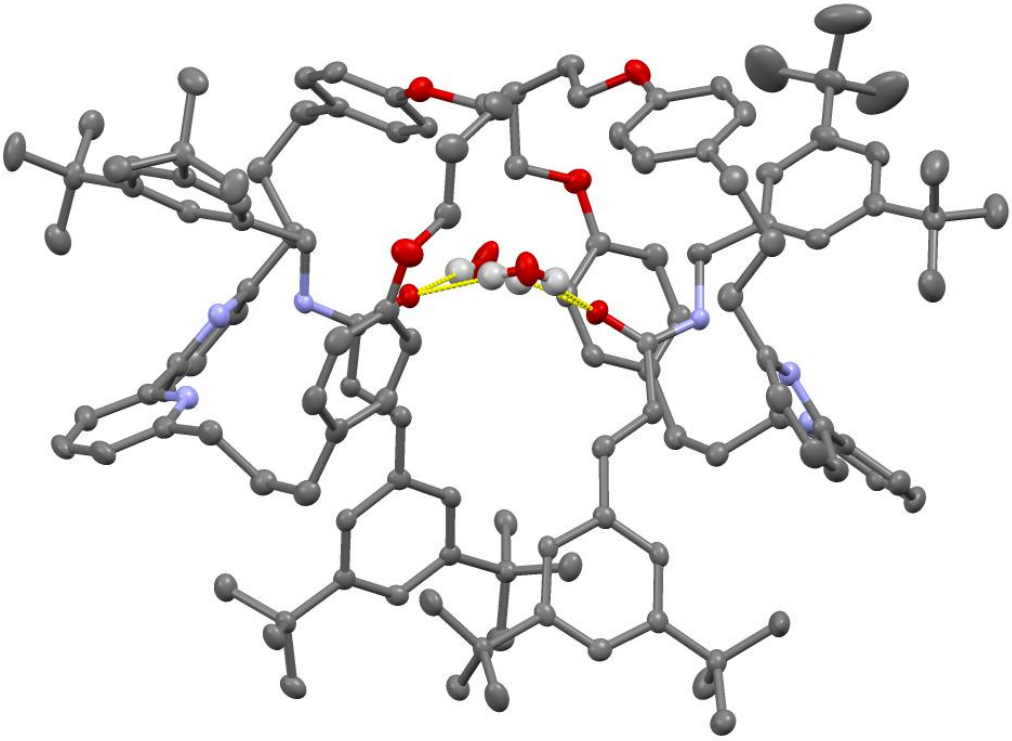

Figure 3.101 Ellipsoid plot of the asymmetric unit of **220** (ellipsoids shown at 50% probability). Hydrogen atoms omitted for clarity, except for H11C, H11D, H15L and H15M.

Compound	**206**
Empirical formula	$C_{63}H_{79}N_5O_3$
Formula weight	954.31
Temperature/K	293(2)
Crystal system	monoclinic
Space group	$P2_1/n$
a/Å	13.8964(7)
b/Å	21.8200(10)
c/Å	18.2565(9)
α/°	90
β/°	94.479(5)
γ/°	90
Volume/Å^3	5518.8(5)
Z	4
ρ_{calc}g/cm^3	1.149
μ/mm^{-1}	0.070
F(000)	2064.0
Crystal size/mm^3	0.055 × 0.05 × 0.015
Radiation	MoKα (λ = 0.71075)
2Θ range for data collection/°	4.752 to 52.744
Index ranges	-17 ≤ h ≤ 17, -27 ≤ k ≤ 27, -22 ≤ l ≤ 22
Reflections collected	63066
Independent reflections	11291 [R_{int} = 0.0677, R_{sigma} = 0.0463]

Data/restraints/parameters	11291/0/656
Goodness-of-fit on F^2	1.004
Final R indexes [I>=2σ (I)]	R_1 = 0.0543, wR_2 = 0.1189
Final R indexes [all data]	R_1 = 0.0731, wR_2 = 0.1284
Largest diff. peak/hole / e $Å^{-3}$	0.54/-0.25

Compound	**208**
Empirical formula	$C_{63}H_{79}N_3O_3$
Formula weight	926.29
Temperature/K	100(2)
Crystal system	orthorhombic
Space group	$Pca2_1$
a/Å	17.0247(4)
b/Å	26.2343(10)
c/Å	12.4688(4)
α/°	90
β/°	90
γ/°	90
Volume/Å^3	5569.0(3)
Z	4
ρ_{calc}g/cm^3	1.105
μ/mm^{-1}	0.067
F(000)	2008.0
Crystal size/mm^3	0.2 × 0.07 × 0.035
Radiation	MoKα (λ = 0.71075)
2Θ range for data collection/°	3.92 to 52.746
Index ranges	-11 ≤ h ≤ 21, -18 ≤ k ≤ 32, -15 ≤ l ≤ 15
Reflections collected	21233
Independent reflections	11078 [R_{int} = 0.0474, R_{sigma} = 0.0902]

Data/restraints/parameters	11078/1/637
Goodness-of-fit on F^2	1.026
Final R indexes [I>=2σ (I)]	R_1 = 0.0738, wR_2 = 0.1496
Final R indexes [all data]	R_1 = 0.1213, wR_2 = 0.1810
Largest diff. peak/hole / e $Å^{-3}$	0.31/-0.24

Compound	**217**
Empirical formula	$C_{61}H_{75}N_3O_5$
Formula weight	930.24
Temperature/K	100(2)
Crystal system	monoclinic
Space group	$P2_1$
a/Å	10.8046(5)
b/Å	16.8432(5)
c/Å	15.2219(6)
α/°	90
β/°	105.545(4)
γ/°	90
Volume/Å^3	2668.80(19)
Z	2
ρ_{calc}g/cm^3	1.158
μ/mm^{-1}	0.073
F(000)	1004.0
Crystal size/mm^3	0.1 × 0.05 × 0.02
Radiation	MoKα (λ = 0.71075)
2Θ range for data collection/°	5.876 to 52.744
Index ranges	-13 ≤ h ≤ 13, -20 ≤ k ≤ 21, -19 ≤ l ≤ 19
Reflections collected	25741
Independent reflections	10822 [R_{int} = 0.0558, R_{sigma} = 0.0948]

Data/restraints/parameters	10822/1/634
Goodness-of-fit on F^2	1.042
Final R indexes [I>=2σ (I)]	R_1 = 0.0718, wR_2 = 0.1599
Final R indexes [all data]	R_1 = 0.1045, wR_2 = 0.1737
Largest diff. peak/hole / e $Å^{-3}$	0.47/-0.21

Compound	**220**
Empirical formula	$C_{64}H_{83}N_3O_4$
Formula weight	958.33
Temperature/K	100(2)
Crystal system	triclinic
Space group	P-1
a/Å	15.5175(6)
b/Å	16.9490(5)
c/Å	23.3325(6)
α/°	105.257(2)
β/°	100.079(3)
γ/°	93.338(3)
Volume/Å^3	5793.7(3)
Z	4
ρ_{calc}g/cm^3	1.099
μ/mm^{-1}	0.067
F(000)	2080.0
Crystal size/mm^3	0.1 × 0.05 × 0.01
Radiation	MoKα (λ = 0.71075)
2Θ range for data collection/°	5.804 to 52.744
Index ranges	-19 ≤ h ≤ 17, -20 ≤ k ≤ 21, -29 ≤ l ≤ 25
Reflections collected	51024
Independent reflections	22793 [R_{int} = 0.0432, R_{sigma} = 0.0799]

Data/restraints/parameters	22793/0/1309
Goodness-of-fit on F^2	1.155
Final R indexes [I>=2σ (I)]	R_1 = 0.0877, wR_2 = 0.1845
Final R indexes [all data]	R_1 = 0.1236, wR_2 = 0.1990
Largest diff. peak/hole / e $Å^{-3}$	0.89/-0.50

3.5. Bibliography

[1] V. V. Rostovtsev, L. G. Green, V. V. Fokin, K. B. Sharpless, *Angew. Chem. Int. Ed.* **2002**, *41*, 2596–2599.

[2] C. W. Tornøe, C. Christensen, M. Meldal, *J. Org. Chem.* **2002**, *67*, 3057–3064.

[3] B. C. Boren, S. Narayan, L. K. Rasmussen, L. Zhang, H. Zhao, Z. Lin, G. Jia, V. V. Fokin, *J. Am. Chem. Soc.* **2008**, *130*, 8923–8930.

[4] S. G. Agalave, S. R. Maujan, V. S. Pore, *Chem. – Asian J.* **2011**, *6*, 2696–2718.

[5] E. A. Shafran, V. A. Bakulev, Y. A. Rozin, Y. M. Shafran, *Chem. Heterocycl. Compd.* **2008**, *44*, 1040–1069.

[6] J. E. Hein, V. V. Fokin, *Chem. Soc. Rev.* **2010**, *39*, 1302–1315.

[7] M. E. Hermes, F. D. Marsh, *J. Am. Chem. Soc.* **1967**, *89*, 4760–4764.

[8] R. E. Harmon, F. Stanley, S. K. Gupta, J. Johnson, *J. Org. Chem.* **1970**, *35*, 3444–3448.

[9] H. M. L. Davies, J. S. Alford, *Chem. Soc. Rev.* **2014**, *43*, 5151–5162.

[10] O. Dimroth, *Justus Liebigs Ann. Chem.* **1908**, *364*, 183–226.

[11] O. Dimroth, W. Michaelis, *Justus Liebigs Ann. Chem.* **1927**, *459*, 39–46.

[12] T. L. Gilchrist, C. W. Rees, C. Thomas, *J. Chem. Soc. Perkin 1* **1975**, *0*, 8–11.

[13] Y. N. Kotovshchikov, G. V. Latyshev, M. A. Navasardyan, D. A. Erzunov, I. P. Beletskaya, N. V. Lukashev, *Org. Lett.* **2018**, *20*, 4467–4470.

[14] M. Whiting, V. V. Fokin, *Angew. Chem. Int. Ed.* **2006**, *45*, 3157–3161.

[15] F. Himo, T. Lovell, R. Hilgraf, V. V. Rostovtsev, L. Noodleman, K. B. Sharpless, V. V. Fokin, *J. Am. Chem. Soc.* **2005**, *127*, 210–216.

[16] E. J. Yoo, M. Ahlquist, I. Bae, K. B. Sharpless, V. V. Fokin, S. Chang, *J. Org. Chem.* **2008**, *73*, 5520–5528.

[17] K. Namitharan, K. Pitchumani, *Org. Lett.* **2011**, *13*, 5728–5731.

[18] T. Miura, Y. Funakoshi, M. Morimoto, T. Biyajima, M. Murakami, *J. Am. Chem. Soc.* **2012**, *134*, 17440–17443.

[19] N. Selander, B. T. Worrell, V. V. Fokin, *Angew. Chem. Int. Ed.* **2012**, *51*, 13054–13057.

[20] S. H. Kim, D. Y. Jung, S. Chang, *J. Org. Chem.* **2007**, *72*, 9769–9771.

[21] E. J. Yoo, M. Ahlquist, S. H. Kim, I. Bae, V. V. Fokin, K. B. Sharpless, S. Chang, *Angew. Chem. Int. Ed.* **2007**, *46*, 1730–1733.

[22] J. Raushel, V. V. Fokin, *Org. Lett.* **2010**, *12*, 4952–4955.

[23] C. Ebner, C. A. Müller, C. Markert, A. Pfaltz, *J. Am. Chem. Soc.* **2011**, *133*, 4710–4713.

[24] S. G. Newman, M. Lautens, *J. Am. Chem. Soc.* **2010**, *132*, 11416–11417.

[25] Y. Itoh, R. Kitaguchi, M. Ishikawa, M. Naito, Y. Hashimoto, *Bioorg. Med. Chem.* **2011**, *19*, 6768–6778.

[26] J. Hornung, D. Fankhauser, L. D. Shirtcliff, A. Praetorius, W. B. Schweizer, F. Diederich, *Chem. – Eur. J.* **2011**, *17*, 12362–12371.

[27] L. M. Urner, M. Sekita, N. Trapp, W. B. Schweizer, M. Wörle, J.-P. Gisselbrecht, C. Boudon, D. M. Guldi, F. Diederich, *Eur. J. Org. Chem.* **2015**, *2015*, 91–108.

[28] M. G. Freire, C. M. S. S. Neves, I. M. Marrucho, J. A. P. Coutinho, A. M. Fernandes, *J. Phys. Chem. A* **2010**, *114*, 3744–3749.

[29] R. K. Sharma, J. L. Fry, *J. Org. Chem.* **1983**, *48*, 2112–2114.

[30] A. F. Hegarty, J. G. Kelly, C. M. Relihan, *J. Chem. Soc. Perkin Trans. 2* **1997**, *0*, 1175–1182.

[31] X.-M. Sun, X.-G. Wei, X.-P. Wu, Y. Ren, N.-B. Wong, W.-K. Li, *J. Phys. Chem. A* **2010**, *114*, 595–602.

[32] W. Zhu, D. Ma, *Chem. Commun.* **2004**, *0*, 888–889.

[33] J. J. Gassensmith, L. Barr, J. M. Baumes, A. Paek, A. Nguyen, B. D. Smith, *Org. Lett.* **2008**, *10*, 3343–3346.

[34] E. A. Neal, S. M. Goldup, *Angew. Chem. Int. Ed.* **2016**, *55*, 12488–12493.

[35] J. E. M. Lewis, R. J. Bordoli, M. Denis, C. J. Fletcher, M. Galli, E. A. Neal, E. M. Rochette, S. M. Goldup, *Chem. Sci.* **2016**, *7*, 3154–3161.

[36] L. Palatinus, G. Chapuis, *J. Appl. Crystallogr.* **2007**, *40*, 786–790.

[37] L. Palatinus, S. J. Prathapa, S. van Smaalen, *J. Appl. Crystallogr.* **2012**, *45*, 575–580.

[38] G. M. Sheldrick, *Acta Crystallogr. Sect. C Struct. Chem.* **2015**, *71*, 3–8.

[39] G. M. Sheldrick, *Acta Crystallogr. A* **2008**, *64*, 112–122.

Chapter 4: Efficient multicomponent active template synthesis of catenanes

Abstract: This chapter reports the simple and high yielding active template synthesis of catenanes using simple macrocycle precursor bearing azide and alkyne functional groups. In addition, our approach was successfully applied to co-macrocyclisation of bis-azides and bis-alkynes as well as oligerisation of azide/alkyne precursor prior mechanical bond formation.

The initial optimisation of the catenane forming reaction, the synthesis and characterisation of catenanes **242**-**245** were carried out by Dr Jamie Lewis. The synthesis of precursors **237** and **240** was carried out by Dr Jamie Lewis. I performed the majority of the characterisation and optimisation of the multicomponent active template synthesis of catenanes.

Prior publication: The totality of this chapter was previously published as part of:

J. E. M. Lewis, F. Modicom, S. M. Goldup, "*Efficient multicomponent active template synthesis of catenanes*" J. Am. Chem. Soc., **2018**, 140, 4787-4791.

4.1. Introduction

The initial reports on the synthesis of mechanically interlocked molecules focused on catenanes,[1–4] however in the following years reports on rotaxanes dominated the field.[5–8] The synthetic challenge involved in the synthesis of catenanes was probably the reason for the growth of rotaxanes compare to catenanes. Rotaxanes can be prepared using threading-then-stoppering approach, whereas catenanes require a macrocyclic ring closure which is competing with the oligomerisation. In order to overcome this competition, strategies were developed.

Passive template synthesis initiated by Sauvage and co-workers was a key discovery for the growth of catenanes.[3,9] The possibility to have strong metal-ligand interactions enabled the pre-organisation of the system before cyclisation to afford catenanes. The efficiency of the macrocyclisation relied on the pre-assembly of the architecture and the successful cyclisation forming the catenanes.

The active template approach initiated by Leigh and co-workers for the synthesis of rotaxanes suggested the possibility to apply this methodology for the synthesis of catenanes.[10,11] Despite the efforts of Saito and co-workers and Leigh and co-workers, the synthesis of catenanes using the active template requires the use of a large excess of macrocycle precursors to obtain reasonable yield.[12–14]

Small macrocycle modification of Leigh active template copper mediated azide-alkyne cycloaddition (AT-CuAAC) reaction considerably improved the efficiency of the synthesis rotaxanes.[10,11,15,16] This approach was applied for the rapid iterative synthesis of oligorotaxanes in high yield.[17] The rapid reaction suggested that catenanes could be synthesised under pseudo-high dilution conditions, affording catenanes in good yield with short reaction times.

We proposed to develop the AT-CuAAC reaction as an efficient synthesis of [2]catenanes with various functional groups. In order to optimise the efficiency of this reaction, a single azide-alkyne functionalised precursor was synthesised. The optimisation of the reaction was performed, leading to the extremely successful approach for monomeric as well as more sophisticated systems.

4.2. Results and Discussion

4.2.1. Synthesis of azide-alkyne functionalised precursor

In order to carry out the proposed study, a series of substrates was synthesised. The synthesis of an azide-alkyne precursor with a long flexible linker between the functions was performed in a 7 steps synthesis (Figure 1). The aniline function was converted to the azide **229** using the Sandmeyer reaction in good yield (93%). The procedure using *tert*-butyl nitrite and trimethylsilyl azide in acetonitrile was selected in preference to using sodium nitrite and sodium azide in concentrated hydrochloric acid. A double Sonogashira reaction was performed with nonadiyne on methyl 4-bromobenzoate in $^{i}Pr_2NH$. Product **232** was obtained in high yield (86%). The internal alkyne was quantitatively reduced using hydrogen gas in presence of 10% wgt Pd on charcoal. Reduction of the ester function was performed using $LiAlH_4$ in THF at reflux resulting in quantitative formation of **233**. The conversion of the alcohol to the bromide was performed using carbon tetrabromide and triphenylphosphine. Product **234** was obtained in good yield (90%). The addition of one molecule of **229** to **234** resulted in the desymmetrised product. The isolated yield of the reaction was increased by addition of three equivalents of **234** compare to **229**, from 25% yield with one equivalent to 59% yield for three equivalents. Precursor **236** was finally obtained by reacting **235** with propargyl alcohol in presence of sodium hydride in good yield (98%).

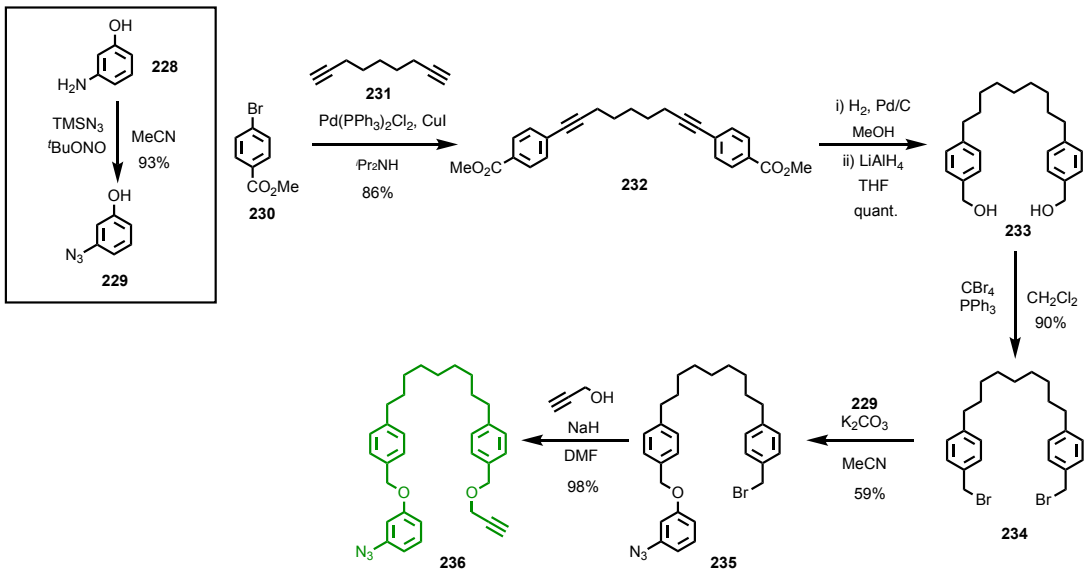

Figure 4.1 Synthetic route to access **236**.

In addition, a series of azide-alkyne functionalised precursor with varying distances between the two functions was prepared from **229**. The precursor **239** with five atoms between the two functions was obtained by reaction **229** with propargyl bromide in good yield (94%). Reaction with pent-4-ynyl tosylate resulted in **238** in 86% yield. Precursor **237** was obtained in a three steps synthesis from 4-hydroxybenzyl alcohol in 79% over three steps. Diazide compound **240** was prepared by treated **234** with sodium azide in 97% yield. Similarly, **241** was obtained from α,α'-dibromo-*p*-xylene in 99% yield.

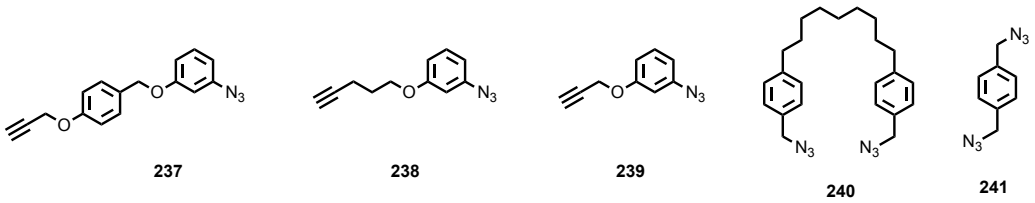

Figure 4.2 Series of precursors for multicomponent AT-CuAAC synthesis of catenanes.

4.2.2. Optimisation of the [2]catenane synthesis using 236

In order to have an efficient procedure for the preparation of [2]catenanes, the effects of varying solvent, temperature, concentration and rate of the addition of **236** were assessed. The initial reaction was performed at room temperature. The addition of **236** as a 25 mM solution in a 1:1 $CHCl_3$/EtOH into a solution containing macrocycle **74** and $[Cu(MeCN)_4]PF_6$ as a 10 mM solution in a 1:1 $CHCl_3$/EtOH over four hours resulted in 82% conversion of the macrocycle **74** into the catenane **242** (Table 4.1, Entry 1). In this case, non-reacted precursor **236** was observed in the crude reaction mixture. Increase of the reaction temperature to 60 °C gave complete conversion of **74** into the catenane structure (Table 4.1, Entry 2). Further increase of the temperature to 80 °C, did not change the outcome of the reaction with complete conversion to the catenane (Table 4.1, Entry 3). It is important to note that the addition of two molecules of **236** into **74** leading to a [3]catenane was never observed. Increase of the concentration of the solution containing the catalyst did not affect significantly the conversion towards the catenane, with 97% and 93% when the concentration increased from 25 to 50 mM (Table 4.1, Entries 4 and 5). A trial was performed at higher concentration (100 mM) of catalyst solution resulted in 92% conversion at 80 °C, over eight hours. The variation of the addition time did not significantly affect the outcome of the reaction, with 98% and 100% conversion for two and eight hours addition respectively (Table 4.1, Entries 7 and 8). For all the reaction performed, the macrocyclisation was

occurring through the macrocycle leading to the formation of catenane. Under the pseudo-high dilution conditions used, the cyclisation appeared to be faster in the cavity of the macrocycle than the oligomerisation in the bulk. The modification of the solvent mixture used during the reaction was crucial for the outcome of the reaction. When $Cl_2CHCHCl_2$ and ^{i}PrOH were used instead of the $CHCl_3$ and EtOH decreased the conversion to 33% (Entry 9). This low conversion was due to the low solubility of the macrocycle-copper complex in the solvent mixture. Under the optimised conditions defined in Table 4.1, Entry 2, it appears that the instantaneous concentration was low enough to favour the intramolecular cyclisation of **236** rather than the oligomerisation of **236**.

Table 4.8 Optimisation of the [2]catenane synthesis using 236

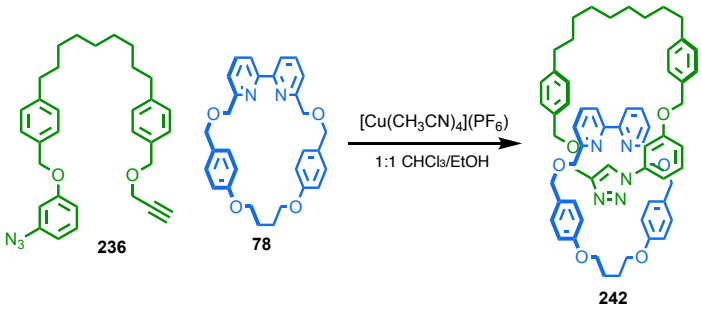

Entry	Initial concentration catalyst (mM)	Final concentration catalyst (mM)	Temperature (°C)	Addition time (h)	Yield[a] (%)
1	10	7	rt	4	82
2	10	7	60	4	100
3	10	7	80	4	100
4	25	13	60	4	97
5	50	17	60	4	93
6	100	50	80	8	92
7	10	7	60	2	98
8	10	7	60	8	100
9[b]	10	7	60	4	33

[a] Determined by ^{1}H NMR, [b] 1 : 1 mixture $Cl_2CHCHCl_2$ / ^{i}PrOH used as solvent.

4.2.3. Variation of the bipyridine functionalised macrocycle

Using the optimised conditions defined above, catenane **242** was obtained in 94% yield from **78** and one equivalent of precursor **236** (Table 4.2, Entry 1). The use of a larger macrocycle **108**, under the optimised conditions, resulted in 88% conversion of the macrocycle into catenane **108**. Attempts at varying the addition rate of the reaction and the temperature did not improve the conversion. Those variations highlighted the fact that **108** presented a lower selectivity for the mechanical bond formation. However, increasing the equivalent of **236** added from one to 1.5 equivalents resulted in complete consumption of **108** into **243**, which was isolated in 96% yield (Table 4.2, Entry 2). Analysis of the crude reaction mixture by ^{1}H NMR of the reaction did not show the formation of other interlocked molecules such as [3]catenane with two molecules of **236** or [2]catenane with a dimeric macrocycle from **236**. The use of a more rigid macrocycle **110**, under the optimised conditions, resulted in a slower and less selective reaction. The analysis of the LC-MS of the crude reaction mixture revealed the presence of macrocycle **110** in solution as well as [2]catenane with a dimeric macrocycle from **236**. In order to overcome this lack of selectivity, addition of 1.5 equivalents of **236** at 80 °C resulted in complete conversion of macrocycle **110** as well as complete selectivity towards the expected [2]catenane. Catenane **110** was isolated in 98% yield (Table 4.2, Entry 3. When the reaction was performed at 80 °C in presence of **95**, 94% conversion of the macrocycle was achieved. The product was isolated in 86% yield due to co-elution during the purification of impurities such as the macrocycle derived from with catenane **95** (Table 4.2, Entry 4). Macrocycle **246** from **236** was prepared using the optimised procedure in a moderate 47% yield.

Table 4.2 Efficient AT-CuAAC synthesis of [2]catenanes

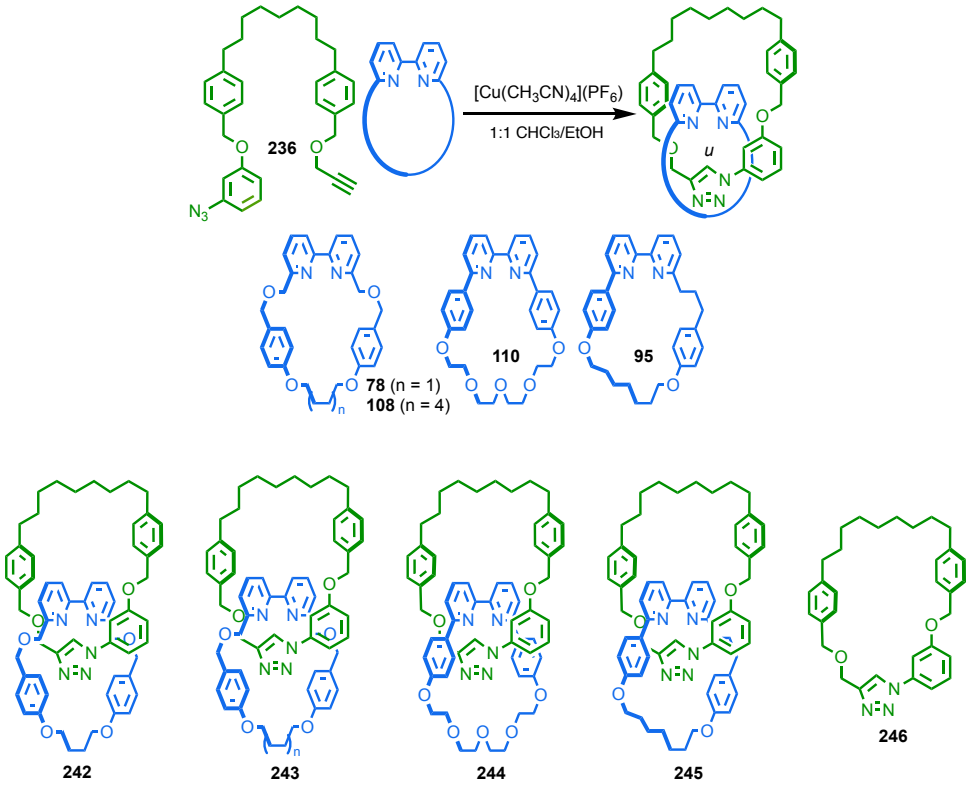

Entry	Macrocycle	Catenane	Equiv. 236	Temperature	Yield
1	**78**	**242**	1.0	60 °C	>99%[a] (94%)[b]
2	**108**	**243**	1.5	60 °C	>99%[a] (96%)[b]
3	**110**	**244**	1.5	80 °C	>99%[a] (98%)[b]
4	**95**	**245**	1.0	80 °C	92%[a] (86%)[b]

Reagents and conditions: **236** in 1:1 $CHCl_3$-EtOH (25 mM) added to **macrocycle** (10 mM), $^{i}Pr_2NEt$ (2 equiv.) and $[Cu(MeCN)_4]PF_6$ (0.99 equiv.) in 1:1 $CHCl_3$-EtOH over 4 h. [a] Determined by ^1H NMR. [b] Isolated yield.

Catenanes **242**, **243**, **244**, **245** were characterised by ^1H NMR (Figure 4.3). In the case of **242**, **244** and **245**, the chemical shift of the triazole proton H_u was higher than the one observed in the case of macrocycle **246**. This change in chemical shift can be explained by the interaction of H_u with the bipyridine unit as hydrogen bond interaction. In the case of **243**, the chemical shift is similar to the one observed in the case of macrocycle **246** highlighting that H_u is not interacting strongly with the bipyridine in solution. The reduction of the

congestion in the larger macrocycle increased the flexibility of the interlocked structure, which allowed the pirouetting of each macrocycle.

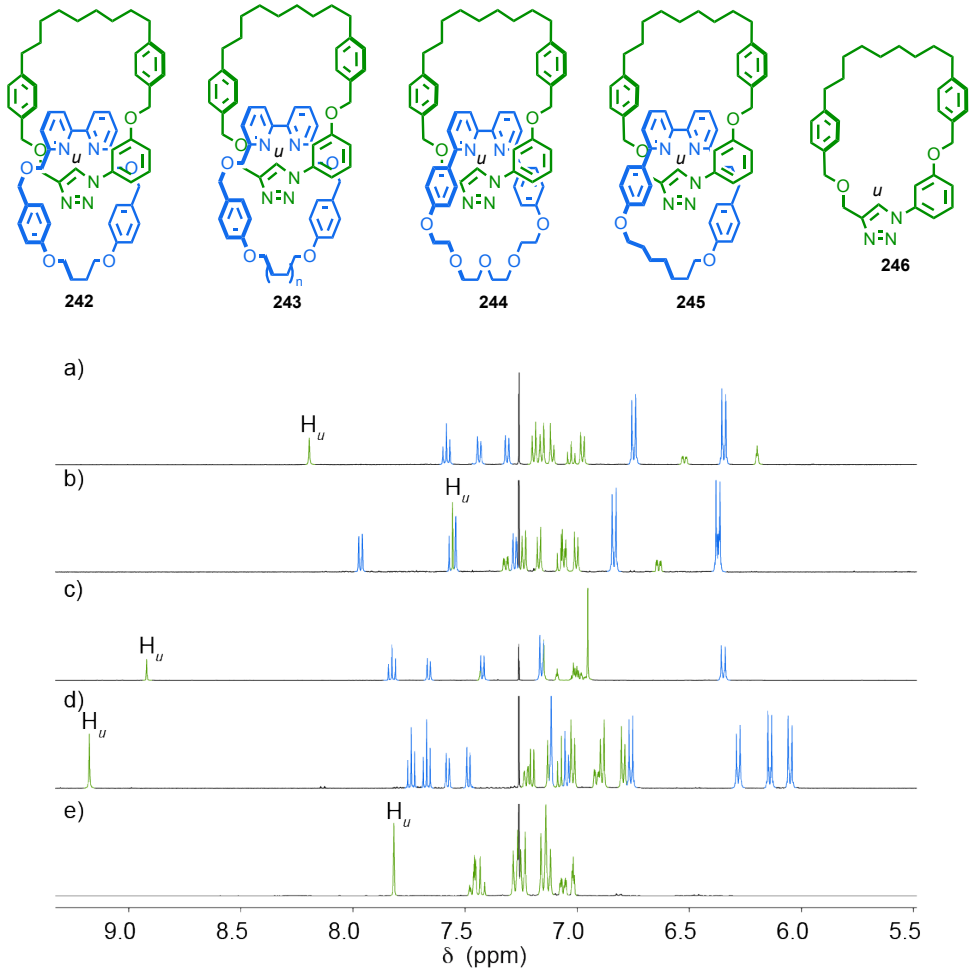

Figure 4.3 Stack partial ^{1}H NMR ($CDCl_3$, 500 MHz) of a) catenane **242**, b) catenane **243**, c) catenane **244**, d) catenane **245**, e) macrocycle **246**.

Catenanes **243** and **245** were characterised by single crystal x-ray diffraction. Their solid-state structures showed crowded structures which can explain why no [3]catenanes were ever observed during the screening of the reaction, even when the large macrocycle **243** was used.

The solid-state structure of **243** did not show any significant stabilising inter-component interactions that are typically observed in interlocked molecules using the passive template approach for their synthesis (Figure 4.4). Catenane **243** was found to adopt coconformations that maximise weak interactions such as C-H H-bonding and C-H-π interactions due to the proximity of both subunits. The solid-state structure of **243** contained a racemic mixture of

enantiomers that are related by points of inversion. Although surprising, due to the presence of C_{2v}-symmetric macrocycle **108** subunit in **243**, the relative arrangement of the ring formed from **236**, compared to the bipyridine macrocycle, desymmetrised the bipyridine macrocycle. This kind of chirality can be defined as coconformationally topologically chiral. In the solid-state, H_u from the triazole was located outside of the cavity of **108** and did not interact with the bipyridine unit, as previously observed in ^{1}H NMR analysis.

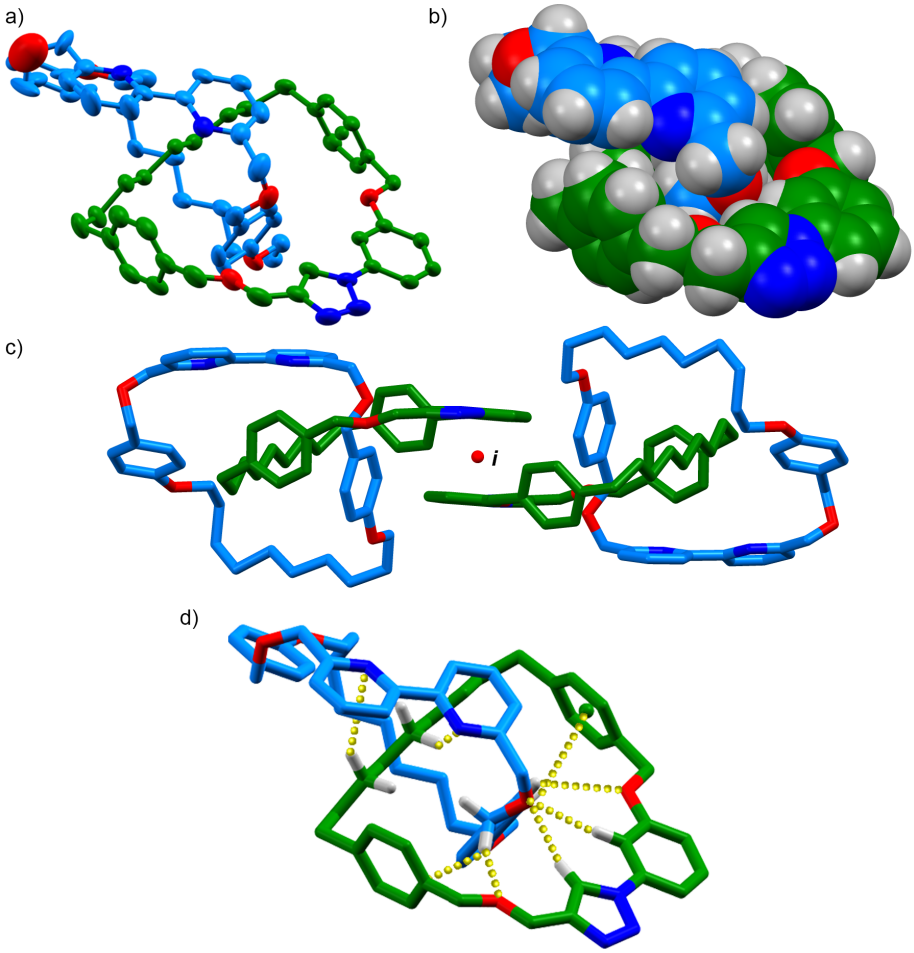

Figure 4.4 a) Ellipsoid plot of the assymetric unit of **243** (ellipsoids shown at 50% probability). Hydrogen atoms omitted for clarity. b) Spacefilling model of **243**. c) Co-conformational enantiomers observed in the solid state related by a point of inversion of **243**. d) Tube representation of **243** showing selected intermolecular contacts (for labelling scheme see characterisation data; distances (Å): H_a–O = 2.55; H_f–N = 3.71; H_n–N = 3.31; H_u–O = 2.38; H_E–O = 2.77; H_E–C = 3.08; H_F–O = 2.94; H_G–● = 3.08).

Catenane **245** was obtained as racemic mixture of enantiomers related by point of inversion (Figure 4.5). In this case, this chirality was the result of the assembly of two C_s-symmetric macrocycles resulting in a topologically chiral catenane. Weak interactions were displayed in the crystal structure, such as C-H H-bonding, C-H-π and π-π interactions.

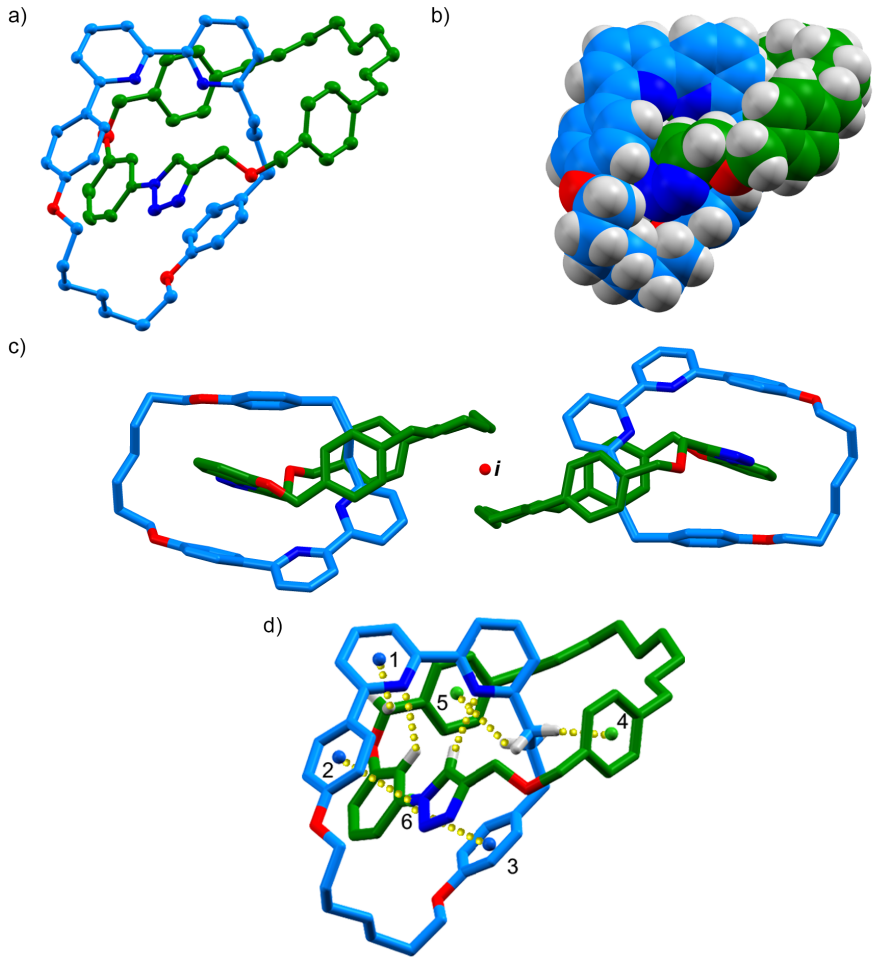

Figure 4.5 a) Ellipsoid plot of the assymetric unit of **245** (ellipsoids shown at 50% probability). Hydrogen atoms omitted for clarity. b) Spacefilling model of **245**. c) Co-conformational enantiomers observed in the solid state related by a point of inversion of **245**. d) Tube representation of **245** showing selected intermolecular contacts (for labelling scheme see characterisation data; distances (Å): H_a–N = 2.88; H_e–●$_1$ = 2.64; H_u–N = 2.43; H_P–●$_5$ = 3.16; H_Q–●$_4$ = 3.00; ●$_2$–●$_6$ = 3.42; ●$_3$–●$_6$ = 3.62).

4.2.4. Multicomponent AT-CuAAC approach for the synthesis of [2]catenane

The excellent selectivity of our new methodology suggested that this reaction could be suitable for a multicomponent cyclisation approach from simple starting materials by a controlled oligomerisation pathway. One of the advantages of this approach would be to produce [2]catenanes on larger scales. In fact, smaller precursors can be prepared in less steps and higher yield than precursor **236**. It is also easier to vary small molecule than large molecule (less than 4 steps compare to more than 7 steps).

In order to illustrate this new approach, a stoichiometric mixture of diazide **240** and propargyl ether **247** was added into the solution containing macrocycle **78** and

$[Cu(MeCN)_4]PF_6$. Analysis of the crude reaction mixture by ^1H NMR revealed full consumption of **74** when 2 equivalents of each precursor were added. LC-MS analysis of the crude reaction mixture revealed the formation of [2]catenane **248** composed of the bipyridine and a second ring containing one molecule of **240** and one molecule of **247** ([1+1] macrocycle). The corresponding [1+1] macrocycle was also detected during the LC-MS analysis. A large number of other organic molecules was detected in the crude reaction mixture, but the identification of their structures was not possible, which could likely be due to oligomeric molecules. Catenane **247** was isolated in a 75% yield (Figure 4.6). Replacing propargyl ether with 2,6-diethylnylpyridine **249** resulted in the same observations. The corresponding [2]catenane **250** was selectively formed during the reaction and isolated in 71% yield (Figure 4.6).

When the reaction was performed with α,α'-diazido-*p*-xylene **241** and propargyl ether **247**, the only detected interlocked structure was composed of macrocycle **78** and a macrocycle containing two molecules of **247** and two molecules of **241** ([2+2] macrocycle). The [2+2] macrocycle represented the smallest macrocycle able to encircle **78**, as the heterodimeric macrocycle was too small to do so. Catenane **251** was isolated in good yield (78%) (Figure 4.6). When propargyl ether was replaced by 2,6-diethynylpyridine **249** in the reaction, the only interlocked structure formed during the reaction was, once again, the [2]catenane **252** constituted of **78** and the [2+2] macrocycle and was isolated in 72% yield (Figure 4.6). The analysis of the LC-MS revealed the presence of a molecule containing one molecule of **241** and two molecules of 2,6-diethynylpyridine, which was consistent with the idea of oligomerisation prior cyclisation.

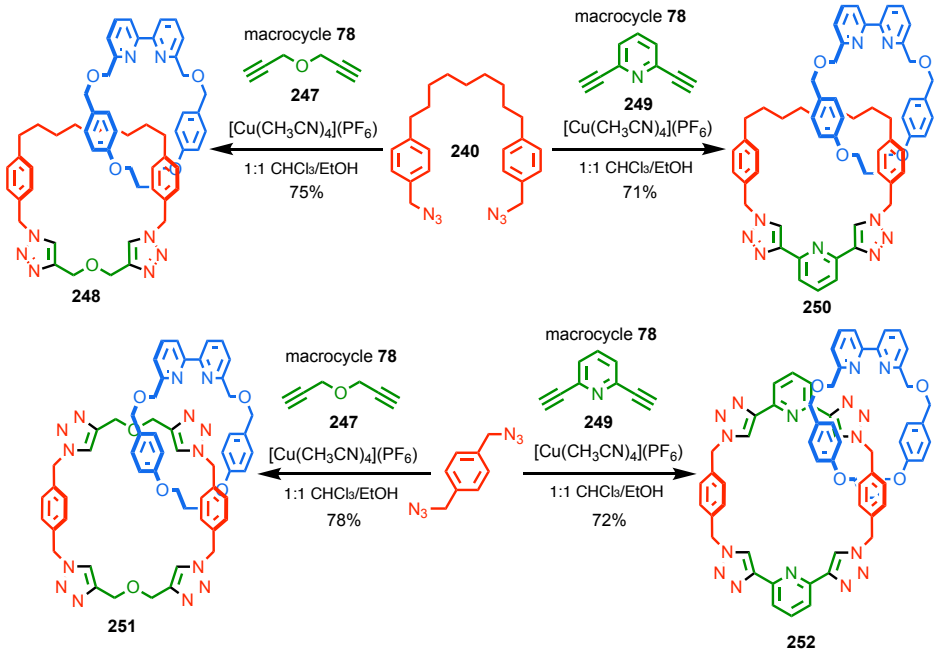

Figure 4.6 Multicomponent active template synthesis of catenanes **248**-**252**.

The hetero-oligomerisation-then-cyclisation approach is a multi-step process. By using 0.96 equivalent of $[Cu(MeCN)_4]PF_6$ with respect to macrocycle **78**, the AT-CuAAC is ensured to occur in the cavity of the macrocycle. Under those conditions, the first AT-CuAAC would generate the first triazole function. However, the absence of a bulky group in the new fragment resulted in a pseudo-rotaxane which dissociated, after protodemetalation of the copper-carbon bond. In the case of the [1+1] system, the closure of the ring occurred during an intramolecular AT-CuAAC cyclisation generating the [2]catenane after protodemetalation of the copper carbon bond. When the azide-alkyne functionalised molecule was too short to undergo an intramolecular cyclisation, the length was extended *via* AT-CuAAC steps. The [2+2] system underwent three AT-CuAAC steps leading each time to an unstable pseudo-rotaxane which could cyclise during the last AT-CuAAC event.

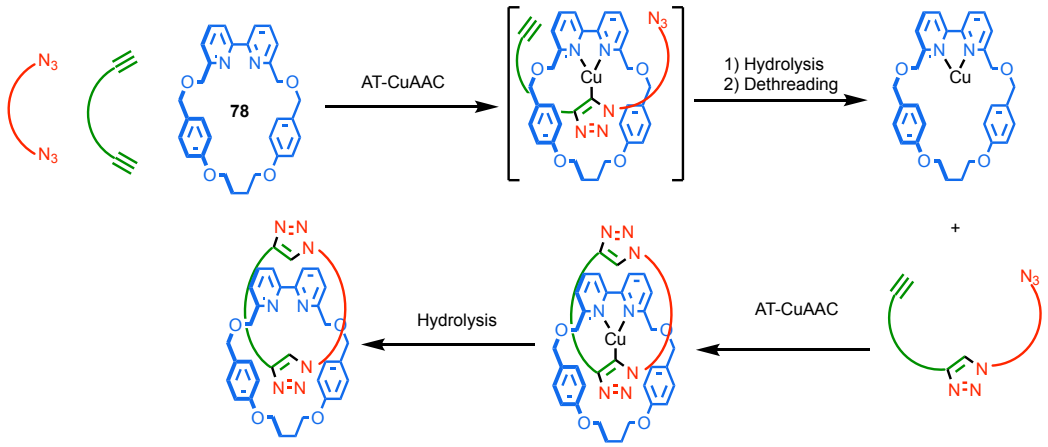

Figure 4.7 General mechanism for the hetero-oligomerisation-then-cyclisation using the AT-CuAAC approach

Similarly to catenane **243**, the solid-state structure of **250** showed a racemic mixture of enantiomers related by point of inversion. The coconformation adopted in the solid-state resulted in the desymmetrisation of each C_{2v}-symmetric macrocycle by the other one. As illustrated in Figure 4.8, the bipyridine-functionalised macrocycle was desymmetrised by the presence of the second macrocycle. The desymmetrisation of the triazole-functionalised ring occurred in the aliphatic region. The interaction between both rings is shown in Figure 4.8. The bipyridine motif interacted with half of the aliphatic chain thus desymmetrising the macrocycle. The chirality in the solid-state for catenane **250** was described as coconformationally topologically chiral.

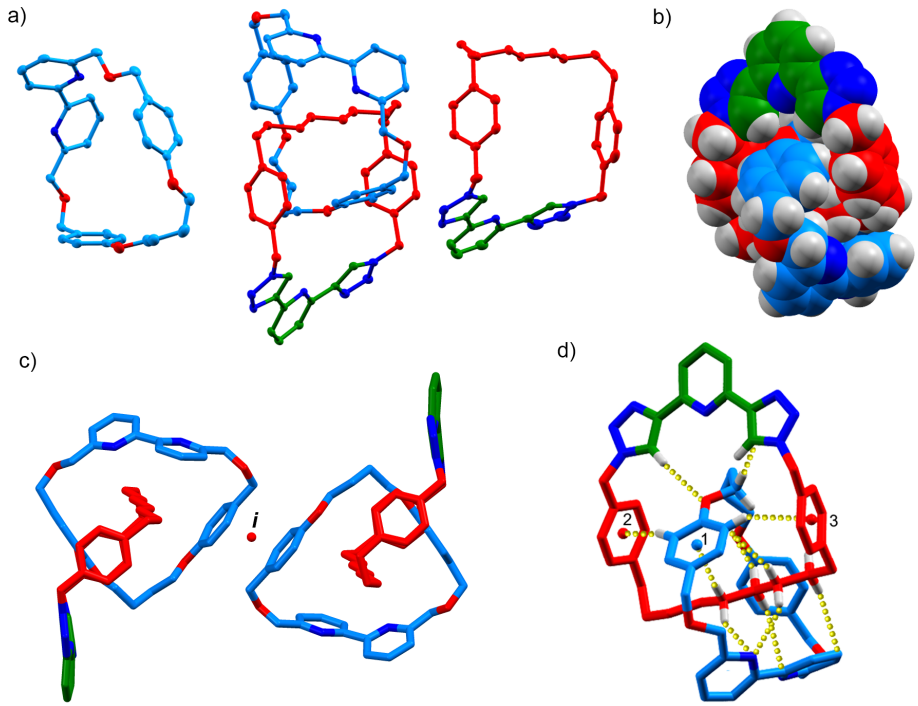

Figure 4.8 a) Ellipsoid plot of the assymetric unit of **250** (ellipsoids shown at 50% probability). Hydrogen atoms omitted for clarity. b) Spacefilling model of **250**. c) Co-conformational enantiomers observed in the solid state related by a point of inversion of **250**. d) Tube representation of **250** showing selected intermolecular contacts (for labelling scheme see characterisation data; distances (Å): H_a–N = 2.88; H_e–●$_1$ = 2.64; H_u–N = 2.43; H_P–●$_5$ = 3.16; H_Q–●$_4$ = 3.00; ●$_2$–●$_6$ = 3.42; ●$_3$–●$_6$ = 3.62).

The solid-state structure of catenane **252** also presented coconformational topological chirality. Due to the congestion of the structure and the presence of a large number of heteroatoms, the number of weak interactions was very high. It is important to note the presence of three C-H- π interactions and several C-H hydrogen bond interactions.

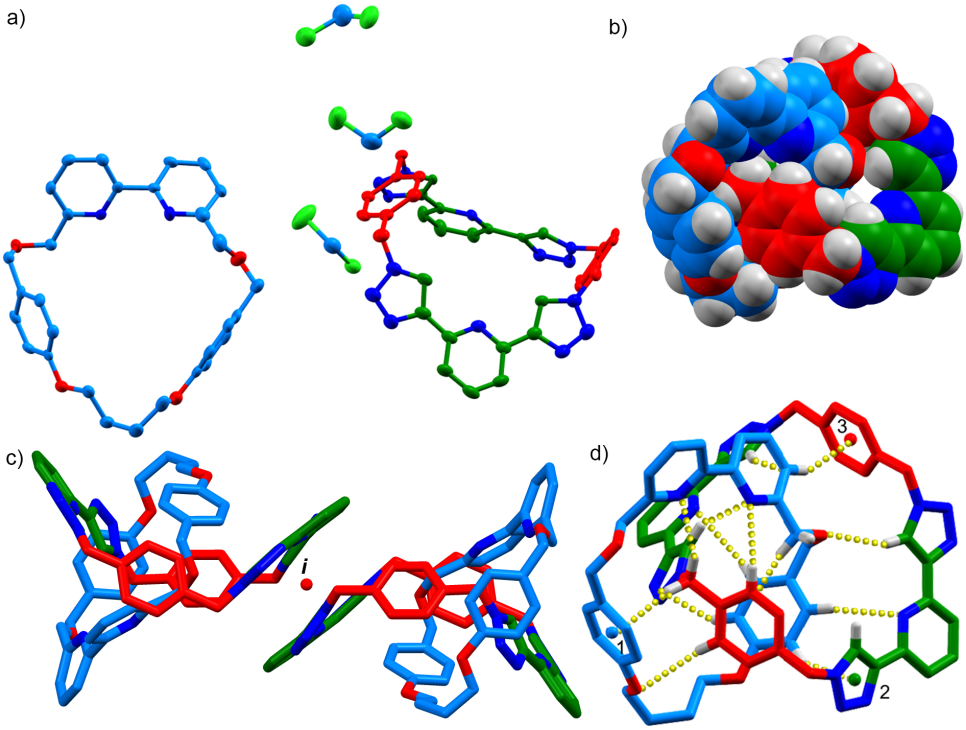

Figure 4.9 a) Ellipsoid plot of the assymetric unit of **252** (ellipsoids shown at 50% probability). Hydrogen atoms omitted for clarity. b) Spacefilling model of **252**. c) Co-conformational enantiomers observed in the solid state related by a point of inversion of **252**. d) Tube representation of **252** showing selected intermolecular contacts (for labelling scheme see characterisation data; distances (Å): H_c–O = 2.43; H_c–C_C = 3.13; H_c–N = 2.84; H_d–N = 2.46; H_d–●$_1$ = 2.66; H_e–N = 2.83; H_e–O = 2.79; H_B–●$_3$ = 2.75; H_D–C_e = 2.81; H_F–N = 2.73; H_F–N = 2.84; H_G–N = 2.78; H_G–●$_2$ = 2.69).

Here, we have demonstrated a highly efficient multicomponent synthesis of [2]catenanes using a hetero-oligomerisation-then-cyclisation approach. In order to push the limit of our method, we were interested in developing homo-oligomerisation-then-cyclisation reactions.

In this approach, the objective was to be able to selectively control the number of repeating unit in the new macrocycle unit. For the first example, precursor **237** in which the azide and alkyne are separated by 11 atoms was slowly added to a mixture of **78** and $[Cu(MeCN)_4]PF_6$ in presence of $^{i}Pr_2NEt$ at 60 °C. The analysis of the crude reaction mixture by ^{1}H NMR revealed complete consumption of **78** as well as the formation of an interlocked structure. The analysis of the crude reaction mixture by LC-MS highlighted the presence of [2]catenane **253** constituted of **78** and a ring with two molecules of **237** (Figure 4.11 a). A [2]catenane with a trimeric macrocycle was also detected in the crude reaction mixture, and represented ~10% of the interlocked structures in the ^{1}H NMR. Catenane **253** was isolated in a good yield (84%) (Figure 4.10). The dimeric macrocyclic unit of catenane **253** was a 28-membered ring.

In order to increase the number of repeating unit in the oligomeric macrocycle, shorter azide-alkyne monomers were used. Monomer **238** presents 7 atoms between the azide and alkyne. The dimeric macrocycle was a 20-membered ring, three atoms per triazole and seven between each triazole, which seemed unlikely to cyclise through **78**. However, the trimeric macrocycle was a 30-membered ring, which appeared more likely to macrocyclise through **78**. When **238** was used in the catenane formation, the major catenane **254** formed was composed of the trimeric macrocycle. The analysis of the crude reaction mixture by ^{1}H NMR suggested the formation of multiple interlocked structure as well as triazole-functionalised macrocycles. The LC-MS analysis confirmed this observation (Figure 4.11 b). The smallest macrocycle formed was composed of two monomers, but trimeric and tetrameric macrocycle were also observed. Catenanes with a tetrameric and pentameric macrocycles were also formed during the reaction. Catenane **254** was isolated in a good 50% yield considering that only 66% of **78** was converted to catenane **254** (Figure 4.10).

When monomer **239** was used, in which the reactive functional groups are 5 atoms apart, 66% of **78** was converted to the major catenane structure. Analysis of the crude reaction mixture by LC-MS revealed that the major catenane **255** formed was composed of a tetrameric macrocycle and **78** (Figure 4.11 c). Higher oligomeric macrocycle containing catenane were observed including homo-heptamer-derived product. The isolation of catenane **255** was more complicated in this case due to coelution with other catenanes. Nevertheless, catenane **255** was isolated in 32% yield (Figure 4.10).

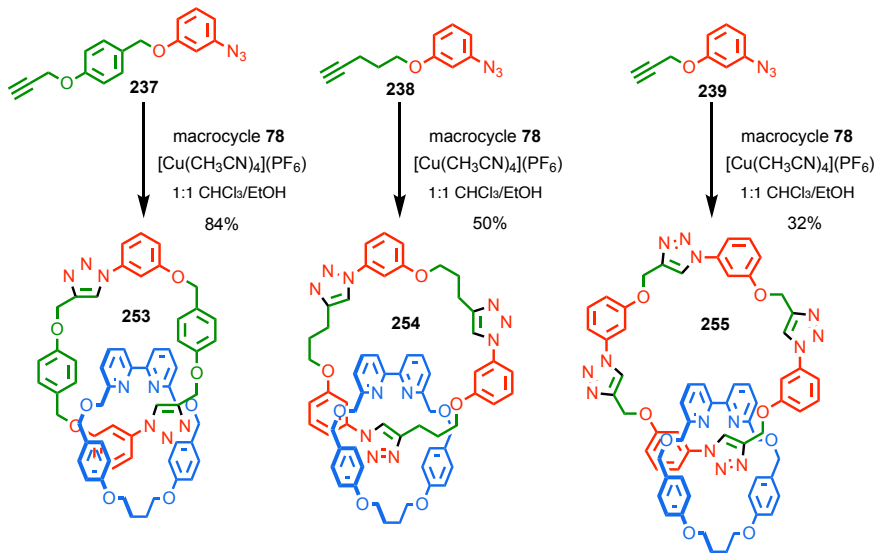

Figure 4.10 Homo-oligomerisation-then-cyclisation approach.

The solid-state structure of catenane **9** presented coconformational topological chirality. Racemic enantiomers were related by glide plane (a solid-state symmetry operation) (Figure 4.12). In this symmetry operation, the reflection in a plane, followed by parallel translation with this plane leaves the structure unchanged. The same desymmetrisation of each ring was obtained by the presence of the second ring inside the first one. The steric congestion of the structure led to the observation of a number of weak interactions such as C-H-π interactions and six C-H hydrogen bond interactions.

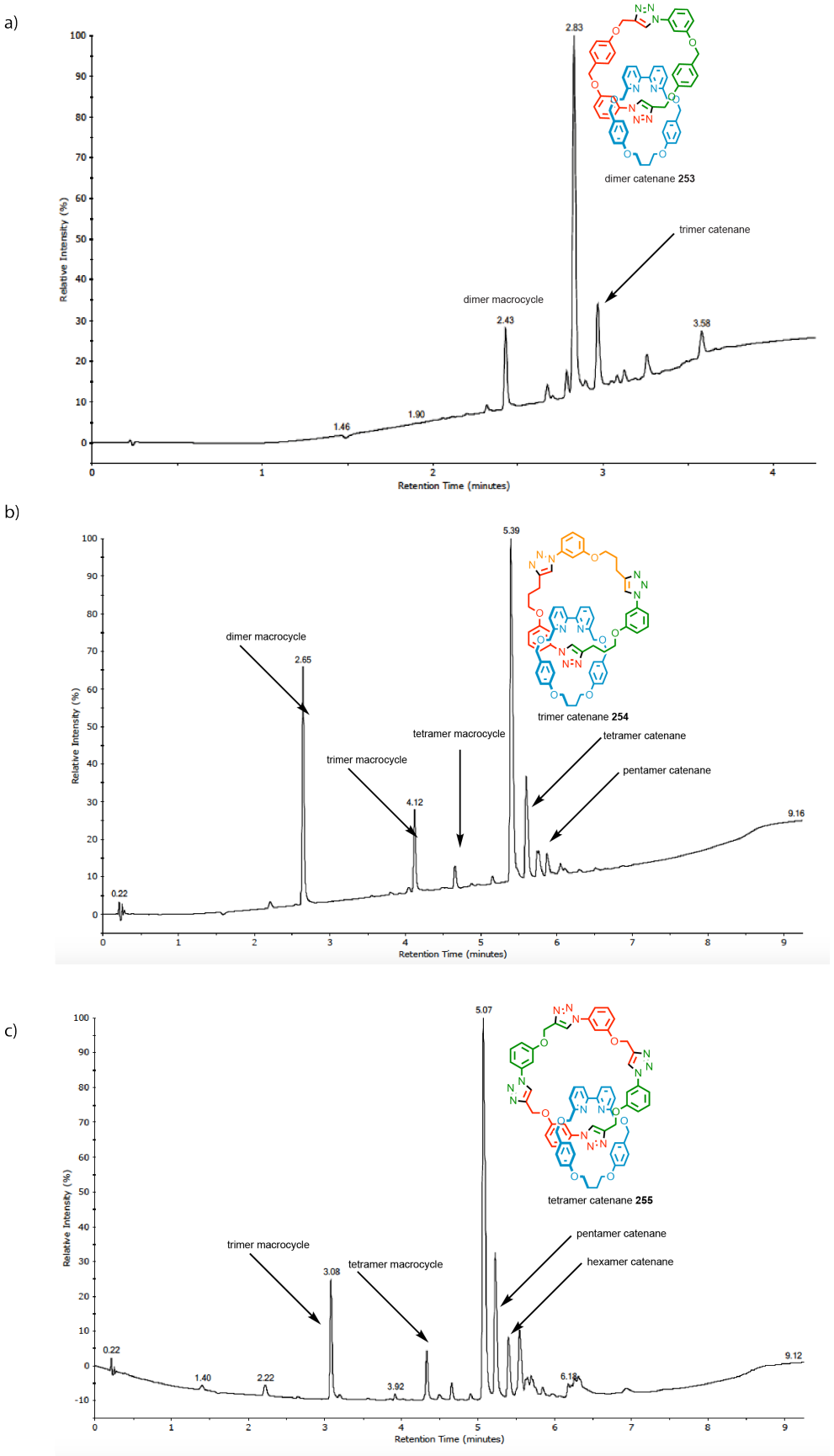

Figure 4.11 LC-MS of the crude reaction mixture for a) catenane **253**, b) catenane **254**, c) catenane **255**.

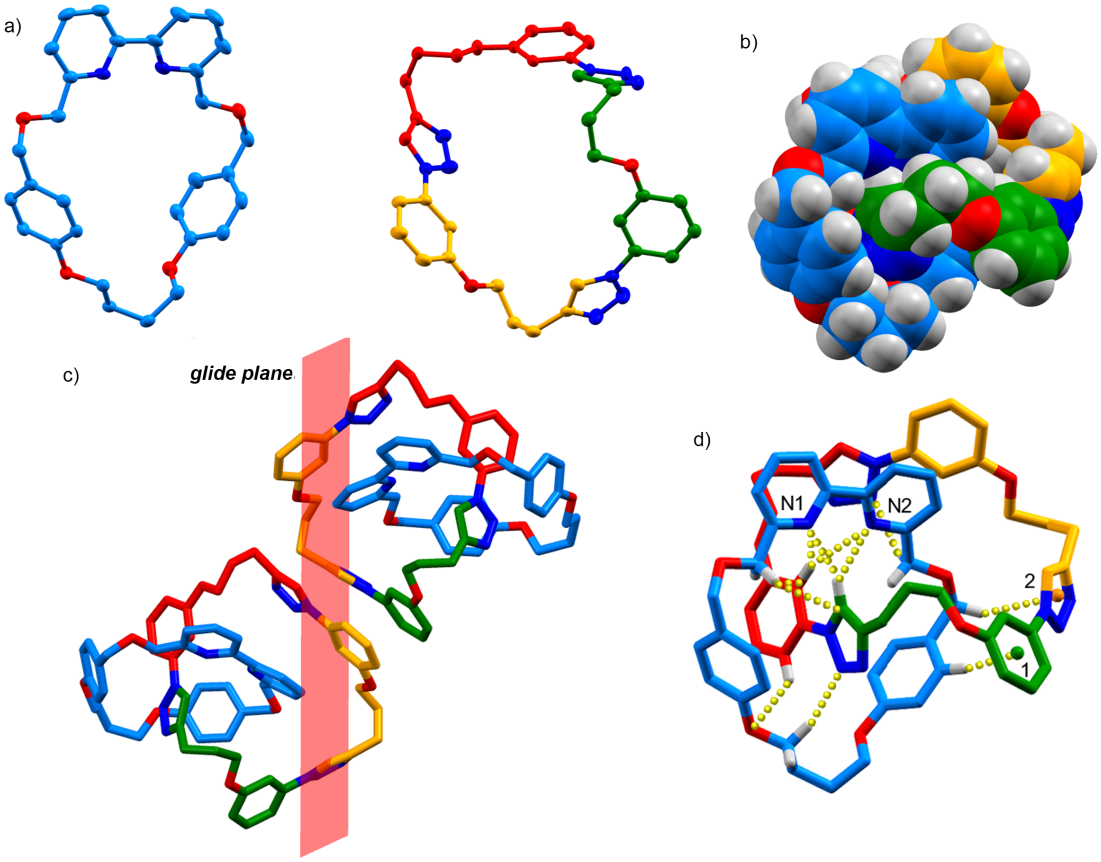

Figure 4.12 a) Ellipsoid plot of the assymetric unit of **253** (ellipsoids shown at 50% probability). b) Spacefilling model of **253**. c) Co-conformational enantiomers observed in the solid state related by a glide plane of **253**. d) Tube representation of **253** showing selected intermolecular contacts (for labelling scheme see characterisation data; distances (Å): H_a–N_1 = 2.34, H_a–N_2 = 2.76; H_a–N_1 = 2.75, H_a–N_2 = 2.77; H_h–O = 2.86; H_D–C_a = 2.94; H_D–C_e = 2.96; H_D–N = 2.99; H_E–●$_2$ = 2.83; H_F–●$_1$ = 2.81; H_H–N = 2.44).

Although efficient, the selectivity for the formation of a single interlocked structure in the case of the homo-oligomerisation-then-cyclisation was lower than the one for the hetero-oligomerisation-then-cyclisation.

4.3. Conclusions and Future Work

A facile, high-yielding and general AT-CuAAC approach was developed for the synthesis of [2]catenanes. This approach is suitable for multi-component approach using precursors that are too small to cyclise *via* hetero or homo-oligomerisation-then-cyclisation leading to the formation of small ring between 26 and 32 atoms. Catenane **242** is composed of a 26 atoms macrocycle and a 28 atoms macrocycle and can be obtained in near quantitative yield. In contrast Sauvage and co-workers reported the synthesis of a catenane containing two 27 atoms macrocycle in only 3.3% yield.[18] The improvement in yield obtained using the AT-CuAAC highlights the powerness of this new approach.

With this new general AT-CuAAC approach, catenanes appeared to be as simple as rotaxanes to prepare. AT-CuAAC-based rotaxanes have proven their efficiency in a large range of applications, such as catalysts,[19] sensors,[20,21] ligands[22] or molecular machine.[23–26] We are expecting, in a near future, AT-CuAAC-based catenanes to prove their applicability in a large range of applications.

4.4. Experimental

The following compounds were synthesised according to literature procedures:

macrocycles **74**, **92**, **108** and **110**.[16]

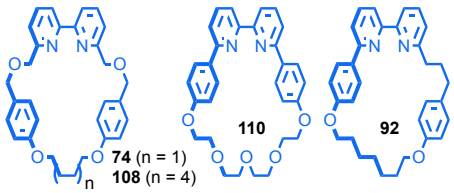

Compound 229

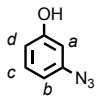

To a solution of 3-hydroxyaniline (2.18 g, 20 mmol, 1.0 eq.) in MeCN (20 mL) at 0 °C was added *tert*-butyl nitrite (4.0 mL, 30 mmol, 1.5 eq.) followed by trimethylsilyl azide (3.2 mL, 24 mmol, 1.2 eq.) via syringe. The reaction was stirred, allowing to warm to rt, for 17 h. The solvent was removed *in vacuo* and following purification by flash column chromatography (CH_2Cl_2) the **229** was obtained as a red oil (2.52 g, 93%). Spectra were consistent with those previously reported.[27] ^{1}H NMR (400 MHz, $CDCl_3$) δ: 7.21 (t, *J* = 8.1, 1H, H_c), 6.65-6.59 (m, 2H, H_b, H_d), 6.51 (t, *J* = 2.2, 1H, H_a). ^{13}C NMR (101 MHz, $CDCl_3$) δ: 156.8, 141.7, 130.9, 112.2, 111.7, 106.4.

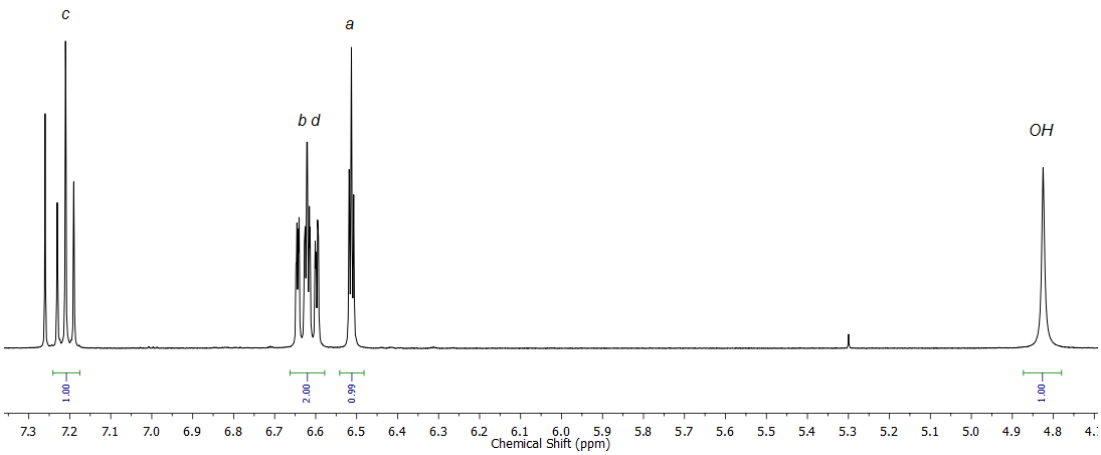

Figure 4.13 ^{1}H NMR ($CDCl_3$, 400 MHz) of **229**.

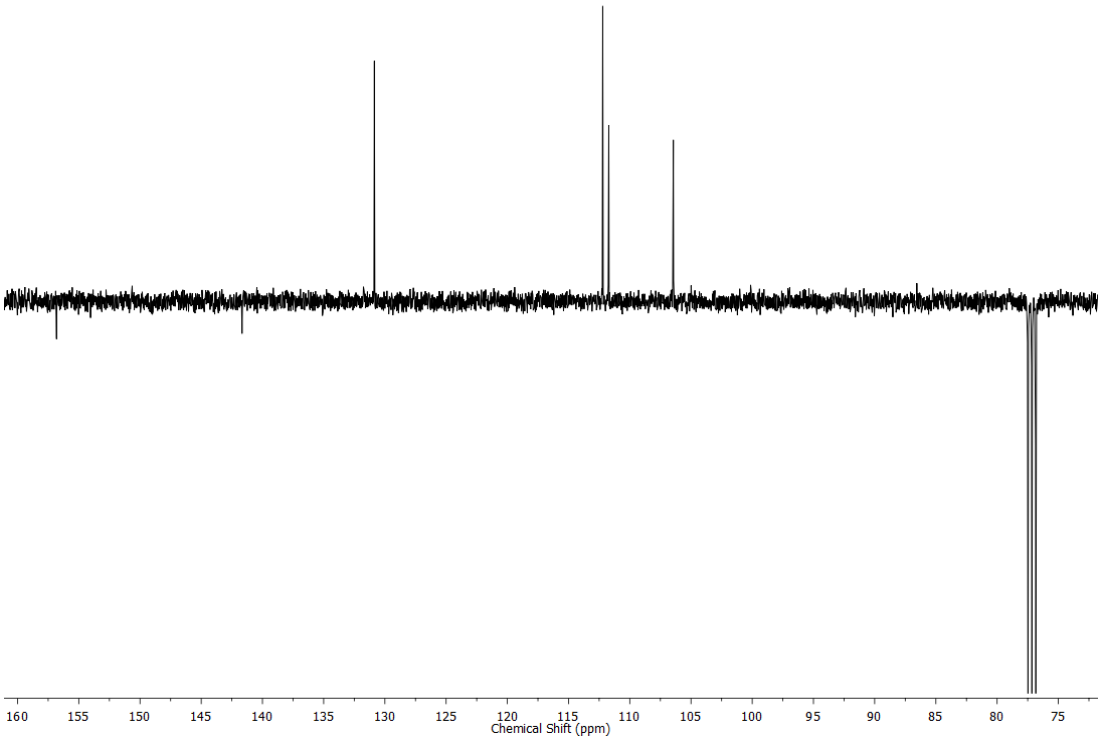

Figure 4.14 JMOD NMR ($CDCl_3$, 101 MHz) of **229**.

Compound 232

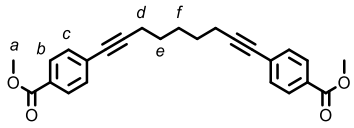

To methyl 4-bromobenzoate (4.73 g, 22 mmol, 2.2 eq.), $Pd(PPh_3)_2Cl_2$ (0.175 g, 0.25 mmol, 0.025 eq.) and CuI (0.095 g, 0.50 mmol, 0.05 eq.) in $^{i}Pr_2NH$ (40 mL), 1,8-nondiyne (1.50 mL, 10 mmol, 1.0 eq.) was added *via* syringe and the reaction stirred at 60 °C for 23 h. The cooled reaction mixture was filtered through celite, washing through with CH_2Cl_2 and the solvent removed *in vacuo*. After purification by column chromatography (petrol with 10% followed by 25% Et_2O) **232** was obtained as a yellow oil (3.35 g, 86%) that solidified on standing. M.p. 53-55 °C. ^{1}H NMR (400 MHz, $CDCl_3$) δ: 7.92 (d, *J* = 8.7, 4H, H_b), 7.42 (d, *J* = 8.4, 4H, H_c), 3.91 (s, 6H, H_a), 2.49-2.46 (m, 4H, H_d), 1.70-1.66 (m, 6H, H_e, H_f). ^{13}C NMR (101 MHz, $CDCl_3$) δ: 166.8, 131.6, 129.5, 129.0, 128.9, 93.7, 80.5, 52.3, 28.2, 28.2, 19.6. HR-ESI-MS *m/z* = 411.1574 $[M+Na]^+$ calc. 411.1567.

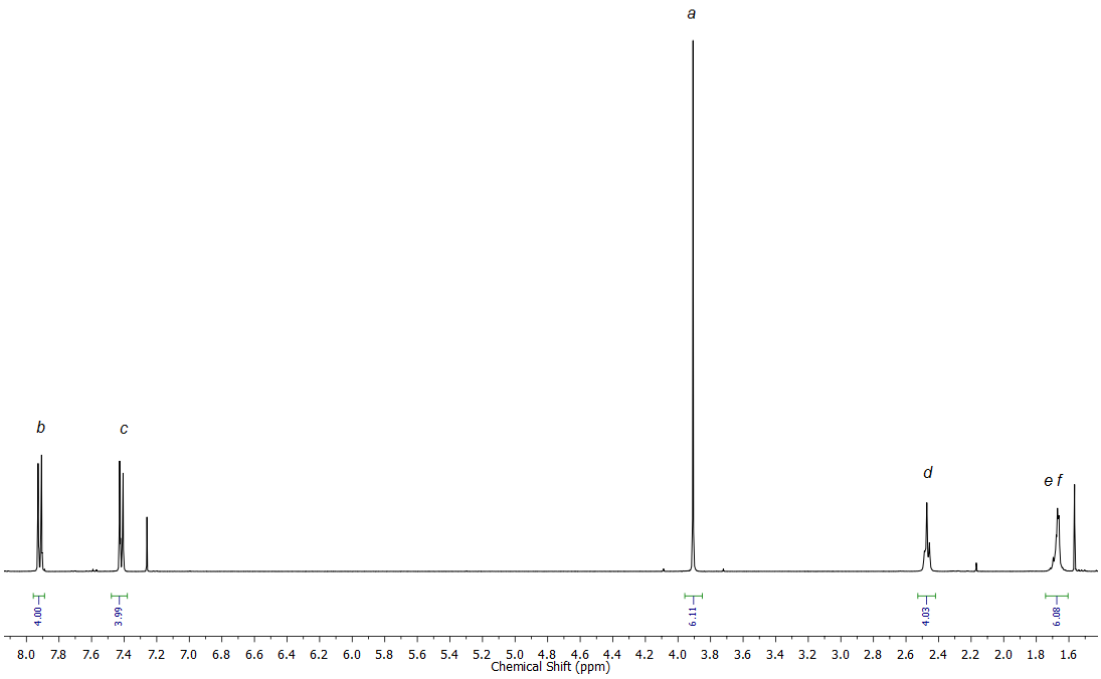

Figure 4.15 ^{1}H NMR (400 MHz, $CDCl_3$) of **232**.

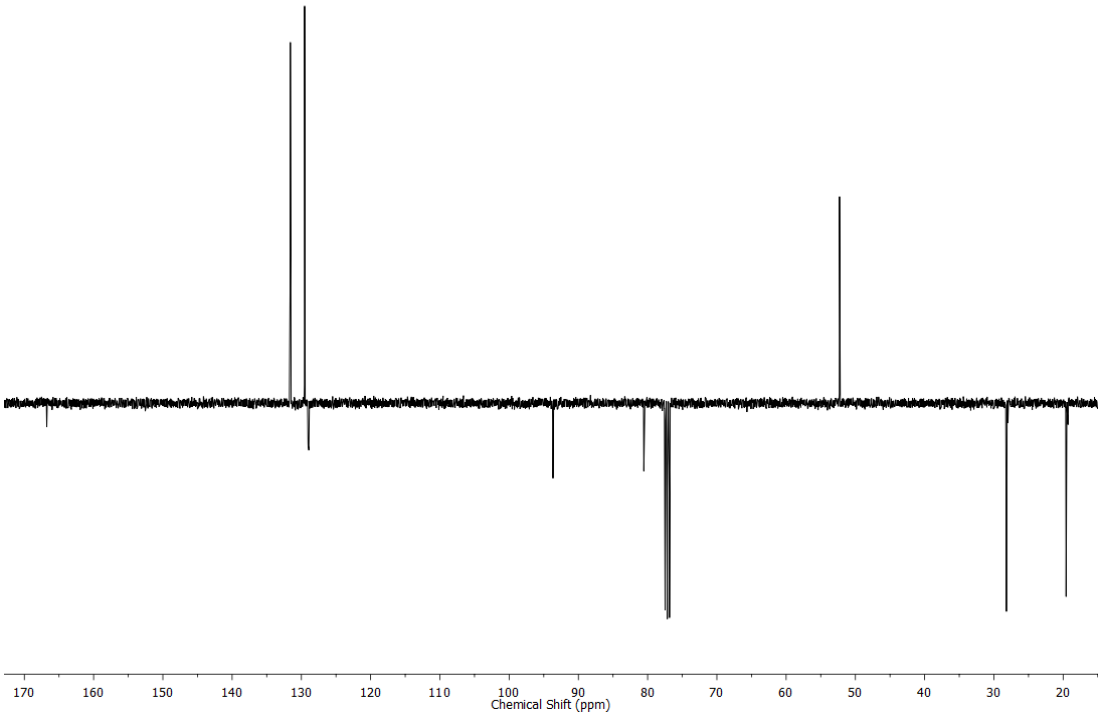

Figure 4.16 JMOD NMR (101 MHz, $CDCl_3$) of **232**.

.

Compound 233

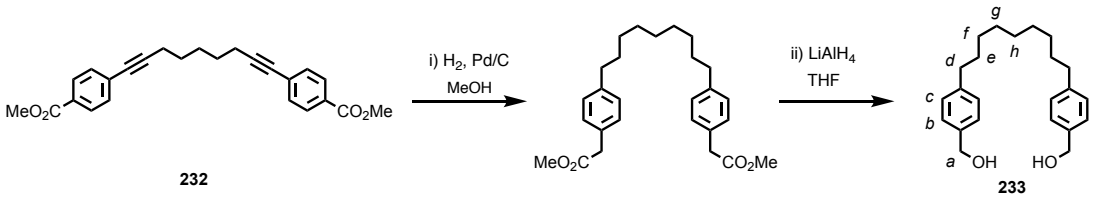

232 (3.75 g, 7.08 mmol, 1.0 eq.) and 10% Pd/C (0.227 g, 0.142 mmol, 0.02 eq.) in MeOH (70 mL) were stirred at rt under an atmosphere of H_2 for 19 h. After filtering through celite the solvent was removed *in vacuo* to give a white solid (2.85 g) which was used without further purification [^{1}H NMR (400 MHz, $CDCl_3$) δ: 7.94 (d, *J* = 8.3, 4H, H_b), 7.23 (d, *J* = 8.3, 4H, H_c), 3.90 (s, 6H, H_a), 2.66-2.62 (m, 4H, H_d), 1.63-1.57 (m, 4H, H_e), 1.28 (br. m, 10H, H_f, H_g, H_h); ^{13}C NMR (101 MHz, $CDCl_3$) δ: 167.4, 148.6, 129.8, 128.6, 127.7, 52.1, 36.1, 31.3, 29.6, 29.5, 29.3]. The residue was redissolved in THF (35 mL) and added dropwise to a suspension of $LiAlH_4$ in THF (70 mL) at 0 °C, before stirring at 60 °C for 4 h. The reaction was cooled to 0 °C and H_2O (20 mL) added dropwise to quench the reaction. 5M $HCl_{(aq)}$ was added to neutralise the reaction mixture before further H_2O (250 mL) was added. After extraction with EtOAc (4 × 100 mL) the combined organic phases were washed with brine (100 mL), dried ($MgSO_4$) and the solvent removed *in vacuo* to give **233** as a white solid (2.13 g, 88%). M.p. 97-99 °C. ^{1}H NMR (400 MHz, $CDCl_3$) δ: 7.28 (d, *J* = 8.0, 4H, H_b), 7.17 (d, *J* = 8.0, 4H, H_c), 4.66 (d, *J* = 5.6, 4H, H_a), 2.61-2.57 (m, 4H, H_d), 1.63-1.54 (m, 4H, H_e), 1.29 (br. m, 10H, H_f, H_g, H_h). ^{13}C NMR (101 MHz, $CDCl_3$) δ: 142.7, 138.3, 128.8, 127.3, 65.5, 35.8, 31.6, 29.6 (×2), 29.4. HR-ESI-MS *m/z* = 363.2292 $[M+Na]^+$ calc. 363.2295.

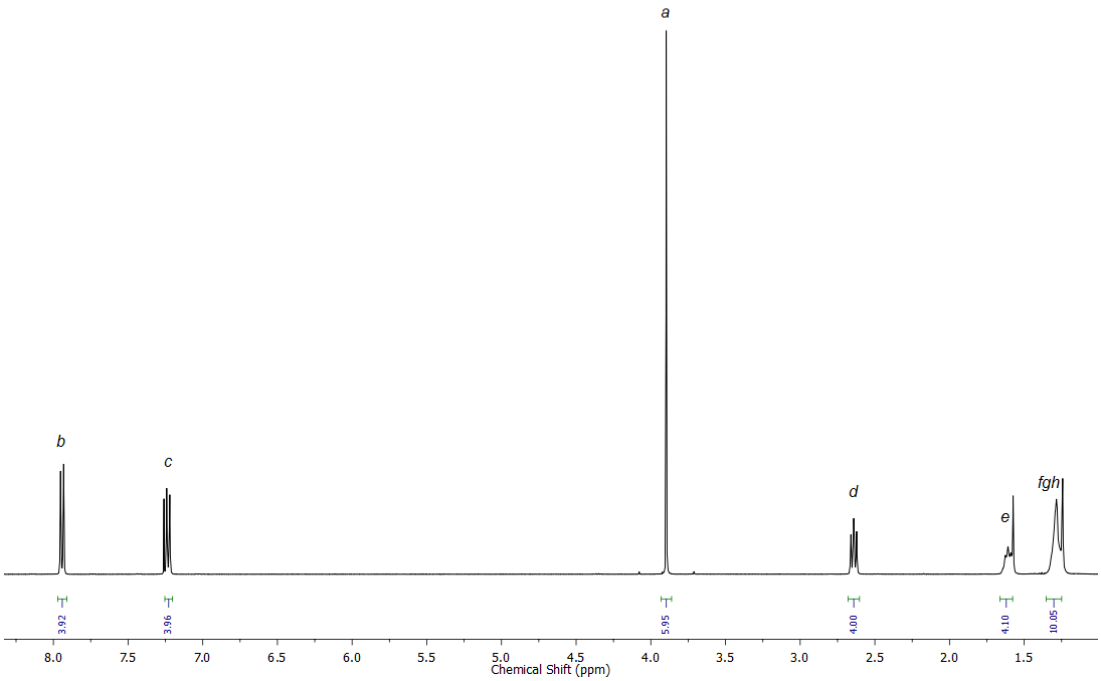

Figure 4.17 ^{1}H NMR (400 MHz, $CDCl_3$) of the crude hydrogenation product of **232**

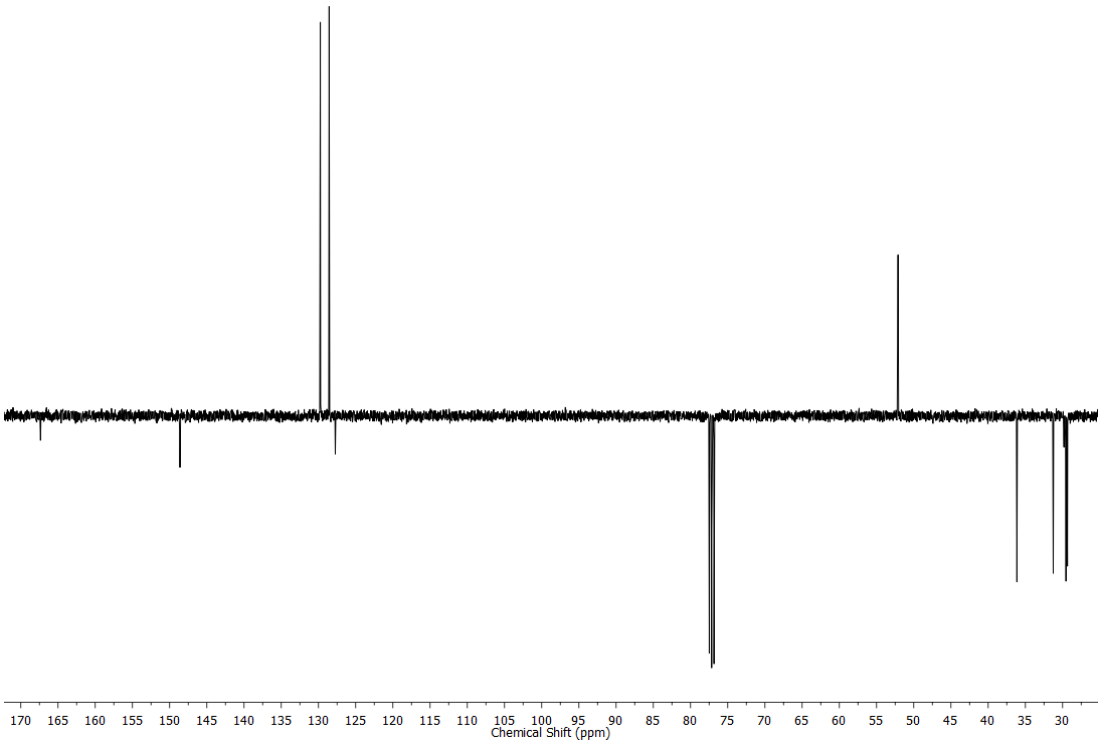

Figure 4.18 JMOD NMR (101 MHz, $CDCl_3$) of the crude hydrogenation product of **232**

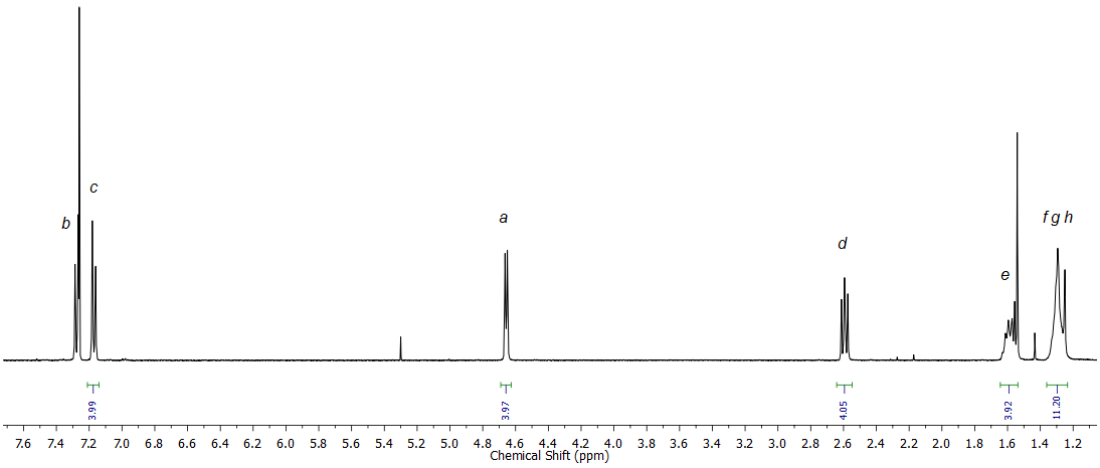

Figure 4.19 ^{1}H NMR (400 MHz, $CDCl_3$) of **233**.

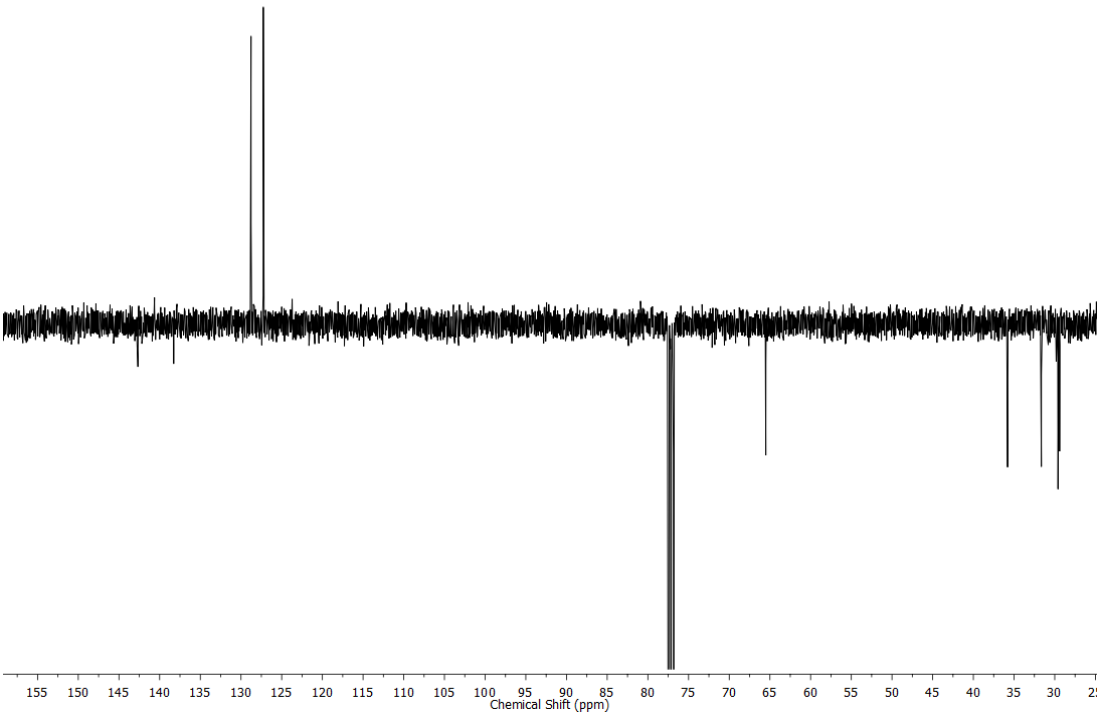

Figure 4.20 JMOD NMR (101 MHz, $CDCl_3$) of **233**.

Compound 234

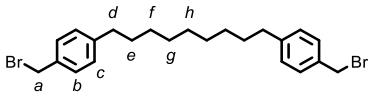

To **233** (2.64 g, 7.75 mmol, 1 eq.) and PPh_3 (6.10 g, 23.3 mmol, 3 eq.) in CH_2Cl_2 (80 mL) at 0 °C was added CBr_4 (7.71 g, 23.3 mmol, 3 eq.) portionwise as a solid. The reaction was stirred, allowing to warm to rt, for 20 h. Silica (8 g) was added and the solvent removed *in vacuo*. Following purification by column chromatography (petrol with a 0 to 100% gradient of CH_2Cl_2) the product was obtained as a white solid (3.25 g, 90%). M.p. 98-100 °C. ^{1}H NMR (400 MHz, $CDCl_3$) δ: 7.30 (d, *J* = 8.1, 4H, H_b), 7.15 (d, *J* = 8.0, 4H, H_c), 4.49 (s, 4H, H_a), 2.62-2.56 (m, 4H, H_d), 1.59 (app. quint., *J* = 7.2, 4H, H_e), 1.29 (br. m, 10H, H_f, H_g, H_h). ^{13}C NMR (101 MHz, $CDCl_3$) δ: 143.6, 135.1, 129.1, 129.0, 35.8, 34.0, 31.5, 29.6 (x2), 29.4. HR-APPI-MS *m/z* = 305.2259 $[M\text{-}Br_2\text{-}H]^+$ calc. 305.2264.

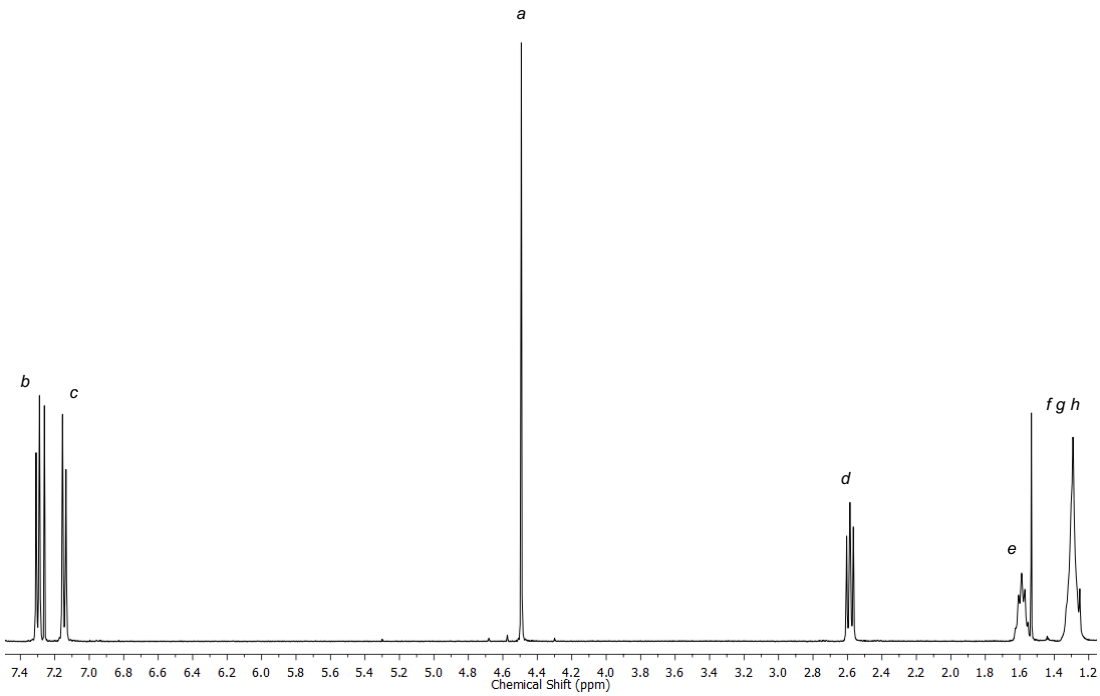

Figure 4.21 ^{1}H NMR (400 MHz, $CDCl_3$) of **234**.

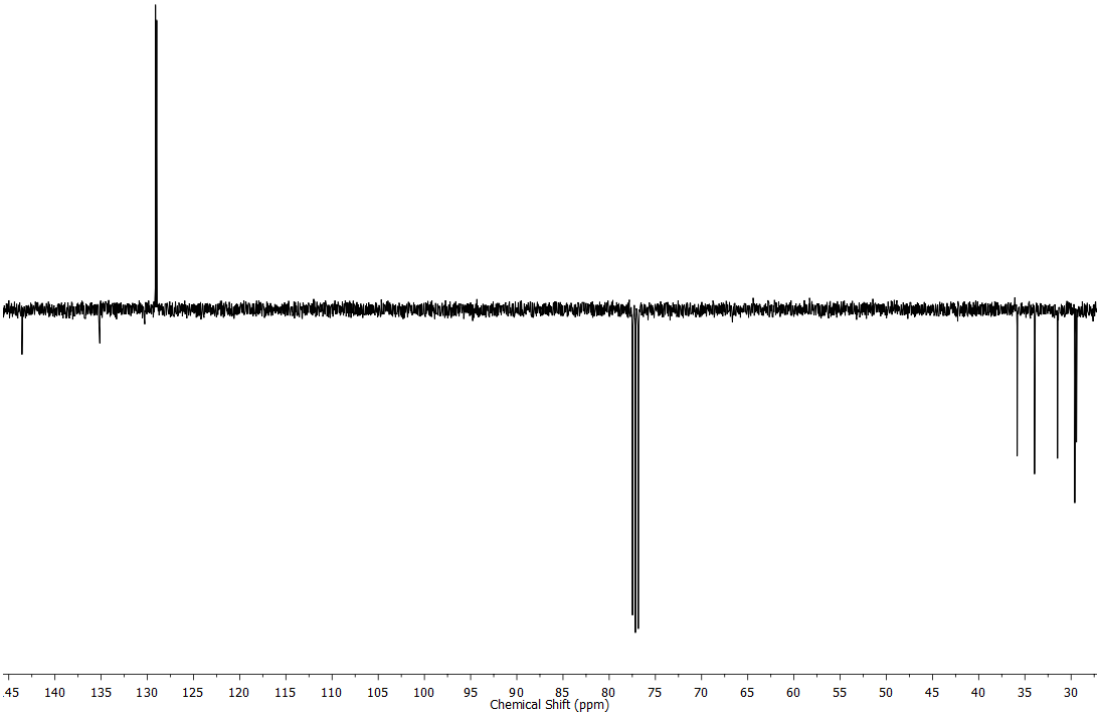

Figure 4.22 JMOD NMR (101 MHz, $CDCl_3$) of **234**.

Compound 235

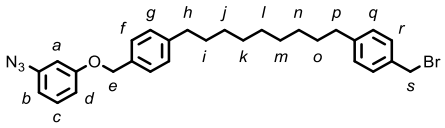

3-Azidophenol (0.135 g, 1.0 mmol, 1.0 eq.), **234** (1.40 g, 3.0 mmol, 3.0 eq.) and K_2CO_3 (0.691 g, 5.0 mmol, 5.0 eq.) were stirred at 70 °C in CH_3CN (50 mL) for 5 h. To the cooled reaction was added H_2O (200 mL) and the resulting precipitate isolated by filtration and washed with H_2O. The residue was dissolved in CH_2Cl_2 (200 mL), dried ($MgSO_4$) and the solvent removed *in vacuo*. Following purification by column chromatography on silica (1:3 $CHCl_3$/petrol) the product was obtained as a yellow oil (0.306 g, 59%) the solidified on standing. M.p. 62-64 °C. ^{1}H NMR (400 MHz, $CDCl_3$) δ: 7.33 (d, *J* = 8.1, 2H, H_g), 7.30 (d, *J* = 8.1, 2H, H_q), 7.27-7.23 (m, 1H, H_c), 7.20 (d, *J* = 8.1, 2H, H_f), 7.15 (d, *J* = 8.1, 2H, H_r), 6.76 (ddd, *J* = 8.4, 2.2, 1.0, 1H, $H_{b/d}$), 6.67-6.63 (m, 2H, H_a, $H_{b/d}$), 5.01 (s, 2H, H_e), 4.49 (s, 2H, H_s), 2.60 (app. q, *J* = 7.7, 4H, H_h, H_p), 1.64-1.56 (m, 4H, H_i, H_o), 1.30 (br. m, 10H, H_j, H_k, H_l, H_m, H_n). ^{13}C NMR (101 MHz, $CDCl_3$) δ: 160.2, 143.6, 143.2, 141.4, 135.1, 133.8, 130.6, 129.1, 129.0, 128.8, 127.8, 111.6, 111.6, 106.1, 70.3, 35.8 (×2), 33.9, 31.6, 31.5, 29.6 (×3), 29.4 (×2). HR-APPI-MS *m/z* = 412.2632 [M-N_2-Br]$^+$ calc. 412.2635; 491.1817 [M-N_2]$^+$ calc. 491.1818.

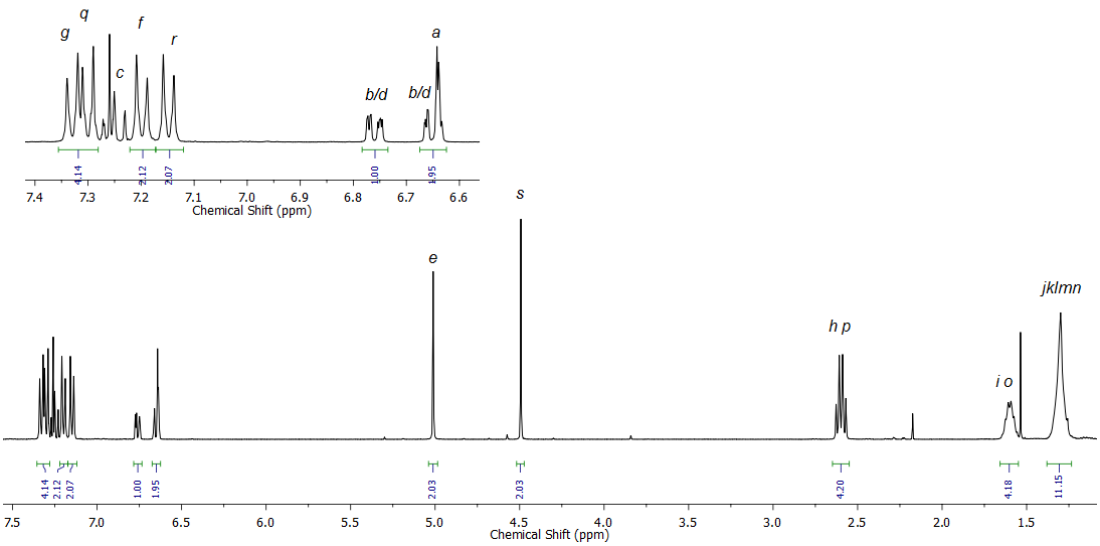

Figure 4.23 ^{1}H NMR (400 MHz, $CDCl_3$) of **235**.

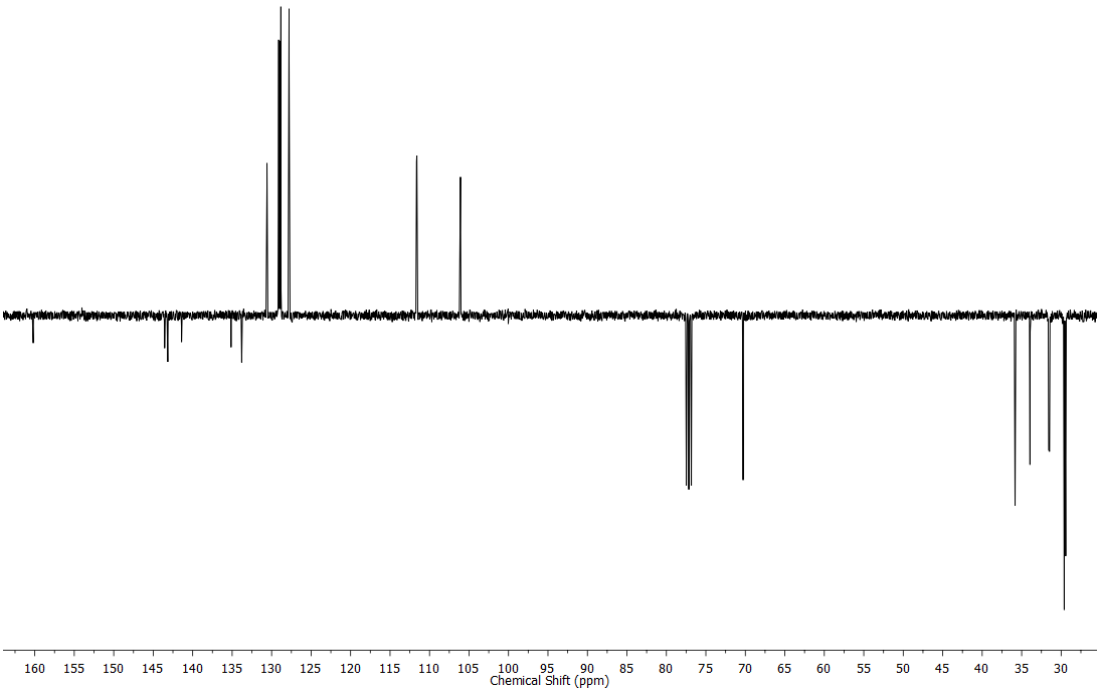

Figure 4.24 JMOD NMR (101 MHz, $CDCl_3$) of **235**.

*Macrocycle precursor **236***

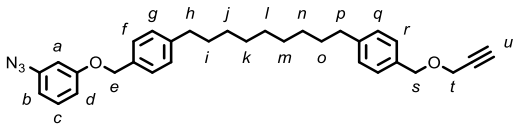

To **235** (0.257 g, 0.494 mmol, 1.0 eq.) and 60% NaH (39 mg, 0.98 mmol, 2.0 eq.) in DMF (15 mL) at 0 °C was added propargyl alcohol (57 µL, 0.99 mmol, 2.0 eq.) in DMF (1.0 mL) dropwise. After stirring at rt for 17 h, H_2O (75 mL) was added and the reaction mixture extracted with EtOAc (4 × 25 mL). The combined organic layers were washed with H_2O (4 × 20 mL) and brine (20 mL), dried ($MgSO_4$) and the solvent removed *in vacuo*. Following filtration through a plug of silica (1:1 CH_2Cl_2/petrol) and removal of solvent *in vacuo* the product was obtained as a yellow oil (0.239 g, 98%). ^{1}H NMR (500 MHz, $CDCl_3$) δ: 7.33 (d, *J* = 8.2, 2H, H_f), 7.27-7.23 (m, 3H, H_c, H_r), 7.20 (d, *J* = 8.2, 2H, H_g), 7.16 (d, *J* = 8.2, 2H, H_q), 6.76 (ddd, *J* = 8.3, 2.3, 0.9, 1H, $H_{b/d}$), 6.66-6.63 (m, 2H, H_a, $H_{b/d}$), 5.01 (s, 2H, H_e), 4.57 (s, 2H, H_s), 4.16 (d, *J* = 2.4, 2H, H_t), 2.62-2.57 (m, 4H, H_h, H_p), 2.46 (t, *J* = 2.4, 1H, H_u), 1.63-1.56 (m, 4H, H_i, H_o), 1.34-1.26 (m, 10H, H_j, H_k, H_l, H_m, H_n). ^{13}C NMR (126 MHz, $CDCl_3$) δ: 160.2, 143.2, 142.9, 141.4, 134.5, 133.8, 130.6, 128.8, 128.7, 128.4, 127.8, 111.6, 111.6, 106.1, 79.9, 74.6, 71.6, 70.3, 57.1, 35.9, 35.8, 31.6, 31.6, 29.6 (×3), 29.4, 29.4. HR-APPI-MS *m/z* = 467.2813 $[M\text{-}N_2]^+$ calc. 467.2819.

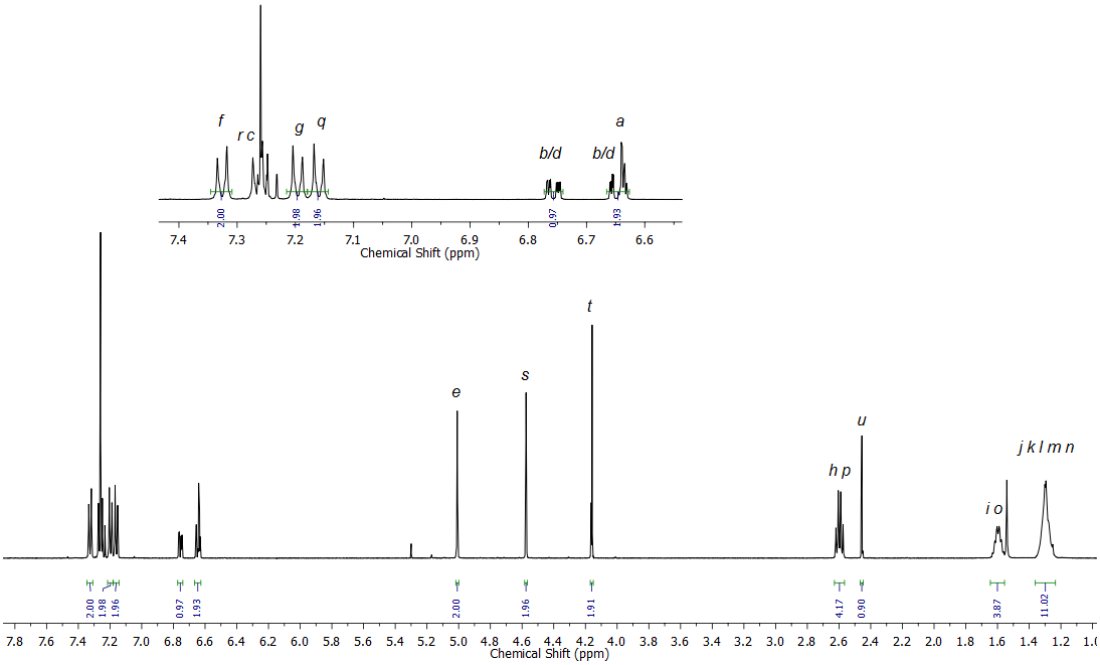

Figure 4.25 ^{1}H NMR (500 MHz, $CDCl_3$) of **236**.

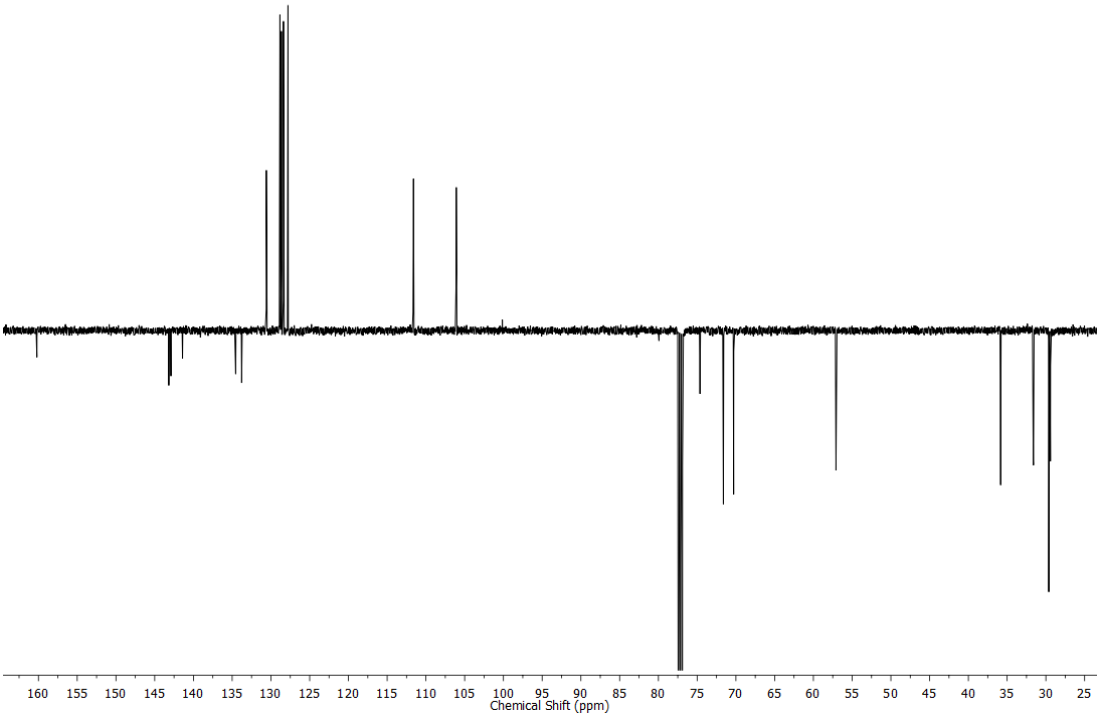

Figure 4.26 JMOD NMR (126 MHz, $CDCl_3$) of **236**.

*Synthesis of Macrocycle Precursors **237**, **238**, **239** and **240***

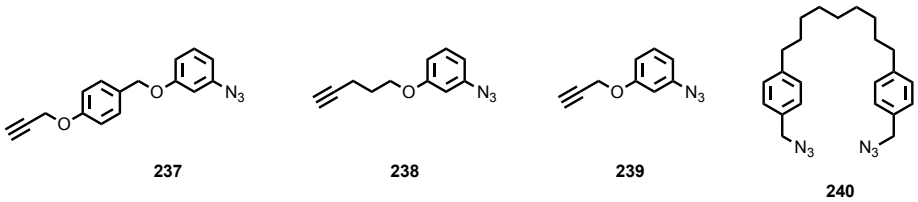

237 **238** **239** **240**

Figure 4.27. Structures of Macrocycle Precursors **237**, **238**, **239** and **240**.

Precursor 240

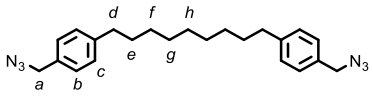

234 (0.933 g, 2.0 mmol, 1 eq.) and NaN_3 (0.325 g, 5.0 mmol, 2.5 eq.) were stirred at 80 °C in DMF (20 mL) for 20 h. The cooled reaction mixture was diluted with H_2O (200 mL) and extracted with EtOAc (4 × 25 mL). The combined organic extracts were washed with H_2O (8 × 20 mL), brine (20 mL), dried ($MgSO_4$) and the solvent removed in vacuo to give the product as an orange oil (0.758 g, 97%). ^{1}H NMR (400 MHz, $CDCl_3$) δ: 7.23 (d, *J* = 8.2, 4H, H_b), 7.19 (d, *J* = 8.2, 4H, H_c), 4.30 (s, 4H, H_a), 2.63-2.59 (m, 4H, H_d), 1.61 (app. quint, *J* = 6.9, 4H, H_e), 1.30 (br. m, 10H, H_f, H_g, H_h). ^{13}C NMR (101 MHz, $CDCl_3$) δ: 143.3, 132.7, 129.0, 128.4, 54.8, 35.8, 31.5, 29.8, 29.6, 29.4.

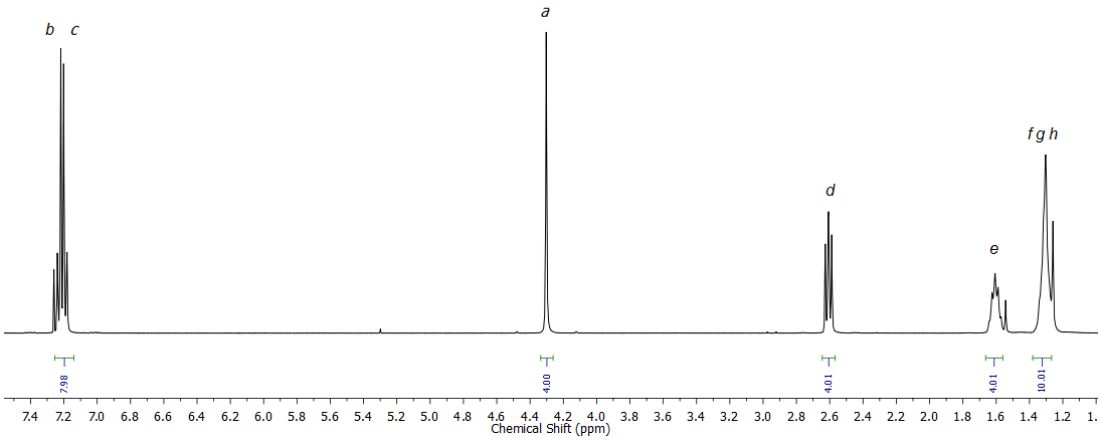

Figure 4.28 ^{1}H NMR (400 MHz, $CDCl_3$) of **240**.

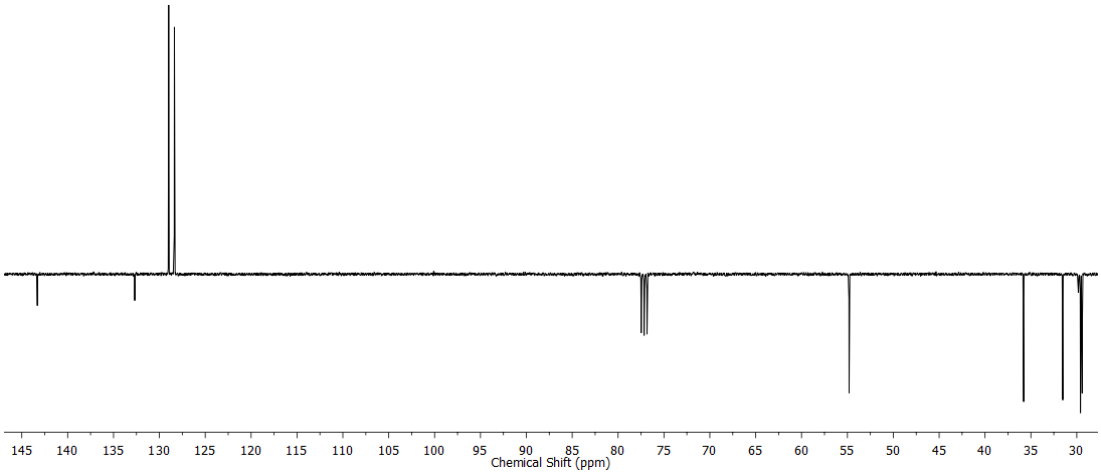

Figure 4.29 ^{13}C NMR (101 MHz, $CDCl_3$) of **240**.

256

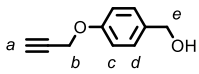

4-Hydroxybenzyl alcohol (0.745 g, 6.00 mmol, 1 eq.), propargyl bromide (80% solution in toluene, 0.80 mL, 7.2 mmol, 1.2 eq.) and K_2CO_3 (4.15 g, 30.0 mmol, 5 eq.) were stirred at 70 °C in CH_3CN (25 mL) for 20 h. The cooled reaction mixture was filtered through celite and the solvent removed *in vacuo* to give **256** as a yellow oil (0.950 g, 98%). Spectra matched literature data.[28] ^{1}H NMR (400 MHz, $CDCl_3$) δ: 7.31 (d, *J* = 8.7, 2H, H_d), 6.97 (d, *J* = 8.7, 2H, H_c), 4.70 (d, *J* = 2.4, 2H, H_b), 4.63 (d, *J* = 3.1, 2H, H_e), 2.52 (t, *J* = 2.4, 1H, H_a). ^{13}C NMR (101 MHz, $CDCl_3$) δ: 157.3, 134.2, 128.7, 115.2, 78.7, 75.7, 65.1, 56.0.

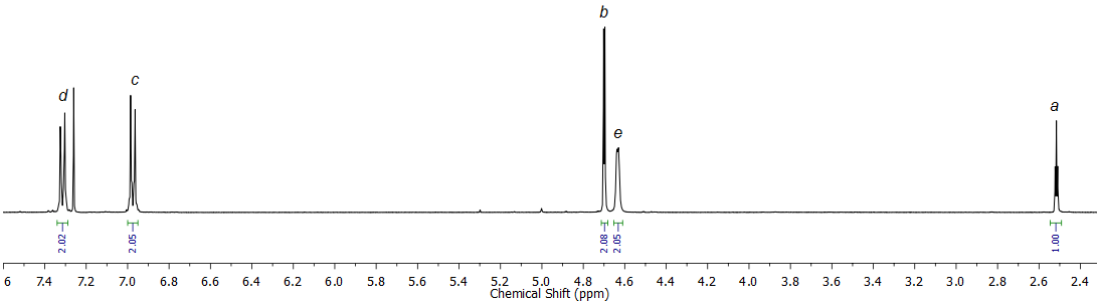

Figure 4.30 ^{1}H NMR (400 MHz, $CDCl_3$) of **256**.

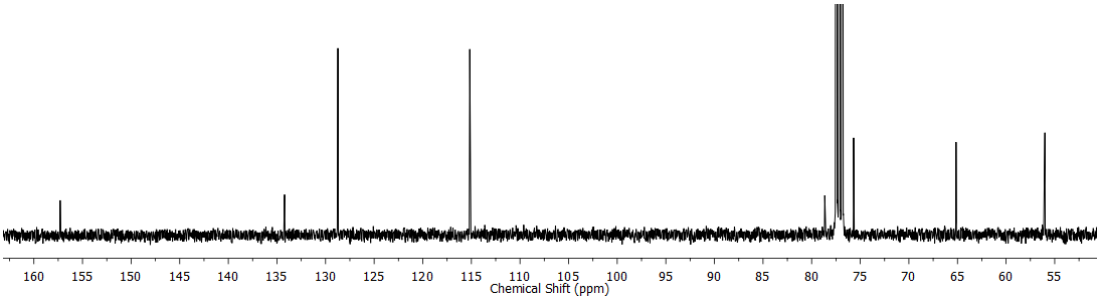

Figure 4.31 ^{13}C NMR (101 MHz, $CDCl_3$) of **256**.

Compound 257

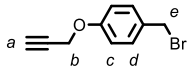

256 (0.356 g, 2.19 mmol, 1 eq.) was stirred in CH_2Cl_2 (5 mL) and HBr (48% w/w aq., 5 mL) at rt for 3 h. H_2O was added (10 mL) and the reaction extracted with CH_2Cl_2 (3 × 10 mL). The combined organic phases were washed with sat. aq. $NaHCO_3$ (20 mL), dried ($MgSO_4$) and the solvent removed *in vacuo* to give the product as a brown solid (0.474 g, 96%). Spectra matched literature data.[29] ^{1}H NMR (400 MHz, $CDCl_3$) δ: 7.34 (d, *J* = 8.7, 2H, H_d), 6.94 (d, *J* = 8.7, 2H, H_c), 4.69 (d, *J* = 2.4, 2H, H_b), 4.50 (s, 2H, H_e), 2.53 (t, *J* = 2.4, 1H, H_a). ^{13}C NMR (101 MHz, CDCl3) δ: 157.7, 131.0, 130.6, 115.3, 78.4, 75.9, 56.0, 33.8.

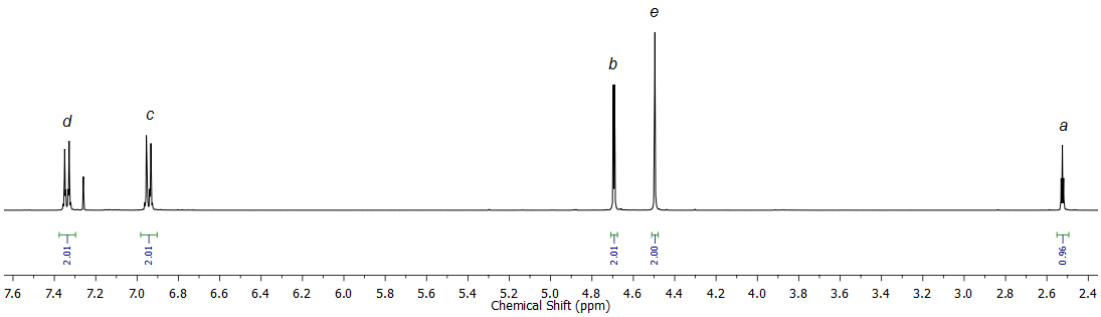

Figure 4.32 ^{1}H NMR (400 MHz, $CDCl_3$) of **257**.

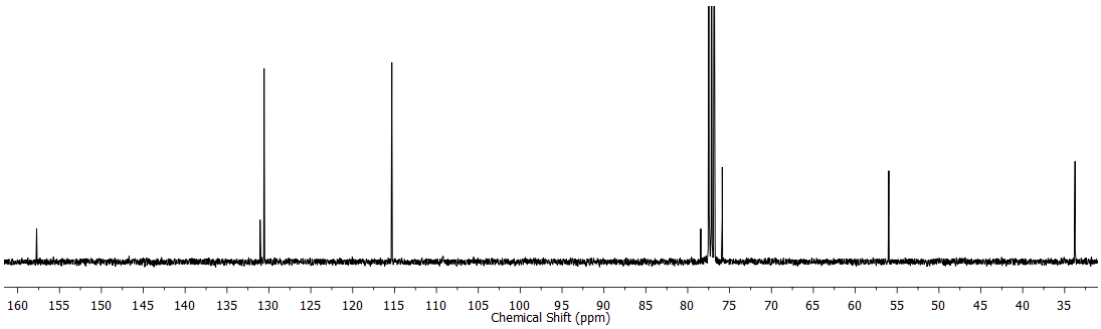

Figure 4.33 ^{13}C NMR (101 MHz, $CDCl_3$) of **257**.

Precursor 237

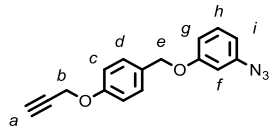

257 (0.438 g, 1.95 mmol, 1 eq.), 3-azidophenol (0.316 g, 2.34 mmol, 1.2 eq.) and K_2CO_3 (1.34 g, 9.73 mmol, 5 eq.) were stirred at 70 °C in CH_3CN (10 mL) for 4 h. The cooled reaction mixture was filtered through celite and the solvent removed *in vacuo*. After purification by column chromatography on silica (1:1 petrol/CH_2Cl_2) the product was obtained as an off-white solid (0.457 g, 84%). ^{1}H NMR (400 MHz, $CDCl_3$) δ: 7.36 (d, *J* = 8.8, 2H, H_d), 7.25 (app. t, *J* = 8.1, 1H, H_h), 7.00 (d, *J* = 8.7, 2H, H_c), 6.75 (ddd, *J* = 8.3, 2.4, 0.9, 1H, H_g or H_i), 6.65 (ddd, *J* = 7.9, 2.1, 0.9, 1H, H_g or H_i), 6.62 (app. t, *J* = 2.2, 1H, H_f), 4.98 (s, 2H, H_e), 4.71 (d, *J* = 2.4, 2H, H_b), 2.52 (t, *J* = 2.4, 1H, H_a). ^{13}C NMR (101 MHz, $CDCl_3$) δ: 160.1, 157.7, 141.4, 130.6, 129.7, 129.3, 115.2, 111.7, 111.6, 106.1, 78.6 (from HMBC), 75.8, 70.0, 56.0. HR-ESI-MS *m/z* = 581.1902 $[M_2+Na]^+$ calc. 581.1908.

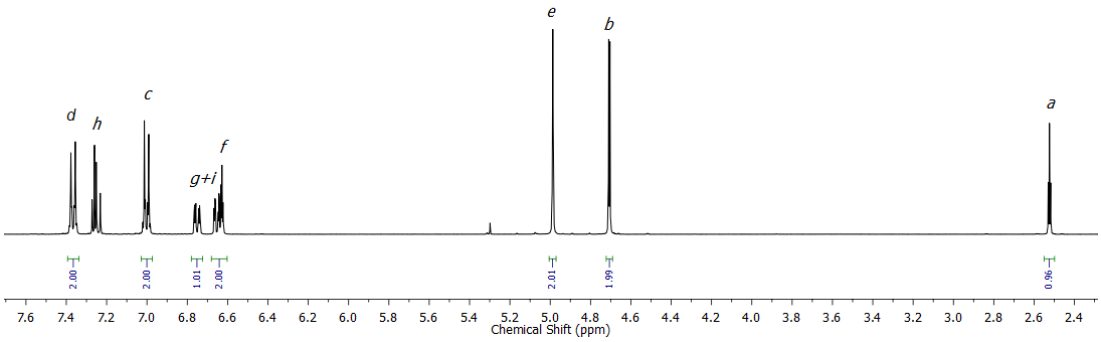

Figure 4.34 ^{1}H NMR (400 MHz, $CDCl_3$) of **237**.

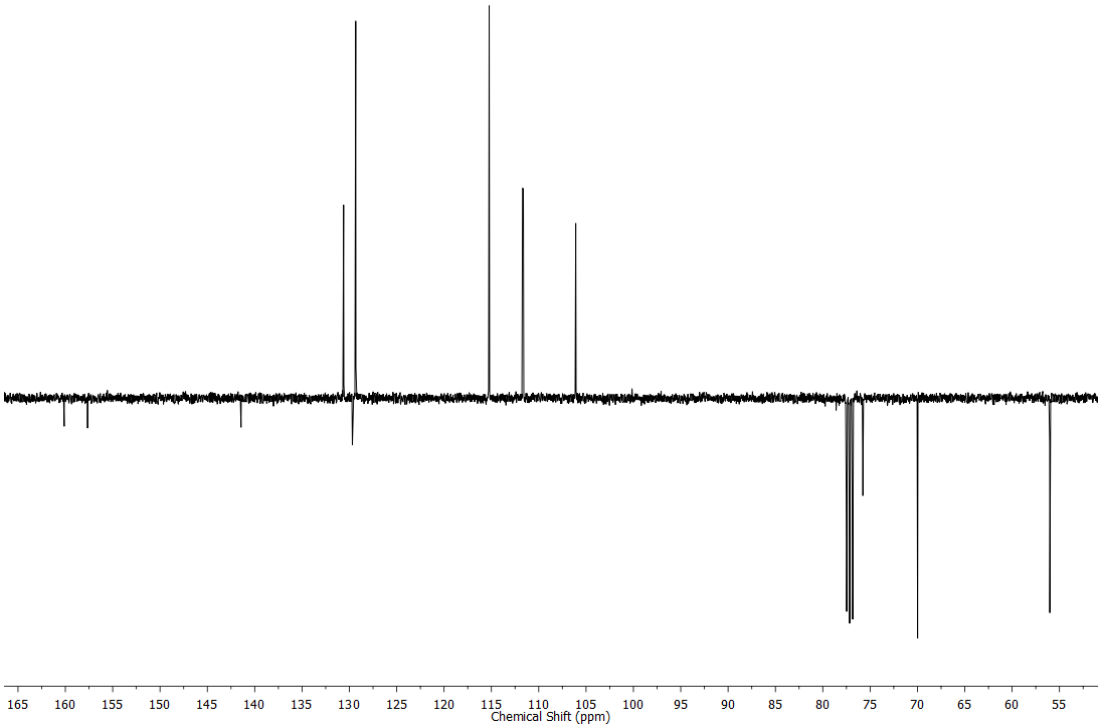

Figure 4.35 JMOD NMR (101 MHz, $CDCl_3$) of **237**.

Precursor 238

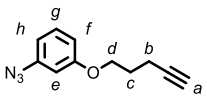

3-Azidophenol (0.124 g, 0.91 mmol, 1 eq.), pent-4-yl tosylate (0.218 g, 0.91 mmol, 1 eq.) and K_2CO_3 (0.629 g, 4.55 mmol, 5 eq.) were stirred at 70 °C in CH_3CN (5 mL) for 24 h. The cooled reaction mixture was filtered through Celite and the solvent removed *in vacuo*. After filtration through a plug of silica (1:1 petrol/CH_2Cl_2) the product was obtained as a light yellow oil (0.158 g, 86%). ^{1}H NMR (400 MHz, $CDCl_3$) δ: 7.26-7.22 (m, 1H, H_g), 6.69 (ddd, *J* = 8.3, 2.4, 0.9, 1H, H_f or H_h), 6.64 (ddd, *J* = 8.0, 2.2, 0.8, 1H, H_f or H_h), 6.56 (app. t, *J* = 2.3, 1H, H_e), 4.07 (t, *J* = 6.1, 2H, H_d), 2.41 (td, *J* = 7.0, 2.7, 2H, H_b), 2.03-1.97 (m, 3H, H_a, H_c). ^{13}C NMR (101 MHz, $CDCl_3$) δ: 160.2, 141.4, 130.6, 111.5, 111.3, 105.7, 83.4, 69.1, 66.4, 28.2, 15.3. *Despite numerous attempts under various conditions MS data could not be obtained for this compound.*

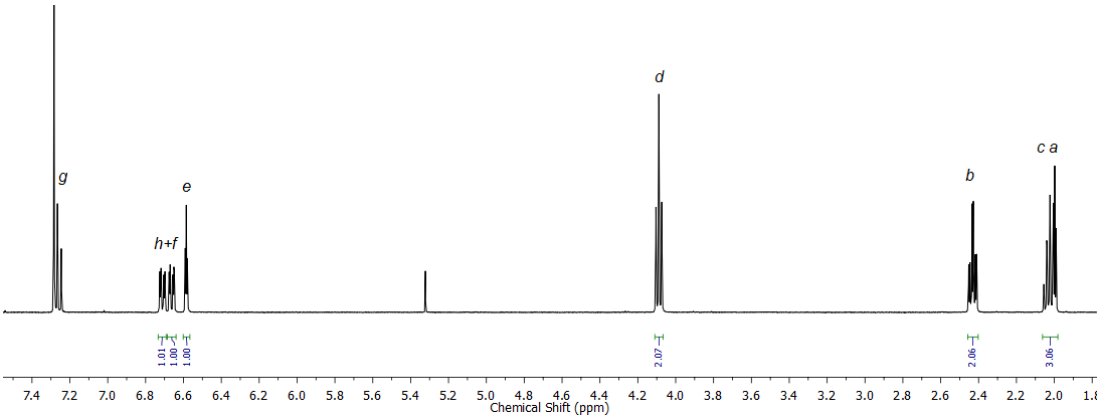

Figure 4.36 ^{1}H NMR (400 MHz, $CDCl_3$) of **238**.

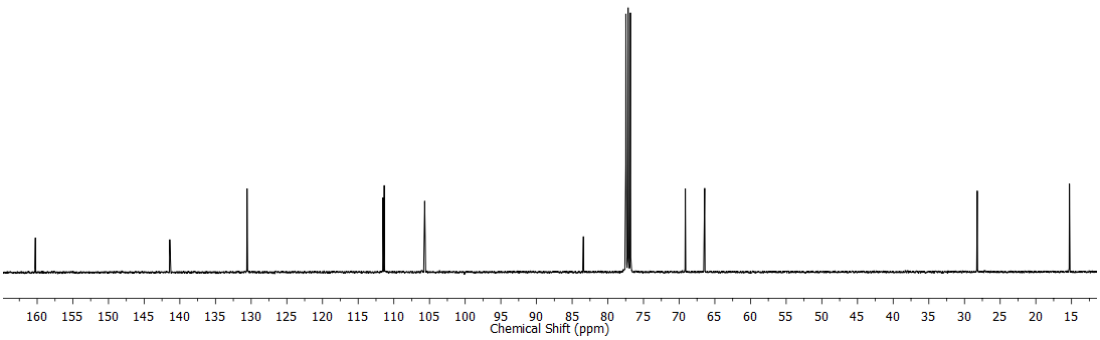

Figure 4.37 ^{13}C NMR (101 MHz, $CDCl_3$) of **238**.

Precursor 239

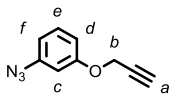

3-Azidophenol (0.135 g, 1.0 mmol, 1 eq.), 80 wt. % propargyl bromide in toluene (0.17 mL, 1.5 mmol, 1.5 eq.) and K_2CO_3 (0.691 g, 5.0 mmol, 5 eq.) were stirred at 70 °C in CH_3CN (10 mL) under air for 4 h. The cooled reaction mixture was filtered through celite and the solvent removed *in vacuo*. After filtration through a plug of silica (1:1 petrol/CH_2Cl_2) the product was obtained as a yellow oil (0.163 g, 94%). ^{1}H NMR (400 MHz, $CDCl_3$) δ: 7.30-7.26 (m, 1H, H_e), 6.76 (ddd, *J* = 8.3, 2.4, 0.9, 1H, H_d or H_f), 6.70 (ddd, *J* = 8.0, 2.2, 0.9, 1H, H_d or H_f), 6.64 (app. t, *J* = 2.3, 1H, H_c), 4.69 (d, *J* = 2.4, 2H, H_b), 2.54 (t, *J* = 2.4, 1H, H_a). ^{13}C NMR (101 MHz, $CDCl_3$) δ: 158.8, 141.5, 130.6, 112.3, 111.5, 106.2, 78.2, 76.0, 56.1. HR-ESI-MS *m/z* = 369.1071 $[M_2+Na]^+$ calc. 369.1070; 347.1254 $[M_2+H]^+$ calc. 347.1251.

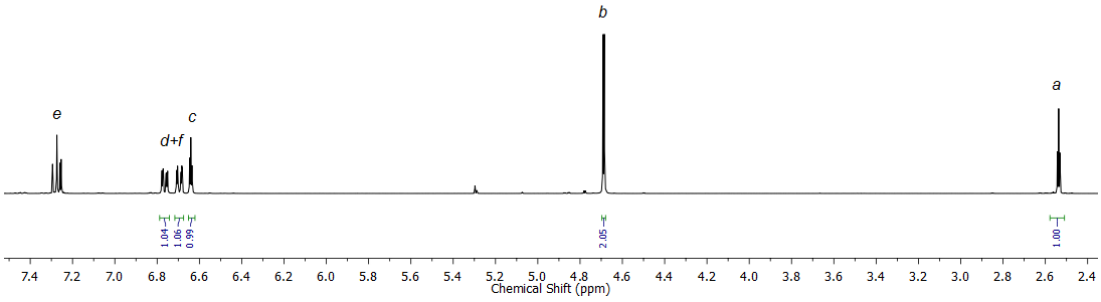

Figure 4.38 ^{1}H NMR (400 MHz, $CDCl_3$) of **239**.

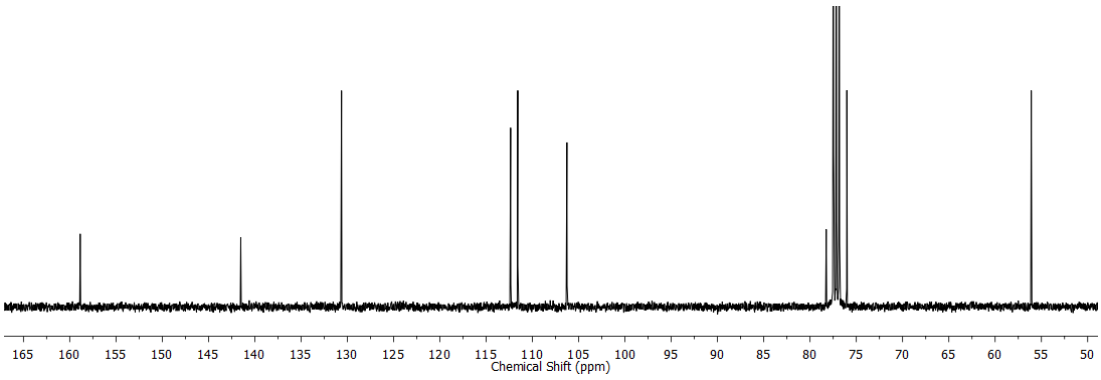

Figure 4.39 ^{13}C NMR (101 MHz, $CDCl_3$) of **239**.

Table 4.9 Optimization of the reaction between **236** and **74** with respect to concentration, temperature and addition time.

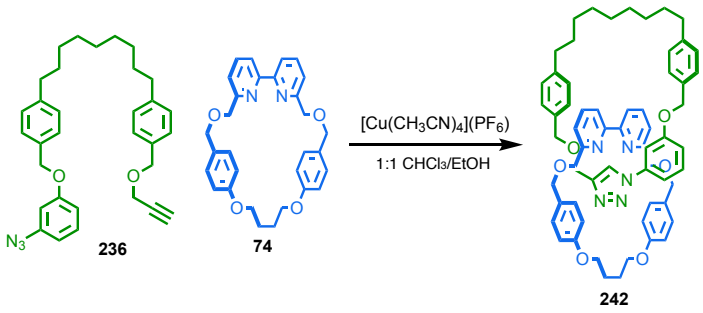

236 **74** **242**

Entry	Initial concentration catalyst (mM)	Final concentration catalyst (mM)	Temperature (°C)	Addition time (h)	Yield[a] (%)
1	10	7	rt	4	82
2	10	7	60	4	100
3	10	7	80	4	100
4	25	13	60	4	97
5	50	17	60	4	93
6	100	50	80	8	92
7	10	7	60	2	98
8	10	7	60	8	100
9[b]	10	7	60	4	33

[a] Determined by ^{1}H NMR, [b] 1 / 1 mixture TCE / ^{i}PrOH used as solvent.

Synthesis and Characterisation of Catenanes

*Catenane **242***

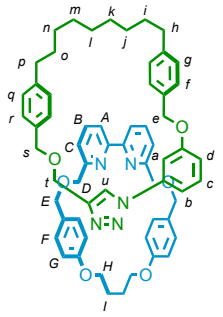

To a solution of **78** (24.1 mg, 0.050 mmol, 1 eq.), $[Cu(CH_3CN)_4]PF_6$ (18.4 mg, 0.0495 mmol, 0.99 eq.), $^{i}Pr_2NEt$ (18 µL, 0.10 mmol, 2 eq.) in 1:1 $CHCl_3$/EtOH (5.0 mL) at 60 °C was added **236** (24.8 mg, 0.050 mmol, 1 eq.) in 1:1 $CHCl_3$/EtOH (2.0 mL) over 4 h. After removal of the solvent *in vacuo*, the residue was dissolved in 1:1 CH_2Cl_2/MeOH (2.5 mL) and KCN (16 mg, 0.25 mmol, 10 eq.) added as a solid. After stirring at rt for 30 minutes the solvent was removed under a flow of air. The residue was dissolved in CH_2Cl_2 (5 mL) and washed with H_2O (4 × 5 mL), dried ($MgSO_4$) and the solvent removed *in vacuo*. After purification by column chromatography on silica (1:1 petrol/CH_2Cl_2 with a gradient of 0 to 20% MeCN over 10 CVs) **242** was obtained as a white foam (46.1 mg, 94%). ^{1}H NMR (500 MHz, $CDCl_3$) δ: 8.19 (s, 1H, H_u), 7.58 (t, *J* = 7.7, 2H, H_B), 7.44 (d, *J* = 7.6, 2H, H_A), 7.31 (d, *J* = 7.5, 2H, H_C), 7.20-7.15 (m, 5H, $H_{b/d}$, H_f, H_r), 7.11 (d, *J* = 8.1, 2H, H_g), 7.03 (t, *J* = 8.2, 1H, H_c), 6.98 (d, *J* = 8.0, 2J, H_q), 6.75 (d, *J* = 8.6, 4H, H_F), 6.52 (dd, *J* = 8.2, 1.9, 1H, $H_{b/d}$), 6.35 (d, *J* = 8.6, 4H, H_G), 6.20 (t, *J* = 2.2, 1H, H_a), 4.56 (s, 2H, H_t), 4.47 (s, 2H, H_e), 4.39-4.37 (m, 4H, 2 of H_E, H_s), 4.32 (d, *J* = 12.1, 2H, 2 of H_E), 4.24 (d, *J* = 12.8, 2H, 2 of H_D), 4.19 (d, *J* = 12.8, 2H, 2 of H_D), 3.92-3.88 (m, 2H, 2 of H_H), 3.82-3.77 (m, 2H, 2 of H_H), 2.57 (t, *J* = 6.7, 2H, H_h), 2.40 (t, *J* = 7.2, 2H, H_p), 1.80-1.75 (m, 4H, H_l), 1.49-1.42 (m, 2H, H_i), 1.21-1.15 (m, 2H, H_o), 1.06-0.87 (m, 8H, H_j, H_n, 4 of $H_{k/l/m}$), 0.76-0.70 (m, 2H, 2 of $H_{k/l/m}$). ^{13}C NMR (126 MHz, $CDCl_3$) δ: 159.0, 158.8, 158.7, 156.4, 146.2, 142.7, 142.5, 137.3, 136.9, 135.6, 134.4, 130.3, 129.8, 129.3, 129.1, 128.7, 128.7, 128.5, 121.8, 120.6, 120.5, 115.5, 113.4, 111.9, 108.0, 73.2, 72.7, 70.8, 69.6, 67.3, 65.0, 35.8, 35.5, 31.7, 31.2, 30.4, 30.2, 29.5, 28.9, 28.5, 25.1. HR-ESI-MS *m/z* = 978.5180 $[M+H]^+$ calc. 978.5164.

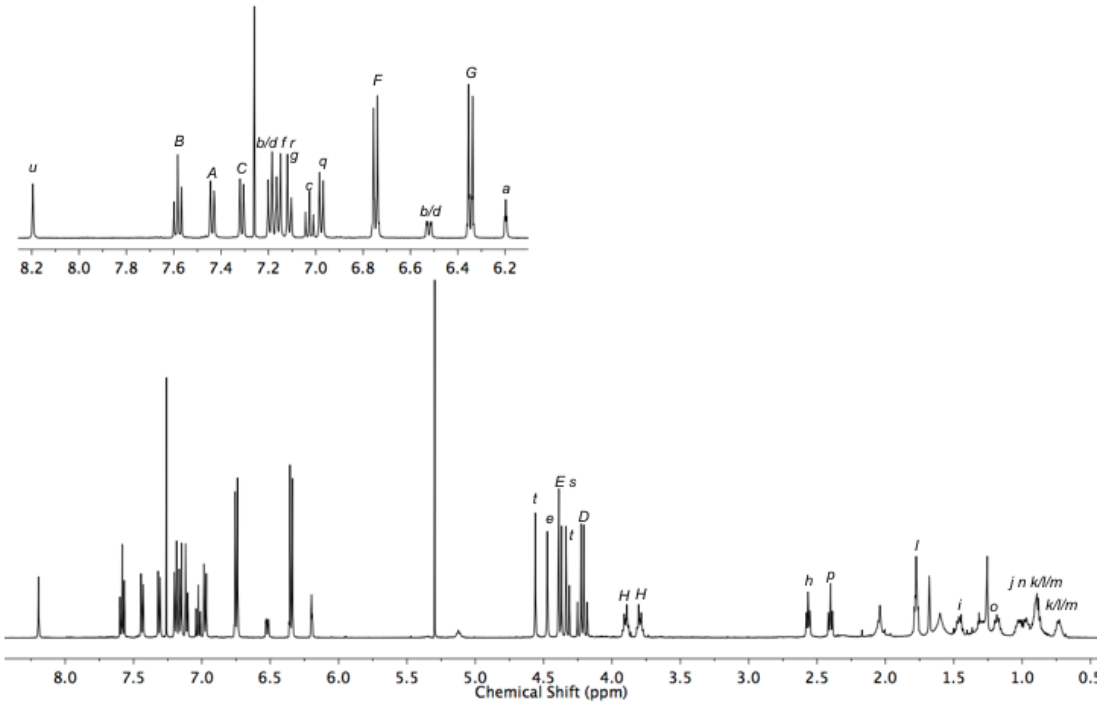

Figure 4.40 ^{1}H NMR (500 MHz, $CDCl_3$) of **242**.

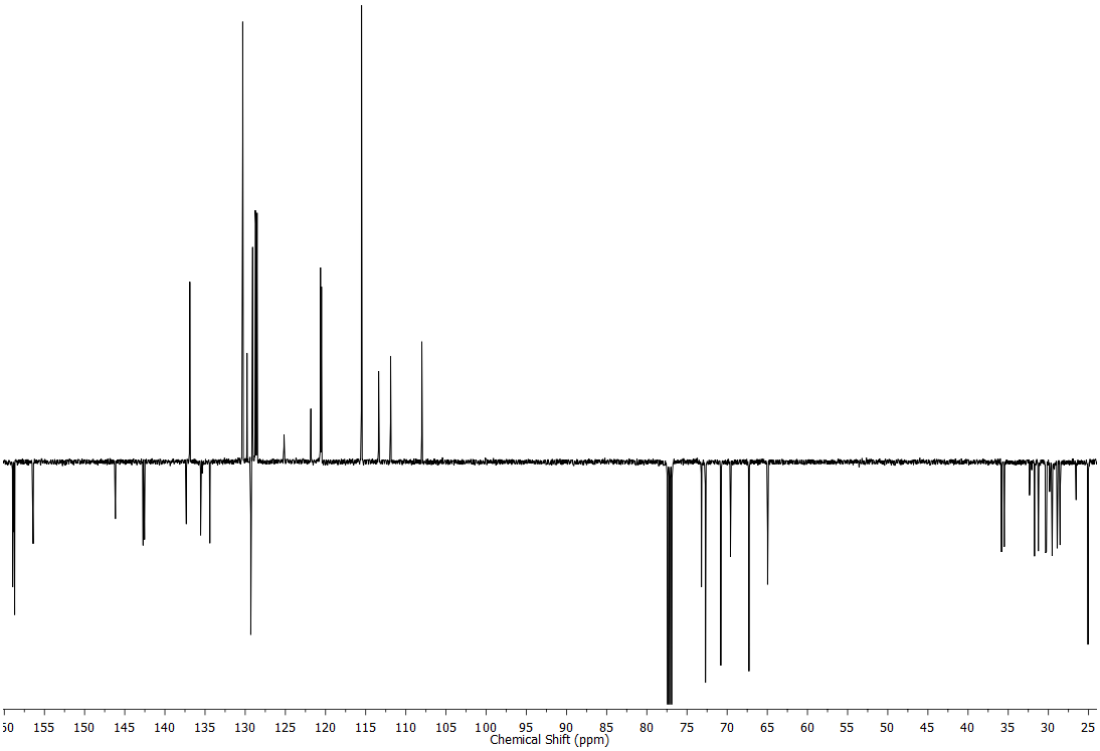

Figure 4.41 JMOD NMR (126 MHz, $CDCl_3$) of **242**.

Catenane ***243***

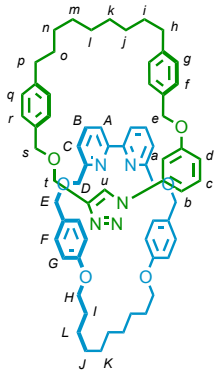

To a solution of **108** (14.2 mg, 0.025 mmol, 1 eq.), $[Cu(CH_3CN)_4](PF_6)$ (9.2 mg, 0.025 mmol, 0.99 eq.) and $^{i}Pr_2NEt$ (13 µL, 0.075 mmol, 3 eq.) in 1:1 $CHCl_3$/EtOH (2.5 mL) at 60 °C was added **236** (18.6 mg, 0.0375 mmol, 1.5 eq.) in 1:1 $CHCl_3$/EtOH (1.5 mL) over 6 h. After removal of the solvent *in vacuo*, the residue was dissolved in 1:1 CH_2Cl_2/MeOH (2.5 mL) and KCN (16 mg, 0.25 mmol, 10 eq.) added as a solid. After stirring at rt for 30 minutes the solvent was removed under a flow of air. The residue was dissolved in CH_2Cl_2 (5 mL) and washed with H_2O (4 × 5 mL), dried ($MgSO_4$) and the solvent removed *in vacuo*. After purification by column chromatography on silica (petrol with a gradient of 0 to 75% Et_2O over 10 CVs) **243** was obtained as a white foam (25.6 mg, 96%). ^{1}H NMR (500 MHz, $CDCl_3$) δ: 7.97 (dd, *J* = 7.8, 0.9, 2H,H_A), 7.57-7.54 (m, 3H, H_B, H_u), 7.32 (ddd, *J* = 8.2, 2.1, 0.7, 1H, H_b), 7.28 (dd, *J* = 7.6, 0.9, 2H, H_C), 7.24 (d, *J* = 8.0, 2H, H_r), 7.17 (d, *J* = 8.0, 2H, H_f), 7.09-7.05 (m, 3H, H_c, H_g), 7.00 (d, *J* = 8.0, 2H, H_q), 6.84 (d, *J* = 8.6, 4H, H_F), 6.65-6.63 (m, 1H, H_d), 6.39-6.36 (m, 5H, H_G, H_a), 4.73 (d, *J* = 0.5, 2H, H_t), 4.70 (s, 2Hm H_e), 4.52 (d, *J* = 1.3, 4H, H_D), 4.50-4.44 (m, 6H, H_E, H_s), 3.67 (t, *J* = 6.5, 4H, H_H), 2.48 (t, *J* = 6.6, 2H, H_h), 2.38 (t, *J* = 7.1, 2H, H_p), 1.52 (app. quint, *J* = 6.6, 4H, H_l), 1.37 (br. m, 2H, H_i), 1.22-1.15 (m, 6H, H_J, H_o), 1.09-1.05 (m, 8H, H_K, H_L), 0.89-0.79 (m, 8H, H_j, H_n, 2 of $H_{k/l/m}$), 0.51 (br. m, 2H, $H_{k/l/m}$).^{13}C NMR (126 MHz, $CDCl_3$) δ: 159.5, 158.5, 158.4, 155.4, 146.7, 143.1, 142.8, 137.8, 136.9, 135.3, 133.8, 130.4, 129.8, 129.7, 129.1, 129.0, 129.0, 128.8, 121.2, 120.3, 119.7, 114.6, 112.2, 111.7, 108.2, 73.8, 72.4, 72.1, 70.4, 67.7, 65.3, 36.0, 35.5, 31.7, 31.3, 30.7, 30.5, 29.5, 29.5, 29.1, 29.0, 28.9, 28.6, 25.9.LR-ESI-MS *m/z* = 1062.61 $[M+H]^+$ calc. 1062.61.

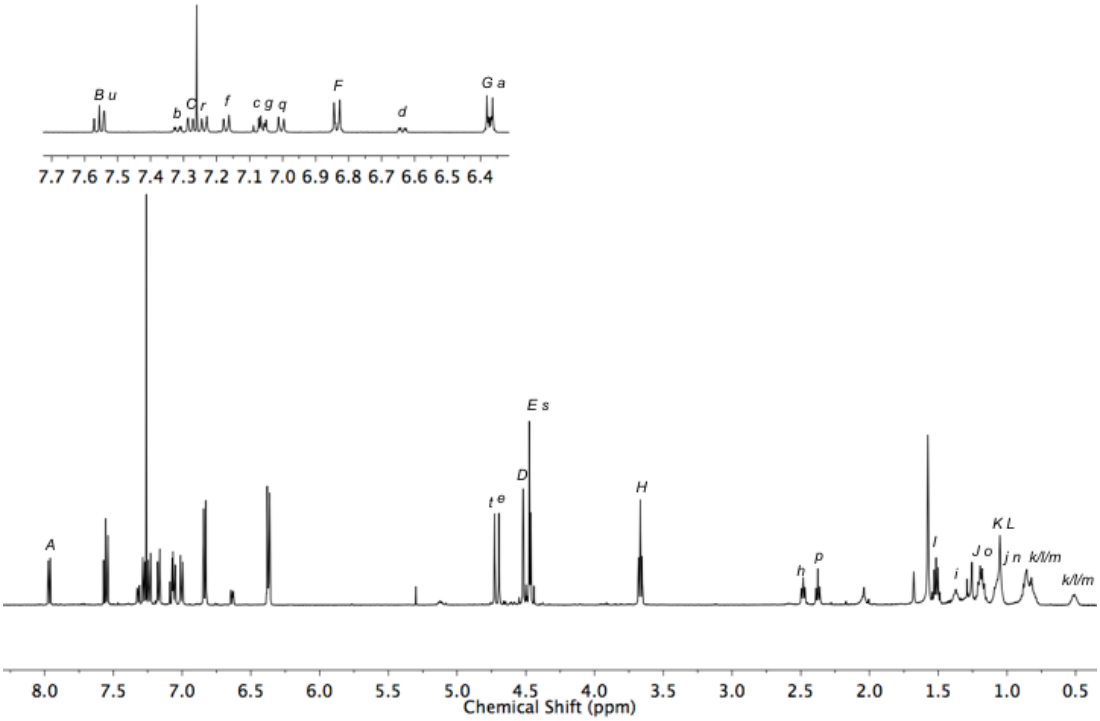

Figure 4.42 ^{1}H NMR (500 MHz, $CDCl_3$) of **243**.

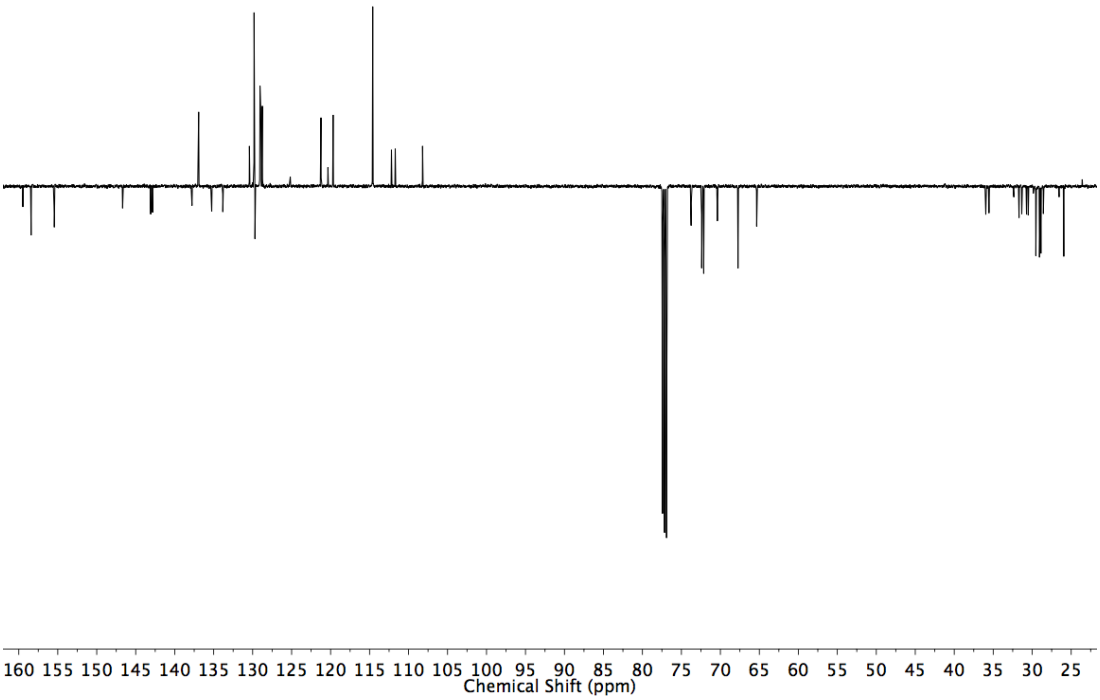

Figure 4.43 JMOD NMR (126 MHz, $CDCl_3$) of **243**.

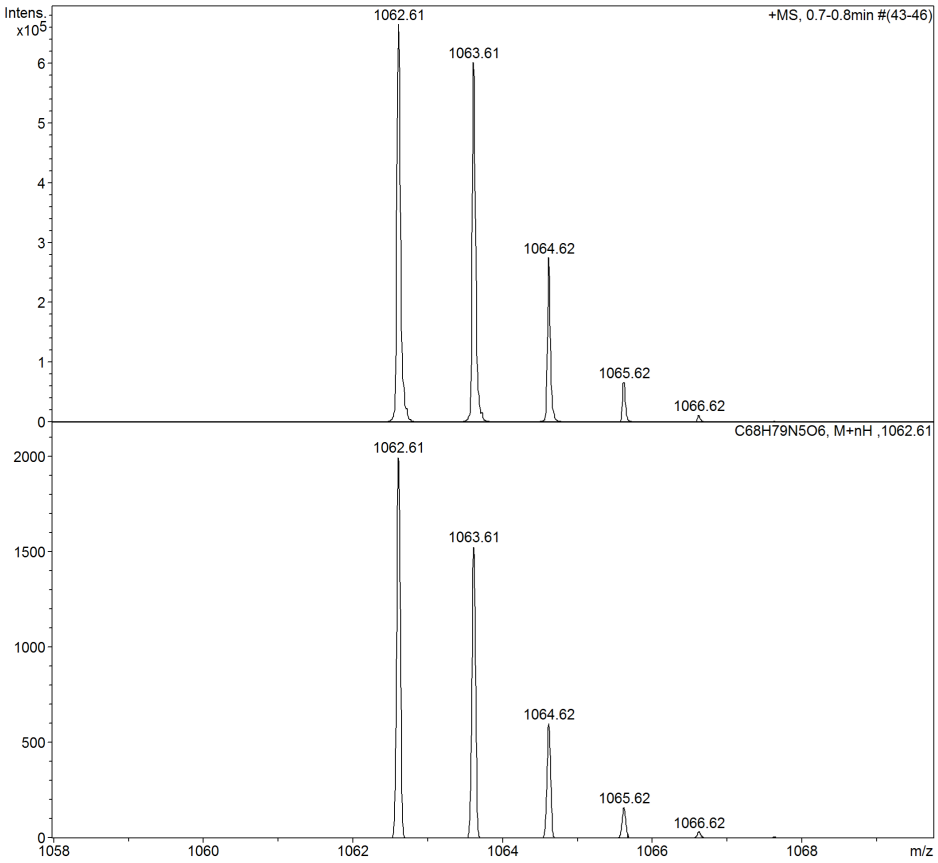

Figure 4.44 Observed (top) and calculated (bottom) isotopic patterns for **243**.

Catenane ***244***

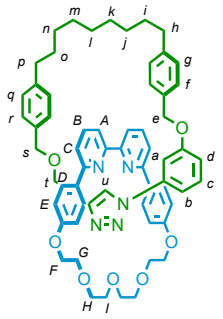

To a solution of **110** (24.9 mg, 0.050 mmol, 1 eq.), $[Cu(CH_3CN)_4](PF_6)$ (18.4 mg, 0.0495 mmol, 0.99 eq.) and $^{i}Pr_2NEt$ (28 µL, 0.15 mmol, 3 eq.) in 1:1 $CHCl_3$/EtOH (5.0 mL) at 80 °C was added **236** (37.2 mg, 0.0750 mmol, 1.5 eq.) in 1:1 $CHCl_3$/EtOH (3.0 mL) over 6 h. After removal of the solvent *in vacuo*, the residue was dissolved in 1:1 CH_2Cl_2/MeOH (5.0 mL) and KCN (33 mg, 0.50 mmol, 10 eq.) added as a solid. After stirring at rt for 30 minutes the solvent was removed under a flow of air. The residue was dissolved in CH_2Cl_2 (10 mL) and washed with H_2O (4 × 10 mL), dried ($MgSO_4$) and the solvent removed *in vacuo*. After purification by column chromatography on silica (1:1 CH_2Cl_2/petrol with a gradient of 0 to 20% MeCN over 8 CVs) **244** was obtained as a white foam (48.8 mg, 98%). ^{1}H NMR (500 MHz, $CDCl_3$) δ: 8.92 (s, 1H, H_u), 7.83 (app. t, J = 7.8, 2H, H_B), 7.66 (dd, J = 7.7, 0.8, 2H, H_A), 7.44-7.41 (m, 3H, H_C, H_b), 7.17-7.15 (m, 6H, H_D, H_r), 7.09 (t, J = 2.1, 1H, H_a), 7.03-6.95 (m, 4H, H_c, H_d, H_q), 6.95 (s, 4H, H_f, H_g), 6.35 (d, J = 8.7, 4H, H_E), 4.69 (s, 2H, H_e), 4.41 (s, 2H, H_t), 4.34 (s, 2H, H_s), 3.96-3.93 (m, 4H, H_F), 3.52-3.43 (m, 10H, H_G, H_H, H_I), 3.38-3.33 (m, 2H, $H_{G'}$), 2.54 (t, J = 6.8, 2H, H_p), 2.47 (t, J = 6.9, 2H, H_h), 1.45 (app. quint, J = 7.2, 2H, H_o), 1.31 (app. quint, J = 6.9, 2H, H_i), 1.07-1.00 (m, 8H, H_n, H_j, 2 of H_k or H_l or H_m), 0.83 (br. m, 2H, H_k or H_l or H_m). ^{13}C NMR (126 MHz, $CDCl_3$) δ: 159.3, 158.7, 158.7, 157.6, 145.2, 142.3, 142.0, 137.6, 137.2, 135.9, 134.6, 133.1, 129.8, 129.4, 128.6 (×2), 128.4, 127.9, 123.5, 119.9, 119.6, 115.0, 114.3, 112.2, 107.9, 72.8, 70.1, 69.9, 69.2, 68.4, 66.7, 64.6, 35.7, 35.6, 31.5, 31.4, 30.4, 30.4, 29.7, 28.8, 28.7. HR-ESI-MS *m/z* = 994.5094 $[M+H]^+$ calc. 994.5113.

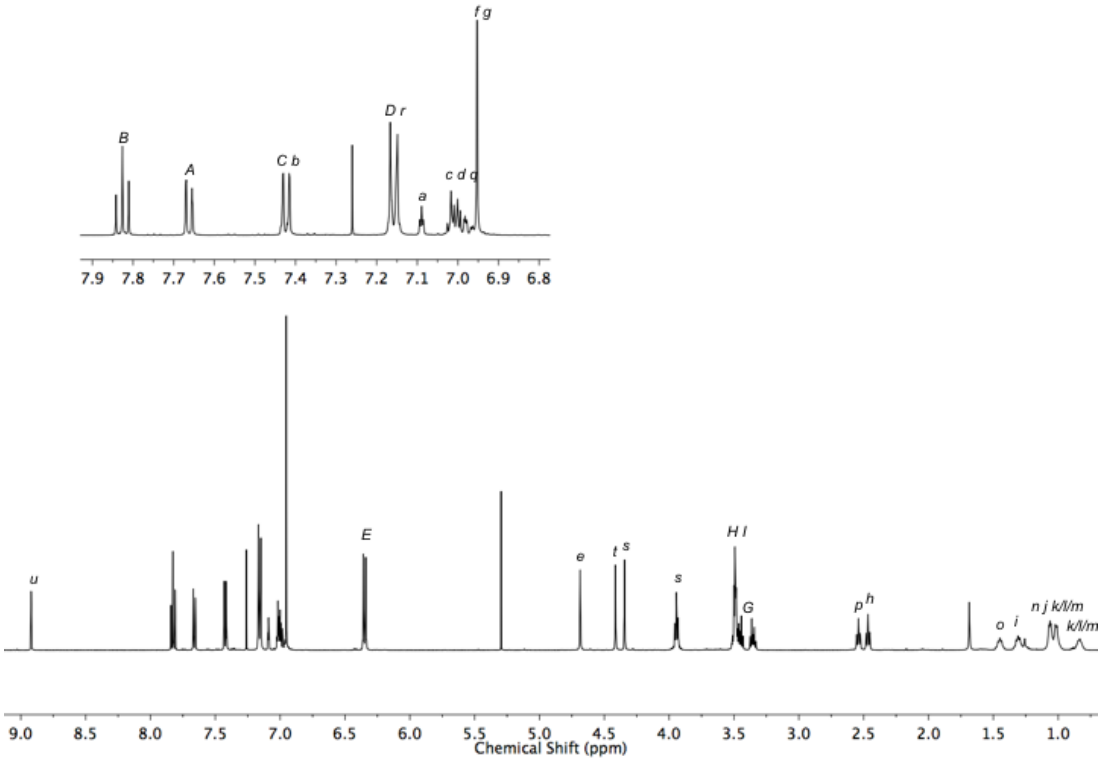

Figure 4.45 ^{1}H NMR (500 MHz, $CDCl_3$) of **244**.

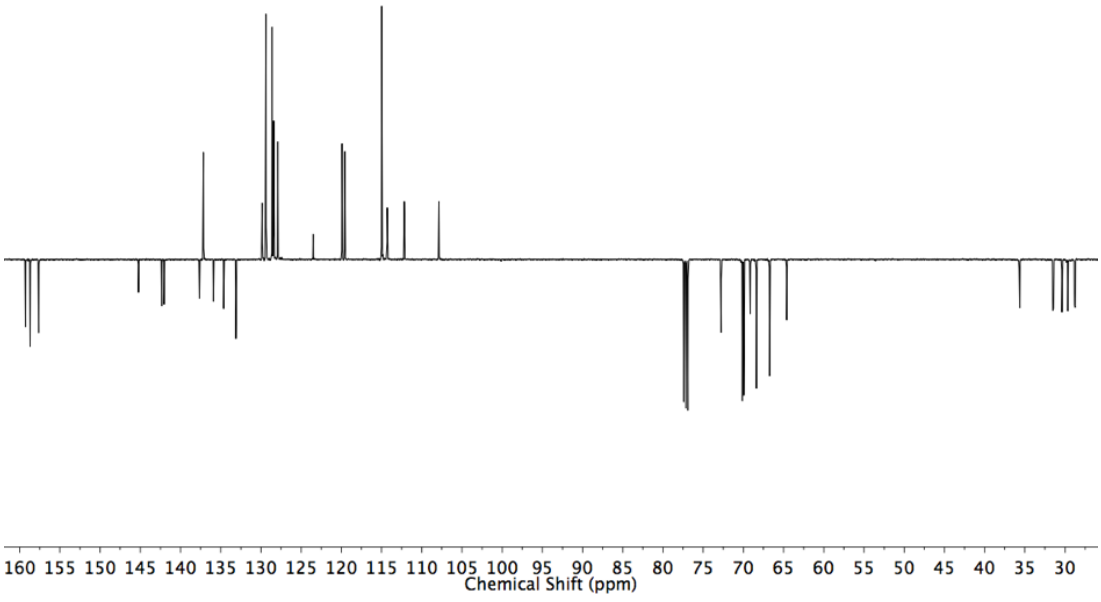

Figure 4.46 JMOD NMR (126 MHz, $CDCl_3$) of **244**.

Catenane ***245***

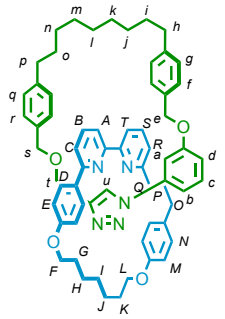

To a solution of **95** (12.0 mg, 0.025 mmol, 1 eq.), $[Cu(CH_3CN)_4](PF_6)$ (9.2 mg, 0.025 mmol, 0.99 eq.) and $^{i}Pr_2NEt$ (9 µL, 0.05 mmol, 2 eq.) in 1:1 $CHCl_3$/EtOH (2.5 mL) at 80 °C was added **236** (12.4 mg, 0.025 mmol, 1 eq.) in 1:1 $CHCl_3$/EtOH (1 mL) over 4 h. After removal of the solvent *in vacuo*, the residue was dissolved in 1:1 CH_2Cl_2/MeOH (2 mL) and KCN (16 mg, 0.25 mmol, 10 eq.) added as a solid. After stirring at rt for 30 minutes the solvent was removed under a flow of air. The residue was dissolved in CH_2Cl_2 (5 mL) and washed with H_2O (4 × 5 mL), dried ($MgSO_4$) and the solvent removed *in vacuo*. After purification by column chromatography on silica (1:1 CH_2Cl_2/petrol with a gradient of 0 to 50% Et_2O over 8 CVs) **245** was obtained as a white foam (20.9 mg, 86%). ^{1}H NMR (500 MHz, $CDCl_3$) δ: 9.18 (s, 1H, H_u), 7.74 (app. t, *J* = 7.7, 1H, H_S), 7.67 (app. t, *J* = 7.7, 1H, H_B), 7.58 (dd, *J* = 7.7, 0.8, 1H, H_T), 7.49 (dd, *J* = 7.7, 0.8, 1H, H_A), 7.23 (ddd, *J* = 8.1, 1.9, 0.8, 1H, H_b), 7.13-7.13 (m, 3H, H_a, H_r), 7.09-7.04 (m, 2H, H_R, H_c), 7.02 (d, *J* = 8.1, 2H, H_q), 6.91 (ddd, *J* = 8.3, 2.3, 0.7, 1H, H_d), 6.89 (d, *J* = 8.1, 1H, H_g), 6.79 (d, *J* = 8.1, 2H, H_f), 6.76 (d, *J* = 8.7, 2H, H_D), 6.28 (d, *J* = 8.5, 2H, H_N), 6.14 (d, *J* = 8.7, 2H, H_E), 6.05 (d, *J* = 8.5, 2H, H_M), 4.63 (d, *J* = 13.5, 1H, 1 of H_e), 4.54 (d, *J* = 13.5, 1H, 1 of H_e), 4.48 (d, *J* = 11.7, 1H, 1 of H_t), 4.41-4.38 (m, 2H, 1 of H_s, 1 of H_t), 4.30 (d, *J* = 10.8, 1H, 1 of H_s), 4.14-4.09 (m, 1H, 1 of H_L), 4.06-4.01 (m, 1H, 1 of H_F), 3.91-3.87 (m, 1H, 1 of H_F), 3.79-3.75 (m, 1H, 1 of H_L), 2.56 (t, *J* = 6.9, 2H, H_p), 2.44 (app. td, *J* = 7.1, 4.1, 2H, H_h), 2.37 (td, *J* = 13.4, 4.7, 1H, H_Q), 2.21 (td, *J* = 13.4, 4.7, 1H, $H_{Q'}$), 2.13-2.08 (m, 2H, H_O), 1.97 (br. m, 1H, 1 of H_H), 1.90 (br. m, 1H, 1 of H_K), 1.84-1.77 (m, 1H, H_G), 1.75-1.63 (m, 4H, H_J, 1 of H_K, $H_{G'}$), 1.58 (br. m, 2H, H_I), 1.50 (br. m, 2H, H_o), 1.32 (br. m, 6H, H_P, H_i, 2 of H_j or H_k or H_l or H_m), 1.11 (br. m, 3H, H_n, 1 of H_j or H_k or H_l or H_m), 0.95 (br. m, 2H, 1 of H_j or H_k or H_l or H_m). ^{13}C NMR (126 MHz, $CDCl_3$) δ: 163.7, 159.4, 158.8, 158.4, 157.6, 157.6, 156.5, 144.3, 141.9, 141.8, 137.7, 136.9, 136.8, 136.2, 134.8, 132.1, 131.7, 129.0, 128.8, 128.4, 128.3, 128.3, 127.9, 126.6, 123.6, 122.4, 120.1, 119.8, 119.5, 114.5, 114.3, 113.5, 112.0, 106.2, 72.2, 68.5, 67.0, 65.0,

64.5, 37.2, 35.8, 35.7, 35.1, 32.6, 31.7, 31.6, 30.3, 30.1, 29.4, 29.4, 29.0, 29.0, 28.8, 28.0, 25.9, 25.8. HR-ESI-MS *m/z* = 974.5584 $[M+H]^+$ calc. 974.5579.

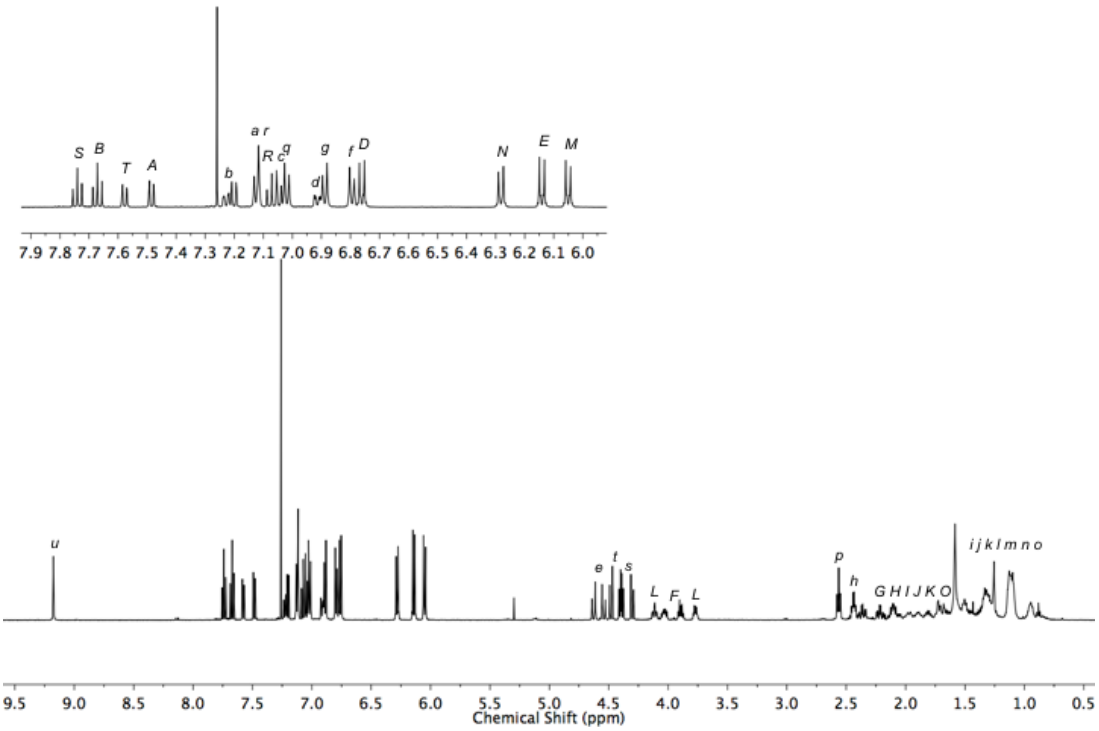

Figure 4.47 ^{1}H NMR (500 MHz, $CDCl_3$) of **245**.

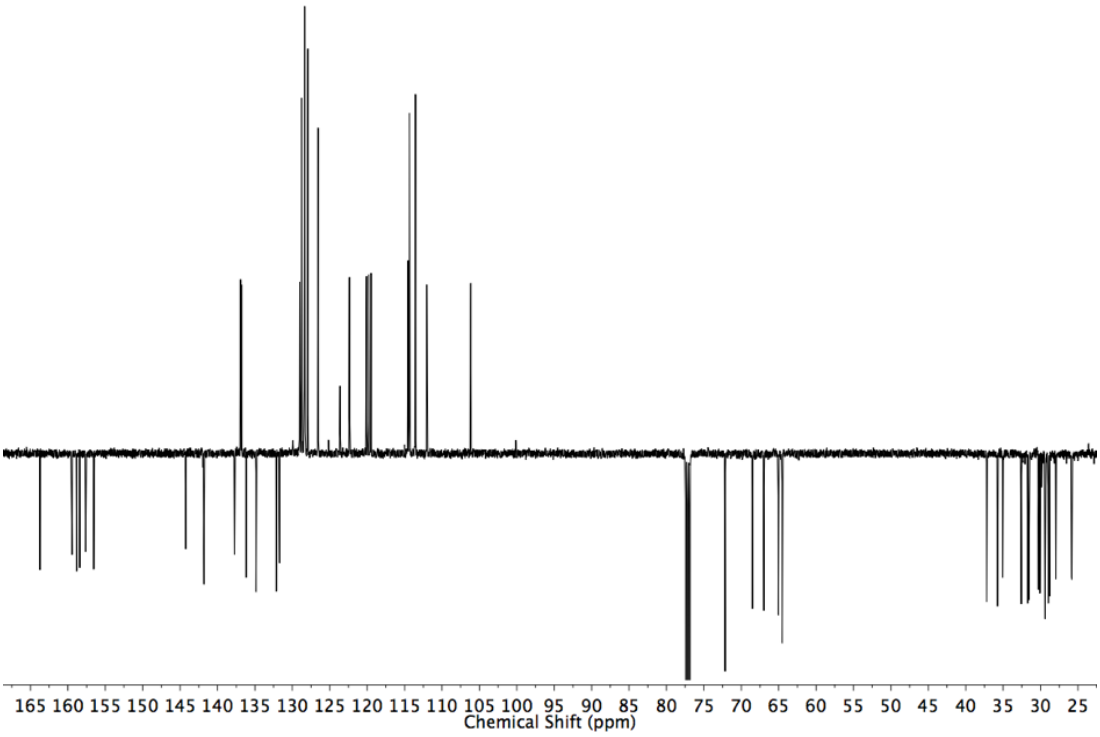

Figure 4.48 JMOD NMR (126 MHz, $CDCl_3$) of **245**.

Macrocycle ***246***

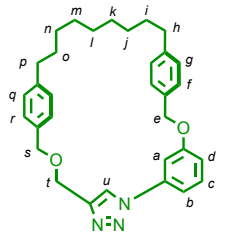

To a solution of $[Cu(CH_3CN)_4](PF_6)$ (7.2 mg, 0.020 mmol, 0.99 eq.) and $^{i}Pr_2NEt$ (3.5 µL, 0.020 mmol, 1 eq.) in 1:1 $CHCl_3$/EtOH (2.0 mL) at 60 °C was added **236** (9.9 mg, 0.020 mmol, 1 eq.) in 1:1 $CHCl_3$/EtOH (0.8 mL) over 4 h. EDTA-NH_3 solution (3 mL) was added and the aqueous phase extracted with CH_2Cl_2 (3 × 5 mL). The combined organic phases were dried ($MgSO_4$) and the solvent removed *in vacuo*. After purification by column chromatography on silica (CH_2Cl_2/Et_2O 98/2) **246** was obtained as a white foam (4.7 mg, 47%). ^{1}H NMR (400 MHz, $CDCl_3$) δ: 7.82 (s, 1H, H_u), 7.49-7.41 (m, 2H, H_c, $H_{b/d}$), 7.28 (d, *J* = 8.1, 2H, H_f), 7.24 (d, *J* = 8.0, 2H, H_r), 7.14 (app. t, *J* = 8.5, 4H, H_g, H_q), 7.06 (ddd, *J* = 7.6, 2.5, 1.6, 1H, $H_{b/d}$), 7.02 (t, *J* = 2.1, 1H, H_a), 5.11 (s, 2H, H_e), 4.82 (s, 2H, H_t), 4.58 (s, 2H, H_s), 2.58 (td, *J* = 7.2, 2.6, 4H, H_h, H_p), 1.61-1.51 (m, 4H, H_i, H_o), 1.21-1.12 (m, 10H, H_j, H_k, H_l, H_m, H_n). ^{13}C NMR (101 MHz, $CDCl_3$) δ: 159.6, 146.7, 143.1, 142.6, 138.1, 135.2, 133.3, 130.9, 129.1, 128.8, 128.3, 127.8, 120.8, 114.7, 113.1, 108.0, 73.2, 70.6, 64.7, 35.7, 35.6, 31.3, 31.0, 29.7, 29.7, 29.2, 28.8, 28.6. HR-ESI-MS *m/z* = 496.2954 $[M+H]^+$ calc. 496.2959.

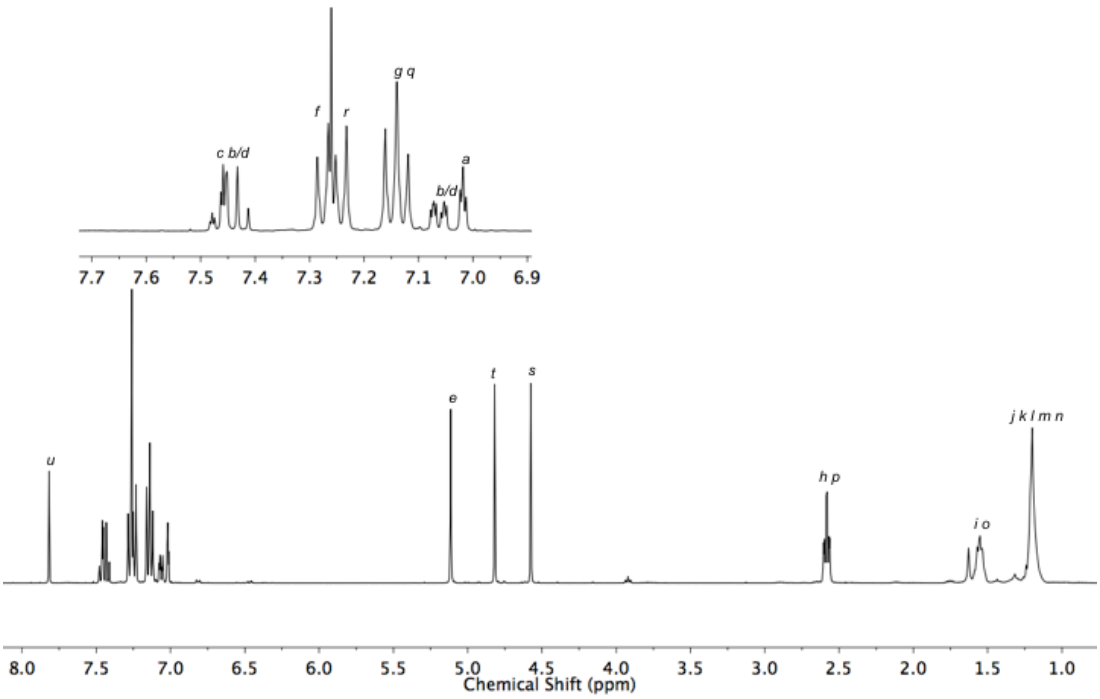

Figure 4.49 ^{1}H NMR (400 MHz, $CDCl_3$) of **246**.

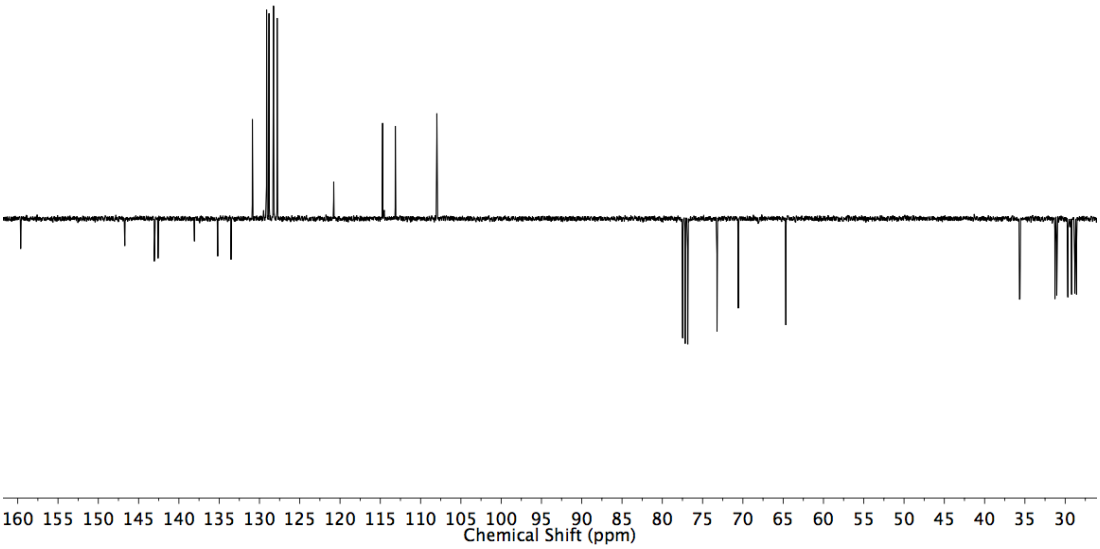

Figure 4.50 JMOD NMR (101 MHz, $CDCl_3$) of **246**.

Catenane ***248***

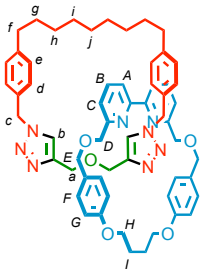

To a solution of **78** (12.1 mg, 0.025 mmol, 1 eq.), $[Cu(CH_3CN)_4]PF_6$ (8.9mg, 0.024 mmol, 0.96 eq.), $^{i}Pr_2NEt$ (18 µL, 0.10 mmol, 4 eq.) in 1:1 $CHCl_3$/EtOH (2.5 mL) at 60 °C was added propargyl ether (5.1 µL, 0.050 mmol, 2 eq.) and **240** (19.5 mg, 0.05 mmol, 2 eq.) in 1:1 $CHCl_3$/EtOH (2.0 mL) over 8 h. After removal of the solvent *in vacuo*, the residue was dissolved in 1:1 CH_2Cl_2/MeOH (2.5 mL) and KCN (16 mg, 0.25 mmol, 10 eq.) added as a solid. After stirring at rt for 30 minutes the solvent was removed under a flow of air. The residue was dissolved in CH_2Cl_2 (5 mL) and washed with H_2O (4 × 5 mL), dried ($MgSO_4$) and the solvent removed *in vacuo*. After purification by column chromatography on silica (Flush 1:1 Et_2O/MeCN, followed by DCM with a gradient of 0 to 50% acetone) **248** was obtained as a white foam (18.0 mg, 75%). ^{1}H NMR (500 MHz, $CDCl_3$) δ: 7.73 (s, 2H, H_b), 7.62 (app. t, J = 7.8, 2H, H_B), 7.43 (d, J = 7.5, 2H, H_A), 7.27-7.26 (m, 2H, H_C), 6.95-6.91 (m, 8H, H_d, H_e), 6.64 (d, J = 8.6, 4H, H_F), 6.50 (d, J = 8.7, 4H, H_G), 5.02 (s, 4H, H_c), 4.25 (s, 4H, H_E), 4.17 (br. m, 4H, H_H), 4.03 (s, 4H, H_a), 3.91 (s, 4H, H_D), 2.45 (t, J = 7.3, 4H, H_f), 1.97 (br. m, 4H, H_I), 1.36 (app. quint, 4H, H_g), 1.10-1.04 (m, 8H, H_h, H_i), 0.89-0.83 (m, 2H, H_j). ^{13}C NMR (126 MHz, $CDCl_3$) δ: 159.3, 159.1, 156.0, 145.3, 143.2, 137.0, 132.2, 130.1, 129.0, 128.7, 128.4, 123.6, 120.9, 120.4, 115.1, 72.9, 70.7, 66.7, 64.5, 53.5, 35.8, 31.2, 29.8, 28.8, 28.7, 24.9. HR-ESI-MS m/z = 989.5043 $[M+Na]^+$ calc. 989.5048.

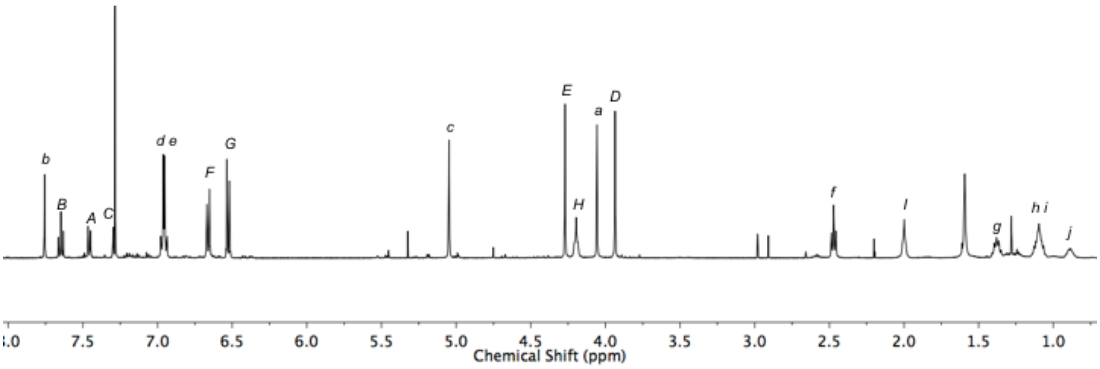

Figure 4.51 ^{1}H NMR (500 MHz, $CDCl_3$) of **248**.

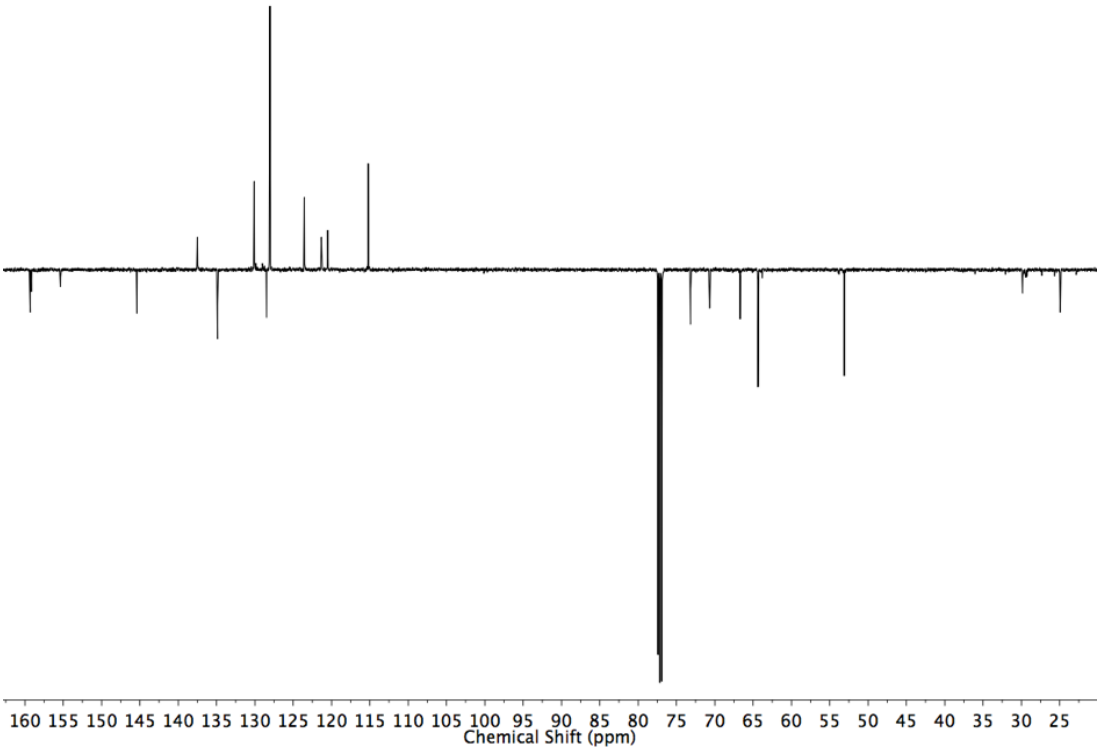

Figure 4.52 JMOD NMR (126 MHz, $CDCl_3$) of **248**.

Catenane ***250***

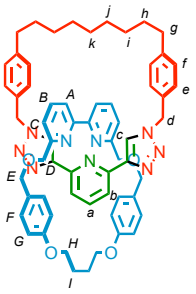

To a solution of **78** (12.1 mg, 0.025 mmol, 1 eq.), $[Cu(CH_3CN)_4]PF_6$ (8.9mg, 0.024 mmol, 0.96 eq.), $^{i}Pr_2NEt$ (18 µL, 0.10 mmol, 4 eq.) in 1:1 $CHCl_3$/EtOH (2.5 mL) at 60 °C was added 2,6-diethynylpyridine (6.4 mg, 0.050 mmol, 2 eq.) and **240** (19.5 mg, 0.050 mmol, 2 eq.) in 1:1 $CHCl_3$/EtOH (2.0 mL) over 8 h. After removal of the solvent *in vacuo*, the residue was dissolved in 1:1 CH_2Cl_2/MeOH (2.5 mL) and KCN (16 mg, 0.25 mmol, 10 eq.) added as a solid. After stirring at rt for 30 minutes the solvent was removed under a flow of air. The residue was dissolved in CH_2Cl_2 (5 mL) and washed with H_2O (4 × 5 mL), dried ($MgSO_4$) and the solvent removed *in vacuo*. After purification by column chromatography on silica (hexane with a gradient of 0 to 100% Et_2O over 10 CVs) **250** was obtained as a white foam (17.0 mg, 71%). ^{1}H NMR (400 MHz, $CDCl_3$) δ: 8.46 (s, 2H, H_c), 8.03 (d, J = 7.8, 2H, H_b), 7.83 (dd*, J = 8.2, 7.4, 1H, H_a), 7.56 (app. t, J = 7.8, 2H, H_B), 7.40 (d, J = 7.5, 2H, H_A), 7.24 (d, J = 7.6, 2H, H_C), 6.84 (d, J = 8.0, 4H, H_f), 6.73 (d, J = 8.6, 4H, H_F), 6.64 (d, J = 7.9, 4H, H_e), 6.52 (d, J = 8.6, 4H, H_G), 4.98 (s, 4H, H_d), 4.24 (br. s, 8H, H_E, H_H), 3.88 (s, 4H, H_D), 2.41 (t, J = 7.3, 4H, H_g), 2.01 (br. m, 4H, H_I), 1.38-1.18 (m, 8H, H_h, H_i or H_j), 1.10 (br. m, 4H, H_i or H_j), 1.01 (br. m, 2H, H_k). ^{13}C NMR (101 MHz, $CDCl_3$) δ: 159.3, 159.2, 156.0, 150.2, 148.6, 142.7, 137.2, 136.9, 132.4, 130.2, 128.8, 128.8, 127.4, 124.2, 121.1, 120.4, 118.7, 115.2, 73.0, 70.7, 66.9, 53.2, 35.6, 31.2, 29.7, 28.8 (×2), 25.0. HR-ESI-MS m/z = 1000.5205 $[M+H]^+$ calc. 1000.5232.

* observed due to slow motion on the NMR timescale

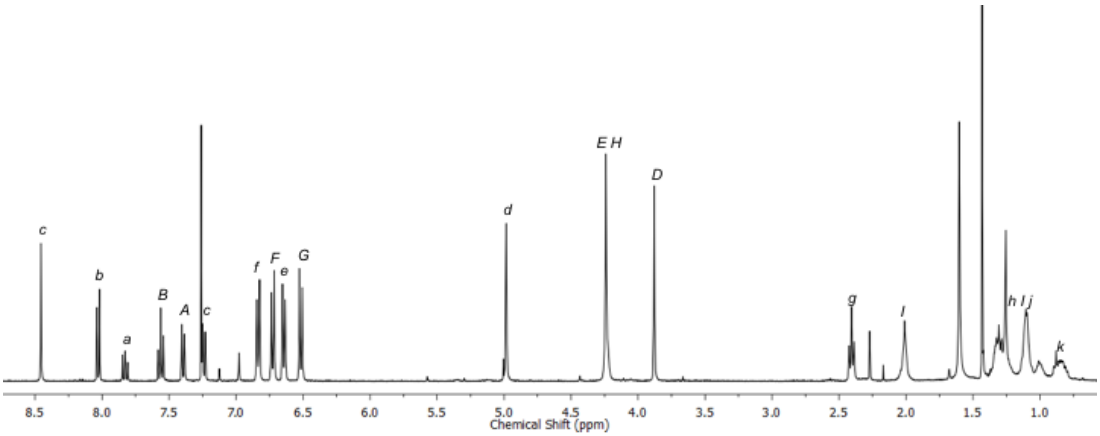

Figure 4.53 ^{1}H NMR (400 MHz, $CDCl_3$) of **250**. Peaks at 6.98, 5.00, 2.27 and 1.43 ppm are due to BHT impurity from the chromatography solvent.

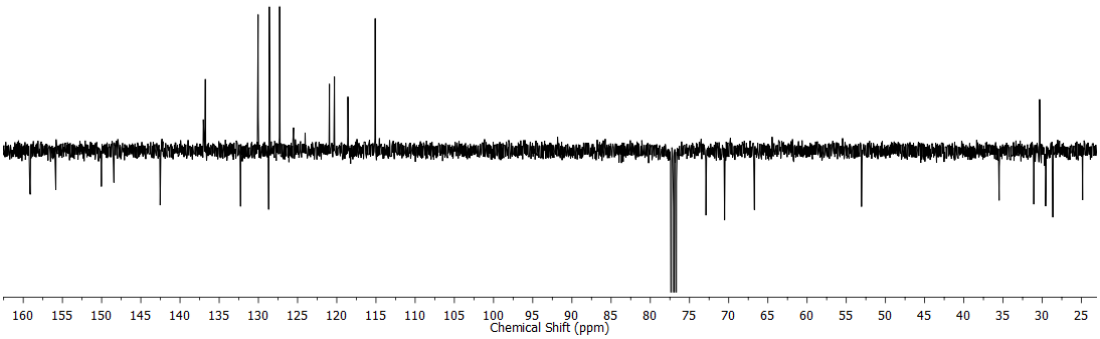

Figure 4.54 JMOD NMR (101 MHz, $CDCl_3$) of **250**.

*Catenane **251***

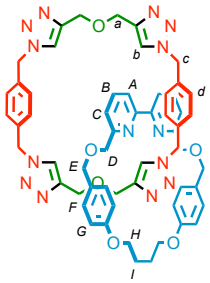

To a solution of **78** (24.1 mg, 0.05 mmol, 1 eq.), $[Cu(CH_3CN)_4]PF_6$ (17.8 mg, 0.048 mmol, 0.96 eq.), $^{i}Pr_2NEt$ (104 µL, 0.60 mmol, 12 eq.) in 1:1 $CHCl_3$/EtOH (5.0 mL) at 60 °C was added propargyl ether (31 µL, 0.30 mmol, 6 eq.) and α,α`-diazido-*p*-xylene (56.4 mg, 0.30 mmol, 6 eq.) in 1:1 $CHCl_3$/EtOH (6.0 mL) over 12 h. After removal of the solvent *in vacuo*, the residue was dissolved in 1:1 CH_2Cl_2/MeOH (5.0 mL) and KCN (16 mg, 0.25 mmol, 5 eq.) added as a solid. After stirring at rt for 30 minutes the solvent was removed under a flow of air. The residue was dissolved in CH_2Cl_2 (20 mL) and washed with H_2O (4 × 5 mL), dried ($MgSO_4$) and the solvent removed *in vacuo*. After purification by column chromatography on silica (MeCN with a gradient of 0 to 8% MeOH over 10 CVs) **251** was obtained as a white foam (41.0 mg, 78%). ^{1}H NMR (500 MHz, $CDCl_3$) δ: 7.86 (s, 4H, H_b), 7.54 (app. t, J = 7.8, 2H, H_B), 7.32 (d, J = 7.8, 2H, H_A), 7.21 (d, J = 7.7, 2H, H_C), 6.71 (d, J = 8.6, 4H, H_F), 6.68 (s, 8H, H_d), 6.61 (d, J = 8.7, 4H, H_G), 5.08 (s, 8H, H_c), 4.47 (s, 8H, H_a), 4.32 (br. m, 4H, H_H), 4.25 (s, 4H, H_E), 3.78 (s, 4H, H_D), 2.07 (br. m, 4H, H_I). ^{13}C NMR (126 MHz, $CDCl_3$) δ: 159.3, 159.2, 155.4, 145.4, 137.5, 134.9, 130.1, 128.5, 128.0, 123.5, 121.3, 120.5, 115.2, 73.2, 70.7, 66.7, 64.4, 53.1, 24.9. LR-ESI-MS m/z = 1047.48 $[M+H]^+$ calc. 1047.47.

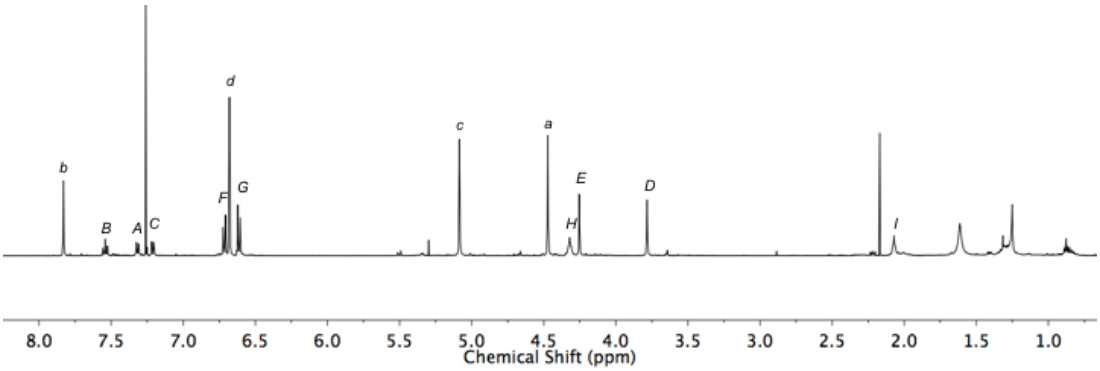

Figure 4.55 ^{1}H NMR (500 MHz, $CDCl_3$) of **251**.

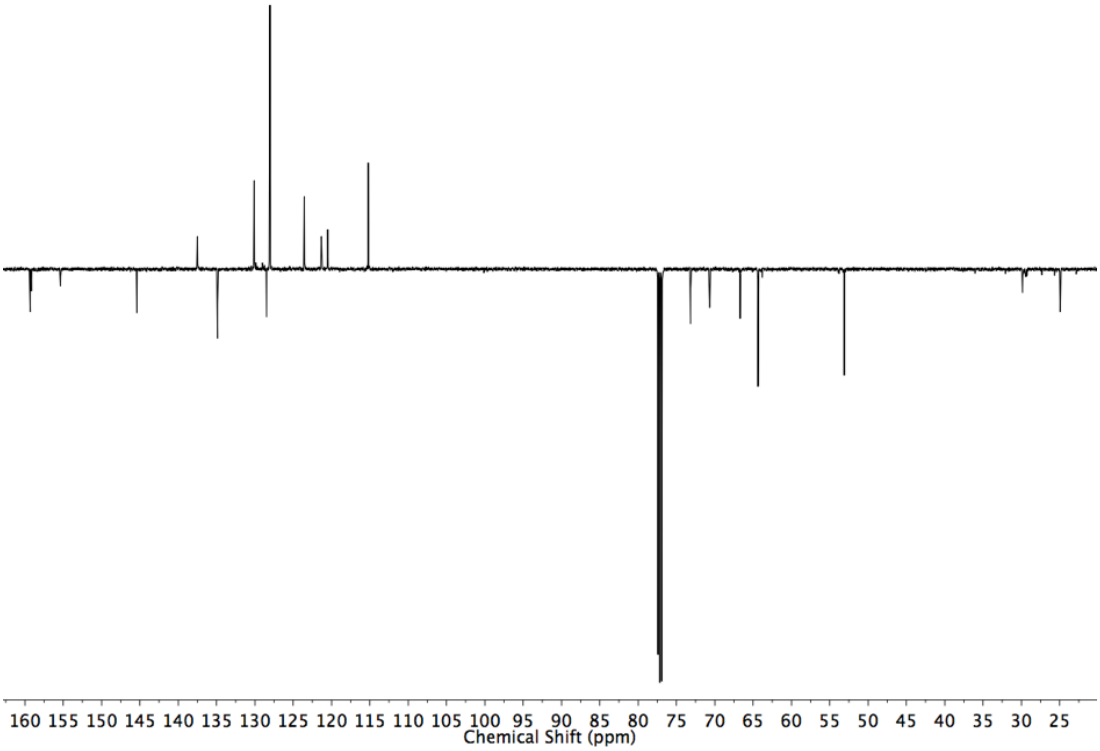

Figure 4.56 JMOD NMR (126 MHz, $CDCl_3$) of **251**.

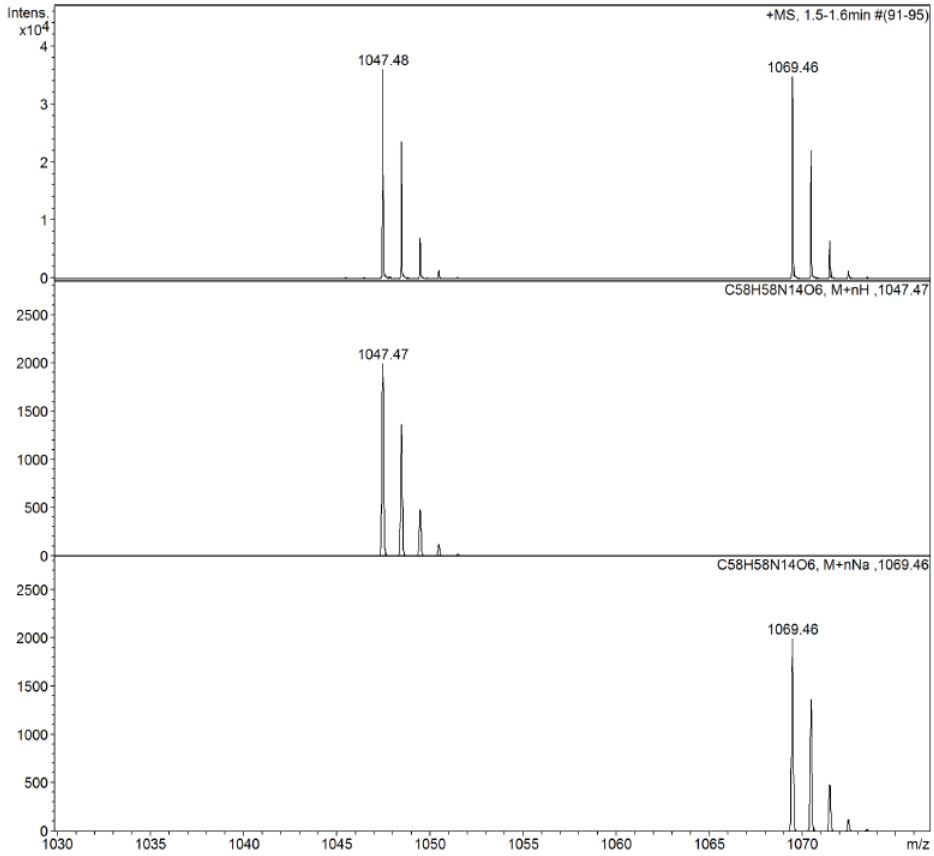

Figure 4.57 Observed (top) and calculated (bottom) isotopic patterns for **251**.

Catenane ***252***

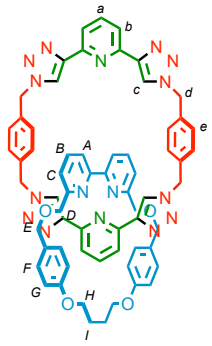

To a solution of **78** (12.1 mg, 0.025 mmol, 1 eq.), $[Cu(CH_3CN)_4]PF_6$ (8.9mg, 0.024 mmol, 0.96 eq.), $^{i}Pr_2NEt$ (52 µL, 0.30 mmol, 12 eq.) in 1:1 $CHCl_3$/EtOH (2.5 mL) at 60 °C was added 2,6-diethynylpyridine (19.1 mg, 0.150 mmol, 6 eq.) and α,α`-diazido-*p*-xylene (28.2 mg, 0.150 mmol, 6 eq.) in 1:1 $CHCl_3$/EtOH (3.0 mL) over 12 h. After removal of the solvent *in vacuo*, the residue was dissolved in 1:1 CH_2Cl_2/MeOH (5.0 mL) and KCN (16 mg, 0.25 mmol, 10 eq.) added as a solid. After stirring at rt for 30 minutes the solvent was removed under a flow of air. The residue was dissolved in CH_2Cl_2 (20 mL) and washed with H_2O (4 × 5 mL), dried ($MgSO_4$) and the solvent removed *in vacuo*. After purification by column chromatography on silica (Et_2O with a gradient of 0 to 25% MeCN over 10 CVs) **252** was obtained as a white foam (20.0 mg, 72%). ^{1}H NMR (500 MHz, $CDCl_3$) δ: 8.24 (br. s, 4H, H_c), 8.11 (d, *J* = 7.8, 4H, H_b), 7.88 (t, *J* = 7.8, 4H, H_a), 7.62 (app. t, *J* = 7.7, 2H, H_B), 7.50 (d, *J* = 7.9, 2H, H_A), 7.28 (d, *J* = 7.8, 2H, H_C), 6.69 (br. m, 12H, H_F, H_e), 6.45 (d, *J* = 8.5, 4H, H_G), 5.18 (br. s, 8H, H_d), 4.20 (br. m, 4H, H_H), 4.14 (s, 4H, H_E), 3.95 (s, 4H, H_D), 1.97 (br. m, 4H, H_I). ^{13}C NMR (126 MHz, $CDCl_3$) δ: 159.3 (×2), 156.3, 150.0, 149.0, 137.9, 137.3, 134.9, 130.2, 128.5, 127.6, 123.2, 121.2, 120.7, 119.2, 115.3, 73.1, 70.5, 66.9, 53.2, 24.9. LR-ESI-MS *m/z* = 1135.45 $[M+Na]^+$ calc. 1135.46; 1113.47 $[M+H]^+$ calc. 1113.47.

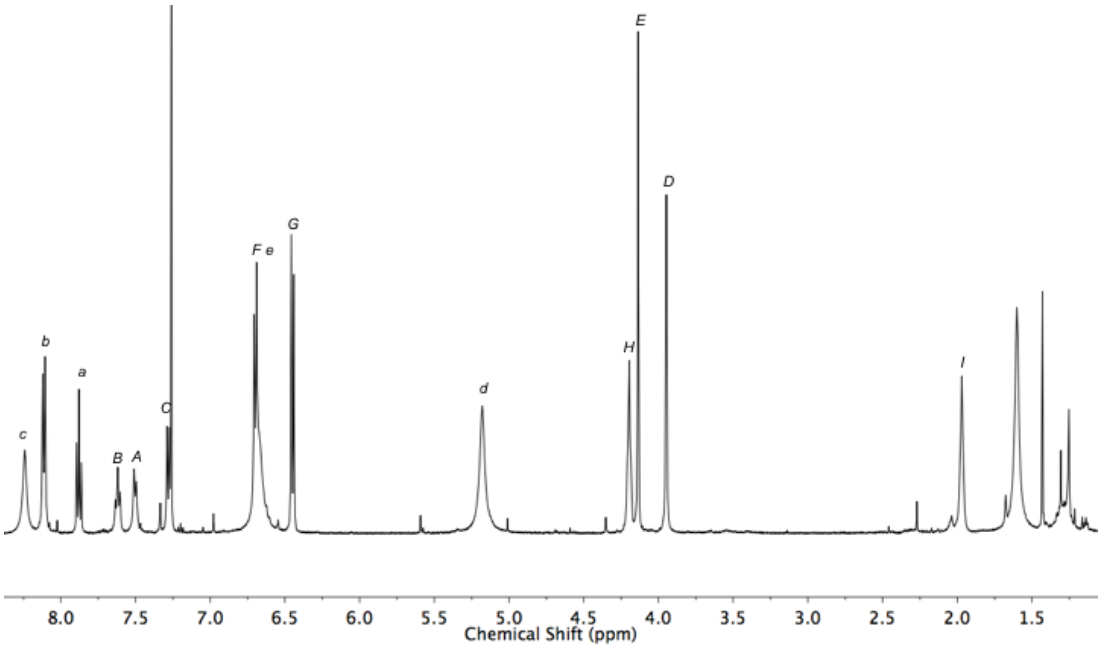

Figure 4.58 ^{1}H NMR (500 MHz, $CDCl_3$) of **252**.

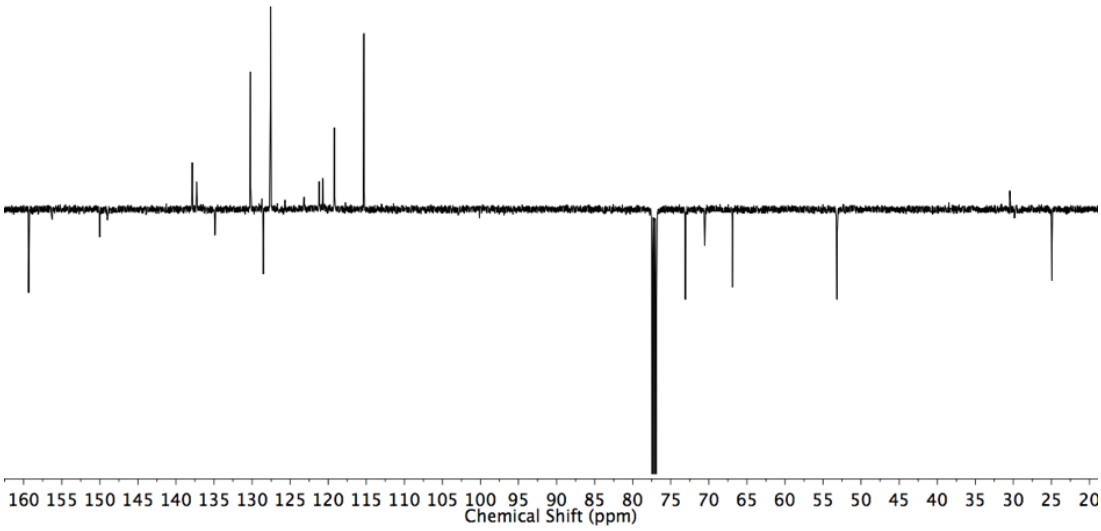

Figure 4.59 JMOD NMR (126 MHz, $CDCl_3$) of **252**.

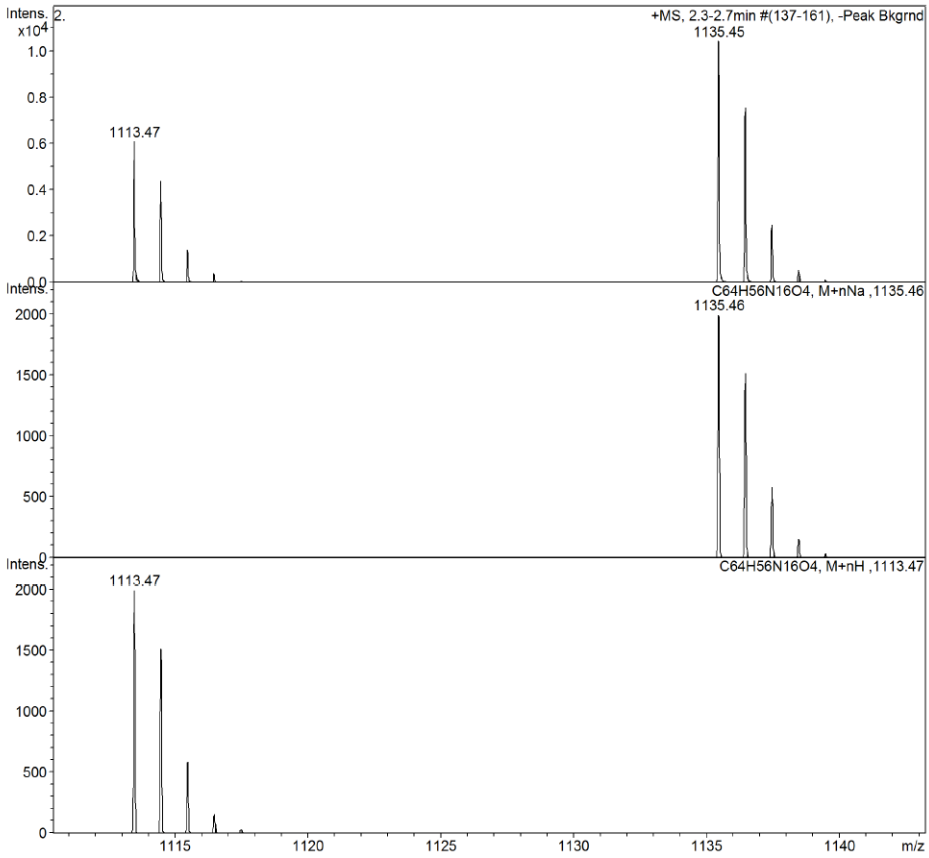

Figure 4.60 Observed (top) and calculated (bottom) isotopic patterns for **252**.

Catenane ***253***

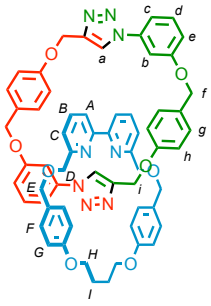

To a solution of **78** (12.1 mg, 0.025 mmol, 1 eq.), $[Cu(CH_3CN)_4]PF_6$ (8.9 mg, 0.024 mmol, 0.96 eq.), $^{i}Pr_2NEt$ (17 µL, 0.10 mmol, 4 eq.) in 1:1 $CHCl_3$/EtOH (2.5 mL) at 60 °C was added **237** (27.9 mg, 0.10 mmol, 4 eq.) in 1:1 $CHCl_3$/EtOH (2.0 mL) added over 8 h. After removal of the solvent *in vacuo*, the residue was dissolved in 1:1 CH_2Cl_2/MeOH (2.5 mL) and KCN (16 mg, 0.25 mmol, 10 eq.) added as a solid. After stirring at rt for 30 minutes the solvent was removed under a flow of air. The residue was dissolved in CH_2Cl_2 (5 mL) and washed with H_2O (4 × 5 mL), dried ($MgSO_4$) and the solvent removed *in vacuo*. After purification by column chromatography on silica (petrol with a gradient of 0 to 100% Et_2O over 10 CVs) **253** was obtained as a white foam (21.9 mg, 84%). ^{1}H NMR (500 MHz, $CDCl_3$) δ: 8.46 (s, 2H, H_a), 7.63 (app. t, J = 7.8, 2H, H_B), 7.50 (dd, J = 7.9, 1.0, 2H, H_A), 7.13 (dd, J = 7.8, 0.9, 2H, H_C), 7.08 (app. t, J = 8.2, 2H, H_d), 6.99-6.97 (m, 6H, H_b, H_h), 6.93 (ddd, J = 8.1, 2.1, 0.9, 2H, H_c), 6.83 (ddd, J = 8.3, 2.4, 0.9, 2H, H_e), 6.78 (d, J = 8.7, 4H, H_g), 6.25 (d, J = 8.7, 4H, H_F), 6.20 (d, J = 8.7, 4H, H_G), 5.17 (s, 4H, H_i), 4.80 (s, 4H, H_f), 4.25-4.20 (m, 2H, 2 of H_H), 4.03-3.99 (m, 2H, 2 of H_H), 3.97 (s, 4H, H_E), 3.68 (d, J = 12.7, 2H, 2 of H_D), 3.62 (d, J = 12.7, 2H, 2 of H_D), 2.10 (br. m, 2H, 2 of H_I), 1.93 (br. m, 2H, 2 of H_I). ^{13}C NMR (126 MHz, $CDCl_3$) δ: 159.2, 158.7, 158.6, 157.4, 155.9, 144.0, 137.5, 137.2, 129.7, 129.5, 129.4, 129.3, 128.3, 122.3, 120.9, 120.5, 115.0 (×2), 114.6, 112.4, 108.2, 72.6, 70.4, 68.8, 66.6, 61.4, 24.9. LR-ESI-MS m/z = 1041.42 $[M+H]^+$ calc. 1041.43.

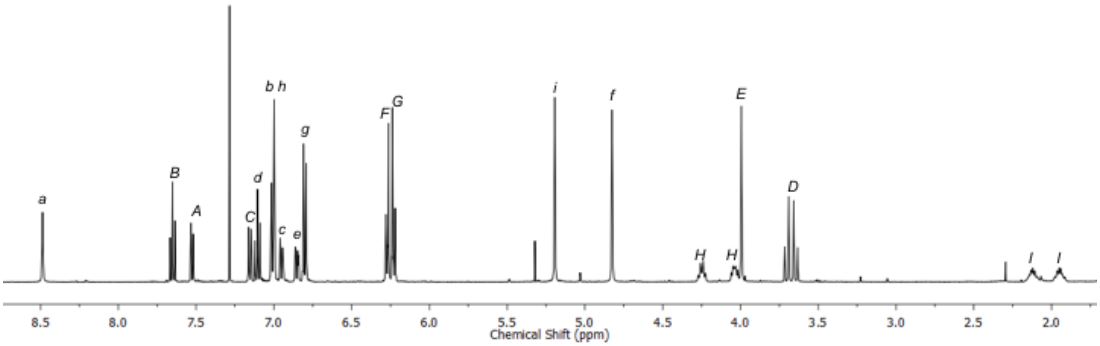

Figure 4.61 ^{1}H NMR (500 MHz, $CDCl_3$) of **253**.

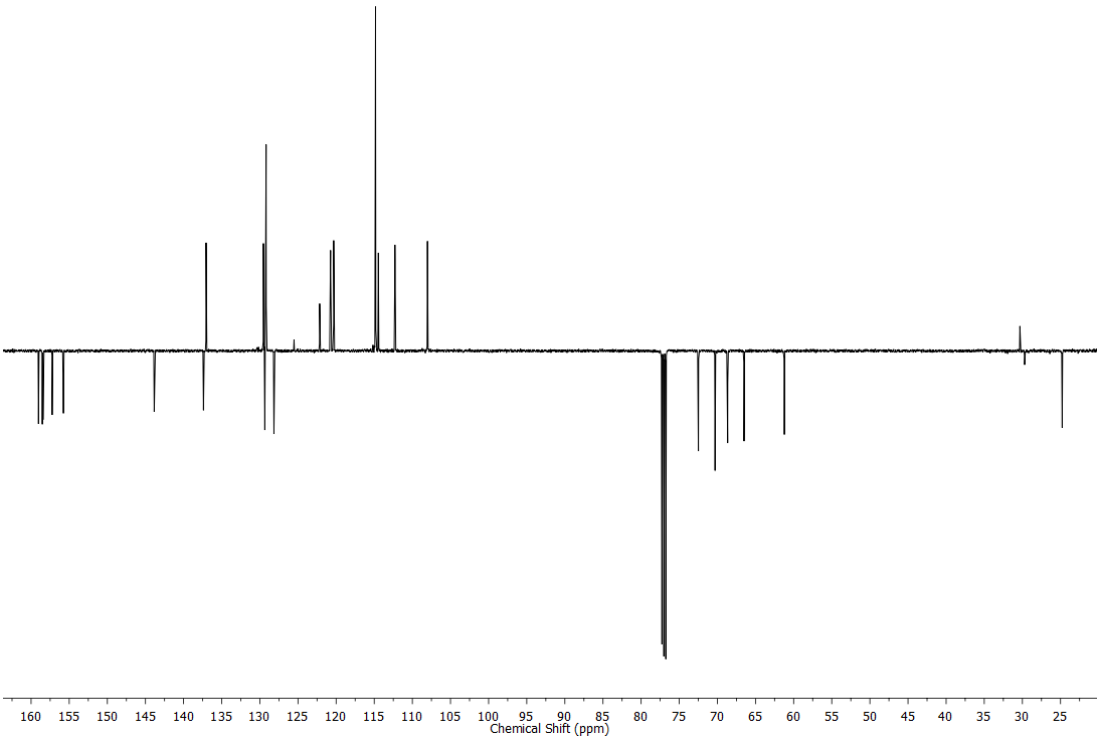

Figure 4.62 JMOD NMR (126 MHz, $CDCl_3$) of **253**.

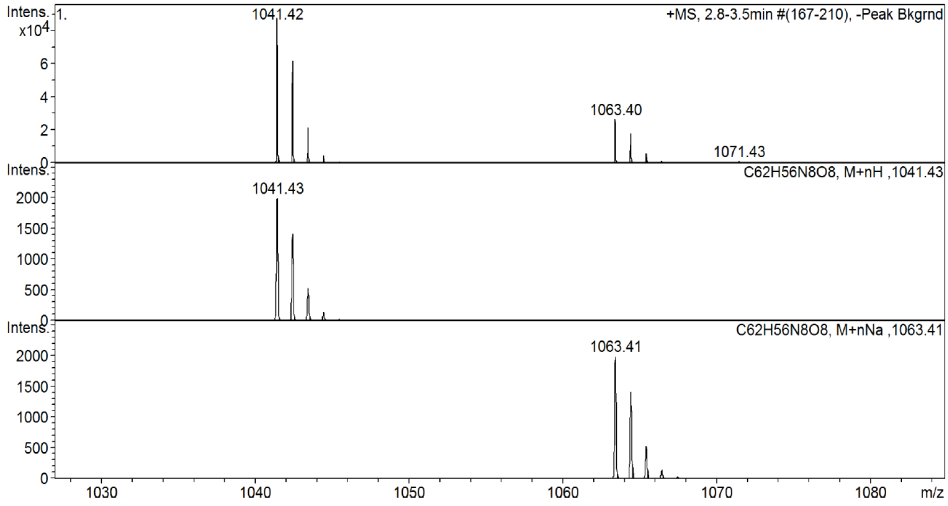

Figure 4.63 Observed (top) and calculated (middle and bottom) isotopic patterns for **253**.

*Catenane **254***

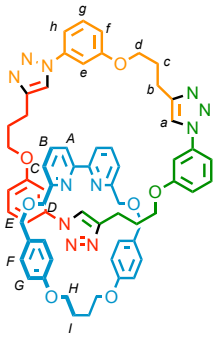

To a solution of **78** (12.1 mg, 0.025 mmol, 1 eq.), $[Cu(CH_3CN)_4]PF_6$ (8.9 mg, 0.024 mmol, 0.96 eq.), $^{i}Pr_2NEt$ (27 µL, 0.15 mmol, 6 eq.) in 1:1 $CHCl_3$/EtOH (2.5 mL) at 60 °C was added **238** (30.2 mg, 0.15 mmol, 6 eq.) in 1:1 $CHCl_3$/EtOH (2.0 mL) added over 8 h. After removal of the solvent *in vacuo*, the residue was dissolved in 1:1 CH_2Cl_2/MeOH (2.5 mL) and KCN (16 mg, 0.25 mmol, 10 eq.) added as a solid. After stirring at rt for 30 minutes the solvent was removed under a flow of air. The residue was dissolved in CH_2Cl_2 (5 mL) and washed with H_2O (4 × 5 mL), dried ($MgSO_4$) and the solvent removed *in vacuo*. Purified by preparative TLC (1:9 acetone/CH_2Cl_2) to give a combined mass of 15.0 mg in a 4 : 1 ratio of catenane **254** to dimeric triazole macrocycle which corresponds to 13.7 mg of **254** (50% yield). A small amount of analytically pure **254** was obtained by crystallisation by vapour diffusion of Et_2O into a CH_2Cl_2 solution of this mixture to allow full characterisation of catenane **254**. ^{1}H NMR (500 MHz, $CDCl_3$) δ: 8.11 (br. s, 3H, H_a), 7.39 (app. t, J = 7.8, 2H, H_B), 7.26-7.26 (m, 3H, H_g), 7.22-7.17 (m, 5H, H_A, H_h), 7.10 (d, J = 7.5, 2H, H_C), 7.06 (app. t, J = 2.0, 3H, H_e), 6.76-6.72 (m, 7H, H_F, H_f), 6.61 (d, J = 8.6, 4H, H_G), 4.39 (d, J = 12.1, 2H, 2 of H_E), 4.34 (t, J = 6.4, 4H, H_H), 4.07 (d, J = 12.1, 2H, 2 of H_E), 3.78 (d, J = 12.3, 2H, 2 of H_D), 3.72 (d, J = 12.4, 2H, 2 of H_D), 3.45 (t, J = 6.2, 3H, H_d), 2.66 (t, J = 6.5, 3H, H_b), 2.18-2.09 (m, 4H, H_I), 1.80 (app. quint, J = 6.3, 3H, H_c). ^{13}C NMR (126 MHz, $CDCl_3$) δ: 159.6, 159.1, 158.8, 155.3, 146.7, 137.9, 137.2, 130.0, 129.7, 128.2, 121.1, 120.3, 120.1, 115.8, 115.1, 111.8, 104.9, 73.0, 70.2, 66.4, 65.7, 27.5, 24.9, 21.1. LR-ESI-MS m/z = 1086.50 $[M+H]^+$ calc. 1086.50.

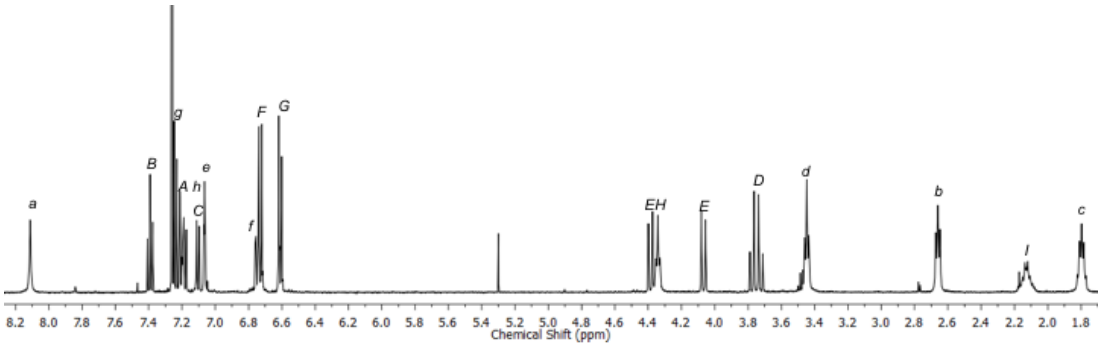

Figure 4.64 ^{1}H NMR (500 MHz, $CDCl_3$) of **254**.

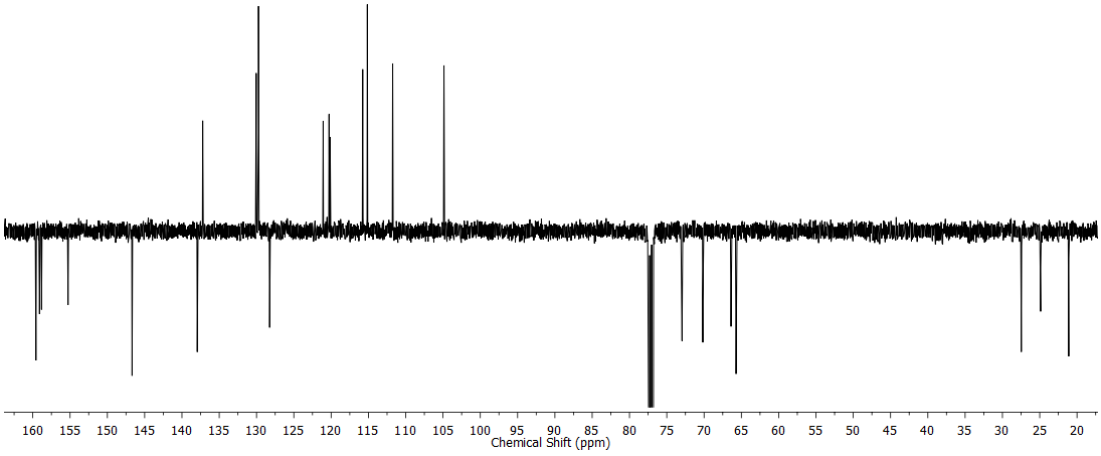

Figure 4.65 JMOD NMR (126 MHz, $CDCl_3$) of **254**.

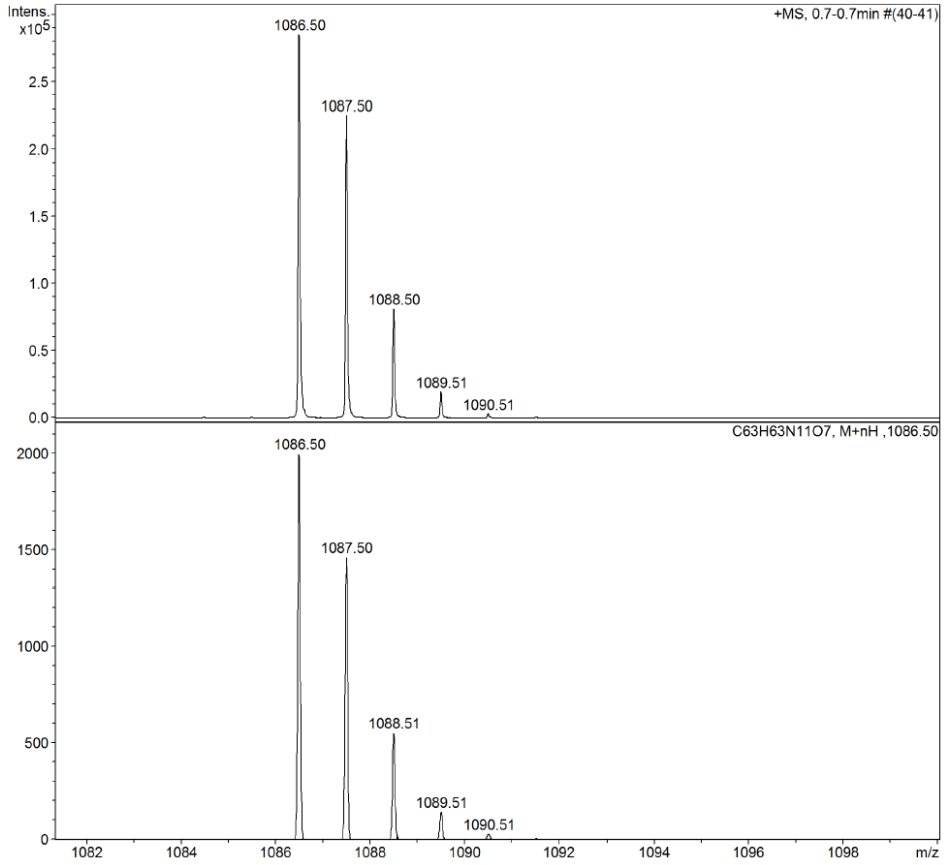

Figure 4.66 Observed (top) and calculated (bottom) isotopic patterns for **254**.

Catenane ***255***

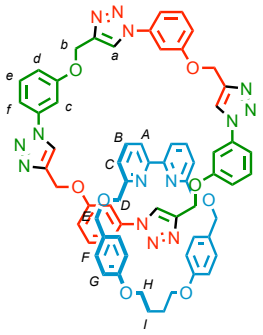

To a solution of **78** (12.1 mg, 0.025 mmol, 1 eq.), $[Cu(CH_3CN)_4]PF_6$ (8.9 mg, 0.024 mmol, 0.96 eq.), $^{i}Pr_2NEt$ (37 µL, 0.20 mmol, 8 eq.) in 1:1 $CHCl_3$/EtOH (2.5 mL) at 60 °C was added **239** (34.6 mg, 0.20 mmol, 8 eq.) in 1:1 $CHCl_3$/EtOH (2.5 mL) added over 8 h. After removal of the solvent *in vacuo*, the residue was dissolved in 1:1 CH_2Cl_2/MeOH (2.5 mL) and KCN (16 mg, 0.25 mmol, 10 eq.) added as a solid. After stirring at rt for 30 minutes the solvent was removed under a flow of air. The residue was dissolved in CH_2Cl_2 (5 mL) and washed with H_2O (4 × 5 mL), dried ($MgSO_4$) and the solvent removed *in vacuo*. After purification by column chromatography on silica (Et_2O with a gradient of 0 to 20% MeCN over 10 CVs) **255** was obtained as a white foam (9.5 mg, 32%). ^{1}H NMR (500 MHz, $CDCl_3$) δ: 8.29 (s, 4H, H_a), 7.53-7.47 (m, 4H, H_B, H_A or H_C), 7.39-7.32 (m, 10H, H_e, H_f, H_A or H_C), 7.22 (app. t, J = 2.1, 4H, H_c), 6.90 (ddd, J = 7.7, 2.4, 1.4, 4H, H_d), 6.74 (d, J = 8.6, 4H, H_F), 6.57 (d, J = 8.6, 4H, H_G), 4.98 (s, 8H, H_b), 4.39 (app. d, J = 12.0, 4H, 2 of H_H, 2 of H_E), 4.31 (d, J = 12.1, 2H, 2 of H_E), 4.30-4.25 (m, 2H, 2 of H_H), 3.94 (s, 4H, H_D), 2.14 (br. m, 4H, H_I).m ^{13}C NMR (126 MHz, $CDCl_3$) δ: 159.2, 159.0, 158.9, 155.6, 144.1, 137.7, 137.5, 130.7, 129.8, 128.6, 121.7, 121.3, 120.5, 115.0, 114.7, 112.9, 107.5, 73.0, 70.4, 66.4, 62.0, 24.9. LR-ESI-MS *m/z* = 1175.46 $[M+H]^+$ calc. 1175.46.

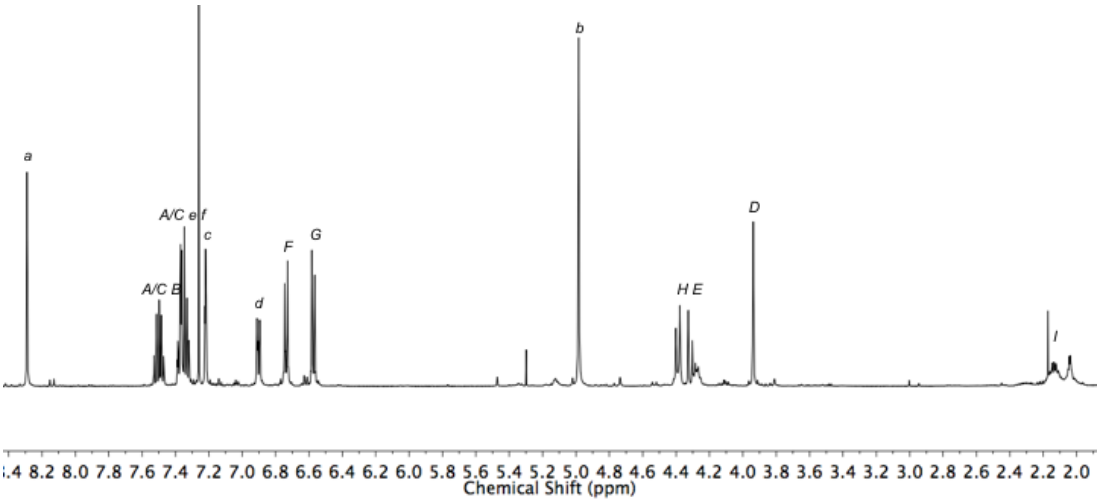

Figure 4.67 ^{1}H NMR (400 MHz, $CDCl_3$) of **255**.

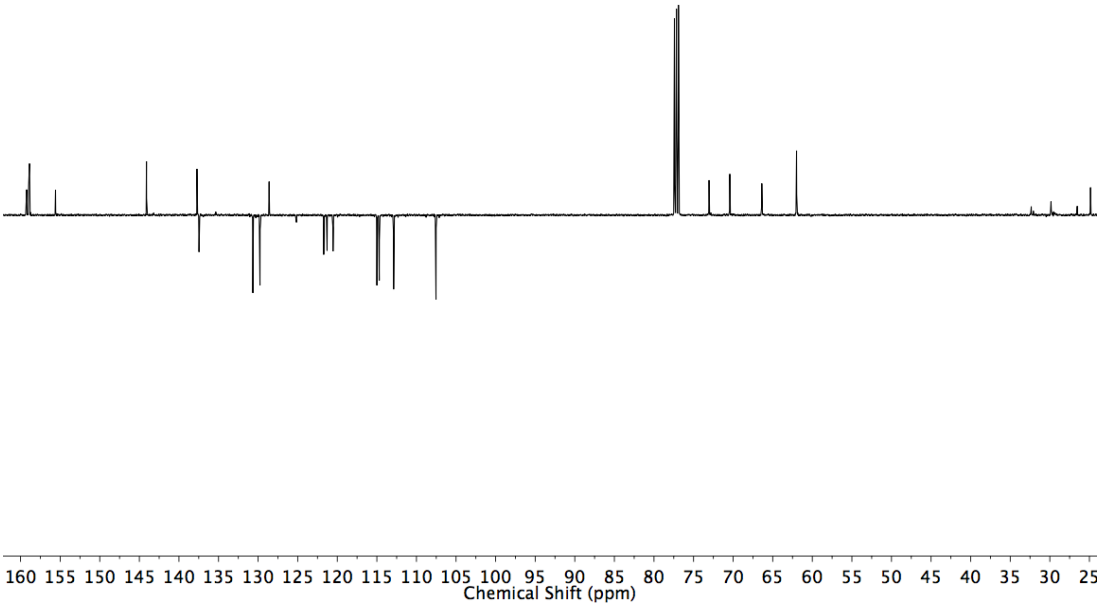

Figure 4.68 JMOD NMR (101 MHz, $CDCl_3$) of **255**.

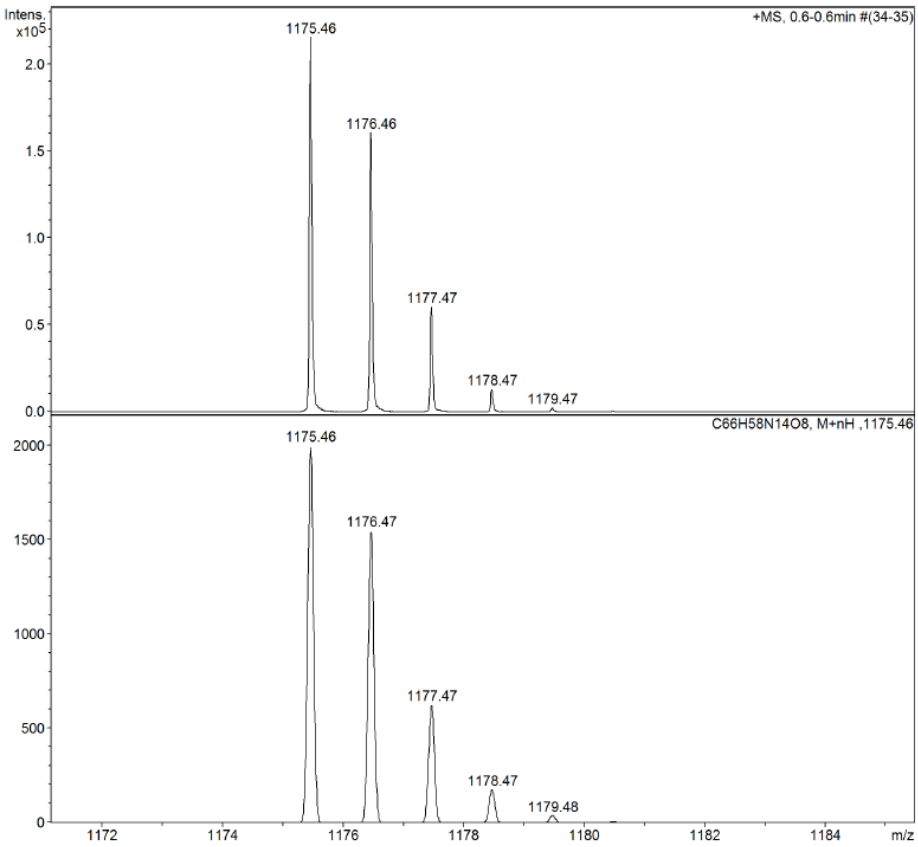

Figure 4.69 Observed (top) and calculated (bottom) isotopic patterns for **255**.

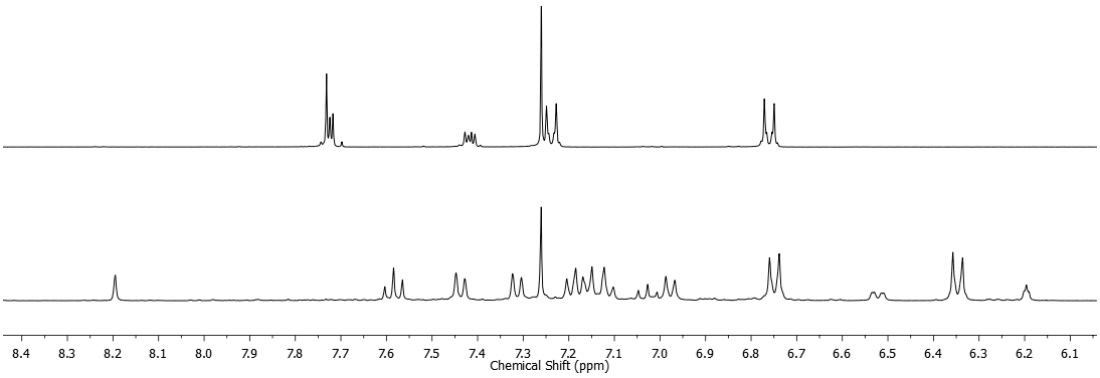

Figure 4.70 Stacked partial ^{1}H NMR (400 MHz, $CDCl_3$) spectra of **78** (top) and crude **242** reaction mixture.

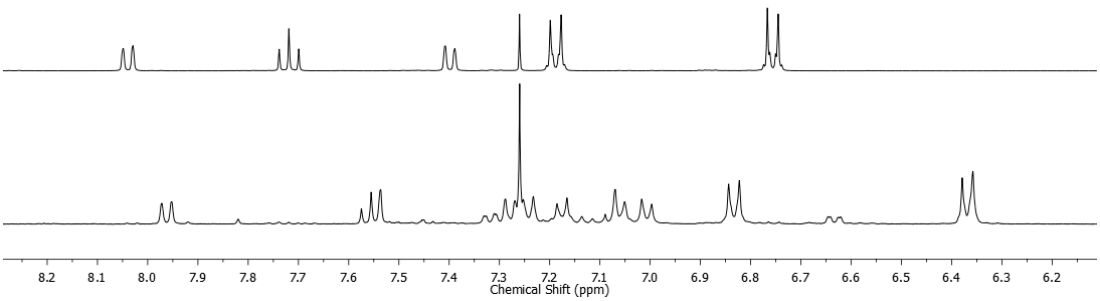

Figure 4.71 Stacked partial ^{1}H NMR (400 MHz, $CDCl_3$) spectra of **108** (top) and crude **243** reaction mixture.

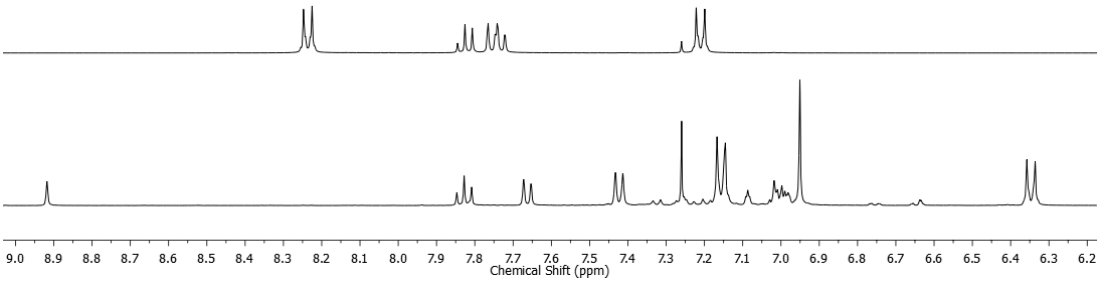

Figure 4.72 Stacked partial ^{1}H NMR (400 MHz, $CDCl_3$) spectra of **110** (top) and crude **244** reaction mixture

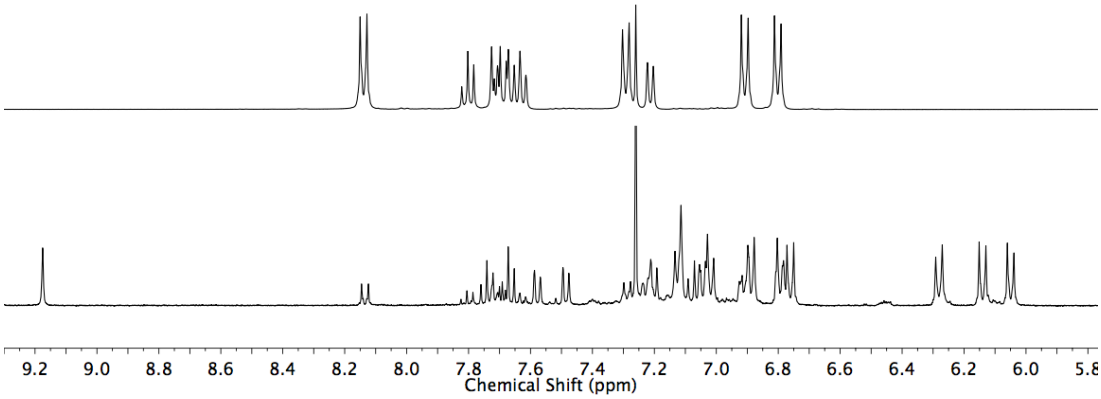

Figure 4.73 Stacked partial ^{1}H NMR (400 MHz, $CDCl_3$) spectra of **92** (top) and crude **245** reaction mixture

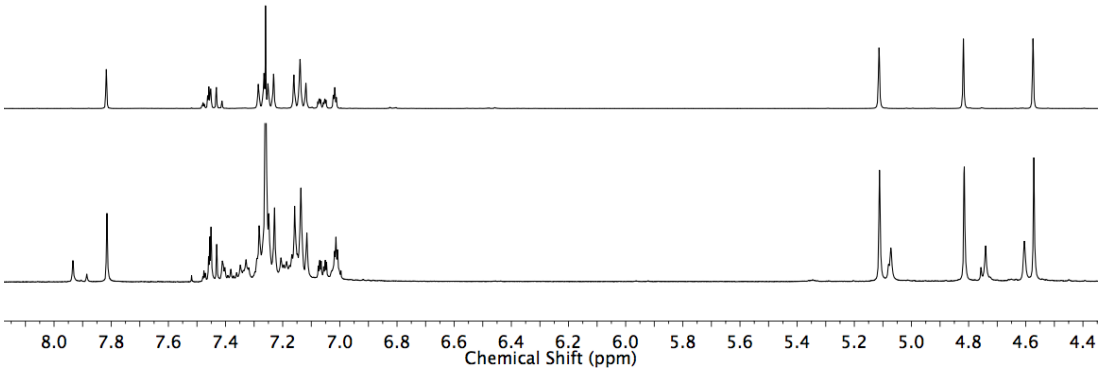

Figure 4.74 Stacked partial ^{1}H NMR (400 MHz, $CDCl_3$) spectra of **246** (top) and crude **246** reaction mixture

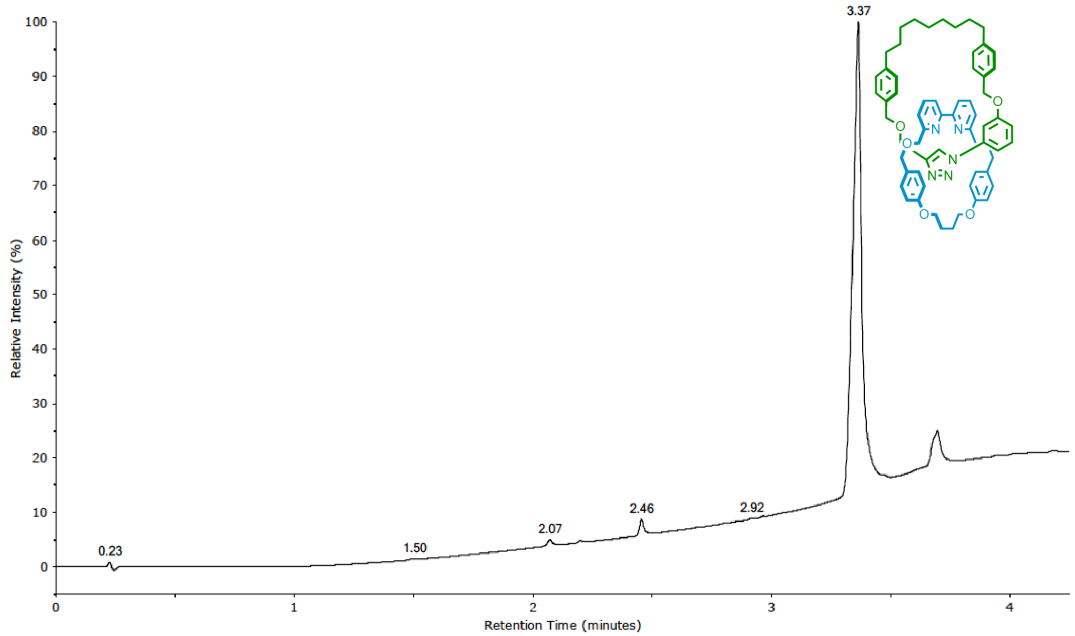

Figure 4.75 LC-MS of the crude reaction mixture for catenane **242**

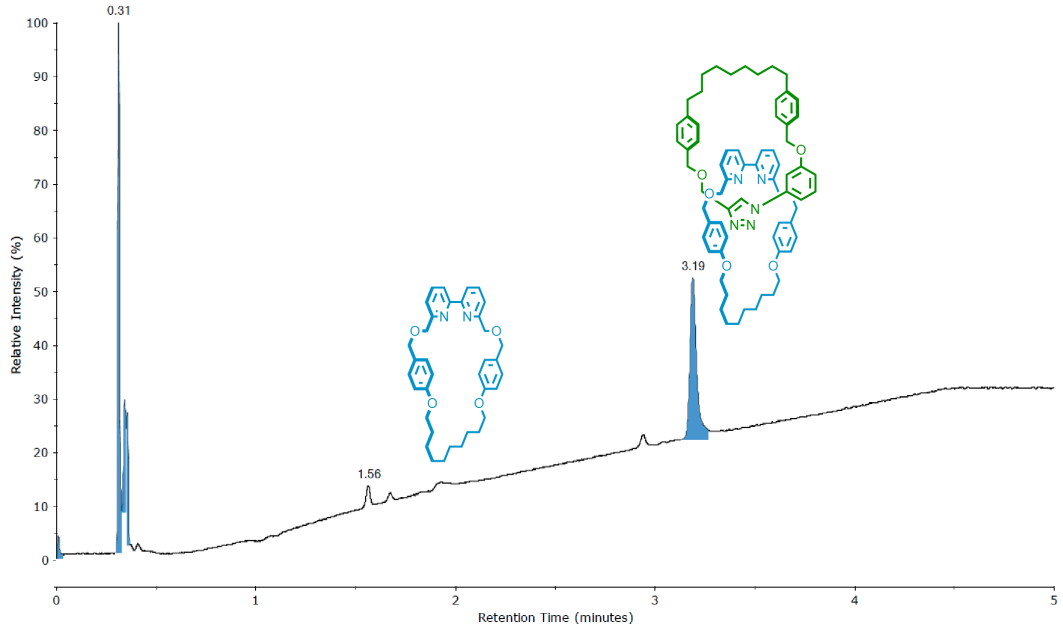

Figure 4.76 LC-MS of the crude reaction mixture for catenane **243**

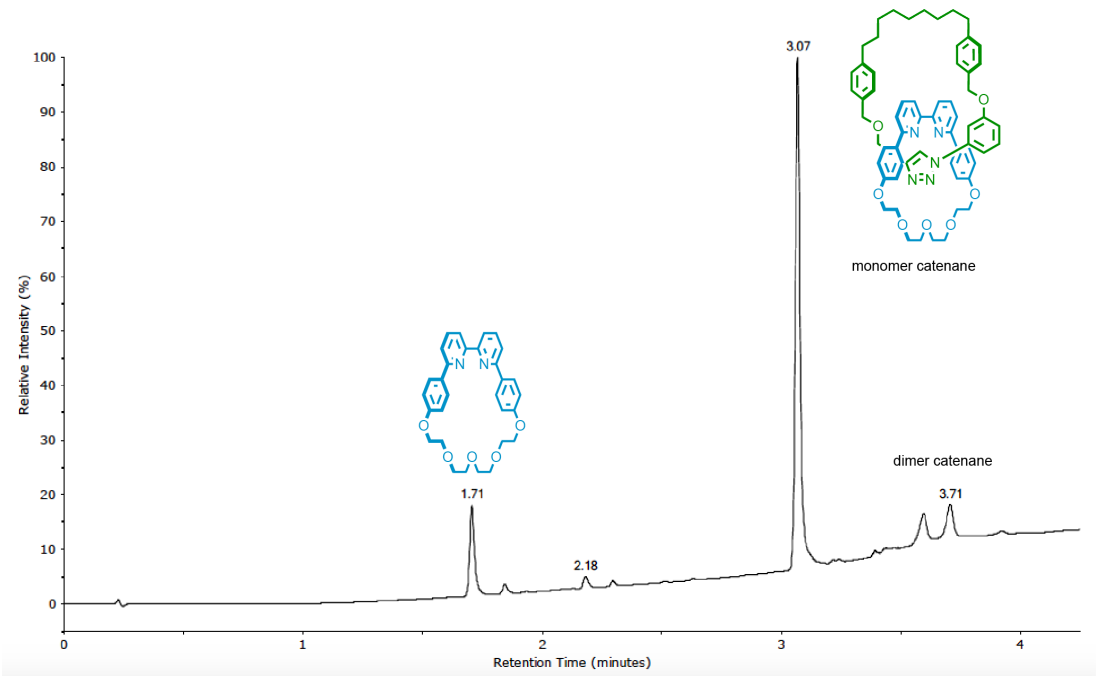

Figure 4.77 LC-MS of the crude reaction mixture for catenane **244**

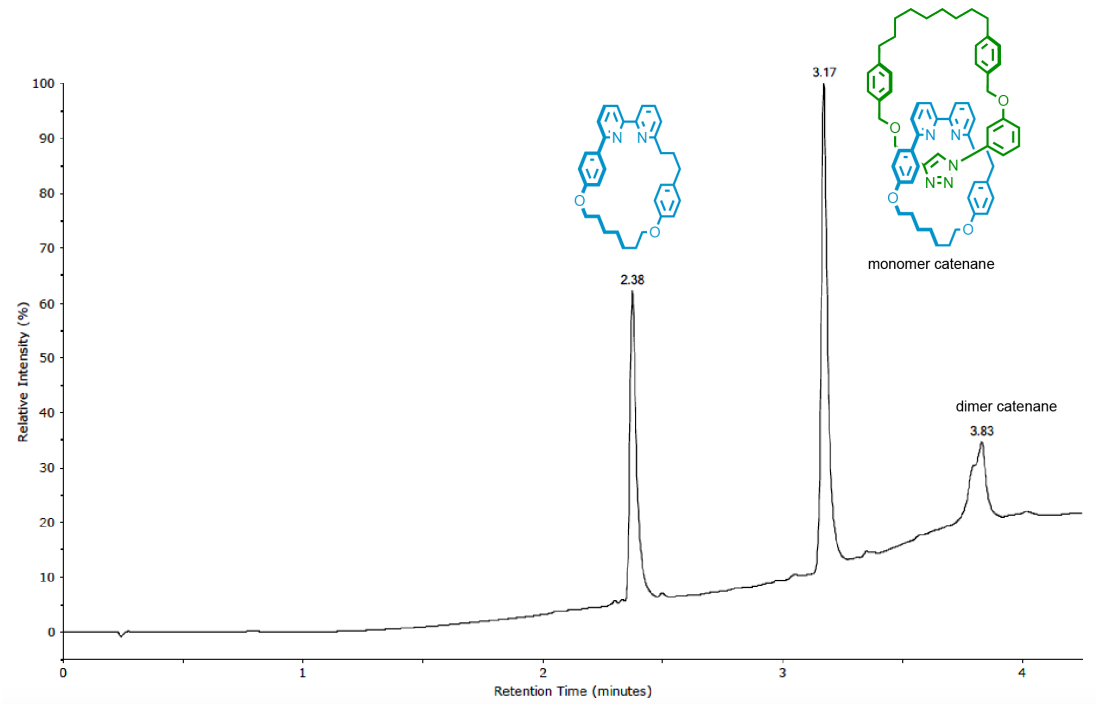

Figure 4.78 LC-MS of the crude reaction mixture for catenane **245**

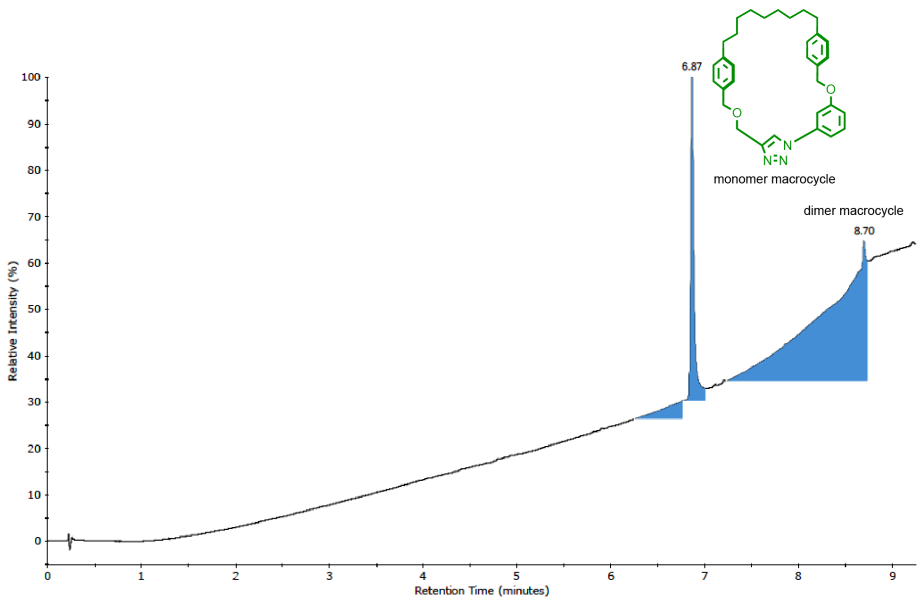

Figure 4.79 LC-MS of the crude reaction mixture for catenane **246**

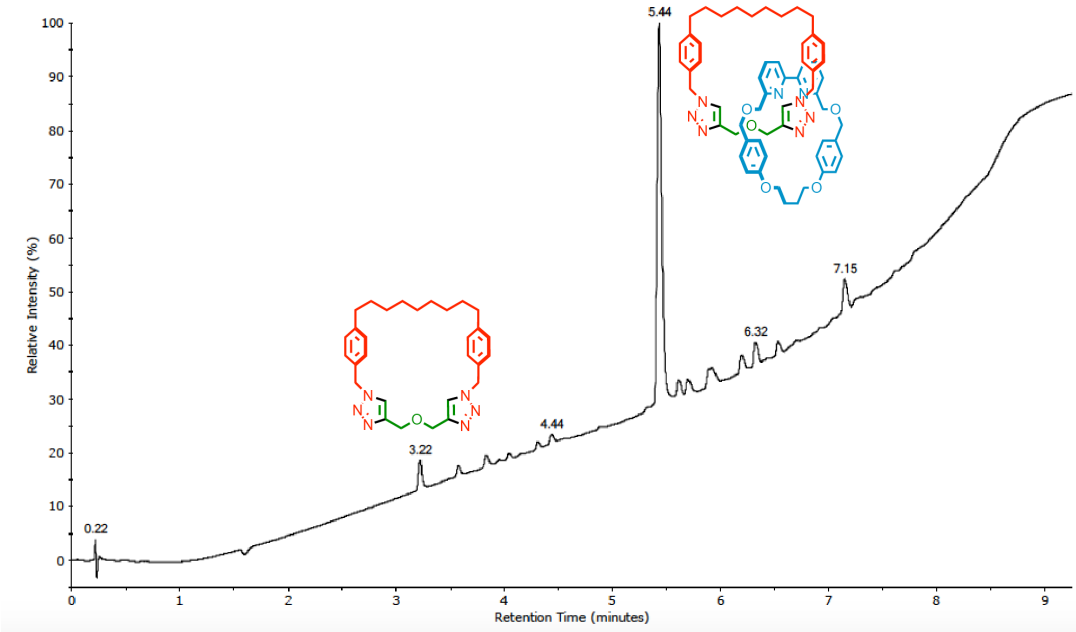

Figure 4.80. LC-MS of the crude reaction mixture for catenane **248**

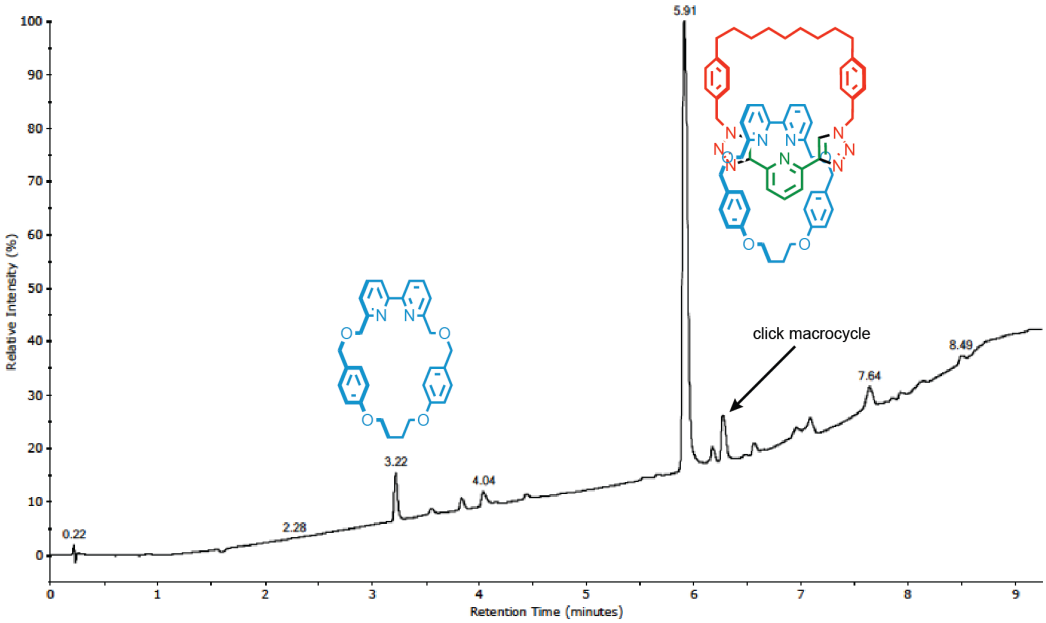

Figure 4.81. LC-MS of the crude reaction mixture for catenane **250**

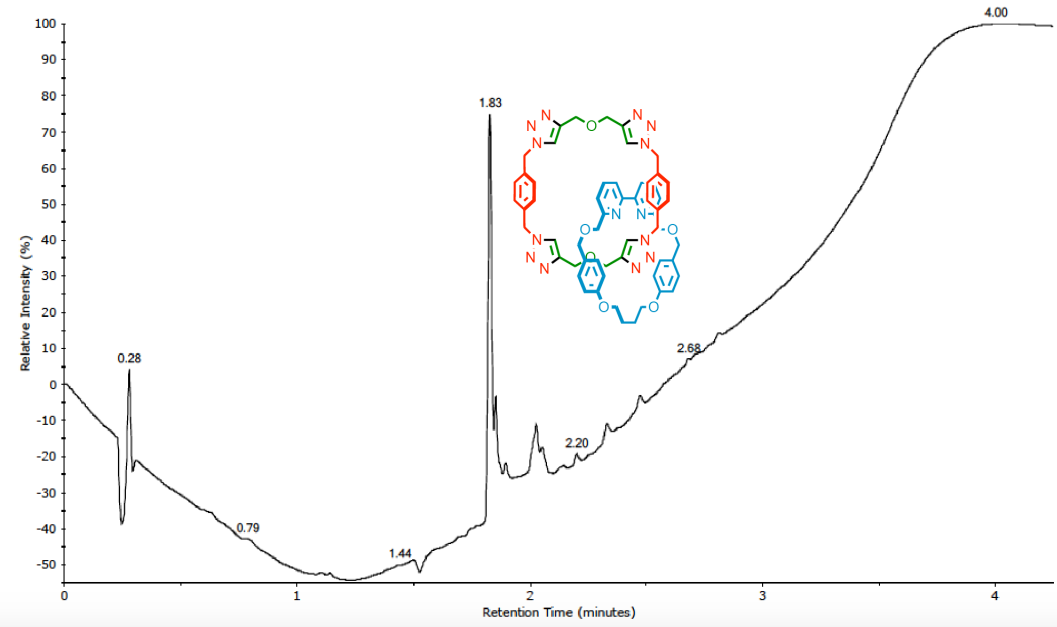

Figure 4.82. LC-MS of the crude reaction mixture for catenane **251**

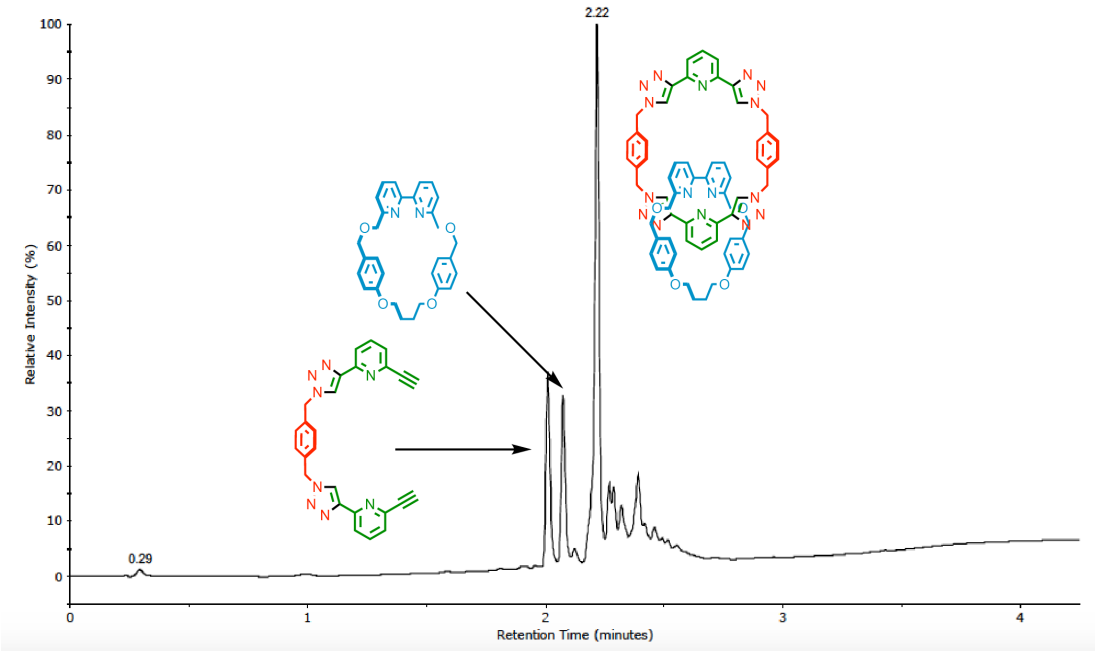

Figure 4.83. LC-MS of the crude reaction mixture for catenane **252**

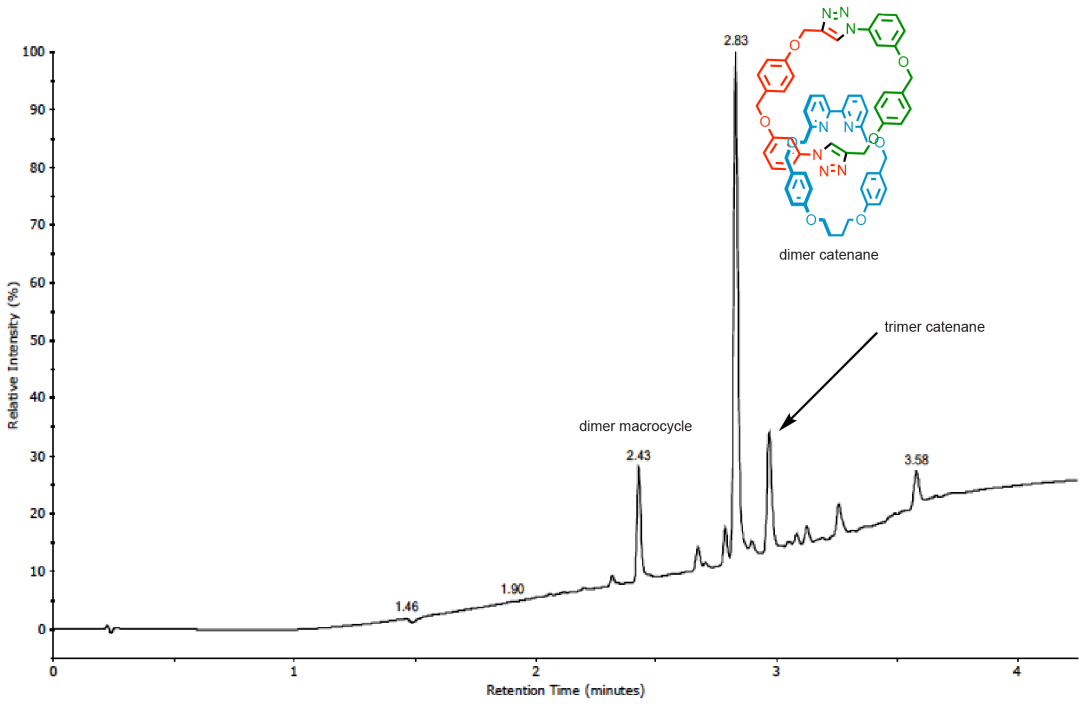

Figure 4.84. LC-MS of the crude reaction mixture for catenane **253**

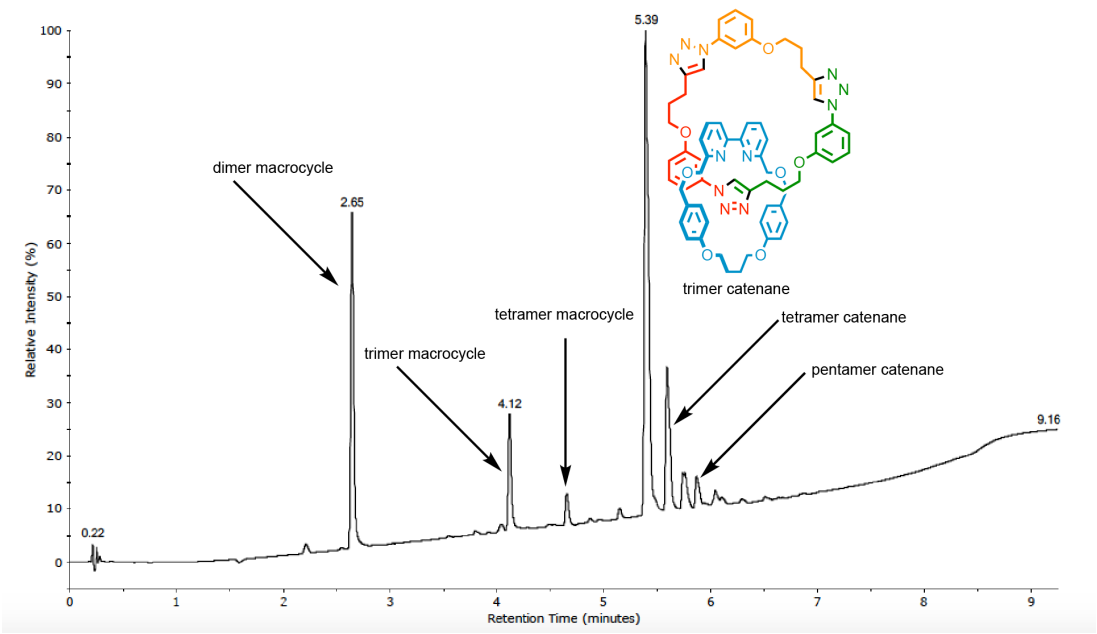

Figure 4.85. LC-MS of the crude reaction mixture for catenane **254**

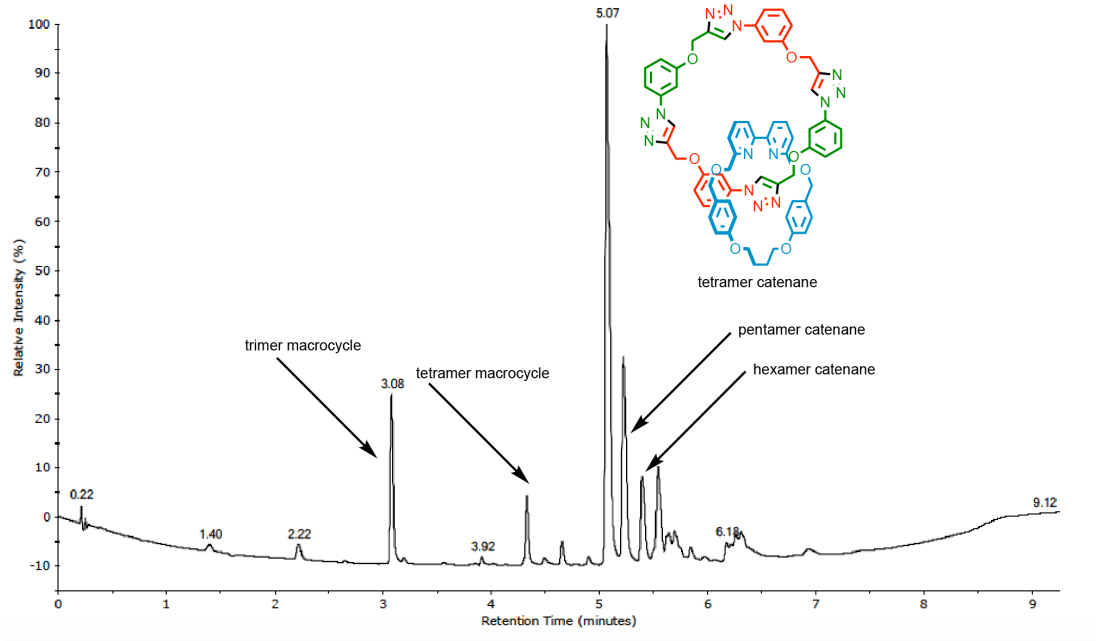

Figure 4.86. LC-MS of the crude reaction mixture for catenane **255**

For **245** and **250**, crystals were grown by vapour diffusion of pentane into a CH_2Cl_2 solution. Crystals of **243** and **252** and **253** were grown by vapour diffusion of Et_2O into a CH_2Cl_2 solution. Data for **243, 250** and **253**, were collected at 100 K using a FRE+ HF diffractometer equipped with a Saturn 724+ enhanced sensitivity detector, data for **245** were collected at 100 K using a Rigaku 007 HF diffractometer equipped with a Saturn 944+ enhanced sensitivity detector and for **250** Data were collected at 100 K using a FRE+ VHF diffractometer equipped with a HYPix6000 enhanced sensitivity detector. Cell determination, data collection, data reduction, cell refinement and absorption correction were performed with CrysalisPro. The structure was solved using SUPERFLIP[30,31] and refined against F_2 using anisotropic thermal displacement parameters for all non-hydrogen atoms using WINGX[32] and software packages within. Hydrogen atoms were placed in calculated positions and refined using a riding model.

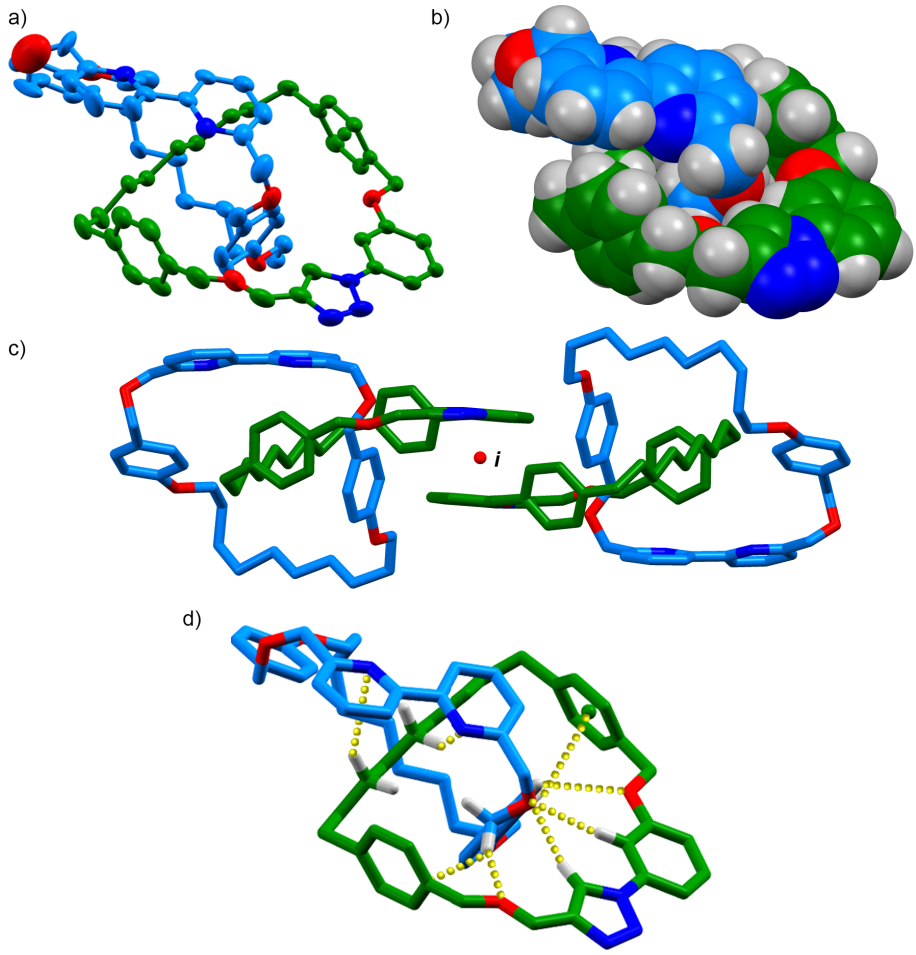

Figure 4.87 a) Ellipsoid plot of the assymetric unit of **243** (ellipsoids shown at 50% probability). Hydrogen atoms omitted for clarity. b) Spacefilling model. c) Co-conformational enantiomers observed in the solid state related by a point of inversion. d) Tube representation showing selected intermolecular contacts (for labelling scheme see characterisation data; distances (Å): H_a–O = 2.55; H_f–N = 3.71; H_n–N = 3.31; H_u–O = 2.38; H_E–O = 2.77; H_E–C = 3.08; H_F–O = 2.94; H_G–● = 3.08).

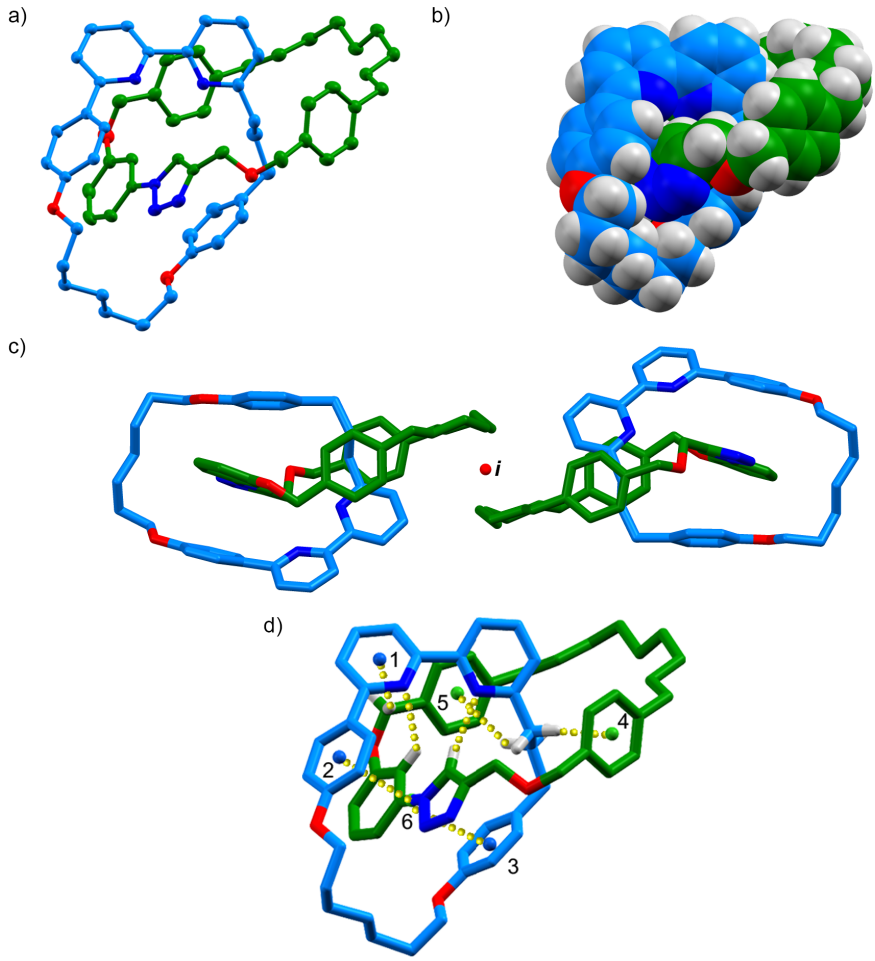

Figure 4.88 a) Ellipsoid plot of the assymetric unit of **245** (ellipsoids shown at 50% probability). Hydrogen atoms omitted for clarity. b) Spacefilling model. c) Co-conformational enantiomers observed in the solid state related by a point of inversion. d) Tube representation showing selected intermolecular contacts (for labelling scheme see characterisation data; distances (Å): H_a–N = 2.88; H_e–●$_1$ = 2.64; H_u–N = 2.43; H_P–●$_5$ = 3.16; H_Q–●$_4$ = 3.00; ●$_2$–●$_6$ = 3.42; ●$_3$–●$_6$ = 3.62).

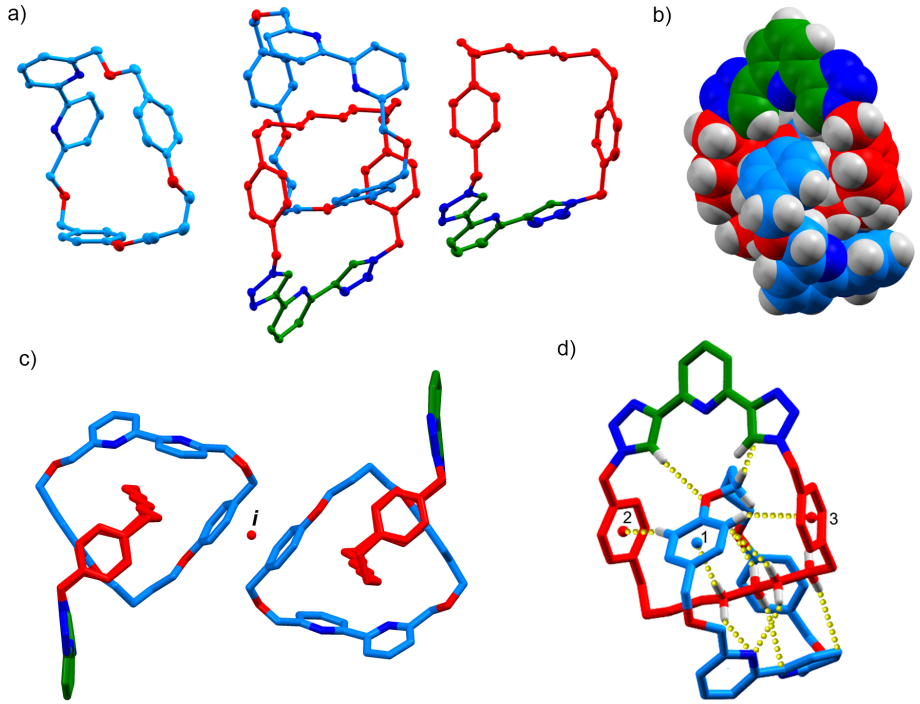

Figure 4.89 Ellipsoid plot of the assymetric unit of **250** (ellipsoids shown at 50% probability). Hydrogen atoms omitted for clarity. b) Spacefilling model. c) Co-conformational enantiomers observed in the solid state related by a point of inversion. d) Tube representation showing selected intermolecular contacts (for labelling scheme see characterisation data; distances (Å): H_c–O = 2.57; H_h–C_B = 2.89; H_f–N = 2.73; H_j–N = 3.09; H_k–N = 2.66; H_k–●$_1$ = 2.91; H_G–●$_2$ = 2.81; H_G–●$_3$ = 2.94; H_H–C_c = 2.94)

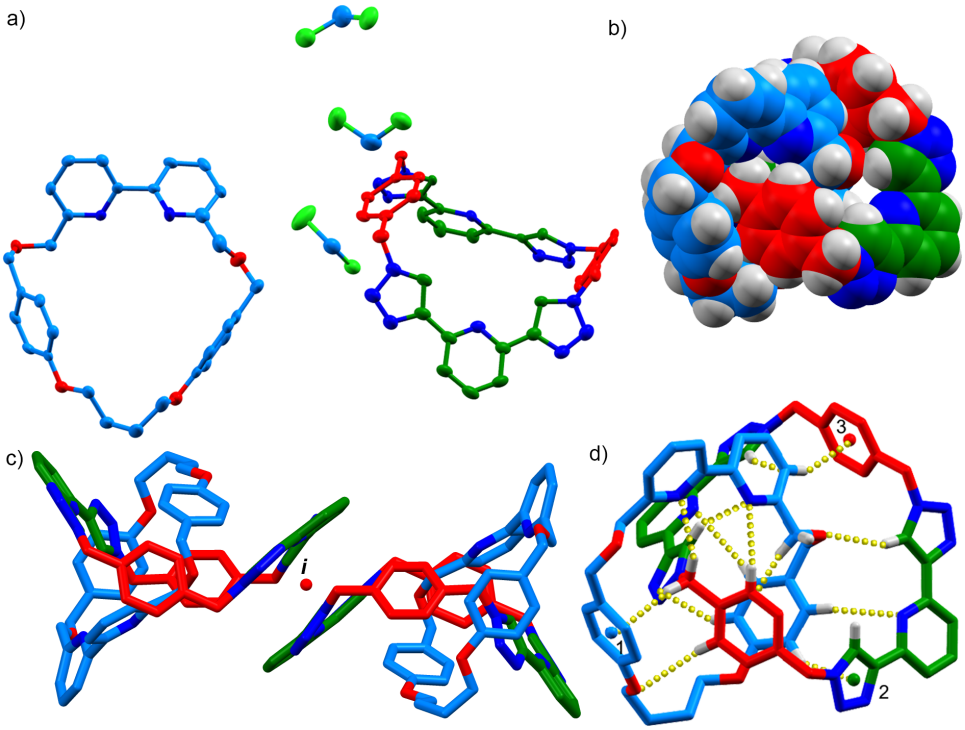

Figure 4.90 Ellipsoid plot of the assymetric unit of **252** (ellipsoids shown at 50% probability). Hydrogen atoms omitted for clarity. b) Spacefilling model. c) Co-conformational enantiomers observed in the solid state related by a point of inversion. d) Tube representation showing selected intermolecular contacts (for labelling scheme see characterisation data; distances (Å): H_c–O = 2.43; H_c–C_C = 3.13; H_c–N = 2.84; H_d–N = 2.46; H_d–●$_1$ = 2.66; H_e–N = 2.83; H_e–O = 2.79; H_B–●$_3$ = 2.75; H_D–C_e = 2.81; H_F–N = 2.73; H_F–N = 2.84; H_G–N = 2.78; H_G–●$_2$ = 2.69).

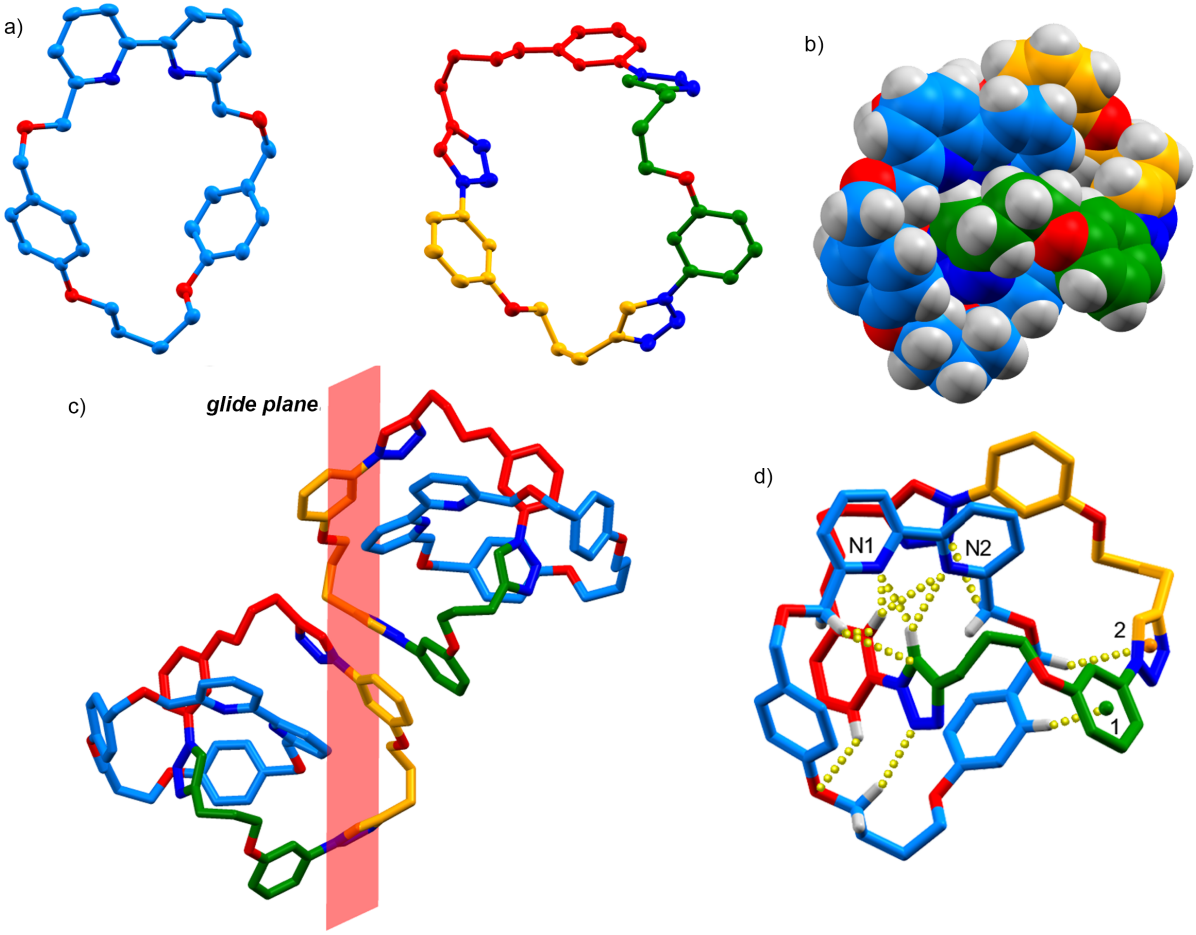

Figure 4.91 a) Ellipsoid plot of the assymetric unit of **253** (ellipsoids shown at 50% probability). b) Spacefilling model. c) Co-conformational enantiomers observed in the solid state related by a glide plane. d) Tube representation showing selected intermolecular contacts (for labelling scheme see characterisation data; distances (Å): H_a–N_1 = 2.34, H_a–N_2 = 2.76; H_a–N_1 = 2.75, H_a–N_2 = 2.77; H_h–O = 2.86; H_D–C_a = 2.94; H_D–C_e = 2.96; H_D–N = 2.99; H_E–●$_2$ = 2.83; H_F–●$_1$ = 2.81; H_H–N = 2.44).

Compound	**243**	
Empirical formula	$C_{68}H_{79}N_5O_6$	
Formula weight	1062.36	
Temperature	100(2) K	
Wavelength	0.71073 Å	
Crystal system	Orthorhombic	
Space group	P c c n	
Unit cell dimensions	a = 43.3239(11) Å	α= 90°.
	b = 25.6455(9) Å	β= 90°.
	c = 10.7279(3) Å	γ = 90°.
Volume	11919.4(6) $Å^3$	
Z	8	
Density (calculated)	1.184 Mg/m^3	
Absorption coefficient	0.075 mm^{-1}	
F(000)	4560	
Crystal size	0.100 × 0.040 × 0.030 mm^3	
Theta range for data collection	2.849 to 23.254°.	
Index ranges	-48<=h<=42, -28<=k<=28, -11<=l<=11	
Reflections collected	80761	
Independent reflections	8535 [R(int) = 0.0545]	
Completeness to theta = 23.254°	99.8 %	
Absorption correction	Semi-empirical from equivalents	
Max. and min. transmission	1.0000 and 0.604000	
Refinement method	Full-matrix least-squares on F^2	
Data / restraints / parameters	8535 / 12 / 748	
Goodness-of-fit on F^2	1.124	
Final R indices [I>2sigma(I)]	R_1 = 0.0890, wR_2 = 0.1752	
R indices (all data)	R_1 = 0.1096, wR_2 = 0.1858	
Extinction coefficient	n/a	
Largest diff. peak and hole	0.896 and -0.553 $e.Å^{-3}$	

Compound	**245**	
Empirical formula	$C_{64}H_{71}N_5O_4$	
Formula weight	974.25	
Temperature	100(2) K	
Wavelength	1.54184 Å	
Crystal system	Triclinic	
Space group	P -1	
Unit cell dimensions	a = 9.0601(2) Å	α= 100.369(2)°.
	b = 10.8306(2) Å	β= 93.561(2)°.
	c = 27.6685(5) Å	γ = 99.092(2)°.
Volume	2625.63(9) $Å^3$	
Z	2	
Density (calculated)	1.232 Mg/m^3	
Absorption coefficient	0.600 mm^{-1}	
F(000)	1044	
Crystal size	0.050 × 0.040 × 0.020 mm^3	
Theta range for data collection	3.262 to 70.262°.	
Index ranges	-11<=h<=11, -13<=k<=13, -33<=l<=32	
Reflections collected	40947	
Independent reflections	9823 [R(int) = 0.0302]	
Completeness to theta = 67.684°	99.3 %	
Absorption correction	Semi-empirical from equivalents	
Max. and min. transmission	1.0000 and 0.73530	
Refinement method	Full-matrix least-squares on F^2	
Data / restraints / parameters	9823 / 0 / 658	
Goodness-of-fit on F^2	1.032	
Final R indices [I>2sigma(I)]	R_1 = 0.0382, wR_2 = 0.0927	
R indices (all data)	R_1 = 0.0460, wR_2 = 0.0978	
Extinction coefficient	n/a	
Largest diff. peak and hole	0.486 and -0.306 $e.Å^{-3}$	

Compound	**250**	
Empirical formula	$C_{62}H_{65}N_9O_4$	
Formula weight	1000.23	
Temperature	100(2) K	
Wavelength	0.71073 Å	
Crystal system	Triclinic	
Space group	P -1	
Unit cell dimensions	a = 11.09990(10) Å	α= 84.8470(10)°.
	b = 20.1467(2) Å	β= 81.6860(10)°.
	c = 24.9074(3) Å	γ = 74.1030(10)°.
Volume	5293.25(10) $Å^3$	
Z	4	
Density (calculated)	1.255 Mg/m^3	
Absorption coefficient	0.080 mm^{-1}	
F(000)	2128	
Crystal size	0.150 × 0.150 × 0.030 mm^3	
Theta range for data collection	2.424 to 31.379°.	
Index ranges	-16<=h<=14, -29<=k<=29, -36<=l<=36	
Reflections collected	144979	
Independent reflections	31480 [R(int) = 0.0456]	
Completeness to theta = 25.242°	99.9 %	
Absorption correction	Semi-empirical from equivalents	
Max. and min. transmission	1.0000 and 0.80293	
Refinement method	Full-matrix least-squares on F^2	
Data / restraints / parameters	31480 / 0 / 1351	
Goodness-of-fit on F^2	1.076	
Final R indices [I>2sigma(I)]	R_1 = 0.0689, wR_2 = 0.1278	
R indices (all data)	R_1 = 0.1001, wR_2 = 0.1410	
Extinction coefficient	n/a	
Largest diff. peak and hole	0.821 and -0.343 $e.Å^{-3}$	

Compound	**252**	
Empirical formula	$C_{67}H_{62}Cl_6N_{16}O_4$	
Formula weight	1368.02	
Temperature	100(2) K	
Wavelength	0.71073 Å	
Crystal system	Monoclinic	
Space group	P 21/c	
Unit cell dimensions	a = 16.0021(6) Å	α= 90°
	b = 20.8606(6) Å	β= 100.792(4)°
	c = 20.1134(7) Å	γ = 90°
Volume	6595.4(4) $Å^3$	
Z	4	
Density (calculated)	1.378 Mg/m^3	
Absorption coefficient	0.323 mm^{-1}	
F(000)	2840	
Crystal size	0.050 × 0.020 × 0.020 mm^3	
Theta range for data collection	2.957 to 26.372°.	
Index ranges	-19<=h<=20, -26<=k<=26, -23<=l<=25	
Reflections collected	62999	
Independent reflections	13449 [R(int) = 0.0678]	
Completeness to theta = 25.242°	99.8 %	
Absorption correction	Semi-empirical from equivalents	
Max. and min. transmission	1.00000 and 0.81046	
Refinement method	Full-matrix least-squares on F^2	
Data / restraints / parameters	13449 / 0 / 838	
Goodness-of-fit on F^2	1.068	
Final R indices [I>2sigma(I)]	R_1 = 0.1127, wR_2 = 0.2785	
R indices (all data)	R_1 = 0.1597, wR_2 = 0.3109	
Extinction coefficient	n/a	
Largest diff. peak and hole	1.517 and -0.879 e.$Å^{-3}$	

Compound	**253**	
Empirical formula	$C_{63}H_{63}N_{11}O_7$	
Formula weight	1086.24	
Temperature	100(2) K	
Wavelength	0.71073 Å	
Crystal system	Monoclinic	
Space group	P c	
Unit cell dimensions	a = 9.6022(2) Å	α= 90°.
	b = 17.0018(2) Å	β= 102.232(2)°.
	c = 17.6771(3) Å	γ = 90°.
Volume	2820.35(9) $Å^3$	
Z	2	
Density (calculated)	1.279 Mg/m^3	
Absorption coefficient	0.086 mm^{-1}	
F(000)	1148	
Crystal size	0.300 × 0.240 × 0.240 mm^3	
Theta range for data collection	2.847 to 32.167°.	
Index ranges	-13<=h<=14, -25<=k<=22, -20<=l<=26	
Reflections collected	37311	
Independent reflections	14940 [R(int) = 0.0304]	
Completeness to theta = 25.242°	99.8 %	
Absorption correction	Semi-empirical from equivalents	
Max. and min. transmission	1.00000 and 0.36265	
Refinement method	Full-matrix least-squares on F^2	
Data / restraints / parameters	14940 / 2 / 730	
Goodness-of-fit on F^2	1.017	
Final R indices [I>2sigma(I)]	R_1 = 0.0478, wR_2 = 0.0917	
R indices (all data)	R_1 = 0.0586, wR_2 = 0.0970	
Absolute structure parameter	-0.2(4)	
Extinction coefficient	n/a	
Largest diff. peak and hole	0.253 and -0.193 $e.Å^{-3}$	

4.5. Bibliography

[1] E. Wasserman, *J. Am. Chem. Soc.* **1960**, *82*, 4433–4434.

[2] G. Schill, A. Lüttringhaus, *Angew. Chem. Int. Ed. Engl.* **1964**, *3*, 546–547.

[3] C. O. Dietrich-Buchecker, J. P. Sauvage, J. P. Kintzinger, *Tetrahedron Lett.* **1983**, *24*, 5095–5098.

[4] P. R. Ashton, T. T. Goodnow, A. E. Kaifer, M. V. Reddington, A. M. Z. Slawin, N. Spencer, J. F. Stoddart, C. Vicent, D. J. Williams, *Angew. Chem. Int. Ed. Engl.* **1989**, *28*, 1396–1399.

[5] J. F. Stoddart, *Chem. Soc. Rev.* **2009**, *38*, 1802–1820.

[6] E. A. Neal, S. M. Goldup, *Chem. Commun.* **2014**, *50*, 5128–5142.

[7] J. E. M. Lewis, M. Galli, S. M. Goldup, *Chem. Commun.* **2016**, *53*, 298–312.

[8] J. E. M. Lewis, P. D. Beer, S. J. Loeb, S. M. Goldup, *Chem. Soc. Rev.* **2017**, *46*, 2577–2591.

[9] C. O. Dietrich-Buchecker, J. P. Sauvage, J. M. Kern, *J. Am. Chem. Soc.* **1984**, *106*, 3043–3045.

[10] V. Aucagne, K. D. Hänni, D. A. Leigh, P. J. Lusby, D. B. Walker, *J. Am. Chem. Soc.* **2006**, *128*, 2186–2187.

[11] V. Aucagne, J. Berná, J. D. Crowley, S. M. Goldup, K. D. Hänni, D. A. Leigh, P. J. Lusby, V. E. Ronaldson, A. M. Z. Slawin, A. Viterisi, et al., *J. Am. Chem. Soc.* **2007**, *129*, 11950–11963.

[12] Y. Sato, R. Yamasaki, S. Saito, *Angew. Chem. Int. Ed.* **2009**, *48*, 504–507.

[13] S. M. Goldup, D. A. Leigh, T. Long, P. R. McGonigal, M. D. Symes, J. Wu, *J. Am. Chem. Soc.* **2009**, *131*, 15924–15929.

[14] K. Ito, Y. Mutoh, S. Saito, *J. Org. Chem.* **2017**, *82*, 6118–6124.

[15] H. Lahlali, K. Jobe, M. Watkinson, S. M. Goldup, *Angew. Chem. Int. Ed.* **2011**, *50*, 4151–4155.

[16] J. E. M. Lewis, R. J. Bordoli, M. Denis, C. J. Fletcher, M. Galli, E. A. Neal, E. M. Rochette, S. M. Goldup, *Chem. Sci.* **2016**, *7*, 3154–3161.

[17] J. E. M. Lewis, J. Winn, L. Cera, S. M. Goldup, *J. Am. Chem. Soc.* **2016**, *138*, 16329–16336.

[18] C. O. Dietrich-Buchecker, A. Edel, J. P. Kintzinger, J. P. Sauvage, *Tetrahedron* **1987**, *43*, 333–344.

[19] M. Galli, J. E. M. Lewis, S. M. Goldup, *Angew. Chem. Int. Ed.* **2015**, *54*, 13545–13549.

[20] M. Denis, L. Qin, P. Turner, K. A. Jolliffe, S. M. Goldup, *Angew. Chem. Int. Ed.* **2018**, *57*, 5315–5319.

[21] M. Denis, J. Pancholi, K. Jobe, M. Watkinson, S. M. Goldup, *Angew. Chem. Int. Ed.* **2018**, *57*, 5310–5314.

[22] J. Winn, A. Pinczewska, S. M. Goldup, *J. Am. Chem. Soc.* **2013**, *135*, 13318–13321.

[23] B. Lewandowski, G. D. Bo, J. W. Ward, M. Papmeyer, S. Kuschel, M. J. Aldegunde, P. M. E. Gramlich, D. Heckmann, S. M. Goldup, D. M. D'Souza, et al., *Science* **2013**, *339*, 189–193.

[24] G. D. Bo, M. A. Y. Gall, S. Kuschel, J. D. Winter, P. Gerbaux, D. A. Leigh, *Nat. Nanotechnol.* **2018**, *13*, 381–385.

[25] S. Erbas-Cakmak, S. D. P. Fielden, U. Karaca, D. A. Leigh, C. T. McTernan, D. J. Tetlow, M. R. Wilson, *Science* **2017**, *358*, 340–343.

[26] G. De Bo, S. Kuschel, D. A. Leigh, B. Lewandowski, M. Papmeyer, J. W. Ward, *J. Am. Chem. Soc.* **2014**, *136*, 5811–5814.

[27] O. Demeter, E. A. Fodor, M. Kállay, G. Mező, K. Németh, P. T. Szabó, P. Kele, *Chem. – Eur. J.* **2016**, *22*, 6382–6388.

[28] J. Luo, C. Pardin, W. D. Lubell, X. X. Zhu, *Chem. Commun.* **2007**, *0*, 2136–2138.

[29] S. Kanamathareddy, C. D. Gutsche, *J. Org. Chem.* **1996**, *61*, 2511–2516.

[30] L. Palatinus, G. Chapuis, *J. Appl. Crystallogr.* **2007**, *40*, 786–790.

[31] L. Palatinus, S. J. Prathapa, S. van Smaalen, *J. Appl. Crystallogr.* **2012**, *45*, 575–580.

[32] L. J. Farrugia, *J. Appl. Crystallogr.* **2012**, *45*, 849–854.

Chapter 5: Stereoselective synthesis of a topologically chiral [2]catenane

Abstract: This chapter highlights a new approach for the synthesis of a topologically chiral catenane. Previous preparations of enantiopure topologically chiral catenane required the use of chiral stationary phase high performance liquid chromatography (CSP-HPLC) making this kind of chirality "inaccessible curiosities". The scalable approach reported in this chapter enabled access to enantiopure materials using standard synthetic techniques.

The initial synthesis and initial separation of **275** were carried out by Dr Jamie Lewis. Crystallography was performed by Dr Jamie Lewis. Dr Mathieu Denis designed and optimised of the synthesis of the chiral amine **262**. Dr Mike Jinks synthesised macrocycle **267**. I optimised the separation of **275**, optimised the cleavage of the chiral group.

Prior publication: None of this work has been previously published.

5.1. Introduction

Chirality in catenanes can come from covalent stereogenic units such as chiral centres, axially chiral units (binaphthyl-containing catenanes) or planar chiral units but chirality can also be induced by the mechanical bond.[1–3] The combination of two C_{1h}-symmetrical macrocycle resulted in a chiral structure, named as "topologically chiral catenane". To date, only two examples are reported on the synthesis of topologically chiral catenanes by Sauvage and co-workers and Vögtle and co-workers, respectively.[4–7] Both examples required the use of preparative CSP-HPLC to access enantiopure materials.

The methodology we proposed to use for the synthesis of topologically chiral [2]catenanes was inspired by the approach developed by Bordoli and Goldup for the synthesis of mechanically planar chiral [2]rotaxanes.[8] We proposed to separate a mixture of diastereoisomeric [2]catenanes which possess the same chiral centre but opposite topological configuration, which resulted from the active template coupling. Once the diastereoisomers were separated, the covalent stereogenic element was chemically removed without affecting the stereochemistry of the mechanical bond and enantiopure topologically chiral catenanes were obtained (Figure 5.1).

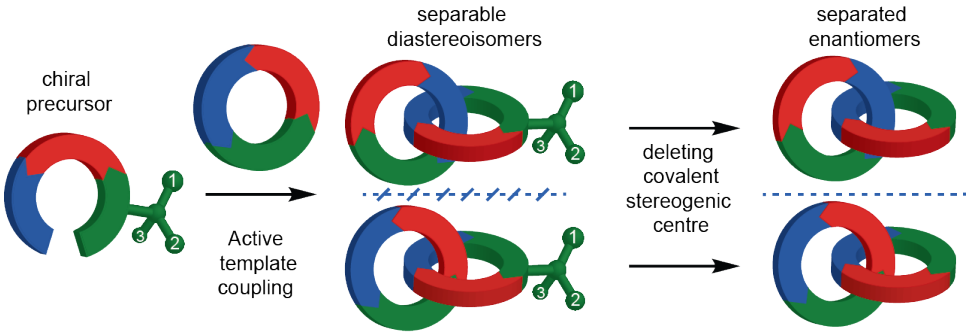

Figure 5.1 Cartoon approach for the synthesis of topologically chiral catenane with separation of diastereoisomers and suppression of the chiral centre.

5.2. Results and Discussion

5.2.1. Synthesis of a precursor bearing a chiral centre

The design of the chiral auxiliary used was based on a commercially available an amino acid, possessing a chiral centre, that has shown excellent result in the development and separation of chiral rotaxanes by another member of the group. The enantiopure precursor was prepared in a multi-step synthesis from commercially available starting material as presented in Figure 5.2. The carboxylic acid function of **258** was esterified by addition of acetyl chloride into a methanoic solution containing **258**. Subsequent protection of the amine with a Boc group and methylation of the phenol led to **259**.[9] The removal of the Boc group was performed using HCl in dioxane, leading to the formation of the ammonium chloride salt **260** (60% yield after recrystallisation). Neutralisation followed by reduction of the ester led to the amino alcohol **261** in 74% yield. Mono-propargylation of the amine was realised using one equivalent of propargyl bromide resulting in **262** in 57% yield. Finally, the alkylation of the amine was performed by addition of **235** in presence of K_2CO_3 leading to **263** in 98% yield.

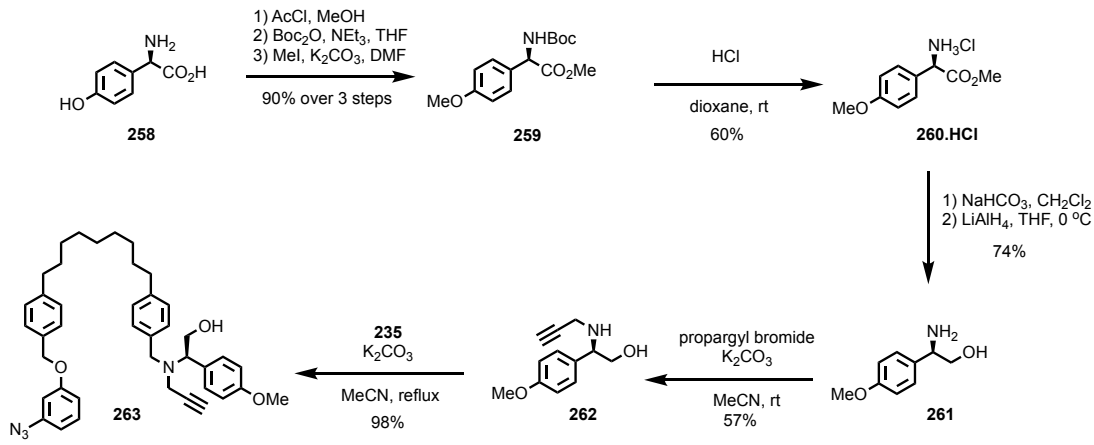

Figure 5.2 Synthesis route to access enantiopure **263**.

The difficulty associated with this synthesis was the access to enantiopure **262**. The enantiopurity of **258** varied from 70 to 95% enantiomeric excess (*ee*). Recrystallisation at different stage of the synthesis was performed. When 95% *ee* **258** was used, the recrystallisation of **259** led to enantiopure crystal of **259**. However, this recrystallisation was not possible when the batch used was only 70% *ee*. The intermediate **262** was also efficiently

recrystallised, leading to enantiopure **262** when the *ee* of the starting material was 95%, but inefficient when the *ee* was 70%. Ultimately, the recrystallisation of **260**.**HCl** led to enantiopure material even if the *ee* of the starting material was 70%.

5.2.2. Synthesis of triazole-containing macrocycles 272 and 274

In order to facilitate the analysis of the catenane reaction mixture, triazole containing macrocycles **264** and **266** were prepared by slow addition of precursors to a mixture containing $[Cu(MeCN)_4]PF_6$ and $^{i}Pr_2NEt$ (Figure 5.3). **264** was isolated in 75% yield from non-enantiopure precursor **263** while **266** was obtained in 32% yield from **265**.

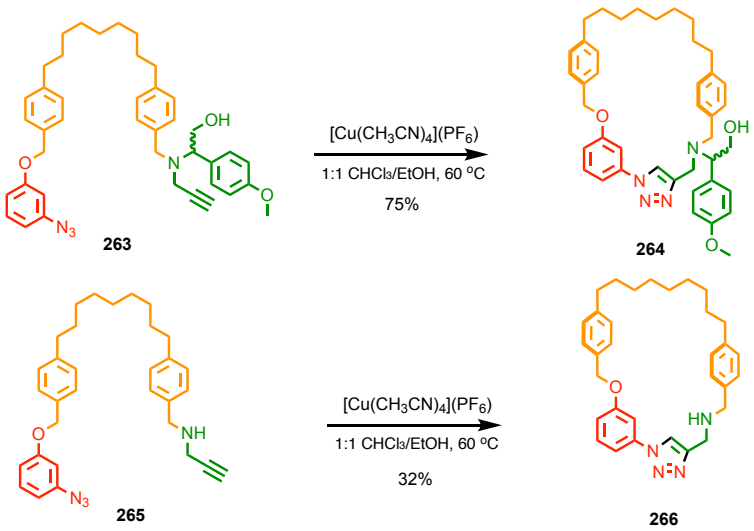

Figure 5.3 Synthesis of triazole containing macrocycles using non-enantiopure precursors.

5.2.3. Attempts to synthesise and separate diastereoisomeric mixture of catenanes.

Macrocycles **95** and **267** were used in first instance as these previously showed excellent results for diastereoselective and enantioselective synthesis of mechanically planar chiral rotaxanes as well as separation of diastereoisomeric mixture of rotaxanes.[8]

We started the investigations with non enantiopure precursor **263** as the optimisation of the synthesis was performed after the preliminary studies.

When precursor **263** was slowly added to a mixture containing **95** and $[Cu(MeCN)_4]PF_6$, the corresponding catenanes were formed as a 1:1 mixture of catenanes **268** and isolated in high yield (72%). Both catenanes displayed the same *m/z*, therefore those two structures were

assumed to be diastereoisomeric [2]catenanes. Despite many attempts to separate these two compounds, the separation was not achieved using column chromatography. Using macrocycle **267** gave a 1:1 diastereoisomeric mixture of catenanes **269** which was isolated in high yield (82%). However, the separation of the mixture of diastereoisomers was not achieved using column chromatography (Figure 5.4).

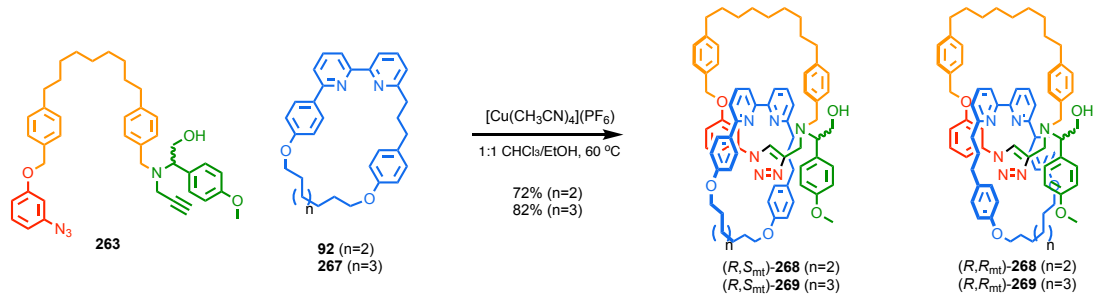

Figure 5.4 Synthesis of diastereoisomeric mixtures of catenanes.

The size increase of the bipyridine-containing macrocycle enabled to improve the yield of the reaction but the separation was not achieved using column chromatography. In order to evaluate the effect of the size of the macrocycle, a smaller macrocycle had to be synthesised.

5.2.4. Synthesis of macrocycle **274**

Macrocycle **274** was prepared similarly to macrocycle **92** (Figure 5.5).[10] Building block **270**, obtained in two steps from commercially available compounds, was reacted with 1,6-dibromohexane in presence of K_2CO_3 leading to the desymmetrised product **271** in 68% yield. **271** was reacted with **272**, obtained in 3 steps from commercially available compounds. These resulted in **273** in 86% yield after purification.[11] The macrocyclisation was performed using the nickel mediated cross-coupling reaction developed by Goldup and co-workers.[10] Macrocycle **274** was isolated in an excellent 71% yield after purification.

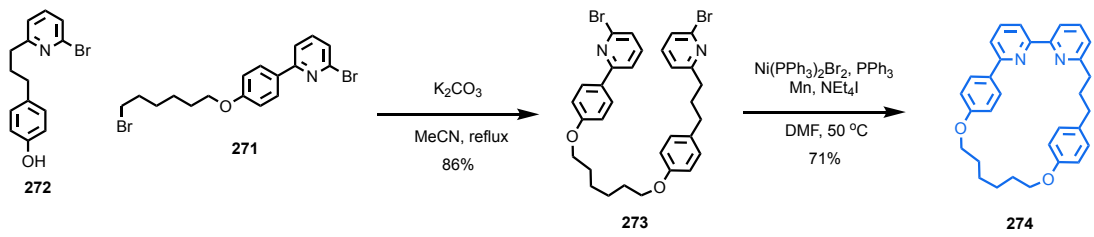

Figure 5.5 Synthesis of macrocycle **274**.

5.2.5. Separation of a diastereoisomeric mixture of catenanes.

The preliminary results for the separation of the catenanes were obtained using non enantiopure precursor **263**. When precursor **263** was slowly added to a mixture containing **274** and $[Cu(MeCN)_4]PF_6$, the corresponding catenanes were formed as a 2:1 mixture of catenanes **275**. After multiple attempts to separate the catenanes using column chromatography, separation was observed but needed optimisation.

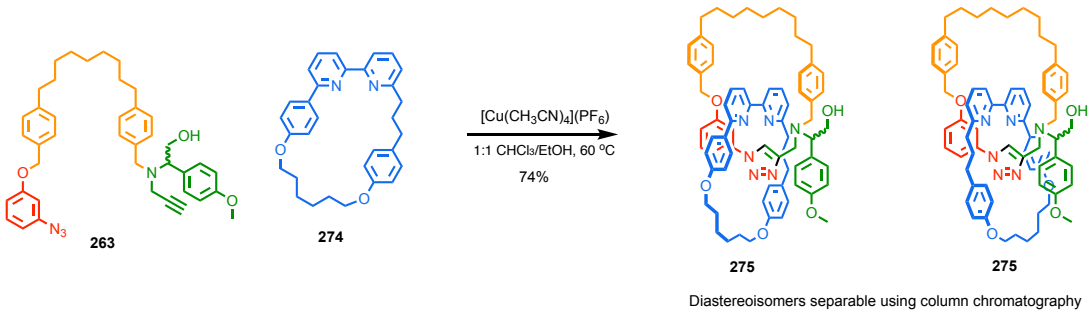

Figure 5.6 Attempts to synthesise and separate a diastereoisomeric mixture of **275**.

Subsequently, the reaction was performed using enantiopure precursor (*R*)-**263** (Figure 5.7). The major diastereoisomer eluted first and was isolated pure in 44% yield. The minor diastereoisomer eluted second and was isolated in good yield (30% yield) but was contaminated by the major diastereoisomer (<3%). Macrocycle **274** therefore had the optimum size and shape for the diastereoselective formation of [2]catenanes as well as allowing the separation of the products.

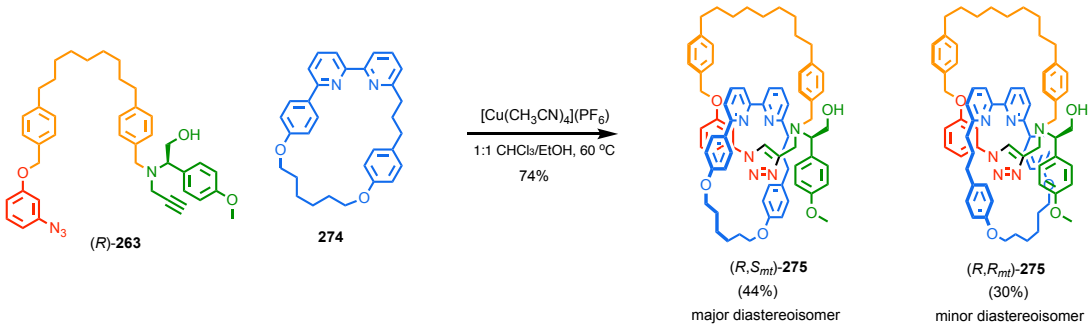

Figure 5.7 Synthesis and separation of a diasteoisomeric mixture of [2]catenanes.

The ^{1}H NMR spectra of the diastereoisomers were clearly different from that of each isolated non-interlocked component (Figure 5.8). The chemical shift of the triazole proton H_u for both [2]catenanes appeared at higher ppm than that observed in the case of the triazole-functionalised macrocycle. This observation suggested a hydrogen bond between the C-H and the bipyridine unit of the macrocycle. Proton H_e from the triazole-functionalised macrocycle, was observed as a singlet in the case of the non-interlocked macrocycle but split into diastereotopic signals in the catenane structure. Many signals (H_D, H_M, H_f) were shifted to lower ppm which is characteristic of an interlocked structure with a crowded environment.

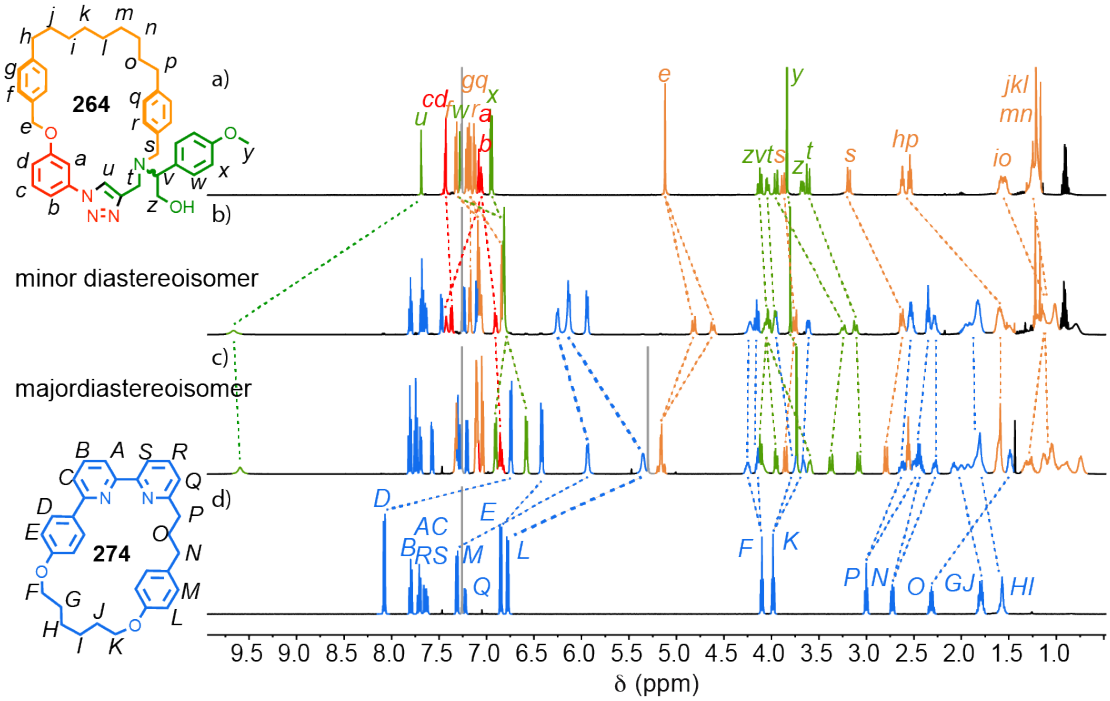

Figure 5.8 Stack ^{1}H NMR ($CDCl_3$, 500 MHz) of a) triazole containing macrocycle **264**. b) minor diastereoisomer of **275**. c) major diastereoisomer of **275**. d) macrocycle **274**.

To enable the assignment of the absolute stereochemistry of each diastereoisomer, single crystals were grown from a racemic mixture of the major diastereoisomer by diffusion of pentane into a CH_2Cl_2 solution containing the interlocked structure. The solid-state structure contained both enantiomers related by mirror plane (Figure 5.9). It can be noted that the interaction between the triazole proton H_u previously observed by ^{1}H NMR was also observed in the solid state. When the same method was used to grow crystals of enantiopure sample of the major diastereoisomers, no crystallisation occurred.

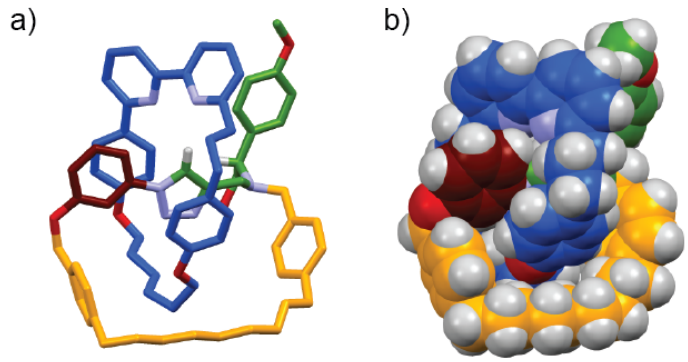

Figure 5.9 Solid-state structures and selected distances and angles of the major diastereoisomer of **275**. a) sticks representation. b) spacefilling representation.

The stereochemistry of the mechanical bond is assigned as follows:[3]

- For each ring, using the Cahn-Ingold-Prelog rules, identify the highest priority atom and call it A.
- Determine the highest priority atom connected to A, allowing the assignment of the orientation of the macrocycle (A-> B vector).
- Orientate the assembly with the vector of one ring passing through the cavity of the other ring.
- Observe the orientation of the second macrocycle from A to B; a clockwise orientation is assigned as R_{mt}, anti-clockwise is assigned as S_{mt}.

The orientation of the triazole containing macrocycle was determined using the red labels included in Figure 5.10 from A to B. The highest priority oxygen in the bipyridine-containing macrocycle was blue-labelled A. In this case, B was the quaternary aromatic directly connected to A. Using the approach described above, the stereochemistry of the mechanical bond was assigned as R_{mt}. Ultimately, the major isomer was assigned as (S,R_{mt}) or (R, S_{mt}) depending on the enantiomer of **263** used. By elimination, the minor isomer was assigned as (S, S_{mt}) or (R, R_{mt}).

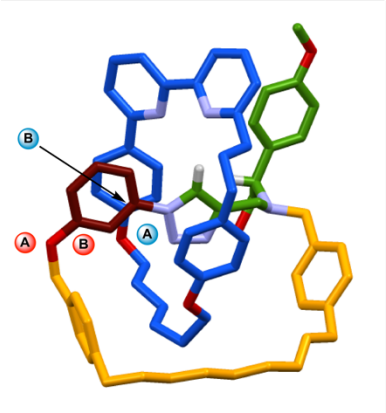

Figure 5.10 Labelled solid-state structure for the assignment of the absolute stereochemistry of the major diastereoisomer of **275**.

Unsurprisingly, the circular dischroism (CD) spectra of the diastereoisomers were different (Figure 5.11). The minor diastereoisomer (*R*,R_{mt})-**275** displayed two maxima at 264 nm and 302 nm, while an additional peak at 290 nm appeared for the major diastereoisomer (*R*,S_{mt})-**275**. The most important observation was that one spectrum is roughly mirror image to the other, suggesting that the topological chirality dominated the CD signal.

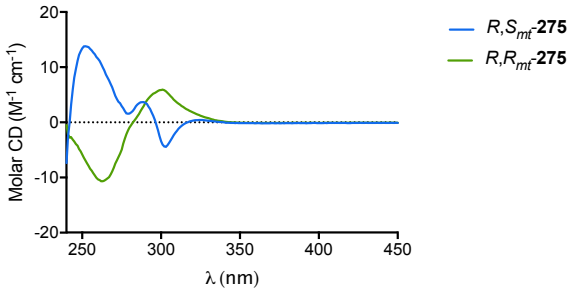

Figure 5.11 Circular dichroism of (*R*,S_{mt})-**275**, (*R*,R_{mt})-**275** (35.0 μM in $CHCl_3$, 293K).

5.2.6. Attempts to remove the stereogenic centre

As the separation of the diastereoisomeric mixture of chiral catenanes was achieved, the next challenge was to remove the chiral centre without breaking any bond of the triazole-functionalised macrocycle. The presence of a substituted *para*-methoxybenzyl protecting group suggested the use of traditional strategies to remove it. The treatment of the [2]catenane with TFA in CH_2Cl_2 resulted in the opening of the triazole-functionalised macrocycle at 80 °C and room temperature (Table 5.1, Entries 1 and 3).[12] When milder acetic acid was used, the same decomposition of the triazole-functionalised macrocycle was

observed at 80 °C (Table 5.1, Entry 2). However, no reaction was observed at room temperature (Table 5.1, Entry 4). The use of oxidants such as DDQ or CAN led to the decomposition of the triazole-functionalised macrocycle, which was potentially due to the presence of multiple benzylic groups in the core of the macrocycle (Table 5.1, Entries 5 and 6).[13,14] The presence of a proton at the α-position of the alcohol also suggested the possibility to eliminate water and remove the chiral centre. Addition of dehydrating reagent (Burgess reagent) was expected to convert [2]catenane **275** to [2]catenane **276** with loss of water and tautomerisation. However, the expected product was not observed (Table 5.1, Entry 8). The conversion of the alcohol to a leaving group using mesityl chloride in presence of base led to the same structure observed in Table 5.1, Entry 7 (Table 5.1, Entry 8). This structure appeared to contain an aziridinium function based on crude ^{1}H NMR and LC-MS, but no further investigations were carried out in the isolation and elucidation of the structure.

Table 5.10 Attempts to remove the chiral auxiliary

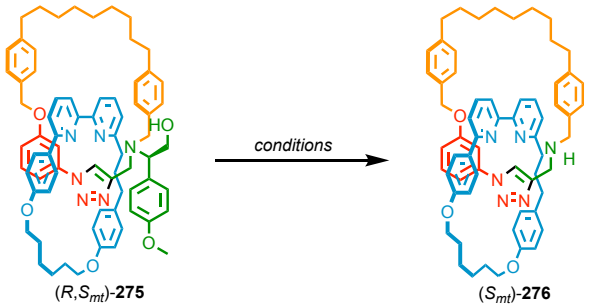

Entry	*Conditions*	Outcome
1	TFA, CH_2Cl_2, 80 °C	Decomposition
2	AcOH, CH_2Cl_2, 80 °C	Decomposition
3	TFA, CH_2Cl_2, RT	Traces + decomposition
4	AcOH, CH_2Cl_2, rt	NR
5	DDQ, CH_2Cl_2, rt	Decomposition
6	CAN, MeCN, rt	Decomposition
7	Burgess reagent, toluene, 80 °C	Aziridinium
8	MsCl, DBU, CH_2Cl_2, rt	Aziridinium

Finally, the conversion of the alcohol to an aldehyde, followed by treatment with acid to isomerise the α–amino aldehyde to the α–hydroxy iminium tautomer was attempted (Figure 5.12). In order to do so, Dess-Martin reagent was added to the [2]catenane but no oxidation of the alcohol was observed. Swern oxidation using two equivalents of activated DMSO completely oxidised the alcohol function. When the aldehyde was treated with acetic acid in isopropanol, the product was isolated in a good 40% yield over two steps. The best yield (68% over two steps) was obtained when the tautomerisation was performed in $CHCl_3$.

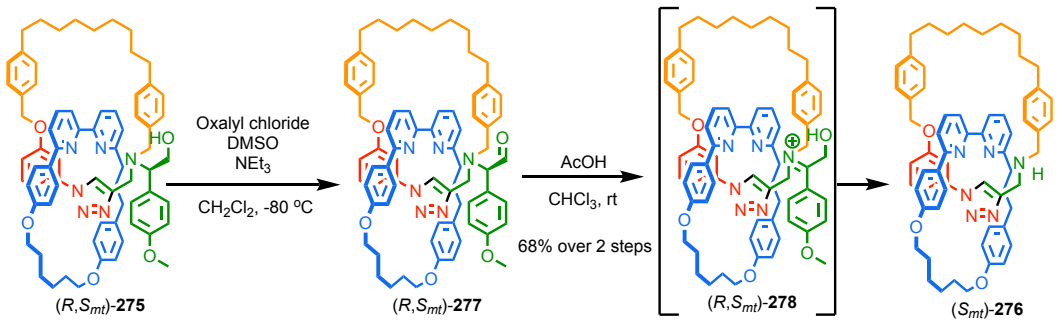

Figure 5.12 Cleavage of the chiral auxiliary via Swern oxidation followed acid hydrolysis.

During the cleavage of the auxiliary, the relative orientation of one macrocycle compared to the other one remained unchanged. In other words, during the cleavage, the structure was not dissociated and re-associated with modification of the relative orientation. Therefore, (*R*,S_{mt})-**275** gave (S_{mt})-**276**. In order to access the second enantiomer, the isolation of the (*S*,R_{mt})-**275** was realised using *S*-**263**, which led to (R_{mt})-**276** after removal.

Analysis of each enantiomers by ^{1}H NMR confirmed that both enantiomers were chemically identical which was expected by the sole presence of the topological chirality (Figure 5.13). The chemical shift of the triazole proton H_u for [2]catenane **276** was at higher ppm than the one observed in the case of the triazole-functionalised macrocycle **266**, which was attributed to a hydrogen bond between the C-H and the bipyridine unit of the macrocycle. Protons H_e and H_t, from the triazole-functionalised macrocycle, were observed as a singlet in the case of the non-interlocked macrocycle but split into diastereotopic signals in the catenane structure. Many signals (H_D, H_M, H_f) were shifted to lower ppm which is characteristic of an interlocked structure with a crowded environment.

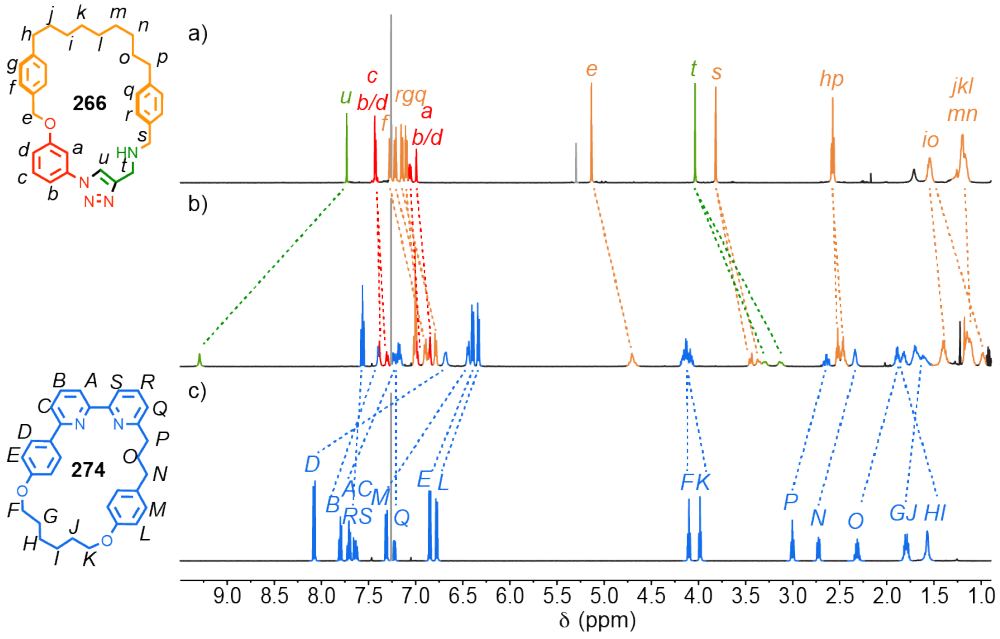

Figure 5.13 Stack ^{1}H NMR ($CDCl_3$, 500 MHz) of a) triazole containing macrocycle **266**. b) catenane **276**. c) macrocycle **274**.

In order to evaluate the enantiopurity of the topologically chiral catenane, separation of each enantiomer was performed using CSP-HPLC (RegisCell column with and isocratic gradient of 98:2 hexane-IPA) (Figure 5.14). The racemic mixture allowed the optimisation of the

separation with return to the baseline. When S_{mt}-**276** was injected, only one enantiomer was detected meaning that the enantiopurity was greater than 99.5%. When R_{mt}-**276** was used for the analysis, the purity was 98.2%. The lower enantiopurity of R_{mt}-**276** can come from the presence of a small amount of the second diastereoisomer before removal of the chiral auxiliary or can be due to a slightly lower enantiopurity of the amine used for the synthesis of *S*-**263**.

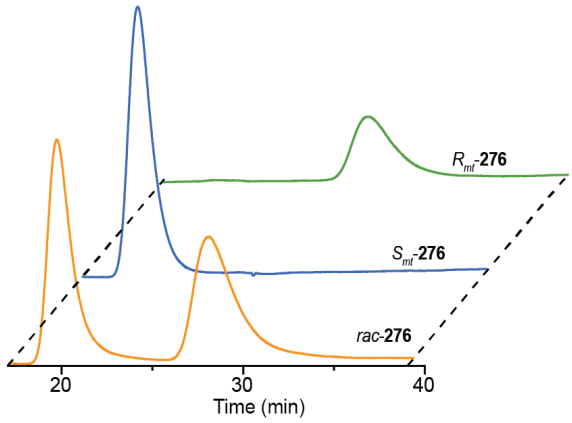

Figure 5.14 CSP-HPLC (RegisCell, 98:2 hexan-IPA, 0.5 mL/min) of (front to back) *rac*-**276**, S_{mt}-**276** and R_{mt}-**276**.

The enantiomeric nature of the structures was confirmed by the identical but mirror image circular dichroism spectra obtained for both enantiomers of **276** (Figure 5.15) The racemic mixture of **276** displayed a silent CD spectrum.

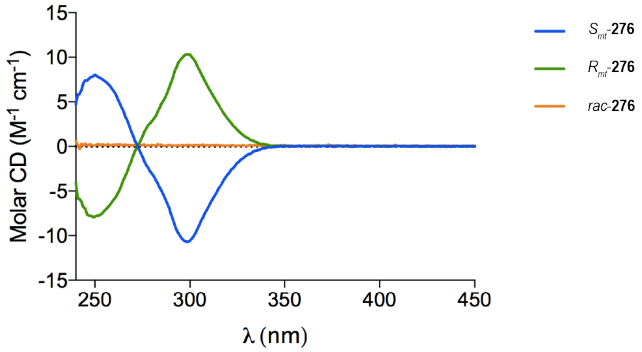

Figure 5.15 Circular dichroism of *rac*-**276**, R_{mt}-**276**, S_{mt}-**276** (35.0 μM in $CHCl_3$, 293K).

5.3. Conclusions and Future Work

The first mechanically topologically chiral [2]catenane was successfully synthesised without the use of preparative CSP-HPLC. The approach used for this synthesis involved the separation of topologically chiral catenanes bearing a chiral centre, resulting in a pair of separable diastereoisomers. The removal of the covalent stereogenic element was achieved by successive oxidation and tautomerisation leading to the production of more than 200 mg of enantiopure topologically chiral [2]catenane.

This approach is technically simple and, given the versatility of the AT-CuAAC catenane forming reaction, it is now possible to prepare topologically chiral catenanes without the need for CSP-HPLC separation. Thus, topologically chiral catenanes are now accessible for investigation in catalysis or sensing.

Experimental

The following compounds were synthesised according to literature procedures:

Azide **235**,[15] macrocycle **95**,[15] compound **270**,[10] compound **272**.[11]

Macrocycle **267** was provided by Dr Mike Jinks. Enantiopure amine **260** was provided by Dr Mathieu Denis.

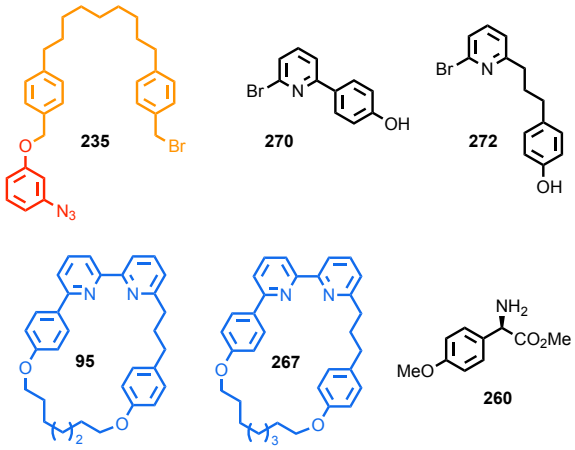

Compound 271

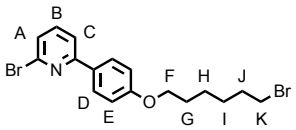

To a solution of **270** (1 g, 4 mmol, 1 eq.) in MeCN (20 mL) was added K_2CO_3 (2.2 g, 16 mmol, 4 eq.) as a solid. After stirring for 30 minutes, 1,6-dibromohexane (1.53 mL, 2.5 mmol, 2.5 eq.) was added and the reaction was stirred at reflux for 18 h. The cooled reaction mixture was filtered through celite. The solvent was removed *in vacuo*. The residue was purified by column chromatography (Petrol with a gradient from 0 to 50% CH_2Cl_2) to give **271** as a white solid (1.1 g, 68%). m.p. 94-96 °C.^{1}H NMR (400 MHz, $CDCl_3$) δ: 7.94 (d, *J* = 8.9, 2H, H_D), 7.61 (dd, *J* = 7.7, 0.9, 1H, H_C), 7.54 (t, *J* = 7.7, 1H, H_B), 7.34 (dd, *J* = 7.7, 0.9, 1H, H_A), 6.96 (d, *J* = 8.9, 2H, H_E), 4.02 (t, *J* = 6.4, 2H, H_F), 3.43 (t, *J* = 6.7, 2H, H_K), 1.97-1.87 (m, 2H, H_J), 1.87-1.77 (m, 2H, H_G), 1.60-1.45 (m, 4H, H_H, H_I). ^{13}C NMR (101 MHz, $CDCl_3$) δ: 160.6, 158.4, 142.2, 139.0, 130.3, 128.5, 125.6, 118.2, 114.8, 68.0, 33.9, 32.8, 29.2, 28.1, 25.4. HR-ESI-MS *m/z* = 411.9910 $[M+H]^+$ calc. 411.9906.

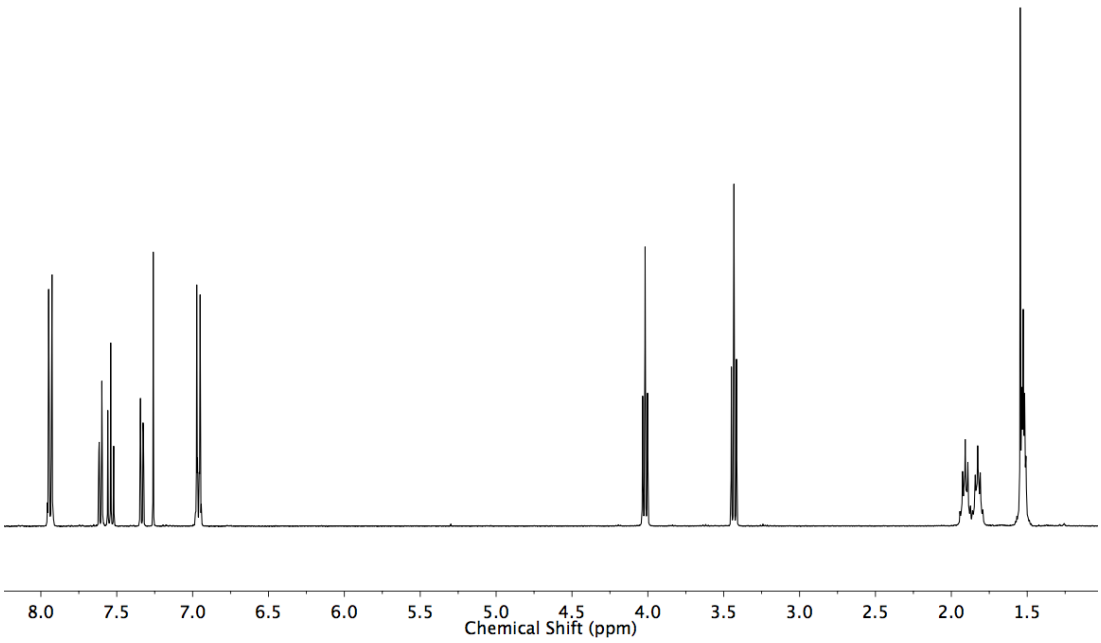

Figure 5.16 ^{1}H NMR (400 MHz, $CDCl_3$) of **271**.

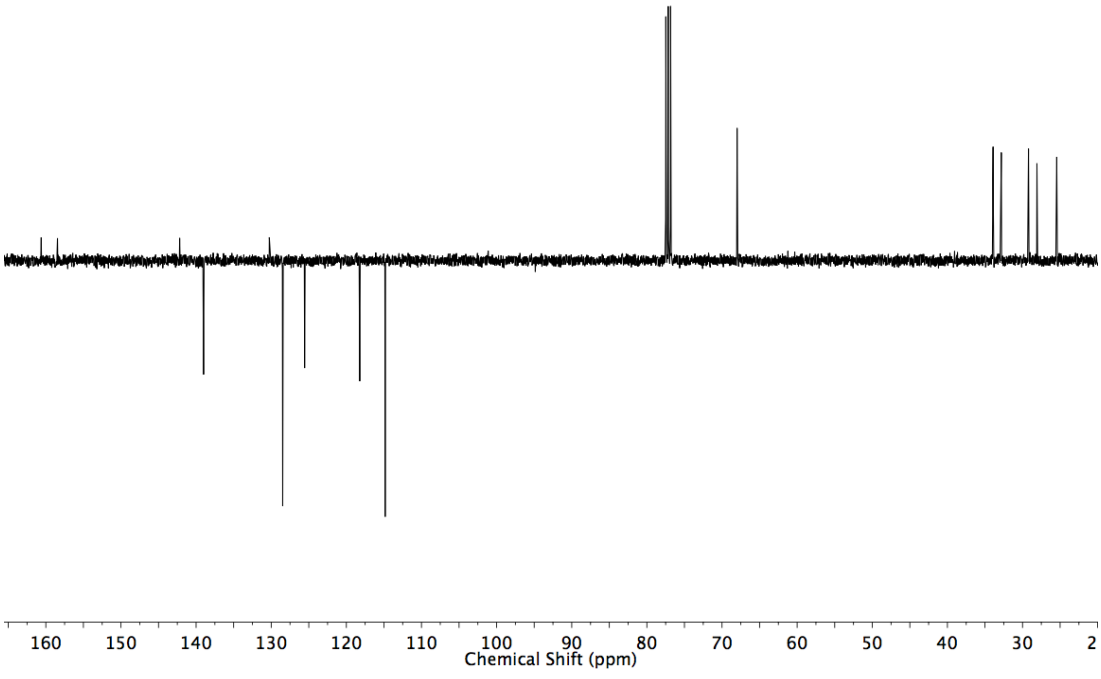

Figure 5.17 JMOD NMR (101 MHz, $CDCl_3$) of **271**.

Compound 273

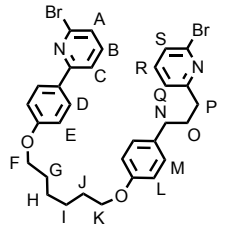

To a solution of **272** (4.5 g, 15.3 mmol, 1.2 eq.) in MeCN (70 mL) was added K_2CO_3 (2.76 g, 20.0 mmol, 1.7 eq.) as a solid. After stirring for 30 minutes, **271** (5.0 g, 12.1 mmol, 1.0 eq.) was added as a solid and the reaction stirred at reflux for 18 h. The solvent was removed *in vacuo* and the resultant solid dissolved in CH_2Cl_2 (500 mL), washed with H_2O (100 mL) and brine (100 mL), dried ($MgSO_4$), filtered and the solvent removed *in vacuo*. After purification by column chromatography (Petrol/CH_2Cl_2 1/1 with a gradient to 80% CH_2Cl_2), **273** (6.5 g, 86%) was obtained as a white solid. m.p. 96-98 °C. ^{1}H NMR (400 MHz, $CDCl_3$) δ: 7.94 (d, *J* = 8.8, 2H, H_D), 7.60 (dd, *J* = 7.7, 0.9, 1H, H_C), 7.54 (t, *J* = 7.7, 1H, H_B), 7.43 (t, *J* = 7.7, 1H, H_R), 7.33 (dd, *J* = 7.7, 0.9, 1H, H_A), 7.29 (dd, *J* = 7.7, 0.9, 1H, H_S), 7.13-7.04 (m, 4H, H_M, H_Q), 6.96 (d, *J* = 8.9, 2H, H_E), 6.82 (d, *J* = 8.5, 2H, H_L), 4.02 (t, *J* = 6.5, 2H, H_F), 3.95 (t, *J* = 6.4, 2H, H_K), 2.78 (t app, *J* = 7.8, 2H, H_P), 2.61 (t app, *J* = 7.6, 2H, H_N), 2.07-1.95 (m, 2H, H_O), 1.90-1.76 (m, 4H, H_G, H_J), 1.61-1.50 (m, 4H, H_H, H_I). ^{13}C NMR (101 MHz, $CDCl_3$) δ: 164.0, 160.7, 158.5, 157.5, 142.2, 141.7, 139.0, 138.7, 134.0, 130.2, 129.5, 128.5, 125.5, 125.4, 121.6, 118.2, 114.8, 114.6, 68.1, 68.0, 37.6, 34.7, 31.7, 29.4, 29.3, 26.1. HR-ESI-MS *m/z* = 623.0907 $[M+H]^+$ calc. 623.0903.

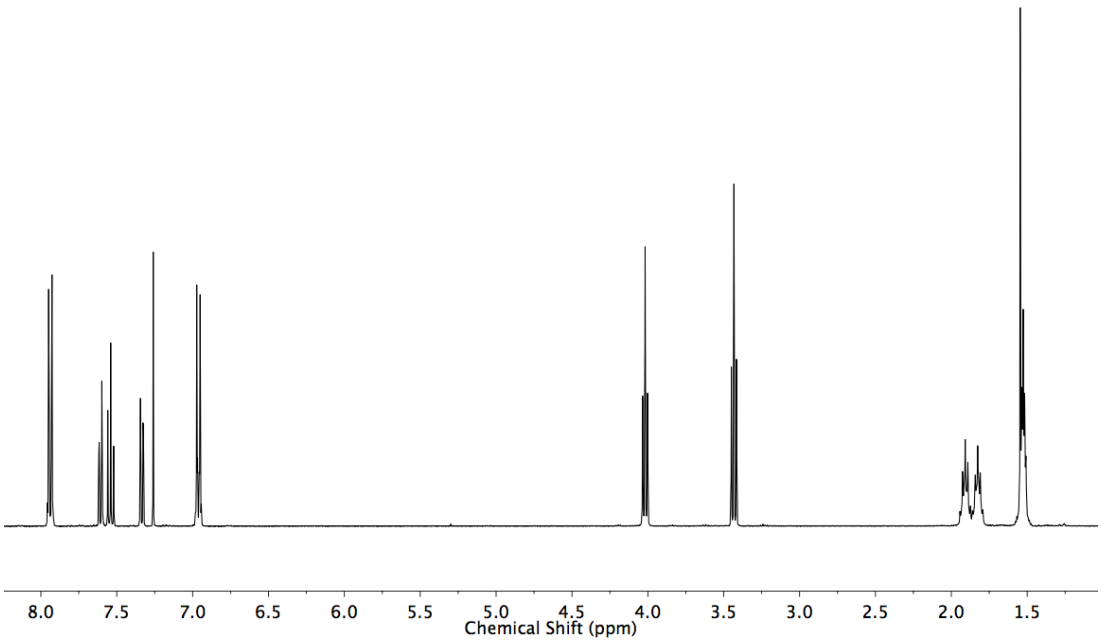

Figure 5.18 ^{1}H NMR (400 MHz, $CDCl_3$) of **273**.

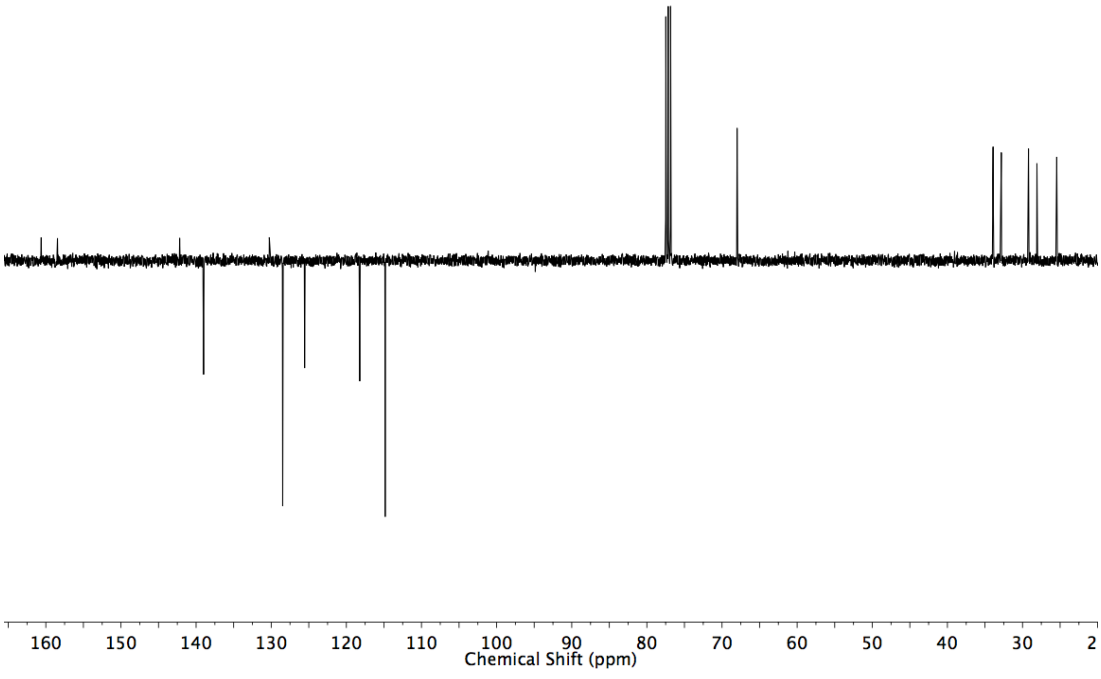

Figure 5.19 JMOD NMR (101 MHz, $CDCl_3$) of **273**.

Macrocycle 274

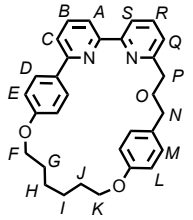

$[Ni(PPh3)_2Br_2]$ (1.49 g, 2.00 mmol, 1 eq.), PPh_3 (1.05 g, 4.00 mmol, 2 eq.), Mn (1.10 g, 20.00 mmol, 10 eq.) and NEt_4I (0.514 g, 2.00 mmol, 1 eq.) in DMF (20 mL) were sonicated for 10 min, followed by stirring at 50 °C for 1 h. To this catalyst mixture was added **273** (1.25 g, 2.00 mmol, 1 eq.) in DMF (20 mL) via syringe over 4 h, followed by additional stirring of the reaction for 1 h. To the cooled reaction was added CH_2Cl_2 (100 mL) and EDTA-NH_3 solution (100 mL). After filtering through a pad of Celite the organic phase was washed with water (2 × 100 mL) and brine (100 mL), and the combined aqueous phases extracted with CH_2Cl_2 (50 mL). The combined organic phases were dried ($MgSO_4$), filtered and the solvent removed *in vacuo*. The crude product was purified by column chromatography (Petrol with a gradient of 0 to 60% $CHCl_3$ + 0.2% EtOH) yielded **274** as white solid (0.653 g, 71%). m.p. 130-132 °C ^{1}H NMR (500 MHz, $CDCl_3$) δ: 8.08 (d, *J* = 9.0, 2H, H_D), 7.80 (t, *J* = 7.8, 1H, H_B), 7.71 (t, *J* = 7.8, 1H, H_R), 7.70 (dd, *J* = 7.7, 0.9, 1H, H_C), 7.65 (dd, *J* = 7.7, 0.9, 1H, H_A), 7.62 (dd, *J* = 7.9, 0.9, 1H, H_S), 7.31 (d, *J* = 8.7, 2H, H_M), 7.22 (dd, *J* = 7.6, 0.9, 1H, H_Q), 6.85 (d, *J* = 9.0, 2H, H_E), 6.78 (d, *J* = 8.7, 2H, H_L), 4.10 (t, *J* = 6.7, 2H, H_F), 3.98 (t, *J* = 6.1, 2H, H_K), 3.00 (t, *J* = 7.2, 2H, H_P), 2.73 (dd, *J* = 8.8, 6.6, 2H, H_N), 2.41-2.20 (m, 2H, H_O), 1.79 (m, 4H, H_G, H_J), 1.66-1.51 (m, 4H, H_H, H_I). ^{13}C NMR (126 MHz, $CDCl_3$) δ: 162.5, 160.0, 157.5, 157.4, 156.7, 156.4, 137.5, 136.9, 135.2, 132.2, 130.1, 128.8, 122.8, 119.5, 119.4, 118.7, 115.3, 114.9, 68.1, 67.7, 37.0, 34.3, 31.4, 28.6, 28.2, 24.8, 24.5. HR-ESI-MS *m/z* = 465.2535 $[M+H]^+$ calc. 465.2537.

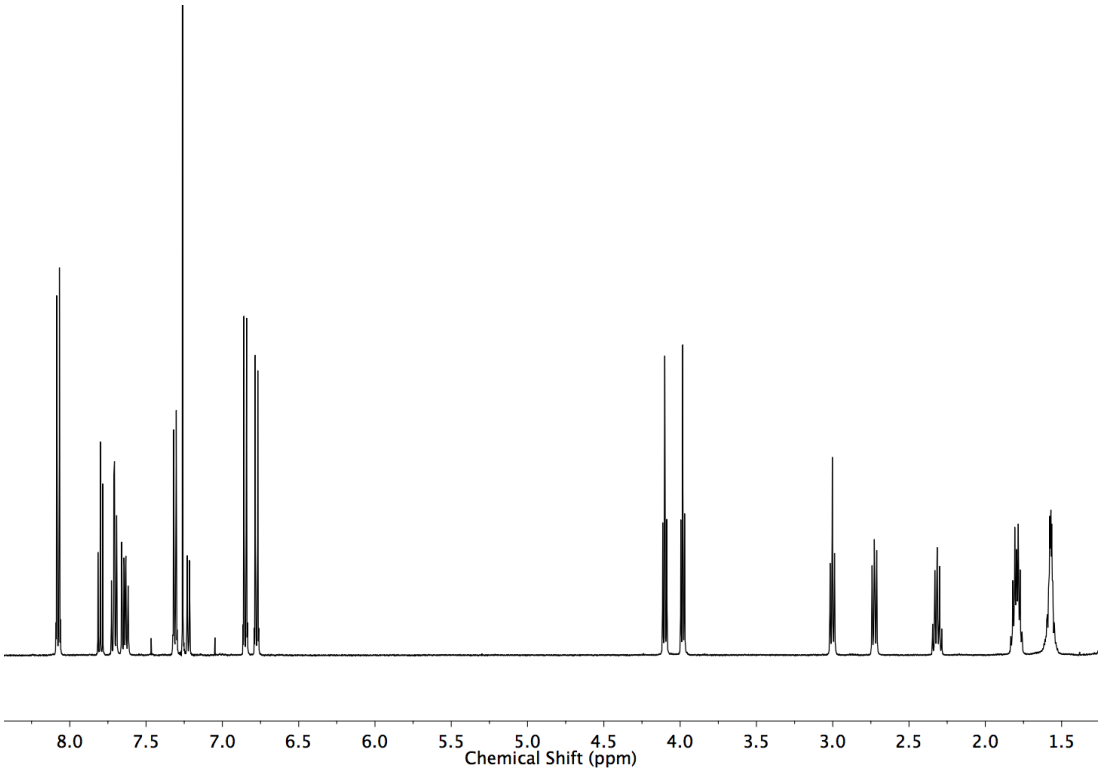

Figure 5.20 ^{1}H NMR (500 MHz, $CDCl_3$) of **274**.

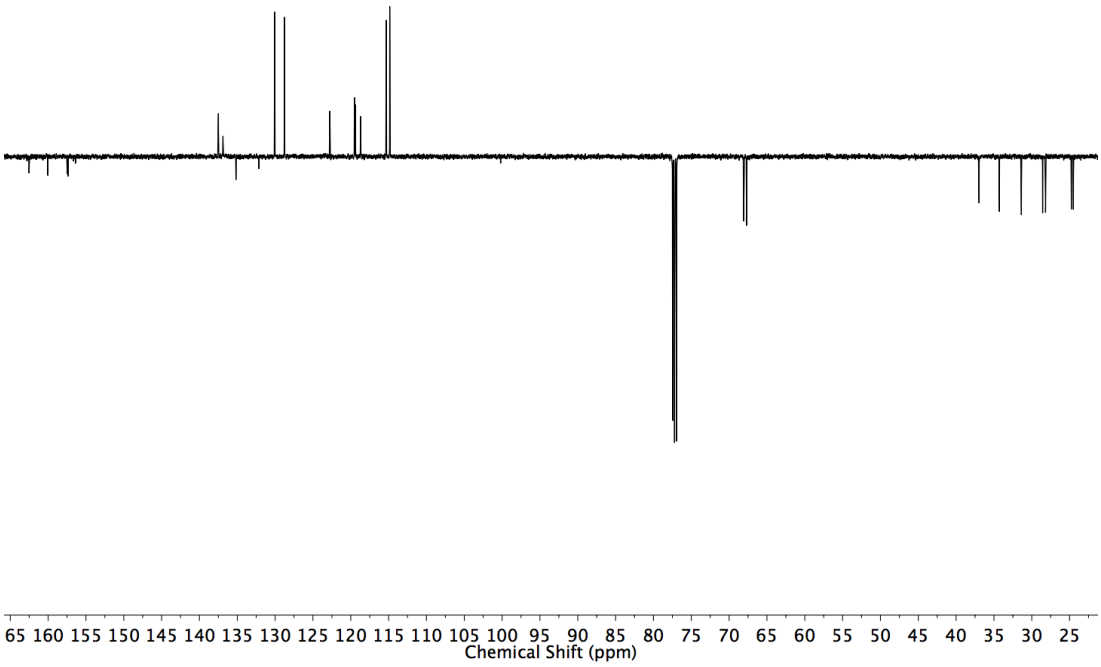

Figure 5.21 JMOD NMR (126 MHz, $CDCl_3$) of **274**.

Compound 262

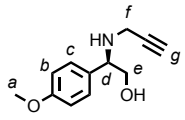

To a suspension of $LiAlH_4$ (0.38 g, 10.0 mmol, 1.5 eq) in THF (20 mL) at 0°C was added dropwise **260** (1.27 g, 6.5 mmol, 1 eq) as a solution in THF (10 mL) after what the reaction mixture was allowed to stir at rt for 16 h. Water (2 mL) was carefully added to the mixture at 0 °C followed by 10 M aq NaOH (2 mL) and the crude stirred for an additional 30 min. The suspension was then filtered through celite with THF and the filtrate concentrated *in vacuo* to give **261** as a pale yellow solid (0.80 g, 74%) which was used without further purification. To a stirred solution of amine **261** (0.80g, 4.8 mmol, 1 eq) in MeCN (20 mL) at rt was added K_2CO_3 (1.40 g, 10 mmol, 2 eq) followed after 15 min by propargyl bromide (80 wt. % in toluene, 0.53 mL, 4.8mmol, 1 eq). The resulting solution was stirred for 16 h then filtered through celite and concentrated *in vacuo*. The crude residue was purified *via* flash column chromatography on silica gel (Petrol/CH_2Cl_2 1/1 with a gradient from 0 to 50% EtOAc), providing the pure product **262** as pale yellow oil (0.45 g, 46%) with an *ee* > 99%. ^{1}H NMR (400 MHz, $CDCl_3$) δ: 7.26 (d, *J* = 8.7, 2H, H_c), 6.89 (d, *J* = 8.7, 2H, H_b), 3.96 (dd, *J* = 8.3, 4.5, 1H, H_d), 3.80 (s, 3H, H_a), 3.73 (dd, *J* = 10.8, 4.5, 1H, H_e), 3.60 (dd, *J* = 10.7, 8.3, 1H, H_e), 3.42 (dd, *J* = 17.0, 2.4, 1H, H_f), 3.20 (dd, *J* = 17.0, 2.4, 1H, H_f), 2.21 (t, *J* = 2.4, 1H, H_g), 1.79 (s, 1H, -*NH*-). ^{13}C NMR (400 MHz, $CDCl_3$) δ: 159.4, 131.6, 128.8, 114.2, 82.1, 71.6, 67.0, 62.4, 55.4, 35.8. HR-ESI-MS *m/z* = 234.1126 $[M+H]^+$ calc. 234.1125.

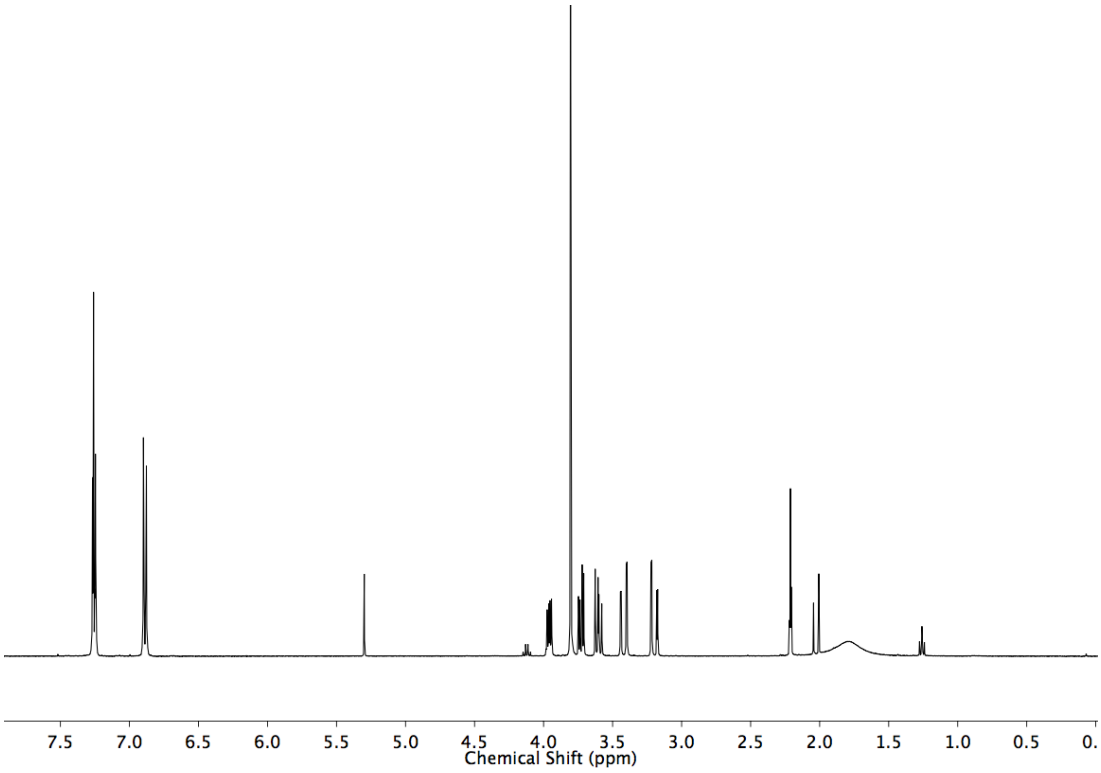

Figure 5.22 ^{1}H NMR (400 MHz, $CDCl_3$) of *R*-**262**.

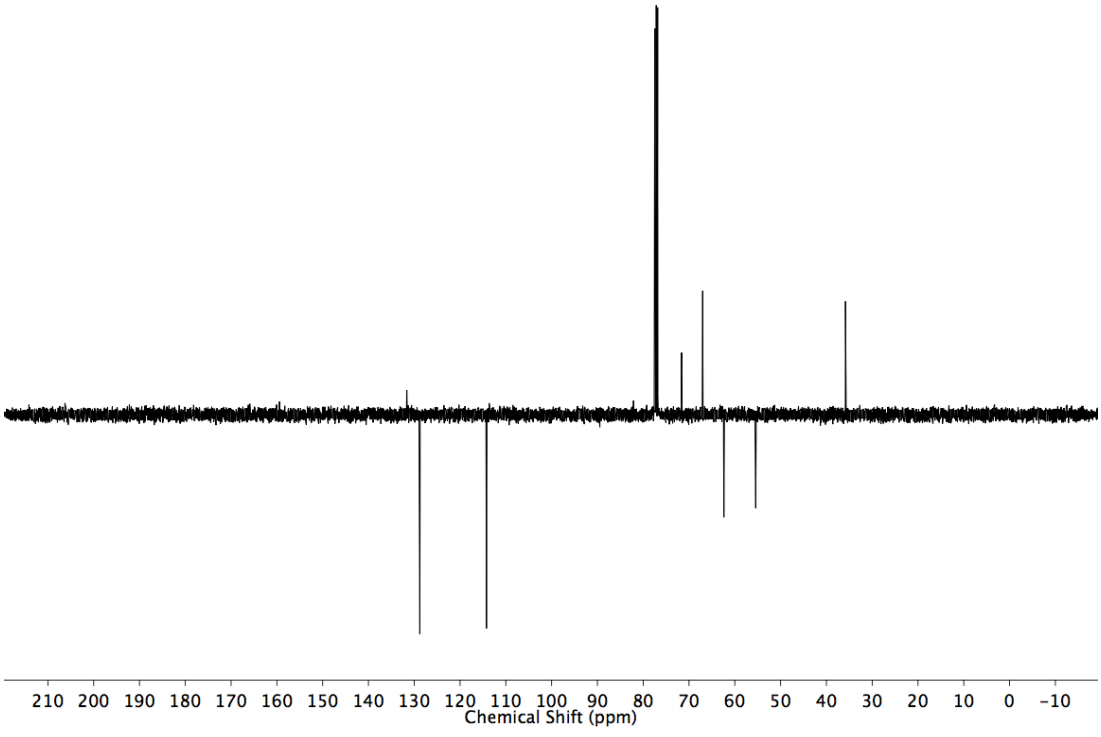

Figure 5.23 JMOD NMR (101 MHz, $CDCl_3$) of *R*-**262**.

*Precursor R-**263***

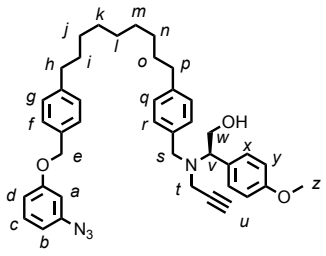

235 (0.296 g, 0.568 mmol, 1 eq.), *R*-**262** (0.140 g, 0.682 mmol, 1.2 eq) and K_2CO_3 (0.785 g, 5.68 mmol, 10 eq.) were stirred at 80 °C in MeCN (25 mL) under air in a sealed vial for 20 h. The cooled reaction mixture was filtered through celite and purified by column chromatography (Petrol/CH_2Cl_2 1/1 with a gradient from 0 to 10% EtOAc) to give the product as a colorless oil (0.362 g, 99%). ^{1}H NMR (500 MHz, $CDCl_3$) δ: 7.33-7.30 (m, 4H, H_f, H_x), 7.26-7.19 (m, 5H, H_c, H_g, H_r), 7.12 (d, *J* = 8.1, 2H, H_q), 6.91 (d, *J* = 8.8, 2H, H_y), 6.76 (ddd, *J* = 8.3, 2.3, 0.9, 1H, H_b or H_d), 6.66-6.63 (m, 2H, H_a, H_b or H_d), 5.01 (s, 2H, H_e), 4.01-3.97 (m, H_v, H_w), 3.84-3.77 (m, 5H, H_s, $H_{w'}$, H_z), 3.41-3.37 (m, 1H, H_t), 3.31 (d, *J* = 13.3, 1H, $H_{s'}$), 3.13 (dd, *J* = 17.2, 2.4, 1H, $H_{t'}$), 2.62-2.56 (m, 4H, H_h, H_l), 2.23 (app. t, *J* = 2.4, 1H, H_u), 1.63-1.55 (m, 4H, H_i, H_o), 1.30 (br. m, 10H, H_j, H_k, H_l, H_m, H_n). ^{13}C NMR (126 MHz, $CDCl_3$) δ: 160.2, 159.5, 143.2, 142.1, 141.4, 135.8, 133.8, 130.6, 130.0, 129.8, 129.0, 128.8, 128.6, 127.8, 114.1, 111.6, 111.6, 106.1, 79.6, 73.3, 70.3, 65.4, 62.8, 55.4, 53.9, 39.0, 35.9, 35.8, 31.7, 31.6, 29.6 (×3), 29.5, 29.4. HR-ESI-MS *m/z* = 645.3799 $[M+H]^+$ calc. 645.3799.

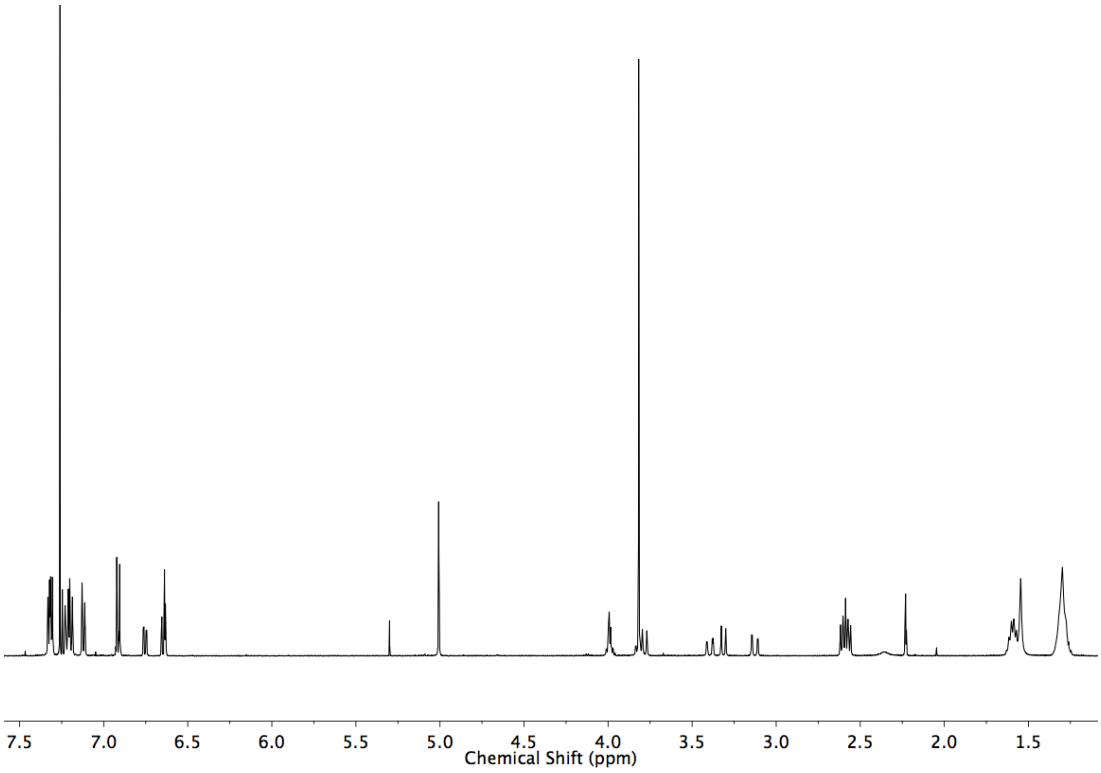

Figure 5.24 ^{1}H NMR (500 MHz, $CDCl_3$) of *R*-**263**.

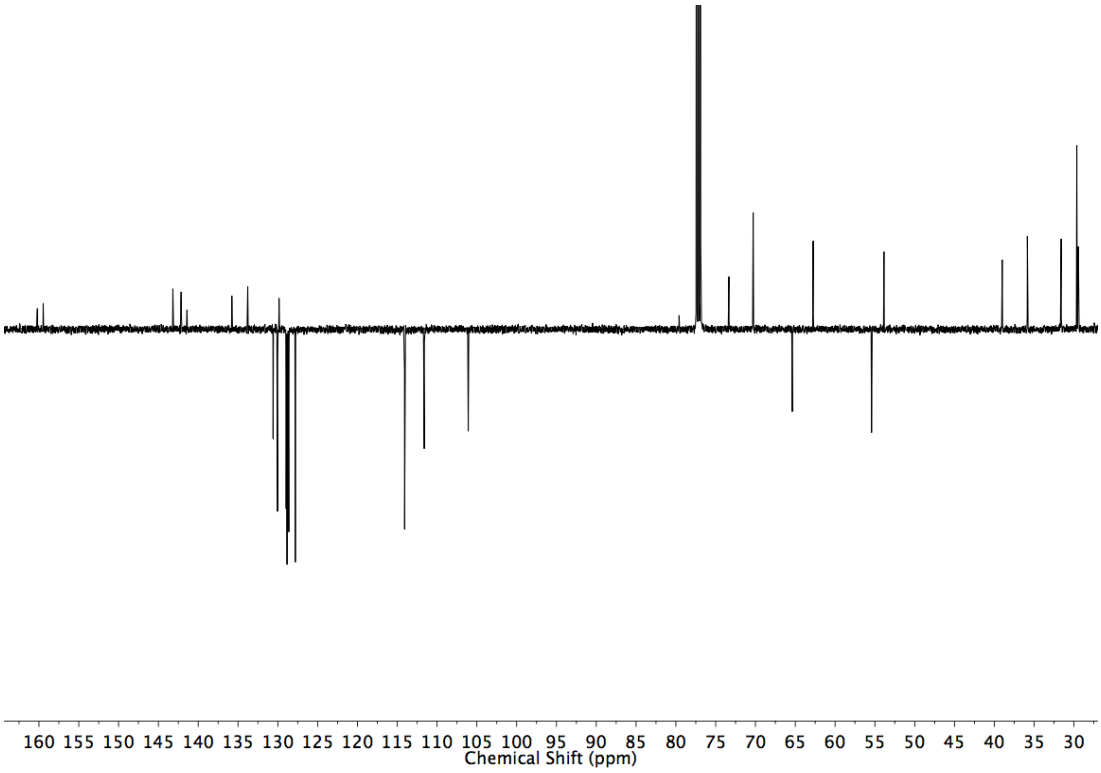

Figure 5.25 JMOD NMR (126 MHz, $CDCl_3$) of *R*-**263**.

*Precursor S-**263***

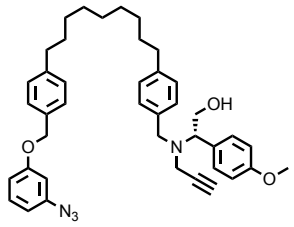

235 (630 mg, 1.21 mmol, 1 eq.), *S*-**262** (308 mg, 1.50 mmol, 1.2 eq) and K_2CO_3 (829 mg, 6.00 mmol, 5 eq.) were stirred at 80 °C in MeCN (50 mL) under air in a sealed vial for 20 h. The cooled reaction mixture was filtered through celite and purified by column chromatography (Petrol/CH_2Cl_2 1/1 with a gradient from 0 to 10% EtOAc) to give the product as a colorless oil (700 mg, 90%). Spectroscopic data were identical to those reported for *R*-**263**.

Precursor 265

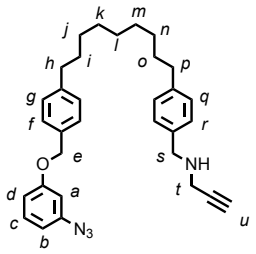

235 (253 mg, 0.50 mmol, 1 eq.), propargylamine (83 mg, 1.50 mmol, 3.0 eq) and K_2CO_3 (83 mg, 0.60 mmol, 1.2 eq.) were stirred at 80 °C in MeCN (3 mL) under air in a sealed vial for 24 h. The cooled reaction mixture was filtered through celite and purified by column chromatography (CH_2Cl_2 with a gradient from 0 to 5% EtOAc) to give the product as a colorless oil (40 mg, 17%). ^{1}H NMR (400 MHz, $CDCl_3$) δ: 7.34 (d, *J* = 8.2, 2H, H_f), 7.28-7.23 (m, 3H, H_r, H_c), 7.21 (d, *J* = 8.2, 2H, H_g), 7.15 (d, *J* = 8.2, 2H, H_q), 6.79-6.75 (m, 1H, H_b or H_d), 6.68-6.63 (m, 2H, H_a, H_b or H_d), 5.02 (s, 2H, H_e), 3.86 (s, 2H, H_s), 3.44 (d, *J* = 2.4, 2H, H_t), 2.61 (td, J = 9.5, 7.5, 4H, H_h, H_p), 2.26 (t, *J* = 2.4, 1H, H_u), 1.69-1.54 (m, 4H, H_i, H_o), 1.39-1.23 (m, 10H, H_j, H_k, H_l, H_m, H_n). ^{13}C NMR (101 MHz, $CDCl_3$) δ: 160.2, 143.2, 142.0, 141.4, 136.7, 133.8, 130.6, 128.8, 128.6, 128.5, 127.8, 111.7 (2xC), 106.1, 82.3, 71.6, 70.3, 52.2, 37.5, 35.8, 35.8, 31.6, 31.6, 29.6 (3xC), 29.4(2xC). HR-ESI-MS *m/z* 495.3121 $[M+H]^+$ calc. 495.3118.

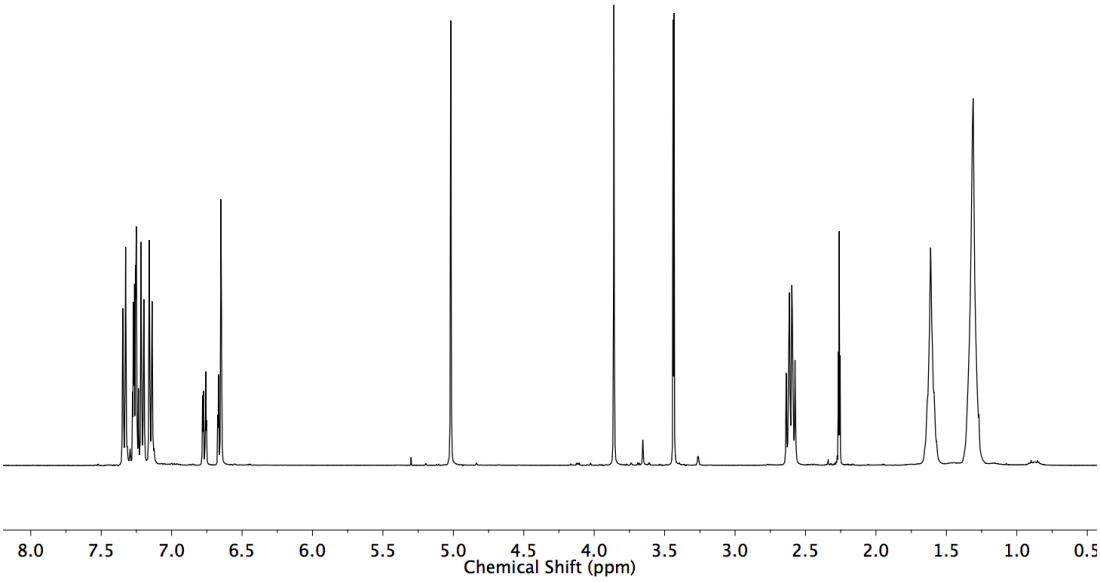

Figure 5.26 ^{1}H NMR (400 MHz, $CDCl_3$) of **265**.

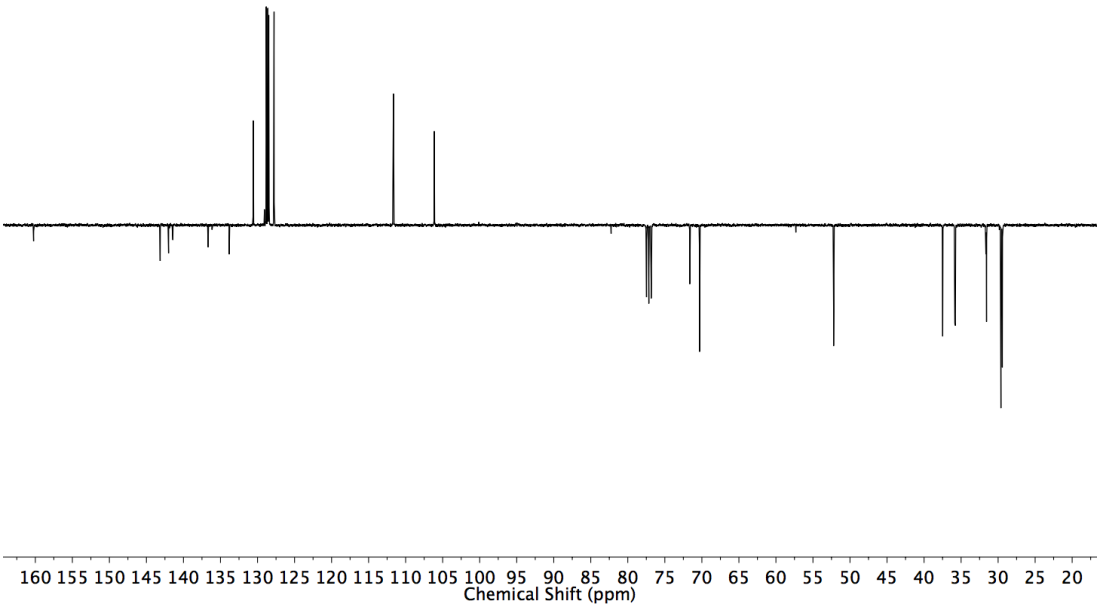

Figure 5.27 JMOD NMR (101 MHz, $CDCl_3$) of **265**.

Syntheses of catenanes

*Catenanes (R,S_{mt})-**275** and (R,R_{mt})-**275***

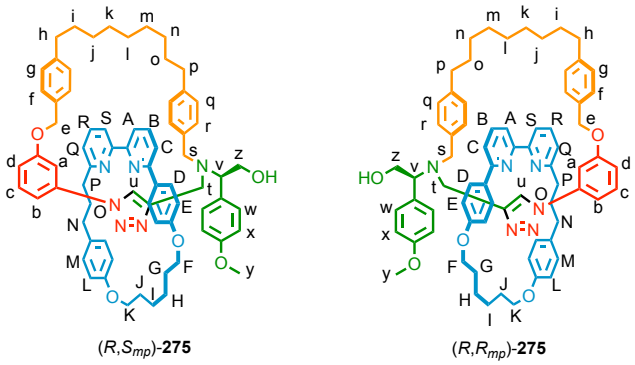

To a solution of **274** (116.2 mg, 0.25 mmol, 1.0 eq.), $[Cu(CH_3CN)_4]PF_6$ (92.8 mg, 0.249 mmol, 1.0 eq.), $^{i}Pr_2NEt$ (87 µL, 0.50 mmol, 2 eq.) in 1:1 $CHCl_3$/EtOH (10 mL) at 60 °C was added *R*-**263** (194.0 mg, 0.60 mmol, 1.2 eq.) in 1:1 $CHCl_3$/EtOH (15 mL) over 4 h. After removal of the solvent *in vacuo*, the residue was dissolved in 1:1 CH_2Cl_2/MeOH (10 mL) and KCN (160 mg, 2.5 mmol, 10 eq.) added as a solid. After stirring at rt for 30 minutes the solvent was removed under a flow of air. The residue was dissolved in CH_2Cl_2 (50 mL) and washed with H_2O (4 × 10 mL), dried ($MgSO_4$) and the solvent removed *in vacuo*. The residue containing catenane (*R*,*R*/*S*$_{mt}$)-**275** (in a 0.67:0.33 diastereoisomeric ratio, Figure 5.27) was purified by column chromatography on silica (Petrol/CH_2Cl_2/AcOEt/Et_2O 140/30/15/15), to yield (*R*,*S*$_{mt}$)-**275** (160 mg, 57%) and (*R*,*R*$_{mt}$)-**275** (90 mg, with 5% of (*R*,*S*$_{mt}$)-**275**, 32%) as a white foams .

Catenane (*R*, *S*$_{mt}$)-**275**. ^{1}H NMR (500MHz, $CDCl_3$) δ : 9.59 (brd. s, 1H, H_u), 7.81 (t, J = 7.8, 1H, H_R), 7.74 (t, J = 7.8, 1H, H_B), 7.69 (dd, J = 7.8, 1.0, 1H, H_S), 7.57 (dd, J = 7.8, 1.0, 1H, H_A), 7.35 – 7.29 (m, 3H, Hc, H_r), 7.27 (dd, J = 7.8, 0.9, 1H, H_C), 7.21 (dd, J = 7.8, 0.9, 1H, H_Q), 7.13 – 7.07 (m, 5H, H_q, H_f, H_a), 7.04 (d, J = 8.4, 2H, H_g), 6.90 (d, J = 8.7, 2H, H_w), 6.88 – 6.81 (m, 2H, H_b, H_c), 6.74 (d, J = 8.7, 2H, H_D), 6.58 (d, J = 8.7, 2H, H_x), 6.42 (d, J = 8.7, 2H, H_E), 5.94 (d, J = 7.8, 2H, H_M), 5.35 (d, J = 7.5, 2H, H_L), 5.22 – 5.15 (m, 2H, H_e), 4.30 – 4.21 (m, 1H, 1 of H_F), 4.19 – 4.04 (m, 2H, 1 of H_z, 1 of H_F), 3.95 (dd, J = 11.2, 4.5, 1H, H_v), 3.85 (d, J = 13.6, 1H, 1 of H_s), 3.75 – 3.72 (m, 4H, 1 of H_K, H_y), 3.70 – 3.63 (m, 1H, 1 of H_K), 3.63 – 6.56 (m, 1H, 1 of H_z), 3.37 (d, J = 14.4, 1H, 1 of H_t), 3.08 (d, J = 14.4, 1H, 1 of H_t), 2.79 (d, J = 13.7, 1H, 1 of H_s), 2.67 – 2.59 (m, 1H, 1 of H_P), 2.56 (t, J = 6.9, 2H, H_h), 2.54 – 2.38 (m, 1H, 1 of H_P), 2.32 – 2.24 (m, 1H, 1 of H_N), 2.13 – 2.04 (m, 1H, 1 of H_N), 2.04 – 1.97 (m, 1H, 1 of H_G), 1.97 – 1.90 (m, 1H, 1 of H_G), 1.90 – 1.73 (m, 6H, H_J, H_H, H_I), 1.67 – 1.55 (m, 4H, H_i, H_j), 1.49 (q, J = 6.9, 2H, H_O), 1.39 – 1.22 (m, 4H, H_n, H_o), 1.19 – 1.10 (m, 2H, H_k), 1.10 – 1.00 (m, 2H, H_m), 0.81 – 0.68 (m, 2H, H_l).

^{13}C NMR (126 MHz, $CDCl_3$) δ : 163.3, 159.9, 159.59, 158.1, 157.9, 157. 6, 156.8, 143.2, 142.2, 141.6, 138.5, 137.3, 136.9, 136.8, 134.5, 132.0, 131.4, 130.2, 129.1, 128.9, 128.8, 128.8, 128.0, 127.9, 127.2, 126.1, 123.4, 122.8, 120.4, 120.1, 119.8, 116.2, 114.9, 114.2, 113.4, 111.8, 105.2, 69.9, 68.7, 65.3, 62.5, 60.6, 55.3, 52.7, 44.7, 37.2, 36.2, 35.8, 35.1, 33.2, 31.7, 31.6, 30.47, 30.4, 29.7, 29.3, 29.2, 28.8, 28.8, 25.3, 24.8. LR-ESI-MS *m/z* = 1109.64 $[M+H]^+$ calc. 1109.63.

Catenane (*R*,R_{mt})-**275**. ^{1}H NMR (500MHz, $CDCl_3$) δ : 9.66 (s, 1H, H_u), 7.80 (t, J = 7.7, 1H, H_R), 7.68 (t, J = 7.7, 1H, H_B), 7.64 (d, J = 7.8, 1H, H_S), 7.47 (dd, J = 7.8, 0.9, 1H, H_A), 7.42 (brd. s, 1H, H_a), 7.37 (dd, J = 7.8, 0.9, 1H, H_d), 7.24 (d, J = 7.7, 0.9, 1H, H_Q), 7.17 (d, J = 7.7, 2H, H_r), 7.14 – 7.03 (m, 7H, H_C, H_c, H_g, H_q), 6.94 – 6.86 (m, 1H, H_b), 6.87 – 6.76 (m, 6H, H_f, H_w, H_x), 6.25 (d, J = 7.8, 2H, H_M), 6.13 (d, J = 8.2, 4H, H_D or H_E, H_L), 5.94 (d, J = 8.1, 2H, H_D or H_E), 4.82 (d, J = 14.4, 1H, 1 of H_e), 4.62 (d, J = 14.4, 1H, 1 of H_e), 4.28 – 4.18 (m, 1H, 1 of H_K), 4.15 (app. t, J = 10.8, 1H, H_F), 4.10 – 4.00 (m, 2H, 1 of H_z, H_v), 4.00 – 3.93 (m, 2H, 1 of H_K, 1 of H_z), 3.80 (s, 3H, H_y), 3.75 (d, J = 13.8, 1H, H_s), 3.61 (dd, J = 10.5, 4.3, 1H, H_F), 3.25 (d, J = 15.0, 1H, H_t), 3.12 (d, J = 15.0, 1H, H_t), 2.68 – 2.48 (m, 5H, H_P, H_h, 1 of H_s), 2.39 – 2.21 (m, 2H, H_N), 2.05 – 1.75 (m, 8H, H_G, H_H, H_I, H_J), 1.66 – 1.45 (m, 6H, H_O, H_i, H_o), 1.25 – 0.95 (m, 8H, H_j, H_k, H_m, H_n), 0.90 – 0.75 (m, 2H, H_l). ^{13}C NMR (126 MHz, $CDCl_3$) δ 163.3, 159.6, 159.2, 159.08, 157.8, 157.5, 156.9, 156.7, 143.3, 141.9, 141.5, 138.3, 137.3, 136.7, 136.6, 134.3, 131.8, 131.7, 130.1, 129.3, 128.7, 128.5, 128.3, 127.9, 125.8, 122.7, 120.1, 119.7, 119.6, 115.9, 114.9, 114.3, 113.5, 112.8, 106.0, 69.9, 67.8, 66.0, 62.4, 61.1, 55.2, 53.3, 45.2, 35.9, 35.7, 33.0, 31.6, 30.2, 30.1, 29.4, 29.2, 29.0, 28.8, 28.8, 25.2, 24.6. LR-ESI-MS *m/z* = 1109.64 $[M+H]^+$ calc. 1109.63.

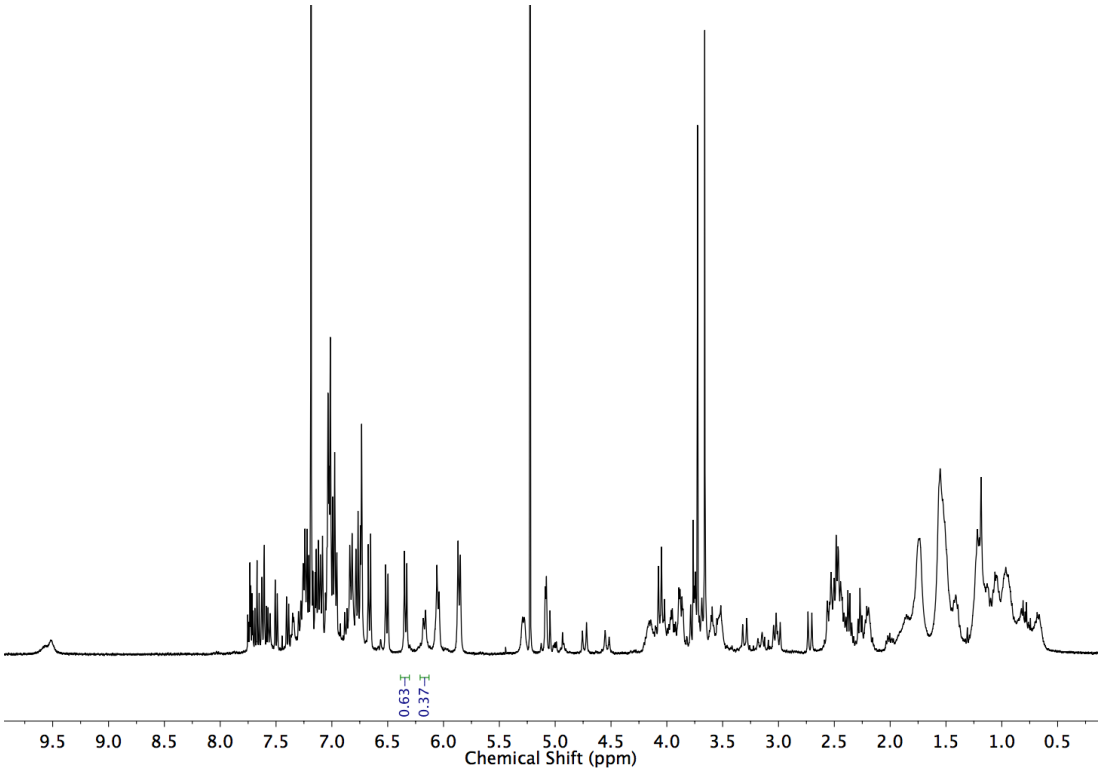

Figure 5.28 ^{1}H NMR (400 MHz, $CDCl_3$) of (R,R/S_{mt})-**275** prior to purification by chormatography.

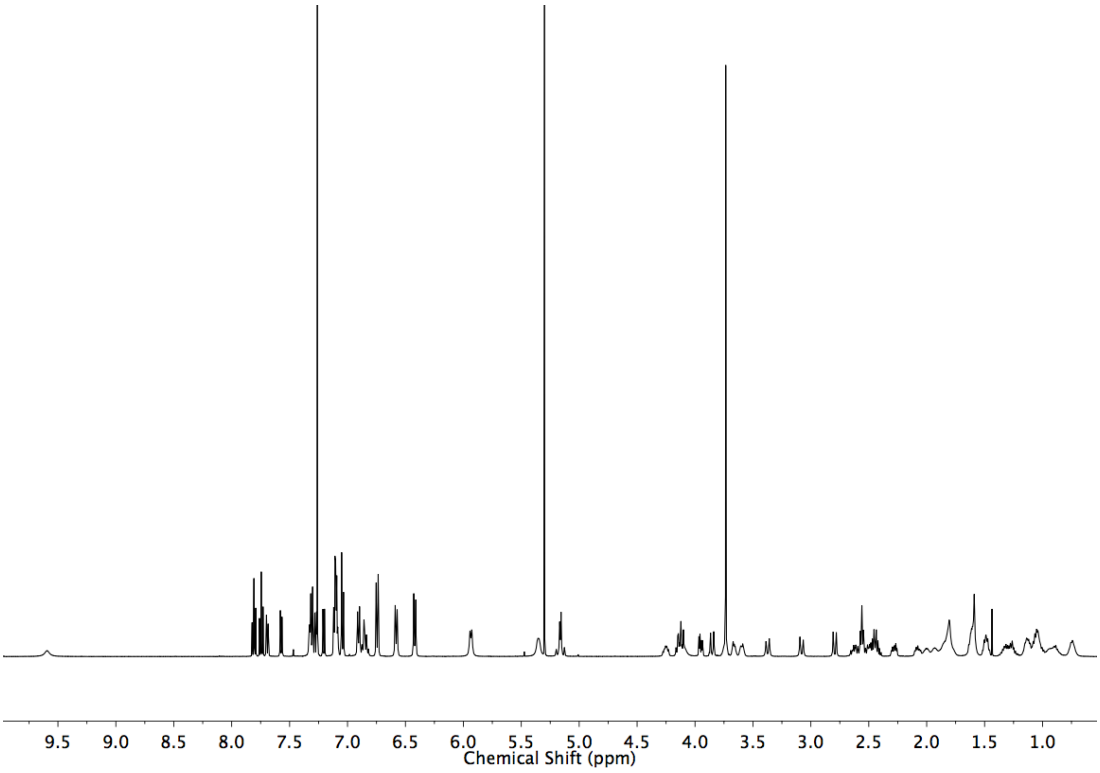

Figure 5.29 ^{1}H NMR (500 MHz, $CDCl_3$) of (R,S_{mt})-**275**.

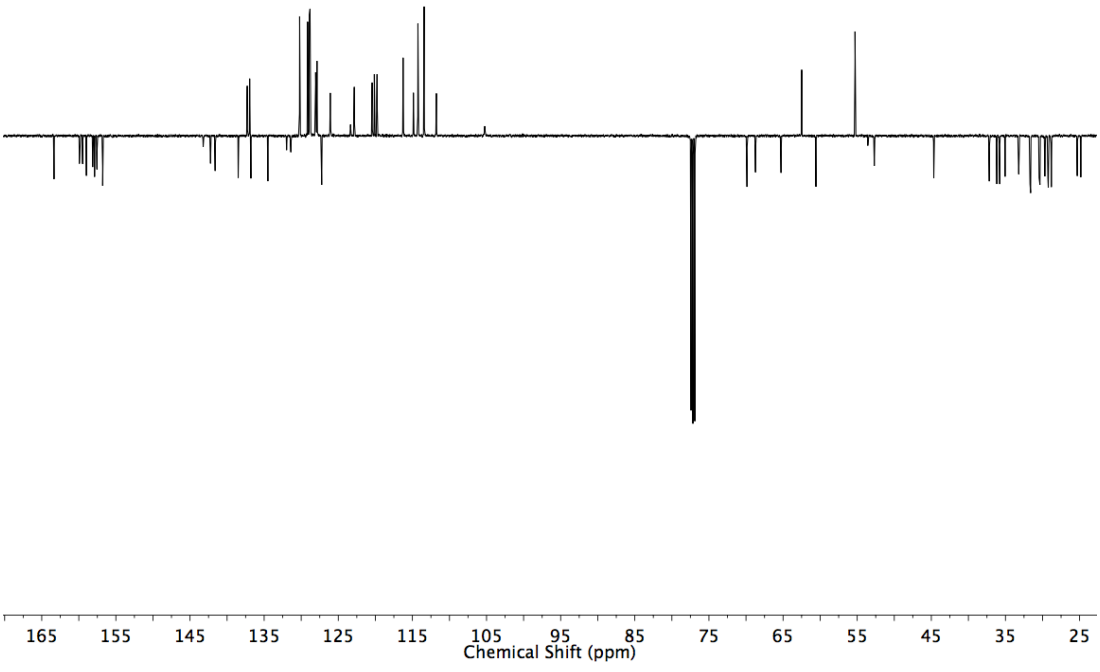

Figure 5.30 JMOD NMR (126 MHz, $CDCl_3$) of (R,S_{mt})-**275**.

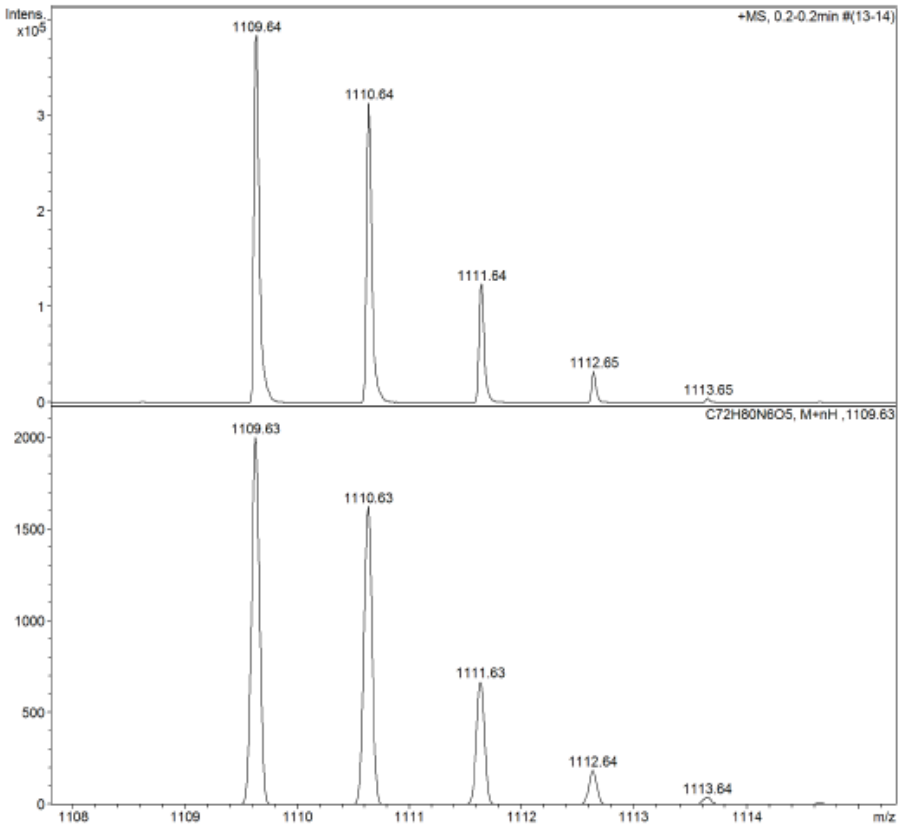

Figure 5.31 Observed (top) and calculated (bottom) isotopic patterns for (*R*,S_{mt})-**275**.

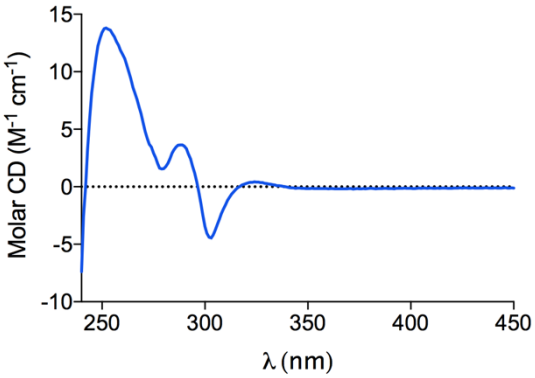

Figure 5.32 Circular dichroism spectrum of (*R*,S_{mt})-**275** (35.0 μM in $CHCl_3$, 293K).

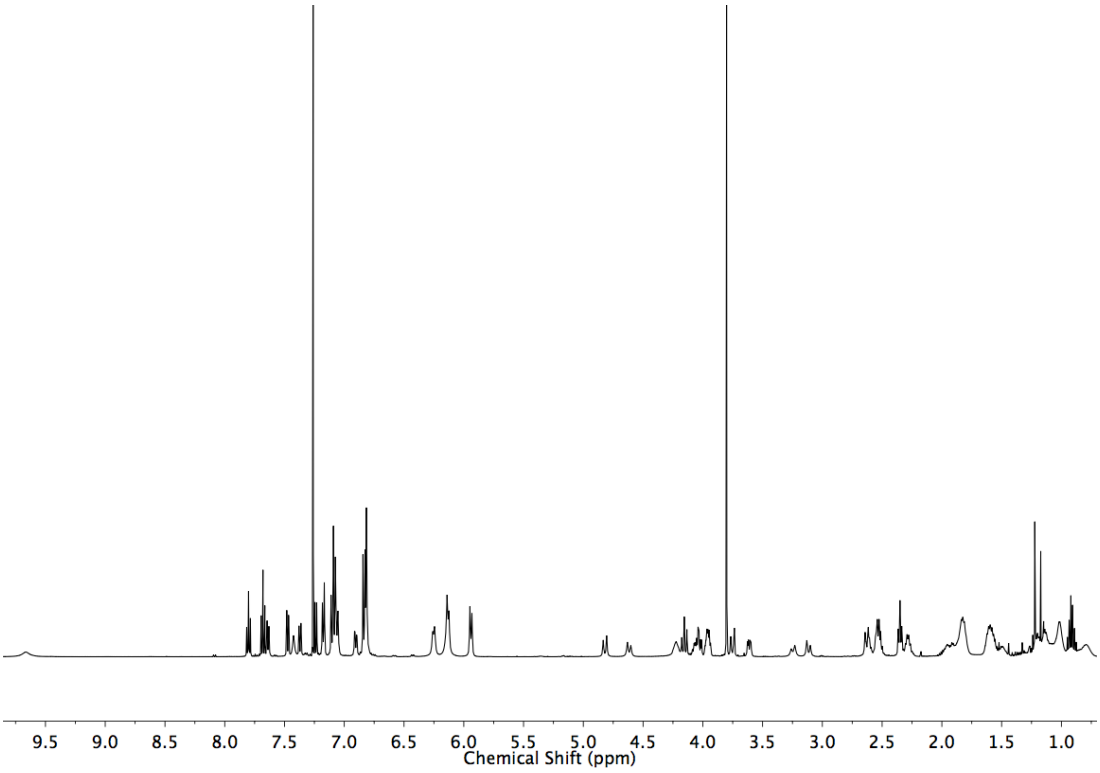

Figure 5.33 ^{1}H NMR (500 MHz, $CDCl_3$) of (R,R_{mt})-**275**.

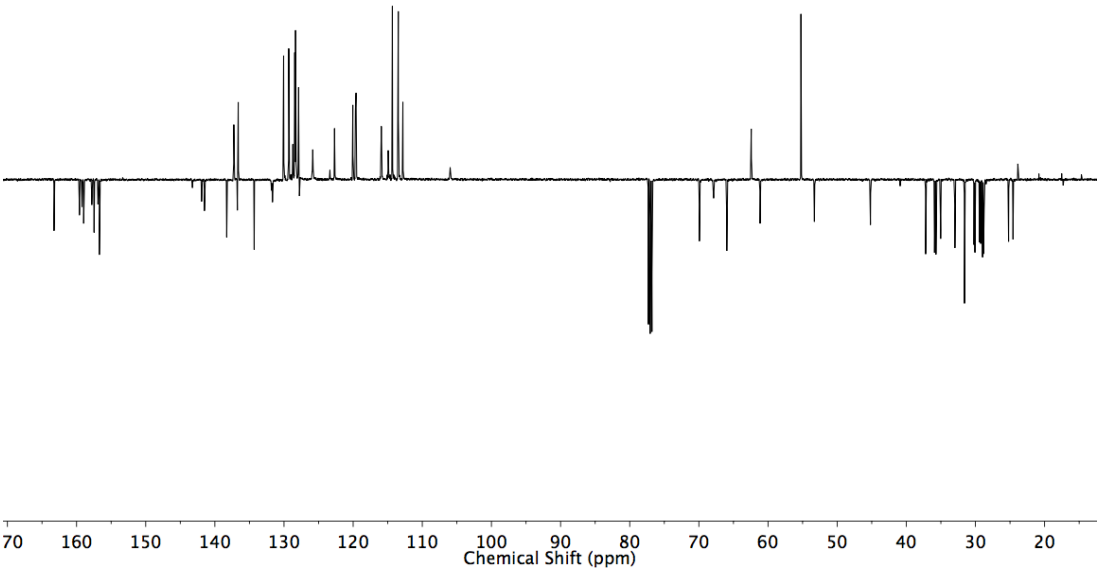

Figure 5.34 JMOD NMR (126 MHz, $CDCl_3$) of (R,R_{mt})-**275**.

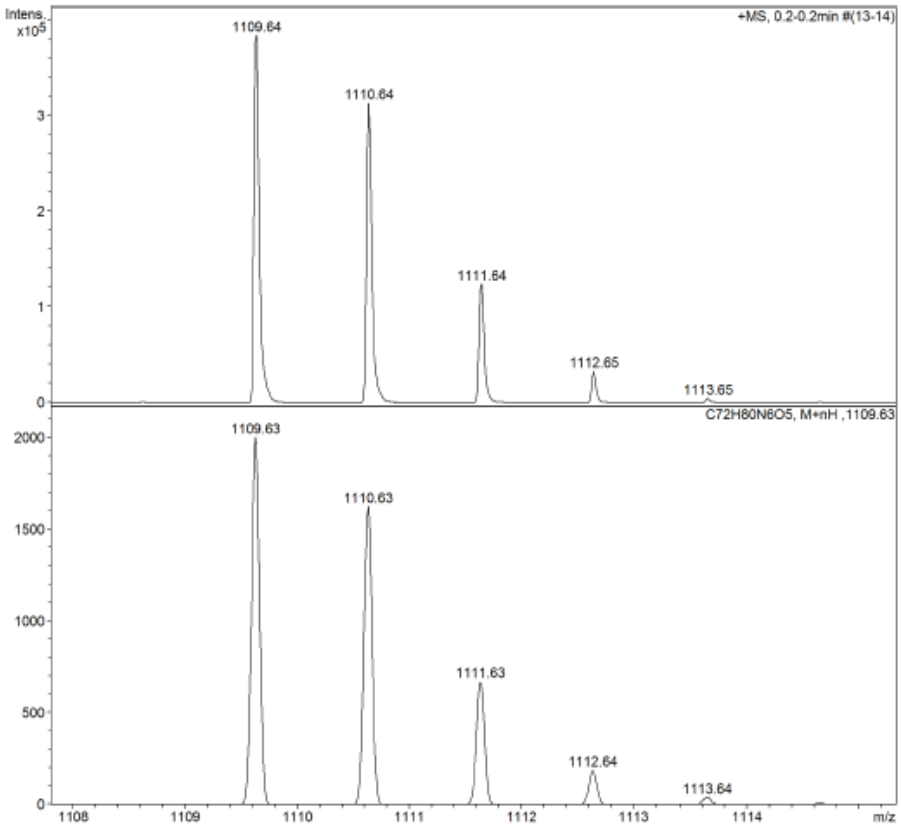

Figure 5.35 Observed (top) and calculated (bottom) isotopic patterns for (R,R_{mt})-**275**.

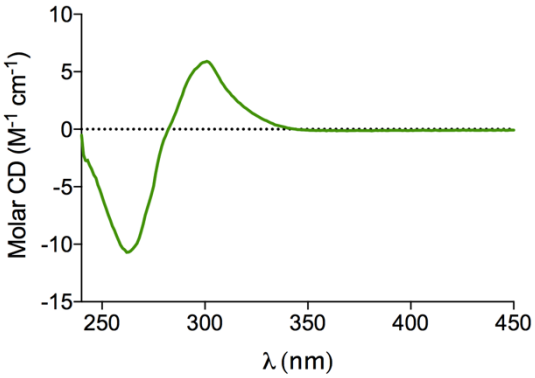

Figure 5.36 Circular dichroism spectrum of (R,R_{mt})-**275** (35.0 μM in $CHCl_3$, 293K).

*Catenanes (S,S_{mt})-**275** and (S,R_{mt})-**275***

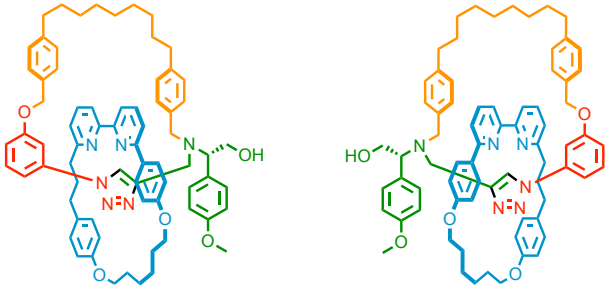

(S,S_{mp})-**275** (S,R_{mp})-**275**

To a solution of **274** (288 mg, 0.62 mmol, 1.0 eq.), $[Cu(CH_3CN)_4]PF_6$ (228 mg, 0.61 mmol, 1.0 eq.), $^{i}Pr_2NEt$ (218 µL, 1.24 mmol, 2 eq.) in 1:1 $CHCl_3$/EtOH (25 mL) at 60 °C was added *S*-**263** (400 mg, 0.62 mmol, 1.2 eq.) in 1:1 $CHCl_3$/EtOH (24 mL) over 4 h. After removal of the solvent *in vacuo*, the residue was dissolved in 1:1 CH_2Cl_2/MeOH (20 mL) and KCN (320 mg, 5 mmol, 8 eq.) added as a solid. After stirring at rt for 30 minutes the solvent was removed under a flow of air. The residue was dissolved in CH_2Cl_2 (100 mL) and washed with H_2O (4 × 20 mL), dried ($MgSO_4$) and the solvent removed *in vacuo*. The residue containing catenane ($S,R/S_{mt}$)-**275** (in a 0.67:0.33 diastereoisomeric ratio) was purified by column chromatography on silica (Petrol/CH_2Cl_2/AcOEt/Et_2O 140/30/15/15), to yield (S,R_{mt})-**275** (300 mg, 44%) and (S,S_{mt})-**275** (200 mg, with 3% of (S,R_{mt})-**275**, 30%) as a white foams. Spectroscopic data were identical to those reported for (S,R_{mt})-**275** and (S,S_{mt})-**275** with the exception of the circular dichroism spectra.

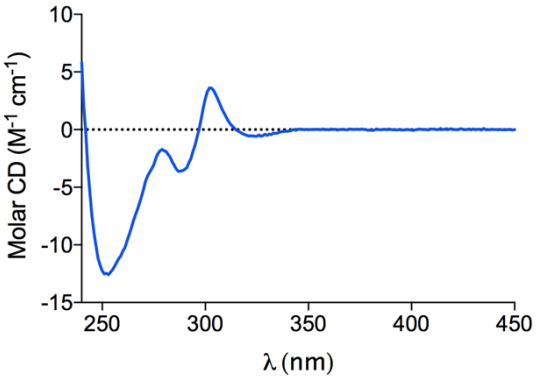

Figure 5.37 Circular dichroism spectrum of (S,R_{mt})-**275** (35.0 µM in $CHCl_3$, 293K).

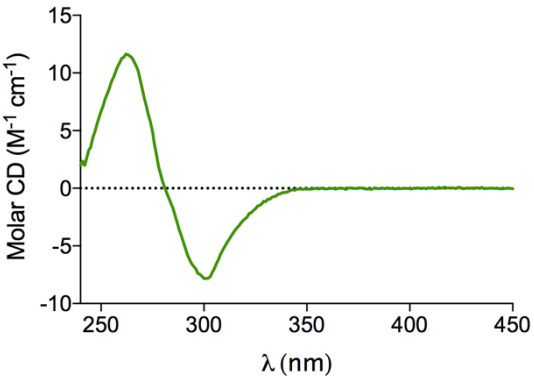

Figure 5.38 Circular dichroism spectrum of (*S*,S_{mt})-**275** (35.0 μM in $CHCl_3$, 293K).

*Catenanes R,R/S$_{mt}$-**268***

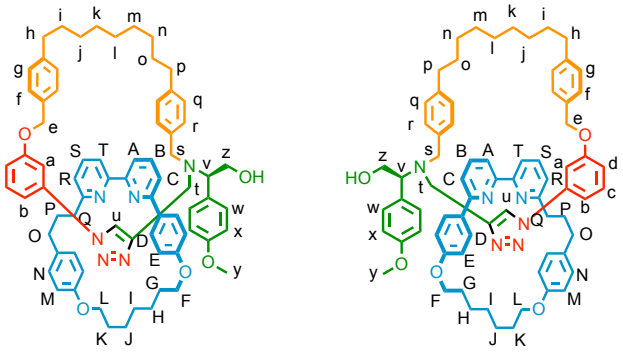

(R,S_{mp})-**268** (R,R_{mp})-**268**

To a solution of **92** (24.1 mg, 0.050 mmol, 1 eq.), $[Cu(CH_3CN)_4]PF_6$ (18.5 mg, 0.0495 mmol, 0.99 eq.), $^{i}Pr_2NEt$ (18 µL, 0.10 mmol, 2 eq.) in 1:1 $CHCl_3$/EtOH (5.0 mL) at 60 °C was added *R*-**263** (40.0 mg, 0.060 mmol, 1.2 eq.) in 1:1 $CHCl_3$/EtOH (2.4 mL) over 4 h. After removal of the solvent *in vacuo*, the residue was dissolved in 1:1 CH_2Cl_2/MeOH (2.5 mL) and KCN (16 mg, 0.25 mmol, 5 eq.) added as a solid. After stirring at rt for 30 minutes the solvent was removed under a flow of air. The residue was dissolved in CH_2Cl_2 (5 mL) and washed with H_2O (4 × 5 mL), dried ($MgSO_4$) and the solvent removed *in vacuo*. After purification by column chromatography on silica (Petrol with a gradient of 0 to 100% Et_2O over 10 CVs) (R,R/S_{mt})-**268** was obtained as a white foam (40.1 mg, 72%, 1 : 1 diastereoisomeric ratio determined by ^{1}H NMR). ^{1}H NMR (400 MHz, $CDCl_3$) δ: 9.24 (s, 1H H_u), 9.19 (s, 1H , $H_{u'}$), 7.82 (t, J = 7.8, 1H, H_S), 7.79 (t, J = 7.8, 1H, $H_{S'}$), 7.74 (t, J = 7.8, 1H, H_B), 7.71 – 7.63 (m, 3H, $H_{B'}$, H_T, $H_{T'}$), 7.57 (dd, J = 7.8, 0.9, 1H, H_A), 7.49 (dd, J = 7.8, 0.9, 1H, $H_{A'}$), 7.40 – 7.32 (m, 3H, H_a or $H_{a'}$ or H_b or $H_{b'}$ or H_c or $H_{c'}$ or H_d or $H_{d'}$), 7.28 – 7.02 (m, 24H, H_C, $H_{C'}$, H_R, $H_{R'}$, H_r, $H_{r'}$, H_w, H_f, H_q, $H_{q'}$, H_a or $H_{a'}$ or H_b or $H_{b'}$ or H_c or $H_{c'}$ or H_d or $H_{d'}$), 7.01 – 6.95 (m, 3H, H_g, H_a or $H_{a'}$ or H_b or $H_{b'}$ or H_c or $H_{c'}$ or H_d or $H_{d'}$), 6.95 – 6.87 (m, 3H, $H_{w'}$, H_a or $H_{a'}$ or H_b or $H_{b'}$ or H_c or $H_{c'}$ or H_d or $H_{d'}$), 6.82 (d, J = 8.7, 2H, H_x), 6.76 (s, 4H, $H_{f'}$, $H_{g'}$), 6.71 (d, J = 8.7, 2H, H_D or $H_{D'}$ or H_N or $H_{N'}$), 6.71 (d, J = 8.7, 2H, $H_{x'}$), 6.28 (d, J = 8.5, 2H, H_D or $H_{D'}$ or H_N or $H_{N'}$), 6.21 (d, J = 8.7, 2H, H_E or $H_{E'}$ or H_M or $H_{M'}$), 6.17 (d, J = 8.3 Hz, 2H, H_q or $H_{q'}$ or H_r or $H_{r'}$), 6.02 (d, J = 8.7, 4H, H_E or $H_{E'}$ or H_M or $H_{M'}$), 5.93 (d, J = 8.3 Hz, 2H, H_q or $H_{q'}$ or H_r or $H_{r'}$), 5.53 (d, J = 8.7, 4H, H_E or $H_{E'}$ or H_M or $H_{M'}$), 5.12 – 4.96 (m, 2H, H_e), 4.80 (d, J = 14.4, 1H, $H_{e'}$), 4.57 (d, J = 14.4, 1H, $H_{e'}$), 4.21 – 3.82 (m, 8H, H_v, $H_{v'}$, H_z, $H_{z'}$, H_F or $H_{F'}$ or H_L or $H_{L'}$), 3.79 (s, 3H, H_y), 3.76 (s, 3H, $H_{y'}$), 3.75 – 3.50 (m, 6H, 1 of H_s, 1 of $H_{s'}$, H_F or $H_{F'}$ or H_L or $H_{L'}$), 3.41 (d, J = 14.4, 1H, 1 of $H_{t'}$), 3.18 (d, J = 14.4, 1H, 1 of H_t), 3.01 (d, J = 14.4, 1H, 1 of H_t), 2.99 (d, J = 14.4, 1H, 1 of $H_{t'}$), 2.86 (d, J = 14.4, 1H, 1 of $H_{s'}$), 2.70 – 2.38 (m, 5H,

H_h, $H_{h'}$, 1 of H_s), 1.96 – 1.78 (m, 8H, H_G, $H_{G'}$, H_K, $H_{K'}$), 1.76 – 1.48 (m, 12H, H_H, $H_{H'}$, H_J, $H_{J'}$, H_i, $H_{i'}$), 1.29 – 1.20 (m, 2H, $H_{i'}$), 1.13 – 0.95 (m, 8H, H_l, $H_{l'}$, H*j*, $H_{j'}$), 0.78 – 0.68 (m, 4H, H_l, $H_{l'}$).

^{13}C NMR (101 MHz, $CDCl_3$) δ 163.6, 163.5, 159.5, 159.3, 159.1, 159.0, 158.6, 158.2, 157.9, 157.8, 157.6, 157.1, 156.7, 156.6, 144.0, 143.7, 142.3, 142.1, 141.6, 141.5, 138.4, 138.3, 137.3, 137.2, 137.0, 136.9, 136.8, 136.7, 134.5, 134.4, 131.6, 131.5, 131.4, 131.3, 130.2, 130.1, 129.3, 129.1, 128.9, 128.9, 128.8, 128.7, 128.6, 128.5, 128.4, 128.2, 128.1, 128.1, 127.5, 126.7, 126.1, 122.7, 122.6, 122.6, 122.4, 120.1, 119.9, 119.8, 119.8, 119.7, 119.6, 115.1, 114.7, 114.5, 114.3, 113.8, 113.7, 113.6, 113.5, 112.7, 112.0, 106.1, 105.7, 68.8, 68.0, 67.6, 67.4, 65.2, 65.1, 62.9, 62.7, 61.4, 60.9, 55.4, 55.3, 53.5, 53.4, 44.9, 44.3, 41.0, 37.3, 36.1, 36.0, 35.7, 35.2, 35.1, 33.4, 33.2, 31.7, 31.7, 31.6, 31.6, 30.4, 30.3, 30.2, 29.4, 29.3, 29.2, 29.1, 29.0, 29.0, 28.9, 28.7, 28.6, 28.2, 28.1, 26.1, 26.0, 26.0, 25.9. LR-ESI-MS *m/z* = 1123.6 $[M+H]^+$ calc. 1123.6.

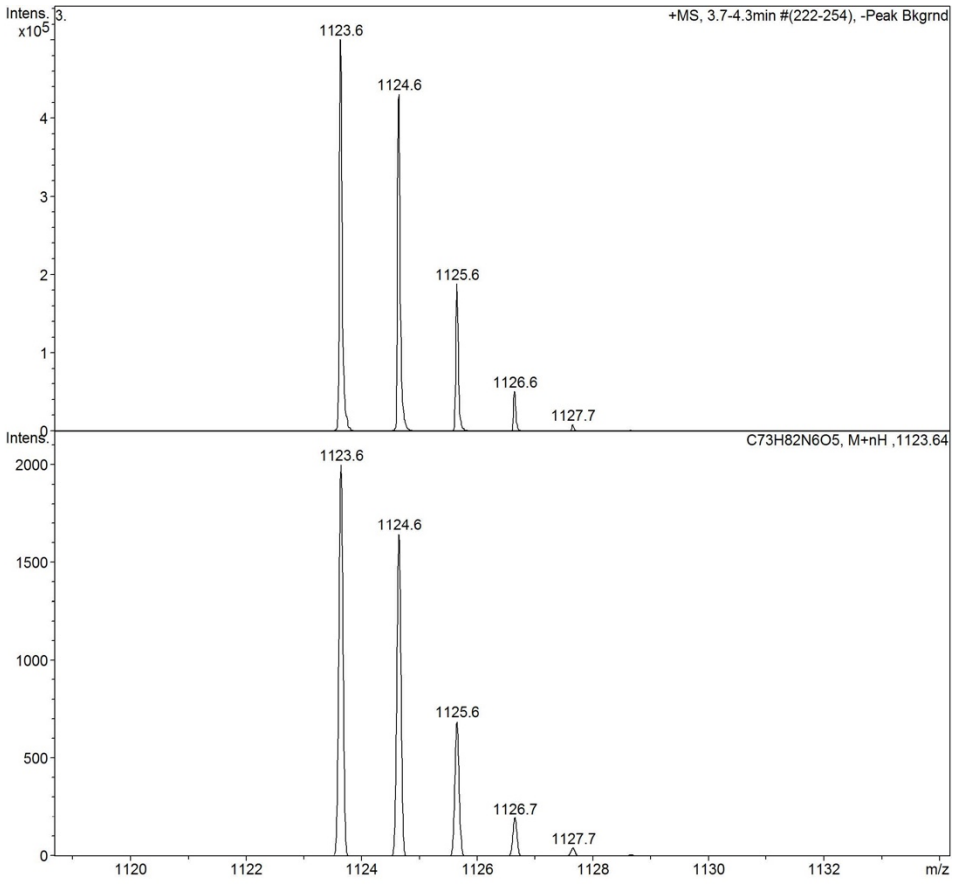

Figure 5.39 Observed (top) and calculated (bottom) isotopic patterns for (*R*,*S*/R_{mt})-**268**.

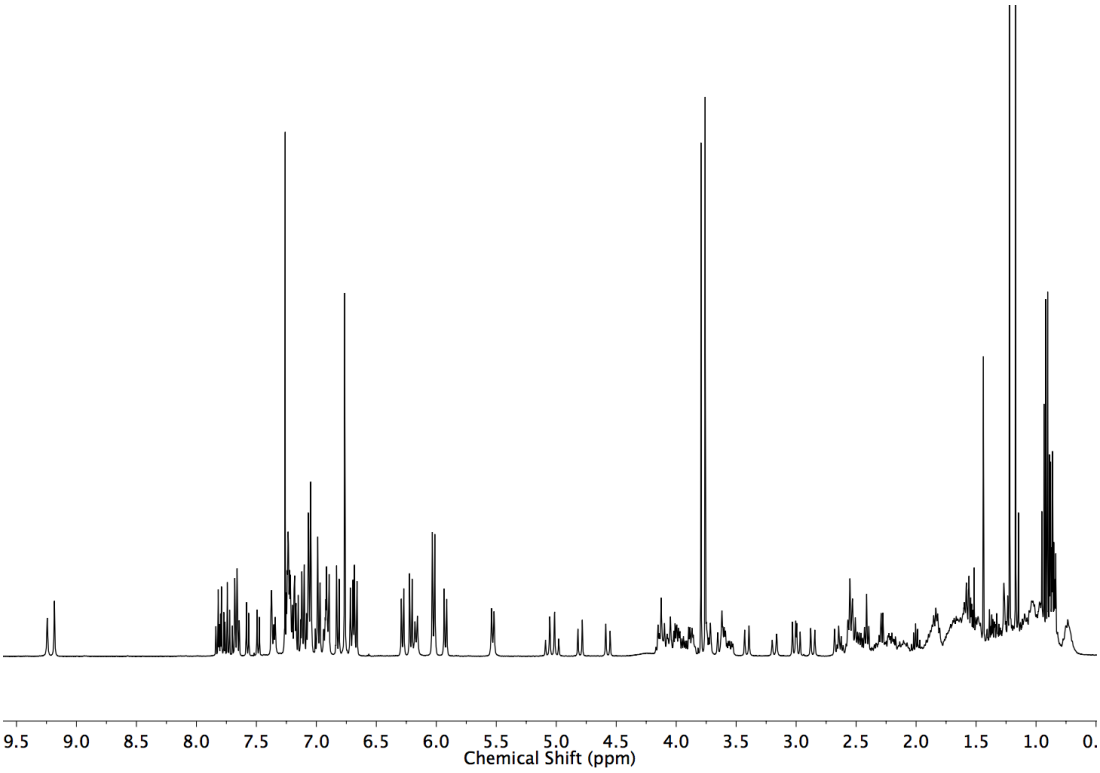

Figure 5.40 ^{1}H NMR (400 MHz, $CDCl_3$) of (R,S/R_{mt})-**268**.

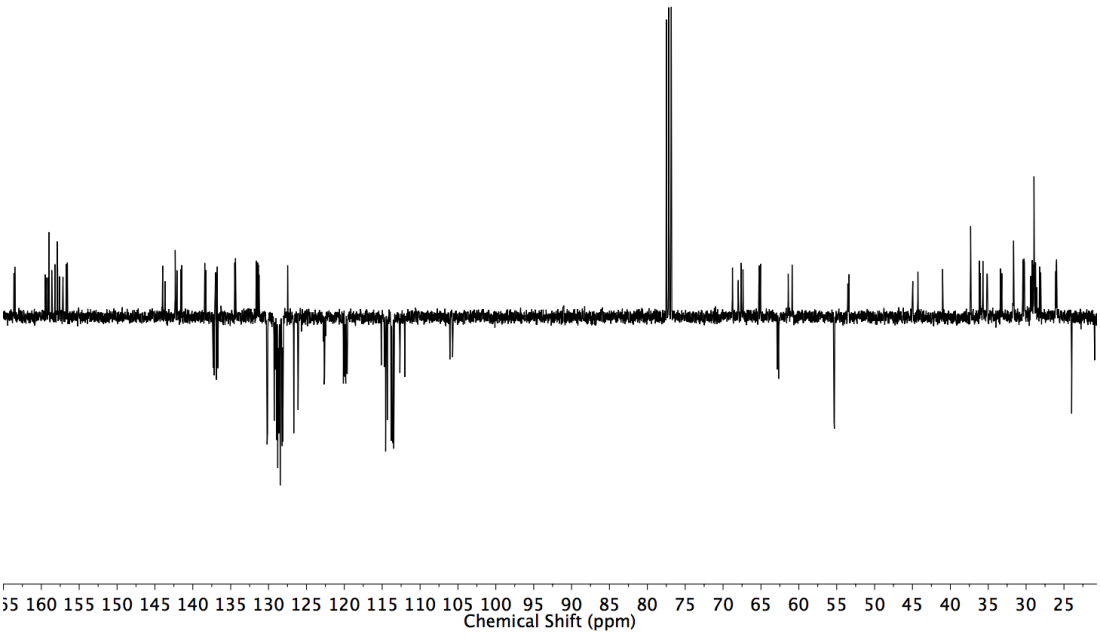

Figure 5.41 JMOD NMR (101 MHz, $CDCl_3$) of (R,S/R_{mt})-**268**.

*Catenanes R,R/S$_{mt}$-**269***

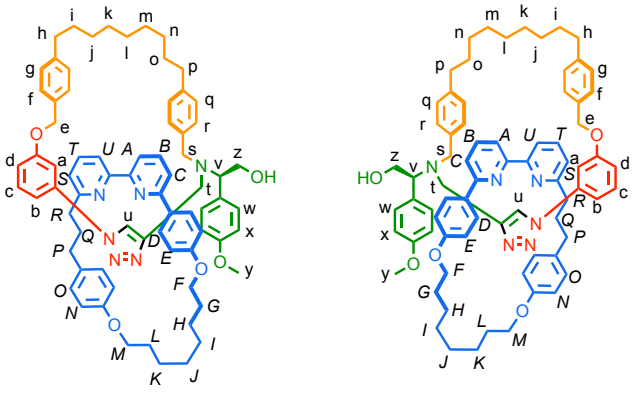

(*R*,*S*$_{mp}$)-**269** (*R*,*R*$_{mp}$)-**269**

To a solution of **267** (21.0 mg, 0.042 mmol, 1 eq.), $[Cu(CH_3CN)_4]PF_6$ (15.1 mg, 0.041 mmol, 0.98 eq.), $^{i}Pr_2NEt$ (18 µL, 0.10 mmol, 2.4 eq.) in 1:1 $CHCl_3$/EtOH (4.2 mL) at 60 °C was added *R*-**263** (38.0 mg, 0.059 mmol, 1.5 eq.) in 1:1 $CHCl_3$/EtOH (2.4 mL) over 4 h. After removal of the solvent *in vacuo*, the residue was dissolved in 1:1 CH_2Cl_2/MeOH (2.5 mL) and KCN (16 mg, 0.25 mmol, 5 eq.) added as a solid. After stirring at rt for 30 minutes the solvent was removed under a flow of air. The residue was dissolved in CH_2Cl_2 (5 mL) and washed with H_2O (4 × 5 mL), dried ($MgSO_4$) and the solvent removed *in vacuo*. After purification by column chromatography on silica (Petrol with a gradient of 0 to 100% Et_2O over 10 CVs) (*R*,*R*/*S*$_{mt}$)-**269** was obtained as a white foam (39.0 mg, 82%, 1 : 1 diastereoisomeric ratio determined by ^{1}H NMR). ^{1}H NMR (400 MHz, $CDCl_3$) δ: 8.83 (s, 1H, H$_u$), 8.78 (s, 1H, H$_{u'}$), 7.72-7.64 (m, 3H, H$_T$, H$_{T'}$, H$_B$ or H$_{B'}$), 7.59 (t, *J* = 7.8, 1H, H$_B$ or H$_{B'}$), 7.54 (dd, *J* = 7.8, 1.0, 1H, H$_A$ or H$_{A'}$ or H$_U$ or H$_{U'}$), 7.48 (dd, *J* = 7.8, 1.3, 2H, H$_A$ or H$_{A'}$ or H$_U$ or H$_{U'}$), 7.37 (dd, *J* = 7.8, 0.9, 1H, H$_A$ or H$_{A'}$ or H$_U$ or H$_{U'}$), 7.27-7.20 (m, 3H, H$_C$ or H$_{C'}$ or H$_S$ or H$_{S'}$), 7.17 – 6.88 (m, 26H,H$_a$, H$_{a'}$, H$_b$, H$_{b'}$, H$_c$, H$_{c'}$, H$_d$, H$_{d'}$, H$_f$, H$_g$, H$_{g'}$, H$_q$, H$_{q'}$, H$_r$, H$_{r'}$, H$_w$, H$_C$ or H$_{C'}$ or H$_S$ or H$_{S'}$), 6.87-6.77 (m, 6H, H$_D$ or H$_{D'}$ or H$_O$ or H$_{O'}$, H$_{f'}$, H$_{w'}$), 6.74 (d, *J* = 8.8, 2H, H$_x$), 6.63 (d, *J* = 8.8, 2H, H$_{x'}$), 6.54 (d, *J* = 8.7, 2H, H$_D$ or H$_{D'}$ or H$_O$ or H$_{O'}$), 6.19 (dd, *J* = 8.7, 2.3, 4H, H$_D$ or H$_{D'}$ or H$_O$ or H$_{O'}$, H$_E$ or H$_{E'}$ or H$_N$ or H$_{N'}$), 6.02 (dd, *J* = 11.7, 8.7, 4H, H$_D$ or H$_{D'}$ or H$_O$ or H$_{O'}$, H$_E$ or H$_{E'}$ or H$_N$ or H$_{N'}$), 5.91 (d, *J* = 8.7, 2H, H$_E$ or H$_{E'}$ or H$_N$ or H$_{N'}$), 5.64 (d, *J* = 8.5, 2H, H$_E$ or H$_{E'}$ or H$_N$ or H$_{N'}$), 5.02-4.88 (m, 2H, H$_e$), 4.78 (d, *J* = 13.9, 1H, H$_{e'}$), 4.65 (d, *J* = 13.9, 1H, H$_{e'}$), 4.00-3.77 (m, 7H, H$_v$, 1 of H$_z$, 1 of H$_{z'}$, 1 of H$_F$, 1 of H$_{F'}$, 1 of H$_M$, 1 of H$_{M'}$), 3.77-3.65 (m, 7H, H$_{v'}$, H$_y$, H$_{y'}$), 3.65-3.48 (m, 6H, 1 of H$_s$, 1 of H$_{s'}$, 1 of H$_F$, 1 of H$_{F'}$, 1 of H$_M$, 1 of H$_{M'}$), 3.49 – 3.36 (m, 2H, 1 of H$_z$, 1 of H$_{z'}$), 3.28 (dd, *J* = 14.3, 3.5, 2H, 1 of H$_t$, 1 of H$_{t'}$), 2.94 (dd, *J* = 14.5, 5.9 Hz, 2H, 1 of H$_t$, 1 of H$_{t'}$), 2.74 (d, *J* = 14.2, 1H, 1 of H$_s$), 2.63 (d, *J* = 13.7, 1H, 1 of H$_{s'}$), 2.57-2.05 (m, 16H, H$_h$, H$_{h'}$, H$_p$, H$_{p'}$, H$_P$, H$_{P'}$, H$_R$, H$_{R'}$), 1.81-1.61 (m, 8H, H$_G$, H$_{G'}$, H$_L$, H$_{L'}$), 1.60-0.65 (m, 46H, H$_i$, H$_{i'}$, H$_j$, H$_{j'}$, H$_k$, H$_{k'}$, H$_l$, H$_{l'}$, H$_m$, H$_{m'}$, H$_n$, H$_{n'}$, H$_o$, H$_{o'}$, H$_H$, H$_{H'}$, H$_I$, H$_{I'}$,

H_J, $H_{J'}$, H_K, $H_{K'}$, H_Q, $H_{Q'}$). ^{13}C NMR (101 MHz, $CDCl_3$) δ 163.2, 163.2, 159.1, 159.0, 159.0, 158.9, 158.9, 158.8, 158.3, 158.2, 157.8, 157.8, 157.7, 157.5, 156.7, 156.6, 144.6, 144.4, 142.4, 142.2, 141.4, 141.2, 138.4, 138.2, 136.9, 136.8, 136.8, 136.6, 136.6, 136.5, 134.4, 134.4, 131.8, 131.6, 131.3, 131.3, 130.2, 130.1, 129.2, 129.1, 129.1, 128.8, 128.7, 128.6, 128.5 (× 4C), 128.3, 128.2, 128.1, 127.5, 127.3, 126.8, 126.3, 122.3, 122.2, 122.2, 122.1, 120.0, 119.9, 119.8, 119.7, 119.6, 114.7, 114.2, 114.2, 114.2, 113.7, 113.6, 113.4, 113.4, 112.5, 112.2, 106.7, 106.4, 76.7, 68.8, 68.5, 67.6, 67.5, 66.2, 66.1, 62.5, 62.3, 61.0, 60.7, 55.2, 55.2, 53.5, 53.3, 44.8, 44.4, 37.4, 37.4, 35.9, 35.9, 35.6, 35.6, 35.0, 34.9, 32.3, 32.1, 31.6, 31.5 (× 2C), 31.4, 30.3, 30.2, 30.2 (× 2C), 29.1, 29.1 (× 2C), 29.0, 28.9 (× 2C), 28.8, 28.7, 28.6, 28.6, 28.5 (× 5C), 25.8, 25.8, 25.6, 25.6. LR-ESI-MS *m/z* = 1137.3 $[M+H]^+$ calc. 1137.7.

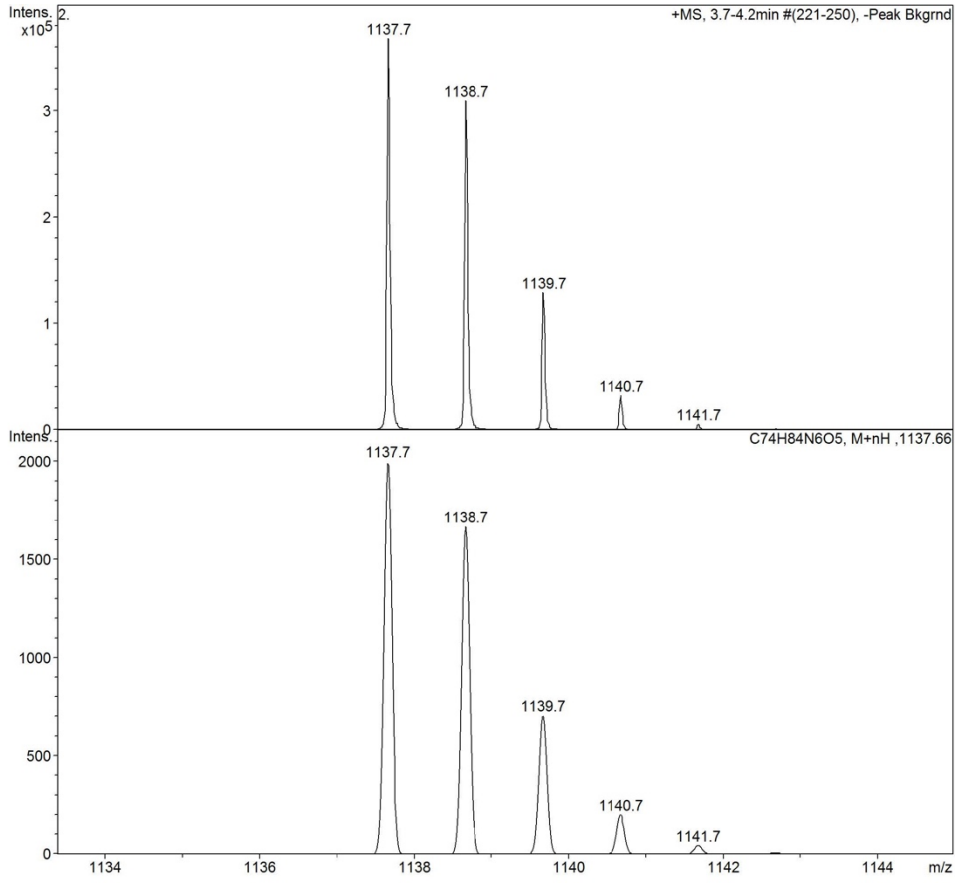

Figure 5.42 Observed (top) and calculated (bottom) isotopic patterns for (*R*, *S*/R_{mt})-**269**.

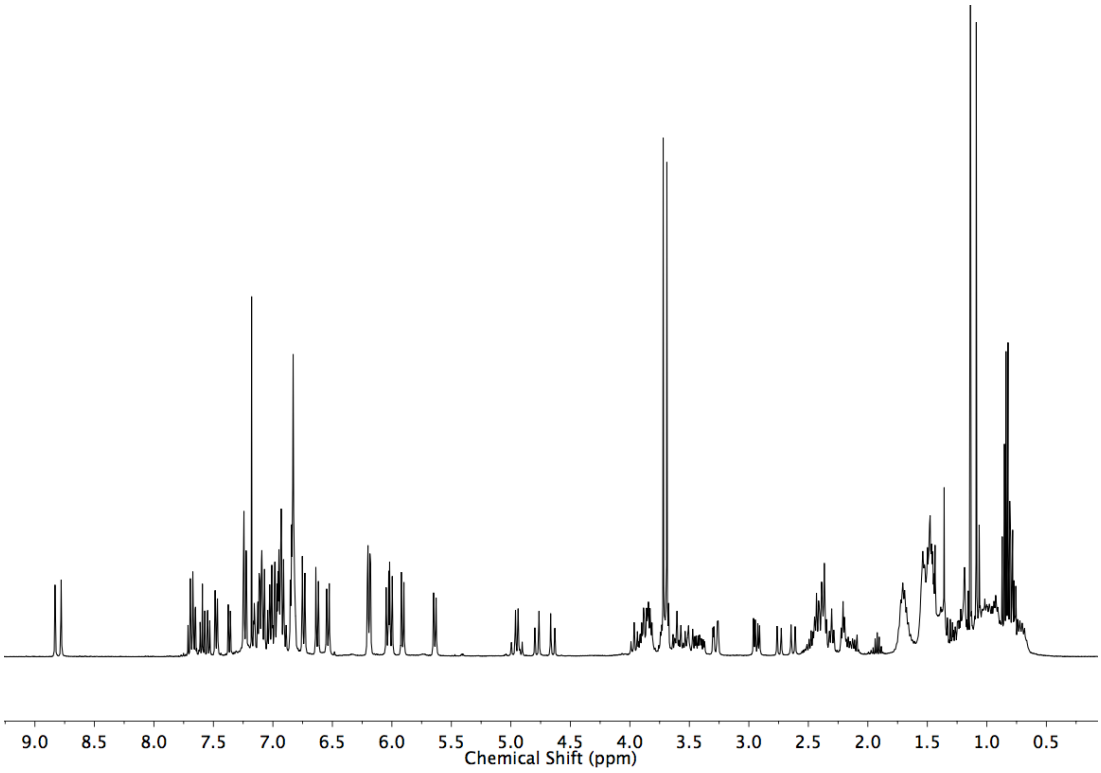

Figure 5.43 ^{1}H NMR (400 MHz, $CDCl_3$) of (R,S/R_{mt})-**269**.

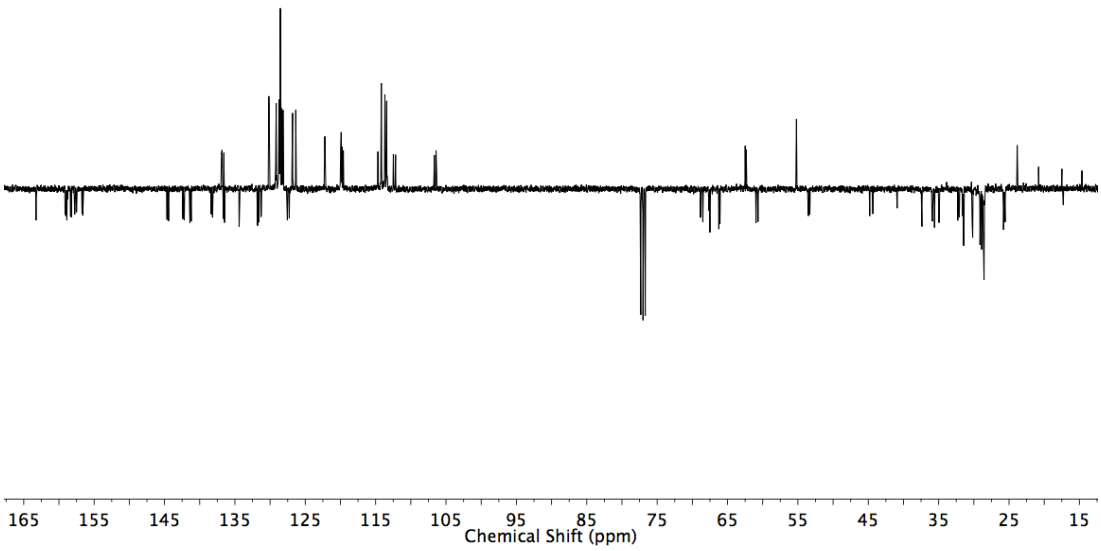

Figure 5.44 JMOD NMR (101 MHz, $CDCl_3$) of (R,S/R_{mt})-**269**.

*Catenane rac-**276***

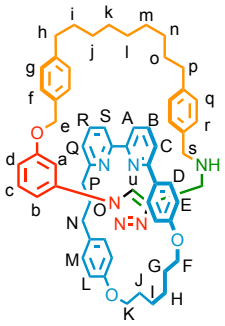

(S_{mp})-**3b**

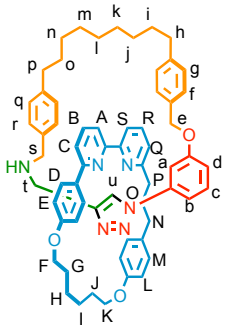

(R_{mp})-**3b**

To a solution of **274** (23.2 mg, 0.050 mmol, 1 eq.), $[Cu(CH_3CN)_4]PF_6$ (18.5 mg, 0.0495 mmol, 0.99 eq.), $^{i}Pr_2NEt$ (18 µL, 0.10 mmol, 2 eq.) in 1:1 $CHCl_3$/EtOH (5.0 mL) at 60 °C was added **265** (24.0 mg, 0.060 mmol, 1.2 eq.) in 1:1 $CHCl_3$/EtOH (2.4 mL) over 4 h. After removal of the solvent *in vacuo*, the residue was dissolved in 1:1 CH_2Cl_2/MeOH (2.5 mL) and KCN (16 mg, 0.25 mmol, 10 eq.) added as a solid. After stirring at rt for 30 minutes the solvent was removed under a flow of air. The residue was dissolved in CH_2Cl_2 (5 mL) and washed with H_2O (4 × 5 mL), dried ($MgSO_4$) and the solvent removed *in vacuo*. After purification by column chromatography on silica (CH_2Cl_2 with a gradient of 0 to 50% AcOEt) *rac*-**276** was obtained as a white foam (33.0 mg, 70%). ^{1}H NMR (500 MHz, $CDCl_3$) δ : 9.29 (s, 1H, H_u), 7.56 (t, *J* = 7.8 Hz, 1H, H_R), 7.43-7.36 (m, 2H, H_B, H_a or H_b or H_c or H_d), 7.30 (m, 1H, H_a or H_b or H_c or H_d), 7.23 (dd, *J* = 5.1, 3.5 Hz, 1H, H_A), 7.21-7.12 (m, 3H, H_C, H_Q, H_S), 7.03-6.96 (m, 5H, H_q, H_r, H_a or H_b or H_c or H_d), 6.90 (d, *J* = 7.6 Hz, 2H, H_f), 6.88-6.83 (m, 2H, H_a or H_b or H_c or H_d), 6.79 (d, *J* = 8.0 Hz, 2H, H_g), 6.68 (d, *J* = 6.6 Hz, 2H, H_D), 6.44 (d, *J* = 7.9 Hz, 2H, H_M), 6.40 (d, *J* = 8.7 Hz, 2H, H_E), 6.33 (d, *J* = 8.7 Hz, 2H, H_L), 4.71 (m, 2H, H_e), 4.21-4.02 (m, 4H, H_F, H_K), 3.45 (d, *J* = 11.6 Hz, 1H, 1 of H_s), 3.36 (d, *J* = 12.1 Hz, 1H, 1 of H_s), 3.30 (d, *J* = 11.3 Hz, 1H, 1 of H_t), 3.13 (d, *J* = 11.8 Hz, 1H, 1 of H_t), 2.64 (td, *J* = 13.6, 4.9 Hz, 1H, 1 of H_P or H_N), 2.52 (t, *J* = 7.1 Hz, 2H, H_h or H_p), 2.50-2.42 (m, 3H, H_h or H_p), 2.40-2.28 (m, 3H, H_P or H_N), 1.94-1.87 (m, 2H, H_G or H_J), 1.86-1.78 (m, 2H, H_G or H_J), 1.76-1.51 (m, 6H, H_H, H_I, H_O), 1.48-1.31 (m, 4H, H_i, H_o), 1.21-1.04 (m, 8H, H_j, H_k, H_m, H_n), 1.04-0.80 (m, 2H, H_l). ^{13}C NMR (126 MHz, $CDCl_3$) δ 163.0, 159.4, 158.8, 158.8, 157.3, 156.8, 156.7, 142.3, 138.3, 137.0, 136.6, 134.2, 132.5, 129.5, 128.9, 128.5 (× 2C), 128.8, 128.4 (× 2C), 127.9, 127.1, 122.2, 120.3, 120.0, 119.3, 116.1, 114.2, 112.1, 106.7, 105.4, 69.4, 69.3, 66.1, 53.7, 44.9, 36.9, 35.7, 35.5, 35.1, 32.3, 31.7, 31.4, 30.3, 30.2, 29.4, 29.3, 29.2, 28.9, 28.7, 25.3, 24.9. HR-ESI-MS *m/z* = 959.5591 $[M+H]^+$ calc. 959.5582.

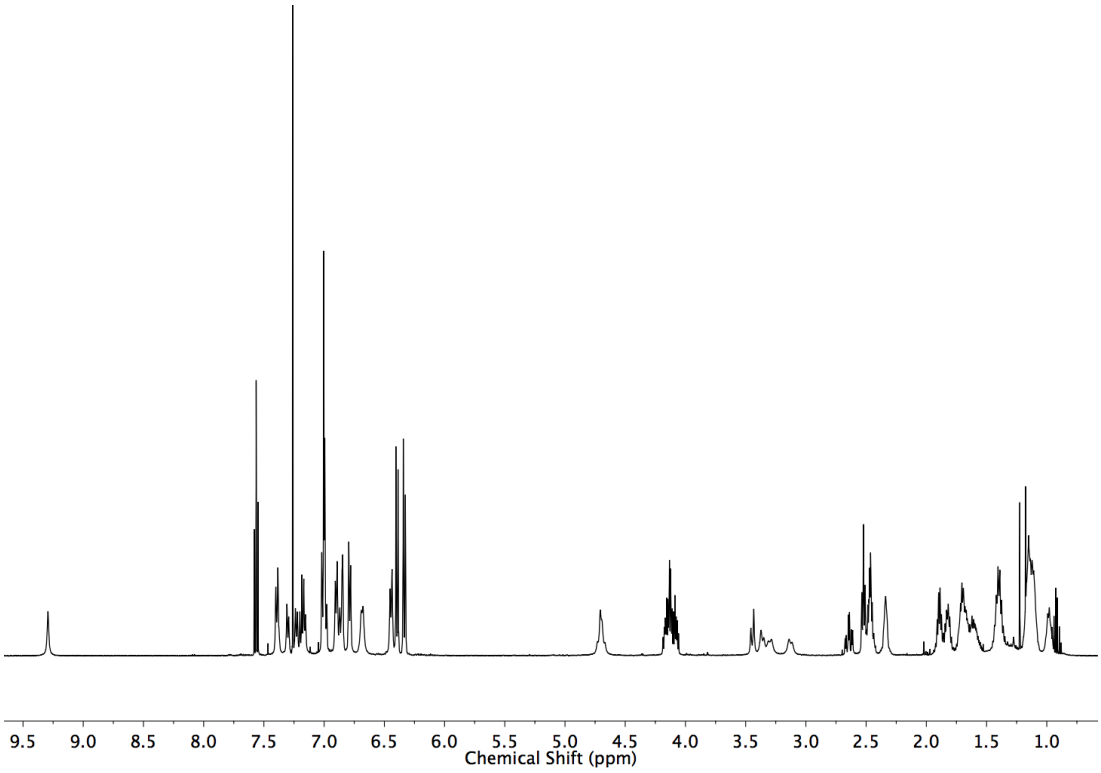

Figure 5.45 ^{1}H NMR (500 MHz, $CDCl_3$) of **276**.

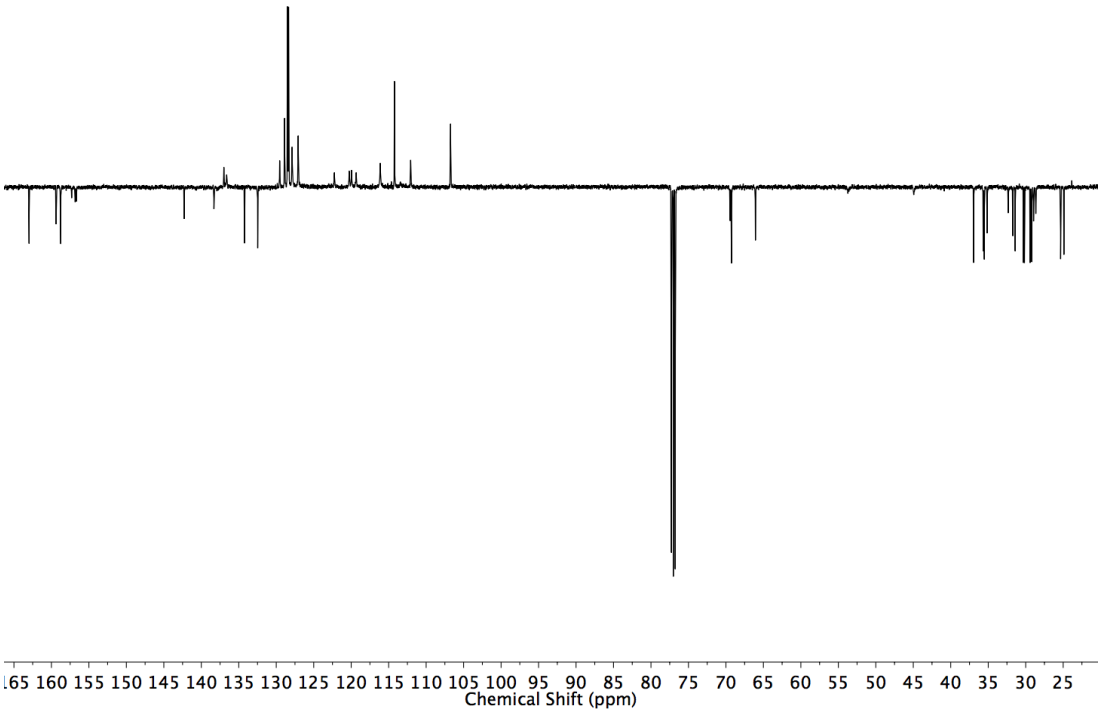

Figure 5.46 JMOD NMR (126 MHz, $CDCl_3$) of **276**.

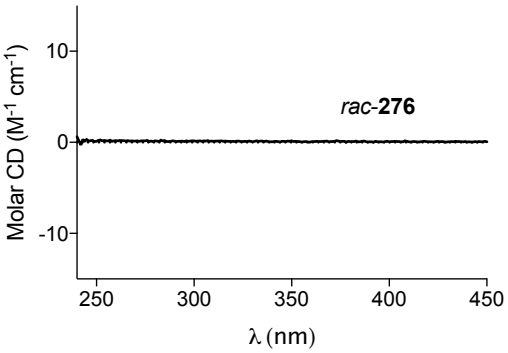

Figure 5.47 Circular dichroism spectrum of *rac*-**276** (43.0 μM in $CHCl_3$, 293K).

*Catenane S_{mt}-**276***

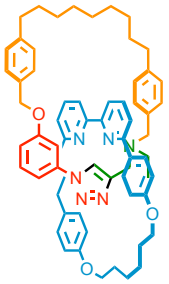

To a solution of oxalyl chloride (140 µl, 1.60 mmol) in dry CH_2Cl_2 (3 mL) at -78 °C was added DMSO (230 µL, 3.25 mmol). The mixture was stirred for 10 minutes at -78 °C before 0.67 mL of the activated DMSO solution was added to (*R,S*$_{mt}$)-**275** (150 mg, 0.135 mmol) in dry CH_2Cl_2 (5 mL) at -78 °C. NEt_3 (91 µL, 0.65 mmol) was added at -78 °C. The mixture was warmed to rt and stirred at rt for 1 h. The reaction mixture was diluted with CH_2Cl_2 (50 mL) and washed with $NaHCO_{3\,(aq)}$ (20 mL), dried ($MgSO_4$) and the solvent removed *in vacuo*. The residue was dissolved in $CHCl_3$ (5 mL), AcOH (1 mL) was added and the mixture was stirred for 3 h at rt. The solvent was removed *in vacuo*. The residue was dissolved in CH_2Cl_2 (100 mL) and washed with $NaHCO_3$ (20 mL), dried ($MgSO_4$) and the solvent removed *in vacuo*. After purification by column chromatography on silica (CH_2Cl_2 with a gradient of 0 to 50% AcOEt) *S*$_{mt}$-**276** was obtained as a white foam (89.0 mg, 68% over 2 steps). Spectroscopic data were identical to those reported for *rac*-**6** with the exception of the circular dichroism spectra.

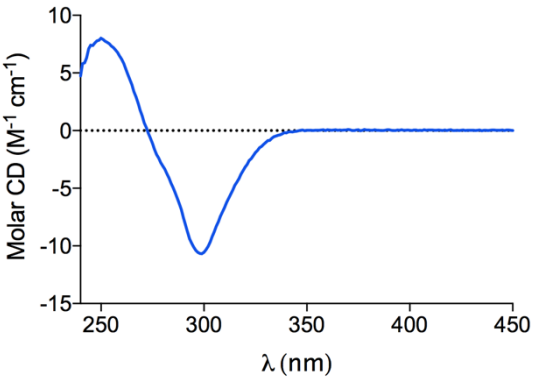

Figure 5.48 Circular dichroism spectrum of *S*$_{mt}$-**276** (43.0 µM in $CHCl_3$, 293K).

Catenane R_{mt}-276

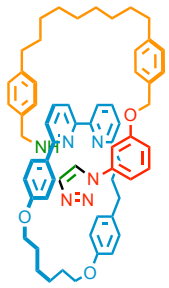

An identical procedure to that for S_{mt}-**276** but employing (S,R_{mt})-**275** afforded R_{mt}-**276** as a white foam (120mg, 50% over 2 steps). Spectroscopic data were identical to those reported for *rac*-**276** with the exception of the circular dichroism spectra.

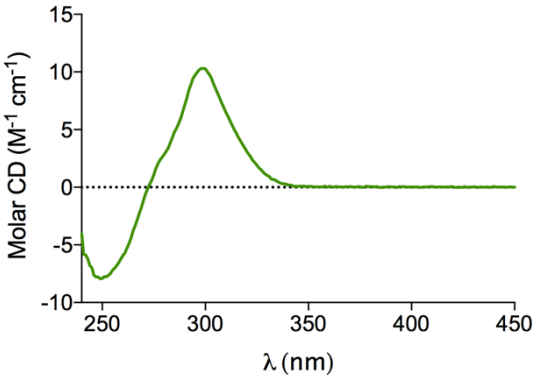

Figure 5.49 Circular dichroism spectrum of S_{mt}-**276** (43.0 μM in $CHCl_3$, 293K).

*Syntheses of triazole-functionalised macrocycles **264** and **266***

*Macrocycle **264***

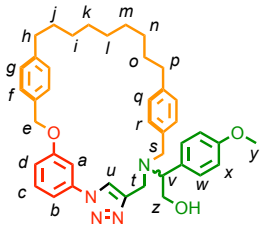

To a solution of $[Cu(CH_3CN)_4]PF_6$ (23.1 mg, 0.062 mmol, 0.98 eq.), $^{i}Pr_2NEt$ (27 µL, 0.15 mmol, 2.4 eq.) in 1:1 $CHCl_3$/EtOH (6.2 mL) at 60 °C was added **263** (40.0 mg, 0.062 mmol, 1.0 eq.) in 1:1 $CHCl_3$/EtOH (2.4 mL) over 4 h. After removal of the solvent *in vacuo*, the residue was dissolved in CH_2Cl_2 (20 mL) and washed with EDTA-NH_3 (2 × 10 mL), dried ($MgSO_4$) and the solvent removed *in vacuo*. After purification by column chromatography on silica (Petrol/CH_2Cl_2 1/1 with a gradient from 0 to 20% EtOAc) **264** was obtained as a white foam (30.0 mg, 75%). ^{1}H NMR (500 MHz, $CDCl_3$) δ: 7.69 (s, 1H, H_u), 7.54-7.41 (m, 2H, H_c, H_b or H_d), 7.32 (d, *J* = 8.2, 2H, H_f), 7.27 (d, *J* = 8.8, 2H, H_w), 7.21 (d, *J* = 8.0, 2H, H_r), 7.17 (d, *J* = 8.4, 2H, H_g), 7.12 (d, *J* = 8.2, 2H, H_q), 7.08 (dt, *J* = 2.4, 1.0, 1H, H_a), 7.07-7.04 (m, 1H, H_b or H_d), 6.95 (d, *J* = 8.8, 2H, H_x), 5.12 (s, 2H, H_e), 4.12 (t, *J* = 10.6, 1H, 1 of H_z), 4.04 (dd, *J* = 10.4, 4.8, 1H, H_v), 3.95 (d, *J* = 15.2, 1H, 1 of H_t), 3.88 (d, *J* = 13.4, 1H, 1 of H_s), 3.84 (s, 3H, H_y), 3.68 (dd, *J* = 10.8, 4.7, 1H, 1 of H_z), 3.61 (d, *J* = 14.6, 1H, 1 of H_t), 3.18 (d, *J* = 13.6, 1H, 1 of H_s), 2.62 (td, *J* = 6.7, 2.4, 2H, H_h or H_p), 2.54 (t, *J* = 7.7, 2H, , H_h or H_p), 1.64 – 1.50 (m, 4H, H_i, H_o), 1.22 (m, 10H, H_j, H_k, H_l, H_m, H_n). ^{13}C NMR (126 MHz, $CDCl_3$) δ 159.5, 159.5, 147.5, 143.0, 142.1, 136.2, 133.5, 130.8, 130.5, 129.2, 128.8, 128.7, 128.1, 127.2, 120.4, 114.2, 113.9, 113.2, 108.3, 70.4, 63.6, 61.0, 55.4, 53.9, 44.7, 35.6, 35.5, 31.2, 30.9, 29.6, 29.2, 29.0, 28.9, 28.3. HR-ESI-MS *m/z* = 645.3813 $[M+H]^+$ calc. 645.3799.

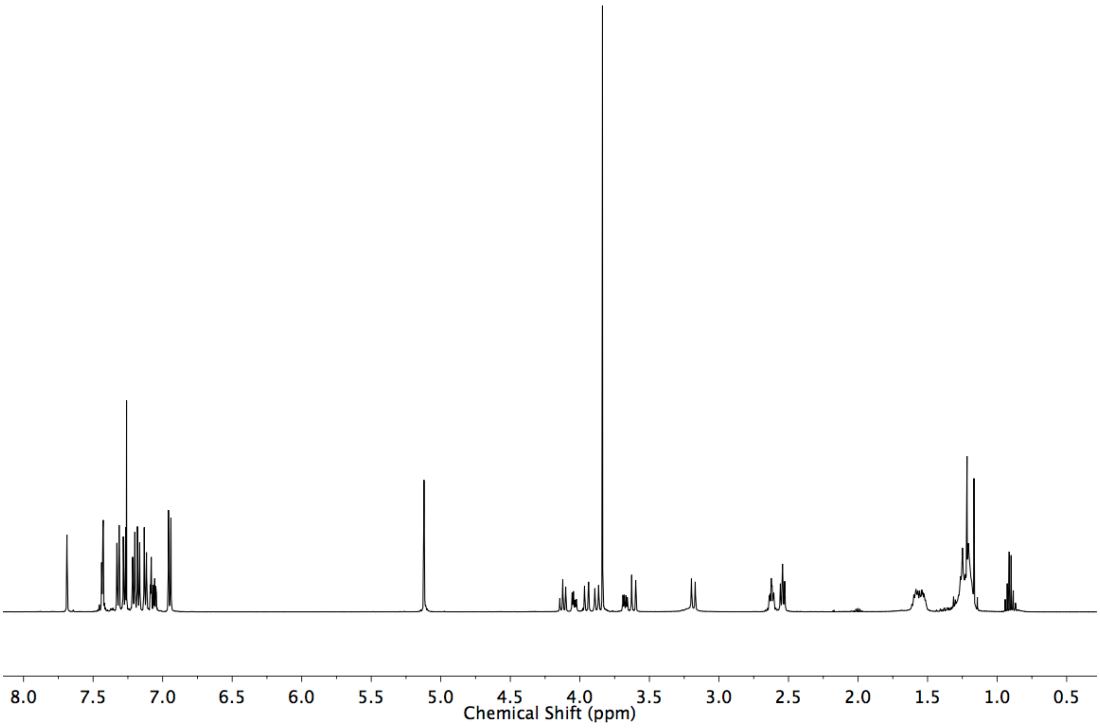

Figure 5.50 ^{1}H NMR (500 MHz, $CDCl_3$) of **264**.

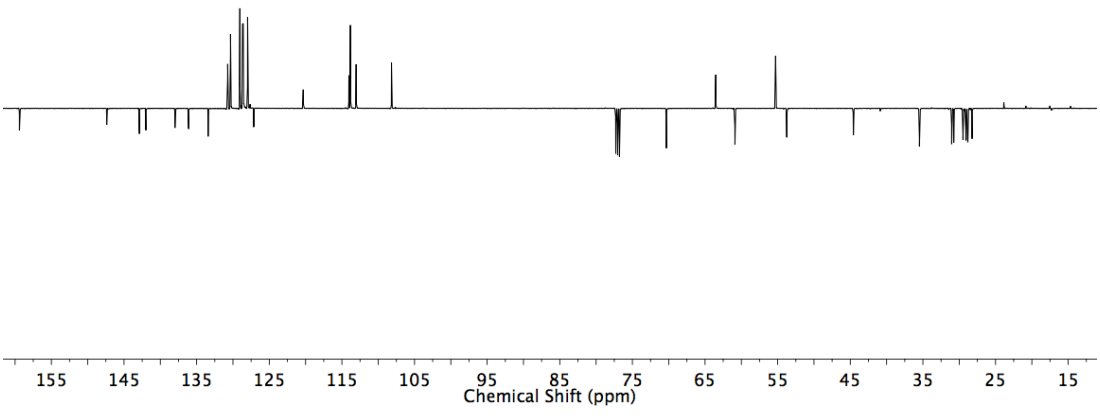

Figure 5.51 JMOD NMR (126 MHz, $CDCl_3$) of **264**.

Macrocycle ***266***

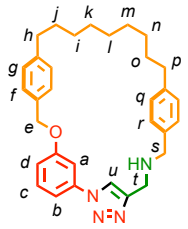

To a solution of $[Cu(CH_3CN)_4]PF_6$ (27.9 mg, 0.075 mmol, 0.98 eq.), $^{i}Pr_2NEt$ (27 µL, 0.15 mmol, 2.0 eq.) in 1:1 $CHCl_3$/EtOH (7.5 mL) at 60 °C was added **265** (38.0 mg, 0.077 mmol, 1.0 eq.) in 1:1 $CHCl_3$/EtOH (3.0 mL) over 4 h. After removal of the solvent *in vacuo*, the residue was dissolved in CH_2Cl_2 (20 mL) and washed with EDTA-NH_3 (2 × 10 mL), dried ($MgSO_4$) and the solvent removed *in vacuo*. After purification by column chromatography on silica (Petrol/CH_2Cl_2 1/1 with a gradient from 0 to 50% EtOAc) **266** was obtained as a white foam (12.0 mg, 32%). ^{1}H NMR (500 MHz, $CDCl_3$) δ: 7.73 (s, 1H, H_u), 7.44-7.41 (m, 2H, H_c, H_b or H_d), 7.27 (d, *J* = 8.4, 2H, H_f), 7.22 (d, *J* = 8.4, 2H, H_r), 7.14 (d, *J* = 8.4, 2H, H_g), 7.10 (d, *J* = 8.4, 2H, H_q), 7.08-7.04 (m, 1H, H_b or H_d), 7.00-6.97 (m, 1H, H_a), 5.13 (s, 2H, H_e), 4.04 (s, 2H, H_t), 3.82 (s, 2H, H_s), 2.57 (t, *J* = 7.3, 4H, H_h, H_p), 1.62-1.50 (m, 4H, H_i, H_o), 1.40-1.05 (m, 10H, H_j, H_k, H_l, H_m, H_n). ^{13}C NMR (126 MHz, $CDCl_3$) δ 159.7, 148.1, 143.0, 141.7, 138.2, 137.2, 133.7, 130.8, 129.1, 128.8, 128.3, 127.6, 120.3, 115.1, 113.2, 107.8, 70.6, 53.4, 44.6, 35.7, 35.4, 31.2, 31.2, 29.6, 29.6, 29.2, 28.9, 28.4. HR-ESI-MS *m/z* 495.3123 $[M+H]^+$ calc. 495.3118.

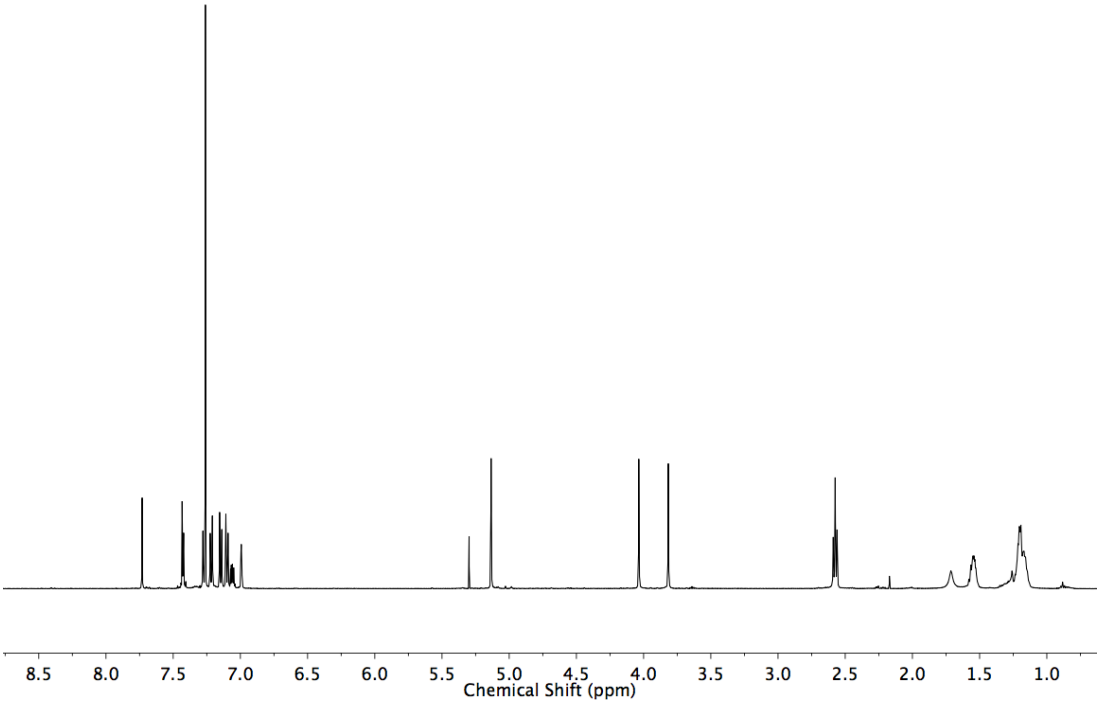

Figure 5.52 ^{1}H NMR (500 MHz, $CDCl_3$) of **266**.

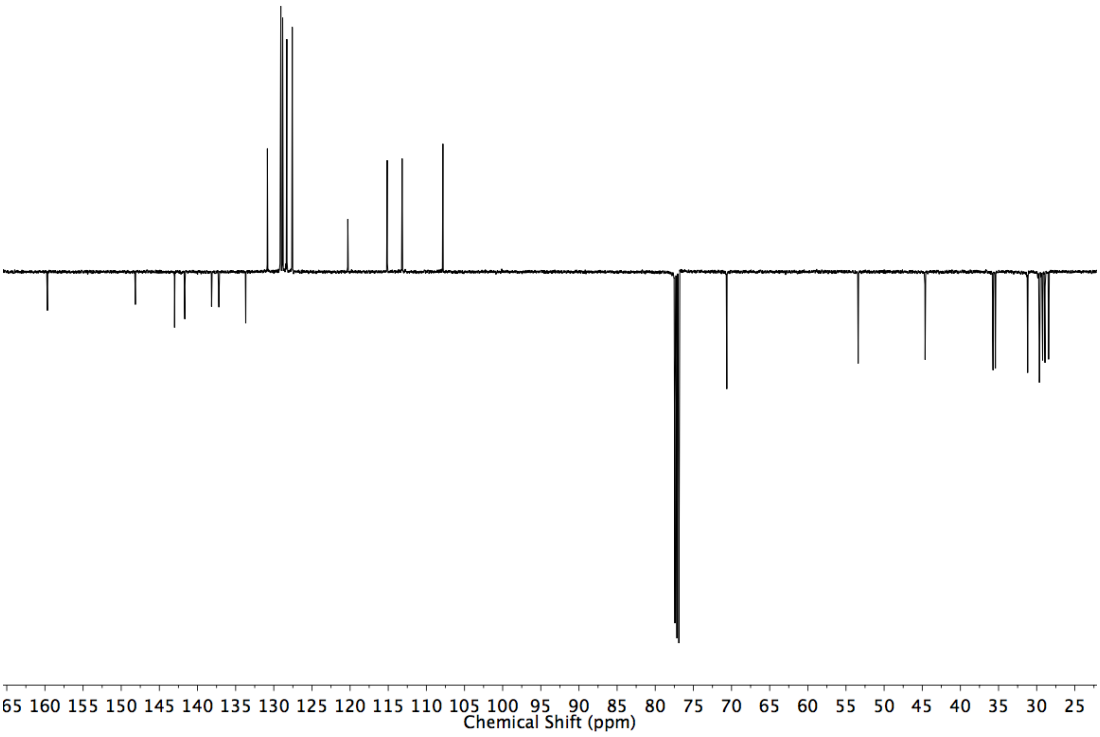

Figure 5.53 JMOD NMR (126 MHz, $CDCl_3$) of **266**.

Chiral Stationary Phase HPLC analysis of enantiopure samples of catenane ***276***

Samples were analysed on a RegisCell column with a concentration of ~ $1x10^{-4}$ M and injection volume = 5 μL, in a solution of 9:1 hexane-IPA, with and isocratic gradient of 98:2 hexane-IPA at a flowrate of 0.5 mL/min.

CSP-HPLC for the racemic catenane ***276***

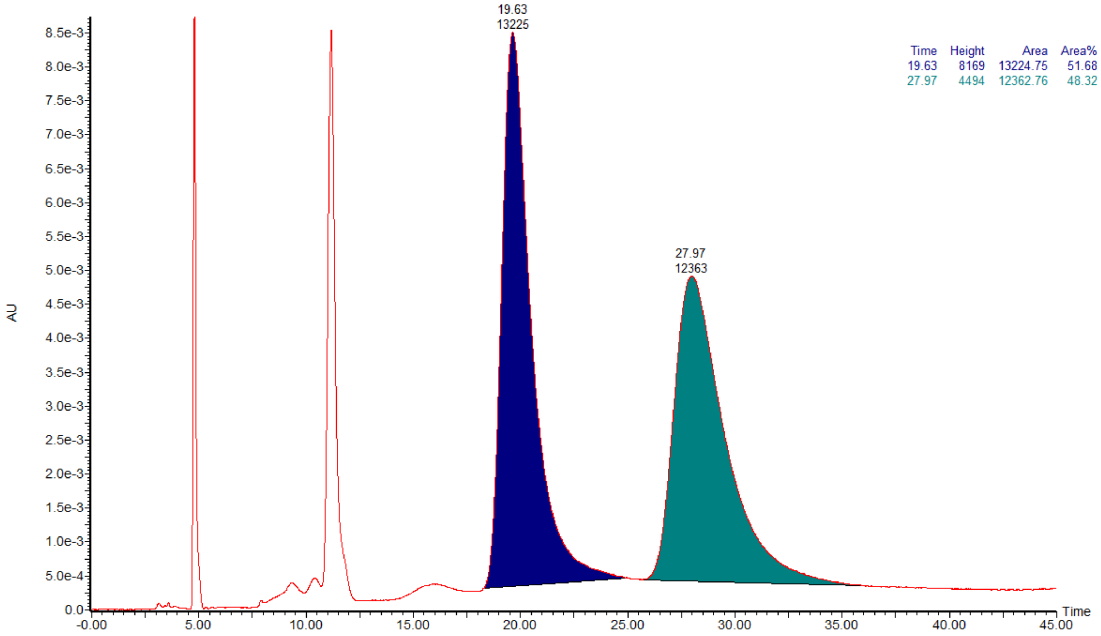

CSP-HPLC for the R_{mt} catenane ***276***

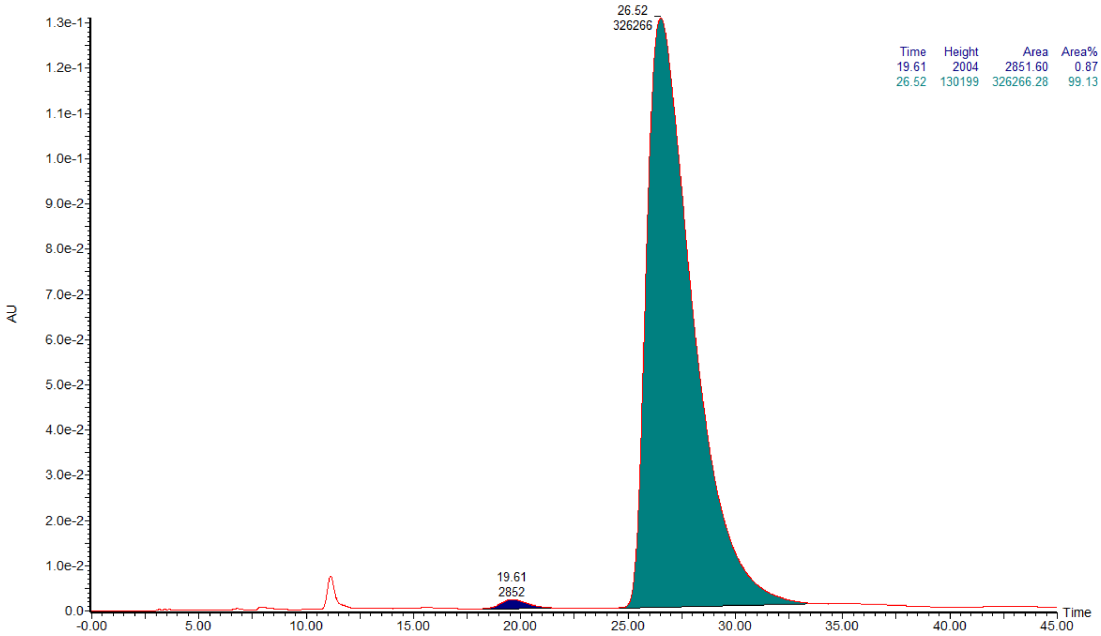

CSP-HPLC for the S_{mt} catenane ***276***

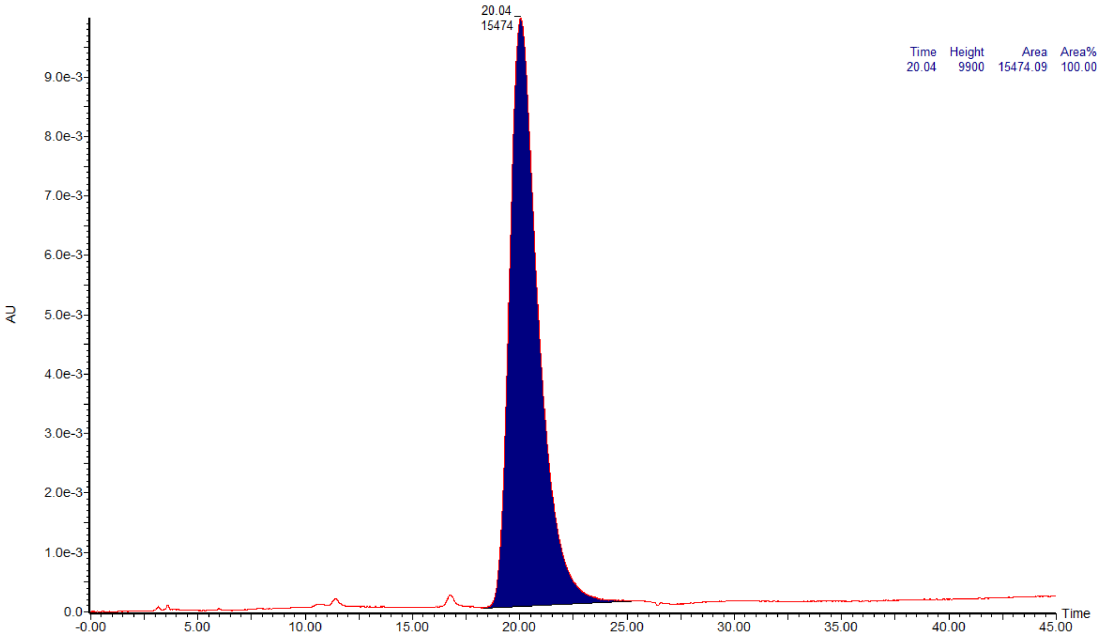

Single Crystal X-ray Analysis of Catenanes

For **275**, crystals were grown by vapour diffusion of pentane into a CH_2Cl_2 solution. Data for **275** were collected at 100 K using a FRE+ HF diffractometer equipped with a Saturn 724+ enhanced sensitivity detector. Cell determination, data collection, data reduction, cell refinement and absorption correction were performed with CrysalisPro. The structure was solved using SUPERFLIP[16,17] and refined against F_2 using anisotropic thermal displacement parameters for all non-hydrogen atoms using WINGX[18] and software packages within. Hydrogen atoms were placed in calculated positions and refined using a riding model.

Compound	(*R*,S_{mp})-**275**	
Empirical formula	$C_{144}H_{158}N_{12}O_{10}$	
Formula weight	2216.81	
Temperature	100(2) K	
Wavelength	0.71073 Å	
Crystal system	Monoclinic	
Space group	$P2_1/n$	
Unit cell dimensions	a = 26.2879(9) Å	α= 90°
	b = 16.1275(5) Å	β= 106.741(4)°
	c = 29.7838(11) Å	γ = 90°
Volume	12091.9(8) $Å^3$	
Z	4	
Density (calculated)	1.218 Mg/m^3	
Absorption coefficient	0.077 mm^{-1}	
F(000)	4744	
Crystal size	0.095 × 0.090 × 0.080 mm^3	
Theta range for data collection	1.500 to 23.256°.	
Index ranges	-29<=h<=29, -17<=k<=17, -33<=l<=33	
Reflections collected	162942	
Independent reflections	17362 [R(int) = 0.1998]	
Completeness to theta = 23.256°	100.0 %	
Absorption correction	Semi-empirical from equivalents	
Max. and min. transmission	1.00000 and 0.72382	
Refinement method	Full-matrix least-squares on F^2	
Data / restraints / parameters	17362 / 0 / 1499	
Goodness-of-fit on F^2	1.038	
Final R indices [I>2sigma(I)]	R_1 = 0.0885, wR_2 = 0.2087	
R indices (all data)	R_1 = 0.1668, wR_2 = 0.2649	

Extinction coefficient	n/a
Largest diff. peak and hole	0.673 and -0.575 e.Å^{-3}

5.4. Bibliography

[1] N. Pairault, J. Niemeyer, *Synlett* **2018**, *29*, 689–698.

[2] N. H. Evans, *Chem. – Eur. J.* **2018**, *24*, 3101–3112.

[3] E. M. G. Jamieson, F. Modicom, S. M. Goldup, *Chem. Soc. Rev.* **2018**, *47*, 5266–5311.

[4] D. K. Mitchell, J.-P. Sauvage, *Angew. Chem. Int. Ed. Engl.* **1988**, *27*, 930–931.

[5] J. C. Chambron, D. K. Mitchell, J. P. Sauvage, *J. Am. Chem. Soc.* **1992**, *114*, 4625–4631.

[6] J.-C. Chambron, C. Dietrich-Buchecker, G. Rapenne, J.-P. Sauvage, *Chirality* **1998**, *10*, 125–133.

[7] A. Mohry, F. Vögtle, M. Nieger, H. Hupfer, *Chirality* **2000**, *12*, 76–83.

[8] R. J. Bordoli, S. M. Goldup, *J. Am. Chem. Soc.* **2014**, *136*, 4817–4820.

[9] K. C. Nicolaou, S. Natarajan, H. Li, N. F. Jain, R. Hughes, M. E. Solomon, J. M. Ramanjulu, C. N. C. Boddy, M. Takayanagi, *Angew. Chem. Int. Ed.* **1998**, *37*, 2708–2714.

[10] J. E. M. Lewis, R. J. Bordoli, M. Denis, C. J. Fletcher, M. Galli, E. A. Neal, E. M. Rochette, S. M. Goldup, *Chem. Sci.* **2016**, *7*, 3154–3161.

[11] M. Galli, C. J. Fletcher, M. del Pozo, S. M. Goldup, *Org. Biomol. Chem.* **2016**, *14*, 5622–5626.

[12] N. Nakajima, K. Horita, R. Abe, O. Yonemitsu, *Tetrahedron Lett.* **1988**, *29*, 4139–4142.

[13] K. Horita, T. Yoshioka, T. Tanaka, Y. Oikawa, O. Yonemitsu, *Tetrahedron* **1986**, *42*, 3021–3028.

[14] J. L. Marco, J. A. Hueso-Rodríguez, *Tetrahedron Lett.* **1988**, *29*, 2459–2462.

[15] J. E. M. Lewis, F. Modicom, S. M. Goldup, *J. Am. Chem. Soc.* **2018**, *140*, 4787–4791.

[16] L. Palatinus, G. Chapuis, *J. Appl. Crystallogr.* **2007**, *40*, 786–790.

[17] L. Palatinus, S. J. Prathapa, S. van Smaalen, *J. Appl. Crystallogr.* **2012**, *45*, 575–580.

[18] L. J. Farrugia, *J. Appl. Crystallogr.* **2012**, *45*, 849–854.